P. Bastian • D. Kranzlmüller • H. Brüchle • G. Mathias
EDITORS

High Performance Computing

in Science and Engineering Garching/Munich 2022

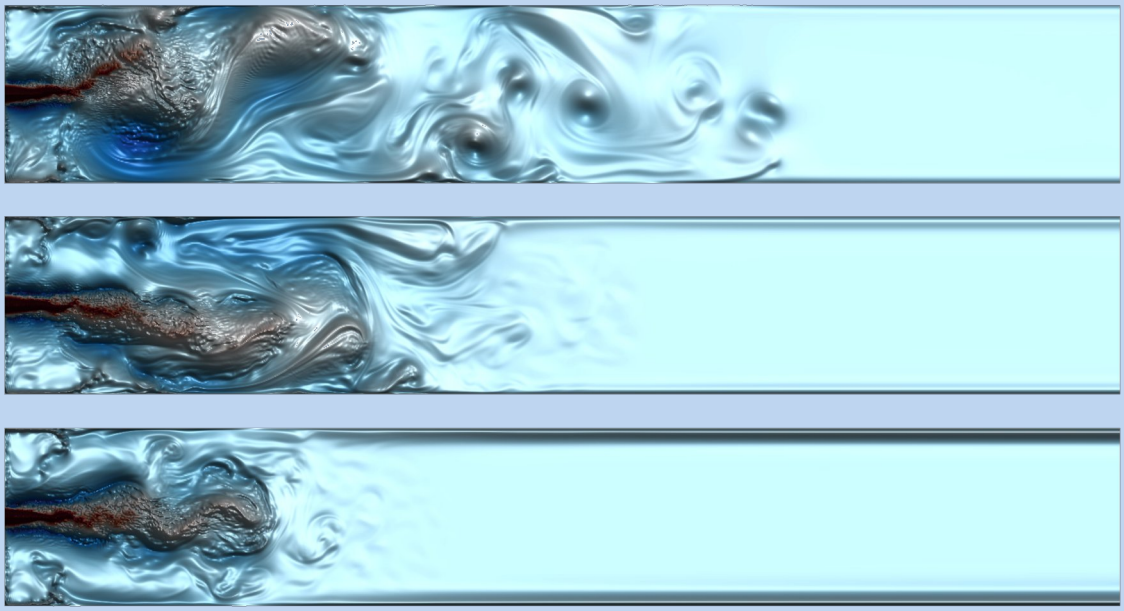

KONWIHR

lrz Leibniz Supercomputing Centre
of the Bavarian Academy of Sciences and Humanities

GCS Gauss Centre for Supercomputing

Titelbild entnommen aus dem Artikel von Jörg Schumacher und Dimitry Krasnov. Die Bilder zeigen Ergebnisse von direkten numerischen Simulationen eines runden Strahls in einem transversalen Magnetfeld. Die drei Teilbilder zeigen Schnappschüsse der Geschwindigkeitskomponente in Strömungsrichting für Wandleitfähigkeiten Cw = 0, 0,01 und 0,1 (von oben nach unten). Das Magnetfeld steht senkrecht zur Bild-Ebene. Weitere Informationen im Artikel ab Seite 110.

Impressum:

Leibniz-Rechenzentrum
der Bayerische Akademie der Wissenschaften
Boltzmannstraße 1, D-85748 Garching bei München
lrzpost@lrz.de, www.lrz.de

Herausgeber: Peter Bastian, Dieter Kranzlmüller, Helmut Brüchle, Gerald Mathias
Redaktion und Layout: Helmut Brüchle
Gestaltungskonzept: Tausendblauwerk, Konrad-Adenauer-Straße 22, 85221 Dachau,
www.tausendblauwerk.de
Druck und Bindung: Mayr & Abel Druck GmbH, Marktplatz 2, 87764 Legau.

Bezugsadresse:

Leibniz-Rechenzentrum (LRZ)
Boltzmannstraße 1, D-85748 Garching bei München
https://www.lrz.de/hpcbooks

ISBN 978-3-9816675-5-4

P. Bastian • D. Kranzlmüller • H. Brüchle • G. Mathias
EDITORS

High Performance Computing

in Science and Engineering Garching/Munich 2022

KONWIHR

Leibniz Supercomputing Centre
of the Bavarian Academy of Sciences and Humanities

GCS
Gauss Centre for Supercomputing

Table of Contents

Preface

Chapter 01 – Astrophysics

Chapter 02 – Chemistry and Material Sciences

Chapter 02 – Chemistry and Material Sciences (cont.)

Chapter 03 – Computational Fluid Dynamics and Engineering

Chapter 04 – Earth, Climate and Environmental Sciences

Chapter 05 – Elementary Particle Physics

Chapter 05 – Elementary Particle Physics (cont.)

Chapter 06 - Life Sciences

Chapter 07 - Plasma Physics

Chapter 08 - Math, Computer Sciences

Appendices

The high-performance computer SuperMUC-NG at the Leibinz Supercomputing Centre is based on Lenovo ThinkSystem SD650 DWC compute nodes and equipped with Intel Skylake Xeon Platinum 8174 processors. The machine hosts 6,336 thin compute nodes, each with 48 cores and 96 GB memory, and 144 fat compute nodes, each with 48 cores and 768 GB memory per node. User operation started in August 2019. (Picture: F. Löchner).

The Editors

Prof. Dr. Peter Bastian
Chairman of the SuperMUC-NG Steering Committee, Interdisciplinary Center for Scientific Computing, Heidelberg University

Prof. Dr. Dieter Kranzlmüller
Chairman of the Board of Directors Leibniz Supercomputing Centre, Bavarian Academy of Sciences and Humanities

Dr. Helmut Brüchle
Editor-in-Chief Computational X Support, Leibniz Supercomputing Centre, Bavarian Academy of Sciences and Humanities

Dr. habil. Gerald Mathias
Head of Computational X Support Leibniz Supercomputing Centre, Bavarian Academy of Sciences and Humanities

Supporting Cutting-Edge Research

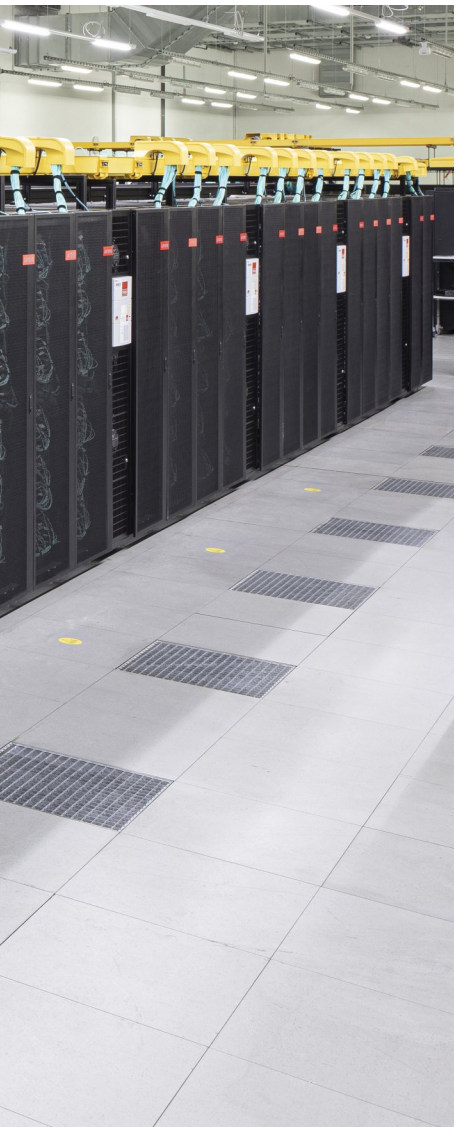

SuperMUC-NG, with its 311,000 compute cores, began user operation in August 2019 and has become a reliable platform for computational science. Today it is still among the worlds fastest supercomputers. The contributions in this book report on the excellent research conducted on the machine between June 2020 and December 2021.

Scientific highlights, like simulating the evolution dynamics of the observable universe (p. 18 and [1]), have only been possible by exploiting all different levels of parallelism in the machine architecture, i.e. from the level of compute nodes, over CPU-cores, down to the vector units. Due to this complex hierarchy, the adaptation and optimization of the scientific codes and workflows is often challenging for domain scientists. Therefore, user support has been extended within the Gauss Centre for Supercomputing (GCS)[2] to offer help on code optimization and efficient workflows. A dedicated mentor is assigned to GCS large-scale compute projects at LRZ. The mentor consults the project if needed and develops tailored solutions together with the compute projects. LRZ staff with a corresponding scientific background provides this high-level support within domain specific labs [3].

A flagship example of high-level support is the development of a new visualization workflow that directly processes the output of massively parallel Lattice-Boltzmann simulations and renders images straight on the compute nodes of SuperMUC-NG. Members of the Computational X Support (CXS) as well as the Visualization and Virtual Reality Centre (V2C) at the LRZ, together with experts from Intel, were able to assist the EU-funded Centre of Excellence CompBioMed [4] in the visualization of human-scale blood flow simulations, as reported at the Supercomputing Conference SC21 (see [5, 6] and page 220).

The upcoming Phase 2 of SuperMUC-NG will be GPU-accelerated and, thus, follows the general trend in high-performance computing, which is imposed by the high GFlop/s per watt power efficiency of GPUs. Code porting to such architectures requires special knowledge, provided by training courses on GPU programming. The rapidly emerging methods of artificial intelligence and deep learning already support GPU architectures within workstations and are now ready to tackle the challenges of high-performance computing. As a first example, the DeToL project, in cooperation with the LRZ, managed to utilize SuperMUC-NG for neural architecture searches during a block operation at full-machine scale (page 248 and [7]), and is now in the starting block for Phase 2.

The broad spectrum of illustrative articles in this book shows that SuperMUC-NG is an outstanding tool for computational scientists to address research problems of broad relevance. Detailed usage statistics on page 260 show how the various science domains utilize the machine.

Acknowledgments

We gratefully acknowledge the continued support of the Free State of Bavaria and the German Federal Ministry of Education and Research (BMBF), as well as the Bavarian Competence Network for Technical and Scientific HighPerformance Computing (KONWIHR), the Gauss Centre for Supercomputing (GCS), the German Research Foundation (DFG), the Partnership for Advanced Computing in Europe (PRACE), and many other institutions promoting high-performance computing. We thank the reviewers and the Steering Committees of GCS and SuperMUC-NG for the reviews of the projects, their insights and helpful remarks. Without their efforts it would not have been possible to sustain the high scientific quality we value in these projects.

Garching bei München, November 2022
Peter Bastian *Helmut Brüchle*
Dieter Kranzlmüller *Gerald Mathias*

[1] https://www.youtube.com/watch?v=2gYsfZ4Gcv8
[2] https://www.gauss-centre.eu/
[3] https://doku.lrz.de/display/PUBLIC/HPC+Application+Labs
[4] https://www.compbiomed.eu
[5] https://sc21.supercomputing.org/proceedings/sci_viz/sci_viz_pages/svs102.html
[6] https://www.youtube.com/watch?v=Sd8_cujMP_4
[7] https://keuperj.github.io/DeToL/

Astrophysics

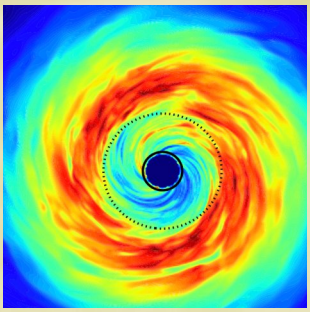

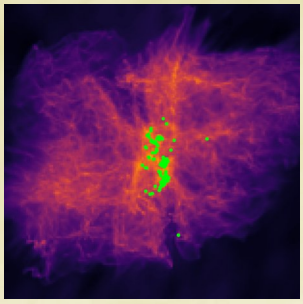

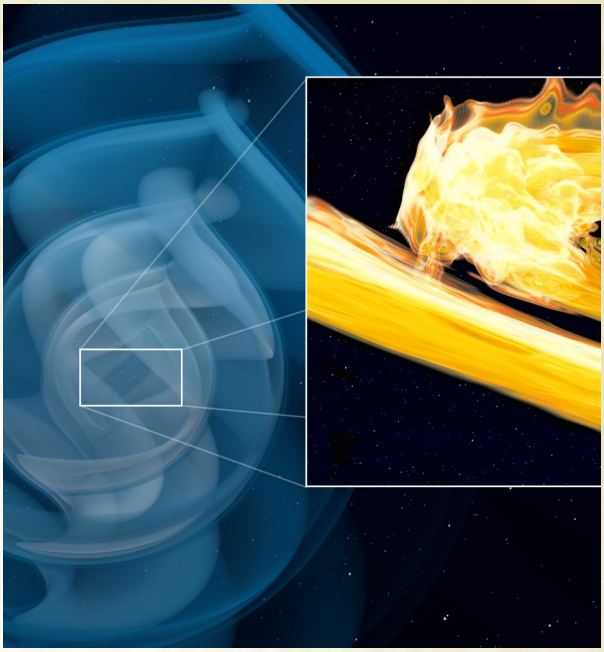

Analyzing and Interpreting Compact Binary Mergers

Research Institution
[1]University of Potsdam

Principal Investigator
Tim Dietrich[1,2]

Researchers
Swami Vivekanandji Chaurasia[3], Henrique Leonard Gieg[4], Nina Kunert[1], Michele Mattei[1], Anna Neuweiler[1], Peter Tsun Ho Pang[5], Maximiliano Ujevic[4], Federico Schianchi[1]

Project Partners
[2]Max Planck Institute for Gravitational Physics, Potsdam
[3]Stockholm University
[4]Federal University of ABC Sao Paulo
[5]Nikhef, Amsterdam

SuperMUC Project ID: pn29ba

Introduction

Since the detection of gravitational waves emitted from the merger of two black holes in 2015, almost hundred binary binary black hole systems have been observed. In 2017 happened another breakthrough discovery namely the first coincident detection of gravitational waves and electromagnetic signals arising from the same system, the merger of two neutron stars. In 2020, the last class of compact binary mergers have been observed, namely a black hole - neutron star system. The conditions present during the merger of a neutron star with another compact object are unreachable with terrestrial processes or experiments. Therefore, neutron star systems provide a unique laboratory to study matter at its extreme limits. However, the extraction of information from such mergers is challenging. To allow an accurate interpretation, one must relate the measured data with theoretical predictions. Concerning gravitational-wave astronomy, this can be done by correlating the observed data with a waveform model until the agreement is maximized. Considering electromagnetic astronomy, one needs to relate the observed signals such as spectra and light curves with the theoretical predictions of the sources. Employing such methods, the observation of GW170817 and its electromagnetic counterparts AT2-017gfo and GRB170817A has provided major leaps forward in several research areas. With the planned upgrades of gravitational-wave detectors and considerable investment in new electromagnetic telescopes, one expects to detect numerous compact binary mergers in the following years. Because of this, we will be able to improve on the existing constraints noticeably. Hence, one also has to improve the existing frameworks and models to ensure that the detected signals are correctly interpreted. This is the main focus of our work using SuperMUC-NG. We aim to better understand the compact binary merger process through numerical-relativity simulations and for improved Bayesian parameter estimation infrastructures to be prepared for the upcoming compact binary merger detections.

Results and Methods

With the help of our allocation, we have been able to publish seven research articles and produced three additional preprints that are currently under review.

Black Hole – Neutron Star Simulations
Numerical-relativity simulations are the only way to describe the final stage of the compact binary coalescence when gravitational fields are strongest, and velocities are largest. Hence, our simulations allow us to characterize the imprint of the intrinsic binary parameters on the binary dynamics, to develop gravitational-wave models, and to relate electromagnetic observations with the binaries parameters. Our numerical-relativity simulations are performed with the BAM code. BAM combines state-of-the-art methods to deal with black hole spacetimes, shock capturing methods for general relativistic hydrodynamics simulations, and mesh refinement techniques to resolve the strong-field region surrounding the compact objects as well as the distant wave zone. The codes use the method of lines with a Runge-Kutta time integration. Every physical configuration is simulated using different numerical resolutions to allow for a proper error assessment and convergence analysis. For this purpose, individual simulations run on a few hundred to a few thousand cores depending on the resolution. While we have focused in the past on the simulation of binary neutron star systems, we have recently extended our code infrastructure to allow the simulation of black hole – neutron star systems [2]. These preliminary studies have been successful but revealed that we have to improve the construction of our initial configurations used for the dynamical simulations. A first step has been done by developing a new code infrastructure [3], and further tests are ongoing. A significant challenge is that in contrast to our binary neutron star simulations, we do not obtain a clear convergence order of characteristic quantities for our black hole – neutron star simulations. Nevertheless, our first simulations have also been important for increasing further the range of physical systems that we can simulate. Furthermore, we could use our

numerical data to create public outreach activities related to the first black hole – neutron star observations, see, e.g. Fig. 1. Our animations based on full 3+1D numerical-relativity simulations have been watched more than 100,000 times, have been used by NASA, and have been taken over by dozens to hundreds of newspapers, including *The New York Times*.

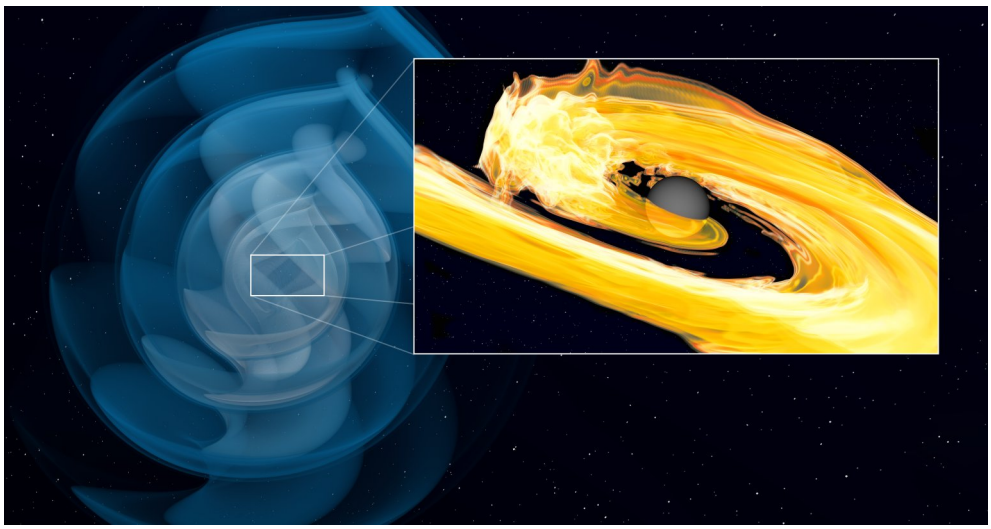

Figure 1: Numerical-relativity simulation of a black hole - neutron star system. The gravitational-wave signal is shown on the left and on the right side we present an inset of the matter distribution. In contrast to the present snapshot, the first detected black hole – neutron star mergers in 2020 were characterized by a plunging neutron star without the formation of a debris disk; see [6].

Comparing Microscopic and Macroscopic Collisions

Multi-messenger data analysis relies on Bayes' theorem to compute the posterior probability distribution functions assuming that the measured data are composed of a signal and noise. The likelihood of obtaining a signal is then calculated by cross-correlating the data with several million theoretical predictions. These predictions have to be computed for various system parameters, have to be fast to compute, and need to describe the system accurately enough to model the measured gravitational-wave or electromagnetic signal. Using a highly-parallel framework to allow efficient usage of SuperMUC-NG's resources, we focus on the multi-messenger of binary neutron star mergers. While the highest matter densities present in our Universe are reached within neutron stars, also terrestrial heavy-ion collision experiments probe matter densities beyond nuclear saturation density. We combined data from astrophysical multi-messenger observations of merging neutron stars, radio and X-ray observations of single neutron stars, theoretical nuclear-theory computations solving the equations of quantum chromodynamics perturbatively, and information from heavy-ion collisions of gold nuclei at relativistic energies to probe matter under extreme conditions. Our analysis [4] showed great consistency between information derived from heavy-ion collision experiments and multi-messenger observations. In fact, it is an astonishing result that data extracted from collisions of gold cores and the collision of neutron stars are in good agreement. Our analysis shows how joint analyses can shed light on the properties of neutron-rich supranuclear matter.

Systematic Biases in Gravitational-wave Models

With upcoming observing runs of advanced gravitational-wave detectors, we expect to observe gravitational-wave signals from multiple binary neutron star systems. As discussed, the combination of these numerous events creates the possibility to place tighter constraints on the neutron star radius and the equation of state at unprecedented accuracy. Despite these promising prospects, it is crucial to quantify systematic uncertainties inherited in gravitational-waveform models to enable more reliable results when multiple detections are combined. Since systematic waveform model uncertainties will become more pronounced when multiple gravitational-wave detections are combined, we performed a large injection campaign and simulated dozens of binary neutron star sources that were analyzed with different models. Some of these simulations were performed on SuperMUC-NG, and jobs ran on 8,192 and 16,384 cores. In our study [5], we were mainly interested in how systematic effects would affect the measurement of the neutron star radius. We found that systematic shifts caused by different gravitational¬wave approximants ended up affecting the radius measurement by about 450 meters. Contrary, due to the large number of detections, the statistical uncertainties decreased up to 250m. These results emphasize that dominant systematic effects are expected for future observing runs with gravitational-wave detectors such as LIGO and Virgo when using currently available waveform models.

Ongoing Research / Outlook

The continuous access to HPC facilities is a crucial prerequisite for our work considering both, the possibility to simulate compact binary systems and also our ability to analyse multi-messenger observations. The main limitation of our multi-messenger simulations was a high memory demand caused by the usage of a Gaussian-Process-Regression framework to compute generic electromagnetic signatures, hence, we used typically 3,072 cores on the fat nodes for our runs. We recently overcame this issue through a neural network approach that reduced the memory footprint by more than two orders of magnitude, which allows us to use SuperMUC-NG's infrastructure more efficiently. Another limitation was the queuing time. Thus, critical simulations, e.g., for the analysis of observational data, have only been performed to some extenti, but we also required local machines for which we had larger run times but shorter queuing times.

References and Links

[1] https://www.uni-potsdam.de/en/theoretical-astrophysics/
[2] S. Chaurasia et al., Phys.Rev.D 104 (2021) 8, 08401.
[3] A. Rashti et al., Phys.Rev.D 105 (2022) 10, 104027.
[4] S. Huth et al, Nature 606 (2022) 276-280.
[5] N. Kunert et al., Phys.Rev.D 105 (2022) 6, L061301.
[6] https://www.youtube.com/watch?v=Rd3p3xPtWn4&t=2s

The genesis of non-thermal radiation in astrophysical objects

1

Research Institution
Leibniz-Institut für Astrophysik Potsdam

Principal Investigator
Mohamad Shalaby

Researcher
Christoph Pfrommer

Project Partners
–

SuperMUC Project ID: pn29wa

Introduction

We observe our Universe primarily though thermal and non-thermal radiation. The thermal component probes gas (including both ionized and neutral components) in thermal equilibrium, whilst the non-thermal emission is emitted by particles such as leptons (e.g. electrons and positrons) or hadrons (e.g., protons and ions of heavier elements) that are not in thermal equilibrium, also known as cosmic rays (CRs). Because of the rarity of collisions of CRs, they survive with their high energies for a long time and emit non-thermal radiation while they travel through the medium in which they have been accelerated.

The prevalent non-thermal emission from CRs spans a vast range of energies: from radio to TeV energies, and occurs in various astrophysical objects spanning many length scales: from Mpc to sub-AU scales. Non-thermal electrons with very high energies (relativistic electrons), which are inferred from many radio observations, have a much higher radiating power compared to heavier ions at the same energy. Thus, understanding their acceleration mechanisms and how these electrons are transported (both in the vicinity and far from their acceleration sites) presents a cornerstone in interpreting current and upcoming observations.

Particle acceleration at shock waves is thought to be the main mechanism for producing CRs (electrons, protons, and heavier ions) in our Galaxy. Protons and heavier ions are transported diffusively near shock fronts and they are accelerated by scattering off of magnetic perturbations that exists near shock waves, a process known as diffusive shock acceleration (DSA) [1]. However, we still lack a detailed understanding of how electrons are accelerated at these shocks to high energies: for electrons and protons traveling with the same speed, the kinetic energy of electrons is much smaller than that of protons owing to their much smaller mass in comparison to protons. Therefore, unlike protons, these electrons can not directly scatter off of these waves. That is, for electrons to get accelerated via DSA processes, their energy needs to be continuously increased, i.e., pre-accelerated, before they can be further accelerated through DSA processes. This is know as the electron injection problem in shocks [2].

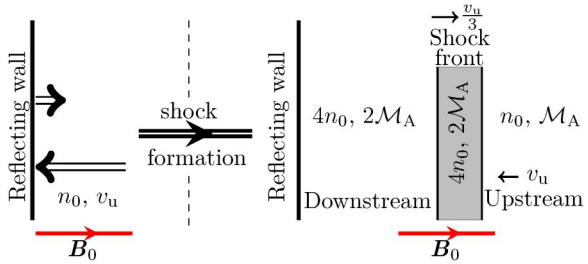

Figure 1: A Schematic representation of shock formation in simulation.

Solutions to this problem have thoroughly been investigated in the literature and in general proceed in two stages: (1) electrons are strongly heated in the downstream of the shock to energies much larger than their initial kinetic energy and (2) further small-scale magnetic wave-modes have to be continuously produced to scatter these hot electrons, which accelerates them to energies that enable them to participate in the DSA process.

The nature of these small-scale waves has been under scrutiny in many recent publications. Typically, they are assumed to be whistler waves that resonate with these hot electrons. However, it has also been shown that whistler waves are strongly damped and thus, they do not have enough energy to accelerate electrons sufficiently in case of quasi-parallel shocks, i.e., shocks that propagate close to the direction of the background large-scale magnetic field [3].

Recently, we discovered a new instability, named “intermediate-scale instability” [4]. This instability drives intermediate-scale ion-cyclotron waves near the shock front and we conjectured these wave-modes to play an important role in solving the electron injection problem. Using our SuperMUC-NG allocation we were able to run direct numerical simulations to show that this conjuncture was true and we now discovered a new mechanism for efficient electron acceleration at parallel electron-ion shocks. A schematic representation for how shocks are formed in simulations is shown in Figure 1.

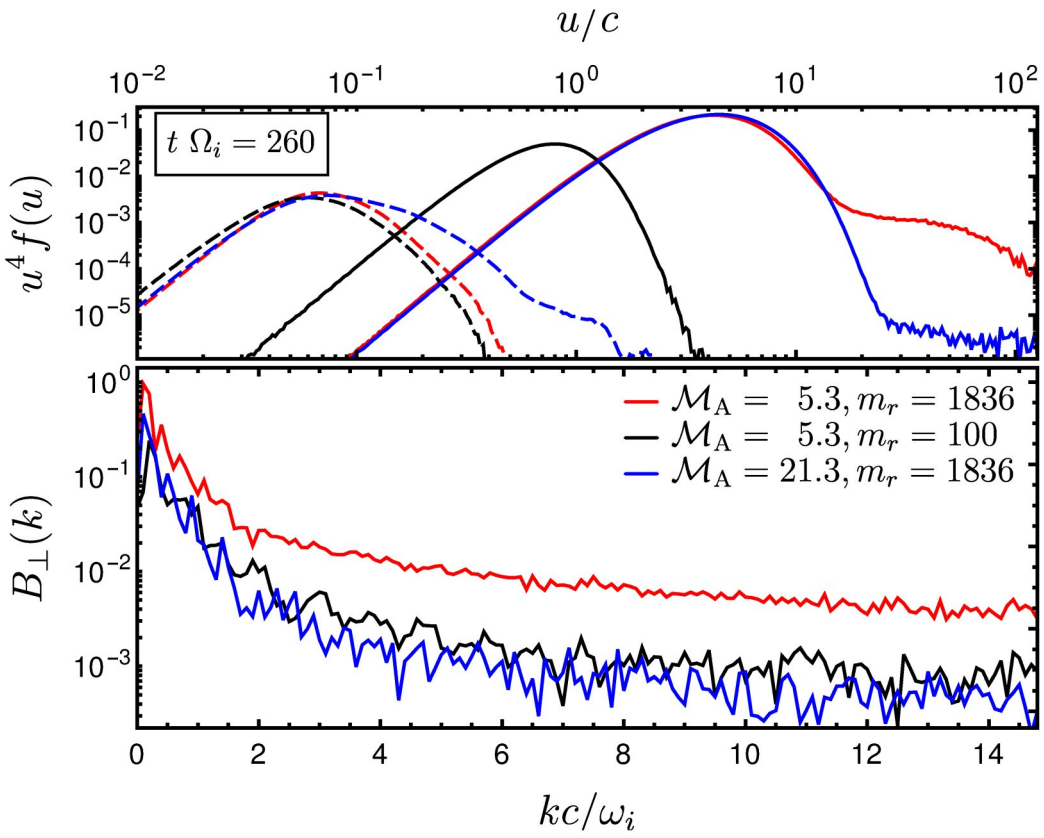

Figure 2: Top: downstream electron (solid) and ion (dashed) momentum spectra in various simulations. Bottom: downstream perpendicular magnetic energy in Fourier space at the same time. This shows that the co-moving (traveling towards the downstream) unstable waves that are driven at the shock front in the red simulation generate a much higher level of small-scale magnetic fields. These increased magnetic fluctuations imply a much stronger scattering and thus, more efficient acceleration of electrons in comparison to the other simulations.

Results and Methods

We run our numerical particle-in-cell simulations using the SHARP code [4,5]. As shown in Figure 1, the shock is formed by sending a supersonic isotropic electron-ion plasma towards a reflecting wall on the left. The interaction of the reflected and the incoming particles leads to shock formation. Our code has an unprecedented ability to avoid numerical heating and thus, enables more faithfully to explore the underlying physical process in our simulations. The memory management and access in our code is optimized to greatly reduce the computational cost for our simulations. For the fist time, this enabled simulations with a realistic ion-to-electron mass ratio and as such, enabled us to discover the physical mechanism responsible for (pre-)accelerating electrons at parallel electron-ion shocks.

To directly test the proposed mechanism for electron injection, we run a simulation where the condition for the new instability is fulfilled (red curves in Figure 2). We then compare this simulation to other two simulations, in which the condition for instability growth is not met. In those two simulations where ion-cyclotron waves are stable, whistler waves are unstable and are excited at the shock front. Figure 2 shows that the red simulation successfully accelerated more electrons and thus, only electrons in the red simulation can successfully participate in the DSA process.

Ongoing Research / Outlook

In all these simulations, we have used parameters relevant for probing the electron acceleration at supernova driven shocks. These results are in good agreement with global, magneto-hydrodynamic modeling of the multi-wavelength emission from the supernova remnant SN 1006 which required more efficient electron acceleration at parallel shocks in comparison to perpendicular shock configurations.

We plan to further investigate the impact of the new instability on the acceleration of electrons at shocks with parameters relevant for merger shocks in the intracluster medium which gives rise to the puzzling class of radio shocks.

References and Links

[1] Blandford, R. & Eichler, D. 1987, Phys. Rep., 154, 1.
[2] Guo, F. & Giacalone, J. 2015, ApJ, 802, 97.
[3] Amano, T. & Hoshino, M. 2010, Phys. Rev. Lett., 104, 181102.
[4] Shalaby, M., Thomas, T., & Pfrommer, C. 2021, ApJ, 908, 206.
[5] Shalaby, M., Broderick, A. E., Chang, P., et al. 2017, ApJ, 841, 52.

Simulating the observable Universe with MillenniumTNG

1

Research Institution
[1]Max Planck Institute for Astrophysics, Garching

Principal Investigator
Volker Springel[1]

Researcher
Simon White[1], Lars Hernquist[2]

Project Partner
[2]Harvard-Smithsonian Center for Astrophysics, Harvard University

SuperMUC Project ID: pn34mo (Gauss Large Scale project)

Introduction

The amazing progress in observational cosmology over the last decades has brought many surprises. Perhaps the most stunning is that we live in a Universe where most of the matter (~85%) is comprised of yet unidentified collisionless dark matter particles, while ordinary baryons produced in the Big Bang make up only a subdominant part (~15%). The initial state of the universe is a hot, nearly featureless soup of dark matter and plasma. But as the cosmos expands and cools, gravity amplifies tiny density perturbations, until they collapse and virialize as non-linear dark matter halos. Baryons radiatively cool and settle in these small potential wells, forming rotationally supported disks. The relentless pull of gravity causes further collapse and fragmentation in the cold gas, leading to star formation and thus to the formation of galaxies. Furthermore, in the last 5 billion years or so, a "dark energy" component has progressively become stronger and begun to overwhelm the matter energy density, driving an accelerated expansion of the Universe. The real physical nature of dark energy, as well as the mass of the neutrinos which contribute a tiny admixture of "hot" dark matter, are profound and fundamental open questions in physics. To make further progress, this firmly established standard cosmological model will be subjected to precision tests in the coming years that are far more sensitive than anything done thus far. Forthcoming cosmological mega galaxy surveys carried out by space missions such as Euclid and Roman, as well as new powerful telescopes on Earth such as Rubin, will map out billions of galaxies through extremely large regions of space. They will primarily use various measures of galaxy clustering and weak gravitational lensing to carry out precision tests of our cosmological model. The primary goals are to detect potential deviations of dark energy from a cosmological constant, signatures for a law of gravity different from general relativity, and new constraints on the mass of the light neutrino flavors. To take full advantage of this rich data, precise theoretical predictions are needed in regions of space equally vast as probed by the observations. In principal, the tool of choice for this are direct hydrodynamical cosmological simulations of galaxy formation that track how the full physics of cosmic structure formation unfolds over more than 13 billion years of evolution. Particular numerical challenges in these computations arise from the non-linear coupling of a range of different physics, including processes such as star formation, supernova explosions, and accretion of gas onto supermassive black holes, combined with the long-range nature of gravity that ties the evolution of dark matter and baryonic material tightly together. The problem however is that these calculations have thus far been restricted to comparatively small volumes, and simply doing them in the volumes required for the cosmological studies is computationally presently still infeasible. In our MillenniumTNG project we have therefore devised a novel, two-pronged approach to cope with this problem by combining key features of our iconic Millennium [1] and IllustristTNG [2] simulations. The idea is to carry out both, a very high resolution dark matter only simulation in the Millennium's original 740 Mpc volume, and a full hydrodynamical simulation using the same initial conditions and the state-of-the-art IllustrisTNG galaxy formation physics model. We then use a comparison of the two calculations to

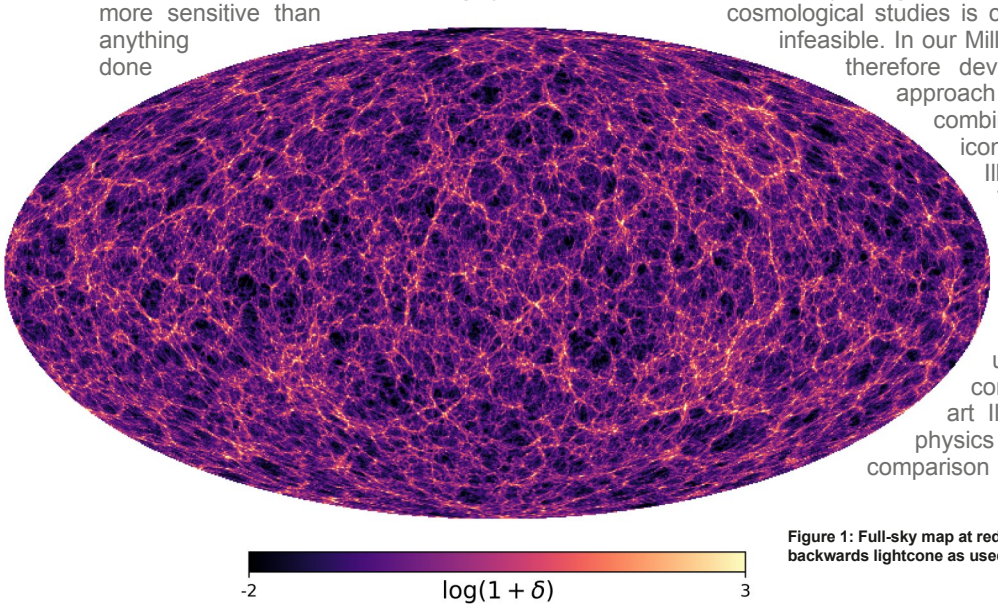

Figure 1: Full-sky map at redshift z = 0.1 of a mass shell projection of the past backwards lightcone as used for our weak gravitational lensing computations.

calibrate a so-called semi-analytic galaxy formation model, which can be subsequently applied to still much larger dark matter simulations of the universe with a size beyond 2 Gpc, but still with an accounting of the impact of baryonic physics on structure formation. This approach is unique in its ability to allow the use of physically based galaxy formation models in the comparison of theory to observations. The realism of the comparison is further boosted by our special strategy to output galaxy properties directly on a perfectly seamless backwards past lightcone, i.e. the hypersurface in space-time that we can actually observe. In addition, we produce special mass shell outputs to facilitate studies of the weak gravitational lensing effect with unprecedented precision. Figure 1 shows an example of such a weak lensing map, which allows us to study this key cosmological probe at an angular resolution of 0.26 arcsec, much finer than possible thus far. Furthermore, we also carry out additional simulations that account for the presence of massive neutrinos as hot dark matter admixture. Neutrinos amount to only about 1% of the matter density, and their fast, relativistic motions at early times prevent them from responding to structure growth initially, but at late times they slow down and begin to accumulate first in galaxy clusters, and later in less massive structures. This leads to subtle, scale-dependent impacts on how cosmic structures grow. Again, the future observational data will be precise enough to detect these percent levels differences, and thus we need simulations which can accurately predict the corresponding scale- and time-dependent effects.

Results and Methods

For the present project, we have developed a new major version of our GADGET code, which is one of the most widely used cosmological codes in the field. GADGET-4 [3] uses a novel approach to shared-memory hybrid parallelization based on MPI-3, where all MPI ranks on a node can bypass the MPI stack and directly synchronize their work via shared memory. One MPI task per shared memory node is set aside to serve incoming communication requests from other nodes, thereby establishing a highly efficient one-sided communication model. The code contains sophisticated on-the-fly postprocessing routines, such as a substructure finder and merger-tree building routines. The other code we have used in this project is our moving-mesh code AREPO, which is particularly well adapted to cosmological hydrodynamical simulations of galaxy formation. We use it to run the hydrodynamical twin of our GADGET-4 dark matter simulations, so that the impact of baryonic physics on cosmic structure formation can be studied in detail, and the semi-analytic galaxy formation code can be calibrated for these effects. The by far most expensive run of MillenniumTNG is a flagship hydrodynamic model in a 740 Mpc box, using 2,560 SuperMUC-NG nodes with 122,880 cores. It consumed slightly more than 100 million core hours to completion, and is by a long shot the largest high-resolution simulation of galaxy formation carried out to date worldwide. It improves on the volume of TNG300, the previous record holder, by a factor of about 15. The restart files of the calculation

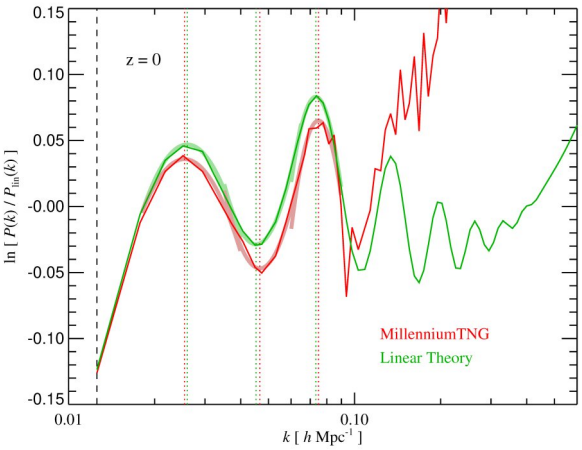

Figure 2: Impact of non-linear cosmic evolution on the baryonic acoustic oscillation on the largest scales. The peak positions are cosmological rulers which are affected at the percent level, an effect that our simulations can for the first time precisely measure.

alone amount to a gigantic size of 70 TB. Indeed, a major challenge of doing the simulation was to fit it into the available memory, and to devise postprocessing strategies that still allow an effective scientific analysis of the hundreds of TB produced by the cosmological model. But the results are rewarding. For example, we can finally study with precision the impact of mild non-linear evolution of the so-called baryonic oscillations measurable in the matter and galaxy distribution at different cosmic epochs. The precise location of these peaks are standard rulers that can be used for a reconstruction of the cosmic expansion history, which in turns gives access to constraining dark energy. Fig. 2 shows a precision measurement from our MillenniumTNG simulations that demonstrates that by the present time the baryonic oscillations are slightly affected even in their first peak, and in particular in its precise location. This effect needs to be accounted for in future cosmological inferences.

Ongoing Research / Outlook

The MillenniumTNG simulations are now complete and their analysis is in full swing. Their rich data sets, including merger trees that link more than 20 billion galaxies at different cosmic times, full matter light-cones of different geometry and redshift depths, as well as galaxy properties such as stellar masses, metallicities and galaxy morphologies, allow precision studies of galaxy clustering and weak gravitational lensing that we expect to be highly informative for theoretical cosmology. The very large data sets we created, of nearly 2 PB in size, will be mined for many years to come and will give rise to dozens of scientific publications. Also, we expect that the new methodologies we developed as part of the project, including the GADGET-4 code, the significant scaling improvements of the AREPO code we needed to realize to successfully scale beyond 10^5 MPI-ranks on SuperMUC-NG, as well as our postprocessing pipelines, will be instrumental for future simulation projects in the field.

References and Links

[1] https://wwwmpa.mpa-garching.mpg.de/mtng
[2] https://www.tng-project.org
[3] Springel V. et al., Nature 435 (2005) 629-636.
[4] Springel V. et al., MNRAS 475 (2018) 676-698.
[5] Springel V. et al., MNRAS 506 (2021) 2871-2949.

Fundamental Physics in the era of gravitational waves

Research Institution
[1]Department of Physics, University of Illinois Urbana-Champaign

Principal Investigator
Helvi Witek[1,4]

Researchers
Katy Clough[2,3], Eugene Lim[4], Josu Aurrekoetxea[3,4], Roberto Emparan[5], Pedro Ferreira[3], Giuseppe Ficarra[4], Leonardo Gualtieri[6], Roland Haas[1,7], Thomas Helfer[4,8], Francisco Jimenez[6,9], Raimon Luna[5], Hector Okada da Silva[10], Paolo Pani[6], Milton Ruiz[1]

Project Partners
[2]Queen Mary University London, [3]University of Oxford, [4]King's College London, [5]University of Barcelona, [6]La Sapienza University Rome, [7]National Center for Supercomputing Applications (NCSA), University of Illinois Urbana-Champaign, [8]John Hopkins University, Baltimore, [9]Albert-Einstein Institute Hannover, [10]Albert-Einstein Institute Potsdam

SuperMUC Project ID: pn34tu (PRACE project 2018194669)

Introduction

The last decade has seen a revolution in modern physics, from the first direct detection of gravitational waves to the measurement of the Higgs boson. Yet, fundamental questions about the Universe remain unanswered: what is dark matter that makes up 26% of the universe's energy budget and drives structure formation? How can we consistently combine gravity and quantum physics? How well do we really understand inflation? Solutions to these puzzles typically require new physics beyond our standard models in cosmology, gravity or particle physics, and will significantly advance our understanding in these diverse disciplines.

Excitingly, the Nobel Prize winning discovery of gravitational waves emitted during the collision of black holes or neutron stars has opened a new window to probe physics in the extreme regimes of gravity. In fact, with more than new 90 detections we are at the dawn of precision gravitational wave observations. To connect the wealth of observations to theoretical models describing the underlying physics in the highly dynamical regime of gravity, we need high-performance numerical simulations. In this project we have investigated (i) the interaction between black holes and new particles that are popular candidates for dark matter; (ii) black holes in quadratic gravity, which is an extension of Einstein's General Relativity motivated by quantum gravity candidates; (iii) cosmic strings; and (iv) initial conditions of inflation.

Results and Methods

The core tool of this project has been numerical relativity, in which Einstein's equations (or modifications thereof) in 3 spatial are evolved in time. They are a set of more than 10 nonlinear, coupled partial differential equations that are split into a set of constraint and a set of evolution equations. The former are solved to provide the initial configuration of a black hole binary at the beginning of a simulation using pseudo-spectral methods. The second set determines the time development using the BSSN or Z4c reformulation of Einstein's equations together with moving puncture coordinates. We employ the method of lines, realizing spatial derivates with finite difference stencils up to sixth order and the time evolution with a fourth order Runge-Kutta integrator. We used adaptive mesh refinement, i.e., the numerical domain is split into a set of refined sub-grids to guarantee high resolution near the black holes while keeping the 3-dimensional grid sufficiently large to extract the simulated gravitational wave signals at distances 100 times larger than the binary.

We employed two different cyberinfrastructures for computational astrophysics and gravitation: the open-source Einstein Toolkit together with the PI's numerical relativity library Canuda [1] and the publicly available GRChombo code developed by members of this team [2].

The computational resources provided by PRACE has led to new discoveries in all four research areas.

Black holes in modified gravity: One of the most popular extension of general relativity, motivated for example by string theory, involves corrections that are quadratic in curvature and couples to a scalar field. In the presence of a black hole, this scalar is excited and leads to "hairy" black holes. Here we have studied the dynamics of the scalar field driven by a binary black hole. For example, scalar dipole radiation is emitted (analogous to two moving electric charges producing electromagnetic radiation like light). After the black holes collide to form a larger mass black hole, the scalar is no longer supported and completely dissipates. We termed this new, nonlinear effect "dynamical descalarization." Figure 1 shows a series of snapshots to illustrate this process, taken from Ref. [3].

Black holes and light fields: Scalar fields around compact objects are of interest for scalar-tensor theories of gravity and dark matter models consisting

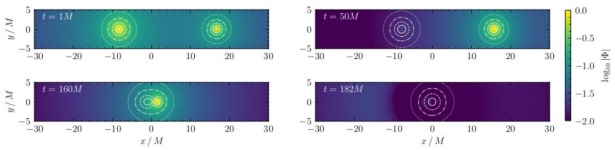

Figure 1: Snapshots showing the evolution of the Gauss-Bonnet scalar field driven by the head-on collision of "hairy" black holes. The bottom right panel shows the dynamical descalarization, i.e., dissipation of the scalar field, after the black holes' merger. Animations can be found in [3].

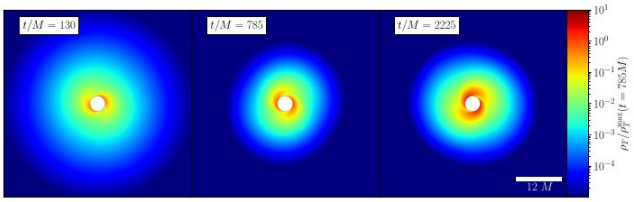

Figure 2: Snapshots showing the superradiant evolution of the energy density of a Proca from an initial transient to a bosonic condensate around a rotating black hole [4].

of a massive scalar. They may form "clouds" around black holes via superradiant instabilities, or via accretion if they form some component of the dark matter. In this series of projects [4], we have investigated the accretion and formation of a bosonic cloud around (single) rotating black holes, as well as the dynamics of a scalar field around a black hole binary. It has been suggested that their presence may lead to a distinctive dephasing of the gravitational wave signal when a small compact object spirals into a larger black hole. Motivated by this, we additionally study numerically the dynamical friction force on a black hole moving at relativistic velocities in a background scalar field with an asymptotically homogeneous energy density. We show that the relativistic scaling is analogous to that found for supersonic collisional fluids, assuming an approximate expression for the pressure correction which depends on the velocity and scalar mass. The approximation we obtain can be used to inform estimates of dephasing in the final stages of an extreme mass ratio inspiral. Superradiance is not unique to scalars and can, in fact, lead to the amplification of any massive boson by extracting energy from a spinning black hole. One interesting possibility is that superradiance may occur for photons in a diffuse plasma, where they gain a small effective mass. We carried out relativistic simulations of a massive Proca field evolving on a Kerr background, with modifications to account for the spatially varying effective mass. This allows us to treat the spin-1 case directly relevant to photons, and to study the effect of thinner disk profiles in the plasma. Studying thin disks we find a leakage of the superradiant cloud that suppresses its growth, concluding that thick disks are more likely to support the instability.

Black hole impostors and Boson stars: Interestingly, the ultra-light fields mentioned in the last section can also clump together to form a new type of stars called "boson stars." We investigated the collision of such boson stars, calculated their gravitational wave signal. We also investigated if their gravitational wave signal may be detectable with current observations and if it can be distinguished from those of black holes.

Cosmic strings: We constructed, for the first time, the time-domain gravitational wave strain waveform from the collapse of a strongly gravitating cosmic string loop in full general relativity [5]. We show that the strain exhibits a large memory effect during merger, ending with a burst and the characteristic ringdown as a black hole is formed. Furthermore, we investigated the waveform and energy emitted as a function of string width, loop radius and string tension.

The results of this PRACE Project have been published in more than 11 peer-reviewed articles.

Ongoing Research / Outlook

Since the beginning of this project gravitational wave astrophysics has matured from the first faint detections to a precision science with more than 90 observations of gravitational wave signals. We expect hundreds of new detections in the coming years as LIGO/Virgo/KAGRA will restart to take data. A crucial ingredient to interpret the observed gravitational wave signals, to infer the properties of the sources and to infer properties of the underlying theory of gravity are numerical simulations of compact binary. Following directly from this project, in which we have performed first proof-of-principle calculations are production level simulations to produce first waveform catalogs in extensions of Einstein's General Relativity. Another line of research that directly builds upon this PRACE project are studies of higher spin fields as a class of dark matter candidates.

In summary, new gravitational wave observations offer a tremendous discovery space for fundamental physics, and PRACE has been instrumental to construct the necessary computational and theoretical infrastructure to facilitate these discoveries.

References and Links

[1] Einstein Toolkit and Canuda, http://einsteintoolkit.org, https://bitbucket.org/canuda/
[2] GRChombo, https://www.grchombo.org; Andrade et al, J.Open Source Softw. 6 (2021) 3703.
[3] H. O. Silva, H.Witek, M. Elley and N.Yunes, Phys. Rev. Lett. 127 (2021) 3, 031101; see also https://bhscalarization.bitbucket.io
[4] G. Ficarra et al, Phys.Rev.D 99 (2019) 10, 104019; J. Bamber et al, Phys.Rev.D 103 (2021) 4, 044059; D. Traykova et al, Phys.Rev.D 104 (2021) 10, 103014; Wang et al, https://arxiv.org/abs/2201.08305.
[5] J.C Aurrekoetxea et al, Class.Quant.Grav. 37 (2020) 20, 204001.

Critical behavior in vacuum gravitational collapse

Research Institution
[1]Friedrich-Schiller-Universität Jena

Principal Investigator
Bernd Brügmann[1]

Researchers
Isabel Suárez Fernández[2], Sarah Renkhoff[1], Daniela Cors Agulló[1], David Hilditch[2]

Project Partner
[2]CENTRA, Instituto Superior Técnico, Universidade de Lisboa

SuperMUC Project ID: pn34vo

Introduction

The science of gravitational waves has achieved major breakthroughs in the last years. Numerical relativity studies have played an important role both in our basic understanding and in the detection of gravitational wave signals. Away from the astrophysical context much about the dynamical behavior of spacetime remains to be understood, however, and in this project we work along this tack, studying the critical collapse of gravitational waves. A key conjecture in mathematical relativity is that of weak cosmic censorship, which states that singularities formed in gravitational collapse should be hidden from observers at infinity by an event-horizon. A natural way to find counterexamples to this conjecture is to look at extreme spacetimes and to examine whether or not such a horizon is present. There is no hope however of finding such spacetimes analytically.

Thus motivated, in the present project we perform parameter studies of gravitational wave spacetimes using the modern pseudospectral numerical relativity code bamps [2]. In particular we consider Brill wave initial data with varying strengths of gravitational wave content. Weak data eventually disperse whereas strong data collapse to form a black hole. We are concerned with the regime that lies between these two end-states. This regime is examined by fixing a family of initial data and performing a bisection search in parameter space towards the expected amplitude at which black holes first form. Data close to this spacetime are expected to exhibit behavior called 'critical phenomena in gravitational collapse', discovered by Choptuik [3] in 1993 in a toy-model, but still relatively poorly understood in the gravitational wave setting. The first study of the critical collapse of gravitational waves was undertaken in 1993 by Abrahams and Evans, but reproducing their results has proven difficult. The state-of-the-art development in the topic was [4], which used our code, and recently [5]. In particular, [4] was limited in scope since only one family of initial data was evolved.

In the present work we finalized the deployment of an upgrade in which we have implemented adaptive mesh-refinement (AMR). We now examine different initial data and expect to answer conclusively the question of whether or not gravitational waves exhibit critical phenomena close to the threshold of black hole formation.

Results and Methods

The numerical method implemented in bamps is designed to permit efficient parallelization; the code is MPI parallel and scales perfectly up to at least 4500 cores and probably beyond (see Figure 1). For our last study we ran predominantly on SuperMuc, where the aforementioned scaling plot was created. Our typical use-case employs several hundred cores (~1,000) and uses the excellent strong-scaling to turn the jobs around quickly. Particularly long jobs are managed in the standard manner by checkpointing and requeuing. Due to the symmetry reduction our memory requirements are not extortionate. During a typical run we will write between 10 - 50 GB of data, which will later be analyzed with postprocessing tools such as horizon finders. Occasionally more data will be written for apparent horizon, visualization and outreach purposes.

The specific workflow is based on running bamps with various families of Brill wave initial data and gauge conditions. The procedure is the following: First, choose a family of initial data parametrized by strength parameter A. Next, within this family fix A. Using bamps we evolve data in time, finishing the run with either the dispersion of the wave, in which case we can classify the initial data as subcritical, or the collapse of the wave to create a black hole. In the second case we need to apply a post processing analysis using AHloc3D, an apparent horizon-locating tool. When the apparent horizon is found in the evolution of the initial data set, we can classify the spacetime as supercritical. As we are interested in finding the critical solution that divides between these two behaviors of dispersion and collapse, we bisect in A towards the conjectured critical amplitude. Repeating this process we obtain the first initial data that collapses to create a black hole, and therefore, find an approximation to the critical spacetime and others in its neighborhood in solution space. The same procedure but with geometrically prolate centered initial data was already carried out in [4].

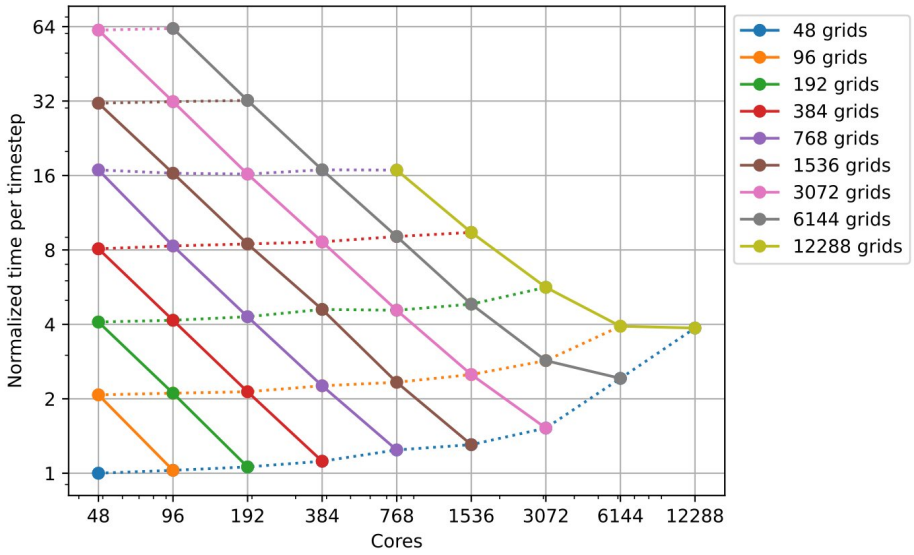

Figure 1: Strong and weak scaling of the code bamps. Solid lines indicate constant total work, dashed lines indicate constant work per core.Considering that this is a challenging AMR problem, the scaling is fully satisfactory in the regime of the runs in the present project.

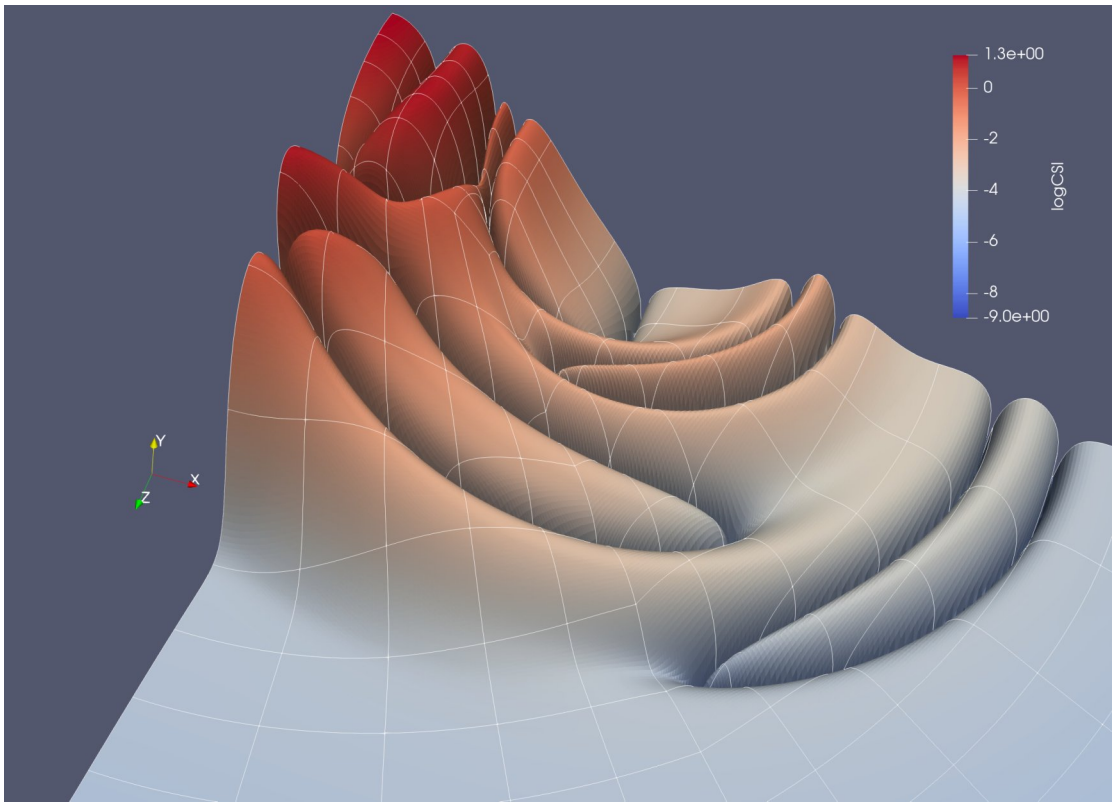

Figure 2: 2-dimensional plot of the logarithm of the Kretschmann scalar at t=6.605 in the evolution of an off-center prolate brill wave (ρ0=5, A=0.0644) before an horizon is formed.

Ongoing Research / Outlook

The family of initial data that we show in Figure 2 are centered Brill waves with positive amplitude. These are the best studied in the literature up to now, because of the ease with which they can be constructed. Studying this type of initial data we are able to develop a comparison with previous results obtained, while significantly improving the resource usage with the new AMR in the code bamps. Moreover, within this type of initial data, we focus for the first time with bamps on geometrically centered and off-center oblate data.

References

[1] https://www.physik.uni-jena.de/en/TPI
[2] D. Hilditch, A. Weyhausen, and B. Brügmann. Phys. Rev. D, 93:063006, 2016.
[3] M. W. Choptuik. Phys. Rev. Lett., 70:9–12, 1993.
[4] D. Hilditch, A. Weyhausen, and B. Brügmann. Phys. Rev. D, 96:104051, 2017.
[5] T. Ledvinka and A. Khirnov. Phys. Rev. Lett., 127:011104, 2021.

Discovering magnetic portals

1

Research Institution
[1]Center for mathematical Plasma Astrophysics, Department of Mathematics, KULeuven

Principal Investigator
Giovanni Lapenta[1]

Researchers
Giuseppe Arrò[1], Francesco Pucci[2], Maria Elena Innocenti[3], Elisabetta Boella[4]

Project Partners
[2]CNR University of Bari, Italy
[3]Ruhr University of Bochum, Germany
[4]University of Lancaste, UK

SuperMUC Project ID: pn29go (Prace project no. 2020225372)

Introduction

The magnetic field moves the motor of electric cars, confines the plasma in fusion energy systems and powers some of the largest explosions in the universe. Magnetic fields store energy on the Sun and release it in spectacular eruptions that produce flashes of light (solar flares) and ejections of matter (coronal mass ejections). These eruptions can affect very severely the Earth. A famous solar storm in 1859, now called by the name of his observer, Carrington, caused severe disruptions of the telegraph lines. Modern studies place the cost of the repeat of one such event in the trillions of euros [1]. Scientists believe Carrington-like events can happen on average every one hundred years with even much more powerful events happening every thousand year. The power grid could be disabled for periods of months and the satellite communication system could be devastated. A study conducted in 2019 by the American Federal Emergency Management Agency (FEMA) identified two main natural risks to our civilisation: a pandemic and extreme solar eruptions [2]. The first has already happened and found us unprepared, we should at least try to prepare for the other.

But the magnetic field also protects the Earth: the field created by the motions of molten rocks in the Earth interior form a dipolar field, with the magnetic poles in proximity of the geographic poles. This field varies in time and with irregular occurrence of thousands to millions of years it nearly disappears to reform with opposite polarity (the north pole becoming south pole and viceversa). Our species survived one of such events, known from the magnetic record left on geological structures as the Laschamps excursion that took place about 42,000 years ago. It is believed that modern homo sapiens evolved about 300,000 years ago. So the disappearance of the Earth magnetic field did not wipe our ancestors out but a recent study points to a mass extinction of bigger prehistoric animals [3].

The point though is that cavemen did not rely on telecommunication, on global positioning and on the electrical grid. We do and some think the social and economic order could not survive another Carrington event nor another Laschamps excursion. We need to prepare and prevent the worst effects.

Let's not get paralysed by fear. Magnetic fields are also a wonderful source of fascinating astrophysical events. Primordial magnetic fields were formed in the universe shortly after the big bang and might have played an important role in its development [4]. Now we observe them for example affecting the formation of solar systems or shaping enormous jets emerging around supermassive black holes at the centre of galaxies and reaching distances comparable to that between galaxies. Magnetic fields also present the best chance to get fusion energy to work and provide unlimited clean and concentrated energy to power the future of humanity.

We need to understand how they operate and we need especially to understand how the magnetic fields exchange their energy within the systems they are embedded in. The research of the last 50 years has focused on one central puzzle: the process of magnetic reconnection. In magnetic reconnection the energy of the magnetic field is suddenly released in the form of fast hot jets, accompanied in some cases by emission of electromagnetic radiations at the most powerful frequencies, reaching even the gamma ray spectrum for the most energetic solar events. The great unknown is how magnetic fields can store so much energy for long periods, of days and months in the case of solar eruptions, and then release it all in a sudden burst lasting sometimes only seconds or minutes.

Results and Methods

The key to this puzzle is to locate and investigate the central region that enables the whole event: the reconnection site, this is the place where magnetic fields of opposite polarity are brought together and mixed (reconnection means breaking the old polarity connection and form a new one). These can be considered as magnetic portals that allow the energy

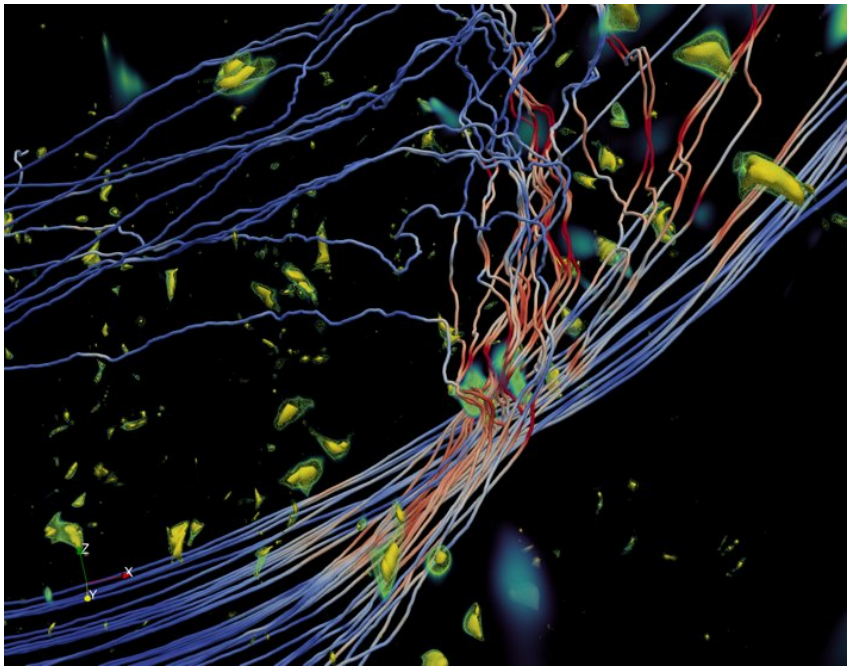

Figure 1: The indicator defined in [5] identifies many reconnection sites visible in the picture as ghostly yellow-green areas. A group of electron flowlines are shown passing one of these reconnection sites and encountering also others. The flow lines are coloured by the intensity of the local electric field that transfers energy between the magnetic field and the electrons, accelerating them and creating a turbulent flow.

stored to pass through. Finding and investigating these portals is a hard task and a grand challenge. Experts have long argued about even the meaning and existence of such portals. In some cases their identification is readily accessible and all can agree one reconnection event is detected. But in other more complex situations it is hard to be sure, especially in observations taken in space with a single spacecraft that only measures one point at a time and does not provide a global view. Often it is not clear even if reconnection is happening at one location or over a broader area and in the latter case whether it is a cluster of smaller events.

The recent work by Lapenta [5] takes a new step in the direction of detecting these magnetic reconnection sites. Lapenta uncovered a peculiar property of these regions that can lead to a very convenient and simple method to detect them. The newly discovered property of reconnection comes from using a famous property of relativity: when an observer moves with respect to a system, the magnetic field and electric field he or she observes are different from those measured by an observer on the system itself. For example, a spacecraft moving with respect to the Earth would measure fields different from those observed on Earth. This difference is small when the speed is small but when the speed is close to the speed of light, the difference becomes dramatic.

Lapenta found that in certain conditions, when the speed of the observer is oriented properly with respect to the system under observation, the magnetic field can be completely eliminated. However, the speed of the observer would have to be faster than the speed of light (an impossibility) almost everywhere, except in close proximity of a reconnection site. Near a reconnection site, the speed needed to eliminate the magnetic field drops below the speed of light and becomes exactly zero at the site proper. The validity of this new approach was shown first in a number of known examples. The new detection meths was applied to new complex cases (see figure), identifying new types of reconnection configurations within complex turbulent systems.

Ongoing Research / Outlook

With this new detection technique we can hunt for the magnetic portals described above and better understand the processes of magnetic energy conversion in laboratory and in the universe.

This new approach is being applied to a series of 3D massively parallel runs completed on SuperMUC to investigate the roled of reconnection (shown as yellow clouds in the figure) in turbulent systems.

The approach can also be applied directly to in situ data and we are applying to a series of 240 crossings of the Magnetospheric Mucltiscale Mission (MMS) to find where turbulent reconnection took place and to characterize the energy exchanges associated with them.

References and Links

[1] Eastwood, J., et. al., Risk Analysis, 37(2), 206-218, 2017.
[2] THIRA. 2019 National Threat and Hazard Identification and Risk Assessment (THIRA), 2019. https://www.hsdl.org/?view&did=827415.
[3] Cooper, A., et. al., Science, 371(6531), 811-818, 2021.
[4] Jedamzik, K., Pogosian, L., Phys. Rev. Lett., 125(18), 181302, 2020.
[5] Lapenta, G., Astrophys. J., 911(2), 147, 2021.

1 Hyper-massive neutron star stability and accretion disk characteristics

Research Institution
[1]Institute for Theoretical Physics, Goethe Universität

Principal Investigator
Luciano Rezzolla[1,2]

Researchers
Elias Most[3,4], L. Jens Papenfort[1], Samuel Tootle[1]

Project Partners
[2]Frankfurt Institute for Advanced Studies
[3]Princeton University
[4]Institute for Advanced Study, Princeton

SuperMUC Project ID: pn56bi (Gauss Large Scale project)

Introduction

Gravitational wave detectors such as LIGO, VIRGO, and KAGRA, have brought about an era of multi-messenger astronomy that has given new insights into the merger of binary compact objects. In all cases, the ability to constrain the characteristics of the compact objects is very limited, especially in the absence of an electro-magnetic (EM) counterpart. Gravitational wave events such as GW190425, however, present a very unique opportunity to study the mass gap regime where the binary could consist of either a black hole and a neutron star (BHNS) or a highly asymmetric neutron star binary (BNS).

The objectives of this project are to extend our knowledge and learn fundamental lessons about the stability of hyper-massive neutron star remnants from the merger of highly asymmetric binary neutron star mergers.

This includes binaries where the neutron stars are not rotating as well as scenarios where the primary can-have up to extremal spins near the mass shedding limit. Additionally, we have looked into BHNS and BNS systems in the mass gap region and compared them against GW190425 to ascertain the phenomenology that distinguishes these two scenarios. Finally, we have performed the first fully general relativistic-magneto-hydrodynamic (GRMHD) evolution from inspiral to ~300ms post-merger using accurate micropysics to characterize the post-merger observables, the remnant disk properties, and determine the possibility of a jet.

Such surveys are the first of their kind due to the computational demand, but more importantly due to a lack of a publicly available initial data solver that is capable of generating the initial conditions that satisfy Einstein-'s field equations for these configurations.

To achieve our goals we use a combination of state-of-the-art numerical-relativity tools, mainly developed in the astrophysics group at Goethe University and have developed the *FUKA* [2] initial data solvers to generate constraint satisfying initial data to obtain the results in [3-5].

Results and Methods

The development of *FUKA* has relied significantly on the pn56bi project to obtain the successful results detailed in [2]. *FUKA* is the first publicly available initial data solver that provides the ability to construct eccentricity-reduced initial data for binary black holes, BHNS, and BNS binaries to include mass asymmetry and spin.

The merger simulations proposed in this project have been carried out using *FIL*, which is a high-order extension of the publicly available general-relativisticMHD code *ILGRMHD*. The basic algorithms in *ILGRMHD* have been developed by the Illinois Relativity Group, but the publicly available version is particularly compact and efficient, providing a speedup factor of almost two when compared with other GRMHD codes. Among the numerous new developments that the FIL code implements, we would like to highlight the fully high-order flux update, the capability for finite-temperature dependent EOSs, an improved primitive-variable recovery, the inclusion of weak-interactions, and a simplified neutrino leakage scheme.

Finally, *FIL* is built on the Einstein Toolkit evolution framework. *FIL* utilizes Carpet, a fixed-mesh box-in-box refinement such that each refinement level doubles in resolution. This allows for flexibility in setting up our evolutions as we can adapt the resolution to the physics we are interested in resolving.

As detailed in [3], we have performed systematic surveys into the post-merger stability of the hyper-massive neutron star remnant from a BNS merger to determine the influence of mass asymmetry and spin. This work has also thoroughly examined the resulting remnant disk masses and the ejected mass to include analyzing the average distribution of the thermodynamic quantities of the ejected mass, the resulting luminosity light curves and the time of peak emission which are critical when comparing to astrophysical observations (Fig. 2).

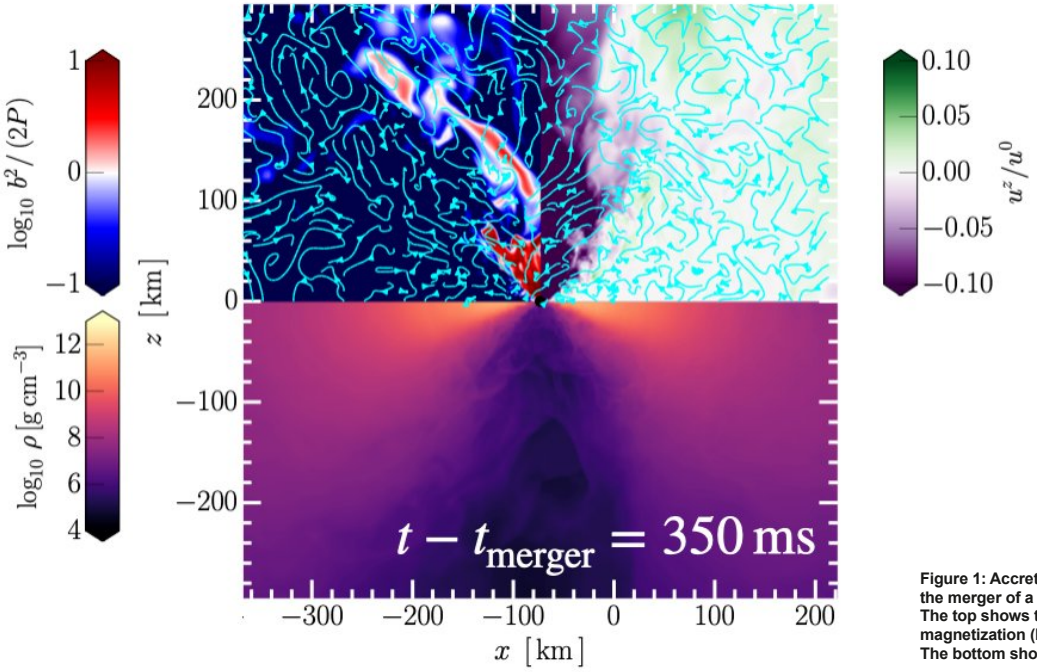

Figure 1: Accretion disk evolved for 350 ms after the merger of a neutron star with a black hole. The top shows the magnetic field lines, magnetization (left) and vertical velocity (right). The bottom shows the baryon density [5].

Furthermore, we have performed a thorough study in the mass gap region specifically targeting GW190425 to determine the ability to distinguish a BHNS merger from a BNS merger. As a result, we have found that fast mass ejecta might be the only distinguishing feature, being accompanied by a distinct class of electromagnetic transients [4].

Finally, we have performed the first GRMHD simulation with accurate microphysics of a BHNS coalescence up to ~350ms post-merger where the NS has an initial magnetic field confined to its interior [5]. We have performed an extensive analysis on the accretion disk properties to facilitate the study of accretion disks in other codes such that the initial conditions can reflect a realistic merger remnant and disk configuration. In addition, we have analyzed the resulting phenomenology to estimate the likelihood of a relativistic jet forming at a later time. Even though a jet is not observed in our simulation, the expected characteristics are present such as funnel clearing and a steady growth in the magnetic field energy (Fig. 1).

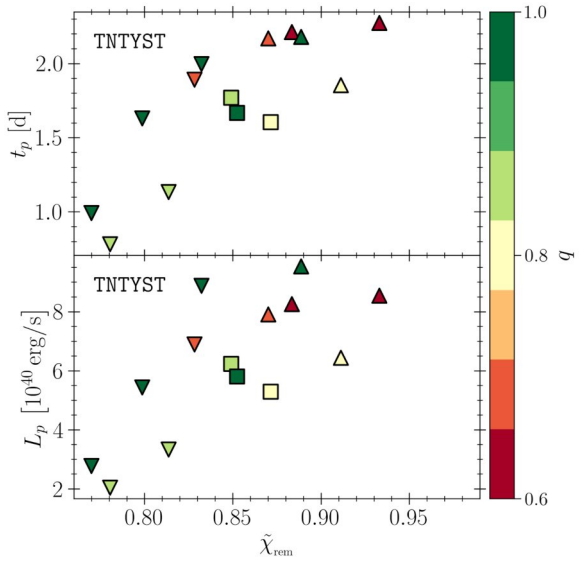

Figure 2: Luminosity and time of peak luminosity as a function of mass ratio and the effective spin of the remnant for the *TNTYST* equation of state [3].

Ongoing Research / Outlook

It is of particular interest to our group to further ascertain the impact of spin from the secondary neutron star on the merger and post-merger dynamics of a BNS. This includes the physics contributing to remnant stability as well as the threshold mass to prompt collapse.

Additionally, we have developed a novel description of nuclear matter using the holographic model which includes a consistent description of nuclear matter in the high density and high temperature regime that is in agreement with QCD. This is of particular importance as this would provide a first insight into a realistic equation of state that incorporates a first order phase transition to quark matter.

References and Links

[1] https://relastro.uni-frankfurt.de/research/
[2] L. J. Papenfort et al., 10.1103/PhysRevD.104.024057.
[3] L. J. Papenfort et al., arXiv:2201.03632.
[4] E.R. Most et al., Astrophys. J. 912 (2021) 1, 80.
[5] E.R. Most et al., MNRAS 506 (2021) 3, 3511-3526.

1 Unveiling the emergence of the first galaxies with state-of-the-art simulations

Research Institution
[1]Max-Planck-Institut für Astrophysik, Garching bei München

Principal Investigator
Enrico Garaldi[1]

Researchers
Rahul Kannan[2], Aaron Smith[3], Volker Springel[1], Mark Vogelsberger[3], Rüdiger Pakmor[1], Lars Hernquist[2]

Project Partners
[2]Center for Astrophysics | Harvard & Smithsonian, Cambridge
[3]Massachusetts Institute of Technology, Cambridge

SuperMUC Project ID: pn56ku

Introduction

In its infancy, more than 13 billion years ago, the Universe went through a period of darkness, with no sources of light. Then, the first stars and galaxies formed and started to pour photons into their cosmic neighborhood, ionizing and heating up gas in the so-called inter-galactic medium (IGM) between galaxies. This is known as the Epoch of Reionization (EoR), and represents the last global phase transition of the Universe, radically altering the conditions in which the progenitors of contemporary galaxies formed. It also represents an evolutionary link between the smooth matter distribution produced by the Big Bang and the large-scale structure observed today.

Despite significant progress over the past decade, little is known about the sources of EoR and their effect on the IGM. However, upcoming facilities will unleash a flood of observations that will usher in a new era of cosmic reionization studies. Most notably, they will detect galaxies in the EoR, and unveil the physical conditions of the IGM at the time when the first stars were born.

To fully exploit these observations, theoretical models need to reach sufficient physical fidelity to make accurate predictions and aid the interpretation of the observational results. This requires a realistic description of galaxy formation in an evolving radiation field. However, this problem is intractable analytically. For this reason, numerical simulations are an essential tool to investigate the EoR. Solving the coupled radiation-hydrodynamics (RHD) equations is numerically challenging, but allows us to model reionization from first principles. In this project we run the most-advanced set of RHD simulations to date, designed to understand the EoR in all its different aspects: from the formation and properties of the first galaxies to their impact on the content of the Universe.

Results and Methods

We have produced a set of state-of-the-art simulations of the EoR [1-4]. They combine for the first time: a realistic model for galaxy formation, cosmic dust evolution, a non-equilibrium primordial chemistry solver, stellar evolution including binary systems, and a self-consistent treatment of gravity, hydrodynamics, magnetic fields, and radiation transport on cosmological scales. These simulations follow a cubic region of the Universe with a side length of 95.5 comoving Mpc, while resolving scales up to 20,000 times smaller (approximately 5 kpc). Specifically, we run a set of simulations with two different resolution levels. Table 1 summarizes the computational and storage requirements for each of them. Science results will be reported primarily from the flagship Thesan-1 run. Overall, our simulations created approximately 11 million files of science output.

Name	RAM	Cores	Core-h	Storage
Thesan-1 (x1)	92 TB	57,600	30 M	220 TB
Thesan-2 (x7)	11 TB	6,730	3.5 M	27.5 TB

Table 1: Computational and storage requirements for the simulations run within this project.

Figure 1 presents an overview of the results from the flagship Thesan-1 run. It shows different simulated quantities (reported in the figure) in a slice through the simulation box centered on the biggest simulated structure. The two circular insets show how the ALMA and JWST telescopes would see the latter. The matter in the Universe organizes itself into a filamentary structure called cosmic web (top left). In the densest spots, stars form and produce photons (left) that ionize the surrounding neutral gas (bottom left) and heat it up by 20,000 K (top right). At the same time, they produce and disperse metals (right) and cosmic dust (bottom right) in the surrounding gas. These processes alter forever the stage where cosmic evolution takes place, transforming a cold and neutral Universe into a hot and ionized one.

The physical processes taking place in the young Universe are not yet fully understood. It is therefore imperative to study different possible scenarios. To this end, we have run a number of simulations varying the

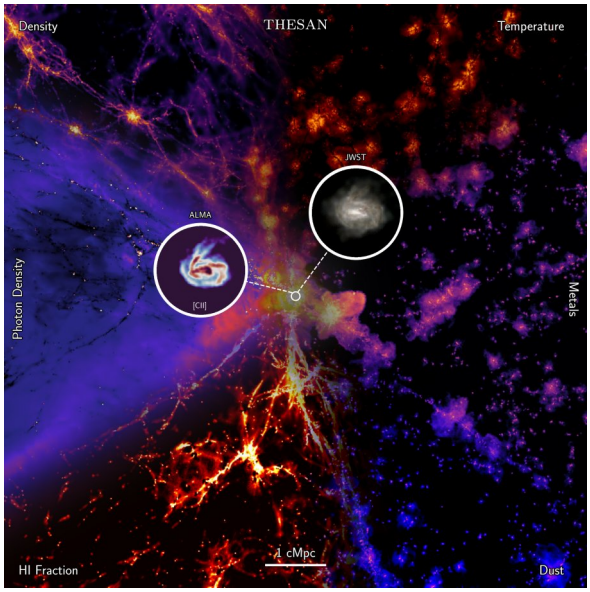

Figure 1: Gas properties in a slice through the simulation box centered around the largest simulated structure. The circular insets show synthetic images of the latter as seen by the ALMA and JWST telescopes.

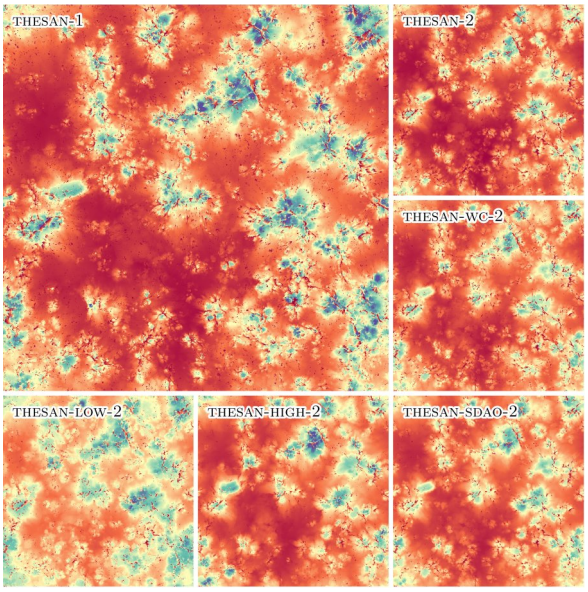

Figure 2: Time of reionization in a slice through the simulation box in the different Thesan physical models.

physics of photon escape from galaxies, the nature of dark matter and the details of the radiation. These are dubbed Thesan-2 and Figure 2 shows an overview of them. Its panels show, in a slice through the simulation box, the time at which the gas in some of the different simulated models was last reionized. Blue colors indicate regions where this process occurred early, and red where this happened late. Comparing the different panels reveals how the physics of the young Universe has a strong effect on the reionization of the latter, and therefore on the evolution of galaxies.

The Thesan simulations have recently been published [2-4]. Among other results, we have shown that Thesan is able to reproduce the number and luminosity of primeval galaxies. This is remarkable since such quantities are usually an input of these kind of simulations, while thanks to our approach that builds on top of previously-gathered knowledge they are now an output. In addition, Thesan reproduces the rate at which new stars are formed, the amount of different elements in the Universe, the evolution of the temperature, density and opacity of the IGM, and the number and mean path of photons produced by stars. Remarkably, Thesan reproduces for the first time the observed modulation of transmitted Ly-alpha radiation in quasar spectra around primeval galaxies. We identify the reason in the superior galaxy formation physics compared to previous studies. Finally, we provide a systematic study of the escape of Ly-alpha radiation from galaxies and its dependence on physical properties of the latter, as well as a study of different emission line tracing the young Universe.

Our code, AREPO [5], was developed explicitly for large parallel simulations. It solves the RHD equations on an unstructured naturally-adaptive Galilean-invariant mesh using a second-order-accurate, un-split, finite-volume Godunov scheme employing an HLLD Riemann solver. In order to achieve the results described above, we faced many technical challenges. First and foremost, we used an unprecedented (for the code employed) number of cores. Therefore, we improved large code parts to optimally scale on almost 60,000 computing tasks, or approximately 1/6 of the entire SuperMUC-NG machine. Two additional important upgrades were the development of a hybrid shared/distributed memory approach and the first time integration of many sophisticated code modules, enabling an unprecedented physical accuracy.

Ongoing Research / Outlook

Our simulations mark the foundation for a large program of investigating the early Universe, following two main branches. On the one hand, we are selecting interesting simulated galaxies and perform a numerical zoom-in on these objects, in order to simulate their functioning to even-greater detail. On the other hand, we are further exploring the still-unconstrained physics of the early Universe by running simulations with additional/ different physical processes at play. For both these numerical quests, the necessary amount of memory and computing cores is unprecedented, driven by the quality of current and forthcoming observations. For this reason, large HPC systems like SuperMUC-NG are vital to such and similar projects, since they allows us to employ vast numerical resources that would be otherwise unavailable to us. In particular, the possibility to get access to the machine through a speedy evaluation procedure allowed us to significantly speed up the project timeline. Additionally, the improved performance of SuperMUC-NG over its predecessor SuperMUC Phase2 allowed us to simulate a three-times larger volume than it would have been possible with the same amount of computing time, improving the statistical power of our predictions.

References and Links

[1] https://www.thesan-project.com
[2] Kannan R. et al., MNRAS in print. (2021).
[3] Garaldi E. et al., MNRAS in print. (2022).
[4] Smith A. et al., MNRAS subm. (2022).
[5] Springel V., MNRAS 401, 791 (2010).

Strong gravity beyond general relativity

1

Research Institution
[1]Queen Mary University of London

Principal Investigator
Pau Figueras[1]

Researchers
Luis Lehner[2], Ramiro Cayuso[2], Guillaume Dideron[2], Tiago França[1], Llibert Aresté Saló[1], Chenxia Gu[1], Tomás Andrade[3], Hans Bantilan[1], Lorenzo Rossi[1]

Project Partners
[2]Perimeter Institute
[3]Universitat de Barcelona

SuperMUC Project ID: pn73do (Prace project no. 2020235545)

Introduction

The detections of gravitational waves produced in mergers of black holes allow to test general relativity (Einstein's theory of gravity) in the strong field regime, that is, when space is highly curved. It is precisely in this regime that the true nature of gravity is most likely to be revealed. One of the main challenges in this area is that almost nothing is known about the strong field regime of alternative theories of gravity. Without this knowledge, only limited tests of general relativity can be carried out. In this project, we investigate black hole binary mergers in alternative theories and extract the corresponding gravitational waves, thus allowing for new tests of Einstein's theory. To further understand gravity at its most fundamental level, we also study the types of singularities (i.e., places where the force of gravity is so strong that Einstein's theory breaks down) that can form dynamically in general relativity.

Results and Methods

The simulations require to solve equations that are typically more complicated than the equations of motion of general relativity that one must solve in the traditional black hole binary problem. The reason is that the theories that we study are mathematically more complex than general relativity or involve more spacetime dimensions or different boundary conditions. This makes the problems much harder from a computational point of view and require higher numerical resolution and greater resources. Furthermore, the formation of singularities in general relativity is a very delicate problem. The reason is that structures can randomly form on different scales and at different times, and they all need to be suitably resolved both in space and in time. We carry out the simulations in our GRChombo code, which is flexible enough to allow us to tackle alternative theories of gravity or higher dimensions. Furthermore, GRChombo has automatic adaptive mesh refinement, which makes it possible to resolve features of the solution that randomly appear on different scales whilst keeping the computational cost of the simulation under control.

We have managed to simulate, for the first time, black hole binaries in certain alternative theories of gravity that contain a scalar field [1,2,3]. These theories have previously been used in cosmology, for instance to study dark matter. Our results have shown that, even if the differences between general relativity and these alternative theories of gravity are small at any given instant of time, these differences can accumulate over time and eventually become large. This is precisely what happens in black hole binaries: during the many orbits of the binary, the differences between general relativity and the alternative theories of gravity build up and, in some cases, they can be so large that current gravitational wave observatories would not be able to detect them. In order to measure this build up effect, it is crucial to treat these alternative theories without making approximations, as we have done in our simulations.

In our other line of research, we have studied the formation of singularities in general relativity. The importance of this topic in the field is reflected by the recent Nobel prize awarded to Roger Penrose. It turns out that certain higher dimensional black holes are unstable under deformations. This should be contrasted with astrophysical black holes, which are believed to be stable. In this project we have investigated the evolution of this instability that affects higher dimensional black holes, first by reproducing previous results in the literature using more modern techniques. The end point of the instability is a singularity but the process by which this singularity is approached seems to be analogous to the process by which a column of fluid breaks. It is important to confirm this picture because it has deep implications for quantum gravity. With our techniques, we will be able to get closer to the singularity than ever before, and hence uncover the details of the singularity formation in general relativity.

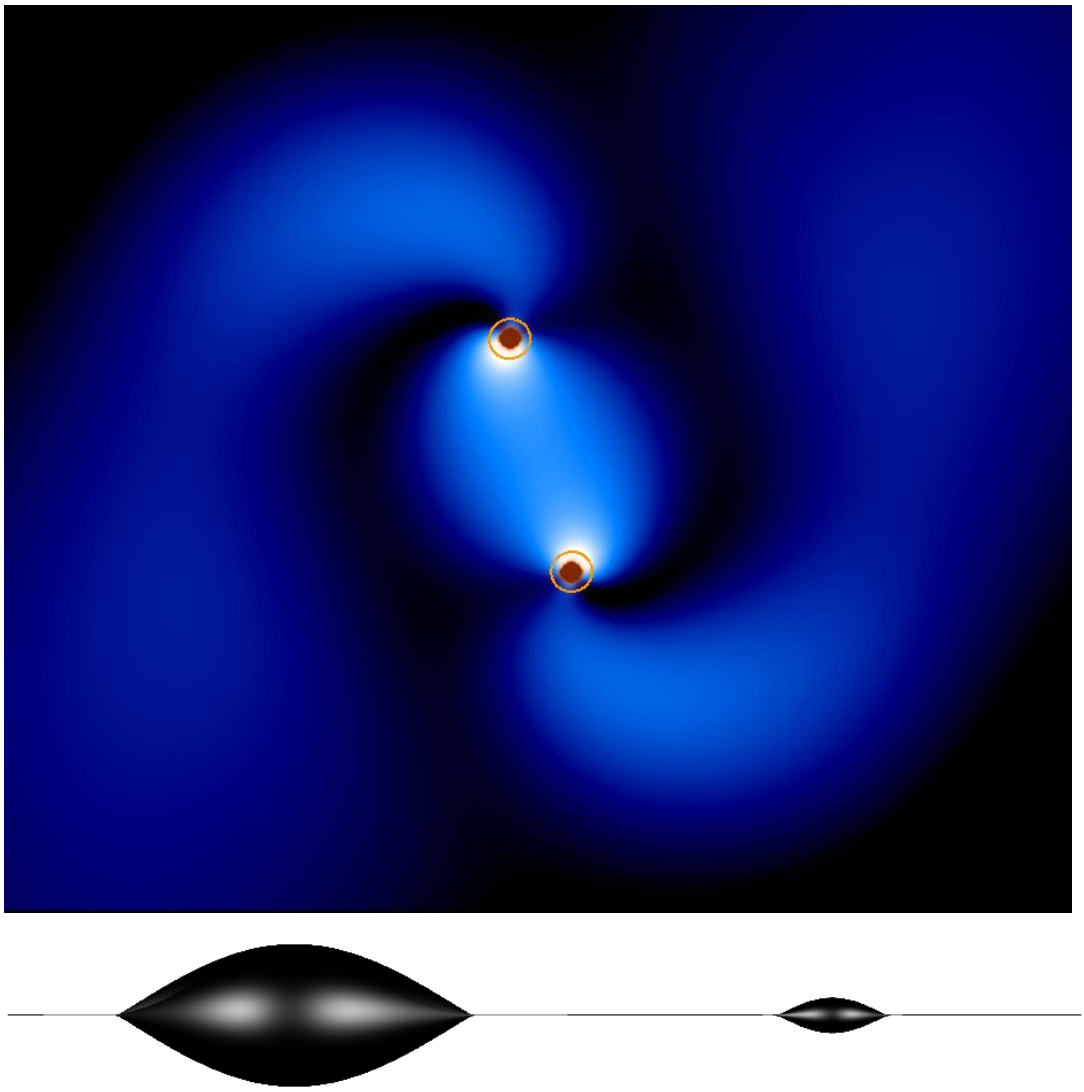

Figure 1: Energy density (in blue) of the scalar field surrounding the binary black holes.

Ongoing Research / Outlook

Currently we are simulating black hole binaries in alternative theories of gravity which are motivated by quantum theories of gravity, such as string theory [4]. The waveforms produced in black hole binary mergers in these theories could allow to detect quantum corrections to Einstein's theory. Understanding how to meaningfully simulate these theories in a computer is by a itself an achievement; in addition, in this project we will be able to make predictions for the waveforms in these theories and hence potentially constraining quantum gravity. In parallel, we are doing very high resolution simulations of these higher dimensional black hole instabilities to confirm that the process by which certain singularities form is indeed quantitatively similar to the breaking of a column of fluid [5]. If that is the case, it would imply that the quantum mechanical details of how singularities form and are resolved by quantum gravity would not matter.

References and Links

[1] https://www.youtube.com/watch?v=uOed4AG1ulg
[2] Figueras et al. Class. Quant. Grav. 37 (2020) 22, 225009.
[3] Figueras et al., [arXiv:2112.15529].
[4] Cayuso et al., ongoing.
[5] Andrade et al., ongoing.

The World's Largest Supersonic, Magnetohydrodynamic Turbulence Simulation

1

Research Institution
[1]Research School of Astronomy and Astrophysics, Australian National University

Principal Investigators
James R. Beattie[1], Christoph Federrath[1]

Researchers
Ralf S. Klessen[2,3], Philip Mocz[4], Salvatore Cielo[5]

Project Partners
[2]Universität Heidelberg, Zentrum für Astronomie, Institut für Theoretische Astrophysik
[3]Universität Heidelberg, Interdisziplinäres Zentrum für Wissenschaftliches Rechnen
[4]Lawrence Livermore National Laboratory
[5]Leibniz Supercomputing Centre

SuperMUC Project ID: pn73fi (Gauss Large Scale project)

Introduction

Supersonic, magnetised turbulence is ubiquitous in-the interstellar medium of galaxies. Unlike incompressible turbulence, supersonic turbulence is not scale-free. The scale that marks the transition from supersonic to subsonic turbulence is the so-called sonic scale, which in the context of star formation may define the critical value for which regions inside of molecular gas clouds collapse under their own gravity to form stars. The sonic scale was recently measured for the first time within a hydrodynamical supersonic turbulence simulation using a grid resolution of $10{,}048^3$ in [1]. This is the only calculation with sufficient resolution to separate the energy injection scale, supersonic cascade, sonic scale, subsonic cascade and dissipation scale of the turbulence. Whilst this calculation brought great insight into the exact position of the sonic scale and the nature of supersonic turbulence, the influence that magnetic fields have on the sonic scale is more or less unknown, yet is of tantamount importance for understanding the nature of supersonic, magnetized turbulence in the interstellar-medium of galaxies.

In this LRZ project, we run the first supersonic, magnetised turbulence simulation that is sufficiently resolved to measure the exact position of the (magneto)-sonic scale, and the supersonic and subsonic energy cascades, to determine how magnetic fields affect the turbulence. We do this by running a magnetohydrodynamical (MHD) turbulence simulation with $10{,}080^3$ grid cells, distributed over almost 140,000 compute cores and run for over 60 million core hours on SuperMUC-NG.

Results and Methods

We use a modified version of the MHD code flash [2]. Our code uses a highly-optimised, hybrid-precision, second-order, positivity-preserving MUSCL-Hancock HLL5R Riemann scheme [3] to solve the ideal, isothermal, compressible magnetohydrodynamic equations in three dimensions with stochastic, large-scale forcing to drive finite time-correlated supersonic turbulence.

We use a block-structured parallelization, with each 3D computational block distributed onto one single compute core. Each block contains 168x210x210 computational cells, which we pass to each of the 138,240 compute cores (2,880 compute nodes on SuperMUC-NG) to give a total grid resolution of 10,080 grid cells in each of the three dimensions, and 3.0PB of data products in total. To ensure numerical convergence of the plasma statistics, such as the turbulent energy spectra, we also perform simulations at $1{,}152^3$, $2{,}520^3$ and $5{,}040^3$ grid resolutions.

In Figure 1 we show the kinetic turbulent energy spectra, $E_{kin}(k)$, where $k=2\pi/l$ is the wavenumber, at the four different resolutions as indicated by the line colour. The different regimes of turbulence are shown by the background colour, with the magneto-sonic transition traced in blue.

We see two distinct regimes of turbulence emerging in the high-resolution simulations. On small k (large spatial scales, coloured green) the turbulence is dominated by networks of interacting shocks, and has an energy spectrum consistent with Burgers turbulence, $E_{kin}(k) \propto k^{-2}$. On large k (small spatial scales, coloured yellow) the energy cascade resembles the incompressible magnetised turbulence Iroshnikov-Kraichnan-like spectrum, $E_{kin}(k) \propto k^{-3/2}$, corre-sponding to magnetised vortices, which exchange energy and cascade the energy to smaller and smaller spatial scales.

In Figure 2 we show a two-dimensional slice of the three-dimensional gas density in the simulation, revealing strong, shocked gas (coloured red to orange for the most extreme) and deep rarefactions (coloured blue and green for the most under-dense), typical of supersonic turbulence in the interstellar medium. The local magnetic field is shown with a line integral convolution filter, highlighting the intricate, complex, small-scale structure of the field.

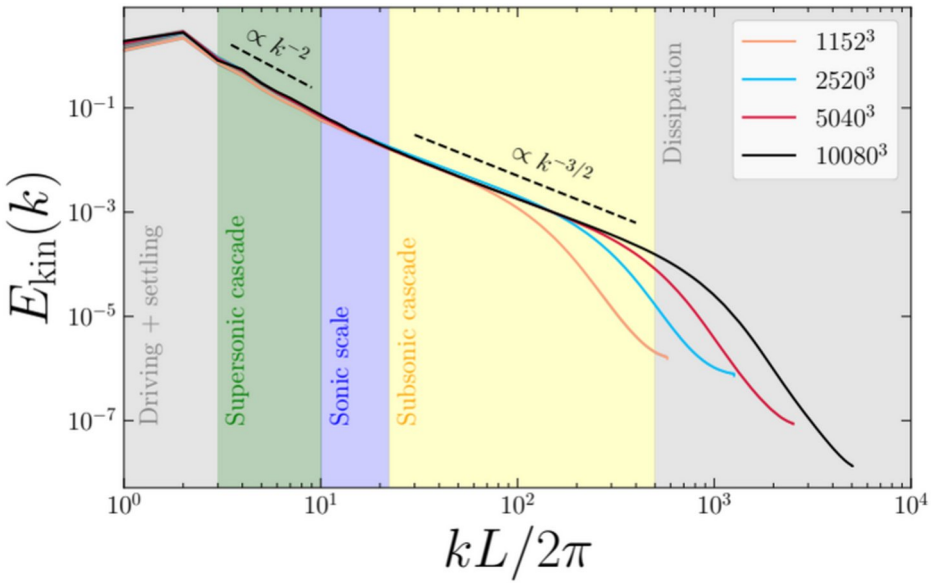

Figure 1: The kinetic energy spectra for compressible MHD turbulence, as a function of wavenumber in units of the box-scale, $L/2\pi$, at different resolutions. We show that in the supersonic cascade, $E_{kin}(k) \propto k^{-2}$, and in the subsonic cascade, $E_{kin}(k) \propto k^{-3/2}$.

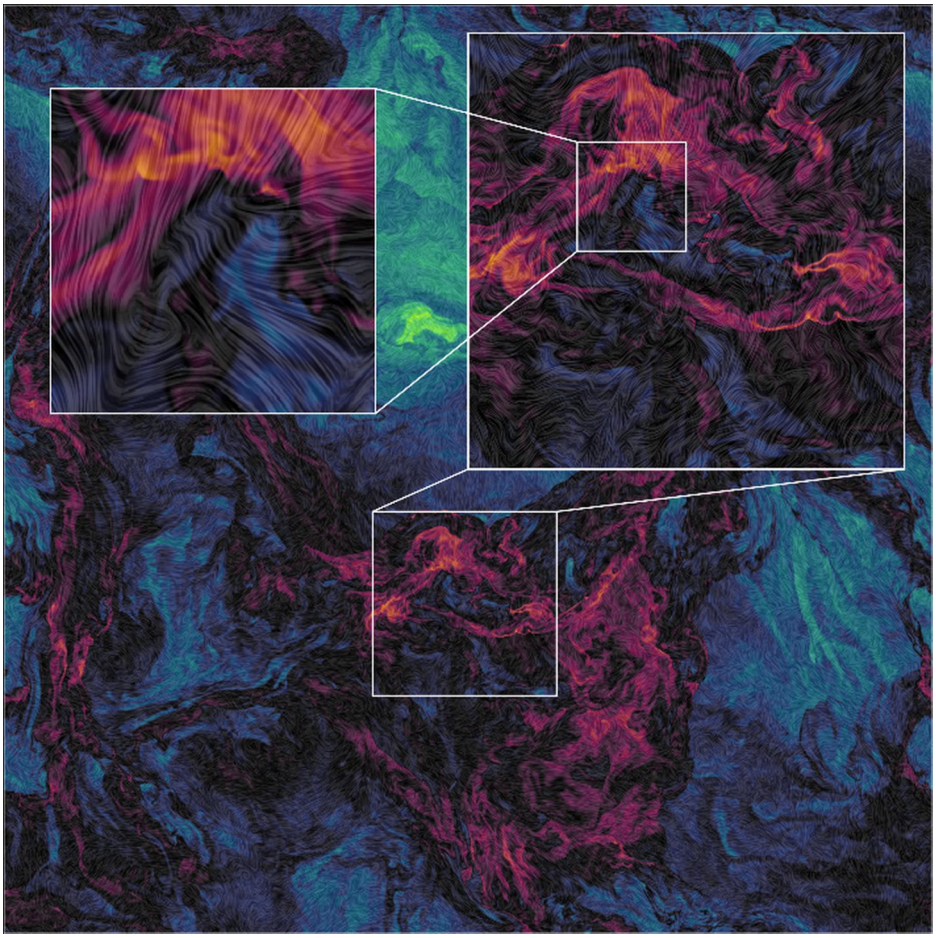

Figure 2: A two-dimensional slice of the three-dimensional gas density (red-orange for over-densities, green-blue for under-densities), with three levels of magnification, showing the detailed structures and scales resolved in the $10{,}080^3$ MHD turbulence simulation. The local magnetic field direction is visualised with a line integral convolution filter (indicated with grey swirls), showcasing the detailed, small-scale structure of the magnetic field.

Ongoing Research / Outlook

We are currently evolving the simulation further on SuperMUC-NG to produce robust measurements of the turbulence on, above, and below the magneto-sonic scale, across multiple correlation times of the turbulent forcing.

References and Links

[1] C. Federrath et al., Nature Astronomy, 5 (2021) 365-371.
[2] Fryxell et al., Astrophys. J. Suppl., 131 (2009) 273-334.
[3] Waagan, Federrath & Klingenberg, J. Comp. Phys., 230 (2011) 3331-3351.

Cracking the convective conundrum

1

Research Institution
Institute for Astrophysics and Geophysics, Göttingen University

Principal Investigator
Petri J. Käpylä

Researchers
—

Project Partners
—

SuperMUC Project ID: pr27li

Introduction

The energy transport in the outer envelope of the Sun is due to motions of gas, or convection. Such gas motions lead to efficient mixing and also to the generation of large-scale flows and magnetic fields. The Sun exhibits both: the solar 11-year sunspot cycle is a manifestation of a large-scale magnetic field continuously maintained by a dynamo in its interior. Furthermore, the Sun rotates differentially such that the rotation period, or the solar day, is longer at the poles than at the equator. The case where the equator rotates faster than the poles is referred to as solar-like differential rotation. Such large-scale flows are crucially important for the solar dynamo, and thus understanding their origin is of prime importance.

Theoretical explanation of the solar differential rotation relies on the interaction of turbulent convection and global rotation of the star, such that in sufficiently rapidly rotating stars a solar-like differential rotation profile appears. However, numerical simulations of solar convection tend to produce anti-solar differential rotation with a slow equator and fast poles which is opposite to what the Sun is doing. Furthermore, analysis of the oscillations of the Sun with helioseismology suggest that the flows in the simulations are too fast in comparison to the Sun. This constitutes the convective conundrum, which is essentially the inability of current simulations to capture the convective flows in the Sun accurately enough. This could imply that our understanding of stellar convection is fundamentally flawed. The current project studies several leads that may crack the conundrum and transform our understanding of the flows and magnetic fields in the interiors of stars. The problem is attacked by means of targeted numerical simulations of convection.

Results and Methods

The simulations were made with the Pencil Code which is an open source solver for ordinary and partial differential equations [1]. The code has switchable modules and can be used to model a wide variety of physical problems ranging from turbulent combustion and astrophysical magnetohydrodynamics to gravitational waves [1]. The code is parallelised with MPI and scales efficiently from laptops to supercomputers employing tens of thousands of CPU cores.

The convective conundrum has been studied with local and semi-global simulations of stellar convection (see Figures 1 and 2). In a recently published study [2], the effects of the Prandtl number (Pr), which is the ratio of microscopic diffusion coefficients relevant for the flow and for the temperature fluctuations, was studied with hydrodynamic simulations. In stars the Prandtl number is very much smaller than unity, which poses a serious challenge for numerical simulations. Thus typical simulations assume Pr = 1 for convenience still today. In [2] the dependence of the dynamics of convection were studied systematically with Pr ranging between 0.1 and 10. In total, more than 30 simulations up to resolutions of 11523 grid points were made. These models used in total more than 20 million core hours and 40TB disk space. The main result is that convection with low Pr is significantly different from that at Pr = 1, such that the efficiency of flows to transport thermal energy is reduced. These results were shown to be robust to the highest resolutions achievable (Figure 1). These findings suggest that most of the current simulations are likely to produce results that are not representative of real stellar convection.

As a follow-up study, a comprehensive set of simulations with varying Prandtl number with semi-global simulations (Figure 2) were made (Käpylä, in preparation). The initial phase of simulations were made with low resolutions (128x288x144 and 144x432x216 grid points) whereas a subset of the simulations were made at higher resolutions (256x576x288 and 288x864x432), some of which are still in progress. These simulations are particularly demanding because reaching a final statistically steady state takes a substantial amount of time while the timestep of the simulations becomes shorter as the resolution is increased. Therefore, a compromise between a sufficiently long run time and spatial resolution is required. More than 30 simulations were made in this study using a total of over 10 million core hours and 20 TB disk space.

This study specifically addresses the issue of the transition from anti-solar to solar-like differential rotation and how it is affected by the Prandtl number and magnetism. In accordance with [2], a clear difference in the dynamics of convection was observed as a function of Pr. More specifically, it is easier to obtain a solar-like

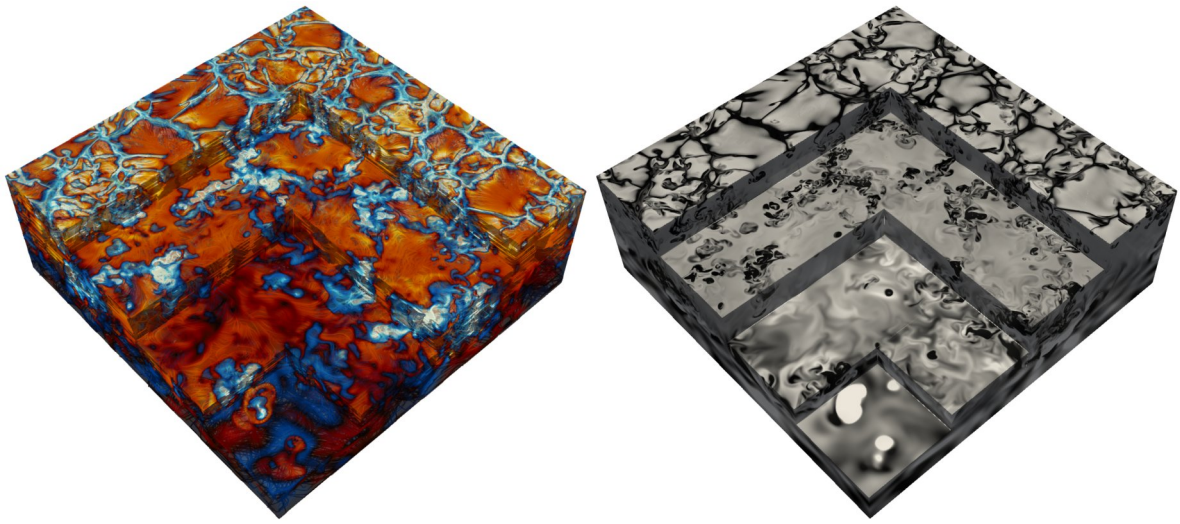

Figure 1: Left panel: Velocity field in a high-resolution simulation of non-rotating convection in Cartesian geometry. Right: entropy fluctuations in the same simulation. Adapted from [2].

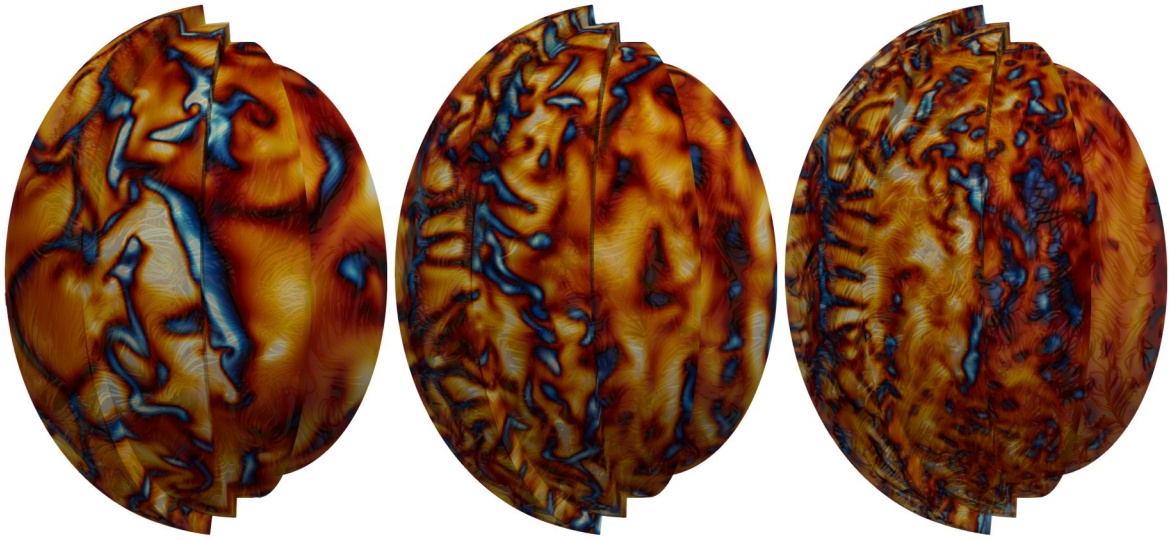

Figure 2: Velocities in semi-global convection simulations with Pr=0.1 (left), Pr = 1 (middle), and Pr = 10 (right) (Käpylä, in preparation).

rotation profile in cases where the Prandtl number is lower than one. This could indicate that the unrealistic Prandtl number in most of the contemporary simulations is at least partially responsible for the mismatch between simulations and solar observations. Furthermore, these convective flows act as dynamos if a weak seed magnetic field is included. Such dynamo-generated magnetic fields make it further easier to obtain solar-like differential rotation. These results provide thus far the most promising leads in the search for a breakthrough in cracking the convective conundrum.

Ongoing Research / Outlook

The SuperMUC-NG resources have been crucial for the successful completion of the current studies and have enabled comprehensive systematic simulations surveys reaching high resolutions and wide parameter coverage. The new results have also opened several new questions that will be addressed in a follow-up resource application at SuperMUC-NG.

Furthermore, the study of differential rotation in semi-global models continues with even higher resolutions which enable more realistic flows and magnetic fields. This is important because even the current highest resolution models are not yet in an asymptotic regime where the results would not change when the resolution is increased further. Additional resource applications from dedicated large-scales calls from the Gauss Supercomputing Centre and PRACE are planned to address specifically this issue.

References and Links

[1] Pencil Code (https://github.com/pencil-code); The Pencil Code collaboration, J. Open Source Softw. (2021), 6, 2807
[2] P. J. Käpylä, Astron. Astrophys. (2021), 655, 78.

1 Testing the limits of magnetized accretion onto black holes

Research Institution
[1]CEA-Saclay, Paris (France)
[2]Max Planck Institute for Astrophysics, Garching (Germany)

Principal Investigator
Matteo Bugli[1,2]

Researchers
Ewald Müller[2], Luca Del Zanna[3],Niccolò Tomei[3]

Project Partner
[3]Università degli Studi di Firenze

SuperMUC Project ID: pr27qu

Introduction

Numerical simulations are an invaluable tool when it comes to investigate the complex dynamics that rule the behavior of astrophysical plasmas. This is even more the case if we consider the fundamental role that General Relativity has in the description of compact objects such as black holes and the magnetized hot accretion disks that are commonly assumed to orbit around them.

In the past decades our understanding of the physics behind accretion processes has vastly increased thanks to an always increasing number of numerical studies, but there are still several uncertainties that make challenging to draw quantitative (and sometimes qualitative) conclusions from them. This fact represents an important incentive for the improvement of numerical models, considering also the extraordinary observational discoveries made in the recent years by the detection of gravitational waves and the first direct imaging of a supermassive black hole.

Our project aims at assessing the degree of accuracy of state-of-the-art general relativistic magnetohydrodynamic (GRMHD) simulations of accretion disks around black holes using the astrophysical code ECHO [1]. We explored the impact of employing different algorithms and numerical implementations by participating to the EHT code comparison project [2] and investigated the limits of an ideal description of the astrophysical plasma by taking into account the turbulent dissipation and amlification of the magnetic field which are usually neglected.

Results and Methods

A significant part of the project focused on the impact of specific choices of numerical implementation, which we investigated within a first code comparison study led by the Event Horizon Telescope collaboration [2]. The 9 different codes employed show a remarkable agreement between the different participating codes, with higher resolutions leading to significant decrease in deviations. The overall structure of the accretion flow is also quite similar among different results, and the same goes for the time variability of the computed light curves, displaying very similar spectra. This agreement was found between codes using different grid geometries (cartesian or spherical coordinates), programming languages (Fortran or C++) and interpolation/integration algorithms.

Name	Grid points	Cores	Runtime [h]	Core-hours [M]	Output size [GB]
Low resolution EHT	192x96x96	560	85	0.05	0.32
High resolution EHT	382x192x192	1,344	490	0.66	2.6
Standard disk	256x256x256	6,840	80	0.55	1.4
High resolution disk	512x512x512	51,840	170	8.81	47

Table 1: Typical models run on SuperMUC Phase 2 and SuperMUC-NG.

The role of numerical dissipation and the limits of an ideal description of the astrophysical plasma can also be very important, as a more efficient diffusion of the magnetic field can affect the global structure of the disk and its accretion properties. By investigating the consequences of assuming a finite magnetic resistivity in the plasma, we show that a weaker MHD turbulence can lead to the formation of non-axisymmetric large-scale structures in the disk which, for an ideal plasma, would otherwise quickly washed out [3] (see Figure 3).

We also explored the impact of a turbulent dynamo mechanism that can amplify the disk's magnetic field and shape its dynamics [4]. Our models can reproduce the results obtained in the EHT code comparison using simple 2D model rather than more expensive 3D ones, showing the importance of the dynamo process. The necessary numerical models make use of a generalized prescription for Ohm's law that accounts for the turbulent dissipation of the magnetic field due to unresolved small-scale motions.

All our three-dimensional simulations of thick magnetized disks were produced using ECHO, a finite-differences Fortran code solving the equations of magnetohydrodynamics in General Relativity. The hybrid MPI-OMP parallelization scheme employed in the code [5] allows for an efficient use of a large number

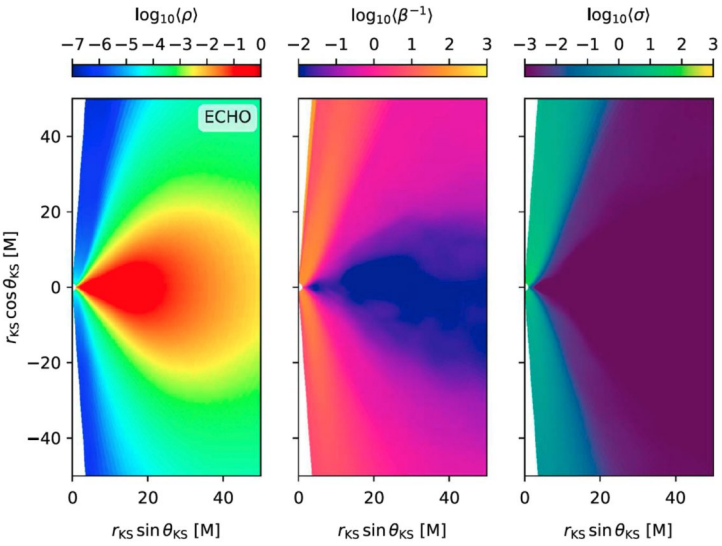

Figure 1: Meridional slices showing rest mass density (left panel), magnetic to thermal pressure ratio (center) and magnetization (right) in logarithmic scale and code units [2].

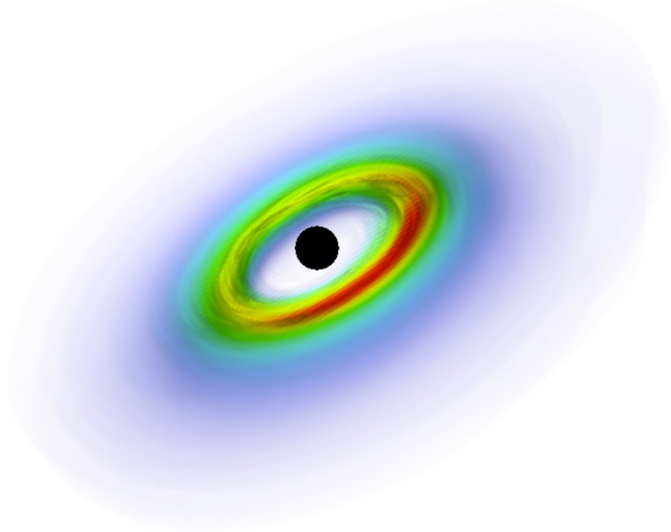

Figure 2: Volume rendering of a thick accretion disk (southern half) with finite resistivity.

of cores (ranging from 560 to 51,840 as shown in Table 1, depending on the model) on SuperMUC Phase 2 and SuperMUC-NG. Each simulation produced between 100 and 1,000 HDF5 outputs (generated with a parallel HDF5-MPI scheme), requiring overall 20 TB of storage volume.

Ongoing Research / Outlook

Thanks to an efficient use of the HPC resources offered by LRZ we explored some important aspects of numerical models of accretion disks, such as the dependency of the results on the specific algorithm choices of the code employed and the effects of magnetic diffusion. A second code comparison project is currently ongoing, which will perform a similar study to the one already published, but will mainly focus on more highly magnetized disk, which are known to trigger the formation of strong polar jets. This work will greatly help assessing to what extent numerical simulations can quantitatively reproduce several important dynamic properties of accreting astrophysical plasmas.

References and Links

[1] M. Bugli, Proceedings of the 26th Euromicro International Conference on PDP, 2018, p. 674-681.
[2] O. Porth et. al., 2019, APJ Suppl. Series, 243(2): 26.
[3] M. Bugli et. al., 2018, MNRAS, 475(1):108-120.
[4] N. Tomei, L. Del Zanna and M. Bugli, 2021, Universe, 7(8): 259.
[5] M. Bugli, L. Iapichino and F. Baruffa, 2018, Intel®Parallel Universe, 34.

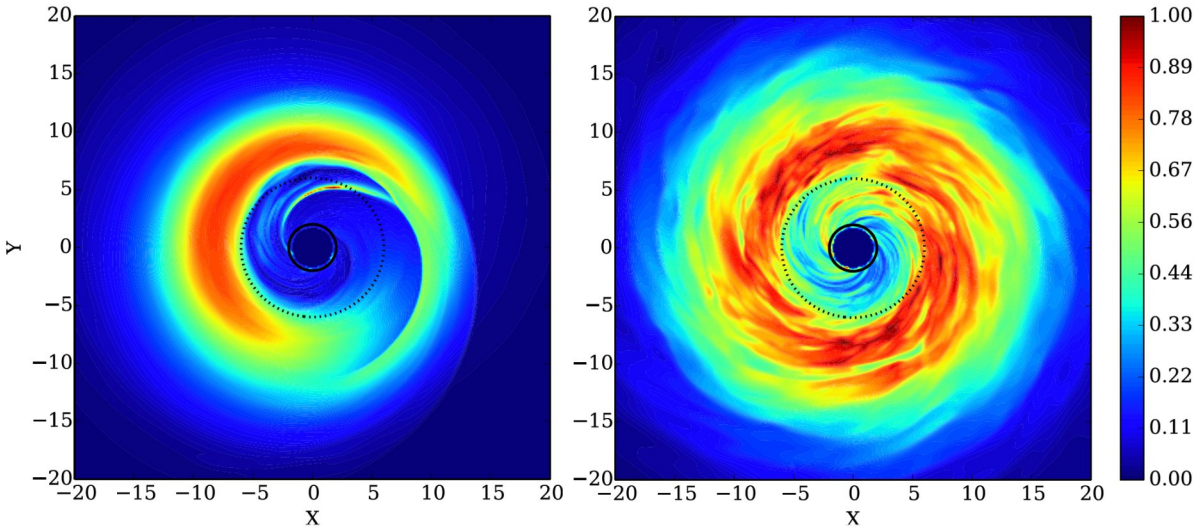

Figure 3: equatorial slices of the accretion disk for a hydrodynamic model (left panel) and a magnetized one (right) showing rest mass density in logarithmic scale normalized by its maximum [3].

Hermeian galaxies: Cosmic messengers between the Milky Way and Andromeda

1

Research Institution
[1]Astrophysics Research Institute, LJMU, UK

Principal Investigator
Oliver Newton[1]

Researchers
Noam I. Libeskind[2], Alexander Knebe[3,4], Miguel A. Sánchez-Conde[3]

Project Partners
[2]Leibniz-Institut für Astrophysik, Potsdam (AIP)
[3]Universidad Autónoma de Madrid
[4]International Centre for Radio Astronomy Research (ICRAR), University of Western Australia

SuperMUC Project ID: pr62ju

Introduction

The environment of the Local Group is an exceptional probe of fundamental theories describing the origin and evolution of the Universe. Detailed observations of its constituent galaxies are facilitating a comprehensive exploration of galaxy formation physics across several orders of magnitude in mass and its population of faint galaxies has also proved to be a compelling test of cosmological models on small astrophysical scales. These developments rely on the predictions of increasingly sophisticated hydrodynamic simulations of the formation and evolution of the Local Group that self-consistently model the interactions of baryons and dark matter. Over the last decade such simulations have revealed a dynamic environment that influences the growth of the Milky Way and Andromeda galaxies (the 'primary' hosts of the Local Group) and has important effects on the evolution of the low-mass galaxy population. In particular, the tidal interactions the low-mass galaxies experience as they pass through the primary hosts increase the concentration of dark matter at their centres. Additionally, baryonic processes efficiently strip them of gas and prevent them forming more stars. We now know that most of these 'pre-processed' galaxies fall into the gravitational potential well of one of the two primary hosts and escape to large distances later on. These are known as 'backsplash' galaxies and they account for as much as half of all systems accreted by the Milky Way or Andromeda. Populations of galaxies with highly concentrated dark matter distributions could be competitive probes with which to constrain the properties of the dark matter. Candidate particles that decay or annihilate with each other in high density regions are predicted to emit electromagnetic radiation, typically in X-rays or gamma-rays. Such signals have been claimed to be observed already coming from dark matter-dominated systems such as the Galactic centre or nearby dwarf galaxies; however, an astrophysical origin of the signal is also possible and has not been ruled out. Gas-poor, pre-processed dwarf galaxies could therefore be attractive targets to distinguish between the two production mechanisms. Using the state-of-the-art magnetohydrodynamic simulations of the Local Group from the HESTIA project [1], we have discovered a new class of pre-processed galaxies that act as intergalactic messengers between the Milky Way and Andromeda [2]. These 'Hermeian' galaxies interact with both primary hosts during the assembly of the Local Group and escape to large distances at the present day. In the process they facilitate the exchange of dark matter, gas, and stars, which leaves chemical signatures in the gas and stellar content of the Milky Way and Andromeda. The interactions also concentrate the dark matter in the Hermeian galaxies and strip them of gas, making them promising targets to detect signals from annihilating dark matter.

Results and Methods

The HESTIA suite consists of 13 medium- and three high-resolution magnetohydrodynamic simulations of the Local Group [3]. The initial conditions are constrained using observations of nearby galaxies to reproduce the major gravitational sources in the local environment. This ensures that at the present day the Local Group analogues are embedded in large-scale structure that is consistent with the observations. The HESTIA simulations are based on the AREPO moving mesh code and use the AURIGA galaxy formation model to incorporate a wide variety of astrophysical processes. In our analysis we used the three high-resolution simulations that each consist of 550 billion particles in a periodic cosmological box with sides of length $100\ Mpch^{-1}$. Each simulation used 4,000 cores per job on SUPERMUC-NG, running for 22 million core hours to produce in excess of 58 TB of data. The HESTIA simulation suite as a whole produced over 900 TB of data across all sets of dark matter-only and full hydrodynamic runs. We identified Hermeian galaxies by reconstructing their trajectories through the simulations and inferred their positions between snapshots using cubic spline interpolation. In Fig. 1, we show the trajectories of Andromeda, the Milky Way, and two Hermeian galaxies in one of the high-resolution simulations. In this example, the Hermeian galaxies accrete gas from Andromeda and transfer it to the Milky Way. The chemical compositions of the primary hosts differ, so when the gas is deposited in

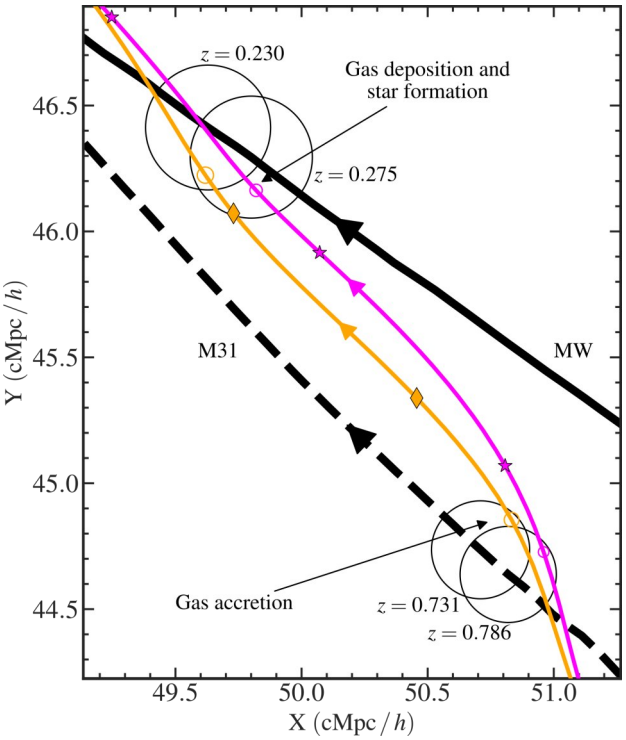

Figure 1: The projected trajectories of Andromeda (M31), the Milky Way (MW), and two Hermeian galaxies. This shows the transfer of gas from M31 to the MW and marks the subsequent formation of stars. Arrow heads indicate the directions of travel of the galaxies and circles show the size of the galaxies and their dark matter.

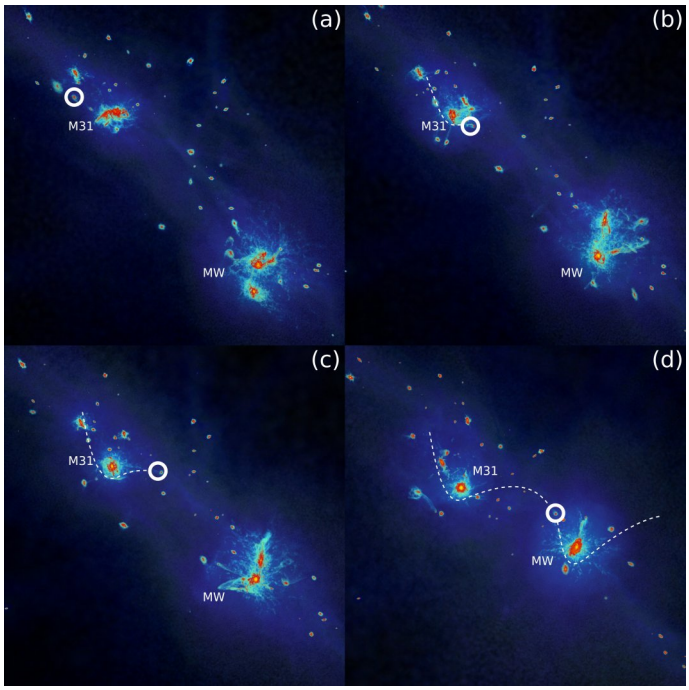

Figure 2: The projected gas density of one of the high-resolution HESTIA Local Group simulations at four snapshots in time showing the passage of a Hermeian galaxy (circled) through the primary hosts. This cosmic messenger traverses the Local Group in 4 Gyr and its trajectory is marked with dashed lines.

the Milky Way it is a source of chemical pollution that could act as a characteristic signature of the passage of the Hermeian galaxy. During deposition the gas pressure increases substantially, causing the formation of stars with unusual chemical compositions compared with the surrounding interstellar medium. This could explain the origin of similar stars that have been observed in the Milky Way. In Fig. 2, we show rendered projections of the Local Group volume at several snapshots in time and mark the trajectory of one Hermeian galaxy through the volume. There is a limited set of trajectories on which galaxies can interact with both the Milky Way and Andromeda and escape to large distances in the time it takes to assemble the Local Group. The trajectory shown in Fig. 2 is therefore typical of Hermeian galaxies in the Local Group and means that the present-day population of Hermeian galaxies is likely to be aligned approximately along the line connecting the Milky Way and Andromeda. As the Hermeian galaxies pass through the primary hosts they experience strong tidal interactions that concentrate their dark matter towards their centres. In HESTIA we find that the dark matter content of Hermeian galaxies is almost twice as concentrated as that of other galaxies that have not interacted with the primary hosts. As the strength of the annihilation signals scales with dark matter density, Hermeian galaxies could be promising targets to detect such signatures of dark matter. We find that the strength of the annihilation signal from Hermeian galaxies is comparable with that expected from more traditional targets, such as dwarf satellite galaxies or galaxy clusters. A recent analysis of Fermi-LAT observations of distant low-mass galaxies in the Local Group predicts annihilation signal strengths that are consistent with those of the Hermeian galaxies in the HESTIA simulations. However, as these field galaxies have not interacted with the primary hosts, their dark matter distributions are less concentrated and the signal they produce is more diffuse.

Ongoing Research / Outlook

The first phase of the HESTIA simulation project is now complete and analysis of the data is underway. Our initial work has uncovered a new class of low-mass galaxies in the Local Group that passed through the primary hosts and escaped to large distances at the present day. We have called these ‘Hermeian’ galaxies after Hermes, the messenger of the gods in Ancient Greek mythology. These cosmic messengers facilitate the exchange of dark matter, gas, and stars between the Milky Way and Andromeda, potentially leaving distinctive chemical signatures of the interactions with the Hermeian galaxies. These processes also concentrate the distribution of dark matter, making them promising targets to search for signals of annihilating dark matter. Hermeian galaxies play an important role in the formation and evolution of the Milky Way and Andromeda and we expect that these first results will motivate further study of these objects using new, higher resolution simulations of the Local Group environment and in forthcoming observational searches.

References and Links

[1] https://hestia.aip.de
[2] O. Newton et al, 2022, MNRAS, submitted.
[3] N. I. Libeskind et al., 2020, MNRAS, 498, 2968.

Star Formation through the Cosmic Ages

Research Institution
Universität Heidelberg, Zentrum für Astronomie, Institut für Theoretische Astrophysik

Principal Investigator
Ralf Klessen

Researchers
Patricio Alister, Li-Hsin Chen, Raúl Dominguez, Philipp Girichidis, Simon Glover, Junia Göller, Glen Hunter, Da Eun Kang, Joseph Lewis, Loke Ohlin, Mattis Magg, Eric Pellegrini, Toni Peter, Brooke Polak, Bastián Reinoso, Stefan Reißl, Matthew Smith, Mattia Sormani, Felix Spanier, Robin Treß

Project Partners
–

SuperMUC Project ID: pr74nu

Introduction

Project pr74nu Star Formation through the Cosmic Ages provides computing time to the star formation group at the Center for Astronomy at Heidelberg University, and allows the members of the team to perform small to medium-sized parameter studies, to develop and validate new numerical code modules, and to prepare for larger-scale highest-resolution numerical simulations on specific topics for which time at national and European supercomputing facilities is being requested in separate proposals.

The research activities of the group focus on identifying and characterizing the physical processes that govern the birth of stars across cosmic time, from the first stars in our universe to young protostellar objects in the solar vicinity. Scientific interests include gas dynamics and chemistry in the multi-phase interstellar medium (ISM), the statistical description of astrophysical turbulent flows, dynamo processes across a wide range of astrophysical scales, gravitational collapse and the formation of stars and stellar clusters, stellar dynamics in the Milky Way, and the development and optimization of numerical algorithms in computational astrophysics. The use of supercomputing resources, as provided by LRZ, is instrumental for these research activities.

This brief report covers the year 2021 and highlights two specific examples of the research activities in the group, one from our efforts to better understand the formation of the first and second generations of stars in the Universe, and the other one from our studies of ISM dynamics and stellar birth in the Milky Way.

Results and Methods

The numerical simulations that form the base of the two studies reported here were carried out using an expanded version of the publicly available moving-mesh AREPO code [10]. We solve the equations of ideal magneto-hydrodynamics, account for the gravitational interaction between gas, stars and – if needed – dark matter, the chemistry of the ISM together with a description of the dominant heating and cooling processes [2,4,9], magnetic fields [8], stellar feedback and radiative transfer [6], and a representation of star formation (in the form of sink particles, see [3]). The code runs efficiently on massively parallel systems, such as SuperMUC-NG.

Metal Mixing in High-Redshift Minihalos
When investigating star formation in the early Universe, the lack of abundance patterns originating in pair instability supernovae in observations of very metal-poor stars in the Milky Way and its satellite galaxies has been a long-standing problem. This class of supernovae is expected to produce an abundance pattern with a strong odd-even effect, making it substantially different from present-day supernovae and easy to identify. As part of the PhD project of Mattis Magg, we use very high-resolution cosmological radiation-hydrodynamics simulations to model such supernovae and the subsequent formation of slightly metal-enriched second generations of stars.

We identify several star-forming minihalos in our simulation before a redshift of 19.5, and we follow the corresponding supernova explosions, the spread of metal-enriched material, and the subsequent formation of new generations of stars. We find a wide range of metallicities, as illustrated in Figure 1. Whereas most of the second generation stars would qualify as extremely metal-poor stars in Galactic stellar archeological surveys [1], we also find several objects with relatively high ([Fe/H] ≥ −2) or intermediate metallicities (−2 < [Fe/H] < −3), at the 20-30% level. All of these are formed by internal enrichment, whereas most of the lowest-metallicity stars are formed by external enrichment. Altogether, our result is at tension with the current (lack of) observations of metal-poor stars with pair instability supernova abundance patterns. We conclude that these very massive stars might have been very rare in the early Universe. Our simulations help us to better understand what drives different modes of recol-lapse and new star formation, and what determines the early enrichment history of the Universe (for further details, see [7]).

Star Formation in Colliding Clouds
Giant molecular clouds (GMCs) are parsec scale, cold clouds within which the stars of a galaxy are born. Due to the dynamics of the galaxy, GMCs will occasionally

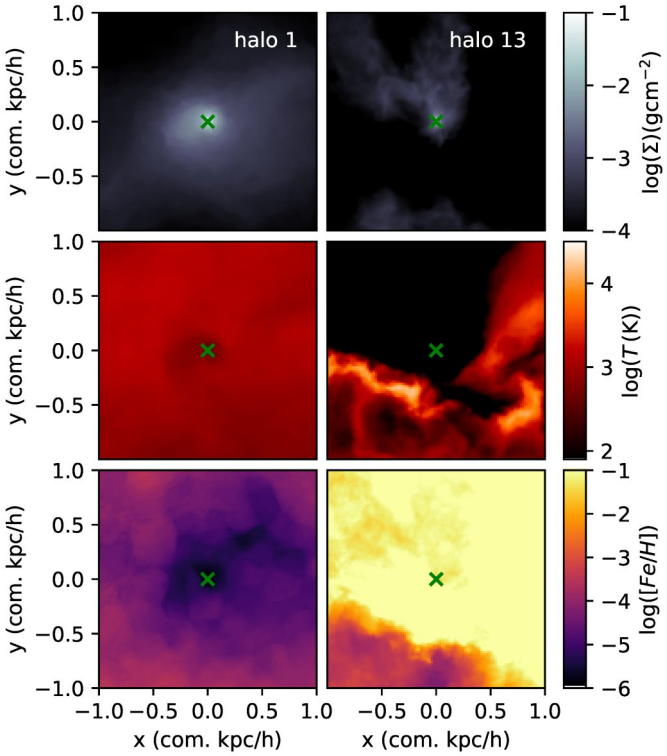

Figure 1: Column density (upper row), average temperature (middle row) and metallicity (bottom row) at the time of recollapse and second-generation star formation (indicated by green crosses). The image illustrates two very different mixing behaviors. To the left, halo 1 has retained very low metallicity and exhibits a steep radial gradient. To the right, halo 13 is highly enriched and has a homogeneous metallicity distribution.

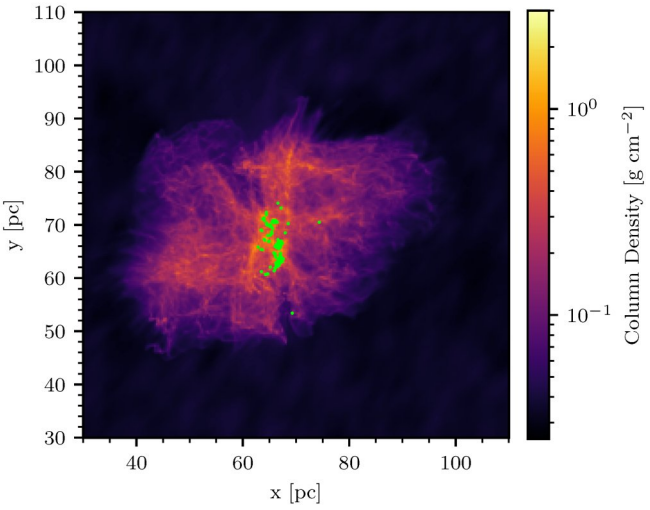

Figure 2: Column density maps of one of the colliding cloud simulations after the system has evolved for 2.48 Myr. The green dots indicate the position of the sink particles (representing young massive stars).

collide with each other. Observations indicate that young stellar clusters are often found near or in these colliding flows suggesting a burst a of star formation as a result of the collision. This prompts the question: does the collision form more stars than if the clouds did not collide?

For this project, as a part of Glen Hunter's PhD studies, we investigate how star formation is affected as a result of GMCs colliding. We perform a series of simulations where two identical GMCs are initialized and allowed to evolve. The series of simulations form the basis of a parameter study where we vary the collisional velocity, magnetic field inclination and resolution to see how the star formation within the clouds responds. The collision results in a turbulent environment, as illustrated in Figure 2, where dense gas forms stars along the collision front. We find that if we increase collisional velocity, we form this dense gas quicker and thus initiate star formation sooner. Magnetic fields misaligned with the collisional axis result in a delay in star formation due to the magnetic field resisting the flow of the gas. We find that collisions increase the rate at which stars form by a factor of 2-5 depending on the simulation setup. For further details, see [5].

Acknowledgements
The star formation group at Heidelberg University acknowledges funding form the European Research Council in the ERC Synergy Grant “ECOGAL” (project ID 855130). They also acknowledge support from the Heidelberg cluster of excellence EXC 2181 “STRUCTURES (ID 390900948), and they are grateful for support from the German Research Foundation (DFG) via the collaborative research center SFB 881 (ID 138713538) ”The Milky Way System” (subprojects A1, B1, B2, and B8). The group also makes use of computing resources provided by the State of Baden-Württemberg through bwHPC and DFG through grant INST 35/1134-1 FUGG. Data are stored at SDS@hd supported by the State of Baden-Württemberg and DFG through grant INST 35/1314-1 FUGG.

References and Links

[1] Beers, T.C., Christlieb, N., ARA&A, 43, 531 (2005).
[2] Clark, P.C. et. al., ApJ, 727, 110 (2011).
[3] Federrath, et. al., ApJ, 713, 269 (2010).
[4] Glover, et. al., MNRAS, 404, 2 (2010).
[5] Hunter, et. al., MNRAS, submitted, arXiv:2109.06195 (2022).
[6] Jaura, O., et. al., MNRAS, 499, 3594 (2020).
[7] Magg, M., et. al., O., ApJ, submitted, arXiv:2110.15372 (2022).
[8] Pakmor, R., et. al., MNRAS, 418, 1392 (2011).
[9] Schauer A.T.P., et. al., MNRAS, 484, 3510 (2019).
[10] Springel V., MNRAS, 401, 791 (2010).

Kinetic simulations of astrophysical and solar plasma turbulence

1

Research Institution
[1]Max-Planck-Institut für Sonnensystemforschung, Göttingen

Principal Investigator
Jörg Büchner[1,2]

Researchers
Daniel Grošelj[3], Patricio Muñoz[1,2], Frank Jenko[4]

Project Partners
[2]Technical University Berlin
[3]Columbia University, New York, USA
[4]Max-Planck-Institut für Plasmaphysik, Garching

SuperMUC Project ID: pr74vi

Introduction

Collisionless astrophysical and space plasmas are usually in a turbulent state. Prominent examples include the plasmas of the solar wind, the interstellar medium (ISM), of galaxy clusters and accretion disks. Despite of the omnipresence of turbulence in the plasma Universe, its properties and consequences are not well understood, yet. One of the main challenges in understanding turbulent collisionless plasmas lies in the complicated kinetic nature of the collective particle interactions at the plasma microscales, where the energy is dissipated. A kinetic, particle description is required to describe the energy dissipation in these systems, such that non-thermal effects and wave-particle interactions are properly taken into account. Two fundamental energy conversion processes in the plasma Universe are in the focus of this SuperMUC-NG project [1]: shock waves and magnetic reconnection. In the first fundamental process, shock waves, the energy of plasma flows is converted into thermal energy (heating) and particle acceleration while the plasma flow is decelerated. It is known that in shock-upstream regions the plasma becomes highly turbulent. Shock waves are observed in situ at space plasma boundaries in the solar wind and ahead of magnetospheres or other obstacles indirectly also, e.g., between exploding supernovae and the interstellar medium (ISM). They play an important role, perhaps, in the formation of gamma-ray bursts (GRBs) out of highly relativistic plasmas. In the first of our SuperMUC-NG sub-project, we investigated the efficiency of particle acceleration by shock waves in GRBs and the role of self-generated turbulence in this highly energetic process. The obtained particle energy spectra are used as input for models of the non-thermal emission due to, e.g., synchrotron and inverse-Compton radiation from GRB afterglows. The second fundamental process of energy conversion in the Universe, magnetic reconnection, is also closely related to plasma turbulence. In the course of reconnection, magnetic energy is converted into plasma flows and heating as well as the acceleration of particles to high energies. Understanding turbulent magnetic reconnection processes is crucial for the understanding of heating, e.g. of stellar coronae, the release of magnetic energy in stellar flares, as well as of the energization of the ISM. Reconnection and turbulence are closely related to each other: reconnection proceeds, if turbulence allows non-ideal plasma responses and ongoing reconnection can cause secondary turbulence via plasma instabilities and the formation of small-scale current sheets. The latter process is the focus of our second SuperMUC-NG sub-project. We concentrated our studies on the not well understood role of the electrons on the energy dissipation, plasma heating and acceleration processes.

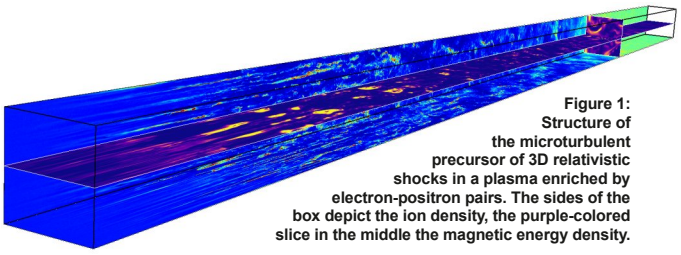

Figure 1: Structure of the microturbulent precursor of 3D relativistic shocks in a plasma enriched by electron-positron pairs. The sides of the box depict the ion density, the purple-colored slice in the middle the magnetic energy density.

Results and Methods

To tackle the outstanding astrophysical problems of collisionless shocks and reconnection in turbulence kinetically, the method of choice are fully kinetic plasma simulations in which the full sets of Vlasov and Maxwell equations are self-consistently solved together with the action of the electromagnetic fields on the charged plasma particles. For this sake we carried out Particle-in-Cell (PIC) simulations which describe the particle motion by a Lagrangian approach and solves for the electromagnetic fields by an Eulerian description allocated on a mesh. The particle distribution functions are the main variables to be obtained by solving Vlasov equations. Hence, the PIC method relies on a sufficiently large number of many macro-particles, in order to statistically reliable reconstruct the particle distribution functions. PIC simulations are, therefore, computationally very demanding: they have to trace in the order of 10^9-10^{11} macro-particles on a mesh consisting of about 10^8 grid points in 3D simulations. This implies that a single particle snapshot requires a memory in the order of one Terabyte, hence, one has to make the particle output as sparse in time as possible. Grid data (e.g.,

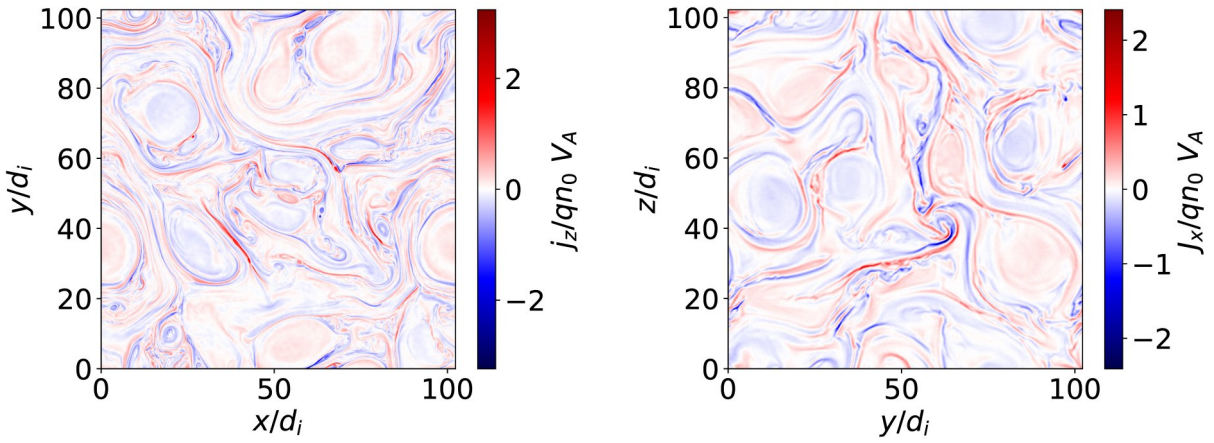

Figure 2: Comparison of out-of-plane current densities in turbulence simulations showing current sheet formation and magnetic reconnection through them. Left panel: fully kinetic model. Right panel. Hybrid-kinetic with electron inertia model.

electromagnetic fields) is less heavy, but this data output should be carried out more frequently in order to correctly understand the evolution of the system. The resulting output field sizes are in the order of a significant fraction of a Terabyte for large production runs. In our project, we utilized the highly efficient parallelized codes OSIRIS [7] and ACRONYM [8]. These codes were proven to run efficiently on the SuperMUC-NG machine. The largest simulations were in the order of a few million core-hours, while parametric studies were done with runs in the order of a significant fraction of a million of core-hours. A typical run requires between a few to tens of thousands cores. With the OSIRIS code we performed the first PIC simulations of relativistic, weakly magnetized electron-ion-positron shock waves and compared them with results obtained for shock waves in a pure electron-ion plasma. Our results apply to the early afterglow of GRBs, where the prompt radiation streaming ahead of the blast wave loads the ambient medium (i.e. the plasma flow ahead of the shock) with electron-positron pairs. The change in the particle composition is characterized by a pair-loading factor Z, the number of loaded electrons and positrons per ion. Another key parameter that controls the energization process is the magnetization Sigma, the ratio of the upstream electromagnetic- to the particle kinetic energy flux. We studied the dependence of the shock properties on both Sigma and Z. We performed 2D and (a limited amount of) 3D simulations [2]). Our runs represent some of the largest and longest simulations of relativistic weakly magnetized shocks to date. In our largest 2D run, we used a spatial grid of size 295,000 x 5,400 and evolved the system for over 600,000 time steps. Figure 1 shows the 3D structure of a relativistic pair-loaded shock (Z=2 and Sigma=0). The simulation ran on 31,104 CPU cores on SuperMUC-NG on a 30,000 x 900 x 900 grid. A microturbulent precursor ahead of the shock is evident, which we analyzed in detail by 2D simulations [2]. This way we could provide estimates for the fraction of energy carried by the post-shock pairs – an important parameter for calculating the radiation emission by the shock. We also constrainted the range of magnetizations and pair-loading factors that allow for efficient particle acceleration. With the ACRONYM code we simulated the evolution of a turbulent plasma at which initially large scale velocity and magnetic field fluctuations are imposed. The energy of the fluctuations is transferred in time to smaller scales, until it is dissipated at the smallest (electron-) kinetic scales. The developed turbulence was of kinetic Alfvénic type as shown in the first part of this project by using OSIRIS [3]. We found that electron-scale current sheets are formed in the turbulence which release and dissipate energy via magnetic reconnection. To understand the underlying process we assessed the role of the electrons by means of comparing fully kinetic with hybrid-kinetic simulations utilizing our newly parallelized CHIEF code [4]. Figure 2 illustrates the importance of considering the fully kinetic electron dynamics, which causes the formation of sub electron-skin-depth-scale structures. We also characterized the resulting deviations of the electron velocity space distribution functions (EVDFs) from a Maxwellian caused by turbulent magnetic reconnection, the stability properties of these EVDFs possibly causing solar radio wave emissions [5,6].

Ongoing Research / Outlook

We are further investigating the partitioning of energy among ions and electrons / positrons in the self-generated microturbulence of relativistic shocks, exploring the conditions for an efficient cosmic ray - particle acceleration. We will further assess 3D kinetically turbulent plasmas, in particular the influence of the electrons of current sheets formed in the turbulent cascade in order to understand energy dissipation, heating and particle acceleration in the plasmas of the Earth's magnetosheath the Sun, and the solar wind. We will submit a SuperMUC-NG proposal to investigate these effects in depth by means of ACRONYM and the newly parallelized hybrid-kinetic CHIEF-code simulations.

References and Links

[1] https://www-astro.physik.tu-berlin.de/node/438
[2] Grošelj, D., Sironi, L., & Beloborodov, A (2022). Astrophys. J., in press.
[3] Grošelj, D., Mallet, A., Loureiro, N. F., & Jenko, F. (2018). Phys. Rev. Lett., 120(10), 105101.
[4] Jain, N, Muñoz P., Tabriz, M.F, Rampp M. & Büchner, J (2022). Phys Plasmas 29, 053902. doi:10.1063/5.0087103.
[5] Yao, X. Muñoz P. & Büchner, J. (2022). Phys. Plasmas, 29(2), 022104. doi:10.1063/5.0061151.
[6] Yao, X. et al. (2022) arXiv:2106.12558.
[7] http://epp.tecnico.ulisboa.pt/osiris
[8] http://plasma.nerd2nerd.org/

A3391/95: a case study from the Magneticum cosmological simulation

1

Research Institution
[1]Universitäts-Sternwarte, Fakultät für Physik, Ludwig-Maximilians-Universität München

Principal Investigator
Klaus Dolag[1]

Researcher
Veronica Biffi[2,1]

Project Partner
[2]INAF – Osservatorio Astronomico di Trieste

SuperMUC Project ID: pr86re

Introduction

The formation and evolution of the large scale structure (LSS) has long been a key target of astrophysical and cosmological investigations. Simulations predict the existence of a thin filamentary structure, the so-called Cosmic Web, connecting the knots where galaxy clusters reside. Observationally, a detailed study of the Cosmic Web structure and evolution can be pursued by investigating the properties of the visible matter tracing the underlying dark matter (DM) distribution. This promoted several investigations aiming for a census of cosmic baryons. Compared to observational estimates, theoretical studies predict that about half of the baryons in the Universe must be indeed undetected. In particular, independently of the use of identification tools used to identify the Web constituents (namely filaments, sheets and voids) cosmological simulations consistently predict that a significant fraction (~40%) of the cosmic baryon budget is in the form of cool intergalactic medium and warm-hot intergalactic medium, with most of it located in filaments. For the first time, the large-scale cosmic structure and a long gas emission filament have been captured by SRG/eROSITA in a direct X-ray observation of the A3391/95 field. We therefore investigated the assembly history of an A3391/95-like system of clusters and the thermo-chemical properties of the diffuse gas in it, connecting simulation predictions to the eROSITA observations, to constrain the origin and nature of the gas in the pair interconnecting bridge.

Results and Methods

Gas bridge between the pair clusters
A debated aspect of the observed A3391/95 system regards the nature of the gas between the two main clusters. Following the common terminology, the gas filament between clusters in close pairs is typically referred to as “bridge”. Depending on the interaction stage of the two systems, this could be either stripped gas from the outer cluster atmospheres or actual filament gas. Distinguishing pure filament gas from outer cluster atmospheres is per se very challenging, in observations but also in simulations. Therefore, it is difficult to define the exact boundaries of the bridge. In our simulations, we define the interconnecting bridge as a three-dimensional cylinder-like volume in between the two main clusters. For simplicity, we define the bridge main axis as the three-dimensional line connecting the centers of GC1 and GC2. For the radius of the cylinder, we assume ~660 kpc. Along the main axis, the bridge is limited to the region outside of r200 of each cluster, see sketch in figure 1.

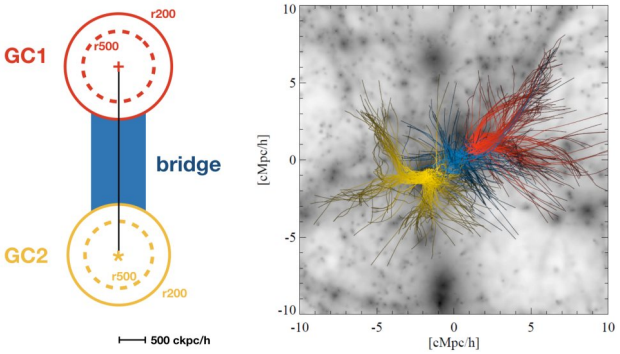

Figure 1: (Left) Schematic view of the simulated system and bridge, rotated to maximize the physical separation between GC1 and GC2. Taken from Biffi et al. 2021. (Right) Gas density maps centered on the cluster pair, encloses a cubic volume of 20 h^{-1} cMpc per side at z = 0.07. Over plotted in red, yellow and blue, the spatial trajectories of the gas particles finally selected within GC1, GC2 and in the bridge at z = 0.07. Each trajectory shows a color gradient with time, from dark at z~2 to light at z=0.07. Taken from [2].

Origin of the pair system
To this end, we select the gas that resides within GC1, GC2 and in the interconnecting bridge at z=0.07, and track it back in time. Figure 1 visually shows the spatial origin of the gas particles of the three aforementioned components through their trajectories towards their final positions at z=0.07. In the background, we report the projected gas density maps in the (20 h^{-1} cMpc)^3 comoving volume centered on the pair. The lines mark the trajectories of the gas in the different components, from their position at z~2 till z=0.07. The colors distinguish the gas in GC1, GC2 and in the bridge between them (red, yellow and blue respectively; as in figure 1), with a color gradient from early times (dark) till z=0.07 (light). In order to ease the visualization, we only show the trajectories for 1,000 randomly-selected gas particles, for each gas component. From the visual inspection of the trajectories, we note that the gas in the bridge (blue lines) is actually collapsing from directions almost orthogonal to the main accretion directions of the gas selected from the clusters (red and yellow lines).

Thermal and chemical properties of the diffuse gas
Given the geometrical configuration presented by this system, with a large physical separation relative to the

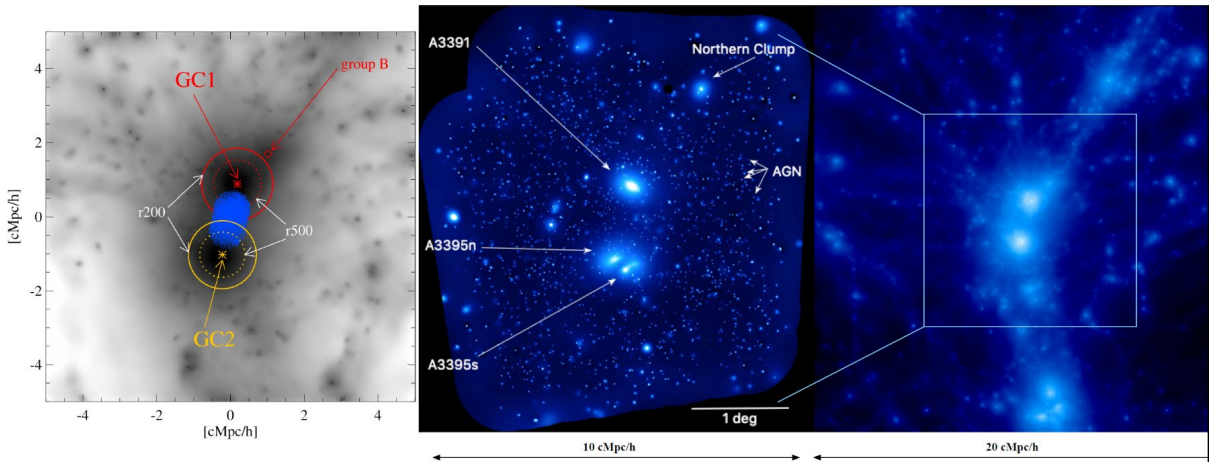

Figure 2: Comparison between the simulated galaxy pair candidate at z = 0.07 and the observed A3391/95 system. Left: zoom onto the projected gas density map of the simulated cluster pair. The image is 10 h^{-1}cMpc per side and projected for 10 h^{-1}cMpc along the l.o.s. We label the two clusters GC1 and GC2 and an in falling group ("group B"), and mark their extent. In blue, is shown the gas in the interconnecting bridge. Middle: eROSITA PV observation of a ~ 15 deg^2 region around the multiple A3391/95 system, with the main clusters and Northern Clump marked (Reiprich et al. 2021). Right: projected gas density map of the simulated cluster pair in its local environment. The map encloses a (20 h^{-1} cMpc)^3 volume, spanning ~ 26 Mpc (physical) in projection, for the chosen redshift and cosmology. Taken from [2].

r200 of the member clusters and a mostly independent origin of the majority of gas in the bridge, this is an optimal target to study the thermochemical properties of the warm-hot gas populating cosmic filaments in comparison to ICM in clusters. Observationally, hints for the presence of colder gas in the interconnecting bridge of the A3391/95 system have been in fact found by eROSITA (Reiprich et al. 2021) as well, encouraging a deeper dedicated analysis of the warm gas in the bridge. For comparison, we show the density temperature diagram for the gas included in the GC1 cluster and the bridge in figure 3. The phase-space diagram is for the cluster only populated at overdensities larger than δ~100 and 75–80% of the GC1 gas mass has T>10^7K and shows a gradient in the Fe abundance: at lower densities the typical metallicity is also lower. This essentially corresponds to the X-ray emitting ICM, for which the radial abundance profile is indeed expected to be a decreasing function of the clustercentric distance. The cluster potential well also comprises high-density cold gas, which is typically found in (or close to) star-forming regions, or within substructures, e.g. galaxies. Typically, this is consequently characterized by large values of the metallicity, as it has been more easily polluted by stellar sources. In contrast we find that in the simulated system ~75% of the gas mass in the bridge is in the warm-hot phase, with a typical temperature of ~1 keV, a median overdensity of ~100 and an homogeneous iron abundance of Z_{Fe}~0.1 $Z_{Fe,solar}$. The colder phase of the WHIM, with T ~ 10^5–10^6 K and δ~100, is not significant. Finally, we find that a minor fraction of the bridge gas mass is characterised by large values of overdensity and iron abundance, and low temperatures (T < 10^5 K). This is halo gas associated to galaxies, either comprised within small substructures or stripped from galaxies at earlier times. Overall, in such a system, the bridge gas closely reflects the chemo-energetic properties of the WHIM, with average temperature and density clearly lower than the ICM within the two clusters. This further supports the conclusion that this is filament-like gas and not stripped ICM due to the interaction between the pair clusters.

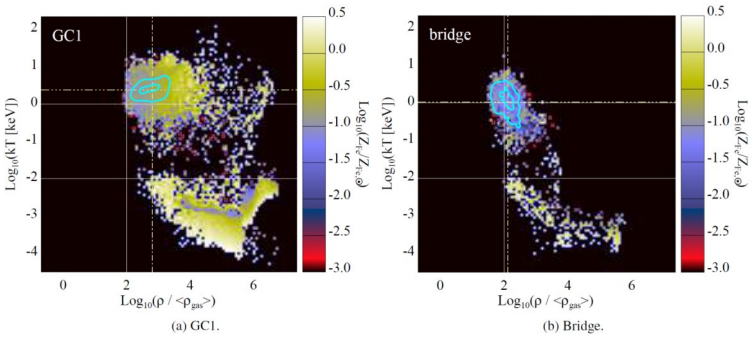

Figure 3: Density-temperature phase-space diagram of the gas within the member clusters GC1 (left panel) and for the gas in the bridge (right panel) between the pair clusters, at z = 007, color-coded by gas Fe abundance (in solar units). Dot-dashed lines mark the average temperature and overdensity. Taken from [2].

Ongoing Research / Outlook

The eROSITA superior soft response and large FoV has allowed for the first direct detection of the faint X-ray emission from the diffuse gas in the bridge and filaments connected to A3391/95, drawing a consistent picture of the LSS that well compares to theoretical predictions. Our conclusions from simulations further support that the geometrical configuration of the A3391/95 system, its pre-merger phase and physical separation, together with the large-scale structure of the field in which it is located, provide an optimal target for unveiling the elusive warm-hot gas that populates the Cosmic Web filaments and for characterising its physical properties. The eROSITA all-sky survey mode will finally enable for a more statistical approach, by providing a significantly larger sample of candidate multiple cluster systems and gas emission filaments. Combined and compared to theoretical predictions from simulations, where samples of binary or multiple cluster systems in various configurations can be statistically investigated as well, this will greatly benefit the baryon census in the Universe, especially through the detailed characterization of the chemo-energetic properties of the diffuse pristine gas.

References and Links

[1] https://www.origins-cluster.de/aktuelles/cluster-news/detail/galaxienhaufen-gefangen-im-kosmischen-netz
[2] Biffi, V., Dolag, K., et al. 2021, A&A, arXiv:2106.14542.
[3] Reipricht, T., et al. 2021, A&A, 647, 2.

Simulating the Local Universe

Research Institution
[1]Universitäts-Sternwarte, Fakultät für Physik, Ludwig-Maximilians-Universität München

Principal Investigator
Klaus Dolag[1]

Researchers
Jenny Sorce[2], Milena Valentini[1], Nabila Aghanim[2], Elena Hernandez[1]

Project Partner
[2]IAS, Universite Paris Sud, Orsay

SuperMUC Project ID: pn68na (Gauss Large Scale project)

Introduction

Our Cosmic Home, which is the local volume of the Universe centered on us, contains very prominently visible structures, extending over almost one billion light-years. Such structures, ranging from the Local Group over the Local Void and the most prominent galaxy clusters like Virgo, Perseus, Coma and many more, represent a formidable site where extremely detailed observations exist. Therefore, cosmological simulations of the formation of galaxies and galaxy clusters within the Local Universe, rather than any other, randomly selected part of the cosmic web, are perfect tools to test our formation and evolution theories of galaxies and galaxy clusters down to the details. However, at these detailed levels, such simulations are facing various challenges, from the computational point as well as from the treatment of various physical processes needed to properly capture the evolution of galaxies and galaxy clusters. Doing this within constrained simulations on the one hand allows a deeper understanding of the evolution of the non-thermal components and thereby improves our understanding of cosmic ray physics and on the other hand sheds light on galaxy formation processes. Including magnetic fields allows us to additionally address questions about the propagation of ultra high energy cosmic rays (UHECRs) and other messenger particles. Figure 1 shows a full sky map of the thermal Sunyaev Zeldovich effect, e.g. the shadow of the prominent local structures caused onto the cosmic microwave background, as predicted by the first, hydro-dynamical simulations performed within this project.

Results and Methods

Validating the reproduction of local clusters
As the observations put constraints in different quality across the simulation volume, it is very important to understand in detail what are the corresponding structures within the simulations and the observations. Especially cross checking the results against independent observations delivers quite a good understanding of the level of matching between simulated and observed structures. We started to do a detailed comparison based on our large set of dark matter simulations, as well as on our first hydro-dynamical simulations.

Figure 2a shows a comparison of the mass of clusters, inferred from different observations, namely dynamical mass (from galaxy position and velocities), Sunyaev Zeldovich effect (the shadow of the ICM on the CMB) and X-ray Temperature measurements. Besides the large uncertainties in the observations reflected in the different masses obtained from the different (and independent) observations, a very clear trend is visible that the constrained simulations re-produce the cluster masses on individual bases for many of the systems quite well. The next steps will be to use directly the observational properties (like SZ and X-Ray signal) from the first hydro-dynamical counterparts.

The additional advantage of the simulations is that this now also allows to investigate the evolution of these objects within their (constrained) environment, as for example discussed for the Virgo cluster (see Sorce+ 2021). Here we can now extend this to many galaxy clusters in the local universe, as shown in figure 2b, which displays the evolution of the mass of some of the simulated, local clusters. Strikingly, one can immediately see that Coma has a recent major merger (as expected from observations), while Perseus has a very quiet recent accretion history, as expected by being observed as a cool-core cluster. Next step will be to more quantitatively derive the dynamical state of the simulated clusters directly from observables (mainly SZ and X-Ray) and directly compare them to the ones derived from the real clusters. We will also investigate, how well merger driven, non-thermal emissions like the radio halo of the Coma cluster can be reproduced within the MHD/CR versions of the simulations.

Galaxy cluster dynamics from velocity waves
Galaxy clusters are excellent cosmological probes provided their mass estimates are accurately determined. Fueled with large imaging surveys, stacked weak

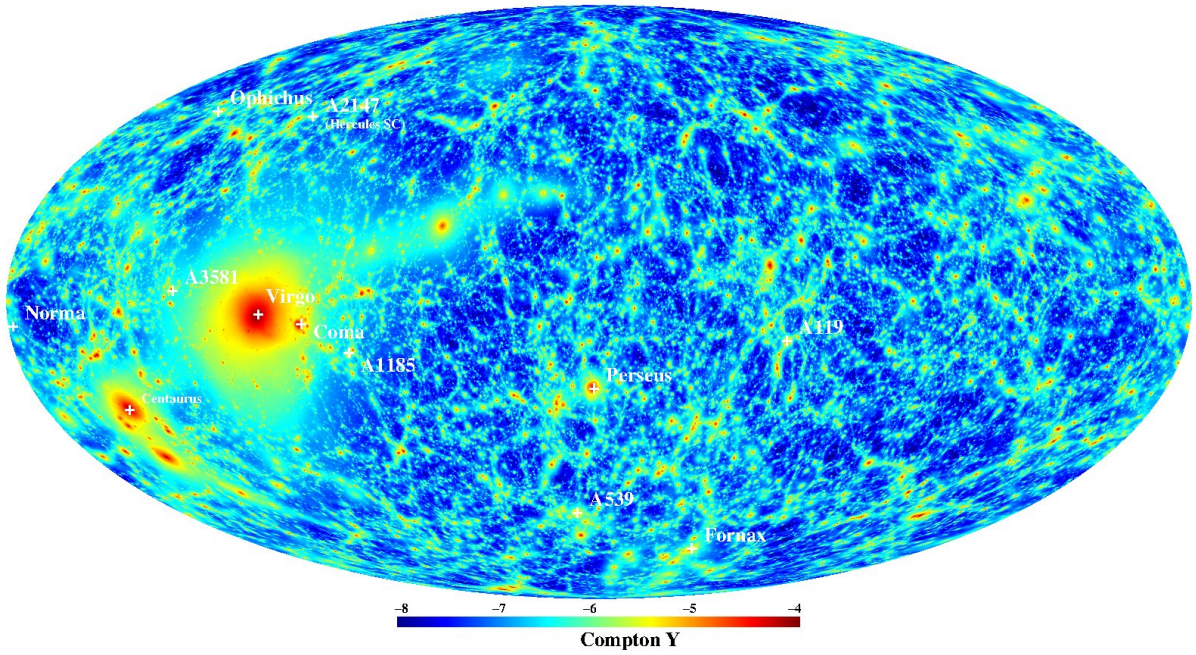

Figure 1: Full sky map of the thermal SZ effect caused by the prominent, local structures as predicted by the hydro-dynamical simulations.

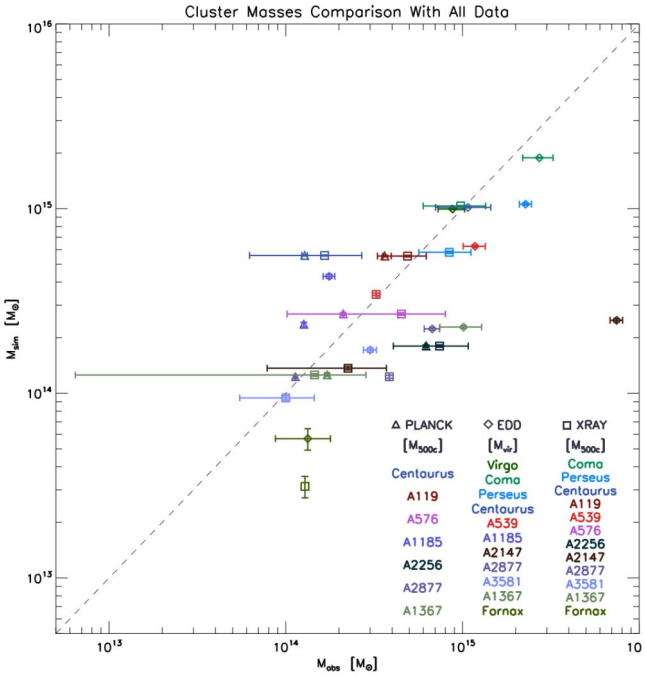

Figure 2a: Comparison of mass inferred from dynamical, x-ray and SZ observations with the mass obtained within the simulations for several, cross identified objects.

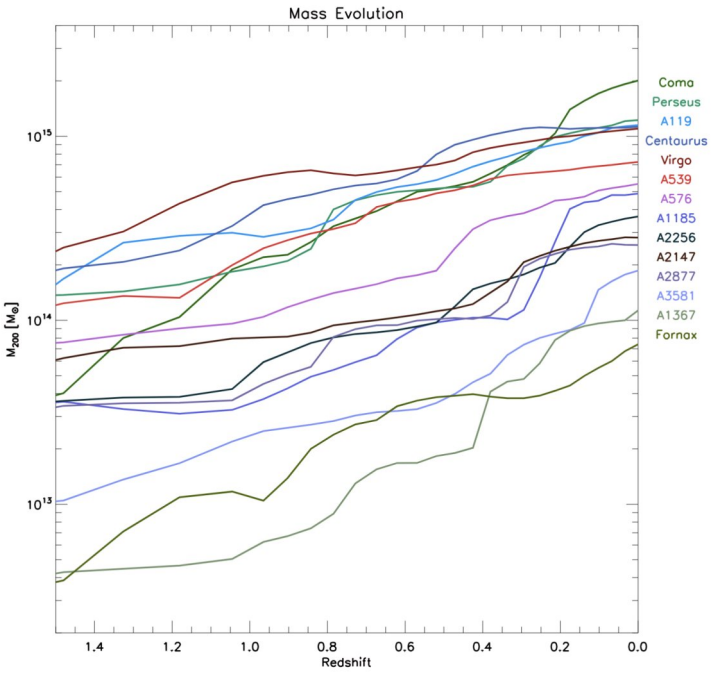

Figure 2b: Shown is the (recent) mass accretion history of prominent galaxy clusters in the local universe as predicted by the constrained simulation.

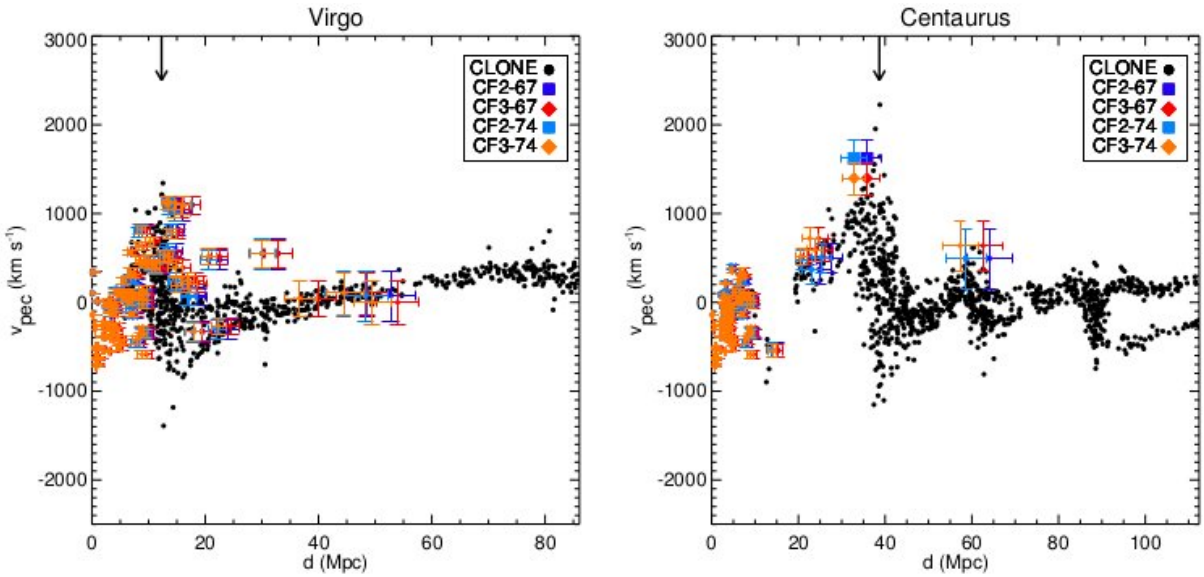

Figure 3: Radial peculiar velocities of simulated dark matter (sub-)halos (black) and observed galaxies (orange, blue and red) as a function of the distance from the synthetic observer and us respectively. Error bars stand for uncertainties on observational distance and velocity estimates. Orange and light blue (red and dark blue) filled squares and diamonds show observed galaxies.

lensing is the most promising method though it provides mass estimates within relatively small radii. Given the large amount of accompanying redshift and spectroscopic data overlapping the imaging surveys, we must take the opportunity to calibrate also with a reasonable accuracy a method based on galaxy dynamics. Two independent measures hold indeed better constraints on the cosmological model. Infall zones of galaxy clusters are probably the less sensitive to baryonic physics thus systematics and probe large radii. These manifestations of a tug of war between gravity and dark energy provide a unique avenue to test modified gravity theories when comparing resulting mass estimates to those from stacked weak lensing measurements. Combined with stacked weak lensing results, they might even yield evidence that departure from General Relativity on cosmological scales is responsible for the expansion acceleration.

The accurate calibration of the relation between infall zones properties and cluster masses starts with careful comparisons between cosmological simulations and observations. Our cosmological simulations of the local Large Scale Structure have sufficient resolution to study the effect of the gravitational potential of massive local halos onto the velocity of (sub-)halos and compare with that of their observational cluster counterparts, as shown in figure 3. Clear to see that velocity waves stand out in radial peculiar velocity – distance to a box-centered synthetic observer diagram. The agreement between velocity waves, caused by the most massive halos of the simulations and those born from their observational local cluster counterparts, is simply remarkable especially for the clusters the closest to us that are the best constrained (e.g. Virgo, Centaurus). Secondary waves due to smaller groups in (quasi) the same line-of-sight as the most massive clusters stand out equally.

Ongoing Research / Outlook

Currently, several simulations are running, among them a simulation including galaxy formation physics like star-formation and AGN feedback, full MHD simulations including in addition the treatment of cosmic rays.

The result of these simulations will be in addition extensively used within LOCALIZATION [1], a newly formed, collaborative project that is jointly funded by ANR/DFG and started in December 2021. Here especially these and future constrained simulations will be used to investigate the so-called σ8 tension (e.g. the difference between the linearly evolved amplitude of the matter power spectrum measured with the CMB and galaxy clusters), as well as CMB large-scale anomalous features.

References and Links

[1] https://localization.ias.universite-paris-saclay.fr
[2] Sorce, J. Mohayaee, R. , Aghanim, N., Dolag, K. & Malavasi, N., 2022, Submitted to A&A.

MEISTER: Multi-physics Effects In Neutron Star Merger Remnants

1

Research Institution
[1]Friedrich Schiller Universitaet Jena

Principal Investigator
Sebastiano Bernuzzi[1]

Researchers
William Cook[1], Boris Daszuta[1], Albino Perego[3], David Radice[2], Francesco Zappa[1]

Project Partners
[2]Penn State University, USA
[3]University of Trento, Italy

SuperMUC Project ID: pn68wi

Introduction

Mergers of neutron star binaries are primary sources of gravitational waves for ground-based interferometers like LIGO and Virgo and the third-generation's Einstein Telescope. They are also at the origin of high-energy electromagnetic transients like kilonovae and gamma ray bursts, and they provide us with "standard sirens" for cosmology. Merger observations promise to deliver unique insights on the unknown equation of state (EOS) of extreme matter, to clarify the merger's contribution to the origin of heavy (r-process) elements, and to deliver new precision measurements of the Hubble parameter. Detailed three-dimensional merger simulations are crucial to predict the mechanisms powering the emitted radiation and to support future scientific discoveries.

MEISTER is part of an ongoing effort led by Jena and the computational relativity collaboration (CoRe) [1] to perform large-scale simulations of binary neutron star in numerical general relativity. The project's goal is to explore the role of microphysics in the long-term evolution of merger remnants. The dynamics of merger remnants on timescales of hundreds milliseconds post-merger are very uncertain. A complex interplay between gravity, magnetohydrodynamics, nuclear and weak interactions determines whether the remnant collapses to a black hole or settles to a stable neutron star. The gravitational collapse phenomenology also depends on the binary masses, the EOS, the details of the accretion process of the remnant disk and the mass ejecta. The latter are sites of r-process nucleosynthesis that, in turn, powers kilonovae transients. A main open question is how the different merger outcomes impact the mass ejecta and the observed signals. In this context, MEISTER's simulations explored the role of different microphysical EOS models and of different neutrino transport schemes, also considering multiple resolutions for a robust assessment of numerical uncertainties.

Results and Methods

MEISTER's simulations are performed in full 3D (plus time) and study the coalescence process with an *ab-initio* approach. i.e. simulating from the last orbits through merger and to the remnant phases. The simulation's methods include the dynamical evolution of the spacetime in the 3+1 formulation of Einstein equations, relativistic hydrodynamics augmented by a Large-Eddy-Simulation scheme to resolve magneto-hydrodynamics turbulence, the use of microphysical EOS and various radiation transport schemes for neutrinos. During the course of this project we deployed a gray+ neutrino transport scheme based on the truncated moment formalism (shortly, "M1 scheme") [2], that significantly improves the physical accuracy (and consistency) of the computations over more efficient but more simplified leakage schemes. In the merger context, ours is the first M1 implementation to include Doppler effects (at all orders in v/c), retaining all nonlinear neutrino-matter coupling terms. The computational cost of this scheme is significantly higher than the leakage. Efficient computations can be achieved by maximizing the number of threads in a hybrid OpenMP/MPI parallelization scheme so to speed up local operations. Hence, modern architectures with multiple cores per node are ideal for these computations.

The simulation code for the project is the Template Hydrodynamics Code based on the public Cactus/Einstein Toolkit infrastructure. Simulations are set up on structured, Cartesian overlapping grids with seven refinement levels. The grids initially cover from the interior of the stars (resolutions of hundreds meters) to the wave zone (extending for thousands of kilometers), and automatically adapt during the simulation to properly resolve the strong field region. Our largest simulations efficiently scale up to ~2,000 SuperMUC-NG cores (>70%, strong scaling) and run for more than 2M of explicit timesteps.

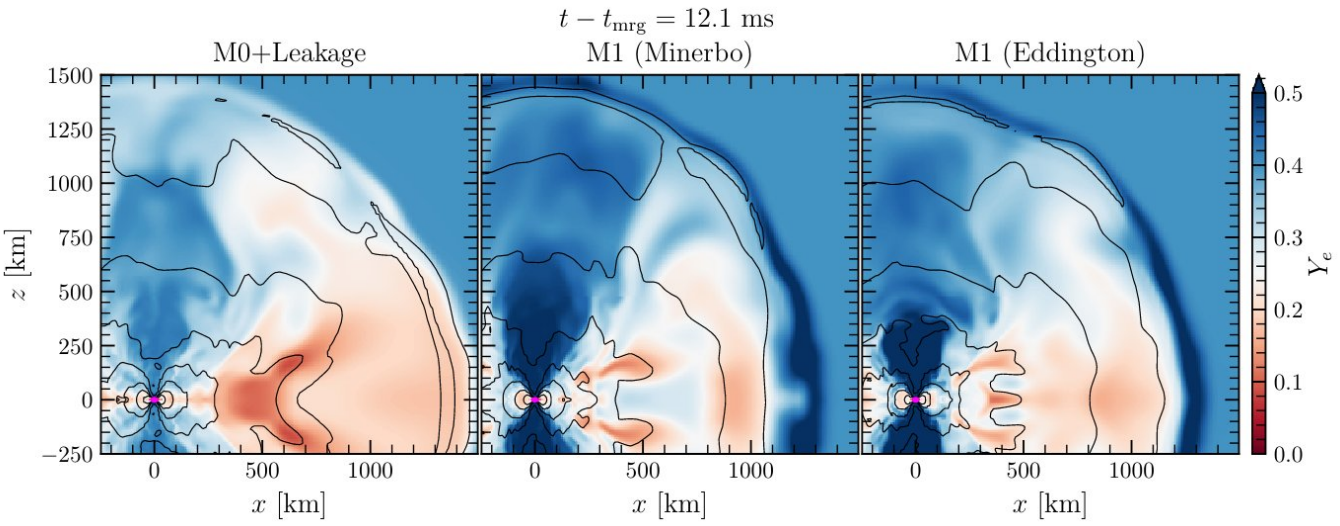

Figure 1: Composition (Electron fraction) of the dynamical ejecta computed with different neutrino transport schemes. Black countours are isodensity levels log10(rho[g/cm^3]) = 5,6,7,8,9,10,11,12. The M1 schemes (central and right panel) predict higher electron fractions than leakage-based schemes.

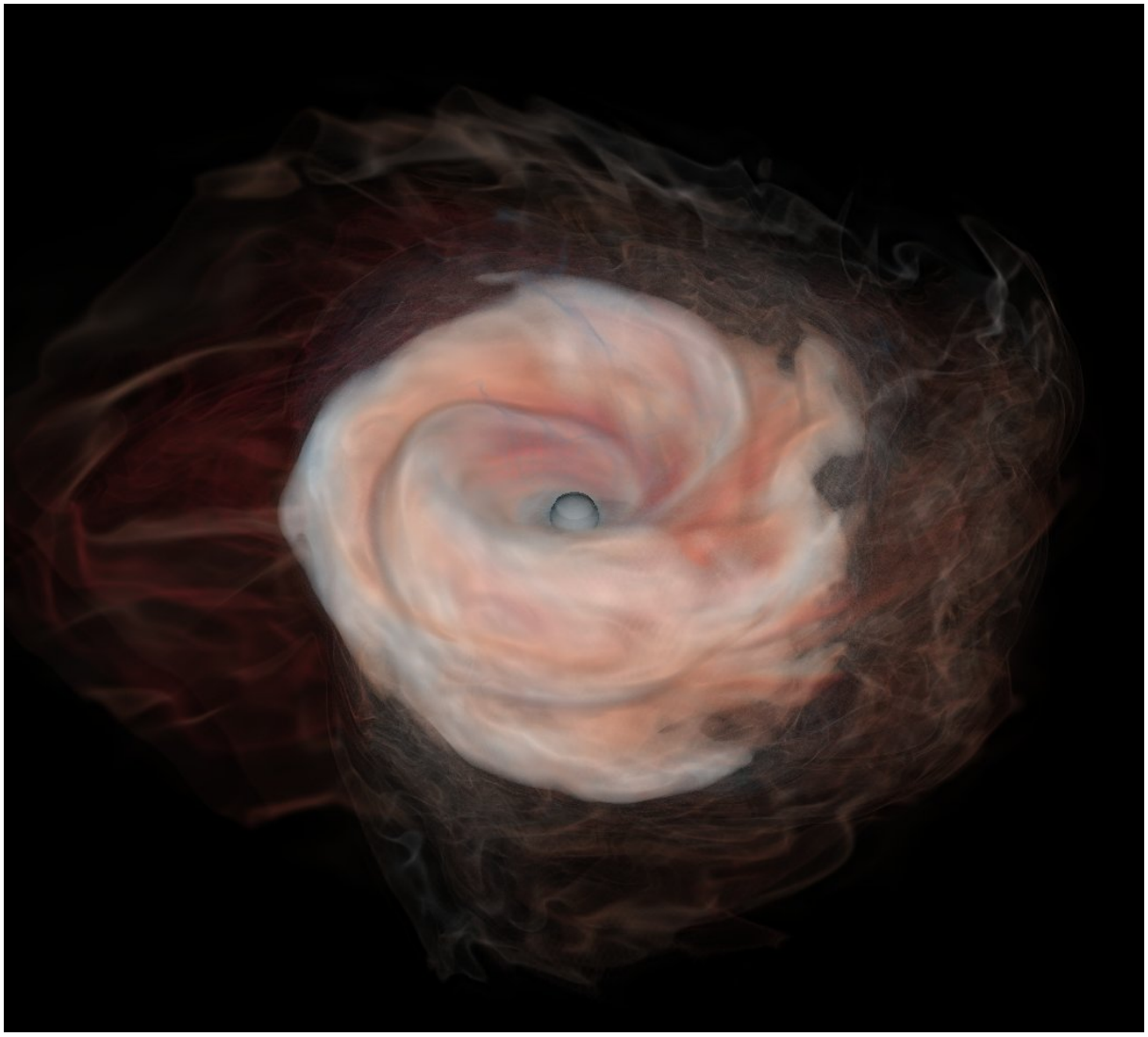

Figure 2: Remnant black hole and accretion disk. The rendering shows the disk composition (electron fraction, Ye) simulated with the M1 neutrino radiation scheme in a box of diameter of ~120 km where red (blue) color correspond to Ye < 0.25 (Ye >0.25). The disk is in a turbulent state far from axisymmetry.

The simulations performed on SuperMUC-NG comprise the longest to-date evolutions with the M1 neutrino radiation transport scheme (~70 milliseconds post-merger). Weak interactions determine both mass and composition of the material dynamically ejected during merger and can drive winds from the merger remnant. Neutrino-matter interactions ultimately determine the final r-process nucleosynthesis yields. Hence, an accurate treatment of neutrino transport in simulations is imperative to obtain quantitative predictions. Comparing the M1 results with those of the leakage scheme, our simulations show systematically larger proton fractions in both the dynamical and early wind, Fig.1. However, the differences in the nucleosynthesis yields are modest and confirm the robustness of the r-process in mergers ejecta. Our simulations reveal the emergence of a neutrino wind that is fed by the neutrinos produced both in the remnant and in the disk. The two neutrino fluxes have different energies and dominate the irradiation of different regions (i.e. polar vs equatorial ejecta). This process effectively enhances the anisotropic character of the kilonova emission. The M1 scheme also correctly captures the trapped neutrino component in the high-density *(log10(rho[g/cm^3]~14)* regions of the remnants. Trapped neutrinos affects the pressure at the few percent level but this is sufficient to alter the stability of the remnant.

A second set of simulations focused on the investigation of the effect of microphysical EOS on prompt black hole formation. A rapid gravitational collapse has strong observational imprints: the gravitational-waves from the black hole remnant are fastly damped (the high-frequency spectrum is effectively suppressed) and, for comparable masses, a light remnant disk is quickly swallowed by the hole. As a consequence, the only expected electromagnetic signal is a dim kilonova triggered by the neutron-rich dynamical ejecta tidally unbind during merger. This is very different from the case of a delayed collapse (or prompt collapse of very asymmetric binaries) described above, in which massive remnant disks and winds are produced, Fig. 2.

Our prompt collapse simulations involved the largest-to-date EOS set for this type of studies, including models with hyperons and phase transitions to deconfined quark at large densities. They allowed a systematic calculation of the mass threshold for the prompt collapse for both comparable masses and asymmetric binaries, and the development of quantitative relations for the prediction of the collapse from the knowledge of the binary properties. These results are key to infer neutron star properties from observational data. For example, based on the LIGO-Virgo GW170817 observation, we improved the lower limit on the minimum neutron star radius (~9.81km, at the maximum mass of the mass-radius diagram) and constrained the radius of a 1.4 solar masses star to be larger than ~11km [3]. Moreover, the simulations revealed that the prompt collapse of asymmetric binaries directly depend on the nuclear incompressibility at the maximum neutron star density [4]. This nuclear physics parameter is currently inaccessible by experiments. We demonstrated that future mergers observations could inform us on the maximum nuclear incompressibility within tens of percent and potentially reveal the presence of hyperons or quarks inside neutron stars.

MEISTER simulations on SuperMUC-NG are still ongoing and the project is an intense phase of data production. Each simulation produces several 3D snapshots of the spacetime, matter and neutrino fields, each snapshot being of the order of few Terabytes. These data will allow us to further probe the physics of merger remnants, of the mass outflows and to establish a robust connection to observations.

Ongoing Research / Outlook

The Jena group and members of the CoRe collaboration are developing the next generation numerical-relativity code for astrophysics GR-Athena++ [5]. The code extends the public Athena++ codebase (J.Stone et al, Princeton) to dynamical spacetimes and showed an unprecedented parallel scaling up to ~10^5 cores on SuperMUC-NG in production binary black hole simulations. GR-Athena++ is currently being upgraded to perform neutron star simulations, notably incorporating microphysics and coupling the M1 neutrino radiation transport scheme with the Einstein and general relativistic magnetohydrodynamics solvers. These advances aim at boosting merger simulations to hundreds of thousand cores and will allow us to maximize the use of resources available on SuperMUC-NG at LRZ.

References and Links

[1] http://www.computational-relativity.org
[2] D. Radice, S. Bernuzzi, A. Perego, R. Haas, Mon. Not. Roy. Astron. Soc., 512, 1499--1521 (2022). 10.1093/mnras/stac589 [arXiv:2111.14858]
[3] K. Rahul, et al., Phys.Rev.D 105 (2022) 10, 103022 e-Print 2111.05183 [astro-ph.HE]
[4] A. Perego, et al., (To appear in) Phys.Rev.Lett. e-Print: 2112.05864 [astro-ph.HE]
[5] Daszuta et al. ApJS 257 25 (2021) arXiv 2101.08289

Turbulent collisionless magnetic reconnection and electron–positron pulsar radiation

1

Research Institution
[1]Max-Planck-Institute for Solar System Research, Göttingen

Principal Investigator
Jörg Büchner[1,2]

Researchers
Patricio Muñoz[1,2], Jan Benáček[2]

Project Partner
[2]Center for Astronomy and Astrophysics, Technical University Berlin

SuperMUC Project ID: pr27ta

Introduction

Electron-scale processes are the last frontier of understanding reconnection — the most efficient mechanism of magnetic energy conversion into plasma bulk flows, heating and particle acceleration in the hot and dilute collisionless astrophysical plasmas. While collisionless magnetic reconnection in the solar system is directly observed, i.e. in situ, its action elsewhere in the Universe can only remotely be recognized via its radiation. For the understanding of the complex non-linear astrophysical reconnection dynamics which takes place in a turbulent plasma environment, numerical simulations have to be carried out. We simulated reconnection with parameters appropriate for turbulent plasmas like those of stellar winds, the interstellar medium and envelops of magnetospheres, where the thermal pressure is comparable with or even exceeds the magnetic pressure (high-plasma β). In sub-project 1 we focused on electron-scale current sheet processes, the last frontier of understanding turbulent collisionless plasmas. The efficiency and properties of magnetic reconnection in this regime are still only poorly under-stood compared with reconnection in low-β plasmas. Moreover, the non- equilibrium electron-scale pro-cesses in turbulent plasmas are practically unex-plored, as the energy dissipation processes in such astrophysical plasmas in general.

To develop the capability of remote diagnostics of astrophysical plasma processes we investigated in sub-project 2 the radiation caused by the interaction of accelerated electrons and positrons in neutron star magnetospheres which are supposed to cause the observed pulsar radio emissions. While the causes of the pulsar radio emissions are still not well understood we investigate the interaction of electron–positrons bunches formed by sparking. We show how the interaction of the electron–positron bunches bunches can become unstable and generate wave packages reminding solitons, which in turn emit coherent radio waves.

Results and Methods

For both sub-projects we utilized the fully kinetic particle-in-cell (PIC) code ACRONYM [6]. This code is appropriate to resolve both electron- and ion-scale processes in collisionless plasmas. It self-consistently solves the Vlasov equation by a Lagrangian tracing of many macro-particle orbits. Other than in fluid codes the main variable of kinetic simulations is the velocity space distribution function of the particles. The code solves the full set of Maxwell equations on a grid where the electromagnetic fields are calculated. The solution of coupled nonlinear equations and the statistical nature of the PIC method makes such simulations computationally very demanding. The ACRONYM code has proven its efficiency and scalability of its MPI parallelization on a number of HPC supercomputers including SuperMUC-NG. The pulsar radiation simulations were carried out using up to one million core-hours and the turbulence simulations utilized three million core-hours, The larger simulation runs used about ten thousand cores. The storage requirements were large, the particle information needed to analyze the distribution functions at a given moment of time could amount up to 4.5 TByte of memory. Note that the simulations run up to hundreds of thousand timesteps.

For sub-project 1 (electron-scale reconnection processes in turbulent collisionless plasmas) we perturbed a 2D thermal plasma by long-wavelength Alfvénic fluctuations. We investigated the influences of: the plasma-β, the size of the plasma domain, ion-to-electron mass ratios and of the number of macro-particles. We used domain sizes of up to 410x410 ion skin depths which we resolved by 9,600x9,600 grid points. We varied the electron- and ion-plasma-β values were varied from 0.1 up to 2. The ion to electron mass ratio between to 25 and 100, the number of particles per cell between 300 and 2,700. corresponding to a total of $5x10^{10}$ traced particles [1].

The results of sub-project 1 show that wave–wave interactions out of the initial fluctuations caused the

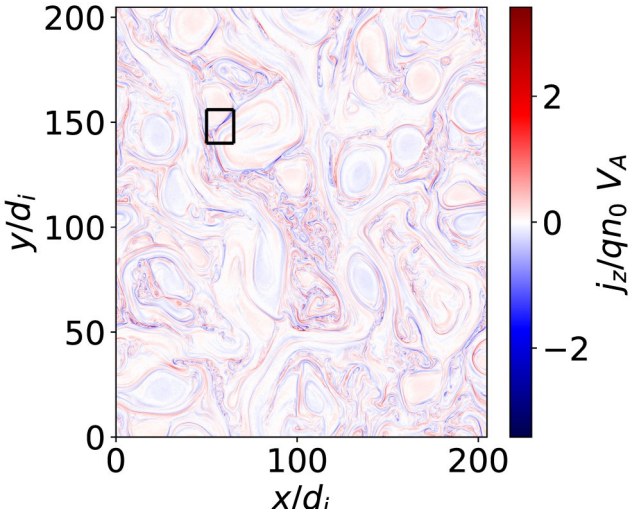

Figure 1: Out-of-plane current density from a turbulence simulation showing the development of current sheets and reconnection through them.

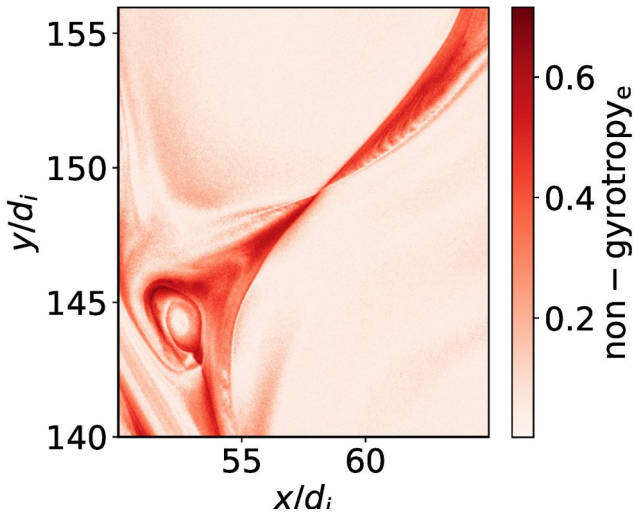

Figure 2: Non-gyrotropy in the small square indicated in Figure 1.

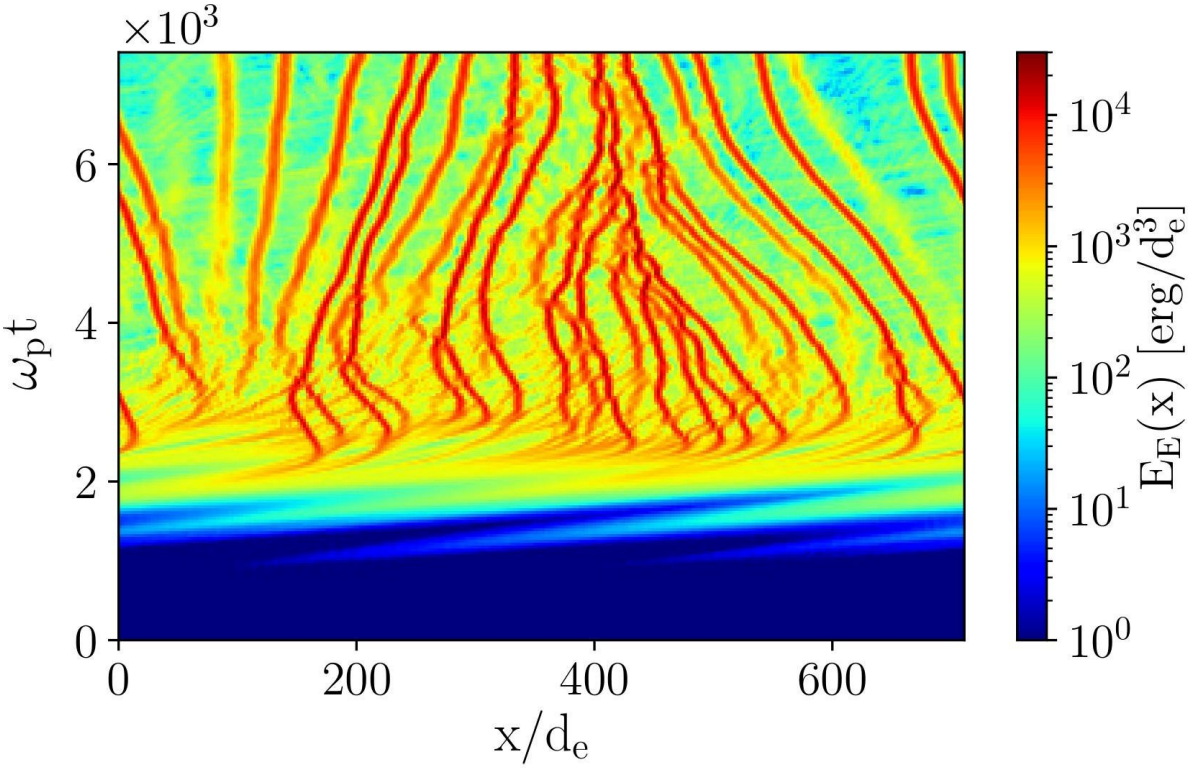

Figure 3: Evolution of the electrostatic energy density illustrating the formation of soliton-like wave structures (in red) [2,3].

development of a turbulence cascade until, finally, new but small-scale structures were formed: current sheets, through which magnetic reconnection occurs (see Fig. 1)

As one of the most important results we could quantify the particle distribution functions which strongly deviate from the initial thermal (Maxwellian) distribution function. We characterized these deviations by means of calculating the elements of the non-gyrotropic, electron pressure tensor including its off-diagonal terms. We could show that the deviations from the electron gyrotropy is concentrated in the current sheets where it balances the reconnection — induced electric fields and in the reconnection outlows (see Fig 2). The non-gyrotropy and the current density maximum diminish in high-β plasmas. This explains why in high-β plasmas the efficiency of reconnection in turbulent plasmas decreases. The higher the ion-to electron mass ratio the stronger the currents carried by the electrons as well as the electron non-gyrotropy. This confirms the suspected need of a correct resolution of the electron dynamics and the use of realistic mass ratios in order to correctly capture the physics of turbulent plasmas, the current sheet formation and the role of reconnection in them in future investigations.

For sub-project 2 (relativistic electron–positron streaming instability in their bunch-bunch interaction) we carried out 1D simulations to obtain a sufficiently high spectral resolution, typically requiring up to $7x10^5$ grid cells and 10^4 particles per cell which we traced over $6x10^5$ timesteps. This was possible only by using high-order solvers and shape functions [2,3].

We analyzed the evolution of relativistic electron–positron streaming instabilities as a possible cause of the observed pulsar radio emissions. We found that streaming instabilities may form solitary-like waves (see Figure 3) that might lead to coherent radio emissions.

We further investigated for the first time the process of coherent radio emission during the nonlinear interaction of electron–positron bunches. We found that the main parameter influencing bunch evolution and radiative power is the mutual drift between electrons and positrons [4]. We estimated the properties of the resulting coherent radio emission by postprocessing the simulation data assuming a linear-acceleration emission mechanism [5]. We found emission properties of the bunch interaction process very similar to the observed pulsar radiation, in particular its spectrum (see Figure 4).

Ongoing Research / Outlook

The resources provided by SuperMUC-NG were essential to achieve the here reported results. Simulations as those described above were never attempted before, in part because of the high computational demand.

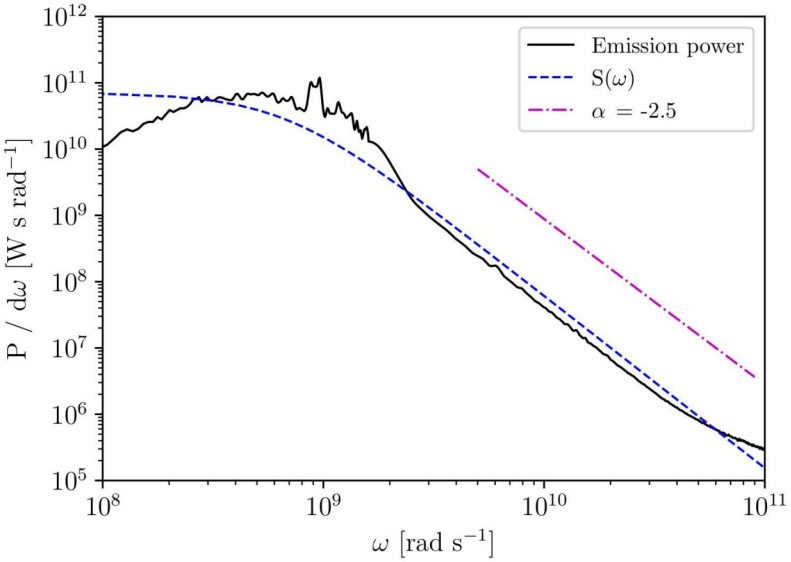

Figure 4: Predicted spectrum of pulsar radio emissions due to a bunch-bunch interaction of positrons and electrons in a neutron star magnetosphere. The parameters of the function S(ω) and power-law index α agree with those obtained by observations [5].

One particular difficulty that we had to overcome was the calculation of the radio emissivity by tracking the individual particle motion, which is very storage demanding, but the standard procedure. For this sake we developed a new particle-aggregated approach, which has not been applied to PIC-code simulation data, yet. Our new approach results in a full wave phase coherence and reduces the amount of required data output by a factor of ~10^3 from a few PBytes to a few TBytes.

For sub-project 1 the processing and interpretation of the wealth of generated data is still ongoing. The publication of those results is in preparation.

For the continuation of sub-project 2 we applied and have already been granted a follow-up project (pn73ne) to further investigate the coherent radio emission process due to electron–positron streaming instabilities in the magnetospheres of neutron stars.

References and Links

[1] https://www-astro.physik.tu-berlin.de/node/439
[2] Manthei, A. C., Benáček, J., Muñoz, P. A., and Büchner, J., Astron & Astrophys., 649, 2021.
[3] Benáček, J., Muñoz, P. A., Manthei, A. C., and Büchner, J., Astrophys J., 915, 2, 2021.
[4] Benáček, J., Muñoz, P. A., and Büchner, J., Astrophys J., 923, 1, 2021.
[5] Benáček, J., Muñoz, P. A., Jessner, A. and Büchner, J., 2022
[6] http://plasma.nerd2nerd.org/

Chemistry and Material Sciences

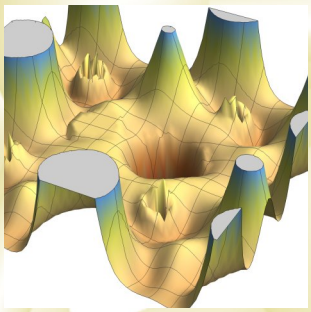

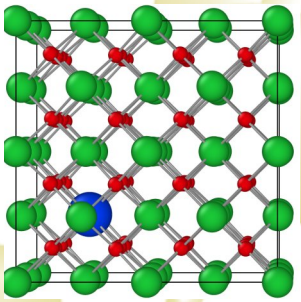

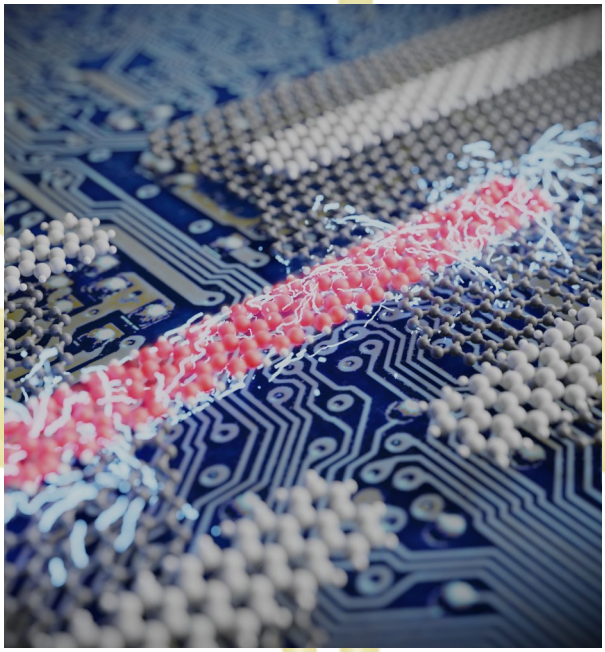

Composition and Structure of β-Ga_2O_3(001) under Realistic (T, p) Conditions

Research Institution
[1]Institut für Physik and IRIS Adlershof, Humboldt-Universität zu Berlin

Principal Investigator
Claudia Draxl[1]

Researchers
Konstantin Lion[1], Matthias Scheffler[2]

Project Partner
[2]NOMAD (Novel Materials Discovery) Laboratory, Fritz-Haber-Institut der Max-Planck Gesellschaft

SuperMUC Project ID: pn29ji (Gauss Large Scale project)

Introduction

This work was performed in the framework of GraFOx, a Leibniz-ScienceCampus partially funded by the Leibniz association [1].

Gallium oxide (Ga_2O_3), a transparent semiconducting oxide with a wide bandgap of around 4.9 eV, has emerged as a promising candidate for future applications in electronics (Schottky barrier diodes, field-effect transistors), optoelectronics (solar- and visible-blind photodetectors, flame detectors, light emitting diodes, touch screens), and sensing systems (gas sensors, nuclear radiation detectors) [2]. The monoclinic β phase is its most stable and studied polymorph. Compared to the bulk properties, research on its surface properties is still sparse. However, these play a crucial role in many processes and applications, such as epitaxial growth and electrical contacts. We have previously shown that surface stability is critical to understanding faceting on β-Ga_2O_3 substrates [3].

Of particular importance is the occurrence of surface reconstructions in reactive environments and under realistic temperature and pressure conditions, which may affect electrical properties and surface stability. To this end, we have applied the recently developed Replica-Exchange (RE) Grand-Canonical (GC) method [4] in conjunction with ab initio molecular dynamics (MD) simulations to obtain an accurate temperature-pressure phase diagram of the β-Ga_2O_3(001) surface in a reactive O_2 gas phase. Compared to the conventionally used ab initio atomistic thermodynamics (aiAT) method, this approach is not only less biased but also includes vibrational contributions with full anharmonicity.

Results and Methods

We consider several replicas of the surface system, each evolving in a different thermodynamical state. During the simulation, each replica has a certain probability to either exchange particles with the oxygen gas phase or perform a RE step. After the particle/RE step, the surface system is diffused in the canonical ensemble via MD simulations. REGC-MD is massively parallel by design, as the replicas communicate only during the RE steps, allowing full use of the SuperMUC-NG architecture. The main cost of the REGC-MD method is associated with the *ab initio* MD simulations. The MD simulations to properly diffuse all replicas were performed at the density-functional theory level with the state-of-the-art all-electron code FHI-aims [5]. It employs a numeric atom-centered orbital basis set that allowed us to add large amounts of vacuum at minimal computational cost. We simulated the surfaces in slab supercells of up to 360 atoms. We considered 60 replicas, with each replica using 10 full nodes (480 cores). Such large and involving calculations were only possible on a Tier 0 computing center. In total, we produced more than 300 GB of data throughout the project.

There are two stoichiometric terminations for the (001) surface, (001)-A and (001)-B, as shown in Fig. 1. The coordination environment at the surface is significantly different for the two terminations. The B termination is much more stable, as only the octahedrally coordinated Ga(II) atoms are under-coordinated, while the tetrahedrally coordinated Ga(I) atoms are under-coordinated in (001)-A. Both terminations occur naturally during growth. We obtained a converged phase diagram for the (001)-B surface, which is given in Fig. 2, where we also compare our results with the more commonly used aiAT approach. The differences are evident. The bare surface and the phase with 14 adsorbates show a region of stability in the aiAT phase diagram. Only by including the full vibrational contributions to the free energy with REGC-MD can we find additional stability windows for several phases. The vibrational contributions also shift the stability window of the bare surface to much higher partial pressures at low temperatures (<1000 K) than given by aiAT. The bare (001)-B surface was remarkably stable throughout the simulation. Oxygen atoms adsorbed preferably on the Ga (II) site, where they then typically formed a bridge-like bond to the O (I) site. However, no significant reconstruction of the surface occurred

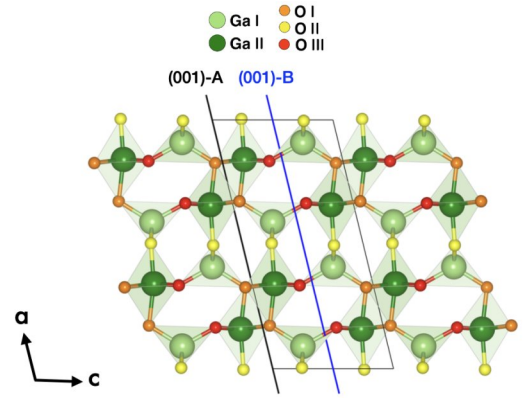

Figure 1: The conventional bulk cell of β-Ga_2O_3. The inequivalent gallium atoms are in light and dark green, while the inequivalent oxygen atoms are orange, yellow, and red. The two stoichiometric (001) terminations, (001)-A and (001)-B, are indicated by the black and blue lines.

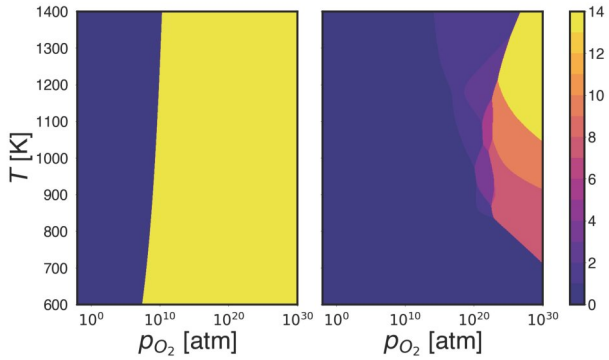

Figure 2: Shown are the phase diagrams of β-Ga_2O_3 (001)-B in contact with a reactive oxygen atmosphere obtained with ab initio atomistic thermodynamics (left) and REGC-MD after 1,000 steps (right). The colors correspond to the number of adsorbed oxygen atoms in the slab.

during the simulation. This suggests that other surfaces with only under-coordinated Ga (II) sites, such as β-Ga_2O_3(100)-B, will also not reconstruct.

We also obtained a preliminary phase diagram for the (001)-A surface. The results are shown in Fig. 3. When including all vibrational effects with REGC-MD, the bare surface is still stable for much higher partial pressures p < 10^{11} atm. In addition, we can see the emergence of several metastable structures. Interestingly, we find that the relaxed bare (001)-A surface is actually not stable at the temperatures considered here. It reconstructs by letting under-coordinated Ga (I) regain their tetrahedral coordination environment. As a result, we find an alternating sequence of tetrahedra-octahedra-tetrahedra at the surface that differs significantly from the bulk environment. When the environment is oxygen-rich, oxygen atoms typically adsorb on the Ga (I) site and prevent the formation of the reconstruction. The structure (001)-A+O_2 with two additional adsorbed oxygen atoms exhibits a large stability range in the phase diagram up to a partial pressure of p < 10^{16} atm. It represents a previously unknown 1/2x1 reconstruction of the (001)-A surface. Here both the dangling bonds of Ga (I) and O (III) are partially satisfied following the adsorption.

We have shown that we can obtain an accurate phase diagram only if we take into account the full vibrational

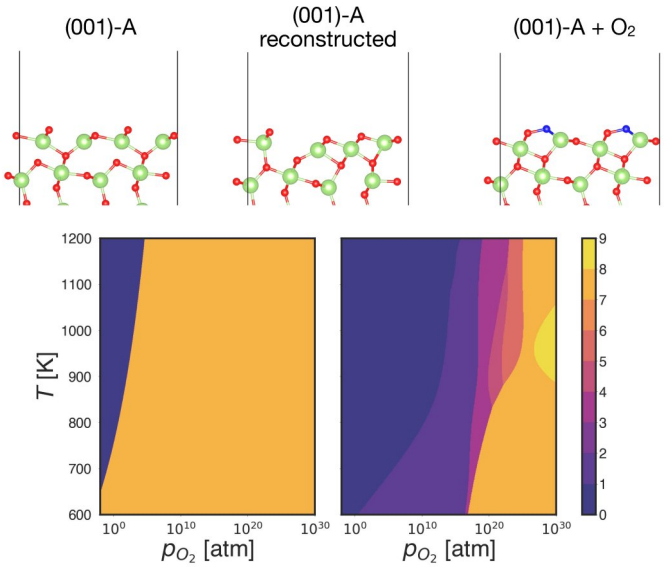

Figure 3: Top: Shown are the phase diagrams of β-Ga_2O_3 (001)-A obtained with ab initio atomistic thermodynamics (left) and REGC-MD after 500 steps (right). The colors correspond to the number of adsorbed oxygen atoms in the slab. Bottom: The unreconstructed bare (001)-A surface (left), the reconstructed bare (001)-A surface (middle), the 1/2x1 reconstruction with two adatoms (right). Gallium atoms are green, oxygen atoms are red, and additional oxygen adatoms are blue.

contributions to the free energy. Our results further indicate that the (001)-B termination is extremely stable even in very oxygen-rich conditions. However, we have found (at least) two possible reconstructions of the (001)-A surface. These results show that we can predict accurate phase diagrams and surface reconstructions of complex surfaces, without prior knowledge or bias.

Ongoing Research / Outlook

One limiting factor of our current approach is that we only simulate an environment with oxygen. During the growth of β-Ga_2O_3 both oxygen and gallium are available. We are currently trying to generalize the REGC-MD method to consider more than one reactive gas in the so-called constrained equilibrium, where different species do not react in the gas phase but only at the surface. In addition, all the data obtained can be reused in subsequent studies. The combination of the REGC sampling and a posteriori analysis allows for the determination of phase diagrams for any (atom position dependent) observables, which provide information on how to adjust the environmental conditions to obtain a material with the desired properties.

References and Links

[1] http://grafox.pdi-berlin.de
[2] Z. Galazka, Semicond. Sci. Technol. 33 (2018), 113001.
[3] R. Schewski et al., APL Materials 8 (2019), 022515
[4] Y. Zhou, M. Scheffler, L. M. Ghiringhelli, Phys. Rev. B 100 (2019), 174106.
[5] V. Blum et al., Comput. Phys. Commun. 180 (2009), 2175-2196.

Electrochemical Interfaces at the Nanoscale

Research Institution
[1]Department of Chemistry, Imperial College London

Principal Investigator
Clotilde S. Cucinotta[1]

Researcher
Matthew T. Darby[1], Marialore Sulpizi[2]

Project Partner
[2]Johannes Gutenberg University, Mainz

SuperMUC Project ID: pn29la (Prace project no. 2020225454)

Introduction

Currently, much effort is devoted to improving the efficiency of energy generation, transformation and storage with the development of advanced electrochemical (EC) devices such as batteries, fuel cells and supercapacitors. Most of the technologically relevant electrochemical transformation in these devices occurs at their electrode-electrolyte electrified (nano-)interface (EI) and the large-scale properties of these devices are the result of their nano-structure and reactions at EIs in operando. However, in spite of their importance, the nano-structure of EIs and reactions occurring therein are still largely unrevealed despite a plethora of experimental data on EC systems having been accumulated over the last century. Indeed, most EC experiments are still restricted to macroscopic observations of electrochemical transformation and cannot be used to answer questions about the relation between atomic/electronic structure and reactivity at the EI. Computational simulations are in principle able to provide an atom resolved picture of EIs. There is a long history of theoretical computational research on single properties of metal surfaces addressing, for instance, ion diffusion within electrolytes, the properties of the neutral electrode-electrolyte interface and some redox transformations at the electrodes in gas phase. However, a comprehensive theoretical description of the mechanisms dominating the interface in operando conditions is still missing. The challenge that prevents a greater progress in this direction is the complexity of the interfacial interactions and the existence of charged phases at EIs, combined with the need for accounting for the subtle interplay of the electronic, ionic and thermal effects therein. This indicates that the only realistic way to describe EC phenomena at the nanoscale is by means of simulations based on first principles of the atom resolved metal/electrolyte solution interface. An explicit treatment of a disordered liquid moiety of the EIs that accounts for the polarizable nature and electrical field properties of the interface necessitates performing ab initio molecular dynamics (AIMD). However, this has been limited in use to rather small systems and short timescales due to the high computational cost of the calculations. In this project we partially bridged the gap between the experimental and theoretical description of EC transformation by having performed atom-resolved, long timescale, ab initio simulations of large Pt-water charged interfaces, providing for the first time a realistic representation of its double layer (DL) nanostructure in operando conditions, and of the free energy profiles for interfacial chemical transformation therein.

Results and Methods

In order to accomplish this, we employed a blend of advanced ab-initio dynamical methodologies based on a technique recently developed in our lab for the simulation of charged electrode/electrolyte interfaces. More specifically, we used second generation Car-Parrinello MD (CP-like) to dynamically advance our systems whilst controlling the simulated electrode potential with our “Ion Unbalance Methodology” (IUB) [2]. We studied an array of technologically relevant interfacial systems designed to facilitate a realistic study of potential dependent EI structures on Pt(111), under reductive (electrolysers/H2 evolution reaction (HER)) and oxidative (fuel cells/O2 reduction reaction (ORR)) conditions. To simulate these conditions, we impose potential control using our novel IUB methodology and determine the equilibrium coverage for given potentials by covering the surface in H (Figure 1) and O/OH, respectively. Further, based on high resolution experimental structures [3], we designed a novel high-index Pt surface model, characterized by reactive, low-coordination edges isolated by using ~1 nm of extended flat Pt facets (Figure 2). The size of this model system is unprecedented, though is a necessity to elucidate the behavior of under-coordinated edge sites that are thought to be key to the observed high-performance of Pt for HER. With this model, we determine the structure of interfacial water under potential control using the IUB method and study the system under reductive conditions. In the remainder of this section we briefly discuss our findings to date, however, due to the vastness of the data set accrued in this project, we note that our analysis is still ongoing. Beginning with our flat Pt(111)|water interfacial models under potential control, we elucidate, as a function of electrode potential, the structure of the electrochemical DL (EDL), the equilibrium coverage of water/H/O/OH and the charge distribution, as well as eliciting the interfacial capacitance and relating our system to known scales using the potential of zero charge (pzc). Initially we studied the “clean” system where Pt is interfaced with water in the absence of surface species. We studied the system at technologically relevant potentials above and below the pzc. We elucidated the EDL structure and determined that the density and orientation thereof are dependent on the

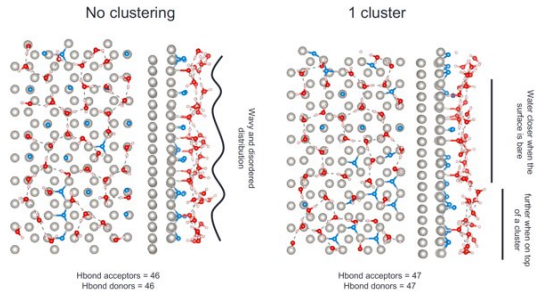

Figure 1: Top-down and side-on views of the EDL on Pt(111) with low (left) and high (right) H coverage.

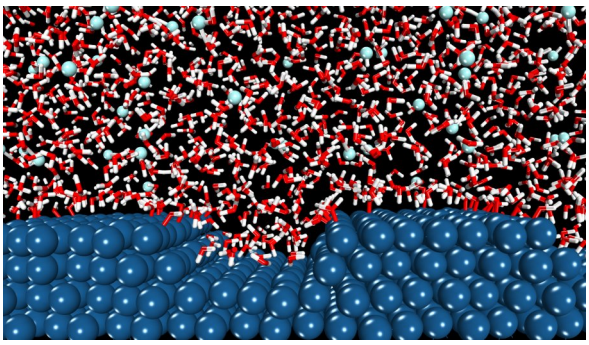

Figure 2: The "edge" of our high-index Pt|water model.

electrode potential. At more negative electrode potentials, the surface charge becomes more negative which is compensated by a reduction in the EDL density and reorientation of the average water dipole moment. Modifying the interfacial structure by adding various coverages of H facilitated the study of the thermodynamics of HER. Contrary to studies in vacuum, the saturation coverage in solution under potential control is shown to be less than 1 monolayer (ML). Moreover, in vacuum H atoms maximize their reciprocal distance, whereas in electrolytic solution, the formation of H clusters is observed, whose structure is potential dependent. This structuring of the H adlayer affects the position and stability of water within the solvation layer. Indeed, the arrangement of water molecules changes depending on the coverage of the surface and opposite polarization of the first water layer is observed, where each water molecule is slightly positive (0.1 |e|) at low coverage and becomes slightly negative at high coverage, when no bond with the Pt surface can be formed due to H site blocking. Further, we elicit the H coverage phase diagram as a function of voltage and note a transition between high and low coverage occurring at 0 and 0.5 V. We identify three possible sites for the HER to occur on the flat surface at i) the bare surface, ii) clusters of H or iii) the interface between the bare surface and a cluster [1]. In a similar vein to our study of HER, we initialized the Pt(111) surface with ORR intermediates (O/OH) and studied these systems, varying the potential. O coverage is shown to inhibit water chemisorption, as is the case for H, whereas OH coverage promotes it. Moreover, we determine that the O adlayer is static whereas OH is dynamic. In fact for the latter, we note facile proton transfer to and from neighboring chemisorbed water, resulting in OH "hopping" across the surface. Furthermore, there is a critical coverage of O that triggers the early stages of Pt dissolution, which is known to occur at high electrode potentials [3]. Indeed we determine that this coverage is lower for more oxidative potentials [2]. On our high-index edge model, the EDL is characterized by two primary features; i) the EDL on the central region of the extended (111) facets exhibits structural similarities to the flat model and is constructed of a layer of chemisorbed water as well as a dynamic second layer. Secondly, at the edge, water strongly chemisorbs and forces the EDL to "wrap" around these sites by drawing more diffuse water closer to surface through H-bonding. Moreover, there is an unusual charge partitioning at the edge that is dictated by surface-water interaction. Indeed in vacuum, Pt edges are negatively charged, however in solution they are positive due to water chemisorption. This charge polarization is likely to have significant implications for the observed reactivity at the under coordinated edge, which will attract electron donors. In the context of electrocatalysis, the adsorption strength of H to the positively charged edge will be weakened bringing the binding closer to thermoneutrality, favouring HER [3]. We studied the effect of the H coverage/distribution along the edge as a function of electrode potential. We elucidated the adsorption energy of H at the edge, and found that there is approximately a 0.1 to 0.2 eV reduction in binding strength in aqueous electrolyte compared to vacuum. Moreover, as the electrode potential was reduced, the binding strength of H increased, which is in line with experimental cyclic voltammetry [3]. We determined a dependence of the coverage on the electrode potential. At high and intermediate potentials the H coverage maximum is 0.33 ML, whereas at lower potentials (closer to the HER operating potential), the equilibrium coverage is 0.66 ML. This is particularly interesting as it suggests that the observed changes in HER activity with potential also depend on the adlayer structure/coverage [4].

Ongoing Research / Outlook

We have gained enormous insight into the various aspects of the EDL of specific systems relevant to HER and ORR. However, these systems are idealized when considering the coverage. In reality there may be mixed phases, depending on the operating potential. In particular we will study the co-adsorption of water, H, O and OH on our high-index edge model at potentials close to boundaries on the phase diagrams derived from this work. We predict that the unique blend of surface adspecies may affect the mechanisms of proton exchange with the electrolyte and believe that this will shed light on the fundamental (electro)chemistry underpinning these microsteps. In our original proposal we intended to use metadynamics (MTD) to accelerate the equilibration of our system by facilitating enhanced sampling of the distribution of slow-moving ions within the electrolytic region. However instead, we initialized our systems by running extensive classical MD simulations that were accessed timescales on the order of microseconds (vs. picoseconds for AIMD). However, MTD has been seldom used in the context of interfacial electrochemical systems. Indeed, we are currently in the preliminary stages of applying MTD to study the equilibrium structure of the EDL of the systems with the most stable coverages of H/O/OH as determined here. Moreover, we plan to progress this towards using MTD to explicitly model the HER and ORR processes from different sites based on these equilibrated structures.

References and Links

[1] https://gow.epsrc.ukri.org/NGBOViewGrant.aspx?GrantRef=EP/P033555/1
[2] R. Khatib et al., Electroch.. Acta, 391 (2021) 138875.
[3] L. Jacobse et al., Nat. Mater., 17 (2018) 277-282.

A New Time-Domain Quantum-Transport Approach for Linear Responses

Research Institution
[1]Center for Advancing Electronics Dresden, Technische Universität Dresden
[2]Department of Chemistry, Technische Universität München

Principal Investigator
Frank Ortmann[1,2]

Researcher
Michel Panhans[1,2]

Project Partners
–

SuperMUC Project ID: pn56hu

Introduction

The Kubo formalism [1] is a powerful and universal theoretical tool to connect the complex microscopic dynamics of condensed matter systems with their macroscopic thermodynamic properties that are measurable in experiments. Central quantities in this framework are linear susceptibilities, which relate any physical observable to any other perturbing quantity that is exerted by the experimenter. For instance, Kubo formulas can explain diverse material properties such as the electrical conductivity or magnetic susceptibility. The Kubo formalism allows particularly for efficient large-scale numerical calculations to describe quantum systems, which elude an analytical description or when disorder, electron-phonon interaction, or electronic correlations are present. Great efforts were therefore spent during the last two decades to work on efficient numerical implementations of Kubo formulae in the field of electronic transport [2]. The application of this theoretical framework to study charge transport in organic semiconductors (OSCs) is therefore a suitable tool to understand the microscopic dynamics of charge carriers in the presence of complex particle interactions and external magnetic fields. Important macroscopic material properties of interest are the dc-Hall and channel conductivities and their corresponding resistivities. An accurate determination of the full electrical conductivity and resistivity tensor yields fundamental insights into the localization behavior of charge carriers and topological properties of the underlying band structure of the OSC material.

Results and Methods

Within the framework of many-body quantum theory, the linear response of an observable to an external force is given by the general Kubo formula [1]:

$$\langle \hat{A}(t) \rangle - \langle \hat{A} \rangle_0 = \int_0^\infty dt' \, f_{AB}(t') F(t - t'),$$

with the linear response function $f_{AB}(t)$ and the time-dependent external force $F(t)$ that couples to the system observable B. During our project, we have developed a new representation of the linear-response function entering the Kubo formula in terms of so-called displacement functions [3]:

$$f_{AB}(t) - f_{AB}(0) = \frac{1}{2\hbar} \tan\left(\frac{\beta\hbar}{2}\frac{d}{dt}\right) D^+_{AB}(t) + \frac{1}{2\hbar} D^-_{AB}(t),$$

with the displacement-operator anticommutator function (DAF):

$$D^+_{AB}(t) = \mathrm{Tr}\left(\hat{\rho}_0 \left[\Delta\hat{A}(t), \Delta\hat{B}(t)\right]_+\right),$$

and the displacement-operator commutator function (DCF):

$$D^-_{AB}(t) = -i\mathrm{Tr}\left(\hat{\rho}_0 \left[\Delta\hat{A}(t), \Delta\hat{B}(t)\right]_-\right).$$

Here $\Delta\hat{A}(t) = \hat{A}(t) - \hat{A}(0)$ denotes the displacement of the quantum mechanical time evolution of observable A with respect to its equilibrium value based on the unperturbed density operator $\hat{\rho}_0$. This new formulation of the linear response function in Eq. (2) can be directly applied to the description of charge transport yielding the electrical conductivity

$$\sigma_{xy} = \int_0^\infty dt \left(\frac{1}{2\hbar} \tan\left(\frac{\beta\hbar}{2}\frac{d}{dt}\right) \frac{d}{dt} D^+_{xy}(t) + \frac{1}{2\hbar}\frac{d}{dt} D^-_{xy}(t)\right).$$

It turns out that this form of the electrical conductivity can be numerically evaluated around *1,000-5,000 times faster* than previous implementations of the electrical conductivity in the time domain [4,5].

To demonstrate the power of the newly developed theoretical approach, we have investigated the topological state of the disordered Haldane model [6] as a nontrivial example of charge transport in topological matter (see below). We first focus on briefly describing the numerical and technical implementation.

The numerical methods and algorithms that run on SuperMUC-NG are implemented in home-made codes and no third-party code has been involved. Our code is written in Fortran90/95. It implements a domain-decomposition scheme for basic matrix-vector multiplications (MVMs), where each domain is handled by a single MPI process. We use pure MPI where the implementation is performed in such a way that communication is initiated and the part of the MVMs that are internal to the MPI-process are carried out subsequently. When this internal work is finished, the communication is finalized and the external part of the MVM is calculated. In this way, communication can operate in parallel to computation on the nodes. The only external library that is required is MPI. In the simulations, we calculate expectation values in an energy-resolved fashion by using an energy projection scheme [2]. This is performed by the Lanczos approach.

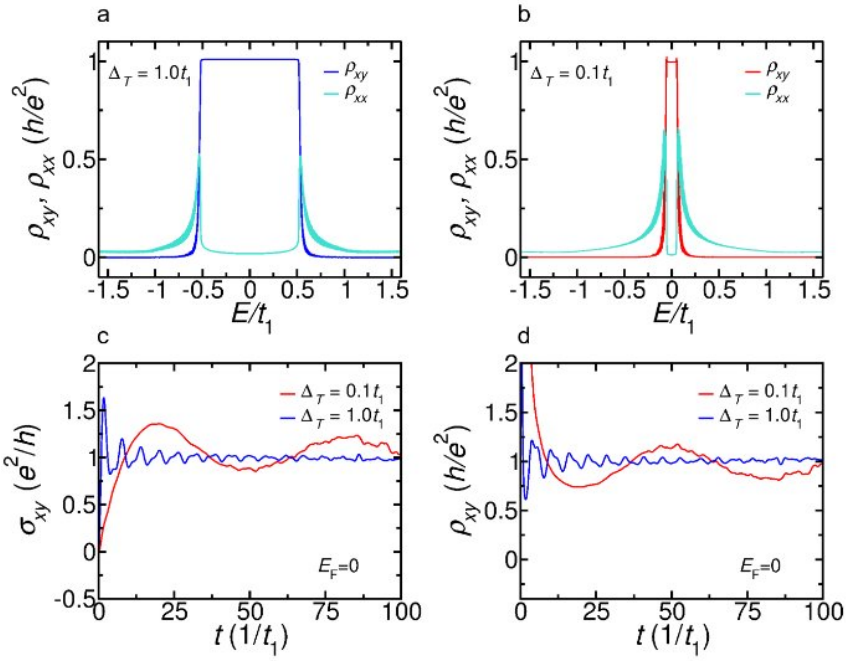

Figure 1: a and b: Energy-resolved resistivity components ρ_{xx} and ρ_{xy} for different topological energy gaps (t_1 is the energy unit), which represent the figure of merit of the QAHE. c and d: Time-resolved transverse conductivity σ_{xy} and resistivity ρ_{xy}, where the time scale is given in inverse energy units. This figure is taken from Ref. [3] with permission from American Physical Society.

The key physical quantities that we calculate are the longitudinal and transverse components of the electrical conductivity and resistivity (cf. Fig. 1). All physical quantities are represented in an effective real-space basis and the supercell approach is implemented. More specifically, a tight binding parametrization for the electronic structure is used which allows to represent the Hamiltonian in a relatively sparse way.

The numerical methods and implementations have been developed by the Ortmann group over the last decade [2,3,4,5,7]. This includes the developed MPI version of the code. The numerical calculations of the conductivities are performed by a Lanczos approach [2] and a subsequent continued fraction expansion to obtain the spectral shape of the corresponding response function at a certain point in time. A single conductivity calculation of a supercell with around 10^8 electronic states with 1,536 cores per run requires about 37,000 core hours (runtime of 24 hours). Besides small output log files, the job output of a single conductivity calculation reduces to the files containing the conductivity spectra at each point in time, which are of MB size. The total output of a single run results in an output of around 2-3 GB. For the above mentioned systems of 10^8 electronic states, a memory capacity of around 1 TB is needed during runtime that depends on the particular realization of the Hamiltonian.

In application of the above approach, we have studied the dynamical evolution of the longitudinal and the transverse conductivities and resistivities (see Fig.1) to characterize the topological state leading to the so-called quantum anomalous Hall effect (QAHE) and its dynamical formation. The unified description of longitudinal and transverse responses makes the development of specific algorithms unnecessary and, at the same time, allows us to study arbitrary linear responses in the time domain. As compared to other linear-scaling time-domain approaches to transverse responses, it benefits from a speed-up factor of 1,000 or more [3,4]. This allows the precise determination of disorder and topological effects in any kind of material (not only for OSCs) in a time-domain approach that has not been established before.

Ongoing Research / Outlook

The SuperMUC-NG cluster is perfectly suitable for our simulations of the charge transport since it provides sufficiently large memory per core and a high speed for massive parallelization that we can exploit to run our code fast and in a highly parallel manner. Due to the high degree of parallelization, most of our jobs require a walltime of only about 12 to 24 hours, which is beneficial for efficient and fast data production.

In future projects we plan to extend and refine our numerical calculations to a large class of materials (organic crystals etc.) that result in further valuable scientific contributions.

References and Links

[1] R. Kubo, J. Phys. Soc. Jpn. 12, 570 (1957).
[2] Z. Fan, et al., Phys. Rep. 903, 1 (2021).
[3] M. Panhans, F. Ortmann. Phys. Rev. Lett. 127, 016601 (2021).
[4] F. Ortmann, S. Roche. Phys. Rev. Lett. 110, 086602 (2013).
[5] F. Ortmann et al. Phys. Rev. B 91, 165117 (2015).
[6] F. D. M. Haldane, Phys. Rev. Lett. 61, 2015 (1988).
[7] F. Ortmann et al. EPL 94, 47006 (2011). 33 (2019) 838-854.

Nanoscale Fluid Interfaces: Evaporating Films and Exploding Droplets

Research Institution
[1]Laboratory of Engineering Thermodynamics, TU Kaiserslautern
[2]Scientific Computing in Computer Science, TU München
[3]Chair of Thermodynamics and Thermal Separation Processes, TU Berlin

Principal Investigators
Maximilian Kohns[1], Simon Stephan[1], Hans Hasse[1], Fabio Gratl[2], Hans-Joachim Bungartz[2], Matthias Heinen[3], Jadran Vrabec[3]

Researchers
Florian Fleckenstein[1], Aditya Kulkarni[1], Dominik Schäfer[1], Sebastian Schmitt[1], Gabriela Guevara-Carrion[3], Simon Homes[3]

Project Partners
–

SuperMUC Project ID: pn56mo

Introduction

Processes across interfaces of fluids, such as evaporation or absorption, play a significant role in many engineering fields, especially in energy technology and chemical engineering. These processes are mainly determined by the properties of the interface on a molecular level. A particularly suited method to gain insight into these small length scales is molecular dynamics (MD) simulation. The interactions between the molecules are modeled by potential functions and Newton's equations of motion are solved numerically for each particle individually. This simulation method allows for the tracking of the motion of the molecules and the energetics in the vicinity of the interface and, therefore, the inference of important interface properties.

Results and Methods

In order to obtain data at high resolution and good statistical quality, molecular systems containing millions of particles must be investigated. This requires using the supercomputer SuperMUC-NG. Our massively parallelized and optimized MD code *ls1 mardyn* [1] is used for running the simulations. Some highlights of recent results are briefly presented in this report.

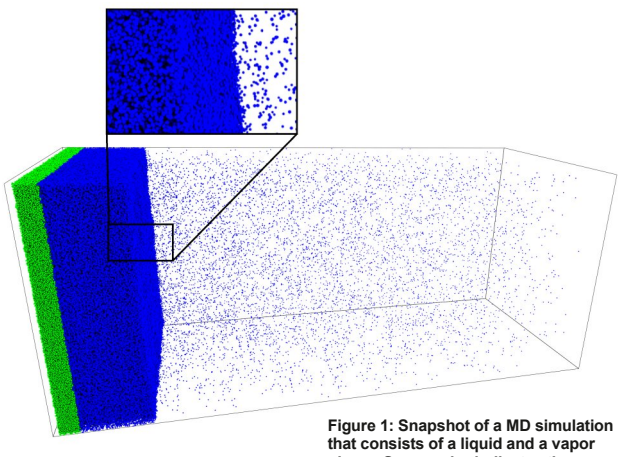

Figure 1: Snapshot of a MD simulation that consists of a liquid and a vapor phase. Green color indicates the replenished particles.

Evaporation processes are stimulated by driving forces, such as gradients of temperature or chemical potential. Those driving forces lead to mass and energy fluxes across the interface. On a physical level, the driving forces and the resulting fluxes are coupled by the Onsager coefficients that play a significant role and can be predicted with MD. In the present work, this was done for the simple Lennard-Jones fluid, which shows an Argon-like behavior. In order to sample the data required for the calculation of the Onsager coefficients, a simulation domain with one liquid and one vapor slab was set up. Depending on the state point, up to 10 million particles were considered. An exemplary snapshot of such a simulation is presented in Figure 1.

The driving force was created by deleting particles in the vapor phase. In order to keep the number of particles constant during simulation, the deleted particles were replenished in the liquid such that this phase was not brought out of local equilibrium [2].

During the simulation runs, physical properties such as the temperature or density as well as the mass and energy fluxes were sampled. Using these data, the Onsager coefficients can be calculated [3]. First, the local heat flux and the local heat resistivity $r_{qq}(z)$ must be derived. In a second step, the local heat resistivity can be integrated to obtain the overall heat resistivities R_{qq}^g and R_{qq}^l across the interface as:

$$R_{qq}^g = R_{qq}^l = \int_{z^g}^{z^l} r_{qq}(z)\mathrm{d}z$$

with z^g and z^l being the spatial limits of the interface. Further resistivities were calculated based on the local heat resistivity and the local enthalpy, which were also sampled during the simulation. In a final step, the Onsager coefficients were determined through the inverse of the resistivities. Examples of the obtained data and the calculated profiles are shown in Figure 2.

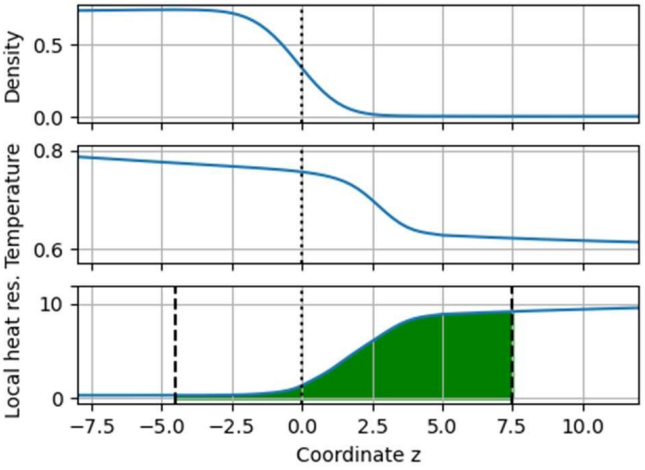

Figure 2: Profiles of density, temperature and local heat resistivity over the spatial coordinate z. The dotted lines mark the interface center, while the dashed lines delimit the interface region. The green area represents one resistivity.

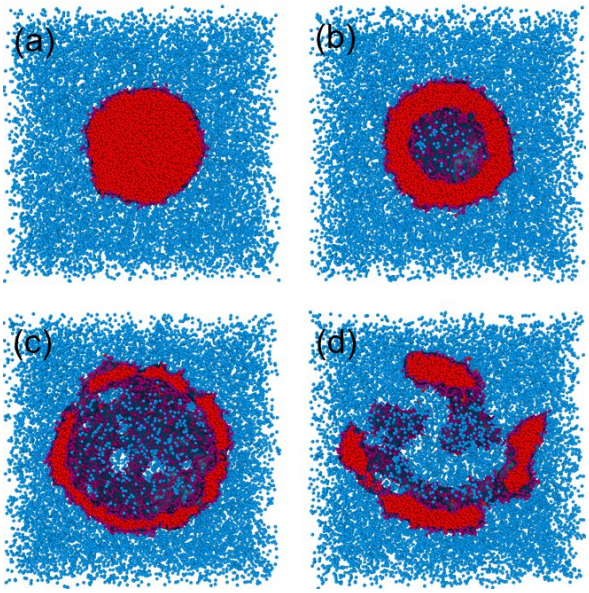

Figure 3: Snapshots of an MD simulation of the explosion of a nanodroplet. The simulation box is sliced in half in order to show the inside of the droplet. (a) Equilibrated starting configuration, (b) Formation of a gas bubble inside the droplet, (c) growing gas bubble starts to tear the droplet apart, (d) fragments of exploded droplet.

Not only flat surfaces, but also curved surfaces occur frequently, most notably e.g. with liquid droplets. In numerous processes, so-called micro-explosions of droplets are important, e.g. in combustion engines and spray flame synthesis processes for the production of nanoparticles. Despite their importance, the mechanisms leading to micro-explosions are not fully understood to date. MD simulations are an ideal tool to study these phenomena on a fundamental level, since they allow for taking a look into an evaporating and exploding droplet, which is difficult to achieve with experimental techniques. We are currently developing simulation scenarios and methods for studying droplet micro-explosions. Snapshots of the course of a representative simulation are shown in Figure 3.

The simulation starts from a droplet in equilibrium with a surrounding vapor phase. Then, the temperature in the center of the droplet is increased abruptly, mimicking e.g. a chemical reaction taking place. In the course of a simulation, a gas bubble inside the droplet forms, fluctuates in size, and grows such that it eventually tears the droplet apart. The great benefit that MD simulations provide is that the radii of the droplet and the gas bubble, heat and mass fluxes, and many more properties that are unavailable in experimental studies are easy to track.

Ongoing Research / Outlook

Future work will focus on the comparison of the present MD simulation results and the predicted Onsager coefficients with data obtained by other simulation methods, such as Riemann solvers and Computational Fluid Dynamics (CFD). As the conducted MD simulations yield data with a high resolution and precision, they will help to further improve and validate the other simulation methods. As the Onsager coefficients depend on the fluid and its state, we are planning series of simulations. To this end, the usage of supercomputers, like SuperMUC-NG, is crucial for our research. Furthermore, we plan to extend our studies of exploding droplets to mixtures.

References and Links

[1] https://www.ls1-mardyn.de/home.html
[2] M. Heinen, J. Vrabec. J. Chem. Phys. 151.4 (2019): 044704.
[3] E. Johannessen, D. Bedeaux. Physica A 370.2 (2006) 258-274.

Understanding Nanoconfined Water

Research Institution
Lehrstuhl für Theoretische Chemie, Ruhr-Universität Bochum

Principal Investigator
Dominik Marx

Researchers
Harald Forbert, Banshi Das, Sergi Ruiz-Barragan

Project Partners
–

SuperMUC Project ID: pn68bu

Introduction

Since recently, nanoconfinement water attracts scientists due to its puzzling and astonishing properties, which could greatly impact on applications in the technological, chemical and biological realms. Transport properties, dielectric responses and chemical equilibria are dramatically affected depending on the topology of the confinement, the strength of the confinement as well as the nature of the wall materials used for confinement [1]. To decipher the effect only due to confinement, recently developed graphene-induced nanoconfinement systems offer us a lot in understanding the change of physical-chemical properties solely due to the confinement effect. Based on our previous work on symmetric confinement [2], we [3] now introduce *asymmetric* confinement to probe the molecular information offered by nanoconfined water using nonlinear vibrational spectroscopy.

Contrary to bare interfaces, where interfacial water is in contact with bulk water and the effects of the interface decay towards bulk, nanoconfined water might feature superposition effects due to stratified interfacial water at both interfaces. To acquire a profound understanding of such systems, experiment and simulation serve as essential complements of each other. For instance, our very recent simulation work on nanoconfined water successfully captured the dramatic change of the dielectric response as compared to bare interfaces [2]. While the dielectric measurement captures collective molecular response from the whole system, vibrational spectroscopy in mid-IR region is capable to probe the local H-bonding environment around a vibrational chromophore, e.g. O-H bonds. In the context of interfacial water, vibrational sum frequency generation (VSFG) spectroscopy has been found to be an excellent tool to extract the molecular details of interfacial H-bonding at bare interfaces down to the sub-monolayer regime. Despite the great efficiency and applicability of VSFG for such open interfaces, its use is hitherto unknown in the realm of very narrow slit pores – hosting nanoconfined water.

To shed light on future applications of VSFG in the framework of nanoconfined solutions, we have computed theoretical VSFG spectral responses for a systematic set of asymmetric model slit pores consisting of graphene and hexagonal boron nitride sheets (thus rendering them VSFG-active) providing large interlayer separations with bulk-like water at the center down to bilayer and monolayer water lamellae.

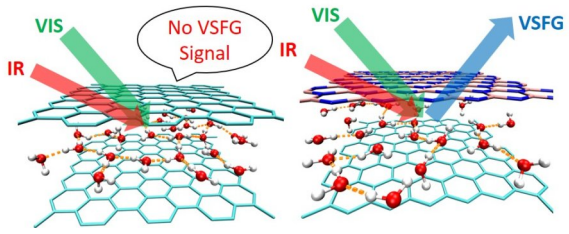

Figure 1:The left panel shows a representative symmetric confinement (GRA-GRA) slit pore setup where there is no VSFG signal due to symmetry, whereas the right panel visualizes the emergence of a non-zero VSFG signal after proper symmetry breaking, thus introducing asymmetry by replacing the upper GRA sheet with HBN .

Results and Methods

We have used graphene (GRA) and hexagonal boron nitride (HBN) sheets with water molecules being intercalated between them to create asymmetric nanoconfined systems being VSFG-active (Fig. 1). The slit pores have been prepared using our rigid piston approach [2]. Initially the HBN and GRA slabs are taken in at a separation of 20 Å while water molecules are placed between them, keeping the overall dimensionality of the simulation box as 34.7484 Å × 34.3920 Å × 60.0000 Å. Controlling the normal pressure to 1 bar within the rigid piston approach, the two sheets come closer and converge to a particular average interlayer distance (dint) depending on the number of water molecules between the sheets. Five representative GRA-HBN slit pore systems have been prepared by increasing the number of water molecules one by one to provide systems in close analogy to the previous symmetric GRA-GRA pores [2]: XS, S, M, L, XL, where the narrow XS and S systems only host monolayer and bilayer water, respectively, whereas the others yield multilayer water. In the XL pore, a bulk-like region forms in the middle of that wide slit pore. For the VSFG calculations, we have used a set of 20 independent NVE simulations for each slit pore size to converge the spectra at controlled thermodynamic conditions corresponding to 300 K and a normal pressure of 1 bar.

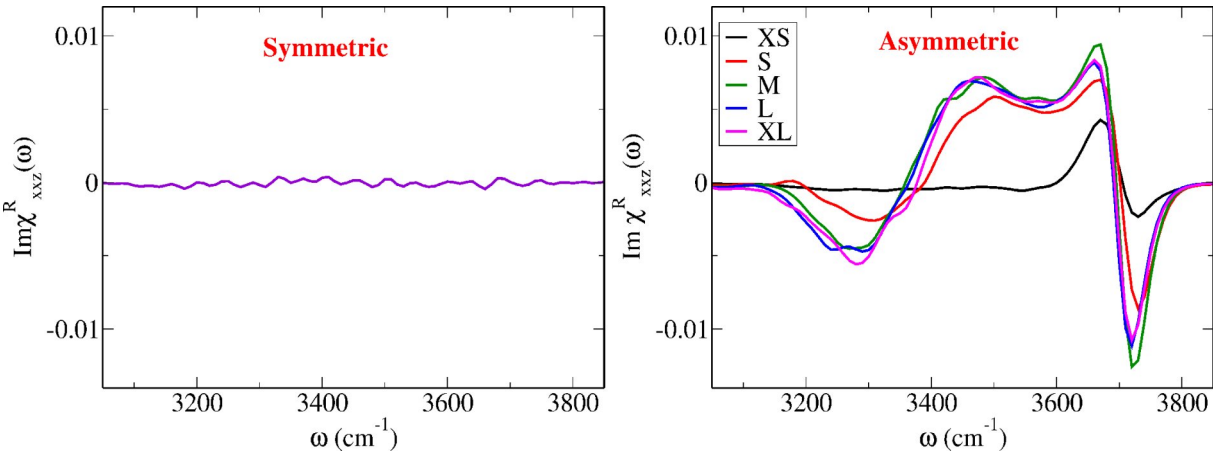

Figure 2: Imaginary part of the VSFG spectral responses from water confined in a symmetric GRA-GRA bilayer slit pore S (left panel) and in five different asymmetric GRA-HBN slit pores (right panel).

We ventured from the most strong confinement limit to weak confinement by changing the distance between the GRA and HBN sheets. At very strong confinement (XS and S), only monolayer or bilayer water is hosted and for moderate to weak confinement, intermediate layers did appear as found earlier for symmetric GRA-GRA confinement. The most important difference we found, with respect to symmetric confinement, is that the density profiles of oxygen and hydrogen atoms along the surface normal are no longer symmetric, rather tilted towards the HBN sheet, which can be attributed to its little stronger interaction with water as compared to that with GRA sheet.

We have adopted a well-established combined electronic structure/molecular dynamics method to calculate the second-order resonant susceptibility within a mixed quantum/classical approach [4]. We indeed found a finite VSFG response even with the incorporation of such mild asymmetry using HBN and GRA sheets (right panel of Fig. 2). As a reference, we also calculated the VSFG response from the symmetric GRA-GRA bilayer system S where, as expected, no signal beyond noise is present (left panel).

By observing the qualitatively different nature of the distinct spectral responses, we can discover three distinct confinement regimes. In the most extreme confinement limit with only a monolayer of water in the XS pore, only the high-frequency part around 3700/cm exists. The spectral responses remain very similar from weak down to moderate confinement (i.e. from XL to L to M). For the bilayer system S, a similar qualitative behavior as that in the multilayer confinement regime is found, yet with a distinctly different lineshape in the low-frequency range. These three different regimes of confinement based on the VSFG spectral response correspond to what was found earlier [2,5] for symmetric nanoconfinement based on H-bonding and electronic structure analyses.

In experiments, one measures the total signal which, in our context, is a combined effect of the responses from the GRA and HBN surfaces. To understand the spectral features due to nanoconfinement, it is useful to compare the total spectral signal with the difference VSFG spectra, which can be defined as the difference between the VSFG spectra of the water/GRA and water/HBN interfaces. We have found that the total VSFG responses from weak (XL) down to moderate (M) confinement can be understood in terms of uncorrelated surfaces, whereas this is clearly not the case of bilayer (S) and monolayer (XS) water.

Ongoing Research / Outlook

Water confined in asymmetric slit pores provided by GRA-HBN sheets shows three different regimes of VSFG responses depending on the strength of the confinement, namely monolayer, bilayer and more weakly confined multilayer lamellae. The interpretation of such VSFG spectra gets complicated due to interference effects between the responses from the two opposite surfaces. This is unlike VSFG spectra from bare interfacial systems, which can at least be qualitatively understood by knowing the chemical nature of that surface in most of the cases. As the total VSFG response of water in slit pores is the result of a huge cancellation of the responses from the water layers adjacent to the HBN and GRA sheets in case of very narrow slit pores, one can probe the effects of nanoconfinement on the properties of monolayer and bilayer water using VSFG techniques. In this context, it would be interesting to study the VSFG response from so-called Janus interfaces, where water is confined between hydrophilic and hydrophobic surfaces, hence the effect of the two different interfaces might become much more pronounced at the level of the observed VSFG signal.

References and Links

[1] D. Muñoz-Santiburcio and D. Marx, Chem. Rev. 18, (2021).
[2] S. Ruiz-Barragan, D. Muñoz-Santiburcio, S. Körning, and D. Marx, Phys. Chem. Chem. Phys. 22, 10833 (2020).
[3] https://www.theochem.ruhr-uni-bochum.de/
[4] B. Auer and J. Skinner, J. Chem. Phys. 129, 214705 (2008).
[5] S. Ruiz-Barragan, D. Muñoz Santiburcio, and D. Marx, J. Phys. Chem. Lett. 10, 329 (2018).

Accurate prediction of Novel Materials

Research Institution
Institute for Physics, Martin-Luther-University Halle-Wittenberg

Principal Investigator
Miguel Marques

Researcher
Jonathan Schmidt

Project Partners
–

SuperMUC Project ID: pn68wa

Introduction

The design of new, stable inorganic compounds remains one of the great challenges of material science. Traditionally, experiments played a key role in the discovery and investigation of materials. However, experimental research is extremely expensive both in terms of resources and equipment as well as time. Furthermore, major material discoveries happened mostly through researchers intuition or even luck.

Theoretical methods, especially those based on density functional theory (DFT) have, in the past decade, drastically sped up this process. We can now perform high-throughput DFT studies of large compound spaces, and nowadays millions of such calculations are available in open databases, such as the Materials Project, Open Quantum Materials Database, AFLOW, or the Computational 2D Materials Database. These resources form an indispensable reservoir to discover candidates for further experimental investigation.

To decide theoretical whether a compound is stable one of the most important quantities is the distance to the convex hull of thermodynamic stability. Materials that form the vertices of the convex hull can not decompose to other compounds (unless the thermodynamic conditions are altered) and are therefore stable. Other entries that are above the hull are either metastable or completely unstable. To construct such hull, and to determine the stability of a given compounds, requires the (free) energy of that compound and of all possible decomposition products. For example, for a binary system of chemical composition AxBy we need the energy of all stable elementary substances An and Bm, as well as of all other binary compounds AnBm. For a ternary compound AxByCz we need the energy of other stable entries in the ternary phase diagram (including also all binaries AnBm, AnCm, and BnCm, and the three elementary substances).

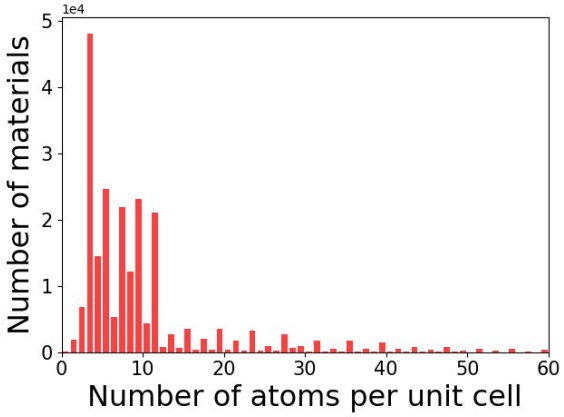

Figure 1: Distribution of number of atoms per unit cell in our compounds.

Naturally, to be able to compare the energies of these compounds all calculations are required to use compatible parameters. So far, high-throughput studies in solid-state material science have relied heavily on the use of the so-called Perdew-Burke-Ernzerhof approximation (PBE). This approximation is extremely successful, and leads to relatively accurate energies and crystal structures. The PBE functional is now over 25 years old. Since its development hundreds of new approximations were developed improving one or more aspects of the PBE. Here we are concerned with two such approximations. In 2007, PBE for solids (PBEsol) was developed, leading to much more accurate crystal geometries, while in 2015, the SCAN functional was proposed leading to more accurate geometries, energies, and electronic band gaps. PBEsol calculations have the same computational cost as PBE, but unfortunately SCAN comes at a higher cost.

The objective of this project was therefore to calculate a database of DFT calculations using these new, more accurate approximations. The geometry was optimized with PBEsol to alleviate the computational effort, while the energy was obtained with both PBEsol and SCAN. This data allows future researchers to have more accurate predictions when determining the stability of potentially stable compounds.

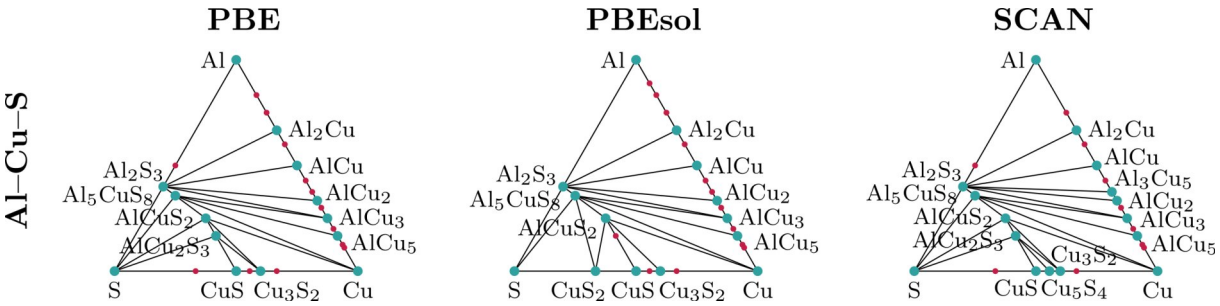

Figure 2: Phase diagrams of the ternary Al-Cu-S system calculated with PBE, PBEsol, and SCAN.

Results and Methods

To select the materials to calculate, we combined our own data with various available databases to accumulate as many stable or close to stable materials as possible [1]. This resulted in a set of 240,000 materials that we reduced to around 223,000 by removing materials with units cell too large for our computational resources. In the end, a large majority of the compounds had between 3 and 12 atoms in the unit cell, although one had as much as 250 atoms in the cell.

All calculations were performed using DFT as implemented in the Vienna ab initio simulation package (VASP). VASP is a very efficient plane-wave code that implements DFT using the projector augmented-wave technique. This code is well tested in high-performance computing environments and can run efficiently in parallel on thousands of cores using MPI. We used a mixed strategy to parallelize our calculations, where several crystal structures were calculated simultaneously, each one using 48-240 cores. The most serious complication concerned memory usage, as the standard parallelization mode of VASP often required more memory per node than available in SUPERMUC-NG. We resolved this problem by developing heuristics that changed the number of cores and the parallelization strategy depending on the system.

Starting from the known ground-state structures in the PBE approximation we optimized the geometries with PBEsol until the forces on the atoms and the internal stresses were converged to a high accuracy. Then, the energy and other physical properties were recalculated with SCAN at the PBEsol geometry. Despite the known numerical instabilities of the SCAN approximation nearly all calculations were converged. These calculations consumed a total of around 20 million core hours.

The resulting data, optimized geometries, bandgaps, forces, stresses, energies etc. can be freely downloaded from the materials cloud archive [3].

We show an example of our calculations in Fig. 2 where we depict the ternary phase diagram of the Al-Cu-S system calculated with the PBE (from the original data) and with PBEsol and SCAN (from the data produced in this work). The blue points denote composition that are thermodynamical stable (forming vertices of the convex hull) while red dots are slightly unstable compositions. We see that overall the three diagrams are similar, but with noticeable differences. In fact some structures that are stable in PBE become unstable with the more accurate SCAN, and vice-versa.

Ongoing Research / Outlook

In Ref. 2 we already developed a well functioning framework that combines DFT and machine learning to predict stable materials. To train the neural networks we used PBE data as this was the only available to us. With the calculations performed in this project, we will be able to extend this machinery to PBEsol and SCAN. Therefore, we will use the networks previously trained on and update them via transfer learning to the precision of SCAN using the new dataset. In a following step, we will use our machinery to scan billions of possible compounds to predict thousands of new stable materials and characterize their properties.

References and Links

[1] Schmidt, J. et al. accepted for publication in Scientific Data (2021).
[2] Schmidt, J. et al., Sci.Adv.7, eabi7948, 10.1126/sciadv.abi7948 (2021).
[3] Schmidt, J et al., https://archive.materialscloud.org/record/2021.164 (2021).

Influence of phase-fractions on eutectic colony formation

Research Institution
[1]Karlsruhe Institute of Technology, IAM-MMS

Principal Investigator
Britta Nestler[1,2]

Researchers
Michael Kellner[1], Marco Seiz[1]

Project Partner
[2]Hochschule Karlsruhe - Technik und Wirtschaft, IDM, Karlsruhe

SuperMUC Project ID: pn69ne

Introduction

During the directional solidification of eutectic multi-component alloys the formation of eutectic colonies can be observed. The formation of these structures is driven by microscopic instabilities in a macroscopic planar solidification front, due to impurities of the components that diffuse from the solidifying phases into the melt. Within the project *pn69ne* [1], the formation of eutectic colonies in the *AlCu-5Ag* system is studied with phase-field simulations including multiple phases and components. For a simultaneous multi-scale representation of the fibrous structure of the eutectic and the multiple times larger structures of the eutectic colonies in a uniform simulation, large solidification fronts with high resolution are needed.

Furthermore, the implementation and adjustment of a nucleation mechanism is required for the simulation of eutectic colonies. This has been elaborated in [2] for the eutectic melt compositions *Al-14.7Cu-5.5Ag* and the three off-eutectic compositions *Al-19Cu-5.5Ag*, *Al-12Cu-8.2Ag* and *Al-14.7Cu-7.4Ag*. The two-dimensional simulation results of [2] show that a change of the chemical compositions ieads to the adjustment of different phase fractions during the simulations of each system.

The focus of the upcoming simulation studies is to investigate the effect of different phase fractions on the three dimensional microstructure evolution during the growth of eutectic colonies.

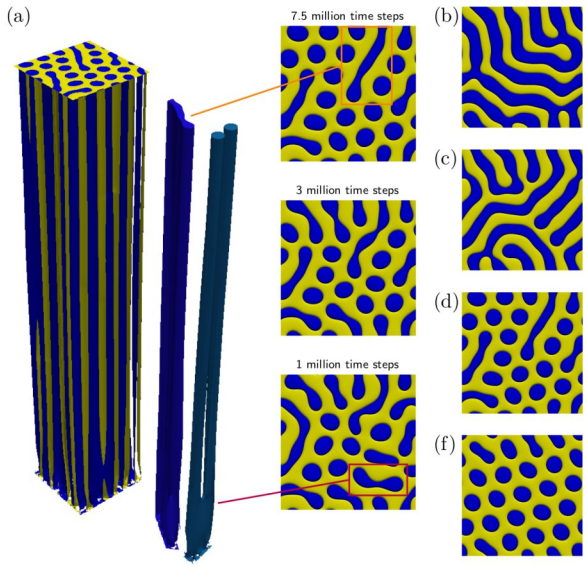

Figure 1: 3D Microstructure evolution of (a) eutectic *Al-14.7Cu-5.5Ag* with selected enlargements of solidification front and resulting final solidification fronts of (b) *Al-19Cu-5.5Ag*, (c) *Al-12Cu-8.2Ag*, (d) *Al-14.7Cu-5.5Ag*, and (e) *Al-14.7Cu-7.4Ag*.

Results and Methods

Following the investigations in Ref. [2], three-dimensional phase-field simulations of the different melt compositions have been conducted within the project pn69ne [1], to study their individual microstructure evolutions. The simulations are performed with a computational domain size of 250x250x300 cells for 7.5 million time steps on 625 cores using the massively parallel multiphysics framework Pace3D [3]. As the simulations are conducted in 3D+t (time), no nucleation mechanism is required to ensure the free evolution of the microstructures.

Figure 1(a) shows the evolved 3D microstructure of the phase-field simulation with eutectic composition *Al-14.7Cu-5.5Ag*. Next to the 3D structure two selected lamellae are exposed. As illustrated by the enlargements of the solidification front after 1, 3 and 7.5 million time steps, some of the initial lamellae split up and form multiple fibers, whereas other lamellae stay constant during the solidification process. The resulting solidification fronts after 7.5 million time steps for the four different compositions are depicted in the images 1(b)-(f). As expected from [2], different phase-fractions evolve dependent on the applied melt composition. The solidification front of the eutectic structure in Figure 1(d) show a mixed structure of fibers and lamellae, whereas the solidification fronts of the off-eutectic structures for Fig. 1(b) and 1(c) show pure lamellar structures. For the last off-eutectic composition *Al-14.7Cu-7.4Ag* the microstructure consists merely of fibers arranging in a hexagonal order.

Next, the parameter ranges for the nucleation mechanism are investigated, to achieve the formation of eutectic colonies. Despite a wide variation of the

parameters, no stable colony growth could be established for the eutectic as well as for the off-eutectic compositions of *AlCu-5Ag*. Either the nucleation mechanism is too weak, leading to a stable planar eutectic solidification front or the nucleation mechanism is too strong, leading to an unstable interface between the phases.

Hence, the influence of the phase fractions on the eutectic colony formation is firstly investigated based on the material system *NiAl-34Cr*, which has been successfully used in previous studies [4,5]. For this, the Gibbs energy parabola of the liquid phase is modified to shift the position of the equilibrium composition of liquid. Due to a consequent adjustment of the melt composition to the newly modeled eutectic compositions, five new material systems are generated. These new material systems do not represent the original *NiAl-34Cr* system. Hence, the new material systems are labeled corresponding to their melt composition with *AB-24E*, *AB-29E*, *AB-39E*, *AB-44E* and *AB-49E*. Additionally, the system *AB-34E* is used which is similar to the original *NiAl-34Cr* system, with *A* representing the original concentration for *Ni*, *B* representing *Al* and *E* representing *Cr*. The letters *C* and *D* are omitted to avoid any possibility of confusion with the chemical symbol of carbon and the variable of the diffusion coefficient matrix, respectively. Subsequently, phase-field simulations are performed in two-dimensional domains of 1,500 x 1,000 cells on 90 cores for 5 million time steps, to validate a matching parameter set of the nucleation mechanism for the formation of eutectic colonies.

Figure 2 shows representative simulation results for the systems *AB-24E*, *AB-34E*, and *AB-44E* with the best aligned and distinct colonies. Hereby the system *AB-34E* with an adjusting phase fraction of 65:35 evolves with three colonies, whereas all other compositions form two cell structures. The systems with higher difference of the phase fractions (*AB-24E* to *AB-39E*) show more distinct colonies, compared to the systems with similar phase fractions (*AB-44E* and *AB-49E*). By analyzing the used nucleation parameters for the presented simulations, a trend to higher amounts of all three values can be observed for decreasing differences between the phase fractions.

The melt compositions of the presented results are located slightly beside the connection line between the equilibrium concentrations of the two solid phases with a higher amount of *A*, which is representing the concentration of *Ni* in the original system. For melt compositions exactly on the connection line, no colony formations occurs. This indicates that a certain misalignment between the equilibrium concentrations of the liquid and solid phases is needed for the formation of eutectic colonies. The lack of such a misalignment could be a reason why no colony formation was achieved in previous simulations in the *AlCu-5Ag* system.

Ongoing Research / Outlook

Due to the granted computational resources on SuperMUC-NG new insights into the growth mechanisms of eutectic colonies could be achieved. Based on the observations made during these studies the following questions arise, which will be addressed in the forthcoming extensive simulation studies predicting material properties and designing new multicomponent materials:

- Is the observed misalignment needed for the formation of eutectic colonies?
- Does a similar misalignment of B show similar results for the formation of eutectic colonies?
- Does larger misalignment lead to more colonies within the same simulation domain?

Depending on the answers to these questions, three-dimensional phase-field simulations of the systems with the most promising configurations for the formation of eutectic colonies are planned to be performed within the next year. For this three-dimensional simulation domains with >1,000³ voxel cells will be used, to achieve the growth of multiple 3D colonies within the simulations. The research of microstructure analysis in alloys is funded through the KIT excellence strategy project ‘’ACDC’’ and Pace3D code optimization to enable large scale parallel simulations is supported within the Gottfried-Wilhelm Leibniz price NE 822/31.

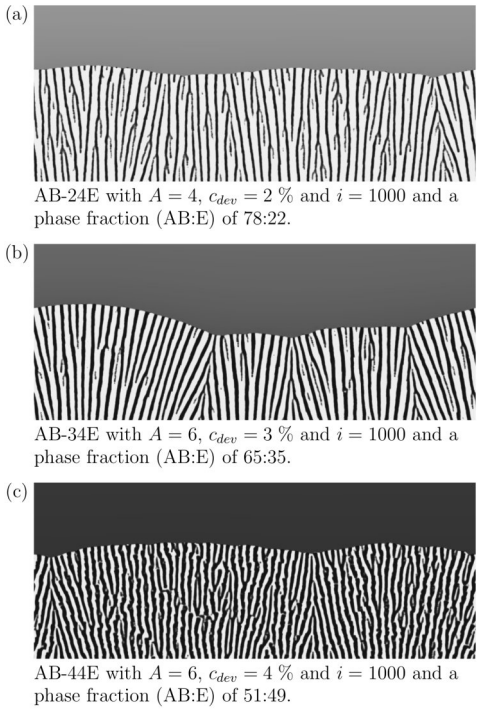

Figure 2: Exemplary plots of eutectic colonies for selected modeled *AB-xE* systems with different phase fractions.

References and Links

[1] https://www.lrz.de/projekte/hlrb-projects/0000000000F43B00.html
[2] F. Hinrichs, M. Kellner, J. Hötzer and B. Nestler, Scr. Mater 186, 89- 94, 2020.
[3] J. Hötzer, A. Reiter, H. Hierl, P. Steinmetz, M. Selzer, and B. Nestler, J Comput. Sci-Neth, 26, 1 – 12, 2018.
[4] M. Kellner, J. Hötzer, E. Schoof, and B. Nestler, Acta Mate. 182, 267–277, 2020.
[5] M. Kellner, 2020, PhD-Thesis, KITOpen, doi: 10.5445/IR/1000119330.

Understanding charge transport in next-generation electronic devices

Research Institution
[1]Institute of Theoretical Physics, University of Regensburg

Principal Investigator
Jan Wilhelm[1]

Researcher
Carlo A. Pignedoli[2]

Project Partner
[2]Swiss Federal Laboratories for Materials Science and Technology (Empa), Dübendorf, Switzerland

SuperMUC Project ID: pn72pa

Introduction

Carbon-based electronics opens a novel way for miniaturization of nanoscale electronic devices (see Fig. 1 for an artistic sketch). One milestone has been the demonstration of the first field-effect transistor based on atomically precise graphene nanoribbons (GNR) in 2017. Since then, a lot of effort has been invested in the design and demonstration of novel GNR based devices. Theoretical investigations of the electronic properties are fundamental to drive experiments towards most promising candidate nanomaterials. We demonstrated in the past years that HPC infrastructures and codes are necessary for that purpose [1]: they allow to tackle with success the simulation problem. In this project, we have improved the underlying algorithms [2] and studied 5-armchair-GNRs [3] and topological organic molecules [4] shedding light on the underlying principles and mechanisms governing their transport properties.

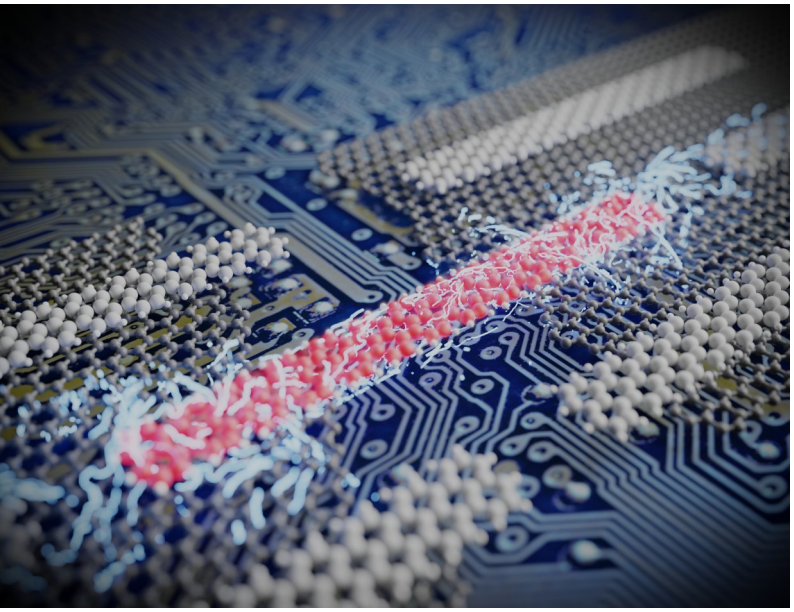

Figure 1: Artistic sketch of future envisaged application of carbon-based nanomaterials. The sketch shows 1D carbon nanomaterials that are fabricated in the nanotech@surfaces laboratory of Empa when integrated into prototypical devices. Both fabrication process and integration into devices require simulations of the structural and electronic properties of the novel nanomaterials in gas phase and on substrates. Credit: M. Perrin (Empa).

Results and Methods

GW is an accurate method for computing electron addition and removal energies of molecules and solids. However, in a conventional GW implementation, the computational cost of GW is $O(N^4)$ in the system size N, which prohibits the application of GW to many systems of interest, We have developed a low-scaling GW algorithm with very high numerical accuracy as we have shown by extensive benchmark calculations on small molecules and phosphorene nanosheets with up to 1,000 atoms [2]. The accuracy of the algorithm is as good as a few tens of milli electron Volt for single-electron levels compared to highly accurate, but computationally much more expensive GW calculations (see Fig. 2). Our work paves the way for numerically well-converged GW calculations of large systems, as they are required for modelling many systems of technological and scientific interest, for example novel materials for electronic devices.

In a recent work in collaboration with Empa, we succeeded in the fabrication of a device demonstrator where an armchair graphene nanoribbon of five carbon rows width (AGNR5), was successfully connected to Pd electrodes in the realization of a FET with HfO_2 gate oxide that demonstrated I_{on} / I_{off} ratios of 10^4 on currents up to 0.4 μA. We used the highly accurate low-scaling GW algorithm [2] to study the energy gap between conducting states of the 5AGNRs. The simulations we conducted were crucial to assess which orbitals contribute to the transport properties of the contacted ribbon, being fully delocalized on the whole nanostructure and allowed to predict the minimal length for the GNRs needed to guarantee that the transport gap would have been stable with respect to GNR length. Indeed, in Fig. 3 we show that for the GNR fabricated in the laboratory, starting from 30 naphtalene units the transport properties are expected to be stable with respect to ribbon length. Moreover, starting form 14 naphtalene units the ribbons start to exhibit a radical character [3].

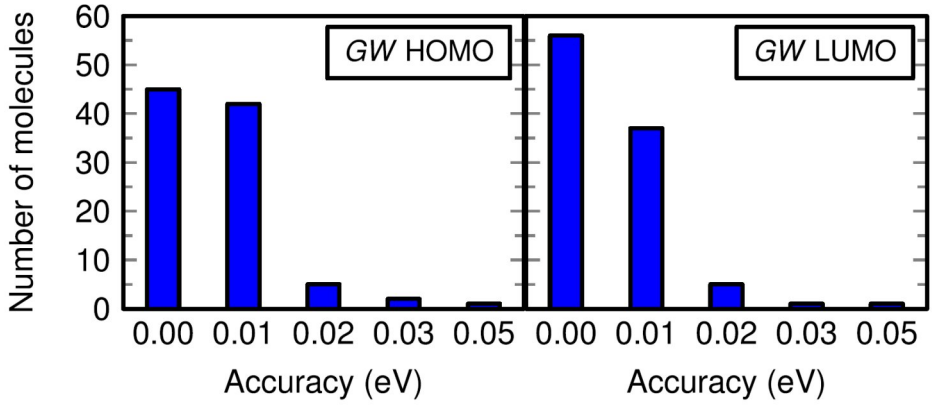

Figure 2: Deviation of GW results from the low-scaling GW algorithm [2] to highly accurate reference data for the highest occupied molecular orbital (HOMO) and the lowest unoccupied molecular orbital (LUMO).

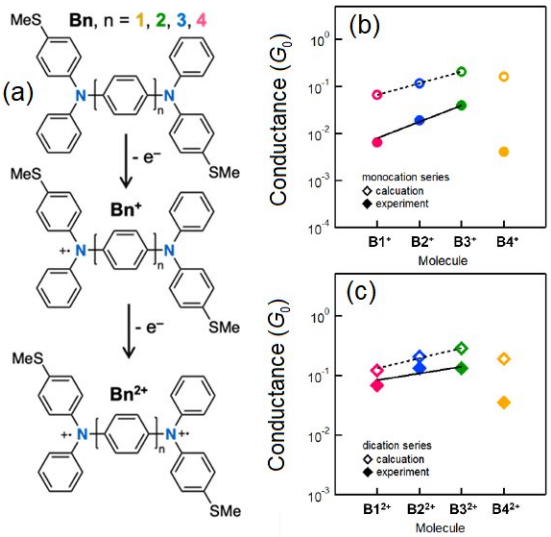

Figure 4: (a) Molecular geometry of neutral Bn molecules, Bn^+ cations and Bn^{2+} dications, (b) conductance for Bn^+ cations with increasing length (from n = 1 to n = 4) and (c) conductance for Bn^{2+} cations with increasing length, both from experiment and theory.

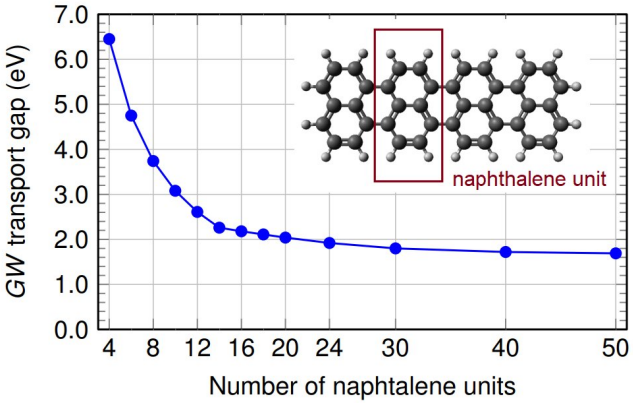

Figure 3: Transport gap of armchair graphene nanoribbon (5-AGNR) as function of ribbon length as computed from GW [2]. Inset: Molecular geometry of 5-AGNR with 4 naphthalene units.

Single-molecule topological insulators are promising candidates as conducting wires over nanometer length scales. However, most conjugated molecular wires exhibit low conductance that decays as the wire length increases. To overcome this limitation, we studied a family of oligophenylene-bridged bis(triarylamines) with tunable and stable (mono-/di-)radicaloid character (see Fig. 4 (a) for a sketch of the wire geometry). The wires can undergo one- and two-electron chemical oxidations to the corresponding radical cation and dication, respectively. Experiments in the group of Prof. Venkataraman (Columbia University, New York) showed that the oxidized wires exhibit high reversed conductance decay with increasing length, as expected from one-dimensional (1D) topological insulators. The champion 2.6 nm long dication displays a significantly high conductance. We carried out quantum transport calculations. Our simulated conductance is sketched in Fig. 4 (b) and (c) for the Bn^+ and Bn^{2+} case together with the experimental result. The conductance increases from $B1^+$ to $B3^+$ and from $B1^{2+}$ to $B3^{2+}$, in agreement with the experimental trend. Our calculations also reproduce the decrease of the conductance when going from $B3^+$ to $B4^+$ and from $B3^{2+}$ to $B4^{2+}$ [3]. We further analyze the origin of this intriguing trend from the underlying electronic states, where report full details in Ref. [4].

Ongoing Research / Outlook

So far, we have carried out static, that means, not explicitly time-dependent calculations. Many important phenomena in charge transport are explicitly time-dependent and we aim at describing the real-time dynamics of the systems under investigation. To this end, we plan to develop a time-dependent GW method to be able to calculate the dynamics of electronic devices as response to ultrashort laser pulses. These calculations rely even more on HPC infrastructures as real-time simulations are computationally orders of magnitude more involved than static calculations.

References and Links

[1] https://www.ur.de/physik/evers/startseite/index.html
https://www.empa.ch/web/s205/home
[2] J. Wilhelm, P. Seewald, D. Golze, J. Chem. Theory Comput. 17, 1662-1677 (2021).
[3] G. Borin Barin et al., G. Borin Barin et al., Small 2202301 (2022, in press).
[4] L. Li et al., Nat. Chem. (2022, in press).

All-electron DFT Simulations of particle-like magnetic objects

Research Institution
Forschungszentrum Jülich

Principal Investigator
Stefan Blügel

Researchers
Daniel Wortmann, Uliana Alekseeva

Project Partners
–

SuperMUC Project ID: pn72qa (Gauss Large Scale project)

Introduction

Complex magnetic textures and localized particle-like structures on the nanometer scale such as chiral magnetic skyrmions (Fig. 1) with non-trivial topological properties are nowadays the most studied objects in the field of nanomagnetism. They offer the promise of new data storage and data processing technologies ranging from racetrack memories to memristive switches for neuromorphic computing. The theoretical and computational description of nanosized magnetic objects usually follows a typical multiscale approach. Ab-initio simulations mostly based on Density Functional Theory (DFT) are utilized to determine fundamental materials properties. Based on these properties simpler purely-magnetic models like the extended Heisenberg model are constructed and spin-dynamics simulations are employed to describe the final complex magnetic structures. While this approach has demonstrated its power and efficiency, it cannot describe fundamental changes in the electronic structure induced by the complex alignment of magnetic moments. In this project we extend the realm of DFT calculations for magnetic systems to significantly larger setups to tackle these challenges from the basic description provided by our ab-initio code FLEUR [1]. Since 2015 FLEUR is one of the flagship codes of the MaX-European Center of Excellence in HPC [2].

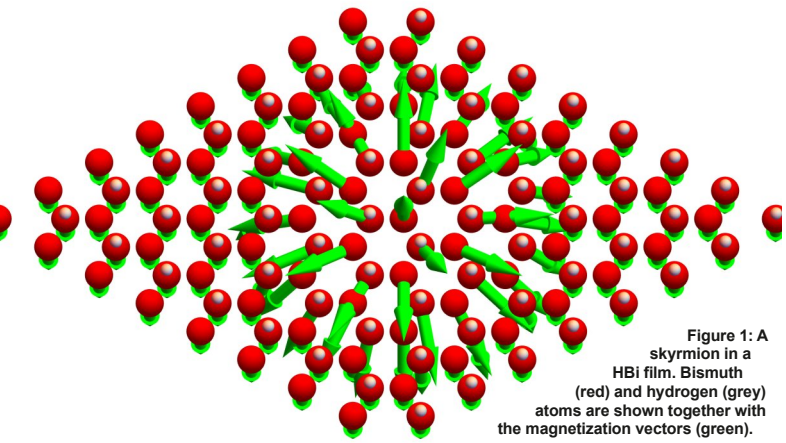

Figure 1: A skyrmion in a HBi film. Bismuth (red) and hydrogen (grey) atoms are shown together with the magnetization vectors (green).

Structure	# atoms	Matrix size	Iteration cost
Globule	1,024	150k x 150k	5,120 core-h
Skyrmion	192	200k x 200k	11,670 core-h

Table 1: Properties of our two magnetic setups, a globule in MnGe (1st row) and a skyrmion in a HBi (2nd row): number of atoms (2nd column), size of dense Hermitian matrices in the generalized eigenvalue problems (3rd column) and number of core-hours needed for one self-consistence iteration (4th column).

Results and Methods

Our project aims at providing insight into the electronic properties of large and complex non-collinear magnetic structures by applying our state-of-the-art all-electron full-potential linearized augmented plane wave (FLAPW) DFT code FLEUR. While the FLAPW method is a numerically complex and computationally heavy approach, it is also considered to provide the ”gold standard” and reference results in DFT. Its accuracy and reliability proven in numerous applications is particularly crucial in the field of magnetism as the fundamental energy scales on which magnetic phenomena occur is usually very small. While DFT simulations of large setups containing many atoms are already possible for quite some time, the simulations we pursue extend the limits of so called all-electron DFT applied to large magnetic configurations. A DFT simulation is an iterative process with 50-120 cycles to achieve a self-consistent solution of the fundamental quantum mechanical equations. A single of these self-consistency iterations contains many different steps like the determination of the potential, the generation of a new density and the density mixing to accelerate the self-consistency process. From the computational point of view, the most relevant task in each iteration consists of the setup of matrices for the generalized eigenvalue problem and its diagonalization. The hybrid MPI/OpenMP parallelization of the FLEUR code allows to utilize machines like SuperMUC-NG [4]. To get insight into the details of the electronic structure which are not in reach of conventional multiscale approaches, we performed simulations with two magnetic setups which are larger than any production-level FLAPW calculations reported so far: i) a globule with two Bloch points in the MnGe 4x4x8 super cell (Fig. 2) and ii) a skyrmion in a HBi film (Fig. 1).

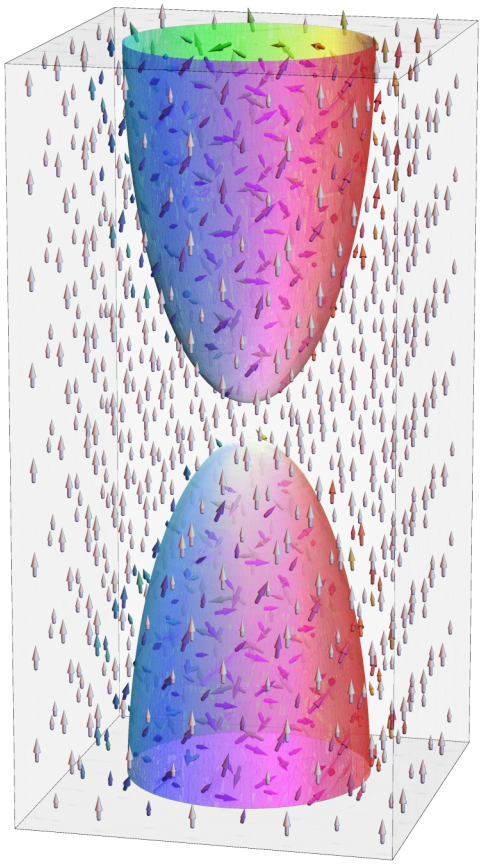

Figure 2: A globule in MnGe super cell 4x4x8. This configuration has two Bloch points at the edges of the globule.

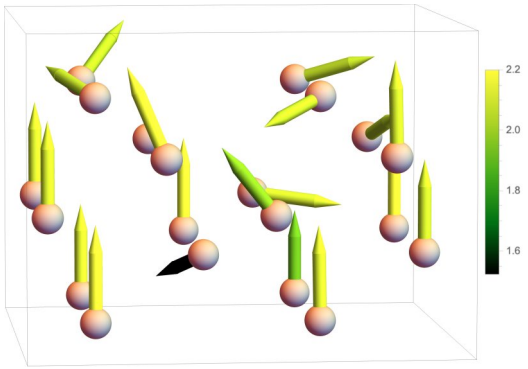

Figure 3: Magnetization values (color-coded, see the legend on the plot) and directions of the atoms close to the upper Bloch point in the MnGe globule from the previous picture.

The setups containing the Bloch points run on 256 nodes with 48 cores for about 25 minutes per iteration. Hence, a single self-consistency cycle consumes about 5,000 core-hours and a full self-consistency with 165 iterations 825,000 core-hours. As we have to compare the different magnetic states for a full analysis of the system and to gain inside knowledge of the interplay between the magnetic and electronic structure of these configurations, we need to obtain self-consistency for several setups. These calculations involve the diagonalization of several complex matrices of size 150k x 150k per iteration. The corresponding data for the second system reported here are given in Table 1. Typical for a DFT calculation, our IO requirements are relatively modest and only few files are generated. In continuous models, a Bloch point manifests itself as a singularity at which the magnetization vanishes. This already indicates that drastic changes in the electronic structure can be expected.

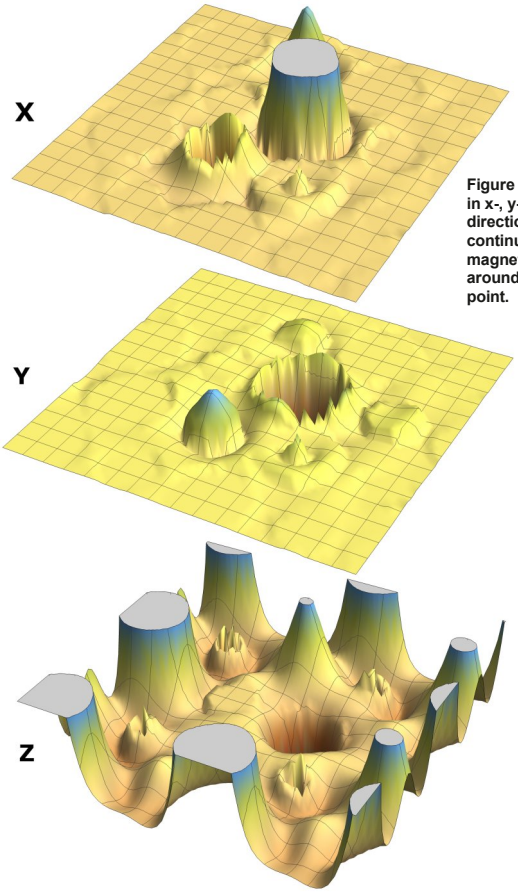

Figure 4: Projections in x-, y- and z-direction of the continuous magnetization field around the Bloch point.

When a system with a Bloch point is simulated with spin-dynamic methods, only the directions of the magnetization vectors are allowed to relax. Our simulations show that the magnetization of the atom most close to the Bloch point is significantly reduced in value (Fig.3). Our simulations also show (Fig. 4) that there is no singularity-like Bloch point in the continuous magnetization field but rather a “Bloch-landscape” with a complicated profile.

Ongoing Research / Outlook

It has been shown [3] that hydrogenated Bi monolayers can exhibit large topological bandgaps and manifest a quantum spin Hall effect. As the partially hydrogenated Bi monolayer is magnetic, the effect of magnetic order on the electronic structure can be significant. In particular the complex interplay between the topological protection in the quantum anomalous state and the magnetic order introduces a rich playground in which details of the electronic structure can be controlled and manipulated by the arrangement of magnetic moments in the system. While such effects have been simulated by means of simple tight-binding models, these models can only indicate the basic phenomenon but fail to grasp the details. We therefore plan to study large unit-cells (as on the Fig. 1 and larger) with non-trivial magnetic order imposed.

References and Links

[1] https://www.flapw.de
[2] http://www.max- centre.eu
[3] C.Niu et al., Phys.Rew. B 91, 041303 (2015).
[4] U. Alekseeva et al., in: Springer International Publishing AG, part of Springer Nature 2018 M. Aldinucci et al. (Eds.): Euro-Par 2018, LNCS 11014, pp. 735–748, 2018.

Ab Initio Molecular Dynamics with Hybrid Functionals and Plane Waves

Research Institution
[1]Friedrich-Alexander-Universität Erlangen-Nürnberg

Principal Investigator
Bernd Meyer[1]

Researchers
Sagarmoy Mandal[1], Ritama Kar[2], Vaishali Thakkur[2], Tobias Klöffel[1], Nisanth N. Nair[2]

Project Partner
[2]Indian Institute of Technology Kanpur, India

SuperMUC Project ID: pn98fa

Introduction

Kohn-Sham density functional theory (KS-DFT) and plane wave (PW) based ab initio molecular dynamics (AIMD) techniques are widely used in investigating structural and dynamical properties of condensed matter systems. The accuracy of KS-DFT calculations crucially depends on the choice of exchange-correlation (XC) functional. Owing to improved accuracy, hybrid functionals are preferred over the commonly used XC functionals using the Generalized Gradient Approximation (GGA). Hybrid functionals incorporate a certain fraction of Hartree-Fock (HF) exchange to the GGA exchange. They give better prediction of energies, structures, electronic properties, reaction barriers, band gaps of solids, and dynamical properties of liquids. However, the prohibitively high computational cost associated with HF exchange energy evaluation makes the hybrid functionals and PW based AIMD simulations extremely time consuming. This limits the routine use of hybrid functionals and PW based AIMD simulations for large condensed matter systems. Recently, we proposed a novel approach called Multiple Time stepping with Adaptively Compressed Exchange (MTACE) to speed up AIMD simulations using hybrid functionals [1,2]. In the MTACE method, the multiple time step integrator scheme was employed based on the Adaptively Compressed Exchange (ACE) operator formalism. The method is able to provide a speed up of 7. In this project, we further improved the performance of the technique by utilizing localized Selected Columns of the Density Matrix orbitals. Through this implementation (s-MTACE), we could achieve one order of magnitude speed up [3]. Subsequently, we implemented the MTACE and s-MTACE method using a task group based parallelization strategy called CP Group as available within the CPMD program [4,5]. These implementations are able to take advantage of large computational resources available on modern supercomputers like the SuperMUC-NG at LRZ. We show that with these developments, AIMD simulations with hybrid functionals can be carried out at a much lower computational cost than what was possible before.

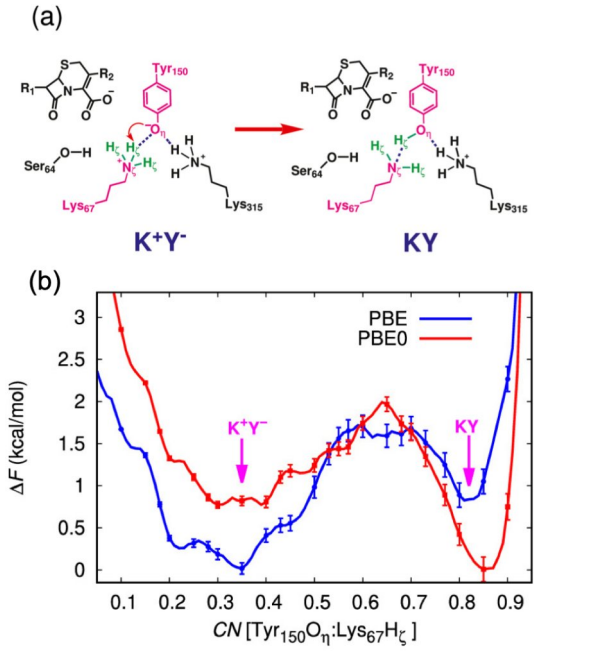

Figure 1: (a) Proton transfer from protonated Lys_{67} to Tyr_{150} in the presence of cephalothin ($K^+Y^- \rightarrow KY$) (b) Free energy as a function of the *CN* [$Tyr_{150}O_\eta$:$Lys_{67}H_\zeta$] coordinate computed for the proton-transfer reaction ($K^+Y^- \rightarrow KY$) using umbrella sampling simulations at the level of PBE (blue) and PBE0 (red) density functionals.

Results and Methods

The most computationally demanding procedure to perform hybrid density functional based AIMD simulations is the evaluation of the HF exchange integrals. In the MTACE method, the ionic forces are partitioned into computationally cheap fast forces using an approximated ACE operator and computationally costly slow forces due to corrections to the approximated ACE operator, which reduces the number of HF exchange energy computations. We employ localized orbitals to improve the performance of the MTACE method by screening the KS orbitals involved in the evaluation of the exchange operator. This approach is named s-MTACE. We obtained a speed up of 10 using this approach. We used this implementation to carry out computationally intensive free energy computations at the level of hybrid density functional theory, in particular, we studied (a) the methyl formate hydrolysis reaction in neutral aqueous media and (b) the proton-transfer reaction within the active-site residues of the

class C β-lactamase enzyme (Figure 1) [3]. We improved the s-MTACE method further by a slightly less rigorous, but a more efficient computational scheme in which a pre-selection of the columns of the density matrix is done. This implementation will be referred as s'-MTACE [5].

In PW based KS-DFT codes, wavefunc-tions and KS potentials are interconverted with the help of 3-dimensional (3D) FFTs between real and reciprocal space. For optimal performance of the 3D parallel FFTs, PW implementations use a slab decom-position of the 3D FFT grids to distribute the data. For typical DFT calculations today, the number of grid points along any direction is a few hundreds, so slab decomposition cannot use a large number of processors. Using CP Group within the CPMD code, the available processors can be divided into several task groups and an array that holds the wavefunctions is replicated among these groups. The total workload of the HF exchange energy computation is divided into several parts and they are distributed evenly among these task groups (Figure 2). Finally, a global summation across these groups provides the total contribution to the HF exchange energy. Our implementations of the MTACE, s-MTACE and s'-MTACE methods with CP Group were tested for their scaling performance on SuperMUC-NG. The number of cores per CP group is chosen to achieve an ideal load balancing. Excellent scaling performance by all the MTACE variants, for different system sizes, has been observed (Figure 3a and 3b). Most importantly, we are able to speed up the computations by two orders of magnitude. For example, the performance of the MTACE method was improved 121 times compared to the conventional hybrid functional calculation. For 7,680 cores and 100 atoms, our method is able to generate 48 ps of hybrid AIMD trajectory per day with a 0.5 fs MD time step, while the conventional implementation could give a best performance of only 0.4 ps per day, with not beyond 120 cores at the same level of theory (Figure 3c).

Ongoing Research / Outlook

Our methods and their implementations allowed us to perform molecular dynamics simulations at the hybrid DFT level of theory with two orders of magnitude speed up in performance. Through this, we are able to apply hybrid DFT for computationally expensive free energy calculations in condensed matter systems. We are now developing new methods to further improve the performance of hybrid functional based AIMD techniques and apply them to study various catalytic reactions.

References and Links

[1] Mandal, S. and Nair, N. N., J. Chem. Phys., 2019, 151, 151102.
[2] Mandal, S. and Nair, N. N., J. Comput. Chem., 2020, 41, 1790–1797.
[3] Mandal, S.; Thakkur, V. and Nair, N. N., J. Chem. Theory Comput., 2021, 17, 2244–2255.
[4] Klöffel, T.; Mathias, G. and Meyer, B., Comput. Phys. Commun., 2021, 260, 107745.
[5] Mandal, S.; Kar, R; Klöffel, T; Meyer, B. and Nair, N. N., J. Comput. Chem., 2022, 43, 588-597.

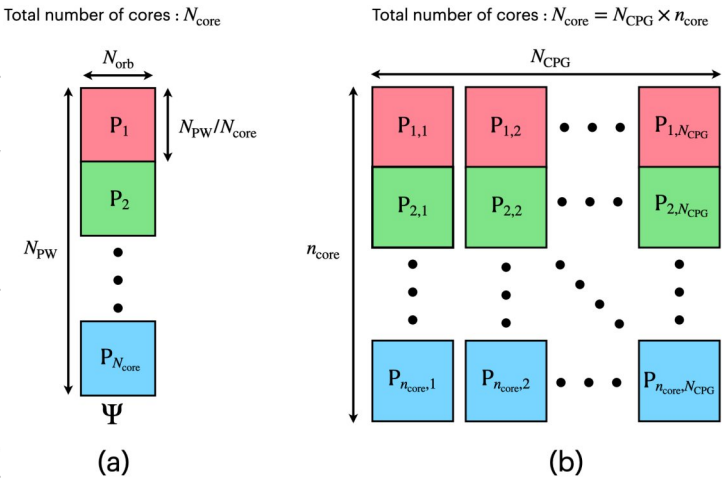

Figure 2: (a) Conventional distribution of the Ψ matrix with N_{core} compute cores. The total number of rows (N_{PW}) is distributed among these available compute cores. (b) The CP Group data distribution is shown for N_{core} compute cores.

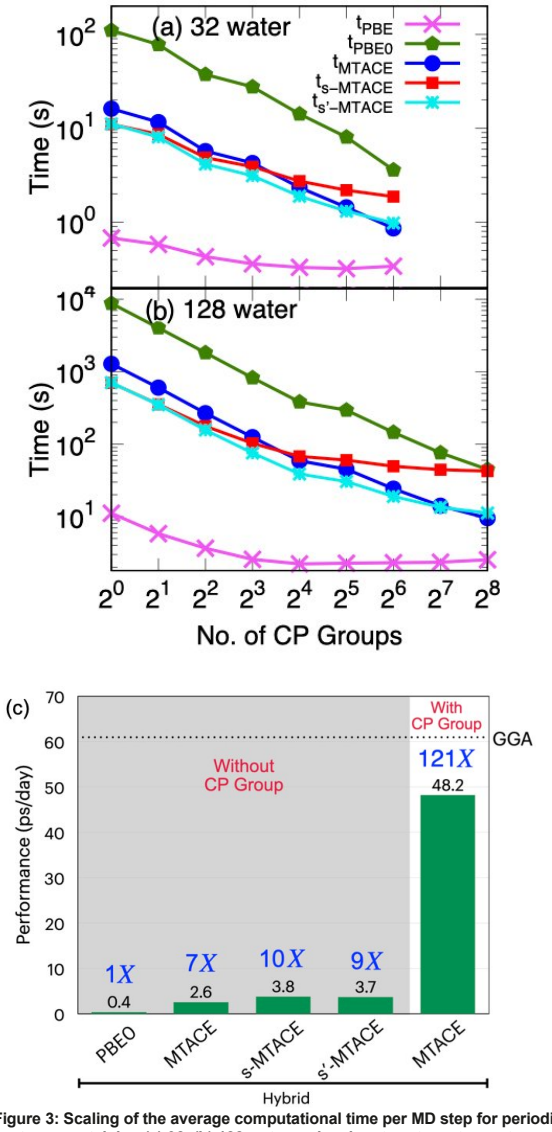

Figure 3: Scaling of the average computational time per MD step for periodic systems containing (a) 32, (b) 128 water molecules. t_{PBE}, t_{PBE0}, t_{MTACE}, $t_{s-MTACE}$ and $t_{s'-MTACE}$ are the average computing time per MD step in PBE, PBE0, MTACE, s-MTACE and s'-MTACE runs. (c) Best performance of these methods for 32 water molecules in the unit of ps/day. Dotted black line shows the performance of PBE calculation with 120 cores. Effective speed-up compared to PBE0 is also indicated here (blue).

Piezoelectric Hafnia and Zirconia

Research Institution
Department of Applied Sciences and Mechatronics, Munich University of Applied Sciences

Principal Investigator
Alfred Kersch

Researcher
Max Falkowski

Project Partners
–

SuperMUC Project ID: pr27su

Introduction

Materials possessing piezoelectric characteristics generate an electric signal as a response to mechanical stress, and mechanical strain if an electric field is applied.

Such materials are indispensable for actuators, transducers and sensors. Piezoelectric devices can be found in the phone and digital cameras, microscope lenses, fuel injectors, micro-pumps, inkjet printers, medical instruments.

The most prominent piezoelectric materials are based on the perovskite crystal structure but may lose their properties in nano-scaled devices.

Recently, a ferroelectric phase was stabilized in HfO_2 and ZrO_2 based thin films which persisted down to a few nanometer thicknesses [3]. In contrast to all prominent piezo electrics, this material is based on the fluorite crystal structure. The scope of the current study is to reveal the possible piezoelectric effects. All ferroelectric films are known to be piezoelectric, but very large piezoelectric constants are found in antiferroelectric materials where the electric field induces a phase transition from a paraelectric to a ferroelectric phase. The large mechanical strain derives then from the volume difference of the participating phases. The field-induced strain mechanism is known to be realized in recently developed lead-free ceramic materials such as barium titanate, $BaTiO_3$ (BT), bismuth sodium titanate, $Bi_{0.5}Na_{0.5}TiO_3$ (BNT), and potassium-sodium niobate, $K_{0.5}Na_{0.5}NbO_3$ (KNN) [4].

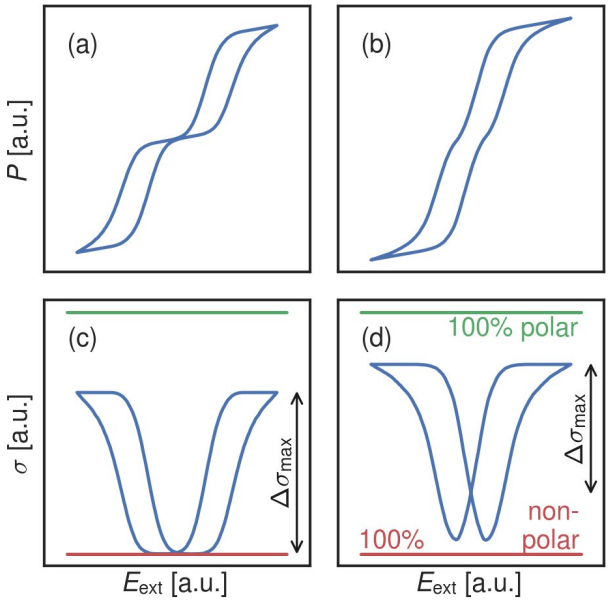

Figure 1: (a) and (b) show the field-induced polarization in differently conditioned antiferroelectric materials. For small electric field, the material is predominantly paraelectric, for larger fields, the polarization increases rapidly in relation to the paraelectric to ferroelectric phase transition. (c) and (d) show the field-induced strain curves where the slope measures the effective piezoelectric coefficient. (Reprinted (adapted) with permission from ACS Applied Materials & Interfaces [1]. Copyright 2020 American Chemical Society.)

Results and Methods

To bring the material into the antiferroelectric state, extrinsic doping can be used [2]. To explore the potential of hafnia and zirconia as piezoelectric and to find the material with the largest strain, a dopant screening study was done. 58 possible dopants were chosen as a dopant in HfO_2 and ZrO_2 in a concentration of 3.125% and 6.25%. Because the dopant can be inserted in several positions, a large number of doped configurations was built to find the energetically most favorable. Because the favored crystal phase is uncertain under these conditions, the structures were considered for all relevant, competing crystal phases, among them the paraelectric and ferroelectric phase in focus.

The calculation of the energy and crystal volume of thousands of structures was then done ab initio with density functional theory calculations. Such calculations require massive parallel computer modelling.

The calculations revealed at first the most favourable dopant configuration and the energetic order of the possible crystal phases. The achieved configuration furthermore depends on the oxygen chemical potential, which is controlled with the production process. The achieved results, therefore, include the recommended production condition.

Then the energetic order of the crystal phases was analysed. In the case of paraelectric and ferroelectric crystal energies with a certain difference, which is suitable to allow a field-induced phase transition, a potential material with the desired antiferroelectric properties was recognized.

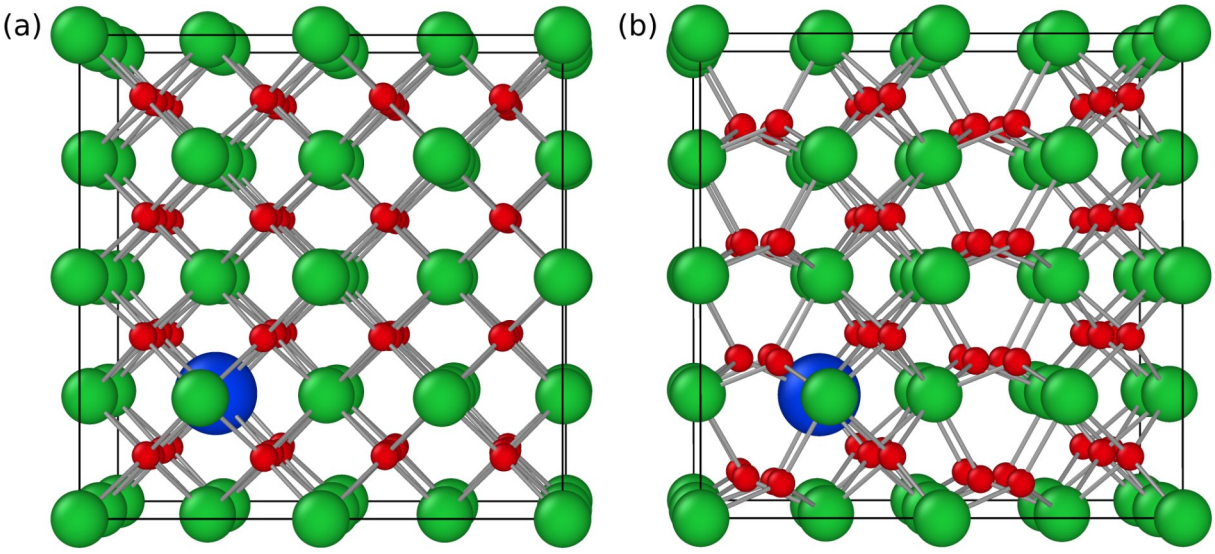

Figure 2: (a) ZrO_2 structure in the paraelectric, tetragonal phase with Yb dopant. (b) ZrO_2 structure in the ferroelectric, orthorhombic phase with the same dopant. The phase transition may be induced with an electric field. © University of Applied Sciences.

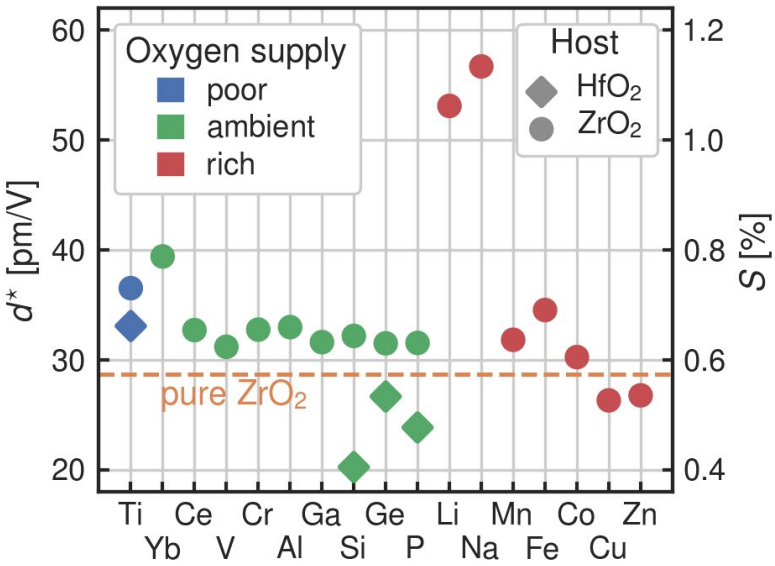

Figure 3: The calculated strains and estimated piezoelectric coefficients stemming from the field-induced transition from the paraelectric to ferroelectric phase. (Reprinted (adapted) with permission from ACS Applied Materials & Interfaces [1]. Copyright 2020 American Chemical Society.)

Last, the volume difference between the paraelectric and ferroelectric phase was searched, and the according effective piezoelectric coefficient calculated. The result in Figure 3 gives calculated coefficients for differently doped materials, including a specification of the required chemical potential for the production process.

In Si-doped HfO_2 thin films, experimentally a piezoelectric coefficient of 20 pm/V was found, which fits well to the predictions. The value compares with 4 pm/V in AlN thin films, the standard material used for mobile communication transducers.

The screening reveals that generally, ZrO_2 based material show larger coefficients then HfO_2 based material. Appropriately doped, ZrO_2 may have a much larger piezoelectric coefficient than for the so far experimentally found materials. The calculated results may serve as a guideline to optimize the piezoelectric coefficient in hafnia and zirconia.

Ongoing Research / Outlook

The ongoing research focuses on the pyroelectric effect in this system, which generates an electrical signal with temperature. The applications are sensorics and infrared sensing. Very large values are expected and again, the optimal dopant is searched.

References and Links

[1] M. Falkowski, A. Kersch, ACS Appl. Mater. Interfaces (2020), 12:29, 32915–32924.
[2] M. Falkowski, Ch. Kuenneth, R. Materlik and A. Kersch, npj Comp. Mat. (2018) 4:60.
[3] Böscke, T. S.; Müller, J.; Bräuhaus, D.; Schröder, U.; Böttger, U., Appl. Phys. Lett. 2011, 99, 102903.
[4] W. Jo, R. Dittmer, M. Acosta, J. Zang, C. Groh, E. Sapper, K. Wang, and J. Rödel, J. Electroceramics 29, 71 (2012).

Numerical simulations of continuum field theories

Research Institution
[1]Institute for Theoretical physics, Würzburg

Principal Investigator
Fakher Assaad[1]

Researchers
Z. Liu[1], J. Schwab[1], B. Danu[1], M. Raczkowski[1], A. Götz1, T. Sato[1], F. Parisen Toldin[1], F. Goth[1], M. Hohenadler[1], Z. Wang[1], Y. Liu[2], D. Hou[2]

Project Partner
[2]Beijing Normal University

SuperMUC Project ID: pr53ju, pn73xu (both Gauss Large Scale projects)

Introduction

The defining properties of our numerical research in the domain of correlated electron systems are the notions of emergence and criticality. It is amazing to realize that starting with a collection of interacting electrons, new particles, corresponding to collective excitations, that carry different quantum numbers than the original electron, can emerge. Emergence only occurs in the thermodynamic limit where the volume of the system is taken to infinity at constant particle number. An example is the canonical spin ½-chain realized for example in $KCuF_3$. Here, a spin-flip carrying spin 1 decays into two spinons that are gapless and perceive no confining potential. This state of matter is critical: it has no length scale and allows for a continuum field theory description. From the theoretical point of view, the one-dimensional spin chain can be described in many seemly different ways. On one hand, one can write the spin 1/2 degree of freedom as a fermion bilinear, with the constraint on one electron per site. A Feynman path integral formulation will lead to compact quantum electrodynamics (QED) in 1+1 dimensions. The spin ½-chain actually has a higher symmetry than the spin rotational symmetry. It has an O(4) one, that unifies seemingly different correlation functions: spin-spin and dimer-dimer ones. The continuum field theory that captures this state of matter is the O(4) non-linear sigma model in 1+1 dimensions with a Wess-Zumino-Witten geometrical term. The above provides one of many examples of why continuum field theories are important in the realm of the solid state: they account for universal and emergent behavior at or in the vicinity of critical points. They equally provide a common language between high-energy and solid state physics.

Results and Methods

To investigate collective phenomena in the solid state without any approximations other than system size, we use auxiliary field quantum Monte Carlo (QMC) methods [2]. This approach samples the Feynman path integral formulation of the grand canonical partition function and is hence a method of choice to study systems in thermodynamic equilibrium. In 2017, we started to develop a generic auxiliary field package, Algorithms for Lattice Fermions (ALF) [2] with the help from DFG and KONWIHR funding. During this grant period, we have released version 2.0 of the software [2], and we are continuously developing it. The challenges we confront when simulating fermionic system include a) the sign problem reflecting the fact that the action is generically complex and b) potentially long autocorrelation times. There has been remarkable progress in understanding how to formulate negative sign free simulations for an ever growing class of problems. In the absence of this problem, the computational cost scales as the third power of the volume, V, times the inverse temperature, β. This scaling and the desire to reach large lattices so as to at best capture critical and emergent phenomena renders the use of supercomputers imperative. Most of the research we have carried out would not have been possible without access SuperMUC-NG. In fact access to substantial compute time has given us the freedom of starting ambitious research projects that have been published in high impact journals.

One of the major achievements of this grant proposal was to provide a Landau Level regularization of the O(5) 2+1 dimensional non-linear sigma model with Wess-Zumino-Witten geometrical term [3]. This continuum field theory is the dimensional generalization of the aforementioned O(4) theory in 1+1 dimensions accounting for the physics of the one-dimensional Heisenberg chain. Aside from the intrinsic interest in understanding the phase diagram of this continuum field theory, it is a candidate theory of so called deconfined quantum criticality that unifies two orders (e.g. anti-ferromagnetism and valence bond solid) into a higher symmetry [4]. For this project, the challenges were the following. i) To simulate a continuum field theory, one needs to provide a regularization. Here we simulate a 2+1 dimensional $N_f = 4$ two component Dirac system akin to graphene, supplemented with 5 anti-commuting mass terms. This model has the desired O(5) symmetry, and in the presence of a gap, integrating out the fermions will generate the desired model. A standard lattice regularization is not an option since it would break the O(5) symmetry of the model. On the other hand, using a Landau level regulariza-

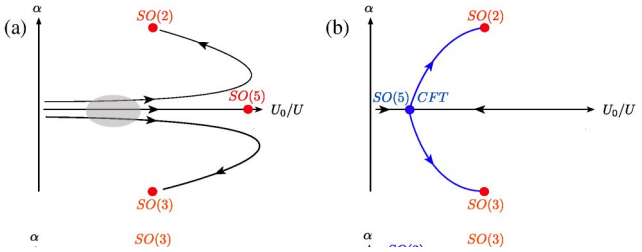

Figure 1: Possible flow diagrams fort he SO(5) non-linear sigma model in the stiffness U0/U versus symmetry breaking term, , plane. Our simulations favor quasi-criticality (a) or an SO(5) CFT (b). See Ref. [3].

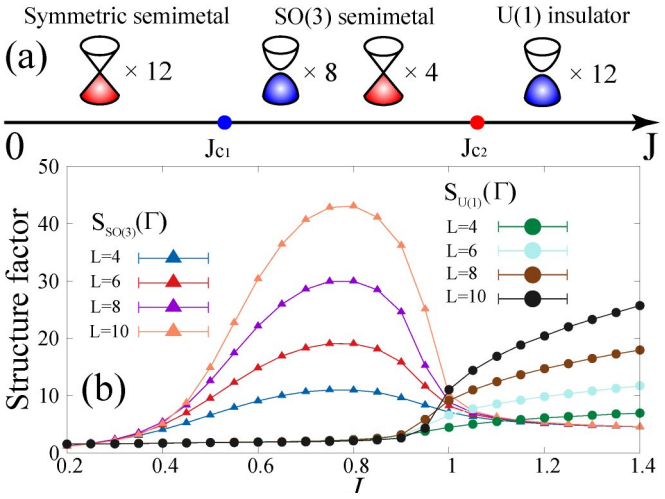

Figure 2: Reproduced from Ref. [5].

tion, by projecting the model onto the lowest Landau level, will do the job. The number of flux quanta defines the degeneracy of the Landau level and the dimension of the Hilbert space in which we will define the simulation. ii) It is amazing to see that this formulation supports a negative-sign free formulation such that large scale numerical simulations are tractable. iii) Even in the absence of the negative sign problem, we were confronted to many difficulties and we refer the interested reader to the supplemental part of our publication [3] for further reading. In short, the projection forces us to work with long-ranged interactions such that the computational cost scales as $V^5\beta$ which is two powers in volume larger than generic simulations with short ranged interactions. Furthermore, the memory cost scales as $V^3\beta$ rather than as $V^2\beta$ for short ranged interactions. Our results are summarized in Fig. 1, and supports the idea that this field theory is close to a SO(5) critical phase, such that the flow diagram of Fig. 1 (c) is supported by the data. Clearly the possibility that the two critical points in Fig. 1 (c) collide so as to produce the quasi-critical behavior shown in Fig. 1 (a) is also a possible interpretation of our data.

Ongoing Research / Outlook

We have recently introduced models of Dirac fermions that show novel quantum critical behavior [5]. The phase diagram is shown in Fig. 2. Here we consider 12 N_f = 2 Dirac cones with an interaction, J, that produces a unique phase diagram. First, at J_{c1}, we observe a partial gapping out of the Dirac cones. This metallic quantum critical point is novel. We have computed exponents, but they are at odds with those computed with a variety of analytical methods. The reason for this mismatch is intriguing and defines a set of novel questions. Are we suffering from quasi-criticality where system sizes beyond reach are required to capture the critical behavior? Is the continuum field theory, SO(3) Gross-Neveu, put forward to understand this transition misleading?

The second transition is even more interesting since the numerical data supports a continuous transition between different broken symmetry phases. Landau forbidden transition between anti-ferromagnets and valence bond solids have attracted considerable attention. In particular the aforementioned SO(5) field theory seems to capture the quasi-universality of this transition. Our instance of a Landau forbidden transition does not fit into the above theory since it involves gapless Dirac fermions. In short, the model and numerical results obtained in Ref. [5] define a set of tantalizing questions that will impact our future research.

The above summarizes only one aspect of our research where Dirac fermions play an important role. Other topics that we are and will continue investigating are heavy fermion systems, frustrated spin systems, electron-phonon problems as well as various lattice gauge theories.

On the algorithmic front, the ALF code is now rather mature. Since, to the best of our knowledge, it is the only general implementation of the auxiliary field quantum Monte Carlo method, we believe that it will set a standard. Of importance for future developments is: i) ease of use and 2) efficiency on novel supercomputing architectures. Concerning ease of use, we have and are developing a Python interface [6] to the Fortran2003 ALF code [7]. As for efficiency, one of our future goals is to provide a GPU version of the ALF code, so as explore possible speedups for large lattice.

References and Links

[1] https://gauss-centre.de/results/materials-science-and-chemistry/article/topology-entanglement-and-critical-phenomena-in-correlated-quantum-matter/
[2] ALF 2.0, Scipost 2022, accepted.
[3] Z. Wang et al. Phys. Rev. Lett. 126 (2021), 045701.
[4] Y. Liu at al. Nat. Comm. 10 (2019), no. 1, 2658.
[5] Z. Liu et al. arXiv:2108.06346 (Phys. Rev. Lett. 2022 accepted).
[6] https://git.physik.uni-wuerzburg.de/ALF/pyALF
[7] https://git.physik.uni-wuerzburg.de/ALF/ALF

Self-consistent-field ensembles of disordered Hamiltonians

Research Institution
[1]Institute of Theoretical Physics, University of Regensburg

Principal Investigator
Ferdinand Evers[1]

Researchers
Matthias Stosiek[1], Ferdinand Evers[1], Bruno Lang[2]

Project Partners
[2]Institute of Applied Informatics, University of Wuppertal

SuperMUC Project ID: pr53lu

Introduction

Our general interest is in self-consistent-field (scf) theories of disordered fermions. They generate physically relevant sub-ensembles ("scf-ensembles") within a given Altland-Zirnbauer class. We are motivated to investigate such ensembles

(i) by the possibility to discover new fixed points due to (long-range) interactions;
(ii) by analytical scf-theories that rely on partial self-consistency approximations awaiting a numerical validation;
(iii) by the overall importance of scf-theories for the understanding of complex interaction-mediated phenomena in terms of effective single-particle pictures.

In particular we investigate disordered thin film superconductors within the Boguliubov-deGennes (BdG) theory of the attractive-U Hubbard model in the presence of on-site disorder; the sc-fields are the particle density n(r) and the gap function $\Delta(r)$.

For this case, we reach system sizes unprecedented in earlier work. They allow us to study phenomena emerging at scales substantially larger than the lattice constant, such as the interplay of multifractality and interactions, or the formation of superconducting islands.

The results generated within our project [1] have led to several publications [2-4] with further publications being in the preparation.

Results and Methods

We observe that the coherence length exhibits a non-monotonic behavior with increasing disorder strength already at moderate interaction strength as seen in Fig. 1.

In Fig. 2 and 3 both the local density of states and the pairing amplitude respectively are shown to exhibit very broad (log-normal) distribution functions, exemplifying the strong mesoscopic fluctuations predicted by analytical theories. With respect to methodology our results are important because we establish that partial self-consistency ("energy-only") schemes as typically employed in analytical approaches tend to miss qualitative physics such as island formation. The fully self-consistent, energy-only with Hartree potential and energy-only schemes are compared in Fig. 4. For a more comprehensive presentation of our results please refer to [2].

To compute our self-consistent fields, we devised an algorithm based on the kernel polynomial method (KPM) [5]. With a KPM based code, we were able to reduce the asymptotic runtime from a cubic to a quadratic dependence on the size of the lattice. Through this we were able to achieve system sizes unprecedented in the literature.

We achieved an approximately ideal parallelization both through the computation of multiple impurity configuration and also the computation of the self-consistent fields on different points in space with negligible communication between processes.

Our code is written in a combination of Python and C, combining the performance of a highly optimized C-kernel with the adaptability and convenience of a high-level language for the non performance critical sections.

It is computationally expensive to find a single solution of the self-consistent fields (~100-1,000 core-h) for one disorder configuration. We need a large number (~100,000) of these configurations to achieve a reliable disorder average and to investigate different regimes of disorder strength, interaction strength, filling fraction and system size.

In total we used 59,424,938 core-h producing approximately 1.3 TB of self-consistent mean-field Hamiltonians across the parameter and impurity configuration space. We generated ~27,000 hdf5 files, where multiple parameter configurations can be saved in the same file for the same impurity configuration. For a typical job we used ~72,000 cores.

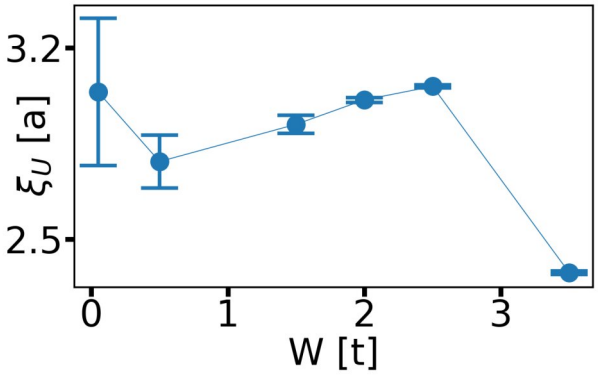

Figure 1: Evolution of the superconducting correlation length with increasing disorder strength W. A clear maximum is visible close to the disorder strength, where island development sets in.

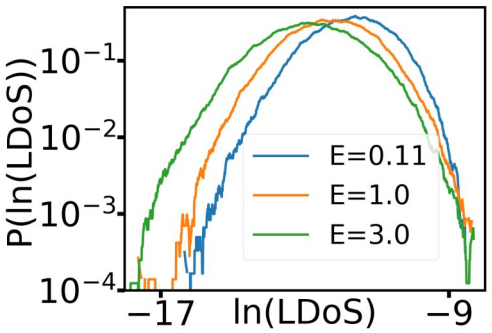

Figure 2: Distribution function of the local density of states at 3 different energies measured from the Fermi energy for moderate disorder and interaction strength.

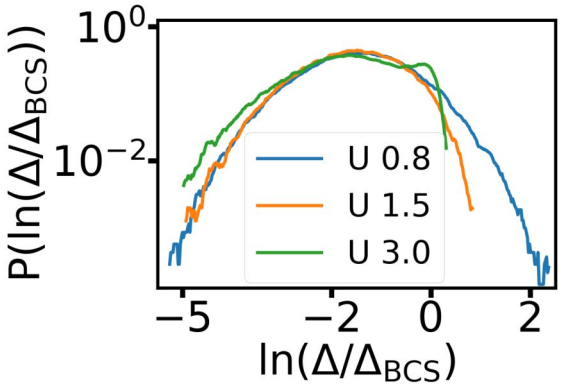

Figure 3: Distribution function of the local density of states at 3 different interaction strengths for moderate disorder.

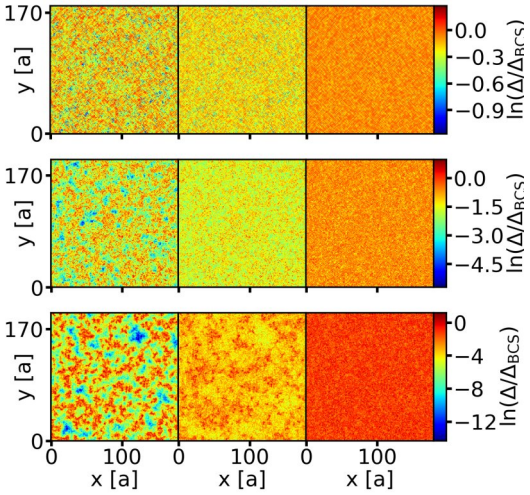

Figure 4: Evolution of the pairing amplitude in real space for full self-consistency (left), energy-only with local Hartree potential (middle) and energy-only. (right) Island formation can be clearly seen in the fully self-consistent scheme. The energy-only scheme with Hartree potential exhibits signs of island formation although it is far less pronounced than in the case of full self-consistency. In the energy-only scheme there is no island formation whatsoever.

Ongoing Research / Outlook

Without the tremendous resources and support of SuperMUC, we couldn't have met the high computational demands that our project entailed. Since the start of the project we have continually improved and optimized our code, most notably with a matrix-free implementation of the Chebyshev expansion [2].

Very interesting related questions remain open. In particular, we are investigating magnetism in disordered superconductors in a follow-up project on SuperMUC-NG. Our focus is on Yu-Shiba-Rusinov bound states around magnetic impurities and the emergence of local magnetism in disordered superconductors with repulsive short-range interactions. For this we extended our self-consistency solver to spin-rotational and time-reversal symmetry broken systems. Data production has been completed and data analysis is ongoing.

References and Links

[1] https://www.gauss-centre.eu/results/elementaryparticlephysics/article/self-consistent-field-ensembles-of-disordered-hamiltonians-efficient-solver-and-application-to-super/
[2] M. Stosiek, B. Lang and F. Evers. 2020. Phys. Rev. B 101, 144503. (April 2020) DOI: 10.1103/PhysRevB.101.144503.
[3] M. Stosiek, F. Evers, and I. S. Burmistrov. 2021. Phys. Rev. Research 3, L042016. (Nov. 2021) DOI: 10.1103/PhysRevResearch.3.L042016.
[4] M. Stosiek, C. Baretzky, T. Balashov, F. Evers, W. Wulfhekel. 2021. arXiv:2107.01646. (Jul. 2021) DOI: https://arxiv.org/abs/2107.01646.
[5] A. Weiße, G. Wellein, A. Alvermann, and H. Fehske. 2006. Rev Mod Phys 78, 275 (Mar. 2006). DOI: https://journals.aps.org/rmp/abstract/10.1103/RevModPhys.78.275.

Gold Solvation in Supercritical Water

Research Institution
Lehrstuhl für Theoretische Chemie, Ruhr-Universität Bochum

Principal Investigator
Dominik Marx

Researchers
Harald Forbert, Jan Noetzel, Philipp Schienbein

Project Partners
–

SuperMUC Project ID: pr86fo

Introduction

Supercritical water and hydrothermal fluids have been focused on a broad range of scientific disciplines, in particular, the geology and geochemistry of the deep seafloor and the earth mantel's crust are intertwined with the solvation properties of water. Pure water reaches its supercritical phase at pressures and temperatures above 221 bar and 647 K, respectively, which defines the supercritical point of bulk water together with a density of 0.322 kg/L. Water is mostly present as SCW in the Earth's mantle and crust where it dissolves minerals and can ejects their solutions through so-called hydrothermal vents located in the deep sea [1]. Remarkably, the solvation properties of SCW can be systematically tuned by the external pressure, which ultimately changes the density of the fluid at a given temperature. This can be roughly understood in terms of the relative permittivity of water which drops from 78 at ambient conditions to 10–25 in the supercritical phase. The latter is in the order of typical apolar organic solvents and thus very different from normal water. Therefore, the solubility of neutral hydrophobic species is typically increased in SCW compared to water at ambient conditions, where they need to be incorporated in void-like structures available in the three-dimensional H-bond network [2]. In contrast, electrolytes do not show such simple trends: From phase diagrams of several binary electrolyte-water mixtures, one can classify electrolytes into soluble and generally insoluble in SCW following the trends in temperature. In the ”gas-like” regime (say below roughly 0.2 kg/L), even the soluble electrolytes get expelled from the homogeneous fluid phase, resulting in so-called ”supercritical phase separation” [3]. In such aqueous hydrothermal fluids, solvation and mass transport processes have been studied since long for many inorganic compounds like silica, sulfites and simples gases. Remarkably, it has been discovered recently that neutral metal clusters – in particular gold nanoparticles – are dissolved in the first place and subsequently transported in hydrothermal fluids, which provides an interesting explanation on how ore deposits are formed in Earth's crust [3]. Using AIMD, we simulate the neutral gold dimer and tetramer in SCW at a temperature of 750 K and a mass density of the solution below 0.3 kg/L. The fundamental aim of the present investigation is to find out how these neutral metal particles integrate themselves into the highly dynamical fluid environment offered by supercritical water. In order to understand their strongly anisotropic interactions with hot water, a detailed investigation of the effective dipole moments of both, the water molecules and the gold clusters as offered by the AIMD technique turned out to be crucial in order to disclose the all-decisive electronic many-body effects.

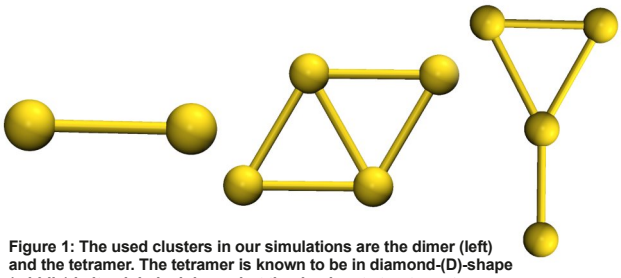

Figure 1: The used clusters in our simulations are the dimer (left) and the tetramer. The tetramer is known to be in diamond-(D)-shape (middle) in its global minimum but the dominant structure at our conditions is the Y-shaped tetramer (right).

Results and Methods

The present ab initio molecular dynamics (AIMD) simulations rely on the same validated electron structure protocol as our previous simulations of pure SCW [4] in line with previous work on aqueous solutions at both, ambient and high pressure conditions [5] using RPBE-D3 based density functional theory with a TZVPP basis at a cutoff of 500 Ry. In particular, all simulations are carried out using the CP2K software suite [6] for Born-Oppenheimer propagation of the electronic structure concurrently with the moving classical nuclei. Core electrons are implicitly considered using norm-conserving relativistic GTH pseudopotentials (leaving 11 valence electrons for Au). The initial gold dimer and tetramer species required for the AIMD simulations of the aqueous solutions as shown in figure 1 were inititally minimized using the electronic structure setup just described. From our previous AIMD studies of pure SCW [4], we used the last configuration often well-equilibrated NVT trajectories of the pure solvent system at 750 K and 0.2 kg/L to initialize pre-equilibrated aqueous solutions of the cluster at these supercritical conditions. Each system was equilibrated for 15 ps using Nosé-Hoover-Chain-based NVT simulations to ensure ergodic sampling at 750 K together with an AIMD integration time step of 0.5 fs. After 16 ps equilibration of each of these NVT simulations, we started to sample every 2 ps indepen-

dent initial conditions for subsequent NVE simulations, generating 24 such conditions for each cluster size. In these NVE simulations, with a length of 40 ps each, the electronic structure was localized every 1 fs for electronic structure analyses based on maximally localized Wannier functions, which allows us to define the dipole classically as sum over charge centers. As for pure SCW [4], we can separate the effective dipole into its main contributions from the water configuration, and the polarization of the electron density, represented by Wannier centers. The significant molecular dipole of water molecules in water at ambient conditions (being μ = 2.86 D for RPBE-D3 water [4]) stems from the pronounced electronic polarization and charge transfer effects (amounting to 1.0 D in the polarizational dipole) in the three-dimensional H-bond network that characterizes liquid water. In SCW at 750 K and 0.2 kg/L, however, the total dipole moment significantly drops to an average value of 2.15 D which is entirely due to the much reduced purely electronic contribution of only ≈ 0.3 D on average (whereas the average configurational contribution ≈ 1.9 D, is largely unaffected and thus constant across the relevant part of the phase diagram of water from ambient thermodynamic conditions to the covered supercritical region [4]), see figure 2A for the corresponding distributions functions. Given these considerations, we now compare the two contributions for all water molecules in the supercritical solution beyond the first solvation shell of the dimer andtetramer in panels B and C of figure 2, respectively, to pure supercritical water SCW in panel A. The corresponding distribution functions is close to perfectly overlap, thus water molecules beyond the first solvation shell around the gold clusters are electronically unaffected. A vastly different scenario is found for solvation water around the dissolved gold species. The electronic polarization and charge transfer effects between the gold clusters and the first shell water molecules lead to a significant enhancement of the polarization to average values of about 1.63 and 1.47 D for the dimer and tetramer, respectively (while the configurational contribution remains the same also in the first shell, as expected, and thus overlays with all other such distributions in figure 2), whereas this enhancement amounts to only ≈ 0.3 D on average in pure SCW. We conclude that water molecules close to gold species in supercritical water get enormously polarized by these neutral metallic solutes. This purely electronic effect explains the massive increase of the average total dipole moment of water molecules from 2.15 D in supercritical water at 750 K and 0.2 kg/L to 3.00 and 3.06 D for solvation water around the dimer and tetramer, respectively, at the same thermodynamic conditions.

Ongoing Research / Outlook

There are pronounced electronic polarization and charge transfer effects found between the neutral gold species and water. These many-body electronic couplings are evidenced by an enormous increase of the effective molecular dipole moment of first shell water molecules by roughly 50 % compared to the gas phase, whereas the second shell is barely affected. The magnitude of this enhanced molecular dipole moment at supercritical conditions even exceeds the one

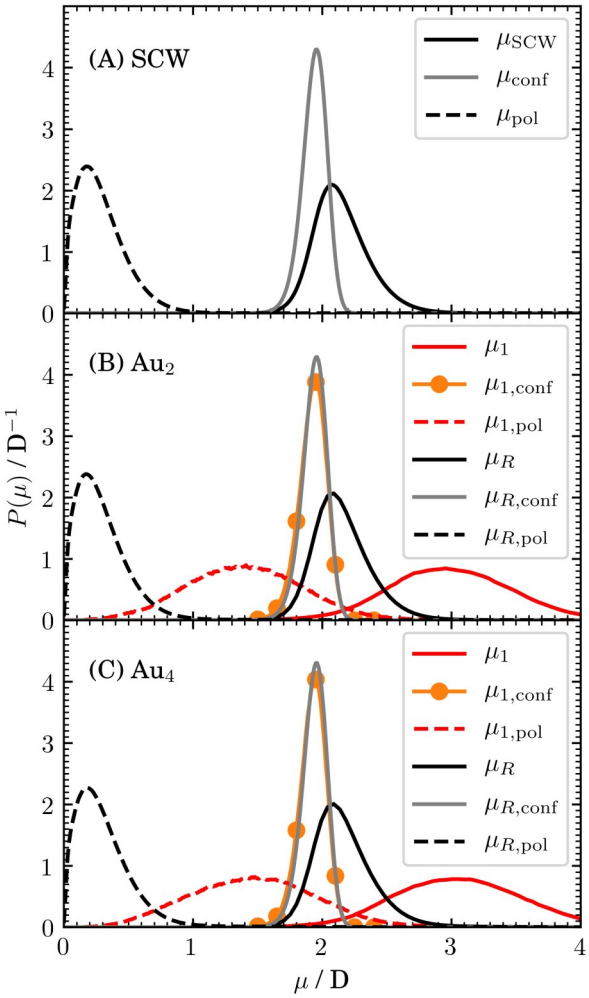

Figure 2: The probability distribution function of the total effective dipole of single water molecules (solid) can be separated into configurational (gray, orange), and polarization contribution (dashed). For the solvation systems, this distributions can be separated for water in the first shell around the clusters (red colors) and non-interacting bulk water (colorless).

in bulk liquid water at ambient conditions. Moreover, such a substantial increase is unknown for water molecules in the first solvation shell of simple ions in ambient water despite their full elementary charge. It is stressed that these crucial electronic effects cannot be generated in molecular dynamics simulations that rely on non-polarizable water models and force fields. Overall, solvation of neutral gold particles is overwhelmingly complex at high temperatures not only relevant to supercritical water but also to aqueous hydrothermal fluids. A next step will be to compute and assign vibrational spectra of these solutions in order to build a bridge from the detailed structural dynamics to experimental spectroscopy of supercritical and hydrothermal aqueous solutions.

References and Links

[1] W. Martin et al., Nat. Rev. Microbiol. 6, 805–814 (2008); A. Koschinsky et al., Geology 36, 615 (2008).
[2] Y. Marcus, Supercritical Water, Wiley-Blackwell 2012.
[3] C.A. Heinrich, Miner. Depos. 39, 864–889 (2005).
[4] P. Schienbein, D. Marx: Phys. Rev. E 98, 022104 (2018); J. Phys. Chem. B. 122, 3318–3329 (2018); Angew. Chem. Int. Ed. 59, 18578–18585 (2020); Phys. Chem. Chem. Phys. 22, 10462–10479 (2020).
[5] S. Imoto et al., Phys. Chem. Chem. Phys. 17, 24224–24237 (2015); S. Imoto, D. Marx, J. Chem. Phys. 150, 084502 (2019).
[6] https://www.cp2k.org/

Transition metal oxide surfaces and interfaces for electronic and energy conversion applications

Research Institution
Department of Physics, University of Duisburg-Essen

Principal Investigator
Rossitza Pentcheva

Researchers
Okan Köksal, Jiongyao Wu, Yuman Peng, Achim Füngerlings, Manish Verma

Project Partners
–

SuperMUC Project ID: pr87ro

Introduction

Artificial transition metal oxide-derived heterostructures offer a plethora of intriguing electronic phases, which are often not present in the bulk counterparts, opening the prospect to discover new materials for electronics, spintronics and energy conversion applications such as water splitting and thermoelectrics. Several examples obtained within pr87ro during the reporting period are selected: Within projects, funded by the DFG, CRC/TRR80, a topologically non-trivial phase was predicted in rocksalt-based EuO/MgO(001) superlattices (SLs) and a link was established between topological properties in systems with broken time-reversal symmetry and an enhanced thermoelectric performance. Moreover, the electronic reconstruction and the effect of strain in the double perovskite Sr_2CoIrO_6 was elucidated and the calculated optical absorption spectra including many body effects were compared to experiment. Finally, within a project funded by the DFG, CRC/TRR247 a detailed insight was gained into the effect of Co substitution on the performance of perovskite anode materials ($LaCo_xFe_{1-x}O_3$) in the oxygen evolution reaction. In particular, not only a reduction of overpotential at both Co and Fe reaction sites was found, Co showing the lowest values, but also involvement of cations from several coordination shells, pointing towards an extended active site.

Results and Methods

Chern insulating phases and thermoelectric properties of EuO/MgO(001) superlattices

Within this project funded by DFG, CRC TRR80 we investigated the topological properties and thermoelectric response in superlattices (SLs) containing the ferromagnetic (FM) insulator EuO and the wide band-gap insulator MgO. The systematic density functional theory simulations with a Hubbard *U* term (DFT+*U*) with the VASP and WIEN2k codes predict that spin-orbit coupling (SOC) opens a sizeable band gap of 0.51 eV in $(EuO)_1/(MgO)_3(001)$ SL strained at the lattice constant of MgO. This occurs due to a SOC-induced band inversion between the occupied majority 4f states and unoccupied minority 5d states of Eu (cf. Fig. 1a). A concomitant reorientation in the spin texture along the contour of band inversion of opposite parity surrounding the Γ point (cf. Fig. 1b) results in a Chern insulating phase with C = -1, accompanied by a broad Hall plateau in the anomalous Hall conductivity (AHC), which is also confirmed by the presence of a topological chiral edge state (not shown here). This Chern insulating phase exhibits promising thermoelectric properties, i.e., a Seebeck coefficient ranging from 400 to 800 μVK^{-1} as well as a power factor PF/τ of 1.2·10^{11} W K^{-2} m^{-1} s^{-1} at 600K (see Fig. 1c). The electronic contribution to the figure of merit $ZT|_{el} = \sigma S^2T/\kappa_{el}$ achieves in- and out-of-plane values of ≈ 0.8/0.9 at the valence/conduction band edges. The enhanced Seebeck coefficient and sizeable electronic conductivity emerge due to the simultaneous presence of localized and dispersive bands along

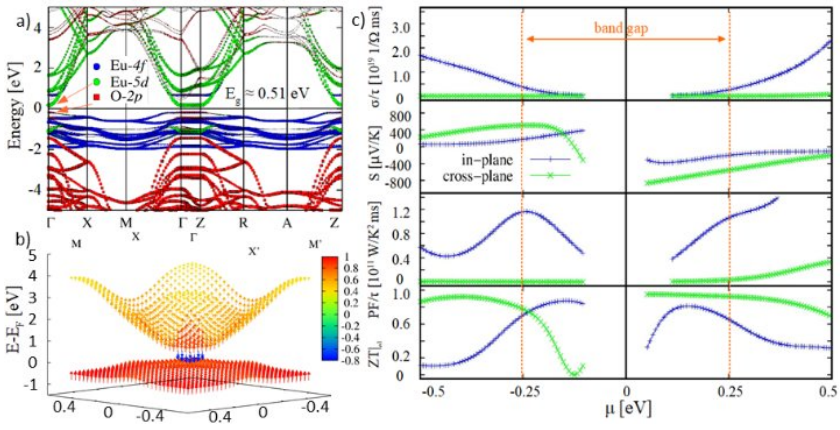

Figure 1: a) Band structure with SOC for FM $(EuO)_1/(MgO)_3(001)$; b) spin texture in k-space from the DFT+U+SOC calculation with magnetization along [001] for the topmost-occupied and lowest-unoccupied bands while the color scale denotes the projection on the z axis with red (blue) indicating parallel (antiparallel) orientation. c) in- and cross-plane components of the electrical conductivity tensor divided by the relaxation time the Seebeck coefficient, PF/τ and the electronic contribution to the figure of merit $ZT|_{el}$ are plotted as a function of the chemical potential μ at 600 K.

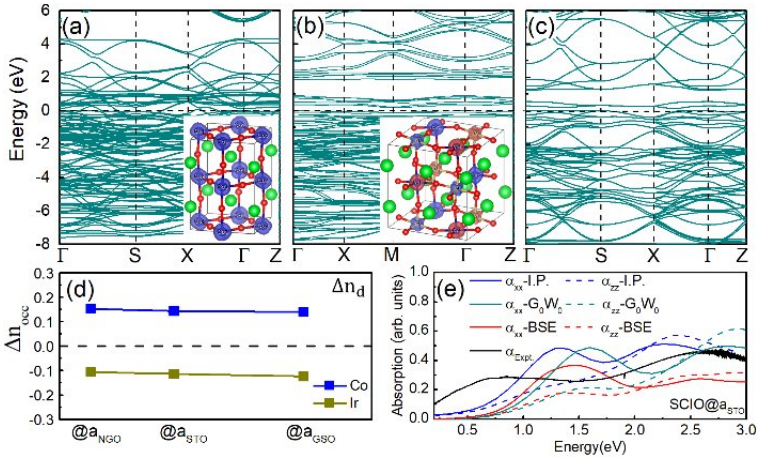

Figure 2: DFT+U+SOC band structure of the end members (a) $SrCoO_3$ and (c) $SrIrO_3$ and (b) Sr_2CoIrO_6 at a_{STO}. In (a) and (b) also the respective spin densities are shown (d) changes in total Co 3d (blue) and Ir 5d (yellow) occupation number in SCIO with respect to the one in the end members SCO, SIO as a function of biaxal strain. (e) The absorption coefficient of I.P. (blue line), G_0W_0 (petrol line) and G_0W_0+BSE (red line) approximation for SCIO@a_{STO} in comparison with the one obtained from transmission measurements (black line). The in- and out-of-plane components are denoted by solid and dashed lines, respectively.

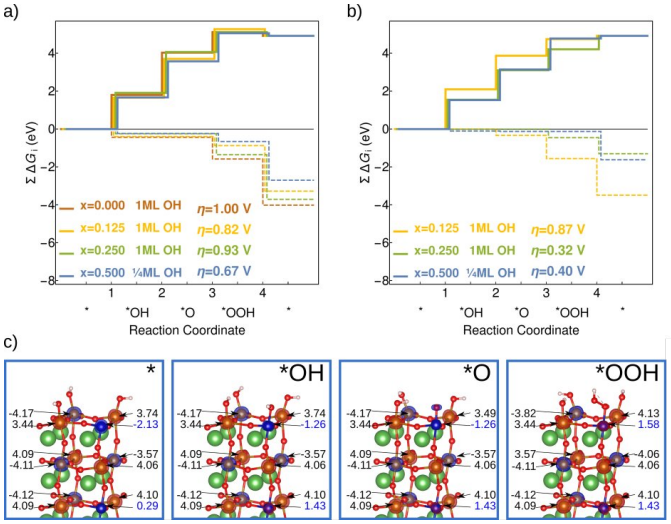

Figure 3: (Cumulative reaction free energies of reaction intermediates and corresponding overpotentials at (a) Fe and (b) Co reaction sites at $LaCo_xFe_{1-x}O_3$(001); (c) magnetic moments of cations in the top three layers of the $LaCo_{0.125}Fe_{0.875}O_3$ (001) slab for the different intermediates during OER.

the Γ-Z direction (cf. Fig. 1a) and highlights the link between Chern insulating behavior and thermoelectric properties.

Electronic reconstruction and charge transfer in strained Sr_2CoIrO_6 double perovskite

The electronic, magnetic and optical properties of the double perovskite Sr_2CoIrO_6 (SCIO) under biaxial strain were studied systematically within density functional theory including a Hubbard *U* term and SOC by employing the VASP code on SuperMUC-NG. The end member $SrCoO_3$ (SCO) is a ferromagnetic metal with a spin and orbital magnetic moment of 2.50 and 0.13 μ_B, respectively (Fig. 2a), whereas bulk $SrIrO_3$ (SIO) is a semimetal with a quenched spin and orbital moment (Fig. 2c). In contrast, the double perovskite SCIO emerges as an antiferromagnetic Mott insulator (Fig. 2b) with a Co spin and enhanced orbital moment of ~2.4 and 0.35 μ_B. Simultaneously, Ir acquires a significant spin and orbital moment of ~1.2 and 0.13 μ_B, respectively.

Analysis of the orbital occupation indicates an electronic reconstruction due to a charge transfer from minority to majority spin states in Ir, leading to the finite magnetic moment and ~0.15e^- from Ir to Co (Fig. 2d) resulting in an $Ir^{4+\delta}$, $Co^{4-\delta}$ configuration. Moreover, the band gap changes nonmonotonically with biaxial strain from 163 meV (a_{NdGaO_3}) through 235 meV (a_{SrTiO_3}) to 187 meV (a_{GdScO_3}). Overall, many body effects improve the agreement of the calculated absorption coefficients with the experimental results (Fig. 2e) [3].

Synergistic Effects of Co and Fe on the Oxygen Evolution Reaction Activity of $LaCo_xFe_{1-x}O_3$ (LCFO)

DFT+*U* simulations carried out on SuperMUC-NG in the framework of CRC/TRR247 show that the overpotential required to facilitate the oxygen evolution reaction (OER), the sluggish half-reaction of electrochemical water splitting, can be decreased by partially replacing iron with cobalt in the perovskite anode material $LaFeO_3$ [4]. In order to examine the influence of Co on the catalytic activity and to shed light on the underlying mechanism, the energetics of different OER intermediates was assessed using LCFO(001) slabs containing ~130 atoms. The cumulative reaction free energies and the resulting overpotentials for Fe and Co reaction sites are shown in Fig. 3a and b. The calculations indicate that the effect of Co incorporation on the catalytic activity is twofold: On one hand, Co exhibits a 0.3 V lower overpotential than Fe; on the other hand, the overpotential is lowered also at the Fe reaction sites in the presence of Co. Overall, the nonmonotonic dependence on *x* was also confirmed experimentally [4]. The spin densities of intermediates shown in Fig. 3c exemplary for *x*=0.125 reveal dynamic changes of magnetic moment during OER in particular for Co with participation even of cations in deeper layers, indicating their participation in the active site [4].

Ongoing Research / Outlook

The access to SuperMUC-NG was essential to achieve the reported results due to the large system sizes and number of studied configurations. Currently, the investigations within CRC TRR80 are extended to further superlattices and thin films [5], whereas further spinel [6] and perovskite surfaces are studied within CRC TRR247 to correlate the structural patterns and environment to the catalytic performance.

References and Links

[1] https://www.uni-due.de/physik/pentcheva/
[2] O. Köksal, R. Pentcheva, Phys. Rev. B 103, 045135 (2021).
[3] J. Wu, M. Zöllner, S. Esser, V. Begum, G. Prinz, A. Lorke, P. Gegenwart and R. Pentcheva, Phys. Rev. B 104, 205126 (2021).
[4] A. Füngerlings, A. Koul, M. Dreyer, A. Rabe, D. M. Morales, W. Schuhmann, M. Behrens, R. Pentcheva, Chem. Eur. J. 27 17145-17158 (2021).
[5] R. Di Capua, M. Verma, M. Radovic, N. C. Plumb, J. H. Dil, Z. Ristic, E. B. Guedes, G. M. De Luca, D. Preziosi, Z. Wang, A. P. Weber, R. Pentcheva, M. Salluzzo, Phys. Rev. Res. 3, L042038 (2021).
[6] Y. Liu, Y. Peng, M. Naschitzki, S. Gewinner, W. Schöllkopf, H. Kuhlenbeck, R. Pentcheva, B. Roldan Cuenya, Angew. Chem. Int. Ed. 60, 16514-16520 (2021).

Planetary Core Properties and Magnetic Field Generation

Research Institution
Earth and Planets Laboratory, Carnegie Institution for Science and LMU Munich

Principal Investigator
R. E. Cohen

Researchers
–

Project Partners
–

SuperMUC Project ID: pr92ma

Introduction

The properties of the iron alloy in Earth's core and in other planetary cores govern the generation of the planetary magnetic field, which is important for the possibility of life on the planet's surface. It is difficult to do experiments at such conditions of pressure and temperatures, millions of atmospheres of pressure and temperatures of many thousands of degrees, so we use first principles theory to help understand deep planetary interiors. We start with electrons and nuclei, at the atomic level, and compute properties of core materials at the extreme conditions of Earth's core and beyond [1]. Earth's core is not pure iron (Fe), and here we address the effects of silicon (Si) on the transport properties of Earth's core. We study the electrical and thermal conductivity of iron alloy with silicon and compare with pure iron. We collaborate with experimentalists who also measure properties at pressures somewhat lower than those in the center of the Earth. This work is also important for modeling exoplants to see whether they can generate a magnetic field and thus support life.

Magnetic fields in planets are generated from convective motion in the liquid core. In the Earth and planets up to 10 times the size of the Earth, the core is mostly iron with small amounts of other elements. The flow that generates a magnetic field depends on the thermal conductivity of the fluid—if it is too high, the core will not convect and generate a magnetic field simply from cooling, but would require an additional mechanism like chemical precipitation to drive flow. Not every planet has a magnetic field. For example, Venus, close in size to the Earth, does not.

Although thermal conductivity is a crucial parameter, it is easier experimentally to determine the electrical resistivity, which is related to the thermal conductivity using the 1853 Wiedemann-Franz law. They are related because the same objects, electrons, carry the electrical charge, and the energy that results in heat flow. However, the accuracy of the Wiedemann-Franz law at extreme conditions is unknown since has not tested at the conditions of planetary cores. Thus, we compute both the thermal and electrical conductivity to better understand the physics, to assist with interpretations of experiments, and to provide information to geodynamicists who model planetary cores.

We can compute properties of both liquids and solids, whereas the experiments are nearly impossible for liquids. Since it is the properties of the liquid outer core of the Earth that flows and causes the formation of the magnetic field, our computations for the liquids are crucial to understand planets, and to apply the experimental results to planets.

Results and Methods

We first simulate iron alloys at extreme conditions of pressure and temperature using first-principles molecular dynamics (FPMD). We solve Newton's law, $F = m \cdot a$, where m is the atomic mass, F is the force on the atom, and a is its acceleration. We evaluate the forces using quantum mechanics within density functional theory (DFT), which allows efficient and accurate solution to find the quantum mechanical forces from all the electrons on each atom. In order to equilibrate the structure and obtain accurate properties such as pressure, we need to simulate 5-10 picoseconds (ps), where 1 ps is 10^{-12} (0.000000000001) seconds. We step forward in time with a femtosecond timestep, 1,000 times smaller than a picosecond. By studying properties at electronic time and length scales (1 angstrom, or 10^{-10} meter), we better understand properties of planetary cores (Earth's core has a radius of 3,486 km) over billions of years (GY). Each time step involves a heavy computation for hundreds of atoms, or over 1,000 electrons, so we need to use a supercomputer like the SuperMUC-NG. Then we need to study many conditions of pressure and temperature and composition in order to understand planetary cores. After we obtain the trajectories from FPMD, we evaluate the transport properties, such as electrical resistivity and thermal conductivity using sophisticated quantum methods.

We found surprisingly that a small amount of silicon (Si) dissolved in iron totally changes its behavior. In iron and other metals, the electrical resistivity at moderate and high temperatures is linear in temperature. That is because the electrical resistivity comes from scattering of electrons by atomic thermal vibrations, and the atoms vibrate more with increasing temperature. However, when we add Si, we find a nearly

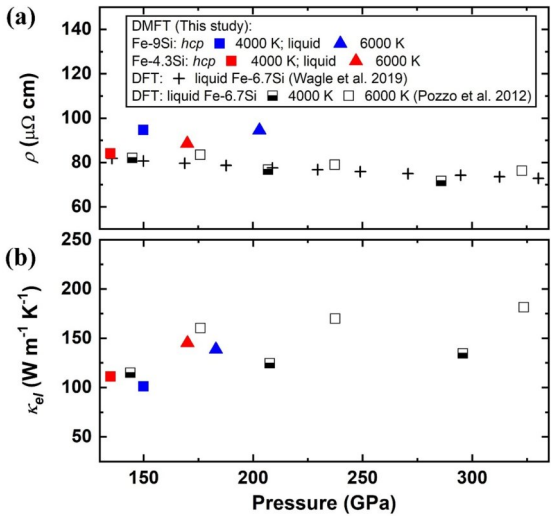

Figure 1: Electrical resistivity from computational theory and experiments for pure iron and for iron-silicon alloy with a few percent silicon. The calculations agree quite well with the experiments, both of which are extremely difficult. From [2].

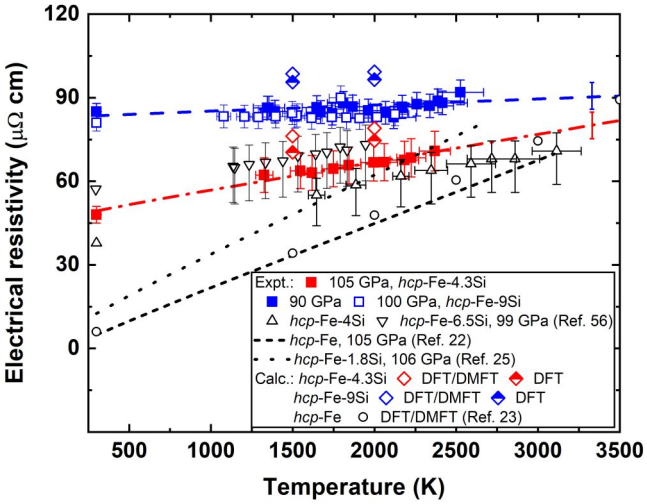

Figure 2: Computed electrical resistivity ρ and thermal conductivity κ versus pressure for Fe-Si alloys, and comparing with previous work. We find good consistency with different studies and little pressure effect. From [2].

temperature independent resistivity (Fig. 1). We find that the resistivity comes primarily from electrons scattering off the Si atoms, rather than from vibrations. Our computational results agree well with experiments that we recently published together [2]. We were also able to compute the thermal conductivity and test the validity of the Wiedemann-Franz law, . We found that it holds quite well, but *L* is not a constant but depends on the composition. Contrary to intuition, a temperature independent resistivity ρ makes the thermal conductivity *κ* more temperature dependent. Therefore, Si may make it harder for a dynamo to work from pure thermal convection. We found that thermal conductivity is not a strong function of pressure (Fig. 2), which is helpful since experiments under core conditions are extremely difficult. However, very high temperatures, difficult to reach in the lab, could change behavior depending on composition.

We found that melting to the liquid causes little or no change in transport properties under extreme conditions. This was a surprise, as people had assumed that the liquid would have a higher resistivity due to disorder. This makes it easier to apply the experimental results directly to understand planets.

Ongoing Research / Outlook

Now we are studying other dopants, including C, H, O, Ni, and N. We are also developing and testing faster methods by using our large scale FPMD simulations as benchmarks to test simpler approximations. We are also studying compounds such as FeS, which is thought to be important in smaller planets like Mars.

Fundamental to understanding planetary interiors is the equation of state, the relationship between pressure, temperature, volume, and composition, and the melting curve. Together with experimentalists we recently published the highest pressure high temperature experiments on the iron equation of state and melting curve [3], and found that indeed iron remains hcp (hexagonal close packed, the structure we studied above) through the Earth and superEarths, that is exoplanets with up to ten times the size of the Earth.

We also study other problems on the SuperMUC-NG, both for planetary interiors and for technological materials. We recently published a study of magnesium germanate Mg_2GeO_4 along with experimental colleagues [4]. Germanates do not form in planets, but silicates form the bulk of planetary mantles, and germanates are analogues to silicates—they form similar crystal structures, but at lower pressures than silicates. Superearths contain different crystals than Earth, due their very high interior pressures. We can find such new structures first by studying germanates. Experiments showed that magnesium and germanium substitute for each other in Mg_2GeO_4 at high pressures and temperatures.[5] This was very surprising because they are very different elements, and do not do so at lower pressures and temperatures. We used computational theory and FPMD to study Mg_2GeO_4 and found indeed that Mg and Ge are disordered, but not completely disordered, making a better interpretation of the experimental data. We are now studying silicates computationally, which are harder to study in the lab at the required higher pressures.

We also study technological materials. We predicted new clathrates [6,7], new polar oxynitrides [8] and new polar metallocenes [9].

References and Links

[1] Y. Zhang et al., Phys Rev Lett 125 (2020) 078501.
[2] Y. Zhang et al., Proc Natl Acad Sci U S A 119 (2022).
[3] R. G. Kraus et al., Science 375 (2022) 202.
[4] R. Dutta et al., (2021).
[5] R. Dutta et al., Proc Natl Acad Sci U S A 119 (2022).
[6] L. Zhu et al., Sci Adv 6 (2020) eaay8361.
[7] L. Zhu et al., Phys Rev Lett 125 (2020) 127601.
[8] L. Zhu et al., Physical Review Materials 5 (2021).
[9] H. Zhang et al., molecules 24 (2019).

Numerical simulations of topological and correlated quantum matter

Research Institution
[1]Institut für theoretische Physik und Astrophysik, Universität Würzburg

Principal Investigator
Florian Goth[1]

Researchers
Armando Consiglio[1], Lorenzo Crippa[1], Philipp Eck[1], Florian Goth[1], Domenico Di Sante[1,2], Giorgio Sangiovanni[1], Ewelina Hankiewicz[1], Andreas Hausoel[1]

Project Partner
[2]Flatiron Institute, New York

SuperMUC Project ID: pr94vu

Introduction

This project provides computational resources to the numerically oriented research lines of the SFB 1170 on Topological and Correlated Electronics at Surfaces and Interfaces. A central pillar of our research is the combination of efforts from numerical and experimental groups. We start this report by showcasing examples of this approach. The first paragraph reports on the detailed microscopic mechanism of adsorption on RuO_2. The second paragraph highlights the numerical prediction of Indenene as a quantum spin Hall (QSH) insulator together with its experimental realization. These results have been mainly obtained using Density Functional Theory (DFT) techniques. The last paragraph broadens the scope to a study of the Bernevig-Hughes-Zhang (BHZ) model with a cluster extension of Dynamical Mean Field Theory (DMFT). Here a detailed study of the structure of the self-energy was performed and the cross over from a local to a non-local behaviour as a function of interaction strength was found. We highlight that only the combination of the computing resources of SuperMUC-NG with numerical techniques made these experimentally relevant findings possible.

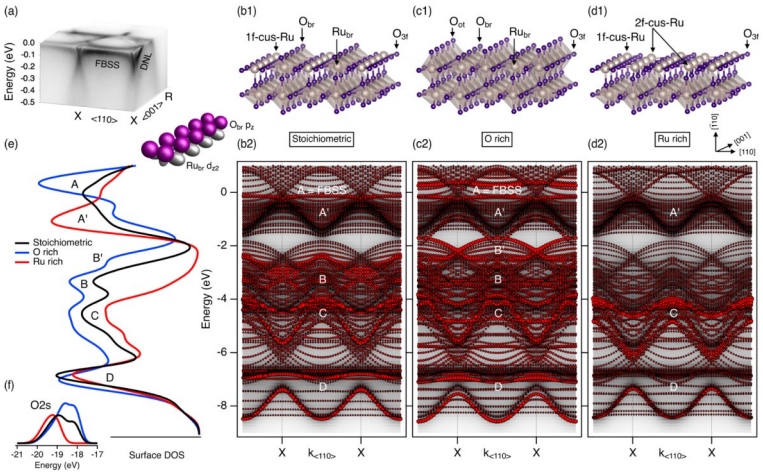

Figure 1: FBSS on RuO_2(110). (a) Angle-resolved photoemission spectroscopy (ARPES) Fermi surface (b-d) Crystal structure and DFT band structure of the stoichiometric (b), oxygen-rich (c), and the ruthenium-rich RuO_2 (110) surface (d). The marker size indicates the surface oxygen character. The gray background is the surface projection of the bulk band structure. (e) Valence and (f) O 2s surface DOS of the stoichiometric (black), the oxygen-rich (blue), and the ruthenium-rich RuO_2 (110) surface (red). Feature "A" labels DOS of preliminary Ru 4dz2 character that forms the FBSS, feature "A' " the DOS composed of under-saturated Ru 4d states. Features "B", "B' ", and "C" are of predominantly O 2p character and feature "D" of mixed orbital character.

Results and Methods

Adsorption of Small Molecules on the (110) Surface of the Dirac Semimetal RuO_2

We studied collaboratively with experimental groups from Würzburg, Berkeley and Auckland the heterogeneous catalysis on the (110) surface of ruthenium dioxide (RuO_2). This particular material gained attention because of its electronic and magnetic properties, that allow to study a variety of catalytic oxidation and dehydrogenation reactions on its surface. The goal was to gain a microscopic electronic understanding of these processes, to complete the picture provided by previous thermodynamic-oriented studies; we then focused on the interplay existing between the catalyst's delocalized electronic band structure and the localized orbitals of its surface reactants. Indeed, the catalytic qualities are directly related to the properties of its Fermi surface, with antiferromagnetic instabilities driven by a particularly large density of states. The electronic structure induced by the crystal symmetry produces a complex Fermi surface composed of Dirac nodal lines and a consequent flat band surface state (FBSS), the latter having an active role in catalytic charge transfer processes at the oxygen bridge sites. Being tuned by surface doping and an electrostatic environment, the FBSS presents an interesting playground for the study of surface chemistry. Well-known surface adsorption processes (e.g. H_2 and CO) have hence been monitored, looking at the response of the electronic band structure and at the orbital origin of the FBSS. The main result of the work, obtained through site-selective surface reactions, is that the delocalized surface electronic band structure of the catalyst actively participate in the catalytic processes. [1]

Indenene: Honeycomb Quantum Spin-Hall Physics on the triangular lattice

QSH insulators hold promises for a more efficient and sustainable technology. At odds with conventional semiconductors, the current flows on their boundaries, with scattering becoming prohibited thanks to symmetry arguments. In the search for new topological materials, most of the theory efforts hitherto have been focusing on two-dimensional atom layers in a honeycomb arrangement. The motivation comes from graphene, the "Drosophila" of the QSH systems. Here we pursued instead an alternative route and discov-

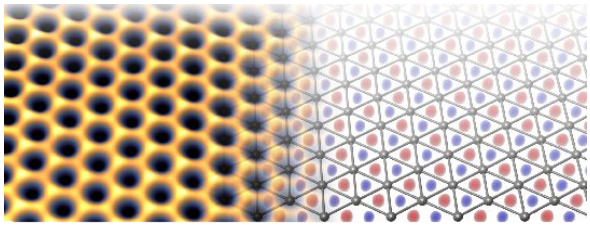

Figure 2: (left half) The calculated electronic charge density (blue and red) of the triangular indium lattice (gray spheres) accumulates not at the atomic positions but instead at the void sites. This classifies indenene as a QSH insulator. (right half) The experimentally measured charge density of indenene shows the predicted honeycomb charge pattern.

ered indenene: a triangular indium lattice on a silicon carbide substrate. This idea was made real in [2] in collaboration with our colleagues from Experimental Physics IV in Würzburg, who have grown the indenene samples with molecular beam techniques. From the very beginning of the project, state-of-the-art *ab initio* DFT simulations were performed on SuperMUC with the aim to calculate the structural and electronic properties of indenene. Further, a detailed analysis of the localization of the electronic wave function unveiled an emergent sublattice pattern, i.e. a charge localization in the voids of the triangular lattice. This hidden honeycomb in combination with modern solid state theory allowed us to identify indenene as a QSH insulator. Lead by the theoretical prediction, the experiment shows indeed a honeycomb charge localization, as summarized in Fig. 2. This allows us to classify indenene as a QSH insulator. The unique materials design that has led to the synthesis of indenene may improve the current technological status in the field of topological electronics: In contrast to graphene, the triangular arrangement allows for a large-gap QSH phase. Therefore, indenene needs not to be cooled down to ultra-low temperatures to manifest its properties as a topological insulator. This is a consequence of the particularly simple triangular lattice. Further, it allows for large structural domains, often a severe bottleneck in the synthesis of other topological materials and an indispensable prerequisite required for device nanofabrication.

Dynamical Mean-Field Theory study of the Bernevig-Hughes-Zhang model

The interplay between the topological properties of condensed matter systems and the effects of electronic interaction has been an interesting topic of research in recent years. It is especially interesting to understand how the momentum-dependent topological properties and the local Coulomb repulsion come together to influence the properties of a solid state system. To this end, many-body techniques such as DMFT have proven to be extremely successful, disclosing some critical topological phenomena beyond the usual non-interacting band theory. A limitation of this approach is, however, the complete locality of the electronic correlation effects, discarding many-body correlations between electrons on different lattice sites. To include these effects, extensions of DMFT have been devised, that study effective clusters of lattice sites in real space, and infer from their properties the correlation patterns of electrons on the original lattice, while keeping the form of the interaction completely on-site, i.e. local. The downside of

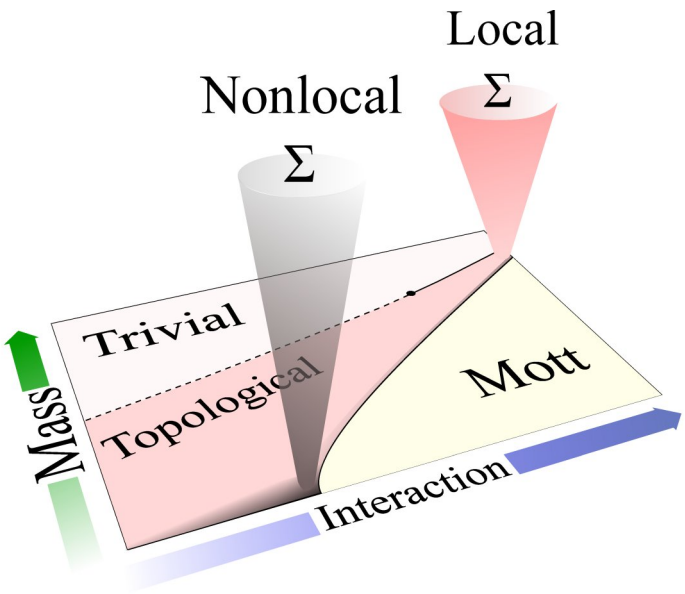

Figure 3: Illustrative phase diagram of the interacting BHZ model, as a function of the local interaction strength U and the atomic orbital splitting M. Three different regions, trivial insulator, topological insulator and Mott insulator are present. The self-energy behavior varies strongly within the same topologically insulating phase in different regions of the phase diagram.

these techniques is the increased computational cost, which especially in an exact-diagonalization based approach involves the solution of an eigenvalue problem whose size in principle scales exponentially with the number of cluster sites. Exploiting the symmetries of the system the overall Hamiltonian can be decomposed in smaller, easy to treat decoupled blocks. In [3] we applied such techniques to a well-known topological insulator, the BHZ model. We inspect the cluster self-energy, an object which encloses all the effects of the interaction at the single-particle level. This is found to change widely in different regions of the parameter space: at one end, nonlocal correlation effects are completely negligible, and in this region the cluster-DMFT results completely agree with their single-site counterparts. At the opposite end of the parameter space, the self-energy becomes strongly non-local, thereby extending and completing the single-site picture and hinting at the possible presence of a wider palette of competing phases. Next steps include the comparison between the BHZ model, where the topology is a consequence of the on-site orbital structure, and the Kane-Mele model, where it follows from the sublattice structure of the honeycomb lattice, hence in principle entailing a bigger role for nonlocal correlations.

References and Links

[1] Jovic et al., ACS Catalysis 2021 11 (3), 1749-1757.
[2] Bauernfeind, M., Erhardt, J., Eck, P. et al., Nat Commun 12, 5396 (2021).
[3] L. Crippa, A. Amaricci, S. Adler, G. Sangiovanni, and M. Capone, Phys. Rev. B 104, 235117 (2021).

Computational Fluid Dynamics and Engineering

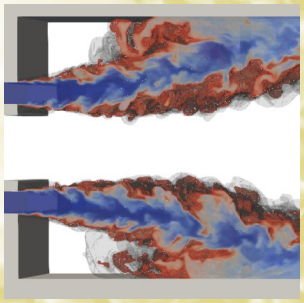

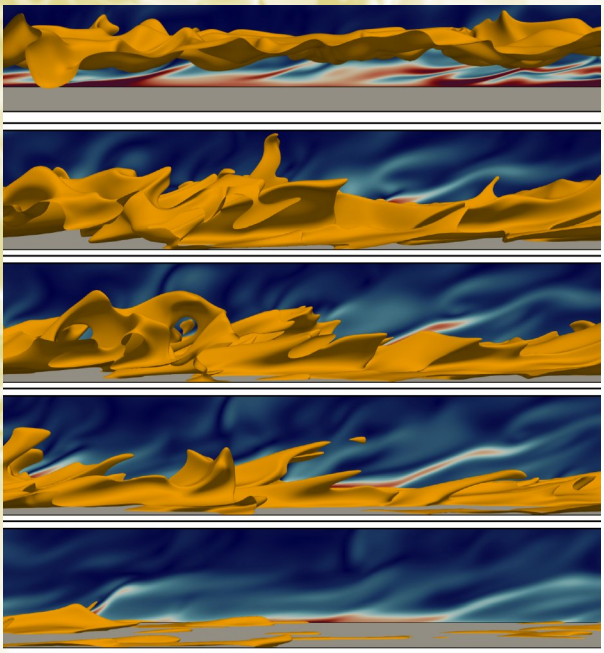

Uncertainty Quantification of Buoyancy-Induced Mixing Processes

Research Institution
[1]Numerical methods in Aerospace Engineering, Bundeswehr University Munich

Principal Investigator
Philipp J. Wenig[1]

Researchers
Ruiyun Ji[1,2], Stephan Kelm[2], Markus Klein[1]

Project Partner
[2]Institute for Energy and Climate Research (IEK-6), Forschungszentrum Jülich

SuperMUC Project ID: pn29ce

Introduction

The overall scientific and technical goal of the present project is to establish a methodology for quantifying the propagation of uncertainties in CFD calculations and the further development of existing methods to optimize the computational effort. Imprecise knowledge of physical properties, model parameters as well as initial and boundary conditions leads to uncertainties in the results of numerical simulations. In some applications, where safety issues are of great importance for the engineering design such as in plant and reactor design, the consideration of uncertainties is essential.

Representative for the later analysis of the THAI-TH32 experiment, which examines the erosion of a stratified helium layer by natural convection in a containment, the Differentially Heated Cavity (DHC) with aspect ratio 4 with superimposed mixing process is investigated. This allows for gradual development of guidelines to quantify the uncertainty of natural convection flows in large-scale industrial applications. The methods for Uncertainty Quantification (UQ) can be transferred to other technical issues and constitute a new cornerstone in the design of reliable engineering applications.

Results and Methods

Three-dimensional large eddy simulations (LES) of the buoyancy-driven mixing process of air and helium within the DHC have been performed. Low Mach number flow of two Newtonian viscous fluids with assumed periodic flow in the third spatial direction is considered. The DHC comprises a hot wall on the left with the temperature T_{left} and a cold wall on the right with the temperature T_{right}. At the top and bottom of the considered cavity temperature profiles were defined. In addition, a vertical temperature gradient $\nabla T|_{wall}$ was defined at the left and right wall. 40 vol% of linear distributed helium was defined in the upper third of the DHC next to air. The simulation setup is schematically shown in Fig. 1.

Several input parameters were considered as uncertain. The thermal boundary conditions like the wall temperature difference ΔT between the left and right walls, the vertical wall-tangential temperature gradient $\nabla T|_{wall}$ at the left and right walls and the temperatures at the top and bottom walls, T_{top} and T_{bottom} respectively. Uncertainty in the initial helium stratification is modeled by a varying linear profile for the mole fraction X. The molecular diffusion coefficient D of the binary mixture is also subject to uncertainty.

The open-source C++ toolbox OpenFOAM v.2006 was utilized for solving the non-linear set of governing equations in a finite-volume framework. The pressure velocity coupling has been addressed by means of the PIMPLE-algorithm. The convective and diffusive fluxes were evaluated by second-order linear upwind and linear schemes, respectively. Temporal advancement was achieved by the second-order Crank-Nicolson scheme. It has been ensured that the Courant number is always below the value of 0.5. Furthermore, the open-source software Dakota 6.12 was utilized as the uncertainty quantification framework. For the evaluation of results non-intrusive Polynomial Chaos Expansions (PCE's) and Karhunen-Loève expansions (KLE's) were applied.

The stochastic processes of quantities, that are important for the evaluation and understanding of the buoyancy-driven mixing process, are represented by the expectation value μ, the standard deviation σ and the quantile functions Q and plotted against the Fourier number Fo, which allows for the dimensionless description of time. In Fig. 2 the stochastic processes of the mixture uniformity Σ_X, the left wall Nusselt-number Nu and the global kinetic energy E_k are visualized. The gradual achievement of the homogenous state can be quantified by the mixture uniformity Σ_X. Σ_X = 1 describes a completely inhomogeneous mixture and Σ_X = 0 characterizes a completely homogenous mixture. The convective heat transfer in the cavity is evaluated by the left-wall Nusselt-number Nu. Effects on the convection mechanisms are described by the global kinetic energy E_k.

The evolution of the mixture uniformity in Fig. 2a reveals that the mixing process consists of the initial diffusive dissolution and the subsequent convective erosion of the helium layer. The transition to the convective erosion phase is evident from larger gradients of the mixture uniformity towards the end of the mixing

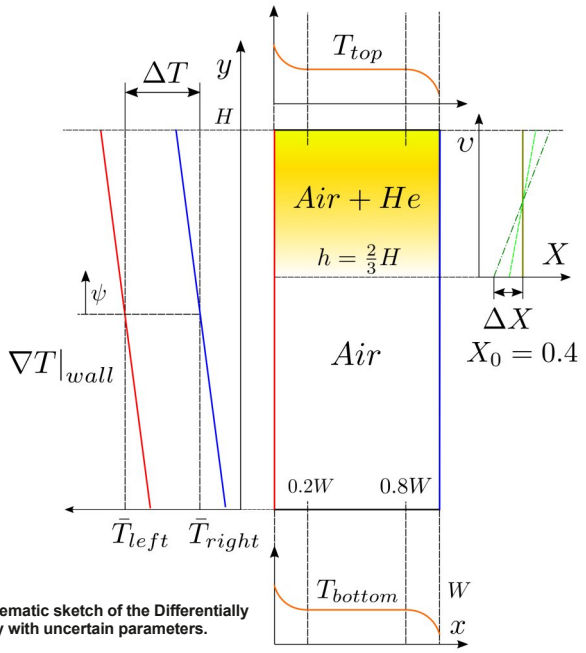

Figure 1: Schematic sketch of the Differentially Heated Cavity with uncertain parameters.

process. Moreover, the duration of the mixing process varies, when the realization of the random input parameters changes. Through the consideration of the stochastic processes of the Nusselt number and the global kinetic energy, shown in Fig. 2b and c respectively, one can see, that a dynamic transient process takes place at the beginning. This is followed by the aforementioned diffusive dissolution phase, which becomes visible through the narrow uncertainty band. Finally, the convective erosion occurs, which involves a larger uncertainty band due to the dynamic transition to the new equilibrium state.

The applied approximation of results by non-intrusive PCE's is distinguished by its efficiency due to its high convergence rate of the stochastic results with an increasing number of simulation runs. Furthermore, the analytical representation of stochastic processes facilitates reliability and risk assessment of engineering applications in the early stage of the design process.

Ongoing Research / Outlook

The selected methodology, which includes the estimation of statistical moments through Deterministic Sampling and the representation of stochastic results by means of PCE's and KLE's, will be applied for the CFD-simulation of the THAI-TH32 experiment, for which there is a large number of uncertainties present in thermal boundary conditions, initial conditions and in the structural model design.

References and Links

[1] P.J. Wenig, R. Ji, S. Kelm and M. Klein. Fluids 2021, 6, 161. https://doi.org/10.3390/fluids6040161
[2] P.J. Wenig, R. Ji, S. Kelm and M. Klein. ETMM-13, 2021.
[3] R. Ji, P.J. Wenig, S. Kelm and M. Klein. NURETH-19, 2021.

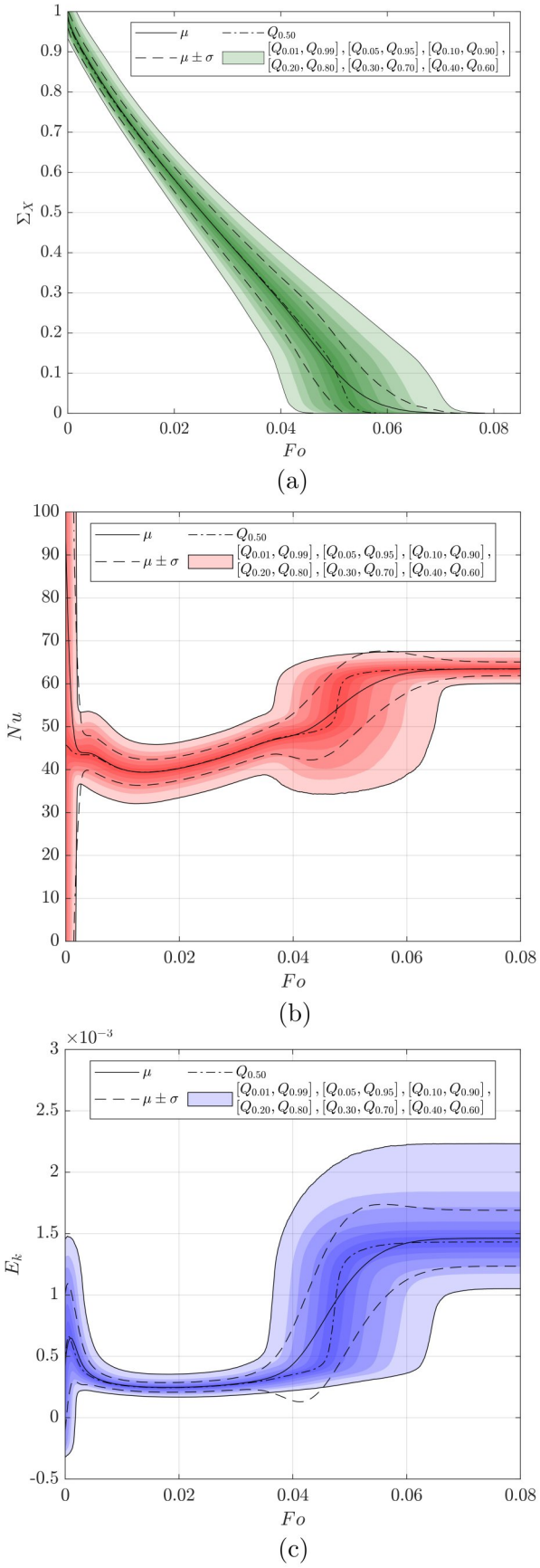

Figure 2: Representation of stochastic processes using expectation value μ, the standard deviation σ and quantile functions *Q:* (a) Mixture Uniformity σ_X, (b) Nusselt-number *Nu* and (c) Global kinetic energy E_k over dimensionless time *Fo*.

The Influence of Flame-Wall Interaction on CO Emissions in Gas Turbine-like Conditions

Research Institution
Institute for Combustion Technology, RWTH Aachen University

Principal Investigator
Heinz Pitsch

Researcher
Kai Niemietz

Project Partners
–

SuperMUC Project ID: pn29gu

Introduction

Renewable energy sources play an increasing role in the energy sector. However, wind and solar power provide decentralized and often fluctuating contributions, which create new challenges in managing the electrical grid and balancing electricity production and consumption. Stationary gas turbines can help balance the electrical grid, since they have faster start-up times and more load flexibility than most other conventional power plants. To increase the incorporability of renewables, the load flexibility of gas turbines needs to be further improved. At low- and part-load conditions, local quenching of the combustion process occurs resulting in increased emissions. The main pollutant in low-load gas turbine operation is carbon monoxide (CO). Generally, CO emissions are reduced by leaner mixtures because the equilibrium concentration is lower. However, it is observed that CO emissions sharply increase at very lean conditions. One of the mechanisms causing this behavior is linked to the fact that the oxidation from CO to CO_2 is disturbed by flame-wall interaction (FWI). This interaction between flame and cold walls "freezes" CO oxidation above the nominal equilibrium value, yielding CO emissions above the chemical equilibrium. This project aims to further investigate the effects of FWI and turbulence on the CO oxidation process by means of direct numerical simulations (DNS). Thereby, all details of the flow and chemical reactions can be thoroughly studied.

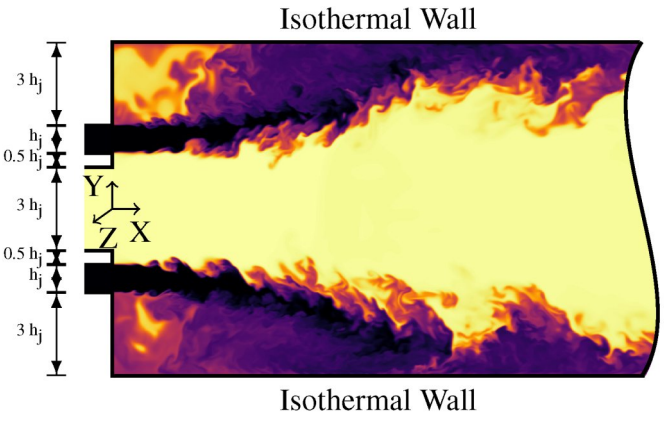

Figure 1: Schematic of the simulation domain. The coloring indicates the temperature field. The inflow consists of two turbulent jets with a pilot in the center.

Results and Methods

Numerical Framework
The governing equations of the DNS are given by the reacting Navier-Stokes equations in the low-Mach limit. For the computation, an in-house code named CIAO is employed. CIAO solves the Navier-Stokes equations along with multi-physics effects. It is a structured, arbitrary order, finite difference code. A low-Mach solver is available within the framework, which uses Crank-Nicolson type time advancement along with a predictor-corrector update scheme. The simulations are run with finite rate chemistry, employing a skeletal mechanism for lean premixed methane/air combustion. Species and temperature equations are discretized by a third order WENO scheme ensuring bounded solutions. Spatial and temporal staggering of flow variables is used to increase the accuracy of the numerical stencils. Temperature and species equations are advanced by introducing the symmetric operator split of Strang. The chemistry operator uses a time-implicit backward difference method, as implemented in CVODE, which is a widespread software package for integrating stiff ODEs. For further details about the applied numerical algorithms and code verification, the reader is referred to [2]. The code uses the widely known message passing interface (MPI) standard for parallelization.

Configuration
The simulations were performed on a domain representing a simplified gas turbine combustion chamber. A sketch of the simulation domain is shown in Figure 1. This setup allows us to study FWI, jet-jet interaction and recirculation effects in conditions relevant to gas turbine combustion. The inflow, on the left side of the domain, consists of two parallel slot jets and a laminar pilot; the outlet is located on the right side. In the spanwise direction the domain is enclosed in walls; the crosswise direction has periodic boundary conditions.

First, a variation of equivalence ratio was performed with adiabatic walls on a half-resolution grid. Three equivalence ratios were investigated: $\varphi = 0.6$ represents a high load reference case, $\varphi = 0.5$ marks

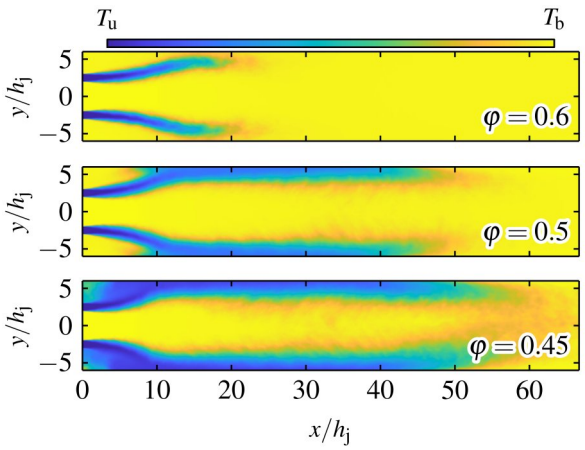

Figure 2: Mean temperature plots for the three cases. The temperatures are scaled with their respective adiabatic flame temperatures. Top to bottom: Case 1 (T_b = 1,960 K), Case 2 (T_b = 1,782 K), and Case 3 (T_b = 1,688 K).

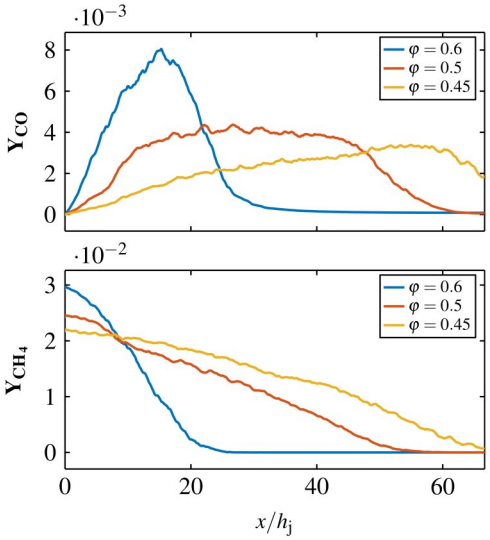

Figure 3: Average streamwise fluxes of the CO (top) and methane (bottom) mass fractions from the simulations with adiabatic walls. Shown are the three equivalence ratios.

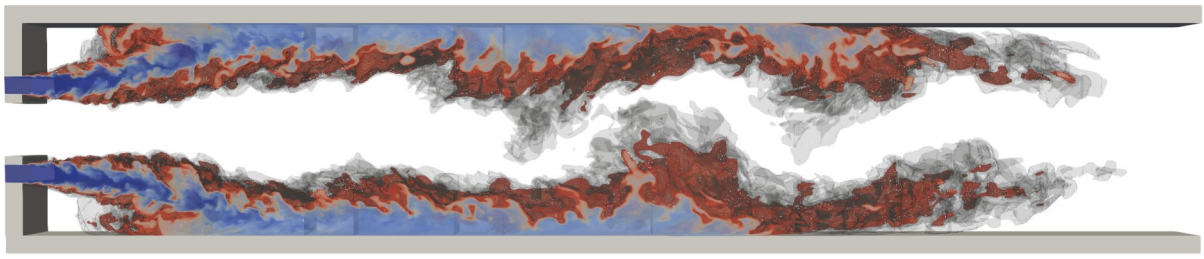

Figure 4: Instantaneous temperature field of the adiabatic case with φ = 0.5. CO concentration is shown in gray.

the transition to increased CO emissions, φ = 0.45 is the lowest stable operating point in this setup. Second, we ran the simulation on the full-scale grid. The equivalence ratio in this case is φ = 0.5. The walls are isothermal with a temperature of 1,000 K.

The full-scale computational grid consists of 3.1 billion grid points. The production runs were performed on up to 49,152 cores, using a total of about 40 million core hours. The total volume of the DNS datasets created is 80 TB.

Results

The average temperature fields from the adiabatic cases are shown in Figure 2. Lowering the equivalence ratio changes the flame shape in the presence of the walls. At φ = 0.6, combustion remains undisturbed by the wall, while the leaner cases display considerable flame-wall interaction. The altered flame shape, combined with the flow field in the domain, changes the mean heat release profile. This, in turn, has a strong influence on the combustion and the distribution of CO in the domain. Figure 3 presents the streamwise fluxes of CO and methane for the three equivalence ratios in the case with adiabatic walls. Particularly the very lean case produces large amounts of CO at the domain outlet [3].

Analysis of the results from the full-resolution case is ongoing. Methane is slowly but consistently consumed along the flame length and is completely depleted at 2/3 of the domain length, well before the end of the domain. After an initial steep increase, the CO concentration reaches a plateau region as seen in the adiabatic cases. After the methane is completely consumed, most CO is oxidized quickly in this area of high temperature. However, a significant portion remains, and oxidation slows as the temperature is reduced downstream. The CO concentration remains significantly higher than the equilibrium value that corresponds to the local temperature, throughout the domain. At the outlet, the CO concentration is approximately 50% above the equilibrium value. We created a DNS dataset of turbulent jets with strong FWI and recirculation along the wall and in the domain center. This dataset covers several important features of gas turbine combustors and offers a unique basis for future analysis.

Ongoing Research / Outlook

The next steps will be formulating a model based on this analysis. The model must account for the slow oxidation of CO, wall heat loss, and strain effects.

References and Links

[1] https://www.itv.rwth-aachen.de/forschung/aktuelle-forschung/nahe-null-emissionen/flammenverloeschen-an-kalten-oberflaechen/
[2] O. Desjardins, G. Blanquart, G. Balarac and H. Pitsch. J. Comp. Phys. 227(15) 7125-7159, 2008.
[3] K. Niemietz, D. Denker, K. Kleinheinz, A. Attili and H. Pitsch. In Proceedings of the 10th European Combustion Meeting, April 14-15, Naples (Italy) / Online, 2021.

High-Fidelity Data for Delta Wing Flow at Transonic Condition

Research Institution
Numerical Methods in Aerospace Engineering, University of the Bundeswehr Munich

Principal Investigator
Tony Di Fabbio

Researchers
Eike Tangermann, Markus Klein

Project Partners
—

SuperMUC Project ID: pn29xa

Introduction

Agile delta wing aircraft configurations operating at high angles of attack typically feature complex flow fields dominated by vortex systems. The understanding and prediction of the vortex and shock waves, generation and evolution, are of essential importance. Classical RANS models, which are very efficient in terms of computational efforts, are not capable of predicting the flow in these configurations accurately enough. RANS models fail to cope with particular challenges like predicting leading edge vortices. On the other hand, since resolving turbulence with DNS or LES methods is far too expensive in terms of computational time, at present, high fidelity predictions can be made using hybrid RANS/LES computations. SuperMUC-NG resources have been employed to achieve hybrid RANS/LES results taking into account generic single and multiple delta wing configurations. The vortex dominated flow around the VFE-2 [2] configuration and the triple-delta wing aircraft model ADS-NA2-W1 [3] have been investigated in detail. All simulations have been performed using the DLR-TAU flow solver developed by the German Aerospace Center.

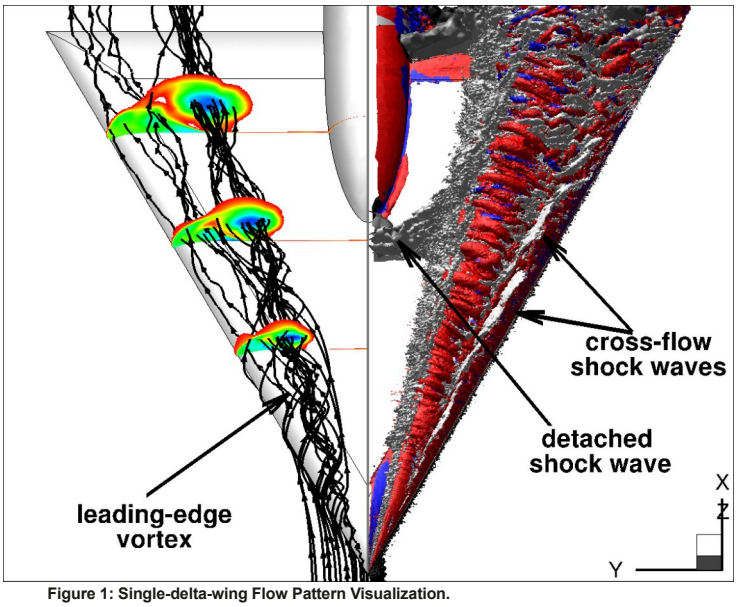

Figure 1: Single-delta-wing Flow Pattern Visualization.

Results and Methods

The complex turbulence fluctuations in the flow field are captured by the underlying turbulence models. Instead of modeling the entire turbulent spectrum, it is possible to resolve parts of the spectrum by means of a scale-resolving simulation. Using hybrid RANS/LES has then became an alternative to accurately capture the unsteady characteristics of various scale vortices. The DDES and IDDES approaches based on Spalart-Allmaras turbulence model [4] have been employed to provide high-fidelity data. In order to stabilize the solver, unsteady simulations have been performed with an implicit dual-time stepping approach. The computation of the fluxes has been performed with a central scheme and the matrix dissipation model has been selected. However, in order to prevent excessive damping of the resolved turbulent structures, a low-dissipation low-dispersion discretization scheme has been used.

Single-Delta-Wing Analysis
Simulations of the sharp leading-edge VFE-2 wing have been performed at transonic conditions with Ma = 0.8, Re = $2 \cdot 10^6$ and α = 20.5° using different levels of temporal and spatial resolution, of which results have been compared. Several turbulence methods and complex flow physics phenomena have been investigated by analysing several details [5]. The surface pressure, the vortex pattern and the position of the shock waves are well captured by the IDDES approach results. For example, as it can be seen in Fig. 1, the hybrid method is able to produce the interaction between the leading-edge vortex and the shock waves generated by the transonic condition and to visualize the formation and breakdown of the primary and secondary vortex.

Triple-Delta-Wing Flow Pattern
The vortex dominated flow around the triple-delta wing ADS-NA2-W1 aircraft has been investigated comparing URANS with scale-resolving DDES results and experimental data [5]. The transonic regime of Ma = 0.85 and Re = $12.53 \cdot 10^6$ with α = 20°, 24° and β = 5° has been selected. The presence of multiple sweep angles further complicates the vortex flow pattern with the presence of vortex merging. The asymmetry of the flow is caused by the side slip angle

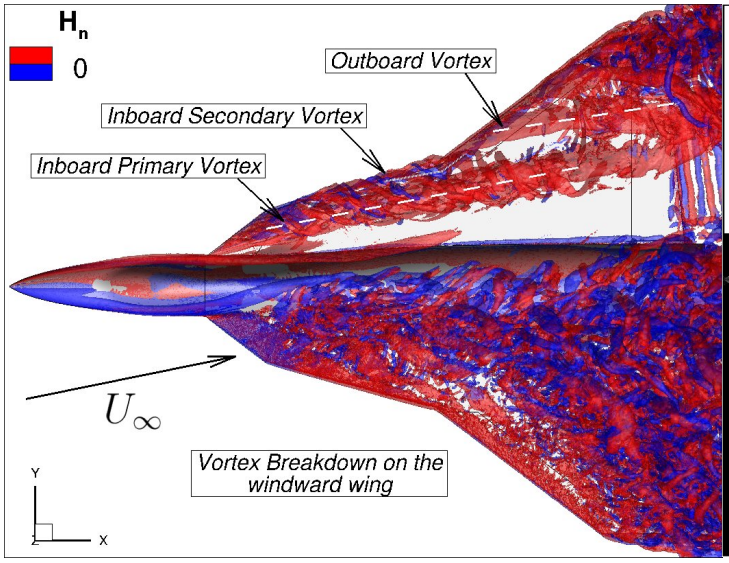

Figure 2: Q-criterion based instantaneous iso-surface with flood contour by instantaneous normalized helicity, DDES with α = 24° and β = 5° [6].

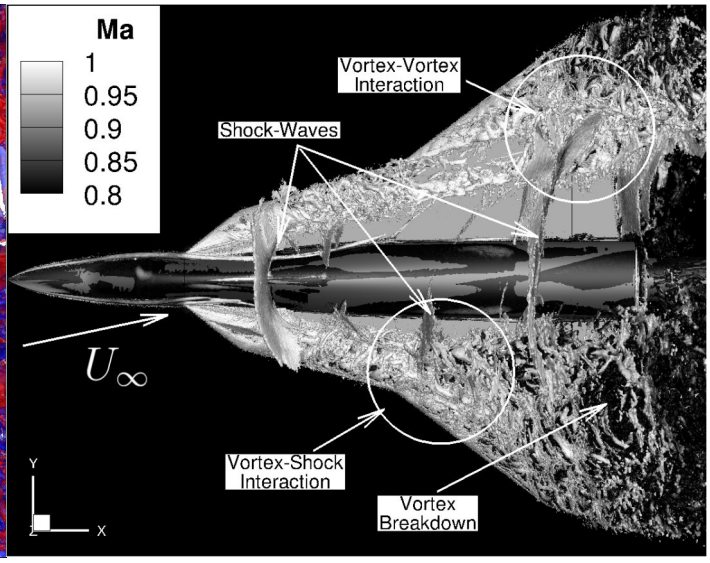

Figure3: Instantaneous x-density gradient iso-surface with flood contour by instantaneous Mach number, DDES with α = 20° and β = 5°.

of β = 5° which generates two different flow conditions on the two wings. Over the wing, the flow undergoes a primary separation at the wing leading edge and subsequently rolls up to form a stable, separation-induced leading-edge vortex. As it can be seen in Fig. 2, at α = 24°, the burst vortex is located on the windward wing and two different main vortices are present on the leeward wing. The first primary inboard vortex induces reattached flow over the wing, and the spanwise flow under the primary vortex subsequently separates a second time to form a counter-rotating secondary vortex outboard of the primary one. The DDES results show the chaotic behaviour of the burst vortex and how the shear layer emanating from the leading edge does not roll up to from a coherent vortex. The chaotic structures captured by DDES show how the burst vortex affects also the starboard wing in the rear part of the aircraft. Moreover, a supersonic area over the wing and consequently different shock waves are caused by the transonic condition. The interaction between shocks and vortices has been investigated, expecially at α = 20°, because it is fundamental for the understanding of the flow physics. It triggers the vortex breakdown on the windward wing and the DDES are able to capture this fundamental phenomenon, as it can be seen in Fig. 3 [6]. The separation of the vortex sheet at the swept leading edge causes a local low pressure region on the suction side which contributes to the overall lift. The so-called vortex lift has a limiting AoA at which the vortex bursts or breaks down. The vortices break down within the second half of the windward wing at the tested flow condition with α = 20°. Downstream of the breakdown, the flow becomes incoherent and turbulent, as only the hybrid RANS/LES results show in Fig. 3, increasing the reliability of the aerodynamic coefficients by comparing them with the experimental data [6].

Ongoing Research / Outlook

The hybrid RANS/LES computations have been carried out as numerical experiment to gain full insight into the three-dimensional flow field for physical understanding of the vortex-dominated flow. Focus of the present research is the accurate reproduction of formation and breakdown of leading edge vortices, taking the importance of the vortex-shock interaction phenomenon at transonic condition into account. The accuracy of predicting the aerodynamic coefficients is mainly related with the prediction of the vortex breakdown onset position and strength because it affects in particular the suction footprint over the wing and consequently the surface pressure coefficient behind the vortex breakdown. Thanks to the SuperMUC-NG resources, promising improvements have been achieved employing the hybrid RANS/LES numerical approach. The qualitatively and quantitatively illustrated results show that all the computational time spent on hybrid RANS/LES approaches has been worth the effort in order to provide a significant advancement in the prediction of (multiple-)delta wing flow. The hybrid method reveals several physics aspects which have not been seen before (vortex-vortex interaction, shock-vortex interaction) with the demonstrated accuracy. The database will be used in future as a reference for improving traditional RANS based closures.

References and Links

[1] https://www.unibw.de/numerik-en/research/turbulence-modelling-of-leading-edge-vortices
[2] R. Konrath, C. Klein, A. Schröder, 46th AIAA Aerospace Sciences Meeting and Exhibit, 7–10 January 2008, Reno, Nevada.
[3] A. Hovelmann, A. Winkler, S.M. Hitzel , K. Richter and M. Werner, New Results in Numerical and Experimental Fluid Mechanics XII, Contributions to the 21st STAB/DGLR Symposium, Darmstadt, Germany, 307-316, 2018.
[4] P. Sagaut, S. Deck, and M. Terracol, Multiscale and Multiresolution approaches in turbulence. LES, DES and Hybrid RANS/LES Methods: Applications and Guidelines, ch. 7, pp. 286–291. Imperial College Press, 2nd ed., 2013.
[5] T. Di Fabbio, E. Tangermann, M. Klein, CEAS Aeronaut J 13, 453–470 (2022). https://doi.org/10.1007/s13272-022-00571-9.
[6] T. Di Fabbio, E. Tangermann, M. Klein, Flow Pattern Analysis on a Delta Wing at Transonic Speed, AIAA SciTech Forum, 3-7 January 2022, San Diego, California.

DNS of premixed flame-wall interaction in turbulent boundary layers

Research Institution
[1]Numerical methods in Aerospace Engineering, University of the Bundeswehr Munich

Principal Investigator
Markus Klein[1]

Researchers
U. Ahmed[2], N. Chakraborty[2]

Project Partner
[2]Newcastle University, Newcastle upon Tyne, UK

SuperMUC Project ID: pn34xu

Introduction

Combustors are increasingly being made more fuel efficient and smaller in size to increase energy density thus leading in many engineering devices, including gas turbines and micro-combustors, to events like flame-wall interaction (FWI). The analysis of FWI poses several experimental challenges in terms of spatial and temporal resolution but remains expensive for direct numerical simulation (DNS) based investigations. While some regimes of analysis are left to experimentation, DNS can provide detailed, 3D and temporally resolved high fidelity datasets which are also enablers for state of the art machine learning algorithms.

In order to obtain a thorough physical understanding of the FWI mechanism and to develop high fidelity turbulence and combustion models more efforts will be needed. The present work constitutes a step in this direction which will help to develop and design more energy-efficient and environmentally-friendly combustion devices.

Results and Methods

Three-dimensional direct numerical simulations (DNS) of two different flow configurations for flames interacting with chemically inert isothermal as well as adiabatic walls in fully developed turbulent boundary layers have been performed. The first configuration is an oblique wall interaction (OWI) of a V-flame in a turbulent channel flow and the second configuration is representative of head-on interaction (HOI) of a planar flame in a turbulent boundary layer. The choice of isothermal and adiabatic wall conditions is made due to the fact that these conditions represent the limiting conditions in the case of an actual combustion device and will serve as a stepping stone in enhancing the understanding of the FWI process. The simulations are representative of stoichiometric methane-air mixture at unity Lewis number under atmospheric conditions. The turbulence in the non-reacting channel is representative of the friction velocity based Reynolds number Re_τ = 110.

A well-known three-dimensional compressible Fortran DNS code SENGA+ has been used for the simulations which employs high-order finite-difference (10^{th} order for internal points and gradually decreasing to 2^{nd} order at the non-periodic boundaries) and Runge-Kutta (3^{rd} order explicit) schemes for spatial differentiation and time advancement, respectively and is parallelised using MPI. The governing equations of mass, momentum, energy, and species mass fractions are solved in a non-dimensional form and a single-step irreversible reaction is used for the purpose of computational economy.

The domain size for the OWI (HOI) case is $10.69h \times 2h \times 4h$ ($10.69h \times 1.33h \times 4h$), h being the channel half height, and has been discretized on 1,920 x 360 x 720 (1,920 x 240 x 720) equidistant grid points. The computational box has been decomposed and run on 4,800 (3,200) cores in parallel. The OWI (HOI) simulations have been performed for approximately 3 (2) flow through times and the data has been sampled once the initial transience have decayed. One simulation consumed about 1,500,000 core hours per case and boundary condition. One result file containing all variables for one time step has a size of about 40 GB and altogether 200 time steps per case have been stored for collecting sufficient statistics and for analysing the temporal development of the flame.

The instantaneous flame structures, represented by the c = 0.5 isosurface along with the normalised vorticity magnitude Ω are exemplarily shown for the HOI case in Fig. 1. During the simulations, the flame propagates into the reactants and moves towards the wall, consequently interacting with the wall and quenching due to wall heat loss in the case of isothermal wall or ceases to exist due to the consumption of the reactants in the case of adiabatic wall.

For both configurations notable differences in the behaviour of the mean progress variable and the mean non-dimensional temperature have been observed between the two wall boundary conditions. Investigation of the mean scalar variance of the progress variable and temperature and their respec-

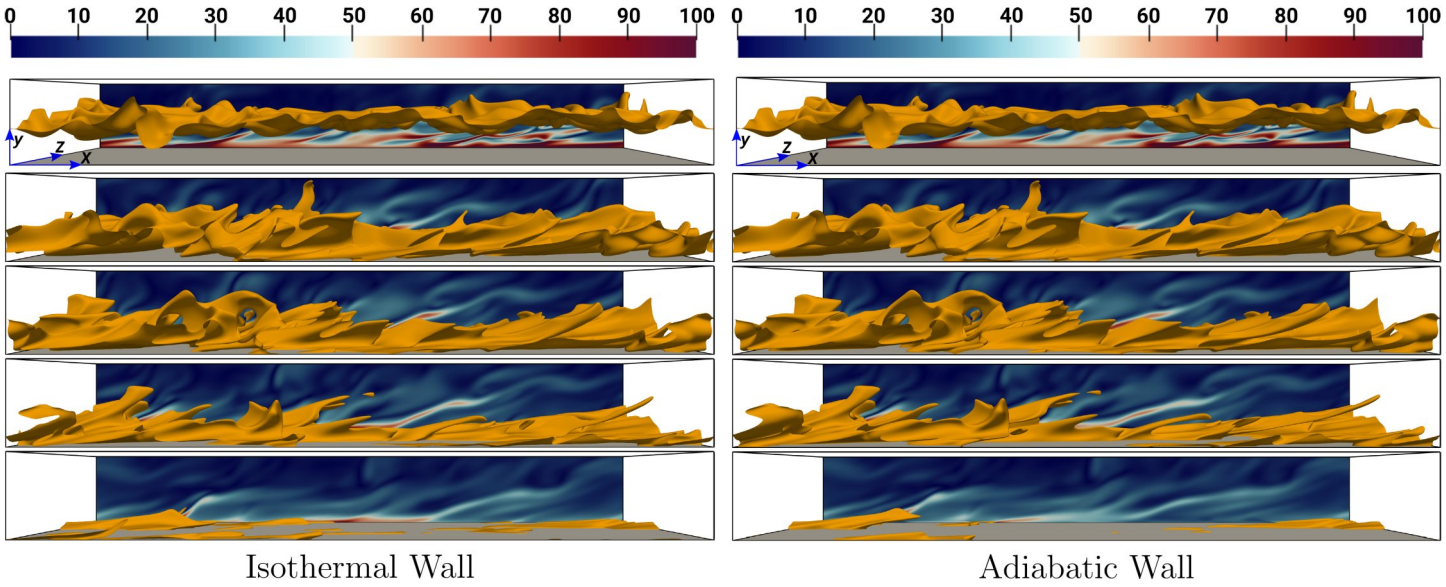

Figure 1: Head-on interaction with isothermal wall boundary conditions (left) and with adiabatic wall boundary conditions (right) at different time instants. From top to bottom t/t_f = 4.20, t/t_f = 10.50, t/t_f = 11.55, t/t_f = 12.60, t/t_f = 14.70. The isosurfaces coloured in yellow represents c = 0.5. The instantaneous normalised vorticity magnitude Ω is shown on the x–y plane at z/h = 4. The grey surface denotes the wall.

tive scalar dissipation rates has revealed that the variances of the progress variable and non-dimensional temperature remain coupled in the case of adiabatic walls while significant differences exist for both flow configurations between the two scalar variances in the vicinity of the wall under isothermal wall conditions. These differences for isothermal wall boundary condition are a consequence of the way the wall boundary conditions are imposed on the species mass fractions and temperature. The mean scalar dissipation rates of progress variable and non-dimen-sional temperature decrease in the near wall region for both wall boundary conditions, but in the case of isothermal walls there is a decoupling between the two scalar dissipation rates and the scalar dissipation rate for non-dimensional temperature remains higher than the scalar dissipation rate for the progress variable. This variation in the scalar dissipation rates is a result of the steep temperature gradients introduced by the low temperature at the isothermal wall. The behaviours of the mean turbulent scalar fluxes of progress vari-able and temperature have been investigated for the two flame configurations and it is found that the scalar fluxes can show both gradient and countergradient type behaviour depending on the flow configuration and also on the proximity of the flame to the wall. In the case of V-flame OWI, the choice of the wall boundary condition has a significant influence on the behaviour of the scalar fluxes, whereas in the case of turbulent boundary layer HOI, no significant differences in the scalar fluxes are observed for different wall boundary conditions. The aforementioned statistics show that improved models are needed for accurate prediction of heat transfer and combustion behaviours in practical combustion devices. It can also be inferred from these statistics that flame orientation with respect to the wall has major implications on the flame and flow behaviour. These variations must be included in the models.

Ongoing Research / Outlook

The choice of the chemical mechanism is unlikely to alter the conclusions of this analysis. However, further analysis will be necessary using detailed chemistry and transport to account for differential diffusion of scalars. Furthermore, the influence of the variation in the friction Reynolds number and the effects of conjugate heat transfer will be considered in future work. Hydrogen is becoming increasingly popular as an alternative fuel for the future and thus it is important to compare and contrast the FWI for hydrogen-air flames with that for conventional hydrocarbon-air (e.g. methane-air) flames under statistically similar conditions. First results for HOQ flames under isotropic turbulence conditions using detailed chemistry and transport have been recently reported in [4].

References and Links

[1] U. Ahmed, N. Chakraborty, and M. Klein. Flow Turbul Combust, https://doi.org/10.1007/s10494-020-00169-3, 2020.
[2] U. Ahmed, N. Chakraborty, and M. Klein. In 13th International Symposium on Engineering Turbulence Modelling and Measurements, Rhodes, May 2021.
[3] U. Ahmed, N. Chakraborty, and M. Klein. Int J Heat Fluid Flow, 92, 108881, 2021.
[4] J. Lai, U. Ahmed, N. Chakraborty, and M. Klein. Int J Heat Fluid Flow, 93, 108896, 2022.

Boundary zonal flows in rapidly rotating convection

Research Institution
Max-Planck Institute for Dynamics and Self-Organization, Göttingen

Principal Investigators
Olga Shishkina, Philipp Reiter

Researchers
Mohammad Emran, Xuan Zhang, Lukas Zwirner

Project Partners
—

SuperMUC Project ID: pn56ga

Introduction

Turbulent thermal convection, driven by buoyancy and subject to background rotation, is ubiquitous in nature; its study is necessary for geophysical and astrophysical flows and for engineering improvements in industrial applications. The classical problem here is turbulent Rayleigh-Bénard convection (RBC), in which a layer of fluid is held between two horizontal surfaces and is uniformly heated from below and cooled from above. The rotation has various effects on the structure of the convective flow and on the global heat transport in the system.

In our recent work [2], it was found that in rapidly rotating turbulent Rayleigh-Bénard convection in slender cylindrical vessels (with an aspect ratio of diameter to height of Γ = 1/2) filled with pressurized gas SF6 (Pr = 0. 8), the classical large scale circulation is suppressed, and boundary zonal flow develops near the sidewall, characterized by a bimodal probability distribution function of temperature, cyclonic fluid motion, and anticyclonic drift of the flow pattern (with respect to that of the rotating frame), see figure 1.

Results and Methods

To solve the Navier-Stokes equations for incompressible flows, we use self-developed highly parallelized, finite-volume and pseudospectral codes, with ideal scaling up to several thousand processors. The conducted numerical simulations are highly demanding, a large number of grid elements is necessary to resolve the highly turbulent flows and long-time statistics must be collected, in order to verify theoretical models. This requires about 20,000-200,000 core-hours per simulation, which would not be feasible without high performance computational support.

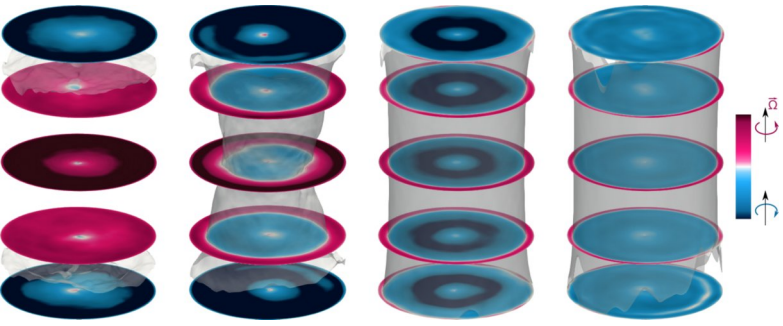

Figure 1: Time-averaged fields of the azimuthal velocity, for different rotation rates. Rotation speed increases from left to right [3].

In our work, we show that the boundary zonal flow transports a disproportionate fraction (>60%) of the total heat transport, even though it is only a fraction of the volume of the experimental cell. This is a valuable finding for the study of rotational convection, since a major purpose of the field is to explore the geostrophic regime in which the main balance of forces is between the Coriolis force and the pressure gradient. So far, it has been assumed that columnar vortices with a typical diameter much smaller than the cell dimension are to be expected at a fast rotational velocity, which is why periodic boundary conditions are usually assumed in numerical studies. Our results show that the boundary zonal flow forms near the sidewall at fast rotation speed, which is crucial for the overall heat transfer.

In [3], the dependencies of the boundary zonal flow properties on external parameters, such as the strength of rotation (Rossby number Ro) and the strength of heating (Rayleigh number Ra), aspect ratio (Γ), different fluid (Prandtl number Pr) are studied in more detail. Through numerous numerical simulations, we obtain important scaling relations (for the width and drift frequency of the boundary zonal flow, see figure 4) that help understand the nature of zonal boundary flows and derive important analytical models.

In the most recent work [4], we connect the boundary zonal flows in turbulent flows to the linear wall mode state that occurs before the onset of bulk convection, through continuity in length and time scales and of convective heat transfer. It is demonstrated that as buoyancy increases at fixed rotation rate, the spatial, temporal and heat-transport properties of the localized state change smoothly and monotonically. By separating the total heat transport into the wall mode contribution and the boundary zonal flow contribution, it shows throughout the wall mode state to the boundary zonal flow, that the near-wall region contribution is essential, and special treatment or attention is needed in considering the heat transport scaling of rotating convection in the rapidly rotating regime for finite geometries.

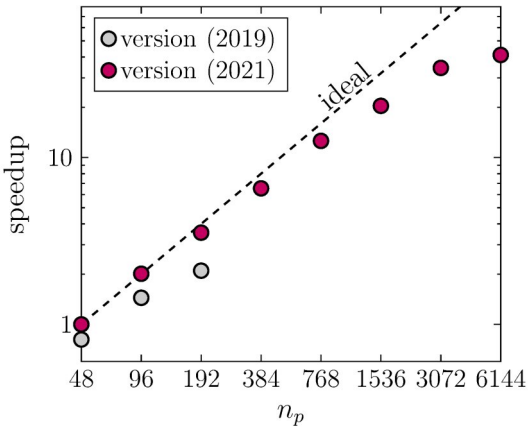

Figure 2: Speedup of our numerical code with respect to the number of processors. The simulation was performed on a grid with 512^3 elements.

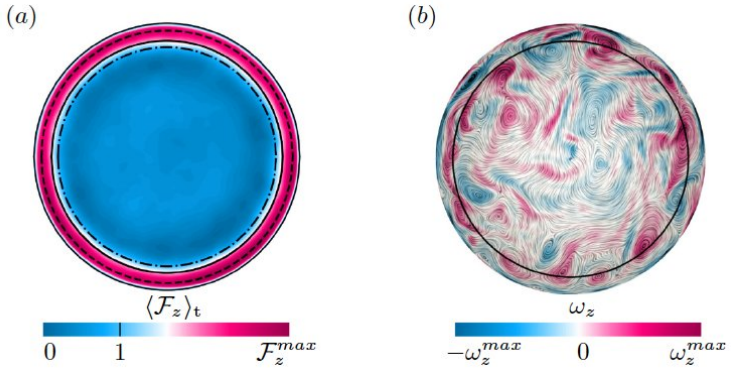

Figure 3: Distribution of in the horizontal plane at mid-height for (a) time-averaged heat flux, (b) instantaneous vertical vorticity [3].

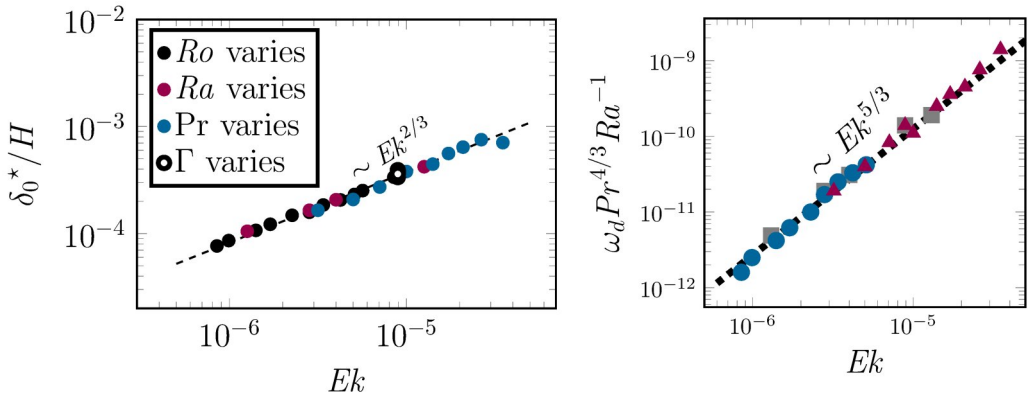

Figure 4: Scalings of length scale (width) and time scale (drift frequency) of the boundary zonal flow for the cases at different rotation rate, heating strength, fluid property and cell aspect ratio [3].

Ongoing Research / Outlook

Further research is ongoing to describe how the transition to a state of bulk convection is influenced by the presence of the wall mode states. It is also very interesting to explore how the sidewall condition (conducting wall) influences the onset of wall mode at rapid rotation rate. Another complexity that comes up during the research is, in very extreme aspect ratio cells (diameter/height ratio being much smaller than 1), the flow organization shows rich possibilities and therefore the local and instantaneous heat transfer also has big variations. It is likely that the bulk onset becomes much more difficult and complicated when the wall mode state occupies a rather big portion of the cell area, and other instability or mechanisms may play a role under such circumstances. This would be an interesting point to investigate further.

References and Links

[1] https://www.lfpn.ds.mpg.de/shishkina/
[2] X. Zhang et al. 2020. Phys. Rev. Lett., 124, 084505.
[3] X. Zhang, R. Ecke and O.Shishkina 2021. J. Fluid Mech., 915, A62.
[4] R. Ecke, X. Zhang and O. Shishkina 2022. Phys. Rev. Fluids, 7, L011501.

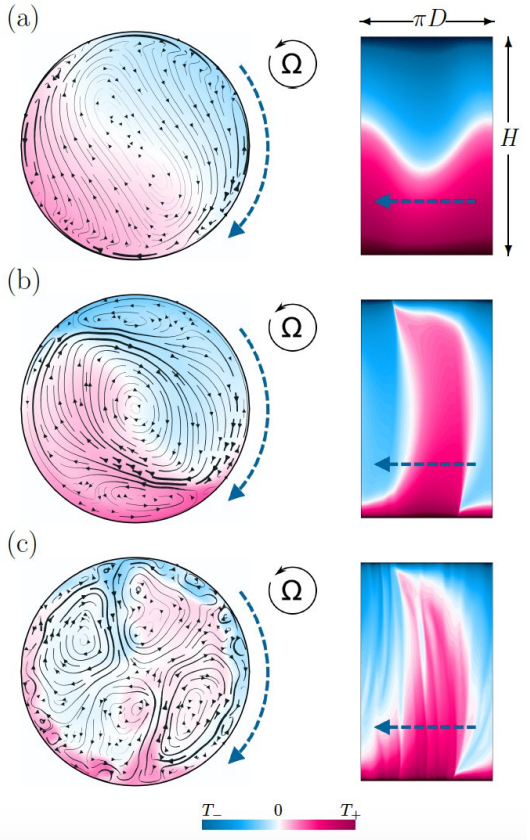

Figure 5: Temperature field at half height and at r=0.95R for (a) linear wall mode near onset, (b) nonlinear wall mode onset of time dependence, (c) bulk mode arising in the presence of wall modes [4].

Scale-Resolving Study of a Fluid-Structure-Acoustics Interaction Test Case

Research Institution
[1]Institute for Parallel and Distributed Systems, University of Stuttgart

Principal Investigator
Miriam Schulte[1]

Researcher
Amin Totounferoush[1]

Project Partner
[2]Technical University of Munich

SuperMUC Project ID: pn56se

Introduction

We present an efficient and scalable communication initialization scheme for partitioned coupled multi-physics simulations. This scheme is implemented in the preCICE coupling library [1]. Numerical methods to solve multi-physics problems can be broadly divided into two categories, monolithic and partitioned. In a monolithic approach, the equations from all occurring physics are discretized and solved as a single large system, while in a partitioned approach, the problem is divided into smaller subdomains according to the governing physic and, hence, separate solvers are used for each sub-problems along with additional software to couple these solvers. This approach allows using the most adapted and well-validated numerical methods for each sub-problem as well as previously developed and computationally optimized single-physic solver codes.

However, using a partitioned approach introduces new challenges, especially when parallel efficiency is concerned, which must be addressed for an efficient simulation. These challenges include, but are not limited to: (i) data communication between solvers, (ii) data mapping between non-matching meshes, (iii) equation coupling at the common interface and, (iv) the inter-solver load balancing.

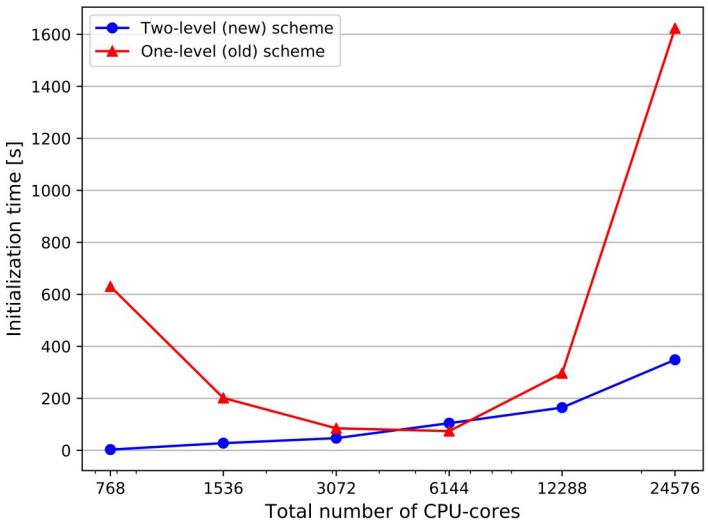

Figure 1: Strong scalability measurements: Total initialization time comparison between the two-level approach and the previously used one-level scheme [3].

In this work, we focus on the initialization of the communication. In a parallel partitioned simulation, ranks of coupled solvers must exchange the values at the common interface. However, since each solver has its communicator, the list of partner ranks and the corresponding data that must be communicated is unknown at the start of the simulation. The purpose of the initialization is to determine partner ranks between coupled solvers and identify the exact list of data that must be communicated during the run time.

Results and Methods

Previously, preCICE used a one-level initialization scheme which required gathering the interface mesh in a master rank and communicating it to the other solver. The master rank of the receiving solver broadcasts the received mesh to other ranks. Individual ranks can determine their partner ranks by comparing their mesh partition with the received mesh. Gathering the mesh in a master rank becomes a bottleneck for the cases with a large mesh size. In addition, the sequential nature of this scheme reduces the parallel efficiency for the cases with a large number of MPI processes.

To effectively address the scalability and memory issues of the communication initialization in preCICE, we introduce a new scheme that breaks down the initialization into two levels. The first level identifies and establishes potentially required communication channels, while the second level specifies the actual list of data to be exchanged.

In the first level, the new scheme uses bounding boxes to determine the list of partner ranks, instead of the actual mesh. Each rank computes a bounding box around its mesh partition. These bounding boxes are gathered in the master rank and communicated to the other solver for comparison. The process is schematically shown in Fig. 2. In the second level, each rank communicates its mesh partition to the partner ranks for final filtering and determining the exact list of data to be communicated during the run time.

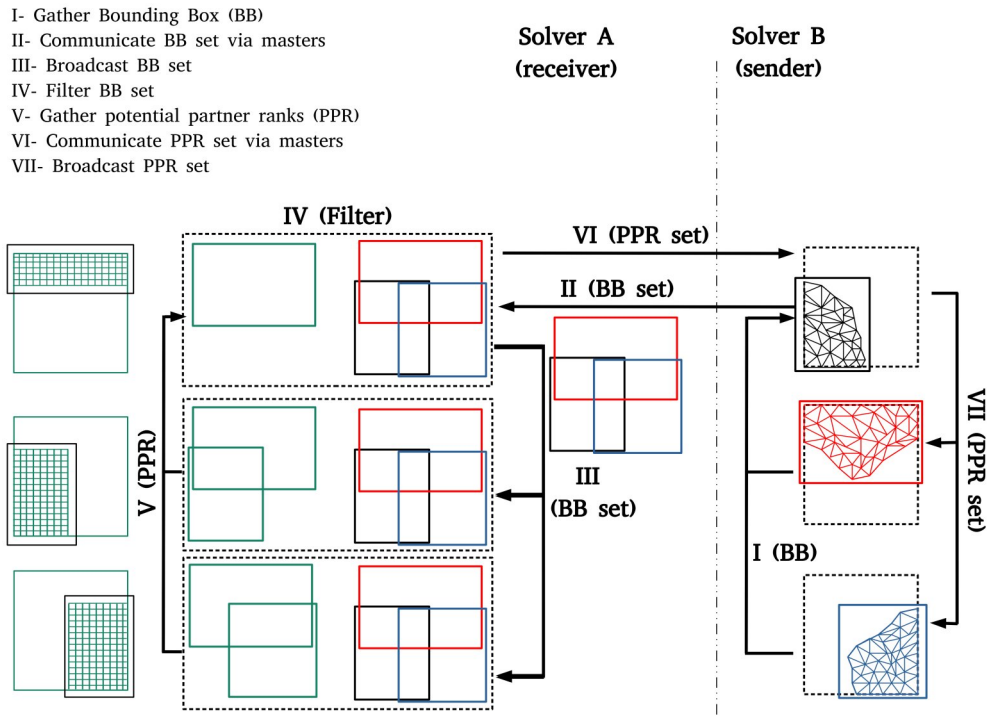

Figure 2: Two-level initialization scheme: the first level exchanges bounding boxes and establishes the communication channels between partner processes. The master process of B gathers the bounding boxes from other processes (I) and communicates them to the master process of solver A (II). The master process of solver A broadcasts the received bounding boxes to all other processes of solver A (III). Each process of A compares the received set of bounding boxes to its own to find the potential partner ranks (PPR) in solver B (IV). The complete set of sent bounding boxes is drawn in black, while the green boxes represent the subset relevant for the respective process of solver A. The list of PPR for all processes of A is gathered in the master process (V) and is communicated to the processes of solver B via master communication (VI) followed by a broadcast (VII), such that not only the processes of solver A, but also the processes of solver B know their potential communication partners [3].

To show the performance and scalability improvements in preCICE, we conduct strong scaling studies for a turbine blade test case in which the fluid-structure interaction between the airflow and the turbine blade is simulated. The details of this test case can be found in [3]. All measurements are carried out on the SuperMUC-NG supercomputer at the Leibniz Supercomputing Centre of the Bavarian Academy of Science and Humanities (LRZ). The strong scalability of the developed initialization scheme is evaluated using a computational mesh with 628,898 vertices. This is the finest mesh resolution that the old one-level scheme can handle due to the memory issue that is explained earlier in this section.

The strong scaling measurements for both schemes are presented in Fig. 1 for total core numbers up to 24,576. This investigation shows that the two-level scheme outperforms the old scheme for larger core numbers. For instance, the two-level scheme accelerates the initialization by a factor of 6 for 24K cores. In addition, the run time breakdown for the new scheme is presented in Fig. 3 for deeper insight. This figure shows that the most time-consuming subcomponent of the new scheme is bounding box communication and comparison in the first level. This corresponds to our expectations since this part is handled sequentially and its performance is expected to decline by increasing the number of processes.

Ongoing Research / Outlook

The performance analysis showed that the two-level scheme improves the scalability and performance of the preCICE initialization significantly. It is also able to completely remove the mentioned memory issue for large meshes. However, the performance breakdown reveals that bounding box communication and feedback are still expensive. This subcomponent can be potentially improved by using more efficient data structures such as linked cells. In addition, even though the mesh communication is handled in parallel, the mesh communication time does not scale as expected. These two issues are currently under investigation for further improvements.

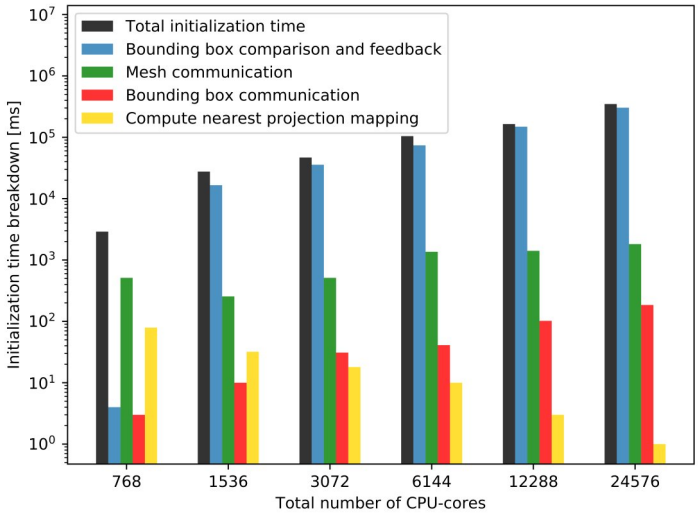

Figure 3: Strong scalability study: Initialization time breakdown for the two-level initialization approach [3].

References and Links

[1] Chourdakis, Gerasimos, et al. arXiv preprint arXiv:2109.14470(2021).
[2] Uekermann, Benjamin Walter. Diss. Technische Universität München, 2016.
[3] Totounferoush, Amin, et al. Algorithms 14.6 (2021): 166.

Thermodiffusive instabilities in lean premixed hydrogen/air flames

Research Institution
Institute for Combustion Technology, RWTH Aachen University

Principal Investigator
Heinz Pitsch

Researcher
Lukas Berger

Project Partners
—

SuperMUC Project ID: pn56vo (Gauss Large Scale project)

Introduction

The recent rise of renewable energy sources is promoting the use of hydrogen as a carbon-free energy carrier. One possibility to harness the energy stored in hydrogen is its usage in thermochemical energy conversion processes such as in gas turbines, industrial burners, or internal combustion engines. However, lean hydrogen/air flames are prone to intrinsic combustion instabilities and, in particular, thermodiffusive instabilities, which can substantially change flame dynamics, heat release rates, and flame speeds. These aspects are highly relevant for the safe operation of any combustion device, e.g., to avoid flame flashback, but can also increase thermal efficiencies. Thermodiffusive instabilities originate from the low Lewis number of hydrogen, which represents the ratio of the thermal and mass diffusivity, where the latter is particularly high for hydrogen. The strong differential diffusion of hydrogen leads to an amplification of small flame front perturbations such that strongly wrinkled flame fronts are observed with a significantly enhanced flame speed and strong variations of the local reaction rates. For example, thermodiffusive instabilities can lead to four times higher flame speeds compared to the unstretched laminar burning velocity in laminar lean hydrogen/air mixtures at ambient conditions [1]. While thermodiffusive instabilities have been extensively studied in laminar flows, combustion applications typically feature interactions of a flame with a turbulent flow, necessitating a comprehensive understanding of thermodiffusive instabilities in turbulent flows. Theoretical works expect flame intrinsic instabilities to be particularly relevant for low Karlovitz numbers, but the exact region of influence in the turbulent combustion regime diagram and the identification of all relevant parameters is yet unclear. However, the effects of differential diffusion and, hence, thermodiffusive instabilities are found to be sustained in turbulent flames for a large range of Reynolds and Karlovitz numbers [2], so it is fundamental to further understand the mutual interaction between turbulence and thermodiffusive instabilities to incorporate these effects into combustion models for predictive simulations of hydrogen flames. In particular, the development process of combustion devices typically involves the use of simulations, e.g. Large Eddy Simulations (LES), to cut the high cost associated with experimental tests. However, high-fidelity, predictive LES of hydrogen/air flames require models that accurately and reliably describe thermodiffusive instabilities. Present-day combustion models developed for hydrocarbon fuels, which are unaffected by such instabilities, cannot capture these effects. To improve prediction capabilities of LES of hydrogen/air flames, detailed data of such flames are needed for model development and validation. However, for three-dimensional thermodiffusively unstable flames, only rare data exist; the available studies only qualitatively highlight the dynamics of these flames, but do not provide enough detail for quantitative model development. The high level of detail and the availability of all desired quantities at all locations motivates the use of Direct Numerical Simulations (DNS) for model development. For example, DNS provide information about reaction rates or higher-order moments, that are challenging to obtain experimentally. Recently, advances in supercomputing have enabled a range of interesting DNS studies and made DNS a powerful tool in combustion science. Within this project, a series of DNS of turbulent premixed lean hydrogen flames is conducted to generate a unique database of thermodiffusively unstable flames. From this database, LES models that account for the impact of thermodiffusive instabilities on turbulent flames can be rigorously developed.

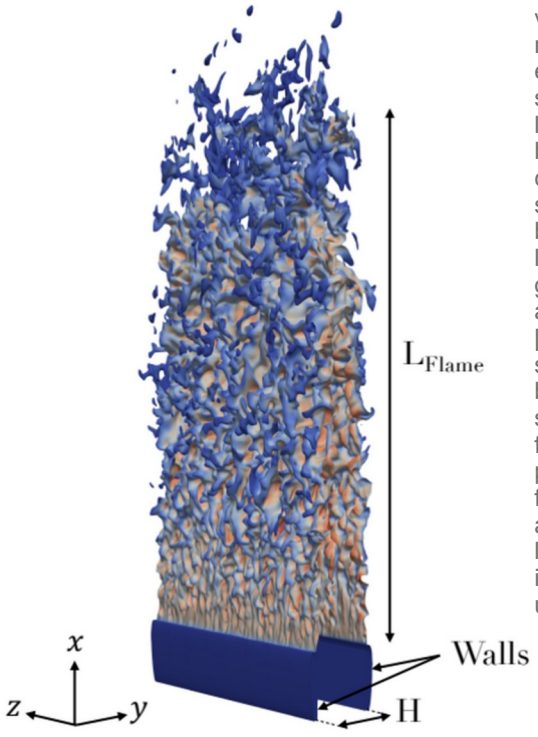

Figure 1: Hydrogen/air flame in slot burner configuration.

Results and Methods

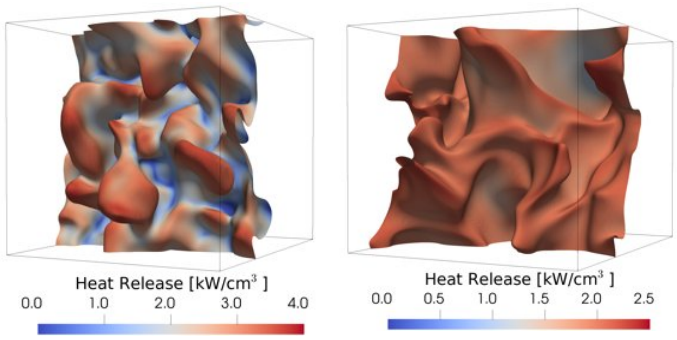

Figure 2: Temperature distribution of hydrogen/air flame with (left) and without (right) instabilities.

The governing equations of the DNS are given by the reacting Navier-Stokes equations in the low-Mach limit. For the computation, an in-house code called CIAO is employed. The code is a high-order, semi-implicit finite difference code that uses Crank-Nicolson time advancement and an iterative predictor corrector scheme. Spatial and temporal staggering is used to increase the accuracy. The Poisson equation for the pressure is solved by the multi-grid HYPRE solver. Momentum equations are spatially discretized with a second-order scheme. Species and temperature equations are discretized with a fifth order WENO scheme. The temperature and species equations are advanced by utilizing an operator splitting according to Strang. The chemistry operator uses a time-implicit backward difference method, as implemented in the stiff ODE solver CVODE. For further details about the applied numerical algorithms and code verification, the reader is referred to Ref. [3]. The code uses the message passing interface (MPI) standard.

The DNS database comprises several turbulent, lean, premixed hydrogen flames in a slot burner configuration at different conditions, where the geometry of the DNS is shown in Fig. 1. All DNS have been performed with a jet Reynolds number of 11,000 using a detailed chemical mechanism. To modulate the interactions of thermodiffusive instabilities and turbulence, three cases have been computed at different Karlovitz numbers, which parametrizes the interaction of the smallest turbulent eddies with the flame. All cases feature realistic transport models that include the differential diffusion of hydrogen, so the characteristic patterns of thermodiffusively unstable flames, such as strong variations of the heat release and super-adiabatic temperatures, are observed. Further, to systematically assess the different contributions of turbulence and thermodiffusive instabilities, an additional case has been considered for the lowest Karlovitz number using a modified diffusivity model to suppress thermodiffusive instabilities. For this, the diffusivities of all species are set equal to the thermal diffusivity (unity Lewis numbers assumption). The significant impact of thermodiffusive instabilities on the turbulent flame dynamics is visualized in Fig. 2, where an instantaneous snapshot of the temperature field is shown for the low Karlovitz number flames with and without thermodiffusive instabilities. In the presence of such instabilities, significant super-adiabatic temperatures of up to 400 K and a much shorter flame are visible, indicating a significantly higher fuel consumption rate in the presence of instabilities. In particular, Fig. 3 shows the variation of the local heat release on the flame sheet for the low Karlovitz number flames with and without

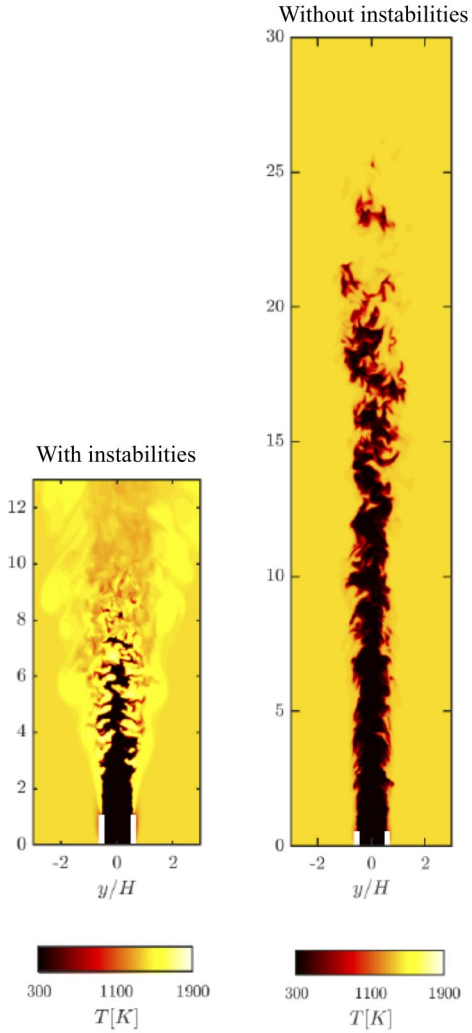

Figure 3: Heat release distribution on the flame sheet of a hydrogen/air flame with (left) and without (right) thermodiffusive instabilities.

instabilities. If the instabilities are suppressed, no significant fluctuations of the local heat release are visible. In contrast, the thermodiffusively unstable flame features a strong variability of the heat release with significantly enhanced peak values compared to a laminar flame at the same conditions, leading to an overall higher fuel consumption rate. Further, the formation of tongue like structures, which are characteristic structures of thermodiffusively unstable flames, is seen. A detailed discussion of all results may be found in [4].

Ongoing Research / Outlook

The analysis of the DNS data reveals a strong impact of thermodiffusive instabilities on the dynamics of lean hydrogen/air flames. As these effects are yet not included in present combustion models, they need to be incorporated into the present LES modeling frameworks and possible model hypotheses need to be validated. For this, the present DNS represent a unique database for model development and validation. Thus, an a priori and a posteriori assessment of different premixed combustion models that are extended to account for the effects of thermodiffusive instabilities will be pursued in future work.

References and Links

[1] L. Berger et al., Proc. Comb. Inst., 37:1879-1886, 2019.
[2] A.J. Aspden et al., J. Fluid Mech., 680:287-320, 2011.
[3] O. Desjardins et al., J. Comput. Phys., 227:7125-7159, 2008.
[4] L. Berger, A. Attili, H. Pitsch, Combust. Flame, 244:112254, 2022

Thermal and magnetoconvection: Small Prandtl numbers and strong magnetic fields

Research Institution
[1]Technische Universität Ilmenau

Principal Investigator
Jörg Schumacher[1]

Researchers
Dmitry Krasnov[1], Ambrish Pandey[2]

Project Partner
[2]New York University Abu Dhabi

SuperMUC Project ID: pn68ni

Introduction

Thermally driven turbulence is one essential process in many astrophysical or technological applications. The dimensionless Prandtl number is then often very small, $Pr \ll 1$. This parameter is defined as the ratio of the kinematic viscosity to the temperature diffusivity. In many cases strong (external) magnetic fields are involved in this turbulence. The dimensionless Hartmann number is then additionally very large, $Ha \gg 1$. Our fundamental understanding of the complex interaction of thermal turbulence with other physical processes, such as its interaction with magnetic fields, is far from being complete. High-resolution direct numerical simulations of the equations of turbulent fluid motion in the simplest setting of a thermally driven turbulent flow, Rayleigh-Bénard convection (RBC) in a layer or a closed vessel and duct that is uniformly heated from below and cooled from above, reveal new insights into the basic mechanisms of turbulent transport of heat and momentum and its connections to characteristic structures and patterns. In our present supercomputing project, we study two extreme cases of RBC that cannot anymore be obtained in a controlled laboratory experiment. We use massively parallel direct numerical simulations that resolve all vortices and thermal plumes to their smallest extension and do not require parametrizations of unresolved turbulence. On the one hand, we push the Prandtl number to values as small as $Pr = 0.001$ which are not anymore obtainable in laboratory experiments. On the other hand, we investigate the turbulence under extremely strong magnetic fields [1].

Results and Methods

We numerically solve the three-dimensional Boussinesq equations of thermal convection which couple the velocity and temperature fields. The external magnetic field enters the Navier-Stokes equations as a Lorentz force term. Our magnetohydrodynamic model uses the quasi-static limit [2]. We apply a second-order finite difference method. The simulation domains are cuboid cells or ducts with no-slip boundary conditions at all walls. The sidewalls are thermally insulated. The biggest direct numerical simulations of a non-magnetic case at $Pr = 10^{-3}$ and a Rayleigh number of $Ra = 10^7$ in a domain with an aspect ratio 25:25:1 requires 144,000 SuperMUC-NG cores for a grid with 20,480 x 20,480 x 1,280 points. One snapshot of the turbulent flow including the three velocity components and the temperature required 17 TBytes storage. In one 24-hour job, we could advance the flow in time for 0.1 convective time units. The simulations with included magnetic fields are smaller in their grid size, but also demanding particularly in terms of the spatial resolution of the thin Hartmann layers at the walls of the duct.

Figure 1 shows results from the MHD simulations of evolving round jet flow at $Re = 1{,}000$ and transverse magnetic field $Ha = 500$ for the grid-size of 2,304 x 512^2 points. This work is conducted as a counterpart to the experiments with liquid mercury [2]. A strong effect of wall-conductivity Cw in destroying quasi-2D turbulence is found in this duct configuration at high magnetic fields. This effect has been inaccessible in experiments. Figure 2 reports results from our largest non-magnetic computations. We compare temperature and vertical velocity fields in horizontal midplane. The geometry and Rayleigh number is the same while the Prandtl number is varied by almost 5 orders of magnitude in the three cases. The figure illustrates clearly how the temperature field structures get coarser with decreasing Prandtl number while the velocity component develops increasingly finer contours that indicate the increasingly vigorous character of the fluid turbulence [3].

Ongoing Research / Outlook

The existing database, which is currently still extended provides a unique possibility to determine turbulent eddy viscosities and diffusivities which are still the backbone for turbulence parametrizations in numerous real-life applications of thermal convection. Our series of high-resolution simulations that vary the Prandtl number Pr for several fixed Rayleigh numbers Ra enable a calculation of the thermal and kinetic energy dissipation rates which are required for such a task. This analysis will be part of our future work on this subject and thus extends existing studies in 2D convection [4].

References and Links

[1] https://www.tu-ilmenau.de/tsm
[2] I. Belyaev et al., arXiv:2112.01600 (2021).
[3] A. Pandey et al., arXiv:2202.09208 (2022).
[4] A. Pandey et al., Phys. Rev. Fluids 6, 100503 (2021).

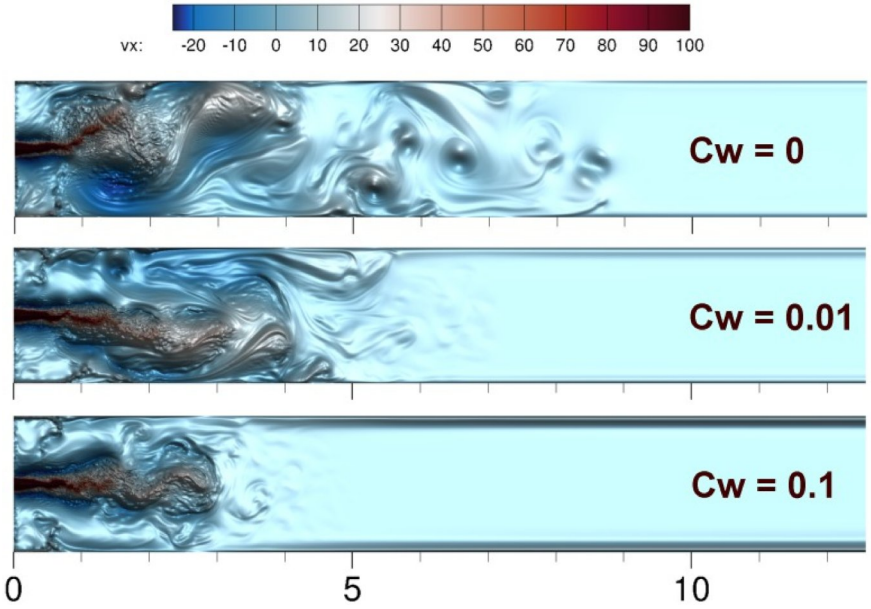

Figure 1: Transformation of a round jet in a transverse magnetic field from a DNS at *Re = 1,000* and *Ha = 500*. Instantaneous snapshots of streamwise velocity *vx* are shown in the *(x,y)*-midplane at *z = 0* for wall-conductivity *Cw = 0, 0.01*, and *0.1*. The magnetic field *Bz* is perpendicular to the *(x,y)*-plane.

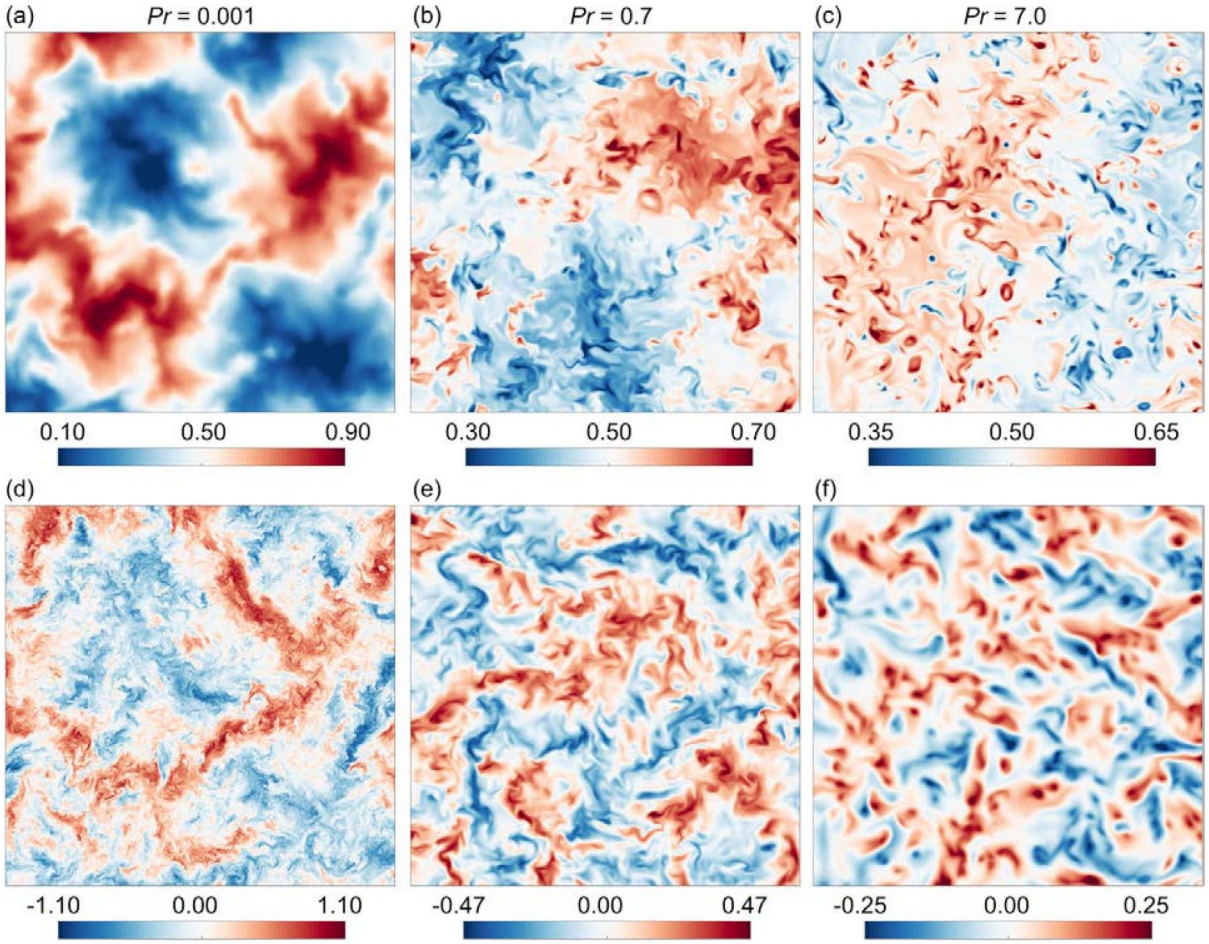

Figure 2: Instantaneous snapshots of temperature *T* (top) and vertical velocity *vz* (bottom) fields in the horizontal mid-plane. Results of DNS show the effect of Prandtl number for and $Ra = 10^6$ and *Pr = 0.001, 0.7*, and *7*.

Numerical Investigation on Reactive Flows of Several Practical Applications

Research Institution
Lehrstuhl für Fluiddynamik, Universität Duisburg-Essen

Principal Investigator
Andreas Kempf

Researchers
Efim Borukhovich, Luis Cifuentes, Linus Engelmann, Timo Lipkowicz, Dominik Meller, Johannes Sellmann

Project Partners
—

SuperMUC Project ID: pn68nu (Gauss Large Scale project)

Introduction

This project collates individual applications from the Fluid Dynamics group at Duisburg-Essen University. The subprojects include the investigation of phenomena from the fields of nanoparticle synthesis, supersonic flows and stratified burners using LES, DNS, and direct chemistry.

Results and Methods

Numerical investigation of spark-ignited combustion engines
This first subproject targeted the assessment of cyclical variations in internal combustion engines using LES in a Lagrangian-Particle framework. HPC facilities for the simulations were required due to the resolution necessary to achieve good results in the complex geometry as well as the run time over several cycles. The inhouse solver PsiPhi was employed to simulate 30 consecutive cycles of the optical research engine at the TU Darmstadt. A density based framework was used to solve the momentum and scalar transport equations using eight-order CDS supported by a tenth order filter for momentum and TVD for the scalar equations. Walls and moving parts were modeled using an efficient Lagrangian-Particle and immersed boundary based method. Flow fields were compared to assess the validity of the proposed method and simulation. Experimental and computational flow fields agreed well. An instantaneous snapshot during intake can be seen in Figure 1. Cyclical variations were assessed by seeding randomly generated Lagrangian tracers in the intake manifold and tracing them down to ignition. Temporal and spatial information of these particles is saved to files and thermodynamical trajectories of the different states experienced by the particles were reconstructed. The proposed method was able to predict the underlying physics well.

Flamelet modeling for the LES of pulverized coal flames
The aim of this subproject was the improvement of simulation tools for solid fuel combustion (biomass, coal, waste) utilizing Lagrangian-particles. Here, LES of the Central Research Institute of Electric Power

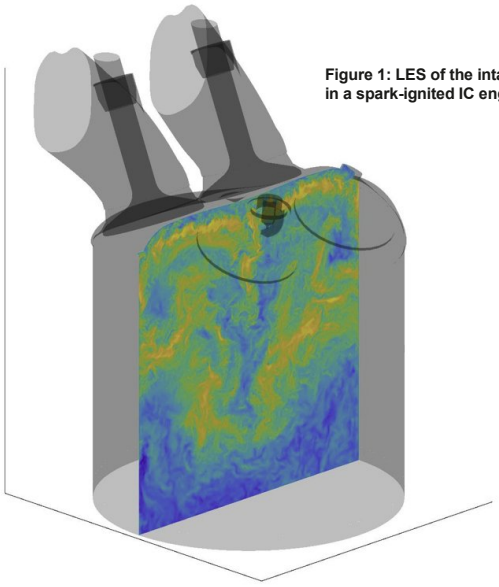

Figure 1: LES of the intake strong in a spark-ignited IC engine.

Industry (CRIEPI) lab pulverized coal flame have been conducted using a four-dimensional flamelet model based on two mixture fractions for volatiles and a hydrogen pilot, a normalized progress variable and the enthalpy [1]. The effect of the suction probe on the scalar field measurements was tested by simulating this probing, observing relative changes up to 50% in various quantities and locations. By consideration of these probe effects, the agreement between the experiment and simulation could be improved significantly; at the same time, the simulation also provided the unperturbed scalar fields, without probing effects. The flamelet model gives a robust and cost-effective prediction of the investigated laboratory flame, provided that the probing effects are considered. The HPC facilities for the simulations were necessary due to the high resolution necessary to get good agreement with experimental results as well as the many test runs to investigate different model parameters and models. Ongoing research in flamelet modeling is made in the context of co-firing of coal and ammonia to reduce pollutants by introducing a hydrogen carrier as a fuel. The introduction of a new fuel stream

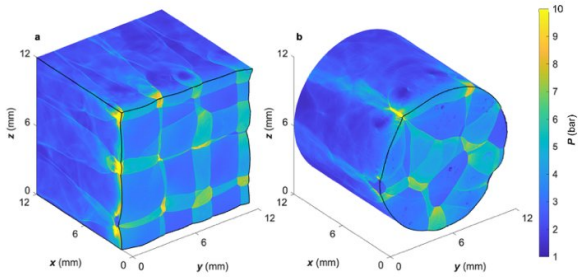

Figure 2: LES of detonation waves propagating in a channel (a) and a tube (b).

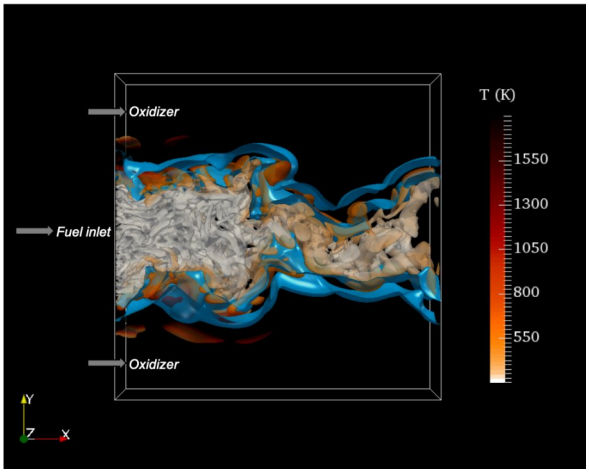

Figure 3: Direct numerical simulation - nanoparticle formation in a non-premixed flame.

complicates the flamelet description and is part of the ongoing work.

Three-dimensional detonation structure
This third sub-project aimed at improving the understanding of detonation cellular structures which in turn is not only important for safe operation of combustion devices that make use of detonations waves but also to prevent unwanted detonations in nuclear reactors or process plants. The resources in this sub project were primarily used for three-dimensional simulations of detonation wave propagation in confined channels and tubes. In particular, the results were used to investigate the influence of the geometry on the propagation dynamics and the structure of the wave. In the past, detonation simulations have been mostly restricted to 2D computational domains, due to immense resolution requirements. While detonation kernels in 2D stem from the collision of two transverse shocks, two classes of detonation kernels exist in 3D, introduced as line kernel blasts and multi kernel blasts, which contain substantially more extreme states. Rectangular channels lead to a highly regular matrix of transverse waves, thus reflecting the confining geometry, while tubes lead to a more complex and chaotic detonation structure (see Figure 2). The results have been presented on ICDERS and are currently under review for publication [2]. A grid resolution of 10 micrometers was necessary to capture important length scales present in the detonation structure, resulting in a total number of 1.7 billion numerical cells. Since a low dissipation Riemann solver with high order reconstruction and, even more important, detailed reaction kinetics were used, i.e. the solution of a stiff system of ODE's was calculated at every point for each time step, the cost of these simulations is very high, making the use of a super computer essential.

Detailed FDF-LES simulations of the SpraySyn burner
The fourth subproject investigates the effect of subgrid stresses on the coagulation kernel with simulations of the SpraySyn burner. The resources were used for three-dimensional LES simulations of the SpraySyn burner. The flame chemistry was resolved with a flamelet generated manifold approach, and each spray droplet was resolved with an individual lagrangian particle. A particular focus was on nanoparticle modeling. Here, a sectional model was used with and without a subgrid model to investigate the effect on the coagulation rate for the first time. Further, detailed measurements of the particle size distribution in the flame became available for the first time and allowed a detailed validation of the simulation results. The simulation required several validation simulations with the largest one having 200 million cells and 0.5 million time steps. As a result, the experimental data could be reproduced sufficiently and confirm the simulations while no significant effect of the subgrid model was observed [3] [4]. For future work on this project, the subgrid effects could be resolved via an FDF-method.

DNS of nanoparticle synthesis in reactive flows
The fifth subproject investigated the formation of nanoparticles in reactive flows using direct numerical simulations. These simulations resolved not only the smallest scales of the turbulent flow, but also the smallest relevant scales of the nanoparticle field - the Batchelor scales. The main objective here is to understand the physics of diffusion, coagulation, and nucleation and to use the DNS database for future modeling efforts. All simulations were performed with the in-house code PsiPhi, using direct chemistry with 8 species and 3 reactions and a sectional model for nanoparticles (20 sections) on a computational domain with 500 x 500 x 100 numerical cells at a grid resolution of Δ =40 µm (see Figure 3). Each simulation required 4M core-h on 25,000 CPU cores. The reasons for the high computational cost were a) the application of direct chemistry and b) the number of sections (and thus transport equations) required for the nanoparticle phase. Figure 2 presents three-dimensional blue iso-surface $Q_1 = 1.0 \times 10^{19}$ [#/m^3] (representing monomers of titanium dioxide nanoparticles) with vortical structures colored by temperature. The simulation of this subproject represents the state-of-the-art in the DNS of flames producing nanoparticles, and will provide meaningful, transferable and sustainable insight into particle formation, to guide the modelling efforts.

References and Links

[1] D. Meller et al., Energy & Fuels 35 (9) (2021) 7133-7143.
[2] J. Crane et al., Proc. Combust. Inst. (2022), under review.
[3] J. Sellmann et al. Powder Techn., under revision.
[4] S.J. Baik et al. ICLASS (1) (2021).

Large-Eddy Simulation of a Delta Wing

Research Institution
[1]Institute of Aerodynamics and Flow Technology, German Aerospace Center, Göttingen

Principal Investigator
Philip Ströer[1]

Researchers
Tobias Knopp[1], Axel Probst[1], Nils Rathje[2], Rolf Radespiel[2]

Project Partner
[2]Technische Universität Braunschweig

SuperMUC Project ID: pn69mu

Introduction

On aircraft engines longitudinal vortices are intentionally generated by strakes to stabilize the flow on the wing in high lift-configurations. Therefore, streamwise vortices are of great practical importance for the design and analysis of aircraft aerodynamics using numerical simulation.

Since several fundamental properties in the streamwise development of these vortices are still under research, high-fidelity Large-Eddy-Simulations (LES) of an inclined delta wing are performed, which are part of a joint numerical and experimental investigation of the stability properties of longitudinal vortices (funded by DFG under grant numbers KN 888/22 and RA 595/252).

Within this project the investigation of vortex wandering is of particular interest. Vortex wandering is a superimposed coherent low-frequency motion of longitudinal vortices. This is visualized in Fig. 1 showing the instantaneous vortex core positions from experiments. For these types of flows, it becomes crucial to distinguish between this large-scale motion of the vortex and the small-scale turbulent motion. Therefore, a data-base is needed to characterize the vortex wandering.

Although vortex wandering has been investigated for several decades now, it is still not clear whether it is originated from the wind-tunnel environment or from inherent flow instability [1,2]. Therefore, one aim of this project is to investigate the stability properties of We consider highly turbulent rotating flows, which provide better insight into geophysical flow phenomena wandering on a fundamental level. For this purpose, methods like proper orthogonal decomposi-tion, dynamics mode decomposition and linear stability analysis will be used.

In the first period of this project [3, 4] numerical methods were used which rely on additional physical models (so called hybrid RANS/LES methods that combine statistical turbulence models with local LES). However, it was shown that these models are not

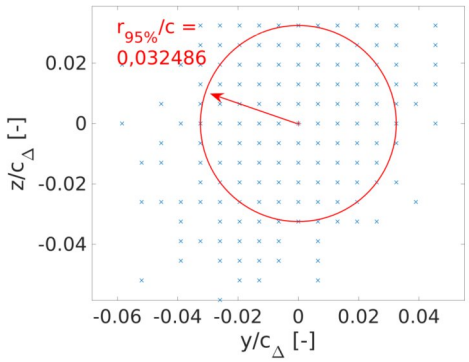

Figure 1: Instantaneous vortex positions at a fixed streamwise position (Plane normal to the flow direction).

capable of reproducing vortex wandering. Therefore, a sub-goal of this project is to improve these so-called hybrid simulation techniques for the simulation of longitudinal vortices based on the new LES database.

Taking everything into account, the top-level scientific goal is to establish an innovative numerical simulation method based on the hybrid RANS/LES approach for the accurate prediction of the interaction of longitudinal vortices and the turbulent boundary layers on aircraft wings in high-lift configuration.

Results and Methods

For this purpose, a highly-parallelized wall-resolved Large-Eddy Simulation (LES) is performed for a chord Reynolds number $Re = 0.99 \cdot 10^6$ and a Mach number $Ma \approx 0.16$ at an angle of attack $\alpha = 8°$.

The simulations on SuperMUC-NG are carried out using the compressible unstructured finite-volume DLR TAU-Code. The convective fluxes are discretized using a low-dissipation numerical scheme.

The hybrid mesh contains approx. $8 \cdot 10^6$ cells. The surface mesh is depicted in Fig. 2. Close to the wing the grid consists of hexahedral elements. The average normalized grid resolution is $\Delta x^+ \approx 40$, $\Delta y^+ \approx 1$, and $\Delta z^+ \approx 20$, where x denotes the streamwise and z the spanwise direction. This complies with the well-known resolution requirements for wall-resolved LES of turbulent boundary layer flow. The chosen computational

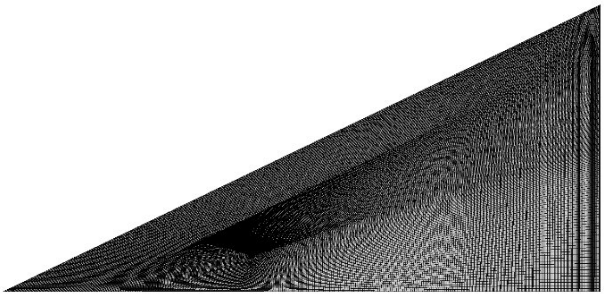

Figure 2: Surface Mesh of the Delta Wing.

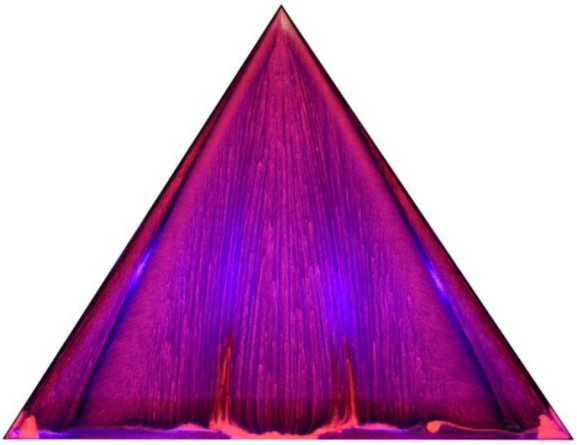

Figure 3: Experimental oil-flow visualization.

time step is based on the temporal resolution requirements known for wall-resolved LES of wall-bounded flows.

Additionally, time-resolved stereo particle image velocimetry (PIV) measurements are performed in the subsonic wind tunnel (MUB) of the TU Braunschweig.

The current status of the still ongoing simulation is shown in Fig. 4. A qualitative comparison of surface streamlines show that a physical vortex pattern arises containing the primary vortex indicated by a lateral flow including a clear reattachment line and a small secondary counterrotating vortex indicated by a tip flow.

This can be also seen from the iso-surfaces that are contoured by c_p at different streamwise positions in Fig. 4. A comparison of the surface streamlines in Fig. 4 with experimental results in Fig. 3 shows a good qualitative agreement. As expected, turbulent structures seem to form on different length-scales which is illustrated by the *Q*-criterion iso-surfaces in Figures 4 and 5.

The simulation is massively parallelized using approx. 10,000 cores. In this way, the number of cells per domain is 80,000. TAU uses geometric domain decomposition of the given problem and starts one process for each domain. Pure MPI is used for inter-process communication, i.e. to exchange the flow variables at the domain boundaries.

Restart data was saved during the simulation multiple times. One restart solution needs 126 GB of storage.

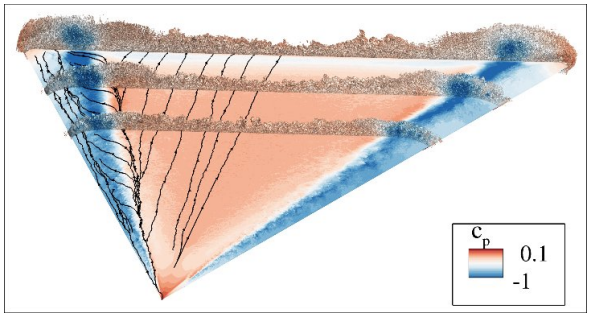

Figure 4: Instantaneous solution of the Large-Eddy Simulation.

The data is transferred to local storage systems on a regular basis.

For the final evaluation of the simulation it is planned to write reduced data sets of the relevant flow regions (sub-volumes, slices) in order to reduce the file sizes that need to be stored and post-processed.

Ongoing Research / Outlook

The future research will focus on the numerical details and the complex post-processing of the LES:

For this purpose, a complex memory-intensive post-processing procedure is applied. The DLR software FlowSimulator is used in order to enable a massively parallelized post processing on SuperMUC-NG. In this way, a reduced postprocessed dataset is written that can be used for further analysis.

This data will be used to investigate the stability properties of the vortex and to provide a database for improving hybrid RANS/LES models. In this way, the final goal is to gain insight into the physics of vortex wandering and to establish an innovate numerical simulation method for reliable predictions of this phenomenon.

References and Links

[1] Devenport, W. J. et al. J. Fluid Mech., Vol. 312, 1996, pp. 67-106.
[2] Bailey, S. C. C., et al. J. Fluid Mech., Vol. 843, 2018, pp. 722–747.
[3] Francois, D. et al. J. Aircr. DOI: 10.2514/1.C036273.
[4] Probst, S. et al. AIAA Scitech 2019 Forum, San Diego, California. DOI:10.2514/6.20190331.

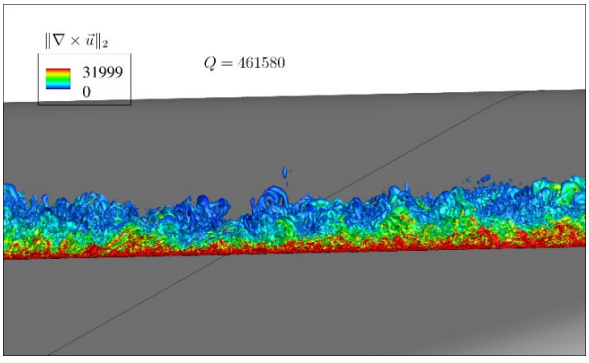

Figure 5: Section of the Delta Wing boundary layer: Q iso-surfaces contoured by the absolute value of the vorticity.

Symmetry based turbulence theory of a turbulent round jet

Research Institution
TU Darmstadt

Principal Investigator
Martin Oberlack

Researcher
Cat Tuong Nguyen

Project Partners
–

SuperMUC Project ID: pn73fu (Gauss Large Scale project)

Introduction

Turbulence has been a topic of research for many decades and finds its applications in many aspects of life. Still, turbulence is not fully understood up until today. The Navier-Stokes equations, which are used to describe the motion of viscous fluids, do not have a general analytical solution. Consequently, many researchers work with specific canonical cases to understand turbulence better.

In the recent years as computers became increasingly powerful, more and more direct numerical simulations (DNS) have been conducted to solve turbulent flows. DNS solve the Navier-Stokes equations without explicitly modeling the turbulence. The main advantage of DNS over experiments is that any imaginable quantity can be generated at any point of the domain. However, with increasing Reynolds numbers *Re* the computational effort rises almost proportional to Re^3 which is why so far DNS is only used for fundamental research as opposed to in industrial applications. Therefore, DNS is not suited for complex geometries until many decades in the future e.g., for DNS of an airplane or a car. In industrial applications the quantities of interest usually only involve mean velocities instead of instantaneous velocity fields. Rather than solving highly complex infinite dimensional hierarchy of moment equations, simplified models are used. However, accuracy of the solution suffers from simplified models of the turbulence.

A method to model turbulence with the infinite dimensional hierarchy of moment equations using Lie symmetry groups has been developed by the PI and his research team. The Lie symmetry principle has been contemplated as a key feature of physics by Einstein's seminal work on special relativity. With the advent of quantum mechanics in the 1920s, symmetries have been established as an axiomatic basis of physics in general. Today it acts as the foremost guiding principle to understand and mathematically model new physical laws to be discovered.

With the recent publications [2,3], we have been able to conduct large-scale DNS of a plane channel flow between two infinite parallel plates at *Re = 10,000* on SuperMUC-NG to test new scaling laws which can be derived directly from theory without any further simplification or modeling. With Lie symmetry analysis, symmetry invariant solutions for arbitrary order of moments have been generated from the infinite dimensional hierarchy of moment equations. One of the key results show that the moments of the streamwise velocity in the channel center follows a power-law scaling with an exponent only dependent of the first and second order moment. The knowledge obtained shall be extended to turbulent round jet flows.

The goal of this project is to validate the scaling laws that have been derived for a turbulent round jet using Lie-symmetry analysis with numerical data. The study of turbulent jet flows is not only interesting as a canonical shear flow. Turbulent jet flow finds applications in acoustic control, mixing of fluids, combustion and even exhalation. It can be described as a stream of fluid that is spreading into an ambient medium through a nozzle. To model the turbulence of a jet flow, a great effort has been made to identify the relevant parameters with experimental and numerical data. Additionally, in jet flow specifically, large computational boxes are needed to capture the spreading of a turbulent round jet. Thus, the simulation of such a flow requires a vast amount of computational resources.

Results and Methods

The CFD code Nek5000 has been used for the direct numerical simulation of a turbulent round jet with and without co-flow. The Nek5000 code is based on the spectral element method (SEM) and solves the Navier-Stokes equations on a hexahedral mesh. The code is well established in the scientific turbulence community and is highly scalable over a million ranks using Message Passing Interface (MPI) for parallelization. As a timestepping method the implicit second order backward differentiation formula (BDF2) scheme is used. The timestep is dynamically controlled and so

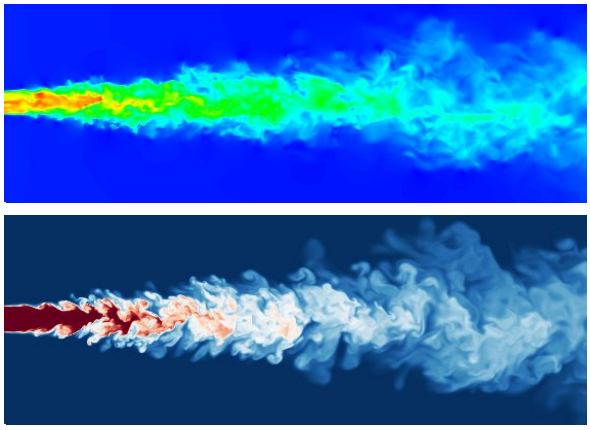

Figure 1: A cross section showing the instantaneous visualization of the velocity magnitude (top). A cross section showing the instantaneous visualization of a passive scalar (bottom).

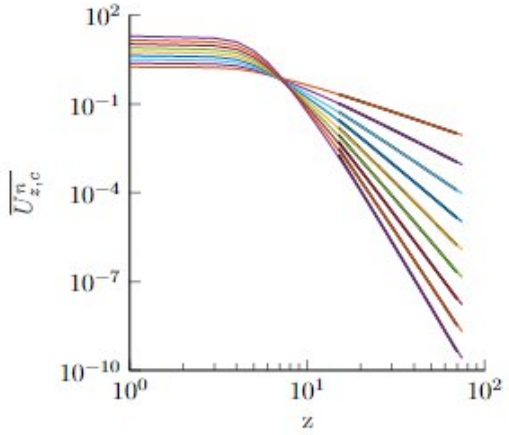

Figure 2: Scaling of the moments of the streamwise centerline velocity over the axial distance from the orifice. The black lines show the scaling laws from the moments 2 (top) to 10 (bottom). The colored lines show the corresponding DNS data.

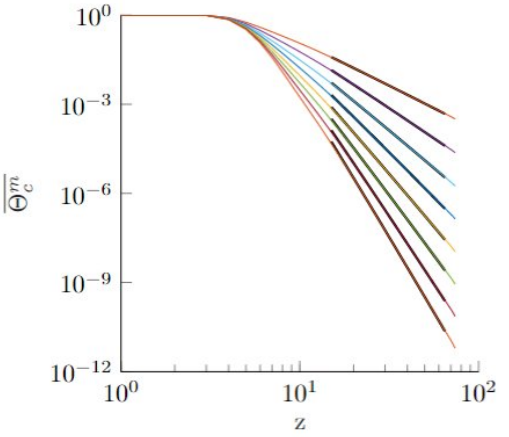

Figure 3: Scaling of the moments of the passive scalar on the centerline over the axial distance from the orifice. The black lines show the scaling laws from the moments 2 (top) to 10 (bottom). The colored lines show the corresponding DNS data.

the computational costs are further optimized. SEM features an exponentially growing accuracy with increase of the order of the polynomial basis functions used.

Currently, we are running two DNS cases on SuperMUC-NG of which one is a DNS of a turbulent round jet at *Re=3,500* without co-flow and one is a DNS of a turbulent round jet at *Re=3,500* with a co-flow velocity ratio of *0.05*. Additionally, a passive scalar equation is solved with *Pr=0.71*. The simulation is carried out on two separate domains. On the first domain, a turbulent pipe flow is generated. Then, the velocity field of the turbulent pipe flow is interpolated onto the main computational box at each time step to generate a turbulent round jet. The main computation is carried out on a truncated cone box with a length of 75 jet nozzle diameters and a radius of 4 nozzle diameters at the inlet and 32 jet nozzle diameters at the outlet. The size of the computational box ensures the full capture of the spreading of the jet and to minimize the influence of the far-field boundary conditions. Altogether the box consists of ~ 90 million grid points, which amounts to ~60 million DOFs.

The figures show the results of the DNS of a turbulent round jet without co-flow. A cross section of the velocity magnitude and the passive scalar concentration of the DNS can be observed in Figure 1. The highly accurate data generated by the DNS allows us to validate the scaling laws that have been derived. The jet scaling laws predict that all the higher moments can be calculated from the exponent of the first and second moment. Figure 2 shows that the exponents of the third up to the tenth moment indeed show great agreement with the theory. The scaling laws of the passive scalar show a similar result in Figure 3.

Ongoing Research / Outlook

The large-scale simulations are currently conducted on SuperMUC-NG. The highly resolved data generated by the simulations enables us to investigate self-similar behavior up to an axial distance of 75 diameters from the inlet nozzle. The Nek5000 code allows us to efficiently run the simulation on 512 nodes in parallel. When the high moment statistics of the co-flow DNS are converged, we will also hope to validate the scaling laws of co-flow jets derived with Lie symmetry analysis. Currently, both DNS are still running to extract statistics for the turbulent budgets. As soon as the turbulent round jet with and without co-flow are better understood, the research is planned to be extended onto different inlet conditions where we expect a higher influence of certain parameters in the scaling laws.

References and Links

[1] https://www.fdy.tu-darmstadt.de/
[2] Hoyas, Sergio, Oberlack, Martin, Alcántara-Ávila, Francisco, Kraheberger, Stefanie V., Laux, Jonathan 2022. Phys. Rev. Fluids 7, 014602.
[3] Oberlack, Martin, Hoyas, Sergio, Kraheberger, Stefanie V., Alcántara-Ávila, Francisco, Laux, Jonathan 2022. Phys. Rev. Lett. 128, 024502.

Interactions between wing wake and horizontal tail plane flow in high-speed stall conditions

Research Institution
University of Stuttgart, Institute of Aerodynamics and Gas Dynamics

Principal Investigator
Thorsten Lutz

Researchers
Johannes Kleinert, Jens Müller

Project Partners
–

SuperMUC Project ID: pn98wo

Introduction

The flight envelope of large transport aircraft is limited in terms of Mach number and angle of attack. At low Mach numbers and high angles of attack, large flow separations occur on the aircraft's wing, which limit maximum lift. At high Mach numbers, however, flow separation occurs at smaller angles of attack due to shocks that form above the wing (high-speed stall). A further increase of Mach number or angle of attack leads to coupled periodic oscillations of the shock and the corresponding boundary layer separation that are denoted as transonic buffet. This in turn causes oscillations of the surface loads that may induce structural vibrations, which can be critical in terms of structural fatigue and flight control. Transonic buffet has been investigated experimentally and numerically for several decades now, mainly for the two-dimensional case, i.e. for airfoils. However, several open questions still exist, especially for swept, tapered wings. In addition, only few studies exist on the development of the separated wake and its interaction with the tail plane under high-speed stall conditions. It is expected that the unsteady wake causes significant load oscillations for the tail plane, possibly leading to fatigue and impacting controllability. The DFG research unit FOR 2895 "Unsteady flow and interaction phenomena at High Speed Stall conditions" [1] aims to further the understanding of transonic buffet and the corresponding high-speed stall phenomena described above. This is pursued by means of experimental and numerical investigations performed on a realistic transport aircraft configuration, the XRF1 research configuration designed by Airbus. In addition, detailed measurements are conducted for a generic tandem wing configuration consisting of two un-tapered and un-swept wing sections. The former has been equipped with a horizontal tail plane (HTP) and Ultra High-Bypass Ratio nacelles (UHBR) as part of the project. The simulations shown here are part of subproject 4 of the research group, which is focusing on the development of the separated wake and its interaction with the tail plane under high-speed stall conditions. As part of the research, it is investigated how the turbulent fluctuations in the wake and the load oscillations of the tail plane resulting from the wake impingement correspond to the buffet phenomena on the wing.

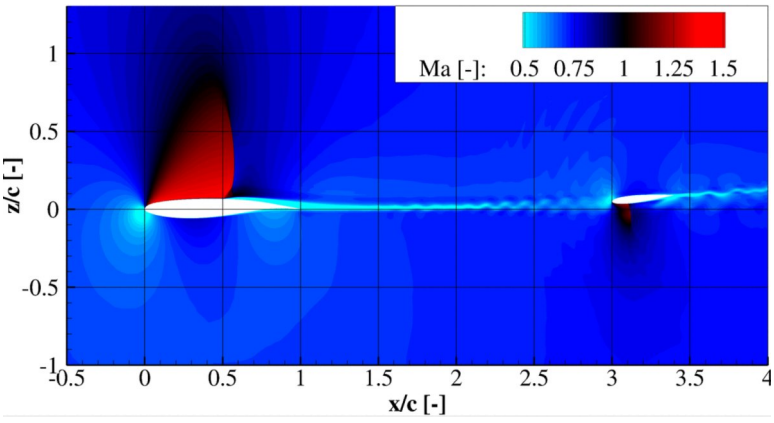

Figure 1: Flow field around the tandem configuration in high-speed stall conditions.

Results and Methods

For the two configurations mentioned above, the tandem wing configuration and the XRF1 configuration, hybrid RANS/LES simulations under high-speed stall conditions are conducted on SuperMUC-NG, using the DLR TAU finite-volume code. The zonal hybrid method AZDES (Automated Zonal DES) developed for transonic flows at the Institute of Aerodynamics and Gas Dynamics is applied. For a typical simulation run, about 600,000 core hours are needed for the tandem and 1.8 million core hours for the XRF1 configuration, respectively, as a sufficient number of convective time scales needs to be computed to achieve convergence of the flow field and turbulence statistics. Several simulation runs are performed varying the inflow conditions, i.e. Mach number, angle of attack and Reynolds number, to study their effect on the buffet and the wake tail plane interaction. For the XRF1 configuration, these runs are performed both without and with UHBR nacelles to evaluate their impact on the high-speed stall phenomena. As the simulations are still in progress, first results and findings are summarized here. For the tandem configuration [2], the impingement of the separated turbulent wake from the front wing, which experiences strong buffet for the investigated inflow conditions, on the rear wing is shown in Fig. 1. This impingement causes a strong fluctuation of

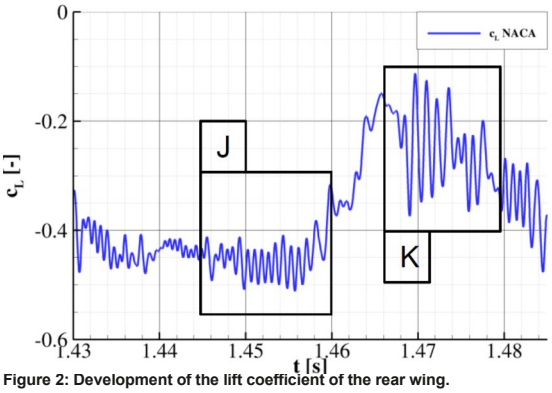

Figure 2: Development of the lift coefficient of the rear wing.

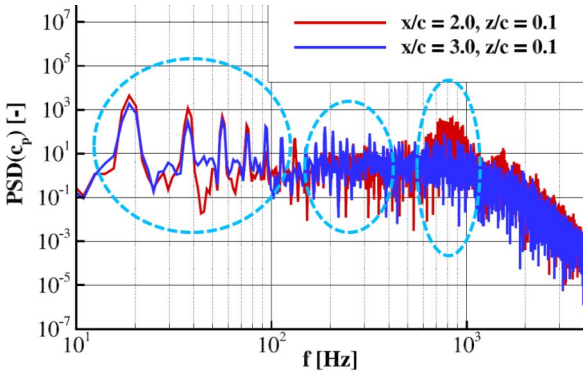

Figure 3: Power spectral density (PSD) of the pressure fluctuation in the wake.

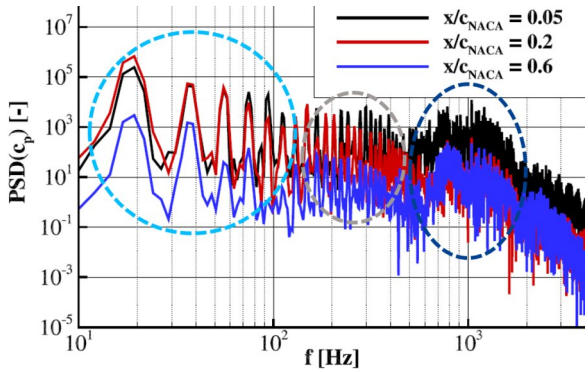

Figure 4: Power spectral density (PSD) of the pressure fluctuation on the surface of the rear wing.

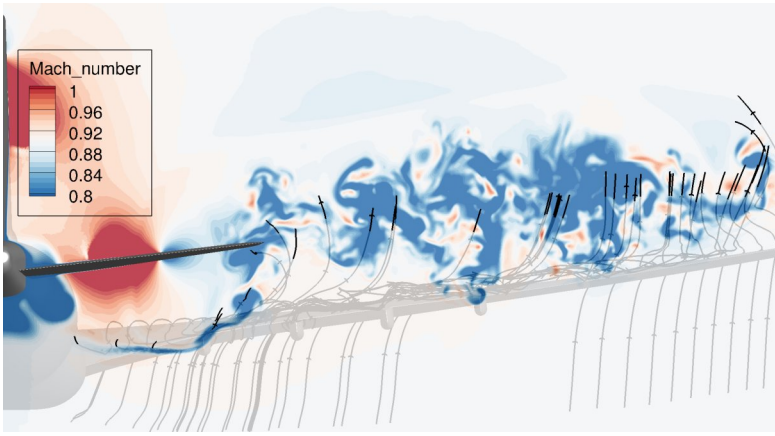

Figure 5: Separated wing wake of the XRF1 configuration in high-speed stall conditions.

the loading of the latter, as seen Fig. 2, which shows the development of the lift coefficient of the rear wing over one buffet period. Here, a low frequency oscillation with a period equal to the buffet period of the front wing can be distinguished from oscillations of higher frequency. The low-frequent oscillation is caused by the change of lift of the front wing during the buffet cycle, which is accompanied by a corresponding variation of the downwash behind it, leading to a change of the effective angle of attack for the rear wing. The high-frequent oscillations, however, are due to the impingement of the turbulent structures onto the rear wing, which evolve from the shear layers at the boundaries of the wake. It is notable that these oscillations vary significantly in amplitude and frequency over the buffet cycle, which corresponds to a variation of the size and strength of the turbulent vortices in the wake over the buffet period. During the phase when there is only a small amount of separation on the front wing, the level of fluctuations in the wake is comparatively small as smaller vortices with higher frequency are formed. During the phase when the separation is large, however, higher fluctuation levels with larger vortices of lower frequency are found in the wake. This is also evident in the spectrum of the pressure fluctuation in the wake, shown in Fig. 3. Besides the oscillation at the buffet frequency of 18.7 Hz itself and its higher harmonics, visible as distinct peaks in the spectrum, elevated amplitudes of pressure fluctuation are visible at higher frequencies that correspond to the turbulent fluctuations of varying size and frequency, at around 200-400 Hz and 800-1,000 Hz. As these vortices impinge on the rear wing, the variation of the rear wing loading shows a strong correlation to the fluctuations in the wake. This can be seen in the spectrum of the surface pressure of the rear wing, displayed in Fig. 4, which is notably similar to the spectrum in the wake, exhibiting the same peaks at the buffet frequency and its higher harmonics and also the increased levels at higher frequencies. For the XRF1 configuration, the impingement of the separated turbulent wake from the main wing on the HTP is shown in Fig. 5. As the flow over the mid- and outboard wing is completely separated, the wake behind it is convected upwards relative to the aircraft according to the inclination of the inflow. In the inboard section, however, there is less separation, and the remaining lift generation creates a downwash, causing the wake to pass the plane of the HTP at a lower vertical position. Due to the gradient in lift generation between those two sections, a notable swirl is introduced into the wake flow in this area. Under the investigated conditions, this swirling part of the wake impinges directly onto the HTP tip, causing pressure fluctuations on its surface that lead to oscillations of the HTP loading.

Ongoing Research / Outlook

The simulations of both configurations will be continued for the remaining inflow conditions. While advancing further simulations, shock motion, pressure spectra on wing and HTP, turbulent fluctuations in the wake and HTP loads will be investigated in more detail. In addition, results from both configurations will be compared with wind tunnel test data from the experimental campaigns.

References and Links

[1] https://www.for2895.uni-stuttgart.de/
[2] J. Kleinert et al., “Numerical simulation of wake tail plane Interactions on a tandem wing configuration in high-speed stall conditions”, DLRK 2021.

Turbulence model conditioning and flow control for aircraft vortical flow

Research Institution
Chair of Aerodynamics and Fluid Mechanics, Technical University of Munich

Principal Investigator
Christian Breitsamter

Researchers
Mauricio Jentys, Christopher Reinbold, Dominik Sedlacek

Project Partners
—

SuperMUC Project ID: pr27ce

Introduction

The Chair of Aerodynamics and Fluid Mechanics (AER) is active in the research on the aerodynamic characteristics of low aspect-ratio wings as well as of transonic transport aircraft wings. A turbulence model conditioning methodology for vortex dominated flows and the controllability and stability investigation of delta wing configurations has provided significant results and play a major role in the academic activity at AER. In this project, the aerodynamics of high agility aircraft are investigated. High agility aircraft often require an operation at extreme flight conditions. The configuration is based on wings with medium to high sweep angle and leading edges small radii. Even at low angles of attack the flow separates at the leading edge or at multiple swept leading edges and forms a vortex or vortex systems, respectively. Extensive investigations on hybrid delta wing configurations were carried out. The project can be divided into three subprojects. In the first subproject, ”Multiple Swept Wings”, funded by the German Research Association (DFG), the vortex dominated flow on hybrid-delta-wing configurations is investigated. The project “Aeroservoelasticity” deals with the development of a numerical method for the investigation of aeroelastic problems including control surface deflections which are modeled with a Chimera approach. The third subproject is based on the investigation of the potential for aerodynamic efficiency increase when coupling hybrid laminar flow control (HLFC) and variable camber (VC) technology. The usage of the High-Performance Computing system has played a fundamental role for the proper development of the simulations. Numerical simulations are routinely employed in parallel to experimental data in the design or investigation of new aerodynamic solutions. Considering a complex geometry and a progressively demanding level of accuracy, the computational grids need to be refined and the numerical methodology improved; both resulting in an increasing computational effort. In this sense, a High-Performance Computing system is essential for the effectiveness of the research. The results and future expectations are reported, showing their importance for the research projects.

Results and Methods

In the project, ”Multiple Swept Wings”, the flow field at hybrid-delta-wing configurations is investigated. The high-performance computing system is used for highly resolved simulations in space and time with different numerical methods. Delayed detached eddy simulations (DDES) are performed for a triple-delta-wing and a double-delta-wing configuration, Fig. 1. The simulations were conducted at subsonic speed, an angle of attack of $\alpha = 24°$ and an angle of sideslip of $\beta = 5°$. For the triple-delta-wing configuration, NA1 W1, the results of the DDES simulations are shown in Fig. 1a by means of isosurfaces of the non-dimensional Q-criterion and colored with the non-dimensional axial velocity. The results indicate a vortex breakdown on the windward side in the front part of the wing and a vortex breakdown on the leeward side in the rear part of the wing. This behavior is caused by the different effective leading-edge sweeps induced by the angle of sideslip. For the NA1 W2 configuration, a similar flow field develops. However, the vortex system on the leeward side is still stable at the trailing edge. The asymmetric flow field results in an abrupt rolling moment reversal and, therefore, flight mechanical instabilities. The next step is the analysis of the flow field at hybrid-delta wings at transonic freestream conditions. The computational time for a fully converged DDES for one configuration at $\alpha = 24°$ is about 1.0 Mio Core-h. The

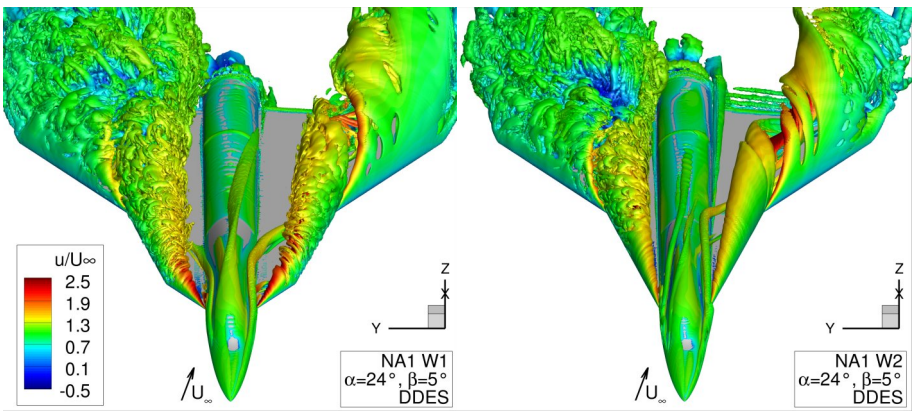

Figure 1: Isosurfaces of the non-dimensional Q-criterion, Q* = 500, colored with the non-dimensional axial velocity u/U∞ for triple-delta (left) and double-delta configuration (right) at α = 24°, β = 5°, and Re = 3.0 · 10⁶.

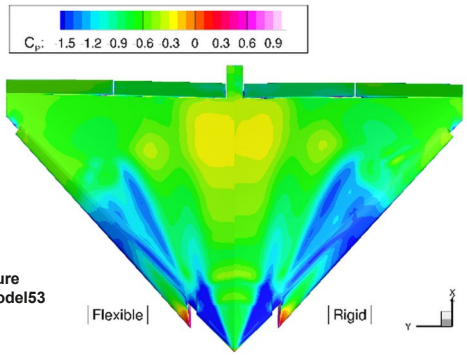

Figure 2: Surface pressure distribution Cp of the Model53 for the rigid and flexible configuration.

RANS simulations with the one-equation turbulence model of Spalart and Allmaras with rotation correction which are the basis of the DDES additionally need about 0.05 Mio Core-h [1]. In the Aeroservoelasticity project, a numerical tool for the computation of aircraft control surface aerodynamics with elasticity effects is developed and investigated. The solution is based on coupled high-fidelity Computational Fluid Dynamics (CFD) and Computational Structural Mechanics (CSM) simulations with the multidisciplinary simulation environment SimServer. In SimServer, the DLR Tau Code is embedded to obtain the CFD solution by solving the Reynolds-Averaged Navier-Stokes (RANS) equations. Structural displacements are computed with a modal solver. The Chimera implementation of SimServer is applied to model the control surfaces. Numerical simulations with the flexible Chimera method have been performed for two validation test cases and for the Model53 wing configuration, Fig. 2, which is a generic delta wing with an inboard and outboard trailing edge flap. Aerodynamic and aeroelastic simulations for several flap deflection angles are conducted in order to investigate the effect of structural deformations on the flow field and control surface effectiveness. The results revealed the significance of taking the structural flexibility into account in order to obtain accurate values and trends of the forces and moments for several flap deflection angles. Compared to the rigid simulation, the computational time increased by a factor of 1.7 for the aeroelastic simulation, which is considered to be acceptable given the considerable improvements in the accuracy of the results [2]. The LuFoVI–I project CATeW (Coupled Aerodynamic Technologies for Aircraft Wings) investigates the potential for aerodynamic efficiency increase when coupling hybrid laminar flow control (HLFC) and variable camber (VC) technology on a transonic transport aircraft wing. While individually, both technologies have proven to possess above mentioned potential, the combination is expected to lead to a higher efficiency increase due to synergistic effects. CFD simulations are performed using the DLR TAU Code on the high-performance computing system. The technology combination is modelled within a (U)RANS context, using special boundary conditions for the boundary layer suction due to the HLFC system and mesh deformation algorithms for reproduction of the VC capabilities. Simulations are performed fully turbulent for a baseline case and considering the effects of boundary layer transition using correlation-based transition transport models. Fig. 3 exemplarily shows the influence of different boundary layer suction mass flows on the transition location for a representative cruise condition. After first exploratory computations for a turbulent reference wing [3, 4], an aerodynamic dataset for the entire cruise flight envelope, considering a plethora of different parameter combinations (suction velocity distributions, VC configurations, operating conditions) needs to be constructed. Although a sampling strategy (e.g. Latin Hypercube Sampling) will be employed to reduce the necessary computational expenses while nevertheless satisfactorily resolving the cruise flight envelope, still a high number of cases need to be simulated. Furthermore, complementary simulations for transition prediction based on linear stability theory are planned for possible assessment and calibration of the transition turbulence model, while the aerodynamic database is planned to provide for training data of reduced order models of the steady-state aerodynamics of the aircraft wing.

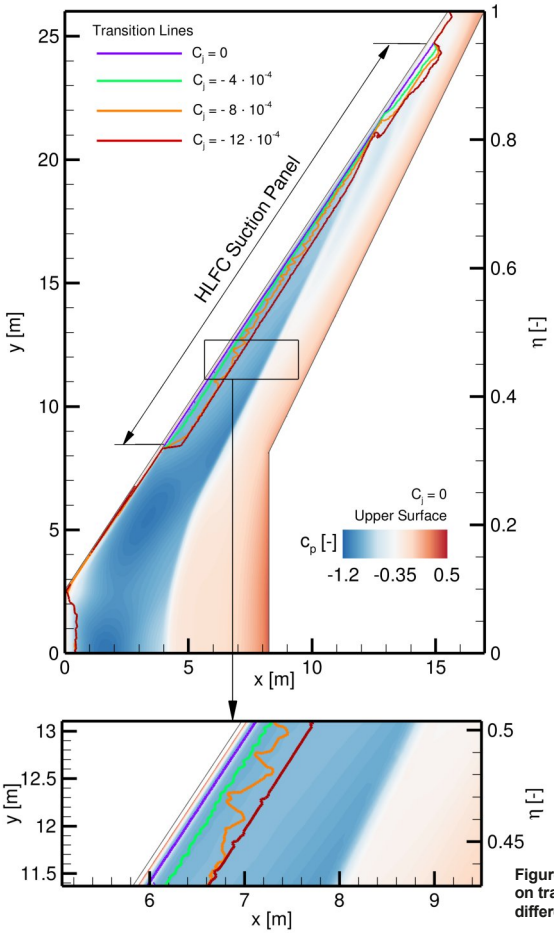

Figure 3: Transition locations on transonic aircraft wing for different suction mass flows.

Ongoing Research / Outlook

The use of SuperMUC-NG is essential to this project. Major investigations have been performed in the past and important and interesting results were achieved. Further numerical investigations are needed in all subprojects for a deeper comprehension of the vortex flows and their structural impact on delta wing configurations.

References and Links

[1] D. Sedlacek, C. Breitsamter, M. Visonneau, E. Guilmineau, J., Wackers: Assessment of Hybrid Delta Wing Vortex Flow Investigation – Part I at Subsonic Conditions. AIAA SciTech Forum, 2022. https://doi.org/10.2514/6.2022-0565

[2] C. Reinbold, K. Sørensen and C. Breitsamter. CEAS Aeronautical Journal, 2021. https://doi.org/10.1007/s13272-021-00561-3

[3] M. Jentys, T. Effing, C. Breitsamter, E. Stumpf, Numerical Analyses of a Reference Wing for Combination of Hybrid Laminar Flow Control and Variable Camber. DLRK, Bremen, 2021.

[4] M. Jentys, C. Breitsamter, Aerodynamic Analysis of Variable Camber and Hybrid Laminar Flow Control Coupling on a Transonic Transport Aircraft Wing. STAB-Workshop, Göttingen, 2021.

Heat Transfer Phenomena in Additive Layer Manufactured Cooling Channels

Research Institution
Chair of Aerodynamics and Fluid Mechanics,Technical University of Munich

Principal Investigator
Steffen Schmidt

Researcher
A. Doehring, T. Kaller, N. A. Adams

Project Partners
—

SuperMUC Project ID: pr48me

Introduction

The SuperMUC-NG project pr48me is part of the subproject D4 of the SFB/Transregio 40 [1] and a General Support Technology Programme (GSTP) by the European Space Agency (ESA). The main objective in the latter case is the investigation of turbulent heat transfer in rocket engine cooling ducts and the influence of rough surfaces on the onset of nucleate boiling. A thorough understanding of cooling channel flows is required for an efficient design of structural cooling in various technical applications. Examples include ventilation systems, electrical vehicle battery cooling to rocket engines. The latter are using the carried cryogenic propellant as coolant in a supercritical state. The correct prediction of the heat transfer within rocket engines cooling channel is crucial for safety reasons and in order to improve the engine's performance. The following results have already been obtained within this SuperMuc project:

- High fidelity simulations of a transcritical channel flow analyzing the influence of strong property variations on the turbulent flow and heat transfer [2].
- High fidelity simulations of a high aspect ratio duct studying the influence of secondary flow on the heat transfer [3].

The development of additive manufactured (AM) technologies as for instance Selective Laser Melting (SLM) offers new possibilities designing regenerative cooling channels. As a consequence, an increased surface roughness is observed in AM cooling channels, leading to an enhancement of the heat transfer but also to an increased pressure drop.

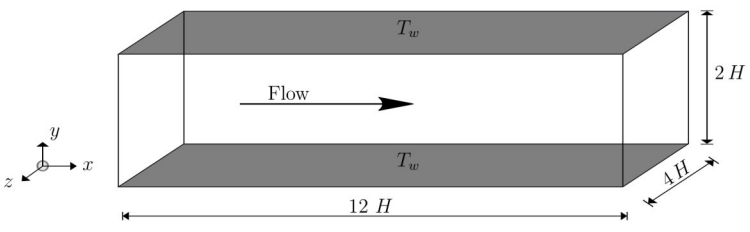

Figure 1: Domain for the well-resolved LES.

In order to investigate the influence of AM cooling channels on the heat transfer and the pressure drop a team of industry and research institutions from Germany and Belgium have started a GSTP research activity. These research activities cover the manufacturing of the cooling channel for experimental investigations and numerical investigations including Large-Eddy (LES) and Reynolds-Averaged Navier-Stokes (RANS) simulations. Within the SuperMUC-NG project pr48me we use numerically expensive well-resolved LES developed within our in-house LES solver. We further compare the obtained results to the more feasible RANS performed by project partners.

Results and Methods

Our LES are carried out solving the three-dimensional compressible continuity, momentum and total energy equations. A finite-volume method is applied in order to spatially discretize the governing equations on a block structured, curvilinear grid. An explicit second-order low- storage four-stage Runge-Kutta method with enhanced stability region is applied for time advancement. A compact four cell stencil approach is used to compute the convective fluxes. A discontinuity detecting sensor functional is used to switch the flux calculation between a linear fourth- order reconstruction for high accuracy and a more stable upwind-biased scheme. A physically consistent subgrid-scale turbulence model based on the Adaptive Local Deconvolution Method (ALDM) is included in the convective flux calculation. Viscous fluxes are determined by a linear second-order centered scheme. Thermodynamic and transport properties are obtained using an adaptive look-up table method based on the REFPROP database . One table is generated for the fluid domain imposing density and internal energy constraints and a second table is used for the boundary conditions imposing pressure and temperature constraints. Thermodynamic and transport properties are extracted from the tabulated look-up database via trilinear interpolation. A generic channel flow configuration with periodic boundary conditions in stream- and

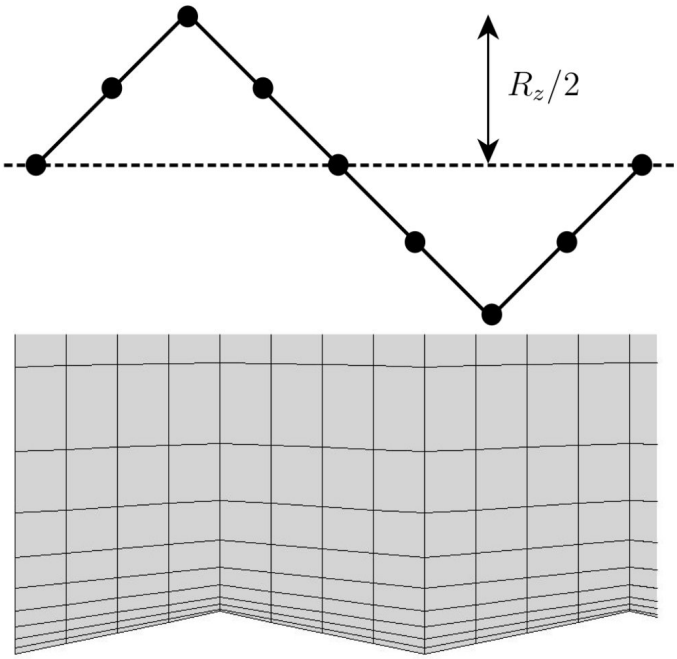

Figure 2: Rough grid modeling by adjusting the nodes close to the walls.

spanwise directions is used, shown in figure 1. Isothermal no slip boundary conditions are applied at the top and bottom walls. The dimensions are based on the channel half-height H with a size of 12H × 2H × 4H in the streamwise, wall-normal and spanwise direction, respectively. In order to fulfill the resolution requirements at walls, we use a hyperbolic stretching law in wall-normal direction, whereas a uniform grid spacing is used in stream- and spanwise directions. The roughness is modeled explicitly by adjusting the nodes close to the walls according to the required roughness height R_z. The node displacement and the grid are presented in figure 2. The triangular roughness shape and the distance between the peaks of 2mm is obtained from small AM channel wall sample prints produced by our project partner. The working fluid is ethanol at 4bar and 306K.

The grid consist of approximately 2.6 million cells and the LES is using 648 core on Supermuc-NG. The time needed to obtain statistical data is 20 runs of 48h. The storage requirements for the 3D data are about 8TB. Figure 3 shows the streamwise velocity u normalized with the bulk velocity ub along three slices in x,y,z direction, respectively. The white spots visible on the Y-slice are the triangular roughness shapes pointing inwards. Close to the wall (Y-slice) streaky structures are observed eluding the roughness peaks. The outward pointing patches are are creating small recirculation zones whereas the inward pointing patches are narrowing the cross section.

Ongoing Research / Outlook

In further investigations the distance between peaks will be reduced from 2mm to 0.5mm in the streamwise and spanwise directions. This is deduced from the sample wall prints where the prominent peaks are 2mm apart, but smaller ones are superimposed with a higher frequency. Furthermore, wall-modeled LES will be performed and compared to the well-resolved LES results to asses the wall modeling capabilities.

References and Links

[1] http://www.sfbtr40.de/
[2] Doehring, A., Kaller, T., Schmidt, S.J., Adams, N.A. (2021). J. Heat Fluid Flow 89, 108781. doi:10.1016/ j.ijheatfluidflow.2021.108781.
[3] Kaller, T., Pasquariello, V., Hickel, S., Adams, N.A. (2019). J. Fluid Mech., 860, 258-299. doi:10.1017/jfm.2018.836.

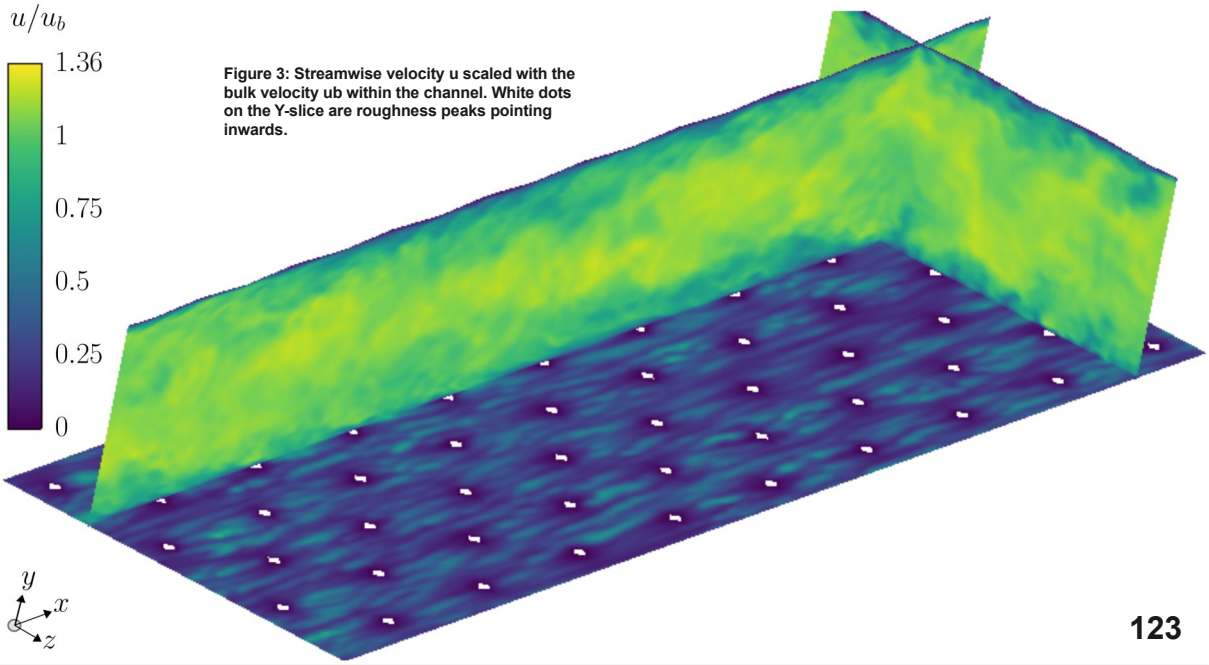

Figure 3: Streamwise velocity u scaled with the bulk velocity ub within the channel. White dots on the Y-slice are roughness peaks pointing inwards.

Heat transport enhancement in rotating Rayleigh-Bénard convection

Research Institution
[1]Max Planck Institute for Dynamics and Self-Organization, Göttingen

Principal Investigators
Detlef Lohse[1,2], Richard Stevens[2], Roberto Verzicco[2]

Researcher
Yantao Yang[2]

Project Partner
[2]Max Planck Center Twente for Complex Fluid Dynamics and Physics of Fluids Group, University of Twente

SuperMUC Project ID: pr74sa (Gauss Large Scale project)

Introduction

A tremendous variety of physical phenomena involve turbulence, such as the dynamics of the atmosphere or the oceans, avian and airplane flight, fish and boats, sailing, heating and ventilation, and even galaxy formation. Turbulent flow is characterized by chaotic swirling movements that vary widely in size, from sub-millimeter, over the extent of storm clouds, to galactic scales. The interaction of the chaotic movements on different scales makes it challenging to simulate and understand turbulent flows. Turbulent thermal convection plays an important role in a wide range of natural and industrial settings, from astrophysical and geophysical flows to process engineering. The paradigmatic representation of thermal convection is Rayleigh-Bénard flow [2] in which a layer of fluid is heated from below and cooled from above. The system is used to test new concepts in fluid dynamics, such as instabilities, non-linear dynamics, chaos, pattern formation, or turbulence. Rayleigh-Bénard convection is a relevant model for countless phenomena ranging from thermal convection in the atmosphere, oceans, and the outer layer of the Sun, to heating and ventilation of buildings and convection in various industrial applications. The Rayleigh-Bénard system is ideal for studying the interaction between the boundary layer and bulk dynamics, which will also shed more light on general wall-bounded turbulent flows.

One of the most striking features of Rayleigh-Bénard flow is the emergence of a large-scale convection roll. This roll is driven by small-scale thermal plumes detaching from the boundary layers at the top and bottom. However, under the influence of rotation [4,5] the flow reorganizes itself to a flow structure with vertically aligned vortices with increasing rotation rate, see figure 2a. Through the experiments by Rossby in 1969 and others, it is known that rotation can enhance heat transport, see figure 1. For water rotation can increase the heat transfer in the system with up to 25%. The heat transport enhancement is caused by Ekman pumping due to which hot or cold fluid near the bottom and top plates is drawn into the vertically aligned vortices and efficiently transported in vertical direction. The efficiency of Ekman pumping, and the rotation rate for which the highest heat transport enhancement is found,strongly depends on the non-dimensional control parameters Rayleigh and Prandtl. The Rayleigh (Ra) number indicates the thermal driving of the system, and the Prandtl (Pr) number the ratio of momentum diffusivity to thermal diffusivity of the fluid.

Results and Methods

For lower Ra the heat transfer at a given Ra and Pr is highest at an optimal rotation rate, at which the thickness of the viscous and thermal boundary layer is about equal. From the scaling relations of the thermal and viscous boundary layer thicknesses, we derive that the optimal rotation rate scales as $1/\mathrm{Ro}_{opt} \approx 0.12\mathrm{Pr}^{1/2}\mathrm{Ra}^{1/6}$, see figure 3. In the low Rayleigh regime the heat transfer is similar in a periodic domain and cylindrical cells with different aspect ratios, i.e. the ratio of diameter to height. This is consistent with the view that the vertically aligned vortices are the dominant flow structure, see figure 1a and figure 2a. For higher Rayleigh the above scaling for the optimal rotation rate does not hold anymore. It turns out that in the high Rayleigh regime, the flow structures at the optimal rotation rate are very different than for lower Rayleigh, see figure 2b. Surprisingly, the heat transfer in the high Rayleigh regime differs significantly for a periodic domain and cylindrical cells with different aspect ratios, which originates from the sidewall boundary layer dynamics and the corresponding secondary circulation, see figure 1b.

We emphasize that the investigation of the phenomena discussed above may find wider applications. It has namely been shown that for relatively low Rayleigh different stabilizing forces, such as horizontal confinement and a second stabilizing scalar field (also known as double diffusive convection), can generate a surprisingly large heat transport enhancement. The heat flux enhancement due to a stabilizing force is observed in an intermediate regime in which the stabilization is enough to re-organize the flow, but not so strong that it severely suppresses the flow motions [3]. The observation that this process may be different

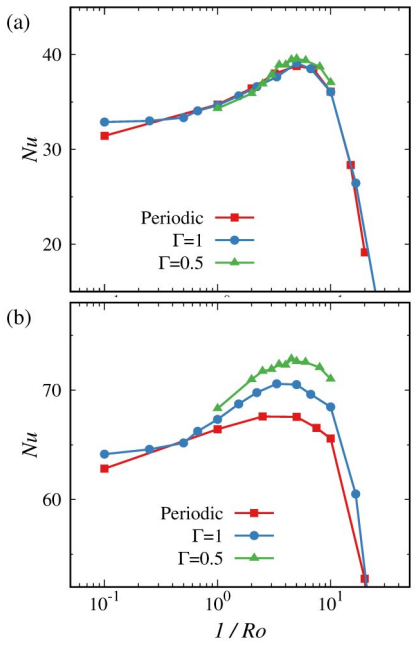

Figure 1: Comparison of the heat transport (Nusselt number) in a periodic and in cylindrical domains with Γ=1/2 and Γ=1 for water for (a) lower Rayleigh (b) higher Rayleigh [2].

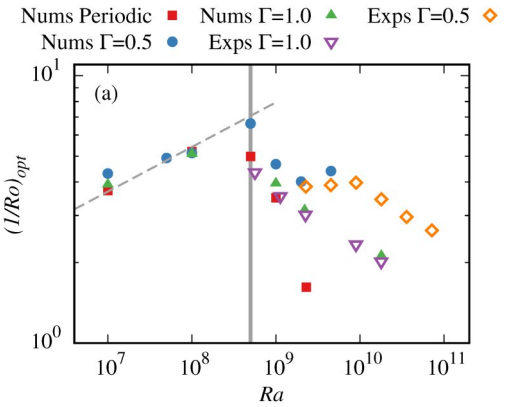

Figure 3: The optimal rotation rate for different Ra for water and different geometries, i.e. a periodic domain and cylindrical domains with Γ=0.5 and Γ=1. The vertical line marks the transition from the low to high Rayleigh regime. The dashed lines indicate the boundary layer scaling law $1/Ro \approx 0.12 Pr^{1/2} Ra^{1/6}$. Figure taken from Ref. [2].

in high Rayleigh number rotating convection may indicate that the effect of other stabilizing forces may be different in other high Rayleigh number settings.

In this project, we perform direct numerical simulations to perform novel simulations of highly turbulent flows. We consider highly turbulent rotating flows, which provide better insight into geophysical flow phenomena. To ensure that all turbulent length and time scales are adequately resolved very large computational grids are required, which requires tens of millions of core hours. Simulations using up to 37 thousand computational cores are performed on SuperMUC-NG and generating overall database of hundreds of terabyte. The benefit of simulations is that they allow one to adjust control parameters arbitrarily and isolate physical effects in an attempt to identify the physical mechanisms that control heat transport in highly turbulent flow. The challenge of these simulations is that they are performed on huge computational domains, making the simulations very time-consuming. To perform these large-scale simulations, we developed an in-house second-order finite-difference flow solver specially developed for cylindrical geometries and periodic domains. To perform landmark simulations, we have completely rewritten our code to optimize its performance on large-scale computing platforms like SuperMUC-NG. Large-scale parallelization is obtained using MPI to divide the computational domain over the outer computational loops, while OpenMP is used to obtain two-dimensional parallelization throughout. This approach is favored since it limits network communication between computational nodes by performing computations within a shared memory environment. To ensure computational efficiency, great care has been taken to vectorize computationally intensive parts of the code, limit memory movement by handwriting and in-lining computational operations and data movements, efficient use of different cache levels, and replace library calls with handwritten routines to perform case-specific optimizations.

Ongoing Research / Outlook

SuperMUC-NG allowed us to perform unprecedented simulations, i.e., the largest turbulence simulations in a fully closed domain, which will be compared to the Göttingen Rayleigh-Bénard convection experiments, which have revealed the transition to the ultimate regime in which the boundary layers along the plates become turbulent and the heat transport increases faster. Computer simulations of such turbulent flows are notoriously computationally demanding due to the extensive range of length and time scales that needs to be resolved. Therefore, groundbreaking simulations can only be performed on the largest supercomputers in the world, such as SuperMUC-NG. Our simulations were only possible due to algorithmic developments that limited the communication between different computational tasks. This improved our code's parallel efficiency. However, even with the massive computational and storage facilities offered by SuperMUC-NG, it is still an enormous challenge to simulate such highly turbulent flows, and more powerful supercomputers are required to study more challenging cases.

References and Links

[1] Group website: https://pof.tnw.utwente.nl;
Project details: https://stevensrjam.github.io/Website/
[2] Y. Yang et al., Phys. Rev. Fluids 5, 053501 (2020).
[3] K.L. Chong et al., Phys. Rev. Lett., 119, 064501 (2017).
[4] R.J.A.M. Stevens et al., Eur. J. Mech. B Fluids 40, 41-49 (2013).
[5] J.Q. Zhong et al., Phys. Rev. Lett. 102, 044502 (2009).

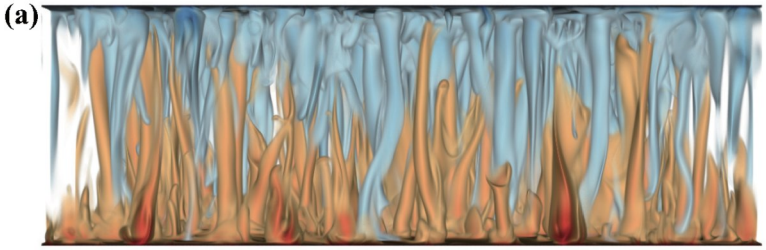

Figure 2: Volume renderings of the temperature field at the optimal rotation rate for (a) lower and (b) higher Rayleigh. The colormap in both panels is identical. The figure shows that the flow structure at the optimal rotation rate is very different in the low and high Ra regime [2].

Modulation of Turbulent Properties in Spray Flame Burning n-Heptane: Direct Numerical Simulation

Research Institution
Laboratory of Fluid Dynamics and Technical Flows (LSS/ISUT), University of Magdeburg

Principal Investigator
Dominique Thévenin

Researchers
Abouelmagd Abdelsamie, Cheng Chi

Project Partners
—

SuperMUC Project ID: pr84qo

Introduction

Our main work on SuperMUC started at the end of 2014; at this time, the main topic was the fundamental investigation of spray flames in a simple geometry using direct numerical simulation (DNS). With the growing power of SuperMUC and with the further numerical optimization done concerning our code, more complex domains could later be handled: in particular, the spray flame in a spatially evolving jet has been computed. Currently, and with the help of SuperMUC, this work is further extended to include additionally models to describe nanoparticle synthesis from a spray flame in a real burner. This is a very challenging task because there are three phases that must be taken into account: a continuous gas phase, liquid droplets, and solid nanoparticles. Additionally, it is necessary to take into account detailed chemistry to describe the complexity of the kinetics. Several papers about this topic have been published by our group with the help of SuperMUC. Without the granted core hours, such studies would have been quite impossible. Even if much has been achieved, further progress is still needed in order to understand better the complex coupling processes between multiphase flow and physicochemical processes.

Results and Methods

The current project relies on the in-house DNS code DINO. DINO is a third-generation, seven-year-old Fortran90 code, which has been developed in our group starting from the beginning of 2013 [1-5]. DINO is a three-dimensional low-Mach number DNS solver code with a 6th order finite-difference spatial discretization for reacting and multi-phase turbulent flows. The code is parallelized in two dimensions using the 2DECOMP&FFT library that acts on top of standard MPI and FFTW. The Poisson equation for pressure is solved by means of FFT for both periodic and non-periodic boundary conditions, but with dedicated pre- and post-processing FFT techniques in the latter case. The ODEs are integrated using a semi-implicit 3rd order Runge-Kutta relying on LAPACK, BLAS, and PyJac (analytical Jacobin matrix solver) libraries. By default, the chemical source terms are computed using the open-source Cantera-2.4.0 library, whereas the transport properties are computed either with the Cantera library or with the EGlib-3.4 library. The discontinuous phase in multi-phase flow simulations (droplets/spray) is tracked by using either a classical Lagrangian point-force approach (for small, non-resolved droplets) or with the Immersed Boundary Method (IBM) technique for fully resolved cases. Nanoparticle synthesis leading to the development of a third solid phase in the code is simulated using the monodisperse model developed by Kruis et al. 1993. In this model three additional equations are solved for three different parameters: nanoparticle number concentration, total surface area concentration, and total volume concentration. Regarding the wall, a novel implementation of IBM, based on directional ghost-cells with a level-set function, has been introduced into DINO in order to consider the walls in a computationally efficient manner [5]. The initial turbulent flow field is generated by inverse Fourier transform of an analytically prescribed energy spectrum (Passot-Pouquet or Von Karman-Pao). In DINO, input/output operations rely on MPI-I/O routines provided by the 2DECOMP&FFT library. These files are used for restarting the simulations, while DINO uses parallel HDF5 saving for actual postprocessing data. The required resources on SuperMUC, until now, for this project are summarized in Table 1.

Total core hours	Overall storage	Typical no. of cores	No. of generated files
55 M	127 TB	4,096	12,000

Table 1: Summary of required resources (over 7 years).

Recently direct numerical simulations (DNS) of nanoparticle synthesis in spray flame have constituted the most ambitious part of the project. This topic itself

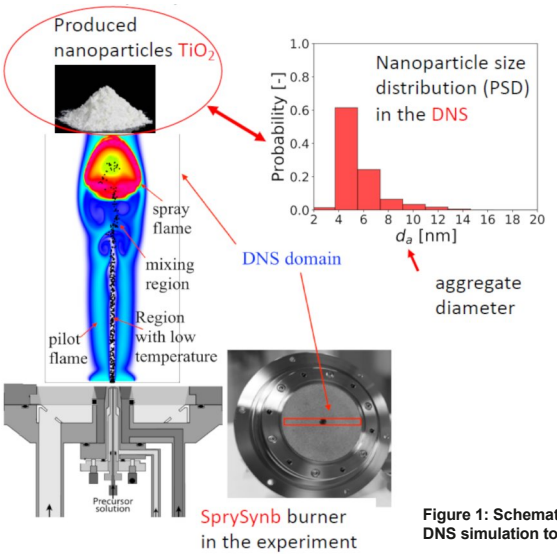

Figure 1: Schematic diagram representing the complete process used in the DNS simulation to predict the nano-particle size distribution [3].

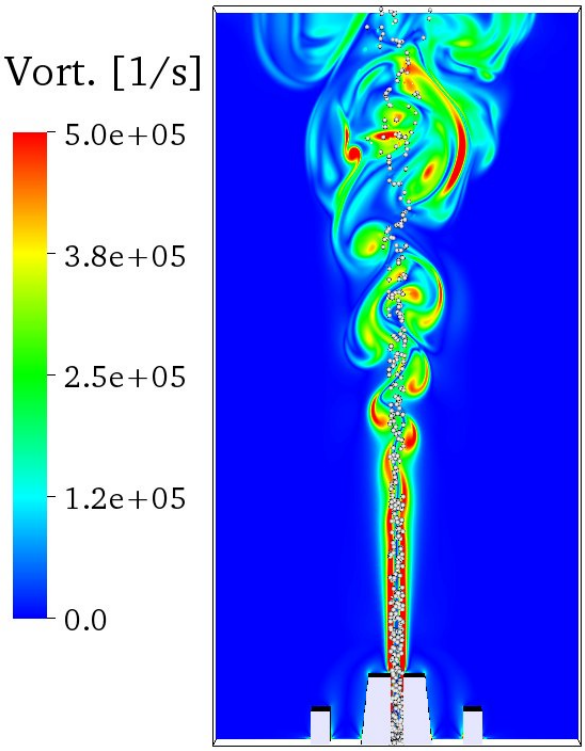

Figure 2: nstantaneous contour of instantaneous gas vorticity magnitude when considering the real injector geometry [4].

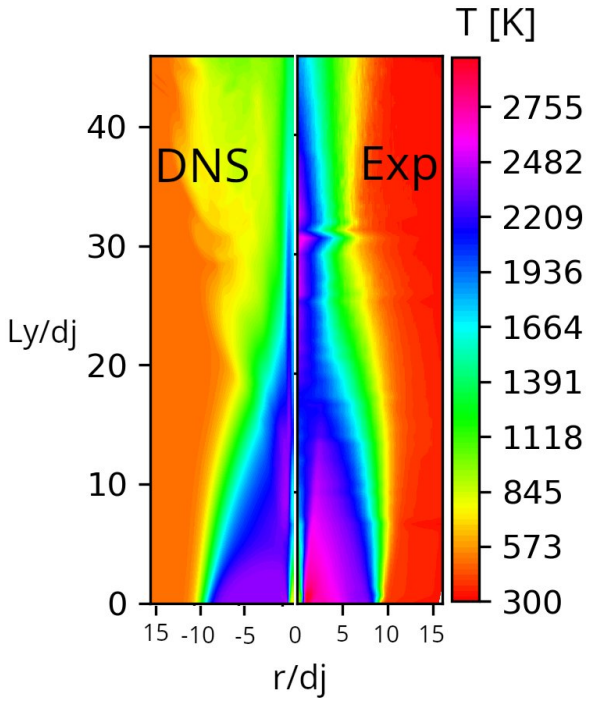

Figure 3: 2D contour of the gas temperature. Comparison between the DNS data and the available experimental data.

is a part of the DFG Priority Program SPP1980; "Nanoparticle Synthesis in Spray Flames, SpraySyn: Measurement, Simulation, Processes". This project started in July 2017 and it is running for six years. The main contribution of our group in this work is to investigate the nanoparticle synthesis in the spray flame and give more details about the complete process, as it will be explained in Sub-project A. In this project, the real geometry of the burner and of the spray injector were included in the simulation. For this purpose, a novel implementation of the immersed boundary method (IBM) was developed as a side project as it will be explained in Sub-project B.

Sub-project A The main purpose of this subproject is to perform direct numerical simulations (DNS) of a burner with conditions similar to that of the SpraySyn burner. The SpraySyn burner is designed as part of a collaborative DFG project (SPP1980) entitled “Nanoparticle Synthesis in Spray Flames SpraySyn: Measurement, Simulation, Processes”. This burner is designed to generate nanoparticles from spray flames. The authors are involved in this collaborative DFG project. During the last granting period of SuperMUC, several publications have taken place documenting the results of this project, in particular [2-4]. In these publications, a relevant part of domain has been simulated while taking into account the real geometry. In this manner, it was possible to estimate the resulting nanoparticle size distribution (PSD) as shown in Fig. 1. A short extension has been selected in the crosswise direction to keep the 3D effects regarding turbulent structures, relevant in particular for spray evaporation, while at the same time reducing the necessary computational time. Different parameters have been changed and investiaged during this work as follows:

(1) the solvents: ethanol or xylene;
(2) droplets injection speed;
(3) droplet size.

Sub-project B The impact of the wall of the SpraySyn burner on the nanoparticle synthesis is a part of the investigation in the DFG project. In order to do that, our DNS code (DINO) needed several modifications. An innovative Immersed boundary method (IBM) developed by our group [5] has been implemented in DINO to consider in a suitable manner the wall effect. During the development of this novel implementation, several cases have been tested and investigated. For example, we started with a simple, standard benchmark: the flow over a sphere. The complete validation procedure has been recently published in Ref. [5]. Later on, far more complex cases have been investigated as well: (1) transient processes controlling ignition by a hot jet issued from a pre-chamber, (2) Internal combustion engine, (3) Biomedical applications, and (4) impact of the wall in the SpraySyn burner [4] as it can be seen from Fig. 2.

Ongoing Research / Outlook

Currently, a huge analysis are performed on the running cases. Part of the current analysis it to compare the DNS with the available experiment as it seen in Fig. 3. The output and published data of the current project can ultimately become a reference data-set for many practical and academic works dealing with turbulent spray combustion. The complete 3D output data generated in the project will thus be gathered in a database accessible for other researchers who would like to validate their own spray evaporation or ignition model by analysis and comparison with DNS data.

References and Links

[1] Abdelsamie A. et al., Comput. Fluids, 131 (2016) 123-141.
[2] Abdelsamie A., Thévenin D. Proc. Combust. Inst. 37 (2019) 3373-3382.
[3] Abdelsamie A. et al., Flow Turbul. Combust, 105 (2020) 497-516.
[4] Abdelsamie A., et al., Turbul. Combust., 106 (2021) 453-469.
[5] Chi C. et al., J. Comput. Phys., 404 (2020) 109122/1-20.

DNS study of the early flame kernel development under engine conditions

Research Institution
Institute for Combustion Technology, RWTH Aachen

Principal Investigator
Heinz Pitsch

Researchers
Hongchao Chu, Temistocle Grenga

Project Partners
–

SuperMUC Project ID: pr89pa

Introduction

Cycle-to-cycle variations (CCV) in spark-ignition (SI) engines depend particularly on the early combustion phase as shown in the experiments by Schiffmann et al. [2]. The early flame kernel initiated by the spark can be influenced by different factors, such as heat loss, spark plug, and the thermo-fluid dynamic states in the vicinity of the spark plug. These effects are typically coupled and influenced by the specific engine geometry and operation conditions. Tailored numerical studies, able to examine the influence of isolated effects pertaining to CCV, can assist and improve the understanding gained from experimental investigations. The effects of inhomogeneous mixture on turbulent combustion have been investigated by computational studies. A detailed review is given by Lipatnikov [3]. However, few studies addressed the flame kernel configuration. The present study investigated the effects of inhomogeneous equivalence ratio on early flame kernel development under engine conditions. For this purpose, datasets of direct numerical simulations (DNS) for idealized engine geometries have been established and analyzed.

Results and Methods

The mixture state and composition in the simulation have been chosen to be representative of direct injection spark ignition (DISI) engine operation at low load. In order to provide well-defined, but engine-relevant flow configurations, flame kernels have been computed in decaying isotropic turbulence. The turbulent Reynolds number, Damköhler Number, and Karlovitz number are specified as close as possible to engine conditions. To be consistent with realistic engine flame development, an ignition heat source has been employed to initialize the flame kernels. The source term is defined to vary smoothly in time and space such that the low-Mach number flow and ideal gas regimes remain valid. Eight realizations were simulated by adding the ignition energy at different locations in the isotropic turbulence field. Figures 1 and 2 show the evolution of the normalized global heat release rate and the global mixture fraction. Significant variations among different realizations can be observed. The local mixture fraction strongly influences the turbulence interactions with the flame kernels. Flame kernels with a mixture fraction close to stoichiometry tend to burn faster. Both local turbulence and mixture fraction are important. Realization r5, which has the mixture fraction closest to stoichiometry, burns slower than realization r1 because of the influence of turbulence. To illustrate the difference in the flame kernel development, a sequence of flame images has been extracted for realizations r1, r4, and r7, and is plotted in Figure 2.

Case	Core-h
Generation of flow field	0.4 M
Eight flame kernels	2 M
Total	2.4 M

Table 1: Summary of the performed simulations.

The present DNS database has been generated with the CIAO code [4] using a time- and space-staggered finite-difference reactive Navier–Stokes solver on Cartesian grids. Mass, momentum, and kinetic energy are conserved discretely in the low-Mach number formulation. In this study, the momentum equations are discretized with a fourth-order-accurate central difference scheme. For the scalar transport equations, a weighted essentially non- oscillatory (WENO5) scheme is used. This scheme has fourth-order accuracy in smooth monotone regions and third-order accuracy near discontinuities. To avoid inconsistencies between discrete mass conservation and scalar convection, a finite-volume mass flux is used in the scalar transport equations. Time integration is performed with a second-order-accurate Crank-Nicolson scheme. For the time-advancement of the Navier-Stokes equations, a variant of the fractional step method is used. The pressure correction is obtained by solving the Poisson equation with the algebraic multi-grid solver Hypre Boomer AMG. To efficiently advance the stiff advection-diffusion-reaction equations for species and temperature, the symmetric operator splitting is used. The resulting system of

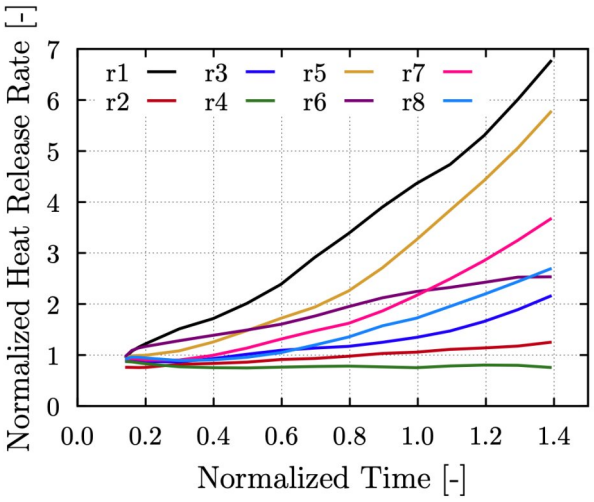

Figure 1: Evolution of normalized global heat release rate.

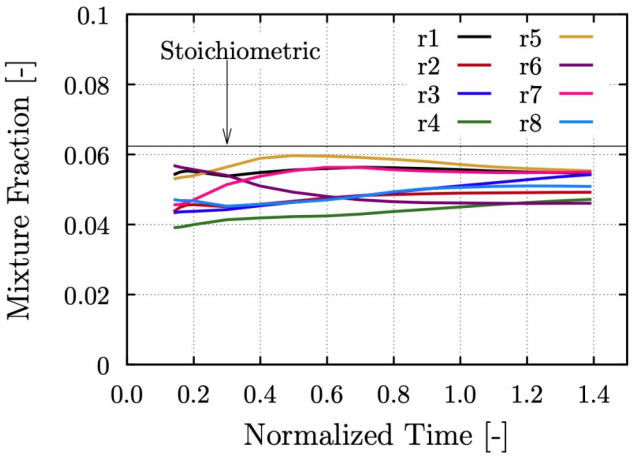

Figure 2: Evolution of the global mixture fraction.

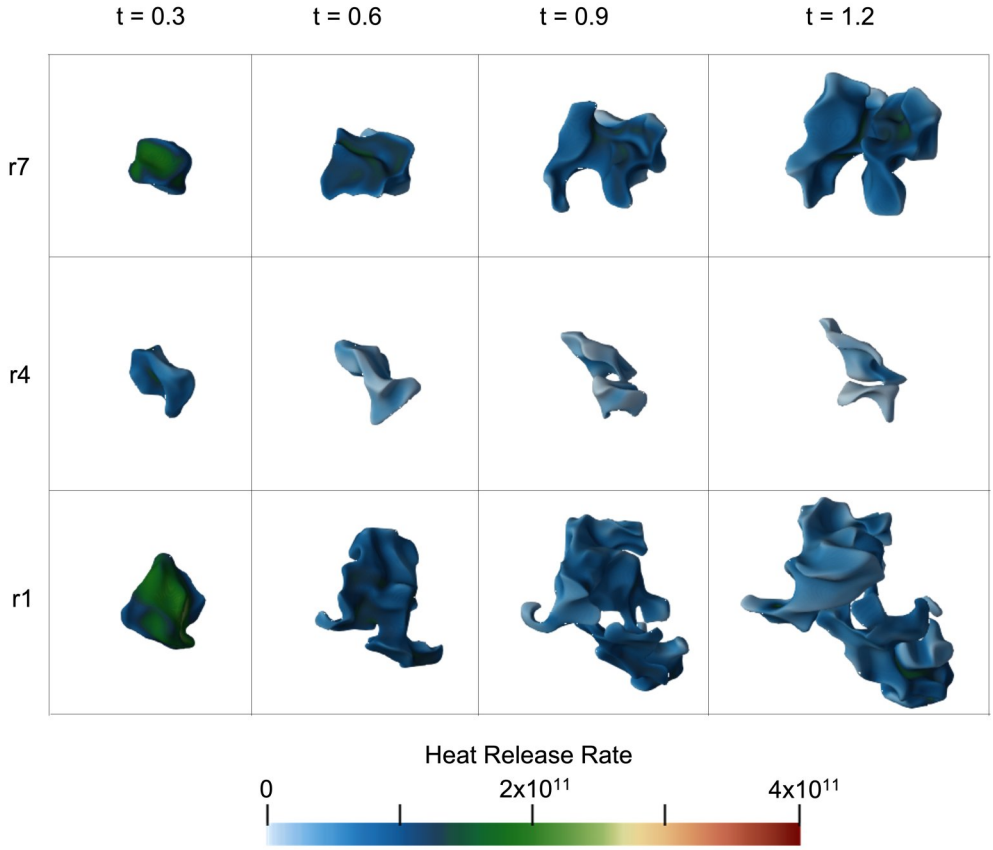

Figure 3: Iso-surfaces of temperature colored with heat release rate for realizations r1, r4, and r7 at different times.

ordinary differential equations for the zero-dimensional homogeneous reactor in each grid cell is solved using a fully time-implicit backward difference method. The Jacobian is evaluated analytically for computational efficiency. All datasets have been computed with grids of 960^3 cells on superMUC-NG with 10,752 cores in "general" partition. A summary of the performed simulations is given in Table 1.

Ongoing Research / Outlook

Current investigations focus on the effects of different fuels. Early flame kernels of anisole and cyclopentanone are studied. Those fuels have high flame speed and thus the potential to increase the thermal efficiency of engines. In addition, flame kernels of lean hydrogen/air mixture are also simulated to investigate the effects of differential diffusion for mixtures with a Lewis number smaller than unity.

References and Links

[1] https://www.itv.rwth-aachen.de/forschung
[2] P. Schiffmann et al., Int. J. Engine Res. 19 (2018) 491–508.
[3] A. N. Lipatnikov, Prog. Energy Combust. Sci. 62 (2017) 87–132.
[4] S. Kang et al., High-Q Club, 2015, http://www.fz-juelich.de/ias/jsc/EN/Expertise/High-Q-Club/CIAO/_node

A Fuel Candidate for the Storage and Re-Conversion of Electricity from Renewable Sources

Research Institution
German Aerospace Center (DLR), Institute of Combustion Technology

Principal Investigator
Georg Eckel

Researchers
Stephan Ruoff, Benedict Enderle, Patrick Le Clercq

Project Partners
—

SuperMUC Project ID: pr92ca

Introduction

The climate protection targets of the Paris climate agreement require complementary strategies incorporating all available technology options. While some sectors and applications can be electrified, hardly any short- and medium-term alternative exists to sustainable biogenic fuels and synthetic fuels (incl. e-fuels) for applications with high energy demand, such as long-haul air transport. Besides, efficient storage of renewable energy remains a challenge. One possibility is that chemical processes and renewable electrical energy are used to produce liquid hydrocarbons, which can be re-converted into electricity or serve as the basis for application-specific synthetic fuels. Fuel design for optimized properties (e.g. reduced emissions) and climate-neutral production in sufficiently large quantity are key aspects of current research activities of the German Aerospace Center (Deutsches Zentrum für Luft- und Raumfahrt; DLR). As the refinement steps (hydro-treating and hydro-cracking) in the fuel production process significantly increase the energy consumption and lead to a lower product yield, the team at the institute of combustion technology investigated whether the “raw” product of the Fischer-Tropsch process (the so-called FT-Crude) could be used directly.

Results and Methods

By means of SUPERMUC-NG, numerical simulations were performed comparing the combustion behavior of traditional kerosene (DLR reference fuel) with the FT-Crude. The test case was a lab scale spray burner producing a highly turbulent swirlstabilized flame. In this test case, the fuel is introduced into the combustion chamber by means of a hybrid prefilming airblast atomizer. The challenge for the prediction was the transient, reacting multiphase flow that combines multiple subprocesses such as atomization, evaporation, turbulent mixing and chemical reactions. All these subprocesses themselves are fuel dependent and highly interdependent. The computations were performed with the DLR in-house CFD-platform THETA-SPRAYSIM. THETA is a 3D finite volume CFD solver for the gaseous phase. Unstructured dual grids allow to incorporate the complex real geometry of the burner. The dispersed liquid phase is computed by the Lagrangian particle tracking code SPRAYSIM. Turbulence was modelled by a hybrid LES-RANS approach. The sub-grid scale model for the scale adaptive simulation was a k-ω based 2-equation model. The convective and diffusive fluxes are discretized using second-order central differencing schemes. The time discretization is based on a second-order Three-Point Backward (TPB) scheme. A projection method is applied to couple velocity and pressure. The Poisson equation for the pressure correction is solved by the flexible generalized minimal residual (FGMRES) method preconditioned by a single multigrid V-cycle. The other transport equations are computed by the BiCGStab method with Jacobi preconditioning.

Chemical reactions are calculated via a Finite Rate Chemistry (FRC) model. In this model, a separate transport equation is solved for each reactive scalar. As characteristic chemical timescales may differ by several orders of magnitude, an implicit stiff chemistry solver with source term linearization is used to avoid extremely small timesteps. Turbulence-chemistry interaction is modelled by an assumed PDF approach.

The chemical analysis of the two liquid fuels yielded the fuel compositions given in Figure 1 and Figure 2. A multi-component vaporization model approximating the discrete species distributions by a continuous description via gamma probability density functions (PDFs) was applied. It is obvious that the composition of the two fuels is very different. In particular, the FT-Crude contains a variety of long chained molecules which are not present in a kerosene product undergoing a fuel refinement process. It is noteworthy that the chemical composition does not only influence the chemical reaction but also the physical properties of the individual fuel. This affects the atomization and evaporation process and finally results in larger droplets (Figure 3). The larger droplets penetrate further into the combustion chamber and lead to a longer flame (Figure 4).

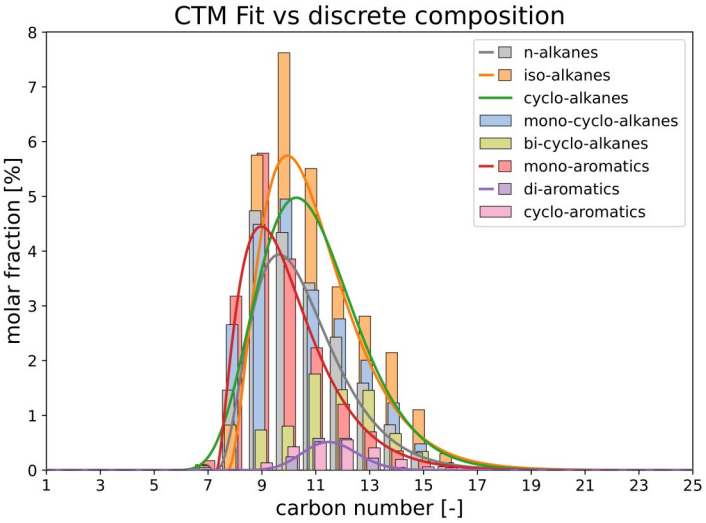

Figure 1: Composition of Kerosene.

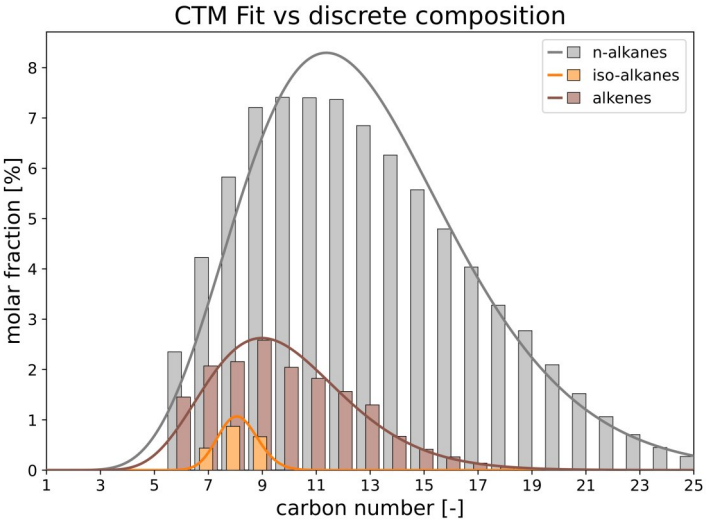

Figure 2: Composition of FT-Crude.

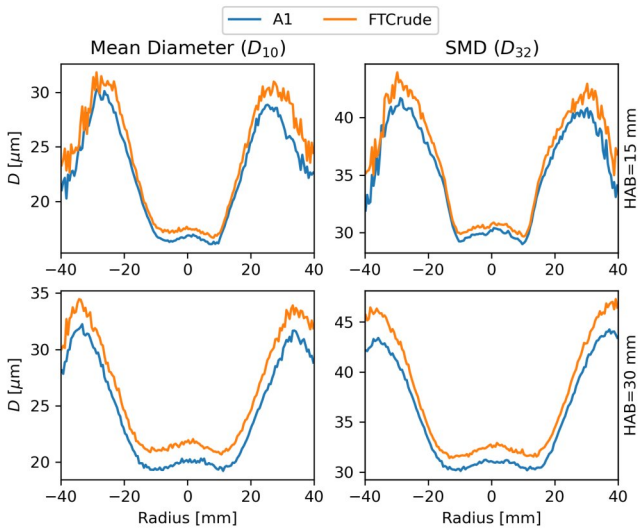

Figure 3: Fuel droplet diameter distribution for kerosene (blue) and FT Crude (orange).

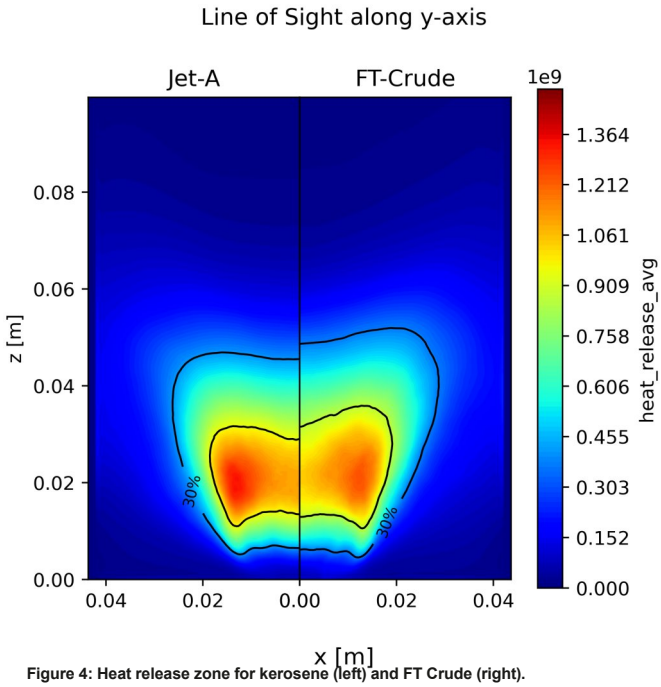

Figure 4: Heat release zone for kerosene (left) and FT Crude (right).

Generally speaking, the investigation showed that the FT-crude is combustible. However, open questions remain concerning pollutant emissions as well as the storage and thermal stability of such a fuel. These aspects are currently under investigation.

Ongoing Research / Outlook

The DLR project “Future Fuels” lay the foundation for the design of sustainable biogenic and synthetic fuels and demonstrated their application. Recently, the new DLR project “NeoFuels” was launched, which has besides aspects of fuel usage a greater focus on the practical production of sustainable fuels. The scientists and engineers within the project aim at a holistic approach (from source to production to use) evaluating the overall environmental impact.

References and Links

[1] https://www.dlr.de/vt/desktopdefault.aspx/tabid-10803/18874_read-43793/
[2] https://www.dlr.de/vt/desktopdefault.aspx/tabid-12479/21760_read-49882/
[3] https://www.dlr.de/vt/desktopdefault.aspx/tabid-9024/15615_read-38735/

Symmetry theory and turbulence

Research Institution
[1]TU Darmstadt

Principal Investigator
Martin Oberlack[1]

Researchers
Sergio Hoyas[2], Stefanie Kraheberger[1]

Project Partner
[2]Universitat Politècnica de València

SuperMUC Project ID: pr92la

Introduction

Wall turbulence is probably one of the open problems in physics with most applications in daily life. Even if the equations determining these flows have been known for almost 200 years, we still lack a complete theory. As wall-bounded turbulence is responsible for the 5% of the CO_2 dumped by humankind into the atmosphere every year, this is a problem of the uttermost importance. Experimental techniques dominated the research of turbulent flows until the eighties of the last century, when supercomputers started to be powerful enough to solve turbulent flows. However, due to the highly non-linear behavior of wall-turbulent flows, Direct Numerical Simulation (DNS) of these flows is restricted to simplified geometries. The most successful of these idealized flows are Poiseuille turbulent channels, where the fluid is confined between two parallel plates and the flow is driven by pressure. Since the seminal paper of Kim, Moin, and Moser in 1987, the friction Reynolds number has grown steadily. In this project, we have run a simulation reaching the 10,000 frontier. This simulation allowed us to study high Reynolds number effects. This friction Reynolds number is still less than the largest flow realization obtained by experimental means. However, the main advantage is that the DNS allows one to compute any imaginable quantity in the whole domain.

Unfortunately, the computational cost of a DNS is very high, such that the DNS of a commercial jet-airliner is several decades away, even for the biggest supercomputers available to date.

Therefore, DNS is not well-suited for design purposes. For most applications, instantaneous flow details are unnecessary, and statistical quantities such as the mean velocity are sufficient. However, considering turbulence as a statistical process leads to an infinite-dimensional hierarchy of moment-equations, which are extremely difficult to solve. Hence, for most applications, a truncated system is considered at the expense of introducing semi-empirical closure models (i.e., RANS methods).

MPI processes	RAM	Memory per task	Restart File	Tape Archive
2,048 4,096	1.8 TB	886 MB 443 MB	262 GB	100 TB

Table 1: Memory requirements in a computational box of (6,144 x 2,101 x 6,144) ~ $8 \cdot 10^{10}$ points.

The PI and his co-workers developed an approach that follows a very distinctive route as it considers the entire infinite-dimensional hierarchy of moment equations using Lie symmetry group methods. Since the work of the mathematician Lie, symmetries have experienced a striking evolution at the heart of physics. In his 1905 seminal work on special relativity, Einstein contemplated the symmetry principle as the key feature of physics. In the 1920s, quantum mechanics established symmetries as an axiomatic basis of physics in general. Today, Lie symmetry group methods act as the foremost guiding principle to understand and mathematically model-new physical laws. This project is the first simulation ever that allows us to test the application of the symmetry-based theory in the field of turbulence.

Results and Methods

The program code, LISO, performs a turbulence simulation using the Navier-Stokes equations for an incompressible fluid in a plane channel between two infinite

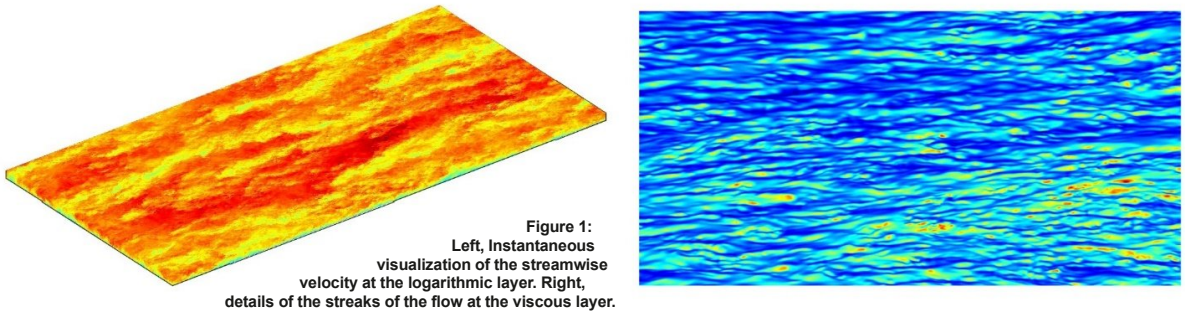

Figure 1: Left, Instantaneous visualization of the streamwise velocity at the logarithmic layer. Right, details of the streaks of the flow at the viscous layer.

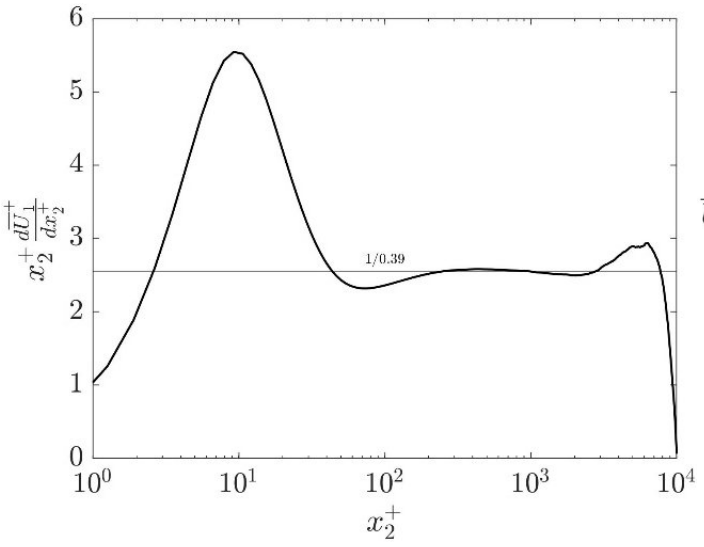

Figure 2: Indicator function. The flat region between 200 and 2,000 indicates the existence of a very long logarithmic layer. The value of 0.39 for the Karman constant can be taken as almost definitive for this range of Reynolds numbers.

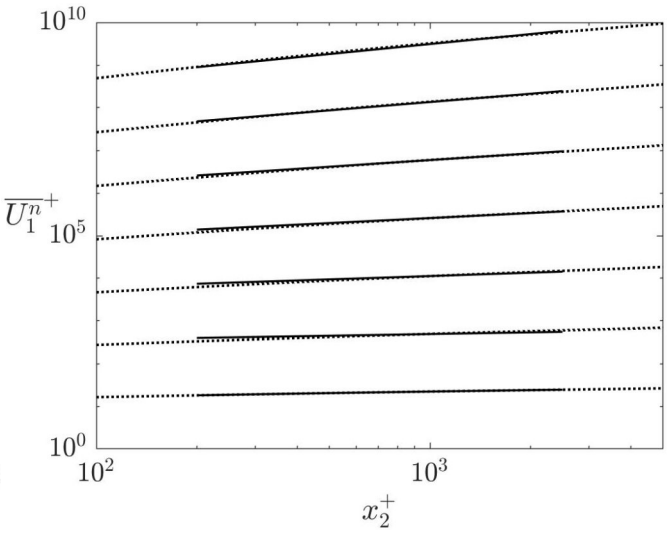

Figure 3: From bottom to top, scaling of moments of the streamwise velocity from 1 to 7. Dot line, data coming from DNS. Continuous line, data from theory.

parallel plates. No modelling is used. The computation is carried out in a doubly periodic domain in the two wall-parallel directions x (streamwise) and z (spanwise), which is chosen large enough to minimize artefacts due to the spurious periodicity. The 10k simulation uses $2\pi h \times \pi h$ where h is the channel half-thicknesses. This is enough to avoid spurious statistics due to the finite length of the box.

The code uses a low-storage third-order semi-implicit Runge-Kutta (R-K) time-stepper for time integration. This R-K scheme allows a longer time step than purely explicit methods while, at the same time, the memory requirements are as low as those of an Euler method. A Fourier discretization in x- and z-directions and a sixth-order Compact Finite Differences (CFD) discretization in the wall-normal y-direction are used for the spatial derivatives. The use of CFD allows greater flexibility in the choice of the mesh, which consists of 6,144 x 2,101 x 6,144 points in space.

LISO is written in Fortran90, and for SuperMUC, it is built with the Intel ifort compiler. It has been carefully checked and optimized for SuperMUC using a test account and In a SuperMUC extreme scaling workshop. The implementation uses FFTW routines for the Fourier transforms (MKL library) and MPI + OpenMP for the parallelization, where Intel MPI is our preferred environment for MPI. I/O routines use the parallel implementation of HDF5 in SuperMUC. It took less than 15sec to save an instantaneous flow realization, with a size of 250 GB. This field was distributed in as many as 4,096 cores. Saving to disk must be done each 7 hours, so the time needed for the I/O routines is negligible.

Due to limitations on the code, the maximum number of processors is 4,096 cores. As we needed to run the code for a considerable time, more than two years, to get enough statistics from the turbulent field, we ran three independent cases simultaneously. In total. In total LISO has been running for about 50M core hours.

This simulation has provided many interesting results about the kinematics of boundary layers [1]. In fact, this is the first simulation where a clear separation of scales can be observed. One of the most important features it that it allowed us to validate the symmetry-based Turbulence theory, where new scaling laws are obtained directly from theory, without any further simplification or modelling [2].

As one example, we can cite the indicator function of figure 2. It was predicted around 1920 that the central part of this function should be a straight line. This indicates that the flow follows a logarithmic profile in this region, which is called, for obvious reasons, logarithmic layer. This layer is the most difficult to model as it is the region of the flow where the largest eddies of the flow, coming from the center, interact with the smaller, and short live eddies that grow from the walls.

The symmetry-based theory not only predicts this logarithmic behavior but also predicts scaling laws for all the moments of the streamwise velocity, and thus characterizing completely the flow. Figure 3 shows the scaling of the moments up to order 7, with an excellent agreement between theory and data. Our final objective is to provide a better knowledge of turbulence and improve the modelling of this thrilling phenomena.

Ongoing Research / Outlook

We sincerely think that Symmetry Theory can be a game changer in the theory of turbulent flows. Thus, we plan to investigate further the theory of symmetry for what we need more statistics from the flow. We have applied for a large project, where we think we will be able to unveil more conservation laws of turbulent wall-bounded flows.

References and Links

[1] Oberlack, Martin, et al., Phys. Rev. Lett. 128.2 (2022): 024502.
[2] Hoyas, Sergio, et al., Phys. Rev. Fluids 7.1 (2022): 014602.

High-fidelity aeroelastic analyses of wind turbines in complex terrain

Research Institution
University of Stuttgart, Institute of Aerodynamics and Gas Dynamics

Principal Investigator
Thorsten Lutz

Researchers
Giorgia Guma, Ferdinand Seel, Patrick Letzgus

Project Partners
—

SuperMUC Project ID: pr94va

Introduction

The report shows high-fidelity Fluid Structure Interaction (FSI) studies applied on the research wind turbine of the

WINSENT project. In this project, two research wind turbines are going to be erected in the South of Germany in the WindForS complex terrain test field. The FSI is obtained by coupling the CFD URANS/DES code FLOWer and the multiphysics FEM solver Kratos [1], in which both beam and shell structural elements can be chosen to model the turbine. The two codes are coupled in both an explicit and an implicit way. A coupling of FLOWer and the FEM solver Simpack has been then used in Guma et al. [2] to simulate the DANAERO wind turbine in both uniform and turbulent conditions, these ones synthetically generated using a Mann box [3].

Results and Methods

One of main differences between a beam and a shell coupling is the number of Degrees of Freedom (DOF) necessary to fully describe the total deformation. A beam element needs 6 DOF (3 translations and 3 rotations) that are calculated in Kratos on prescribed nodes at the shear centers. On the other side, a shell only requires 3 translations because the entire outer shape of the turbine is considered. The choice of the shear centers as communication nodes in the beam coupling is not casual, because a beam model in Kratos is not considering bend-twist coupling. The shear center is the point on which a shear force causes no twist, and a torque moment causes no displacement of the shear center.

The elongation generates a larger surface of the blade with consequent higher loads and therefore larger bending deformations. This is not happening with the nonlinear models applied in this study, as it can be seen in Fig. 1.

The tip deformations in flapwise and edgewise direction are depicted in Figs. 1b and 1c. The

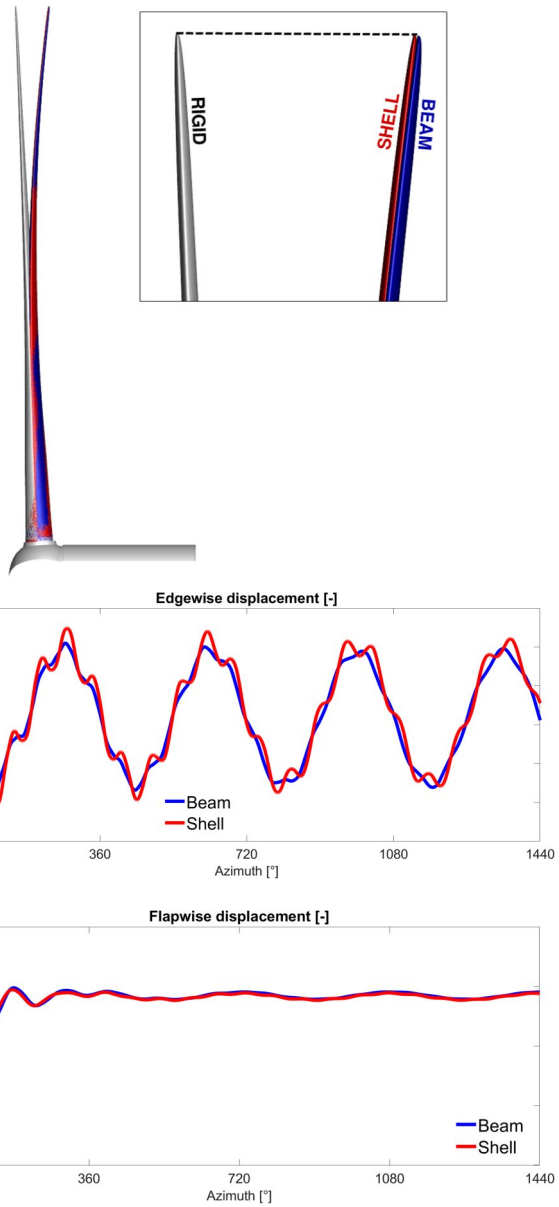

Figure 1: Top: One-third model (OTM), rigid and deformed blade beam vs shell. Middle and bottom: Deformations in two directions normalized according to the blade radius.

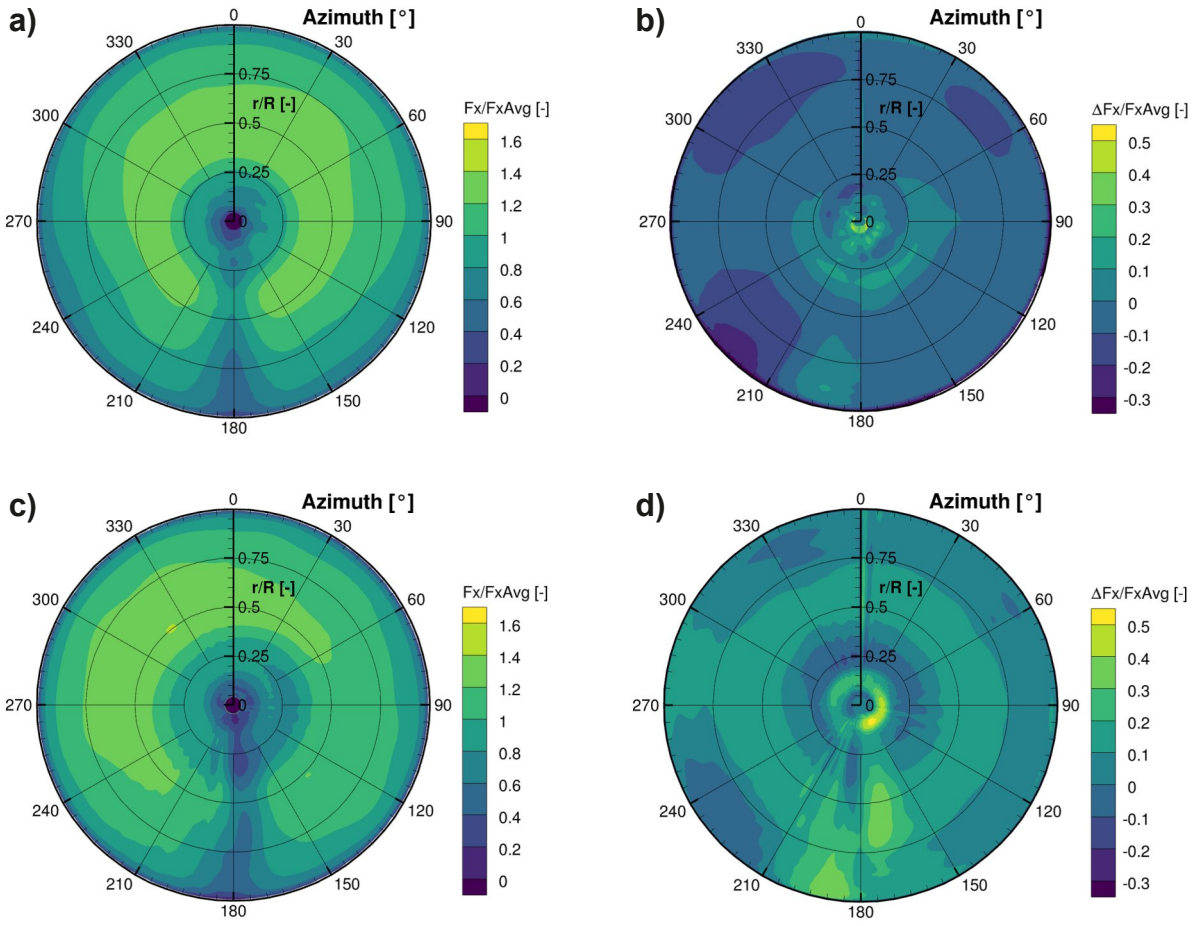

Figure 2: Phase average of the thrust force of one blade calculated over 26 revolutions. Loads are normalized according to the average. a) Rigid case flat terrain. b) Differences by applying shell model. c) Rigid case complex terrain. d) Differences by applying shell model.

Normalized Root Mean Square Deviation (NRMSD) is around 1% and therefore negligible. The sectional torsion has been calculated from the surface output files, because the shell coupling communicates only the displacements in the three directions. A reference section at the tip of the rigid blade has been considered.

The phase averaged thrust force (Fx) calculated over 26 revolutions (about one minute real time) the rigid cases is shown in Figs. 2a and 2c. Figures 2b and 2d show the respective difference in case of shell-coupled FSI simulations. Loads are normalized according to the respective average value in rigid case. It can be seen that in flat terrain the load distribution is mostly symmetric, with lower loads during the tower passage. The tower passage effect can be seen also in the FMC case, although the load distribution between the upper and lower side of the rotor is not symmetric anymore. This results from the inclined flow due to the orography of the terrain. The retreating blade effect leads to a higher AOA on the left-hand side of the plot than on the right-hand side [4]. When both cases are considered as flexible, in flat terrain (2b) and complex terrain (2d) the largest differences occur at the lower rotor half close to the hub and after the blade-tower passage. Directly after the tower region, i.e. between 180° and 230°, the effect of the blade-tower interaction can be depicted.

Acknowledgments

The authors are grateful to the HLRB and to the German Federal Ministry for Economic Affairs and Climate Action (BMWi) for funding the research within the framework of the research project WINSENT (FKZ 0324129).

Ongoing Research / Outlook

The FSI coupled simulations will be validated in the future with real measurement data of the research wind turbine.

References and Links

[1] Guma, G., Bucher, P., Letzgus P., Wüchner, R., Lutz, T.: High-fidelity aeroelastic analysis of wind turbines in complex terrain: FSI and aerodynamic modelling.
[2] Guma, G., Bangga, G., Lutz, T., and Krämer, E.: Aeroelastic analysis of wind turbines under turbulent inflow conditions, Wind Energy Science, 6, 93–110, 2021.
[3] Mann, J.: The spatial structure of neutral atmospheric surface-layer turbulence, Journal of fluid mechanics, 273, 141–168, 1994.
[4] Letzgus, P., El Bahlouli, A., Leukauf, D., Hofsäß, M., Lutz, T., and Krämer, E.: Microscale CFD Simulations of aWind Energy Test Site in the Swabian Alps with Mesoscale Based Inflow Data, in: The Science of Making Torque fromWind (TORQUE) 2020, 28 September - 2 October 2020, online, vol. 1618 of Journal of Physics: Conference Series, pp. Art.–Nr.: 062 021, IOP Publishing.

Numerical investigation on flashback mechanisms in premixed H_2/air swirl combustion

Research Institution
Institute for Simulation of reactive Thermo-Fluid Systems, TU Darmstadt

Principal Investigator
Christian Hasse

Researchers
Wang Han, Arne Scholtissek

Project Partners
—

SuperMUC Project ID: pn29so (Gauss Large Scale project)

Introduction

As a carbon-free fuel, hydrogen (H_2) has the potential of emerging as the leading energy carrier for next-generation, zero-carbon power generation, and hence has received considerable attention. H_2 can offer significant benefits over hydrocarbon fuels, such as wide flammability range, low ignition energy, and high diffusivity. However, the use of H_2 in gas turbines poses considerable challenges, e.g., the risk of flashback due to its high flame speed, which adversely affects the performance of H_2 combustion [1].

Flashback, a problem that occurs in premixed combustors, is the upstream propagation of the flame from the combustor into the premixing tube due to the change in mass flow rate, which could change the combustion process and pollutant emissions as well as cause considerable damage on the combustor [1]. Therefore, a deep understanding of the flashback mechanisms is required before applying pure H_2 or H_2 enriched fuels in combustion systems.

Flashback can occur because of four main mechanisms [1]: (1) boundary layer (BL) flashback in non-swirling or low swirling flow, (2) combustion induced vortex breakdown (CIVB) flashback in a swirling flow without a bluff-body, (3) combustion instability induced flashback, and (4) combined BL/CIVB flashback in a bluff-body swirl burner. The focus of this work is the latter one, because bluff-body swirling flows are typically employed to enhance mixing and flame stabilization. The systematic investigation of BL flashback started with the work by Lewis and von Elbe [2], who proposed a classical critical gradient model to evaluate the flashback in channel flows. In the confined BL flashback configurations where the flame is already inside the premix duct before flashback, the formation of reversed flow pockets ahead of laminar/turbulent flames is one of the main characteristics prior to the onset of flashback, which is attributed to a pressure rise induced by the formation of flame bulges and has been reported both experimentally and numerically. On the other hand, flashback in a swirl combustor without a central bluff body has been studied extensively. It is concluded that the flashback is related to vortex breakdown (i.e., CIVB flashback). This is because the baroclinic torque can produce a negative azimuthal vorticity and then induce a negative axial velocity along the vortex axis, leading to the vortex breakdown and facilitating flashback.

Despite its high relevance for various practical combustor designs, there are only a few studies on flashback in a bluff-body swirl burner. The Clemens group [3] experimentally identified two modes of flame propagation during flashback, i.e., (1) small-scale bulges propagating in the negative streamwise direction; and (2) large-scale flame tongues swirling with the bulk flow while leading flashback. More recently, a new flashback mode was discovered by Ebi et al. [4], and they found that the upstream propagation of flame can be led by flame bulges. Due to the inherent three-dimensional and transient nature of flame flashback, 3D parameter measurements and high-speed detecting devices are required, which leads to a significant challenge for experimental investigations of flashback.

It is noted that the above investigations of flashback in bluff-body swirl burners only provided 2D or local 3D flow field (without flame) measurements due to the limitation of laser-based techniques, which cannot comprehensively capture flow-flame interaction during the swirling flashback. The overarching objective of this project is to provide for the first time a detailed understanding of complex flow-flame interaction during flashback in a bluff-body swirl burner using Direct Numerical Simulation (DNS), which would help to reveal the mechanism(s) allowing the flame to propagate upstream during flashback and to improve practical swirl burner designs.

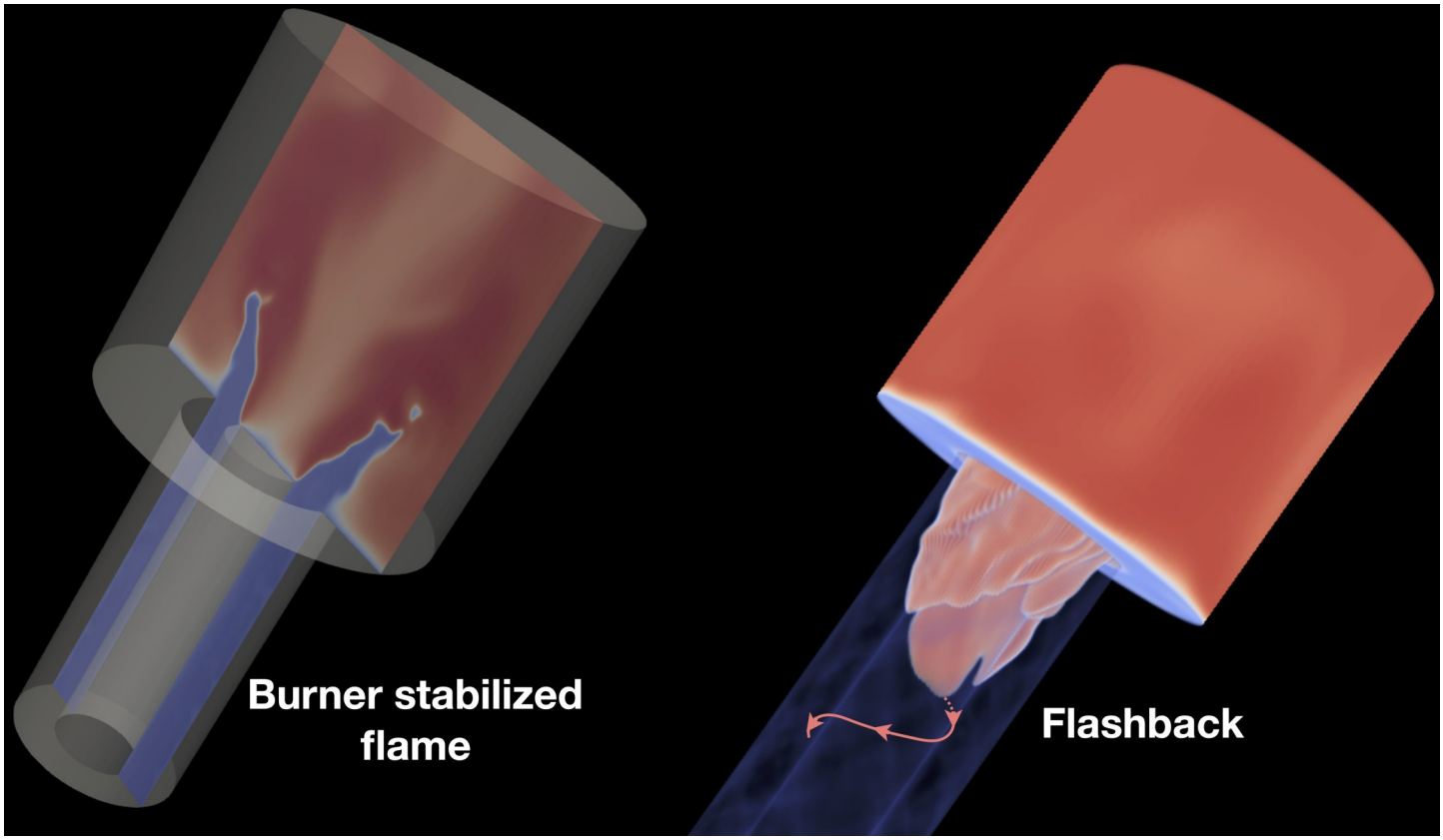

Figure 1: Temperature fields in the burner stabilized flame (left) and flashback (right) cases. Low and high values correspond to blue and red colors. The line with arrows indicates the flashback direction.

Results and Methods

Within this project all simulations and analyses are based on direct numerical simulations (DNS) which are conducted with the DNS code DINO [5]. The solver is designed for the simulation of low-Mach number reactive flows, where spatial derivatives in the governing equations are discretized with 6th order finite differences. The temporal integration is done by a 3rd order semi-implicit Runge-Kutta scheme. Based on the distributed memory architecture of SuperMUC parallelization of the solver is achieved by the message passing interface (MPI), where an excellent scalability up to 65,536 cores is achieved.

The DINO code is parallelized in two dimensions using the 2DECOMP&FFT library that acts on top of standard MPI and FFTW. The Poisson equation for pressure is solved by means of FFT for both periodic and nonperiodic boundary conditions, but with dedicated pre and postprocessing FFT techniques in the latter case. An implicit time integration of the stiff chemical source terms has been implemented, relying on a semi-implicit RungeKutta 3rd order. In the DINO code, the chemical source terms are computed using the opensource Cantera library. The transport properties are computed either with the Cantera library or with the EGlib3.4 library. It is noted that a cylindrical DINO version has been developed with the help of the project to achieve DNS calculations of flashback efficiently.

DNSs of burner stabilized flame and flashback
In this project, two DNSs are performed: (1) DNS of a stable, lean premixed swirling hydrogen/air flame in the bluff-body swirl burner; and (2) DNS of lean premixed swirling hydrogen/air flame flashback in the bluff-body swirl burner. The two DNS results are shown in Fig. 1. Flashback is triggered by disturbing the stable burning flame through impulsively increasing the equivalence ratio (Φ) uniformly at the inlet plane from Φ = 0.5 to Φ = 0.8. The computational domains comprise a region of 291x72x72 or 350x88x88 flame thicknesses for the first DNS or second DNS, respectively. They require 3,200x900x900 and 3,500x1,000x1,000 grid points for the first DNS and second DNS, respectively. Concerning the overall simulation time, the DNS is estimated to run for about 150 ms and 200 ms for stable flame and flashback DNS calculations, respectively. The stable burning case is found to have reached a statistically steady state after 150 ms and the flashback process lasts over a time span of 200 ms which was assessed qualitatively by a visual inspection of the flame front evolution during flashback. It is seen from Fig. 1 that at Φ = 0.8 the flame can propagate upstream and hence flashback occurs. The flame front is swirling around the center body, which is indicated by the red arrow. It is noted that owing to a higher axial velocity near the outside wall, the flame mainly propagates near the bluff-body wall.

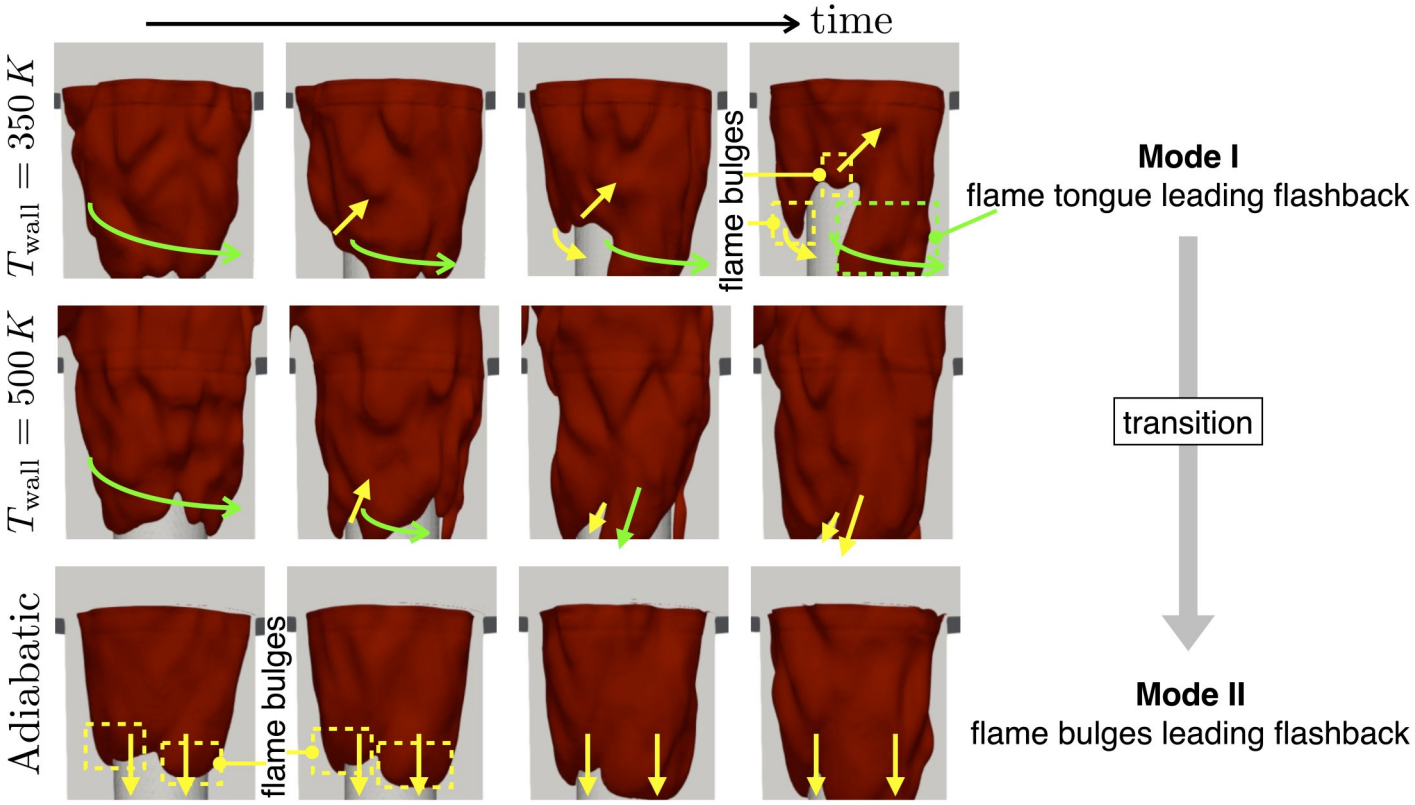

Figure 2: Instantaneous flame fronts during flashback at different boundary temperatures: 350 K (left), 500 K (middle), and adiabatic state (right). The flame tongue and flame bulges are marked by a green and yellow box, respectively. Their propagation directions are indicated by green and yellow arrows, respectively.

Flashback modes

Figure 2 illustrates the instantaneous flame fronts during flashback at different themral boundary conditions. Two flame structures can be observed along the flame front: (1) a large-scale flame tongue, and (2) multiple small-scale flame bulges, which are consistent with experimental observations [3]. Similar to [3], we refer to the rather large, leading part of the flame front as a flame tongue and refer to smaller structures along the flame front as flame bulges which tend to form on the trailing side of the flame tongue. Figure 2 shows that the leading flame tongue tends to swirl upstream (green arrow), while the flame bulges tend to propagate upstream in the negative streamwise direction (yellow arrow). It is found that the flashback process can exhibit different modes when changing the thermal boundary conditions. Specifically, for T_{wall} = 350 K case, the flashback is led by a large-scale flame tongue, and the flame tongue swirls in the direction of the flow upstream and propagates upstream in the mixing tube. At the trailing side of flame tongue, there exist multiple small-scale bulges that are convex to the coming flow. The flame bulges cannot achieve a sustained flame propagation against the swirl flow direction and hence cannot lead to the net upstream flame propagation. In this context, the lowest tip of flame front always locates at the flame tongue rather than these bulges, indicating that flashback in this case is led by the large-scale swirling flame tongue, denoted as Mode I. However, it is seen that for the adiabatic case, the flashback is led by small-scale flame bulges, denoted as Mode II. When the temperature of the central bluff-body is fixed at 500 K, there also exist a flame tongue and multiple flame bulges, like T_{wall} = 350 K case. However, compared to T_{wall} = 350 K case, the flame tongue and flame bulges are separated from each other at T_{wall} = 500 K. More importantly, the lowest flame tip no longer locates at the flame tongue only. Instead, the location of the lowest flame tip switches between the flame tongue and the flame bulges, which indicates that flashback in this case is led by different structures, switching between Mode I (swirling flame tongue) to Mode II (non-swirling flame bulges).

Ongoing Research / Outlook

The preliminary results shown in this report imply that the thermal condition of bluff body has a significant on flashback characteristics. To understand the underlying mechanisms, we are investigating near-wall flame-flow-wall interactions.

References and Links

[1] A. Kalantari, V. McDonell, Prog. Energy Combust. Sci. 61 (2017) 249–292.
[2] B. Lewis, G. von Elbe, J. Chem. Phys. 11 (1943) 75-97.
[3] D. Ebi, N.T. Clemens, Combust. Flame 168 (2016)39-52
[4] D. Ebi, R. Bombach, P. Jansohn, Proc. Combust.Inst. 38 (2021) 6345–6353.
[5] A. Abdelsamie, G. Fru, T. Oster, F. Dietzsch, G. Janiga, D. Thévenin, Comput. Fluids 131 (2016), 123-141.

On the dynamics of streamwise and transverse sediment patterns in turbulent open channel flows

Research Institution
Institute for Hydromechanics, Karlsruhe Institute of Technology (KIT)

Principal Investigators
M. Scherer, M. Uhlmann

Researchers
—

Project Partners
—

SuperMUC Project ID: pn34yi

Introduction

Sediment bedforms such as subaqueous ripples or large desert dunes arise in many natural ecosystems due to a delicate interaction between a shearing turbulent flow and an erodible sediment bed. Despite more than a century of intensive research of these interaction mechanisms, the processes that cause the development of sediment “bedforms” are even nowadays not entirely understood. A fundamental understanding of these physical processes is, however, of crucial importance for engineers and environmental scientists likewise, as it allows to better predict, for instance, the risks during flooding events.

The current project aims to contribute to the fundamental understanding of the physical processes that cause the evolution of sediment bedforms in subaqueous environments, such as natural rivers or man-made canals, and to the development of sediment transport models by providing high-fidelity datasets of sediment pattern formation. In the interface-resolved direct numerical simulations that are performed in this study, all relevant flow scales including vortices of size smaller than the particle diameter are resolved. The analysis of the simulation results focuses in particular on the different formation processes of and the interaction between transverse-oriented ripple-like patterns and streamwise-aligned sediment ridges. Even though both of them evolve from the same initially flat sediment bed, their formation mechanisms fundamentally differ. In this context, a key question is how the presence of lateral domain boundaries such as river banks influence the basic interaction mechanisms, a point that will be further investigated in the current project.

Results and Methods

In order to simulate the time evolution of the fluid-particle system at the highest accuracy, we use an immersed boundary technique [1] to resolve all flow scales including those that are smaller than the particle size. In that framework, spatial gradients are discretised by a second order finite difference scheme on a uniform staggered grid, while the governing equations are integrated in time in the framework of a standard fractional-step method with a mixed explicit-implicit time integration scheme. The dynamics of the spherical sediment grains are determined by numerically solving the Newton-Euler equations for rigid body motion in the framework of a sub-stepping algorithm. Contact forces and torque that become relevant during particle collisions are described by a suitable soft-sphere collision model [2].

The reasons for the necessity of performing the current simulations on a massively-parallel computing system are twofold: on the one hand, the amount of 48 billion grid points required to resolve even the smallest relevant flow scales together with the immense number of around 1.4 million fully-resolved particles in each of the simulations require a sufficiently high number of cores that is able to execute this work in a reasonable wall-clock time. On the other hand, in particular the transverse-oriented sediment patterns evolve rather slowly, such that even on a large-scale system as SuperMUC-NG the current simulations require a pure computing time of several months in order to capture the entire evolution of these bedforms.

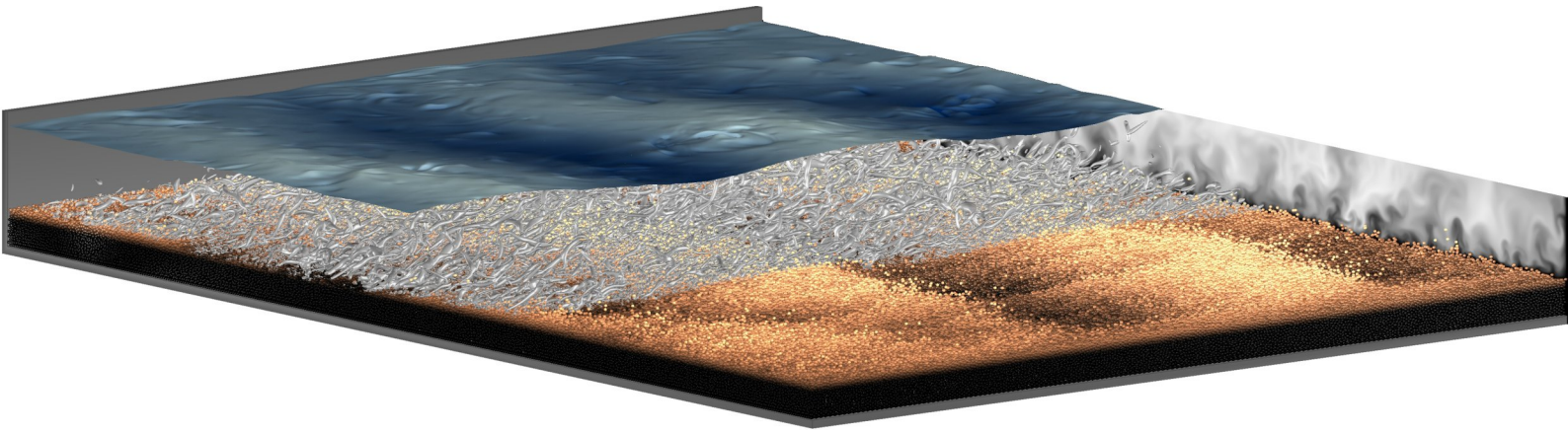

Figure 1: Instantaneous snapshot of the sediment bed in the presence of sidewalls. The particle colour ranges from dark to light brown with increasing distance to the bottom wall. Mean flow is from bottom left to top right. Turbulent vortices are visualized by means of the λ_2-criterion, while pressure fluctuations in the free surface (kept flat in the simulation) are shown as vertical deformation with low (high) values indicated by dark (light) blue colour. At the downstream end of the streamwise periodic domain, a cross-section of the flow field indicates low (high) intensity of the instantaneous streamwise fluid velocity by dark (bright) grey regions. For the sake of visualization, the second sidewall in the foreground has been removed.

In this project, we perform two individual simulations of turbulent open channel flow over a mobile sediment bed reaching intermediate Reynolds numbers Re_b = 3,000 (using the bulk velocity u_b as velocity scale). In one case the channel is laterally bounded by solid sidewalls, whereas in the other case it features spanwise periodic boundary conditions. The dimensions of the computational domain measure in both cases [$12H_f \times 1.5H_f \times 16H_f$] in the streamwise *x*-, wall-normal *y*- and spanwise *z*-direction of a Cartesian coordinate system, where H_f denotes the mean fluid height between the surface of the sediment bed and the flat free surface of the channel. The mobile particles that form the sediment bed have a relative diameter of roughly $D/H_f = 0.04$.

For the current flow configurations, scaling tests of our MPI-parallelised simulation code with different processor arrangements have suggested that a domain decomposition strategy based on a Cartesian processor grid with 48 × 1 × 64 = 3,072 processors in the streamwise, wall-normal and spanwise direction is the most economic way to use the granted computing time. Note that by choosing only one single processor in the wall-normal direction, the load imbalance due to a varying number of particles per core can be reduced to a minimum. For check-pointing and post-processing, snapshots of the flow field and the corresponding state of all particles are saved every 24 hours of simulation run time, each of which has a size of around 160 gigabytes. Until the end of the project, this procedure will lead to a grand total of roughly 45 terabytes for the two simulations.

Data analysis of the obtained simulation results reveals two different evolution stages of pattern formation. The first starts shortly after the onset of the simulation and is characterised by a regular pattern of essentially parallel quasi-streamwise sediment ridges that develops on the surface of the sediment bed. These well-organised sediment bedforms evolve as a consequence of large-scale velocity structures in the turbulent flow field [5], which induce regions of relatively stronger and weaker erosion along the sediment bed, leading to the formation of local troughs and crests of the sediment bed surface. These findings, in turn, highlight that an accurate representation of all turbulent flow scales is of central importance to advance our understanding of the turbulence-sediment interaction processes, and thus simulations at the present level of detail are indeed required.

While in the early phase of the sediment bed evolution streamwise-aligned sediment ridges are the dominant type of bedforms, in later stages of the simulations larger bedforms with transverse-oriented crest-lines, so-called “initial ripples”, grow in size and eventually reach crest heights that are at least three times higher than those of the streamwise ridges. The instantaneous snapshot of the fluid-particle system provided in figure 1 shows two such transverse sediment patterns together with the overlying flow field. Clearly, the presence of these sediment patterns alters the global system of vortical structures in the flow and affects even the pressure fluctuations along the upper free-slip plane of the channel. These observations extend the findings gained in the recent works which have exclusively focused on the formation of transverse patterns [3,4]. In these studies, the authors have studied the flow in domains significantly narrower than those considered in the current project to intentionally suppress other sediment structures and possible spanwise heterogeneities. In the current project, on the other hand, the large dimensions of the computational domains allow us, for the first time, to study the evolution of sediment bedforms in an essentially spatially unconstrained context. In particular, the current simulations provide an important dataset of the development of pattern three-dimensionality: As can be observed in figure 2, the sediment bed gradually transforms from a ridge-covered to a ripple-covered bed, going through different transient phases during which localised three-dimensional sediment patches develop, later connecting with their lateral neighbours to form large ripple structures that span the entire channel width of 16 times the clear fluid height H_f.

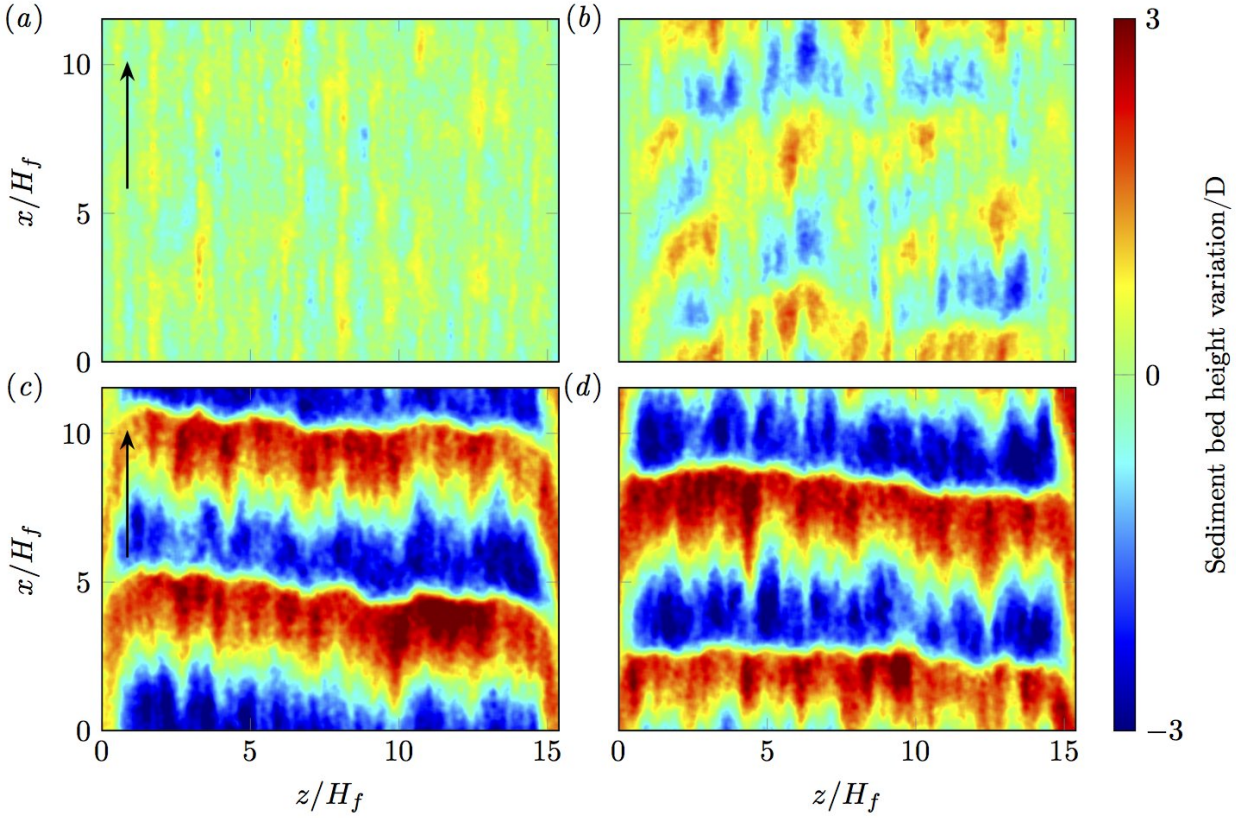

Figure 2: Top view of the sediment bed height variation for the case with lateral sidewalls in different phases of the simulations, time is increasing from the top left to bottom right. Details on the definition of the sediment bed surface can be found in [4]. Mean flow is from bottom to top in each panel.

Ongoing Research / Outlook

Thanks to the granted computing time and the hardware provided on SuperMUC-NG, we have been able to create a new database of high-fidelity simulations of sediment pattern formation in turbulent open channel flows in the presence and absence of lateral sidewalls. The current numerical simulations at this level of detail in a similarly long and wide physical domain represent a novelty in the field and have contributed to a better understanding of the physical processes that are responsible for the evolution of sediment ridges [5]. In this context, it would be of high interest to perform simulations at higher Reynolds numbers that allow for a clear scale separation between the smallest and largest eddies, which was, in virtue of the enormous computational costs of such simulations, out of the scope of the current project.

References and Links

[1] M. Uhlmann. J. Comp. Physics, 209(2):448–476, 2005.
[2] A. G. Kidanemariam and M. Uhlmann. Int. J. Multiphase Flow, 67:174–188, 2014.
[3] A. G. Kidanemariam and M. Uhlmann. J. Fluid Mech., 818:716–743, 2017.
[4] M. Scherer, A. G. Kidanemariam, and M. Uhlmann. J. Fluid Mech., 900: A1, 2020.
[5] M. Scherer, M. Uhlmann, A. G. Kidanemariam, and M. Krayer. J. Fluid Mech., 930:A11, 2022.

Aerodynamic Investigation and Design Optimization of Helicopter and Propeller Configurations

Research Institution
Chair of Aerodynamics and Fluid Mechanics, Technical University of Munich

Principal Investigator
Christian Breitsamter

Researchers
Andreas Kümmel, Ulrich Hartmann, Catharina Moreira

Project Partners
–

SuperMUC Project ID: pn69ni

Introduction

The chair of Aerodynamics and Fluid Mechanics (AER) is active in the research on the aerodynamic characteristics of innovative rotorcraft and propeller configurations. Therefore, experimental, and numerical analysis of different helicopter and multi-copter configurations as well as isolated propeller configurations have been performed.

The present project can be divided into three subprojects, which deal with the development of environmentally friendly aircraft and propulsion systems.

Within the first subproject, different propeller configurations are investigated. The focus is on the design optimization of the propeller blades with respect to the aerodynamic efficiency as well as the noise footprint. In addition to highly accurate CFD simulations low-fidelity methods are implemented for the optimization task. On the one hand the SuperMUC-NG is used for the validation of the low fidelity methods and on the other hand within an optimization framework to investigate promising candidates. SuperMUC-NG enables us to perform the CPU intensive CFD simulations to investigate the complex aero-acoustic flow problems.

The second and third subproject deal with multi rotor configurations, which are typically used for urban air mobility (UAM) concepts. Therefore, numerical investigations regarding the aerodynamics and the aeroacoustics of different concepts are conducted.

The interaction noise of a multi-rotor vehicle can be significantly influenced by design and mission-specific aspects. Parameters of particular interest are the arrangement of the rotors, the functional separation of the rotors and strategies for avoiding aero-acoustic interactions. In addition to aeroacoustics, the aerodynamic performance of the aircraft must also be considered in the design measures for the noise reduction. Furthermore, the specific flight conditions of multicopter (high inflow angles at low advance ratios) pose a challenge for accurate numerical simulations due to the strong interactions. The usage of the SuperMUC-NG enables a high temporal and spatial resolution of the simulations, which is required to calculate the flow field in a time-resolved manner. The results are used to derive recommendations for aircraft design purposes.

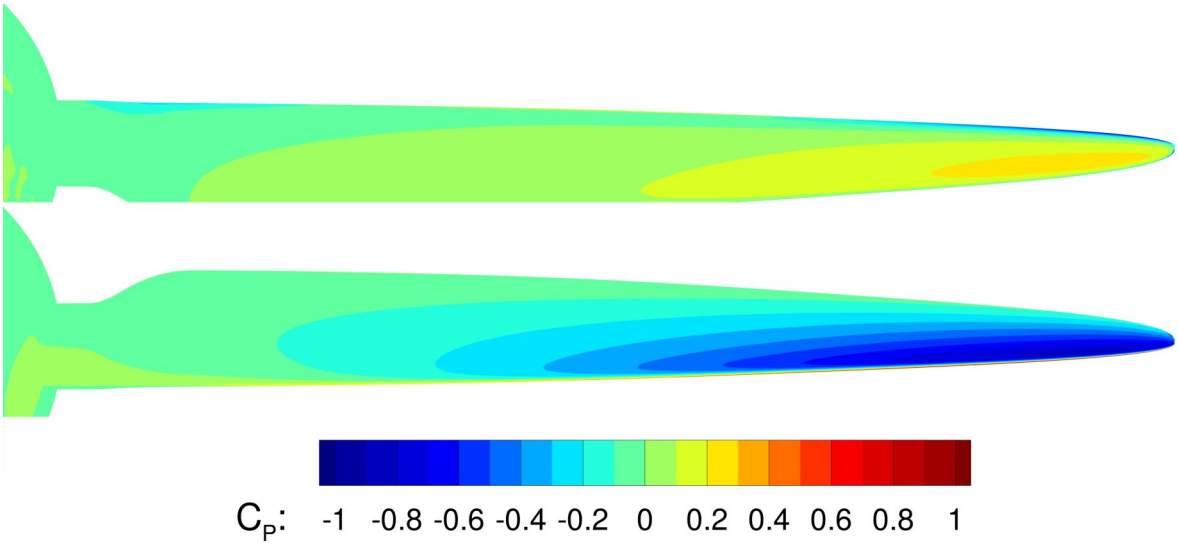

Figure 1: Surface pressure distribution of the propeller for the upper (top) and lower (bottom) side of the blade.

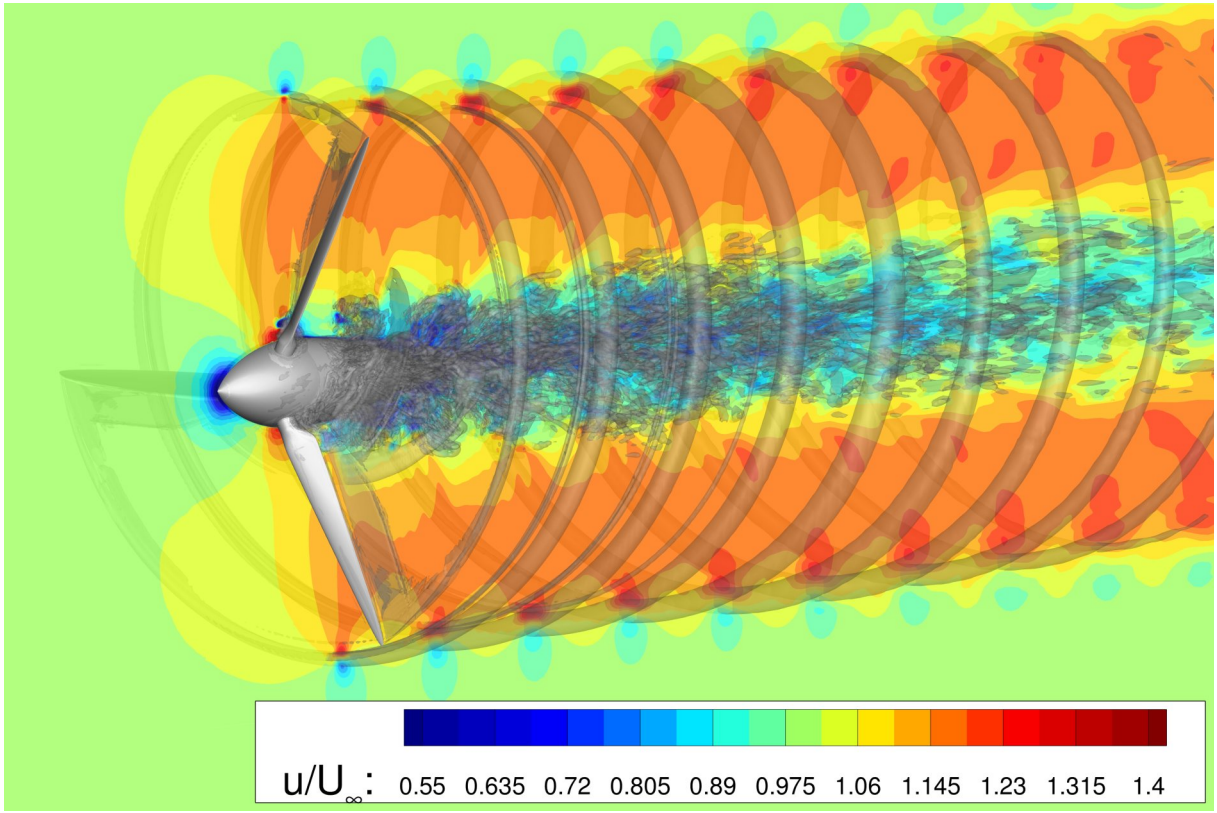

Figure 2: Y-Slice along the propeller axis colored by the normalized axial velocity and an Isosurface of the Q-criterion colored in grey.

Results and Methods

The first subproject deals with the optimization of the propeller shape to improve the aerodynamic performance and reduce the noise emissions. The optimization is divided into several steps. Starting with a pure aerodynamic optimization the level of complexity is steadily increased and structural properties and aeroacoustics are also considered. Therefore, a multi-disciplinary optimization approach is applied. For the optimization process, a fully automatic optimization tool chain is implemented. CFD simulations are applied for a detailed aerodynamic investigation of promising designs. Thereby, the Ffowcs-Williams Hawkings (FW-H) method is used for the acoustic analysis. A very fine computational mesh in combination with a high-fidelity stress-blended eddy simulation (SBES) is applied to preserve all relevant flow characteristics for the FW-H analysis and reduce the dissipation.

For the unsteady flow simulations, ANSYS Fluent 2020.R1 was used and for the creation of the block-structured hexahedral mesh ANSYS ICEMCFD. The mesh contains approximately 80 Mio. cells. The SuperMUC-NG allows CPU intensive flow and aero-acoustic simulations of multiple designs and operating conditions. The simulations are conducted on 16 nodes using 768 cores. Considering 12 revolutions, approximately 110,000 Core-h were needed.

Figure 1 exemplarily shows the surface pressure distribution of the propeller blade. The smooth distribution without high gradients indicates low aerodynamic losses and no regions of flow separation. Furthermore, Figure 2 illustrates the highly complex wake flow of the propeller, which is shown by an axial slice through the propeller colored with the normalized axial flow velocity. Additionally, the vortex system is visualized by an Iso-Surface of the Q-criterion in grey. Here, the blade tip vortices and a highly turbulent region downstream of the propeller hub can be seen.

Within the other subprojects, different design concepts for multi-rotor configurations are investigated. In a first step, single and tandem rotor concepts are compared to each other. Moreover, different flight conditions like hover and forward-flight are analyzed regarding the aero-acoustic footprint for both configurations.

ANSYS Fluent is used for the meshing and solution process of the CFD simulations. The mesh is an unstructured poly-hexcore mesh containing approximately 35 Mio. cells for a single rotor configuration and 50 Mio. for a tandem rotor configuration. The Scale-Adaptive Simulation (SAS) turbulence model is used for the unsteady flow simulations. This helps to reduce the dissipation which is important for the subsequent aero-acoustic analysis with the FW-H method.

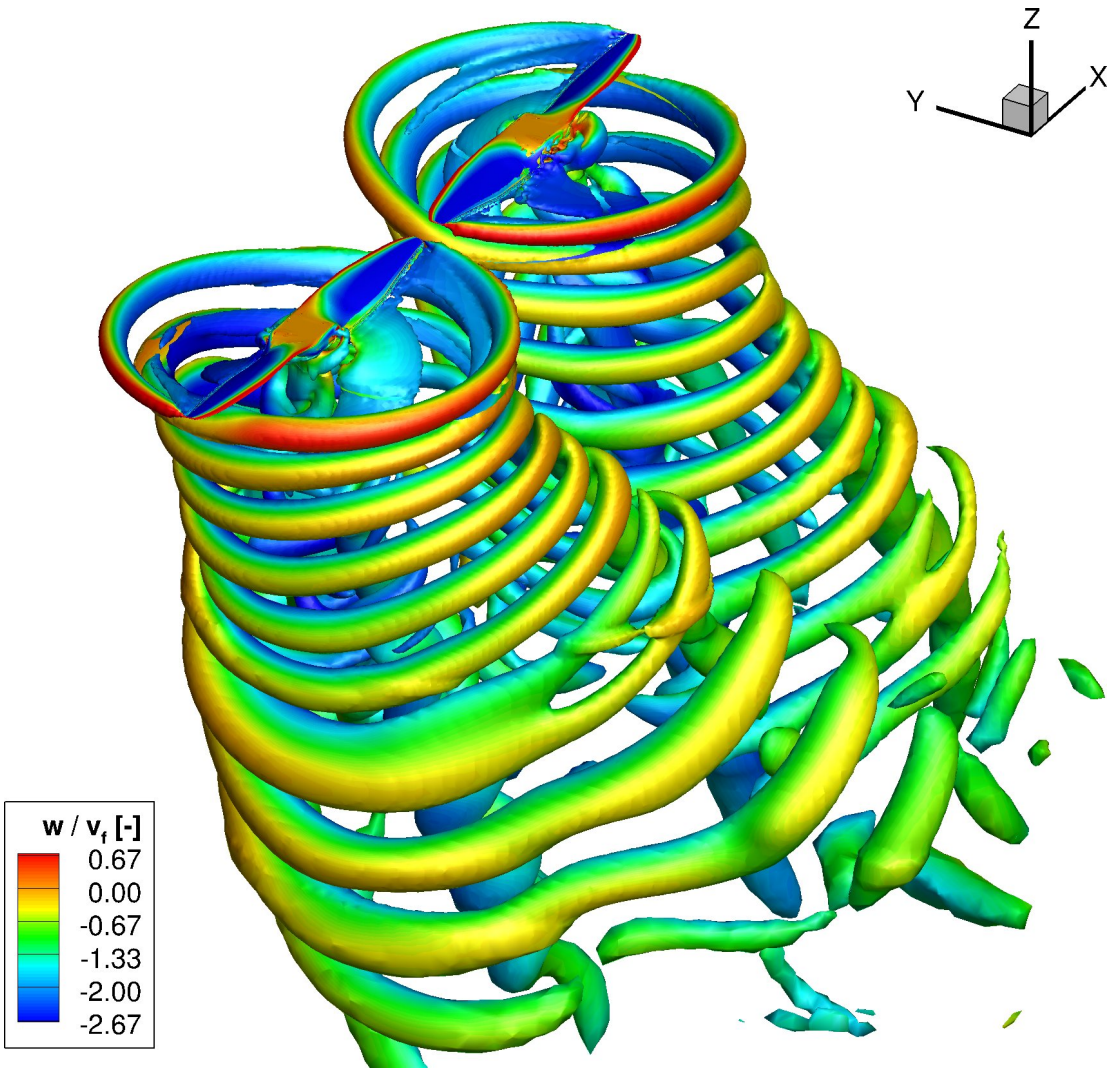

Figure 3: Iso surface of the Q-criterion colored with the non-dimensional downwash velocity for a tandem rotor configuration.

The usage of the SuperMUC-NG enables the calculation of the flow field with high temporal and spatial resolution allowing for a detailed analysis of the flow field characteristics.

Figure 3 shows the vortex system of a tandem rotor configuration for an advance ratio of 0.22 and 60° of inflow angle. The blade tip vortices for both systems are clearly visible, as well as the interaction downstream of the rotors.

Figure 4 shows the directivity of the radiated rotor noise for different forward flight conditions with different inflow angles and at hover flight. In general, a distinctly higher overall sound pressure level can be detected for the forward flight configurations, especially at an azimuthal angle of approximately 315°.

Ongoing Research / Outlook

The use of SuperMUC-NG is essential to this project and to perform the complex and CPU-intensive flow simulations within this project. Further, numerical investigations are required in all subprojects to achieve a deeper understanding of the generation of rotor noise and interactions between multiple rotors. Especially with the upcoming trend of UAM, the importance of these topics is strongly increasing and further research is of major importance.

References and Links

[1] Kuemmel, A and Breitsamter, C.: IOP Conf. Ser.: Mater. Sci. Eng. 1024 012060, 2021.
[2] Poelzlbauer, P.; Kuemmel, A.; Desvigne, D. and Breitsamter, C.: Aerospace 8 (3), 2021.
[3] Cerny, M.; Faust, J. and Breitsamter, C. IOP Conf. Ser.: Mater. Sci. Eng. 1024 012034, 2021.

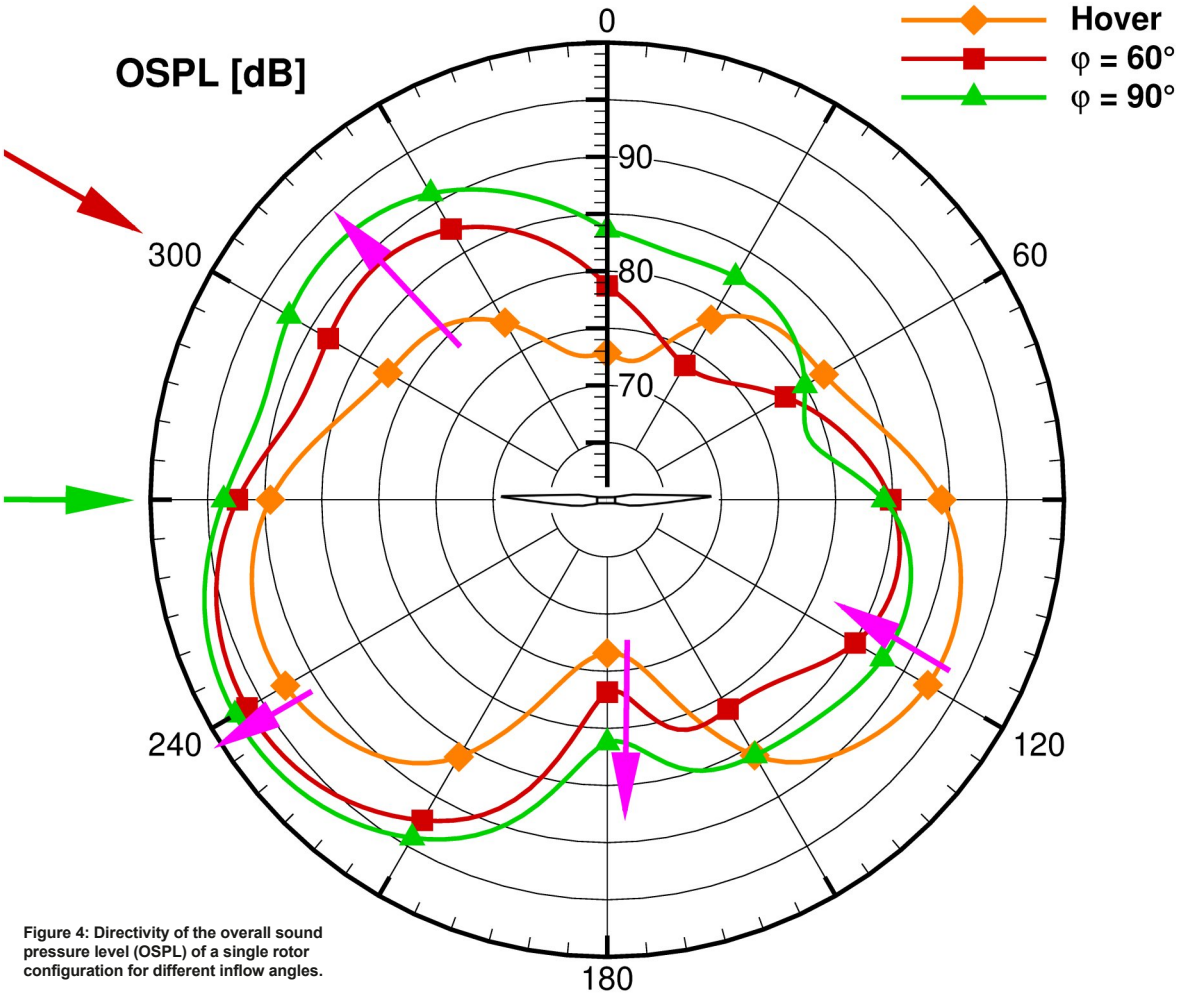

Figure 4: Directivity of the overall sound pressure level (OSPL) of a single rotor configuration for different inflow angles.

Latest studies on vortical flow Interaction on Airborne High Speed Vehicles

Research Institution
German Aerospace Center, Institute of Aerodynamic and Flow Technologies, Göttingen

Principal Investigator
Christian Schnepf

Researcher
Michael Werner

Project Partners
–

SuperMUC Project ID: pn72xu

Introduction

The requirement of high maneuverability is a major design goal for state-of-the-art airborne high-speed interceptor vehicles. This requirement demands that the vehicle must be able to perform maneuvers at high angles of attack and roll angles at the edge of the flight envelope. Flow fields under these flight conditions are characterized by large-scale separations and multiple vortices (Figure 1). These separations and vortices and the accompanied flow phenomena have a major influence on the surface pressure distribution of the vehicle and thus on its aerodynamic performance.

Large scale vortices are created, for example, on the nose of the vehicle or on the leading edges of the specially designed wings (Figure 1). During the lifetime of these vortices, they often interact with each other or with control surfaces of the vehicle. The vortex-vortex interaction can even end in vortex merging and the loss of one vortex. In addition, at high speeds (M > 0.85) shock waves occur and a vortex-shock interaction is likely. These interactions can significantly alter the trajectory, strength and lifetime of vortices. The latter is closely related to a phenomenon called vortex burst or vortex breakdown. This phenomenon is characterized by an abrupt change of the vortex trajectory like in the case of spiral vortex breakdown or by a sudden pressure rise within the vortex core and a significant expansion of the vortical structure (Bubble-type breakdown). All mentioned vortex related phenomena and vortex interactions significantly affect the aerodynamic performance of the vehicle and its flight stability. Therefore, an accurate prediction of these flow features is crucial for the design of a vehicle operating at the edge of the envelope. However, the physics of flow separation, vortex roll-up and interaction are still difficult to model numerically with state-of-the-art turbulence models and Reynolds-Averaged Navier-Stokes (RANS) flow solver [1]. In terms of accuracy, hybrid RANS-LES methods have been shown to allow for better performance than conventional RANS methods in predicting the turbulent properties of vortices convecting in downstream direction e.g [2].

The goal of this project is to investigate the performance of HYBRID-RANS-LES methods in comparison to RANS methods for a generic delta wing configuration and a generic, highly maneuverable transonic missile configuration. For both configurations, large flow separations and multiple vortices occur for the flow conditions investigated. In addition to these realistic configurations, the vortex shock interaction is studied in more detail using a simplified interaction scenario between an analytically defined vortex and an oblique shock, which allows better control of the interaction parameters.

Results and Methods

The missile and delta wing configurations investigated are the outcome of DLR design studies. A detailed description of both test cases are in [3,4]. Numerical simulations were carried out for various turbulence models. Furthermore, scale resolving simulations (SRS) for an SST-IDDES model were performed. For both, the unstructured finite volume flow solver DLR-TAU Code was used to determine the flow field for a Mach number of 0.85. A typical IDDES simulation consumed about 500,000 core hours to perform about 4,000 physical time steps with a time step size between $5 \cdot 10^{-6}$ s and $1 \cdot 10^{-6}$ s for numerical mesh sizes of $30 \cdot 10^{6}$ nodes to $90 \cdot 10^{6}$ nodes. A total of 17.5 million core hours has been used for the project so far, which would not have been possible without the grant for SuperMUC-NG HPC.

Missile configuration LK6E2
Since the last status report, SRS calculations have been carried out in addition to the RANS simulations for a Mach number of 0.85, a roll angle of 45° and an angle of attack of 17.5°. Figure 1 shows a comparison of both types of simulations with the k-ω SST turbulence model. The general flow topology like the topology, as shown in Figure 1 is not affected by SRS. However, the exact development of the flow separation and the vortex flow changes noticeably, which can be seen well on wing 2. The shape of the leading edge separation and the trajectory of the

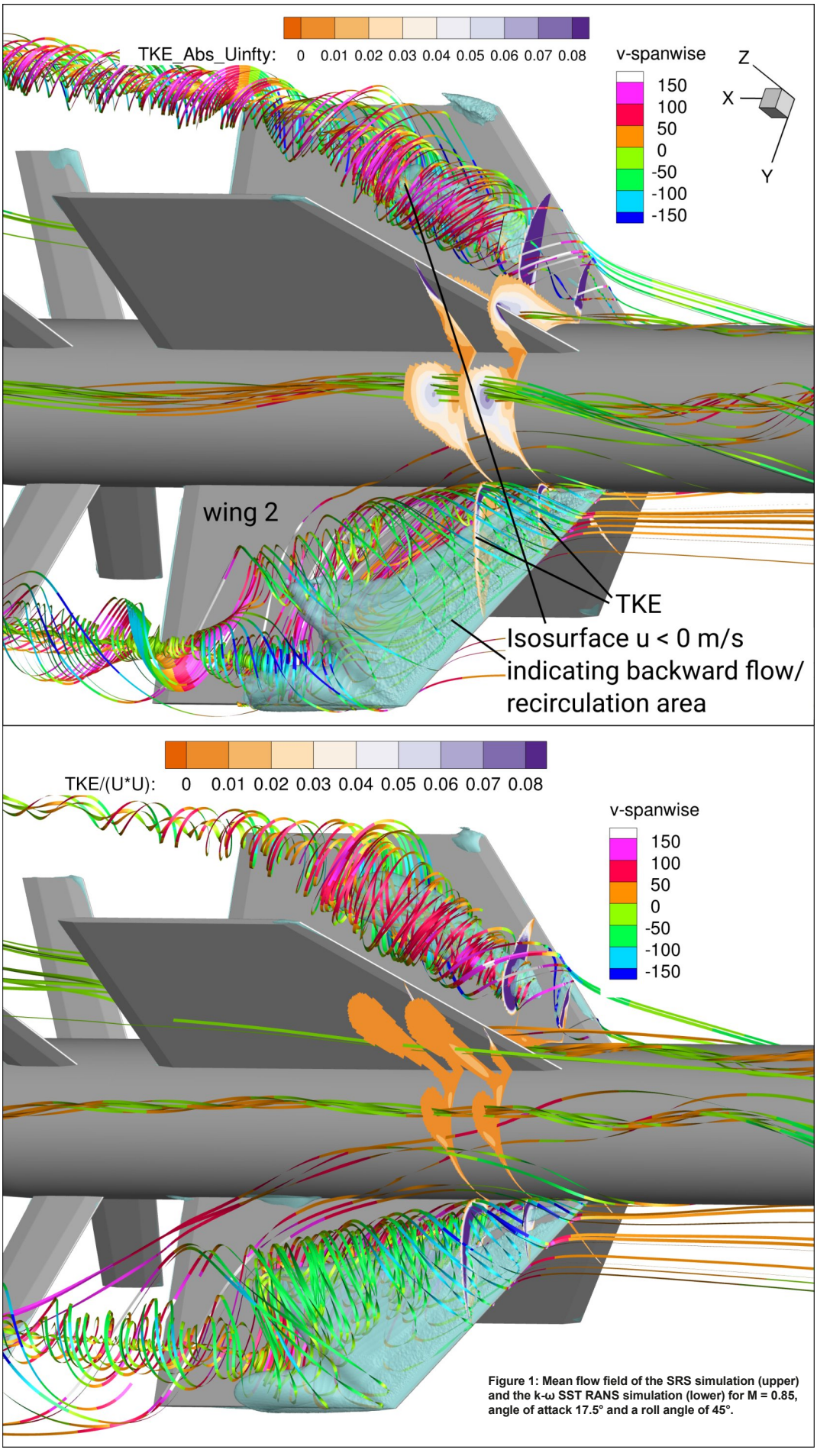

Figure 1: Mean flow field of the SRS simulation (upper) and the k-ω SST RANS simulation (lower) for M = 0.85, angle of attack 17.5° and a roll angle of 45°.

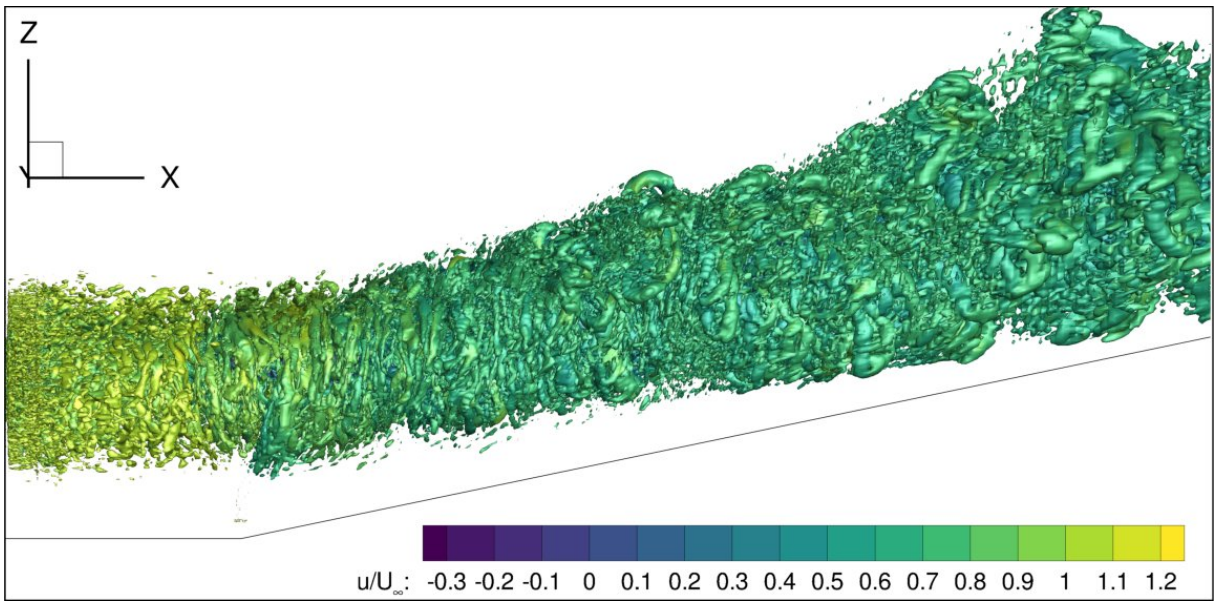

Figure 2: Instantaneous isosurface of the λ_2 criterion, colored by x-component of the velocity, Γ = 4.0, δ = 0.2.

streamlines within the separation is influenced by the choice of method, for example. Figure 1 also shows the value TKE_Abs_Uinfty for the SRS which corresponds to the turbulent kinetic energy (TKE) in the RANS simulation. Compared to the SRS, the RANS simulation shows significantly larger TKE values in the shear layer emanating from the leading edge. This might lead to higher dissipation in the case of the RANS simulation, explaining the different flow development at wing2 in Figure 1. In this context, RANS simulations with a laminar boundary layer near the leading edge, and therefore low TKE values, showed a similar flow field as the SRS in Figure 1. More detailed analysis and further conclusions will be included in the final report.

Analytical Vortex-Shock Interaction

In addition to the work done on the missile configuration, since the last status report a major focus was placed on the third sub-project, the investigation of the interaction between analytically prescribed vortices and an oblique shock. For this simplified interaction scenario, the shock was created by a ramp in supersonic flow, with a ramp angle of . At this resulted in a shock angle of . A vortex was then introduced by modifying the inflow boundary condition upstream of the ramp. In a first step, laminar Navier-Stokes simulations as well as conventional (turbulent) RANS simulations were performed to identify the onset of vortex breakdown, depending on circulation Γ and axial velocity deficit δ of the vortices.

In a second step, scale resolving IDDES simulations were performed for selected parameter combinations. By using a synthetic turbulence approach in the area immediately downstream of the inlet, turbulent fluctuations were introduced into the flow. In Figure 2 the instantaneous flow for one IDDES result is visualized by the vortex criterion. By performing a dynamic mode decomposition (DMD) of the unsteady flow field, large scale structures similar to spiral vortex breakdown could be identified, compare Figure 3.

Ongoing Research / Outlook

The majority of the planned simulations has been successfully completed. Currently, postprocessing and analysis of the gathered data is taking place. A broader and more detailed overview over the results will be given in the final report.

References and Links

[1] Rizzi, et.al., “Historical development and use of CFD for separated flow simulations relevant to military aircraft”, Aerospace Science and Technology, 2021.
[2] Probst, Axel. “Scale-Resolving Simulations on Unstructured Meshes with a Low-Dissipation Low-Dispersion Scheme”. New Results in Numerical and Experimental Fluid Mechanics XI. Springer, Cham, 2018. S. 489-498.
[3] Schnepf, Christian, et al., “Comparisons of predicted and measured aerodynamic characteristics of the DLR LK6E2 missile airframe”. AIAA SCITECH 2022 Forum. 2022.
[4] Werner, Michael et al., “Turbulence Model Effects on the Prediction of Transonic Vortex Interaction on a Multi-Swept Delta Wing”. AIAA SCITECH 2022 Forum. 2022.

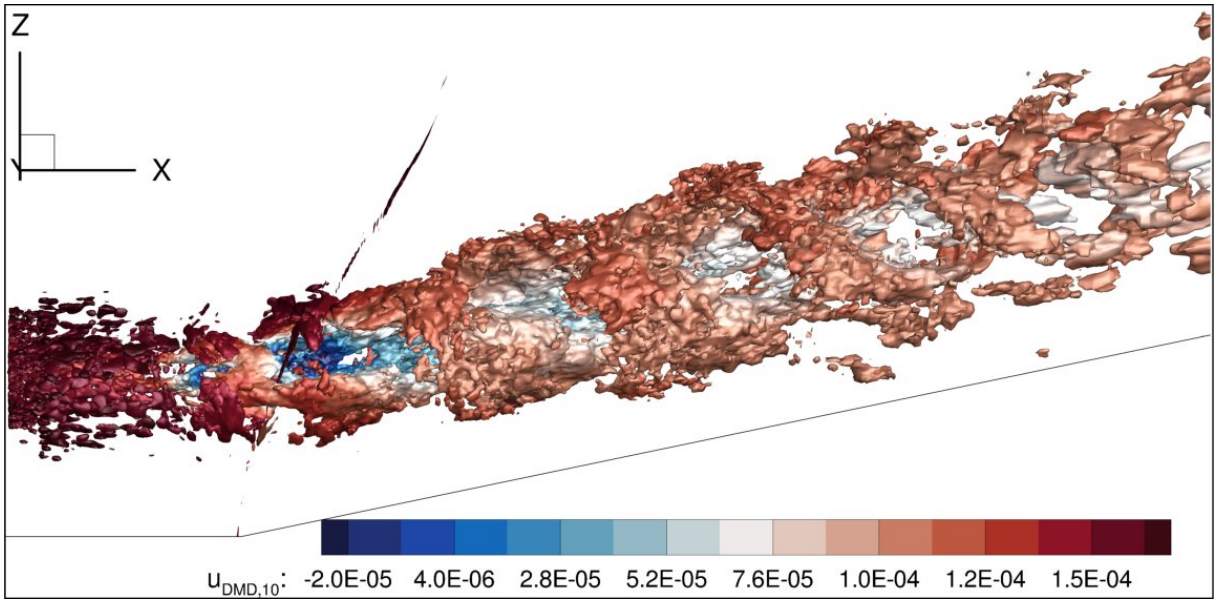

Figure 3: Isosurface of the fourth DMD mode, Γ = 4.0, δ = 0.2.

Numerical Investigations on Green Propellants for Applications in Rocket Engines

Research Institution
Institute for Space Propulsion, Technical University of Munich

Principal Investigator
Oskar J. Haidn

Researchers
Daniel Martinez-Sanchis, Andrej Sternin

Project Partners
—

SuperMUC Project ID: pr53we

Introduction

Turbulence is the largest unclosed problem in classical physics. Turbulent flows are chaotic by definition, and deterministic methods are unsuitable for approaching them. Therefore, it is necessary to use statistical methods to characterize their behavior. The core problem lies in developing mathematical models for the space and temporal evolution of these statistics. During the last decades, several models have been proposed. However, their application range is often restricted to very specific standard conditions i.e. subsonic, incompressible, non-reacting, isotropic… etc. The flow conditions that take place in the combustion chamber of a rocket engine challenge the classical assumptions in turbulence. In the injection region of a rocket engine, the flow is highly anisotropic, and density can change by nearly two orders of magnitude in a matter of microns. As a consequence, conventional turbulence models are unsuitable for accurate prediction in this sort of environment. The design and optimization of modern rocket engines are limited in one way or another by this challenge. The current project aims to improve the understanding of turbulent flows in such conditions.

Results and Methods

Direct Numerical Simulations (DNS) have been performed to investigate this problem. This kind of simulations resolve all the relevant scales and processes, without using any sort of statistical modelling. Due to their unrivaled fidelity, DNS results can be used to develop new statistical models. Nevertheless, the computational cost is extremely expensive, and only high-performance supercomputers are capable of executing these simulations within reasonable time frames. Detailed chemistry, and high Reynolds numbers enhance the computational cost significantly. The simulation of a single flame has a computational cost in the order of 2 M core hours, although this number may vary considerably depending on the combustion regime. It is usually necessary to use over 10,000 cores for several days. The reconstruction of the simulation's output takes several days, and it often accounts for 1-10 Tb. Processing the statistics of such data is only feasible through supercomputers.

Turbulent flames in similar conditions as what can be found in a rocket engine were simulated in the last year to investigate the turbulent properties. An example can be visualized in Fig 1. This figure corresponds to a premixed Methane-Oxygen flame, with similar conditions to that found in modern rocket combustors. The right side of the picture represents the flow's density, and it serves to allocate the flame front. On the right side, enstrophy can be visualized. This parameter represents the fluid's local tendency to rotate, and it is indicative of the turbulence levels. It can be seen that this indicator is maximized at the regions where the flame front is perpendicular to the main flame propagation's direction. This effect is generated by a misalignment between density and pressure gradients which generates a torque that promotes a local spinning, increasing the kinetic energy of vortexes.

Non-premixed turbulent flames were also simulated within the present project's frame. An example of such a setup can be observed in Fig 2. As it can be seen, oxygen is injected at the center bottom, and it burns to generate an exothermic expansion. The right side of this figure represents the normalized second invariant, which indicates the presence of eddies. Red colors indicate the presence of vortexes, and blue the absence. As it can be seen, combustion has a dramatic effect on the size of vortical structures. This effect is vital in the development of combustion. Turbulence can increase the burning rate of propellants, and this increase is governed by the size and geometry of these structures. In conventional models, it is necessary to rely on rough assumptions to estimate these sorts of variables. These simulations provide us access to the actual geometries and characteristics of these structures, which is a piece of invaluable information to optimize the size of future combustion chambers.

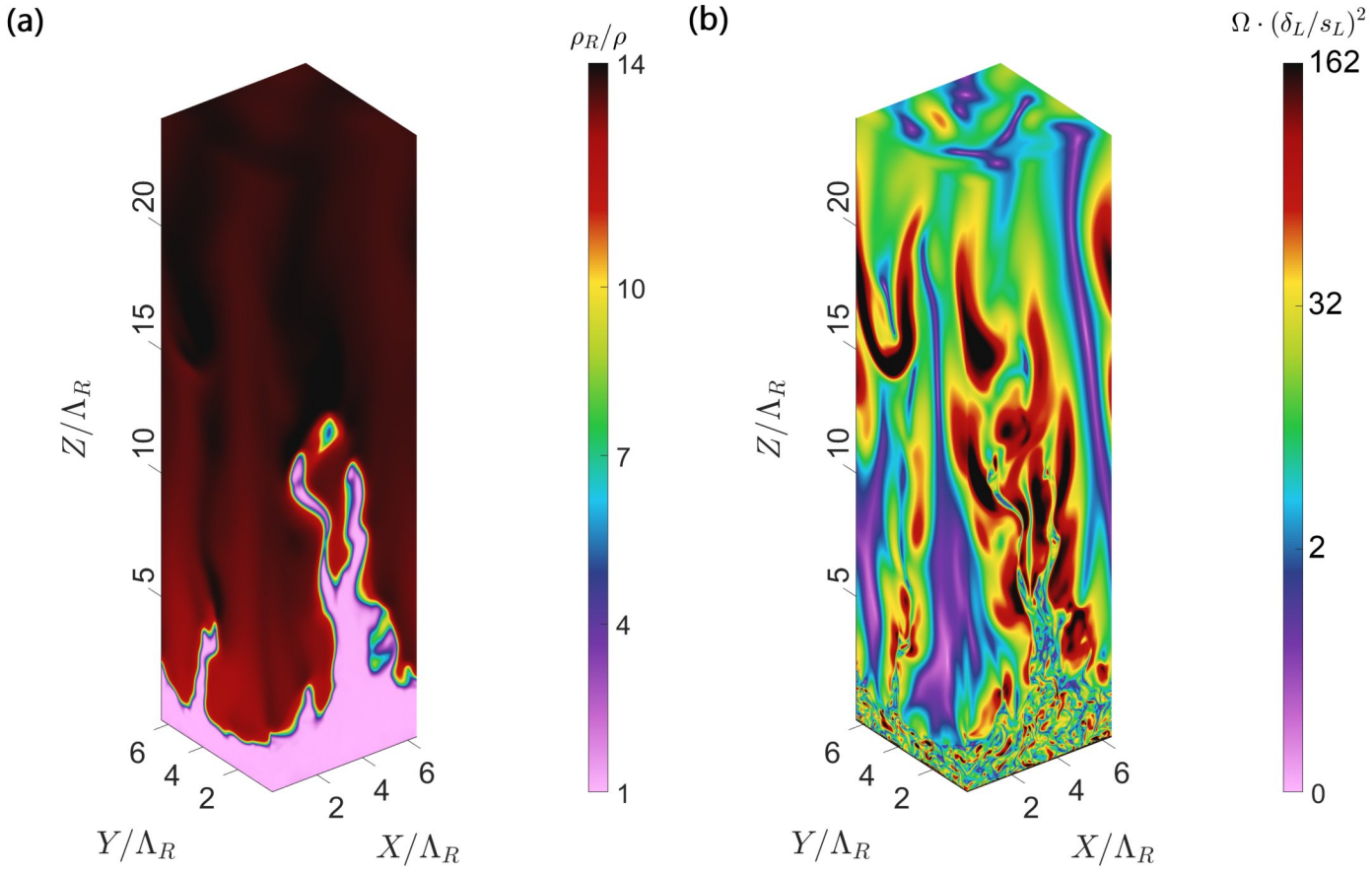

Figure 1: Instantaneous field in turbulent premixed flame: Density ratio (left), Enstrophy (right).

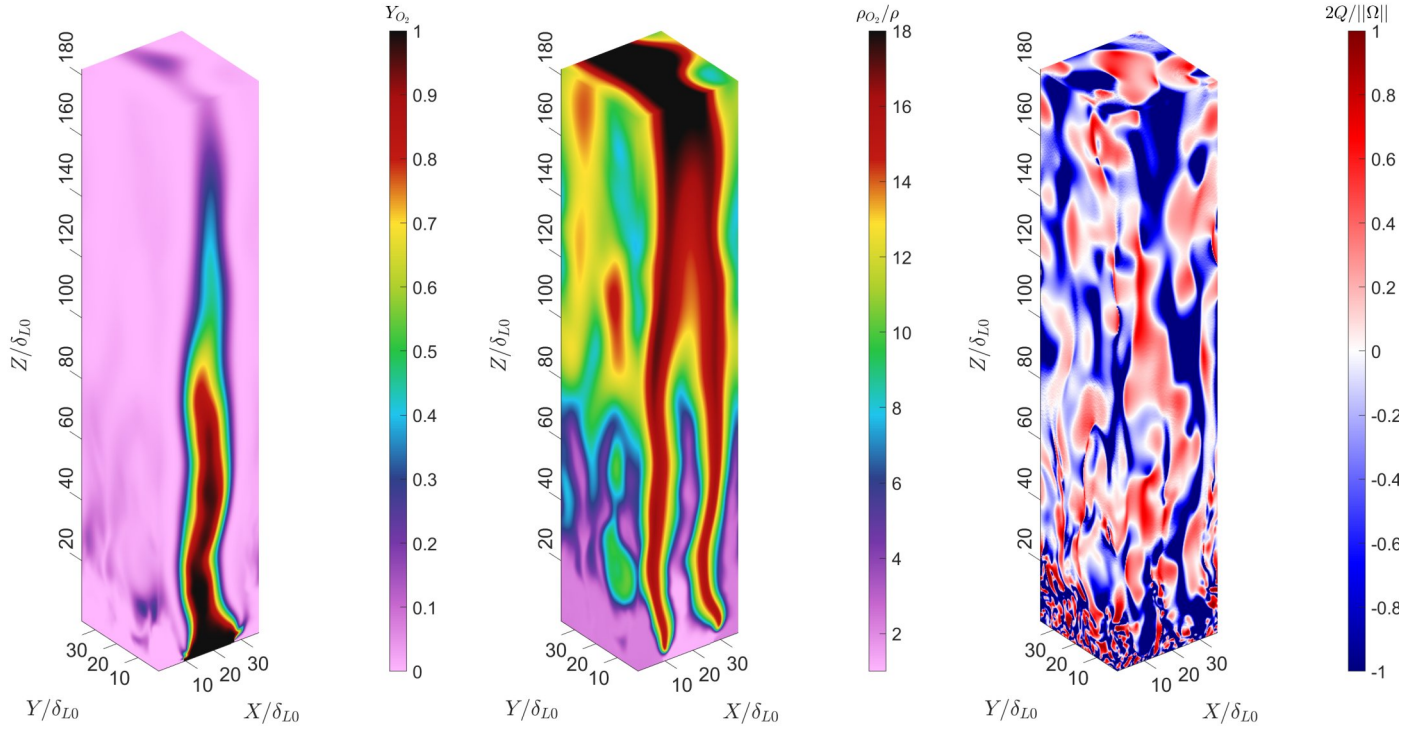

Figure 2: Instantaneous field in turbulent diffusion flame: Oxygen mass fraction (left), Density ratio (center), Normalized second invariant (right).

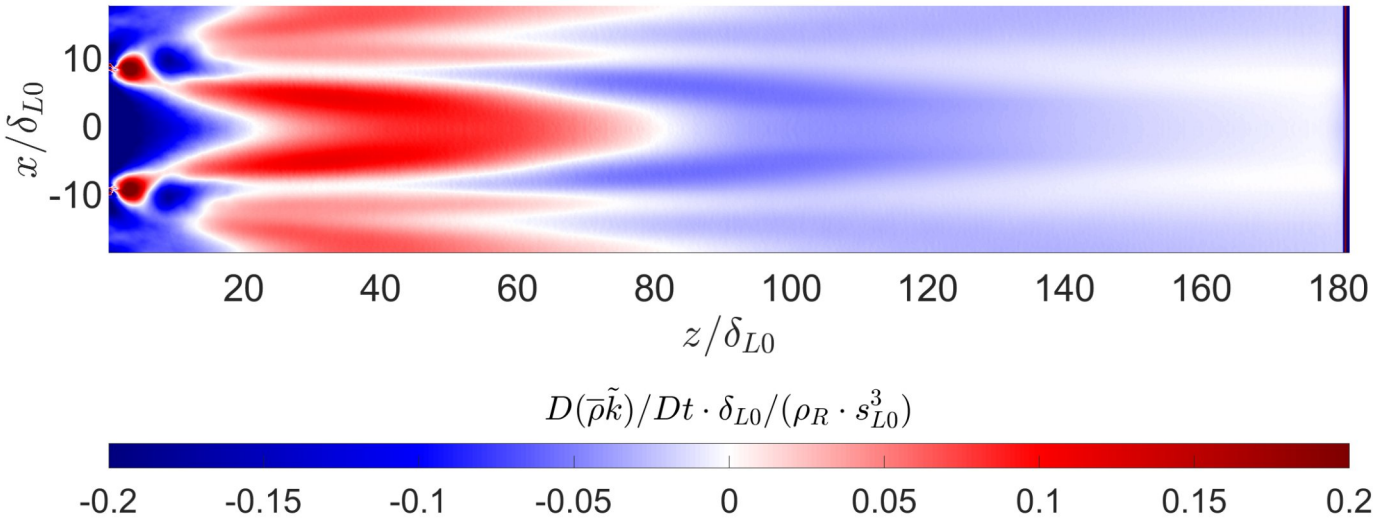

Figure 3: Turbulent transport in diffusion flame.

Instantaneous values such as the ones presented in Fig 1 and Fig 2 allow to visualize the most relevant physical processes. However, building models requires to study the time-averaged statistics. An example of such result is presented in Fig 3. In this illustration, the transport of turbulent kinetic energy in a methane-oxygen non-premixed turbulent flame displayed. Here, red colors indicate that turbulence is created, whereas blue point out turbulence dissipation. A significant generation of turbulent kinetic energy in the first regions of the shear layer can be observed. These results oppose the usual predictions of conventional models. As the viscosity increases through the flame, a higher dampening of vortexes is expected, implying the destruction of turbulence. This simulation's results exhibit the opposite outcome. Understanding the physical motivations behind this result is an intensive research topic. Our preliminary results point to the small-scale interactions between turbulence and chemistry as the responsible elements for this behavior. The local curvature of the flame can decrease or enhance the heat transfer, which is crucial for the combustion progress. If flame wrinkles are very small, the heat transfer experiences a local enhancement, generating local velocity fluctuations, which accentuate the flow's chaotic behavior.

Ongoing Research / Outlook

The obtained results constitute an extremely valuable data source for investigating the behavior of flames operating in extreme conditions. The collected results will be used as a basis to train models for machine learning and artificial intelligence applications. Future simulations will be performed to cover a broader range of operation regimes. More detailed geometrical aspects of the injection region will be simulated to investigate flame-wall interactions.

References and Links

[1] D. Martinez-Sanchis et al., Flow Turbul. Combust. (2022).
[2] D. Martinez-Sanchis et al., Phys. Fluids (2022).

Training CNN to estimate SGS scalar variance and dissipation rate

Research Institution
[1]Simulation of reactive Thermo-Fluid Systems, TU Darmstadt

Principal Investigator
Christian Hasse[1]

Researchers
Wang Han[1], Felix Dietzsch[1], Arne Scholtissek[1], Dominique Thévenin[2]

Project Partner
[2]ISUT, Otto von Guericke University, Magdeburg

SuperMUC Project ID: pr74li (Gauss Large Scale project)

Introduction

Currently, more than 80% of power and propulsion is achieved by combustion of fossil fuels, which significantly contributes to carbon and NOx emissions. To meet stringent pollutant regulations, in the development of next-generation piston and aero engines, one of the main concerns is the reduction of pollutant emissions, such as soot, nitrogen oxides (NOx) and carbon monoxide (CO). To this end, the challenges in combustion research are therefore to advance fundamental understanding of combustion chemistry and dynamics from molecule scales to engine scales and to develop quantitatively predictive models. While numerical simulation is of increasing importance in the development of advanced engines, numerical modeling of reacting flows in practical combustion devices with a detailed or comprehensively reduced chemical mechanism remains a formidable challenge. One of the main reasons is that realistic kinetic mechanisms involve hundreds of species and thousands of reactions. The significant disparities of characteristic time scales of different species and reactions force one to solve many stiffly coupled scalar transport equations. To overcome this challenge, two main strategies have been proposed: chemical reduction techniques and flamelet-based chemistry models. The focus of this work is these latter methods.

In the context of the flamelet-based chemistry model, the complex chemical structures of the flame can be decoupled from the flow dynamics [1]. This decoupling of scales constitutes an important advantage of flamelet models compared to other combustion models, as it allows for a pre-tabulation of thermochemical states based on a small number of independent parameters, e.g., mixture fraction Z and its dissipation rate .

On the other hand, in large eddy simulation (LES) of turbulent combustion, the modeling of sub-grid scale (SGS) mixing between fuel ($Z = 1$) and oxidizer ($Z = 0$) is crucial for the accurate use of the Z - χ based flamelet model. The SGS mixing can be characterized by two variables, mixture fraction variance (Z_{var}) and dissipation rate (χ_{sgs}). The former quantifies the level of unmixedness at the scales not resolved by LES, and the latter describes the rate of mixing between fuel and oxidizer that will lead to a decay of the variance. Typically, Z_{var} and χ_{sgs} are modeled by assuming that the local production of subfilter variance is exactly balanced by scalar dissipation, leading to algebraic models for both quantities [2]. However, the local equilibrium assumption (LEA) derived models for Z_{var} and χ_{sgs} have been found to yield erroneous predictions of scalar mixing (and hence scalar dissipation rate), which can significantly alter predictions of lift-off heights of flames, soot formation and evolution, and gas-phase pollutant emissions.

With this background, the part objective of this SuperMUC project is to train Convolutional Neural Networks (CNN) to estimate SGS mixture fraction variance and dissipation rate using the DNS databases created by this SuperMUC project.

Results and Methods

Within this project all simulations and analyses are based on direct numerical simulations (DNS) which are conducted with the DNS code DINO [3]. The solver is designed for the simulation of low-Mach number reactive flows, where spatial derivatives in the governing equations are discretized with 6th order finite differences. The temporal integration is done by a 3rd order semi-implicit Runge-Kutta scheme. Based on the distributed memory architecture of SuperMUC parallelization of the solver is achieved by the message passing interface (MPI), where an excellent scalability up to 65,536 cores is achieved.

The DINO code is parallelized in two dimensions using the 2DECOMP&FFT library that acts on top of standard MPI and FFTW. The Poisson equation for pressure is solved by means of FFT for both periodic and nonperiodic boundary conditions, but with dedicated pre and postprocessing FFT techniques in

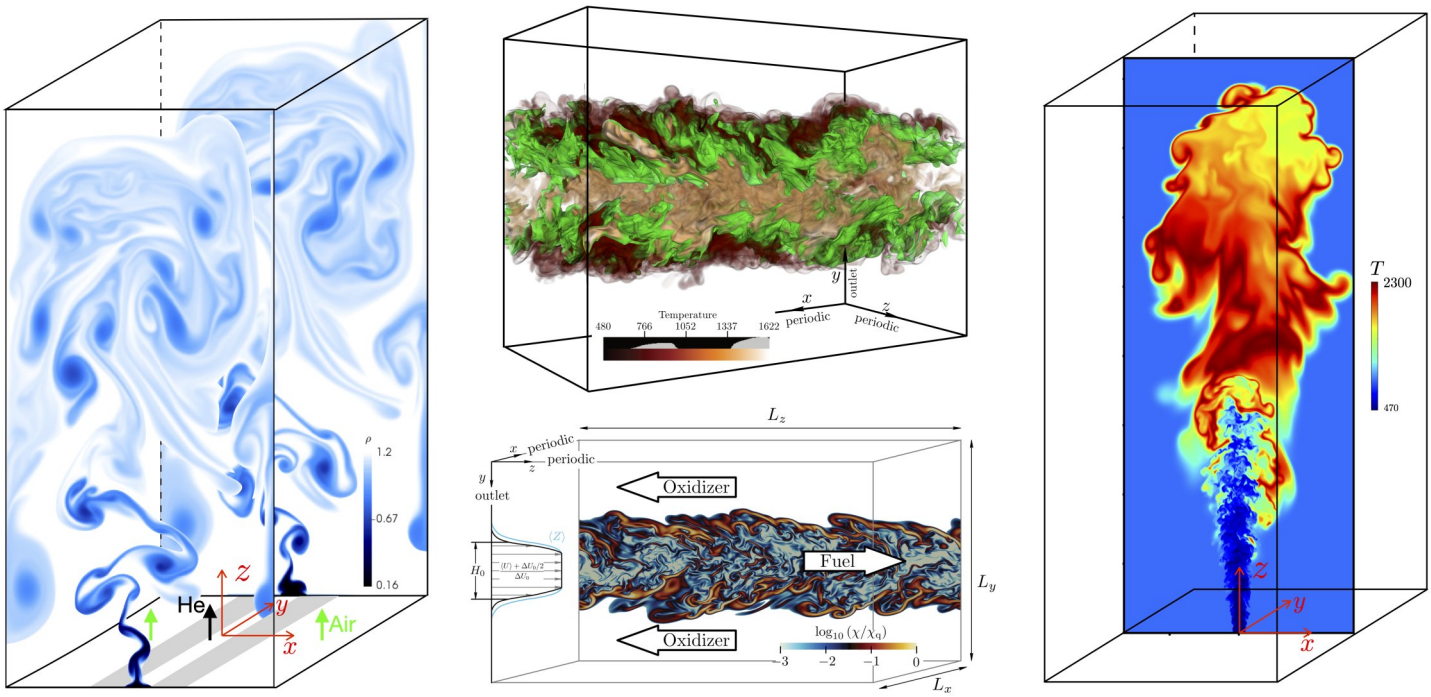

(a) Turbulent Helium plume (test data, Re=1000)

(b) Temporally evolving jet flames (training/validation/test data, Re=4500, 9000)

(c) Spatially evolving jet flame (test data, Re=17000)

Figure 1: DNS databases used to train, validate, and test CNN models for Z_{var} and χ_{sgs}. The spatially evolving jet flame is from Ref [4].

the latter case. While in the lowMach number solver the time step restriction associated with acoustic waves is removed, the restriction of time step due to chemistry stiffness is still present. For that reason, an implicit time integration of the stiff chemical source terms has been implemented, relying on a semi-implicit RungeKutta 3rdorder. In the DINO code, the chemical source terms are computed using the open-source Cantera library. The transport properties are computed either with the Cantera library or with the EGlib3.4 library.

Building the training database

In this project, two DNSs of temporally evolving turbulent jet flames were conducted, which provides valuable databases for training and validating the CNN models for Z_{var} and χ_{sgs}. Figure 1(b) schematically illustrates the flow configurations of the two DNSs. In the top, the fuel stream is composed of 65%H_2 and 35%N_2 by volume with the initial velocity of 97.5 m/s, and the oxidizer stream is composed of 30%O_2 and 70%N_2 by volume with the velocity of -97.5 m/s. The jet Reynolds number is 4,500. In the bottom, the fuel stream is composed of The fuel stream is composed of 50%CO, 10%H_2, and 40%N_2 by volume with the initial velocity of 138 m/s, and the oxidizer stream is composed of 25%O_2 and 75%N_2 with the initial velocity of -138 m/s. The fuel jet Reynolds number is 9,000.

The first DNS calculation consumed 5 M core hours on 12,000 cores and generated roughly 10 TB of raw data. The second DNS calculation consumed 10 M core hours on 23,904 cores and generated roughly 30 TB of raw data.

The above two DNS databases are used to train, validate, and test the CNN models for Z_{var} and χ_{sgs}. To examine the performance of the CNN models in the cases beyond the training databases, other two DNS databases (see Fig. 1a and 1c) of spatially evolving jets are used to test the CNN models. It is noted that the turbulent Helium plume jet DNS databases (Fig. 1a) were created within the project and that the jet DNS databases with Re-17,000 were provided by Sandia National Labs, USA [4].

Training and validating CNN models

This work aims to train U-net CNN models using resolved mixture fraction (Z) as input. Therefore, the DNS databases produced on the DNS mesh are first filtered with a Gaussian filter (see Fig. 2). It is noted that the input field naturally falls the range of 0-1 which is favorable for machine learning. Figure 2 shows the training strategy, in which the input and target outputs of the CNN are indicated.

Figure 3 compares the LEA-based models with CNN-based models using the test data. It is seen that the CNN models perform better than the physics-based LEA models.

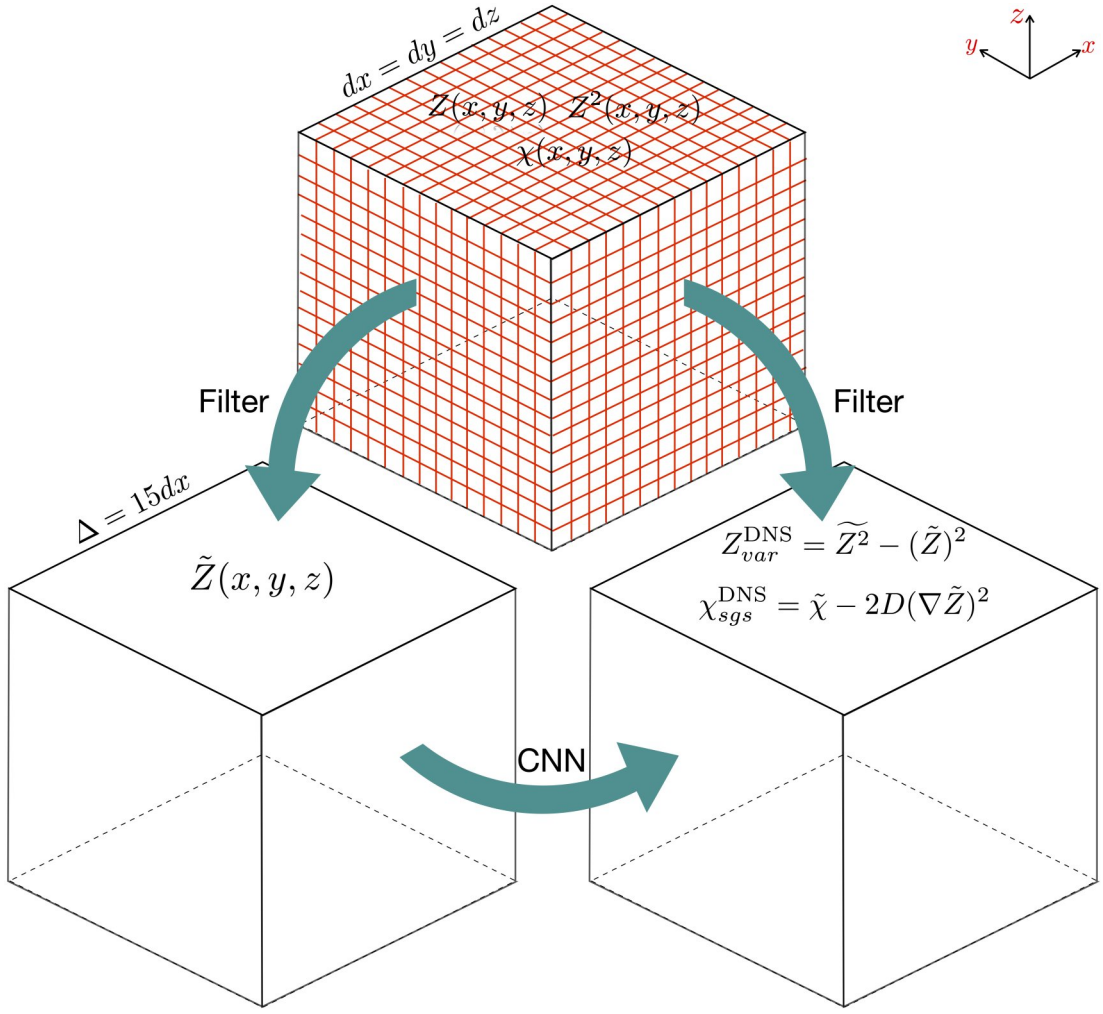

Figure 2: Training strategy to estimate SGS mixture fraction (Z) variance and dissipation rate. The DNS field of Z is filtered to produce input ($\tilde{Z}$) and target outputs (Z_{var} and χ_{sgs}) of CNN on an 'LES' mesh that is 15 times coarser than the DNS. The CNN is trained on the dataset to approximate the functions $Z_{var}^{DNS} = f_{CNN}(\tilde{Z})$ and $\chi_{sgs}^{DNS} = f_{CNN}(\tilde{Z})$.

Ongoing Research / Outlook

The preliminary results shown in this report imply that the data-driven CNN approach is very promising for modeling SGS mixture fraction variance and dissipation rate. This will be further investigated by testing the CNN models using other DNS databases beyond the scope of training databases, e.g., two jet flows illustrated in Fig. 1a and Fig. 1c. Moreover, this work complements the analysis of turbulent reacting flows by means of dissipation elements [5], tangential diffusion, and Soret diffusion conducted in previous SuperMUC project by providing a new insight into the modeling of SGS scalar variance and dissipation rate.

References and Links

[1] Heinz Pitsch. 2006, Annu. Rev. Fluid Mech. 38, 453-482.
[2] Colleen M. Kaul, Venkat Raman, Edward Knudsen, Edward S. Richardson and Jacqueline H. Chen. 2013, Proc. Combust. Inst. 34, 1289-1297.
[3] Abouelmagd Abdelsamie, Gordon Fru, Timo Oster, Felix Dietzsch, Gábor Janiga and Dominique Thévenin. 2016. Comput. Fluids 131, 123-141.
[4] Xu Wen, Martin Rieth, Wang Han, Jacqueline H. Chen and Christian Hasse. 2021, Proc. Combust. Inst. 38, 5605-5613.
[5] Michael Gauding, Felix Dietzsch, Jens Henrik Goebbert, Dominique Thévenin, Abouelmagd Abdelsamie and Christian Hasse. 2017. Phys. Fluids 29.

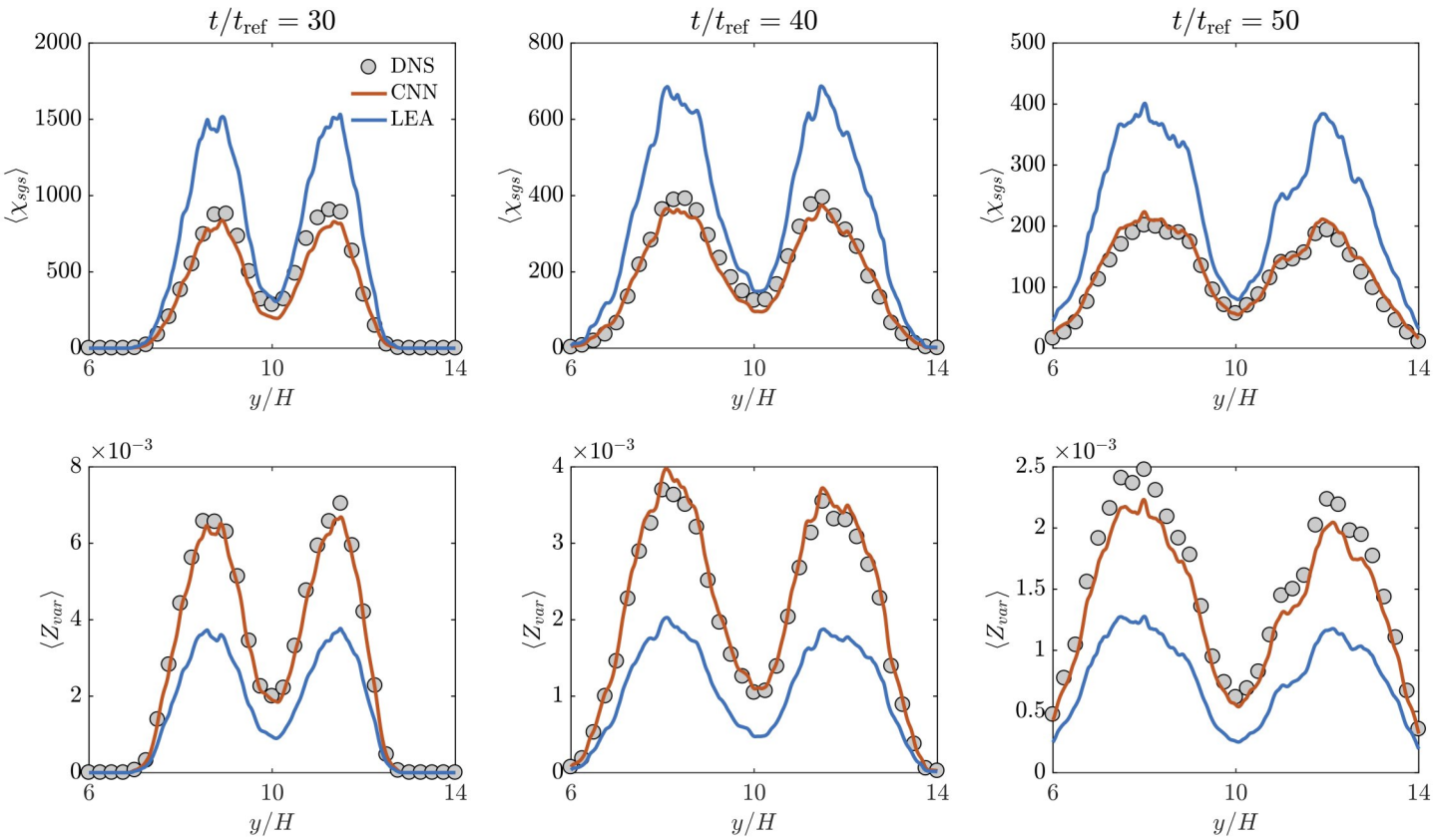

Figure 3: Comparisons between the physics-based LEA models and data-driven based CNN models for predicting SGS mixture fraction variance (bottom) and dissipation rate (top).

Toward simulation-assisted statistical theories of turbulence

Research Institution
[1]Max Planck Institute for Dynamics and Self-Organization, Göttingen

Principal Investigator
Michael Wilczek[1]

Researchers
Cristian C. Lalescu[1,2], Markus Rampp[2], Bérenger Bramas[3]

Project Partners
[2]Max Planck Computing and Data Facility, Garching
[3]Inria, Nancy – Grand-Est

SuperMUC Project ID: pr53ru

Introduction

Turbulence is virtually everywhere. It governs our atmosphere, our oceans as well as their interaction. Turbulent flows feature a broad range of dynamically active scales with a continuous transfer of energy between them. Turbulence, therefore, plays an important role for the energy budget of geophysical flows, it triggers precipitation by enhancing droplet growth in clouds and provides the main mixing mechanism for combustion processes, pollutants in the atmosphere, urban environments, and marine micro-organisms in the ocean.

Since turbulent flows are chaotic and random, theories of turbulence necessarily have to be of a statistical nature. Despite decades of research, developing such theories, which ultimately all modeling applications rely on, remains one of the outstanding scientific challenges.

From a physics perspective, fully developed turbulence constitutes a paradigmatic problem of a strongly driven system with an enormous number of interacting degrees of freedom. The challenge of developing a statistical theory of turbulence arises from multi-scale flow structures, which introduce long-range correlations and give rise to complex, scale-dependent statistics. Numerical simulations can provide key insights into the emergence of these structures, their dynamics, and the resulting statistics.

Results and Methods

For our simulation-driven theoretical investigations, we study highly turbulent flows from two complementary perspectives: The Eulerian frame, i.e. a fixed frame of reference, is well suited to investigate spatial features of turbulence. In contrast, the Lagrangian frame, i.e. following tracer particles, is particularly useful to study spatio-temporal phenomena such as turbulent mixing.

We have developed the simulation framework TurTLE (Turbulence Tools: Lagrangian and Eulerian), a flexible pseudo-spectral solver for fluid and turbulence problems implemented in C++ with a hybrid MPI/OpenMP approach. TurTLE allows for an efficient tracking of a large class of particles by means of a parallel programming pattern that is easy to adapt and implement [1]. TurTLE scales well up to $O(10^4)$ computing cores for problem sizes up to $4{,}096^3$ grid points and up to 10^9 particles.

For the largest problem size ($4{,}096^3$) that we considered so far, the simulation of an integral time (characteristic time for large-scale flow features) requires several million core-h on SuperMUC-NG using jobs with up to 512 nodes. A single flow field requires 1.65TB of disk space, such that a database spanning several integral time scales requires on the order of 100TB. Figure 1 is a visualization of the velocity field from one of our large-scale simulations. It illustrates the multi-scale nature of turbulence: while the velocity shows correlations comparable to the domain size, a considerable degree of small-scale structure in the form of coherent vortices is evident from these visualizations.

Ongoing Research / Outlook

Over the past years, simulations on HPC infrastructures such as the systems provided by LRZ have been instrumental in informing new fundamental theories for turbulence and in tackling a number of applied problems.

For example, analyzing millions of particle tracks from large-scale simulations, we made the observation that the ensemble of tracer trajectories, based on their acceleration signature, can be categorized into classes of fluid particles with much simpler statistics [2]. This led us to develop a comprehensive theoretical framework for single-particle statistics. This work pointed toward the exciting possibility to finally unravel the complex statistics of turbulence in a data-driven theoretical approach, which inspires novel statistical field theories of turbulence. We also showed that the transport of tracer particles can be predicted from spatial features of the flow [3]. Essentially, this means that a snapshot

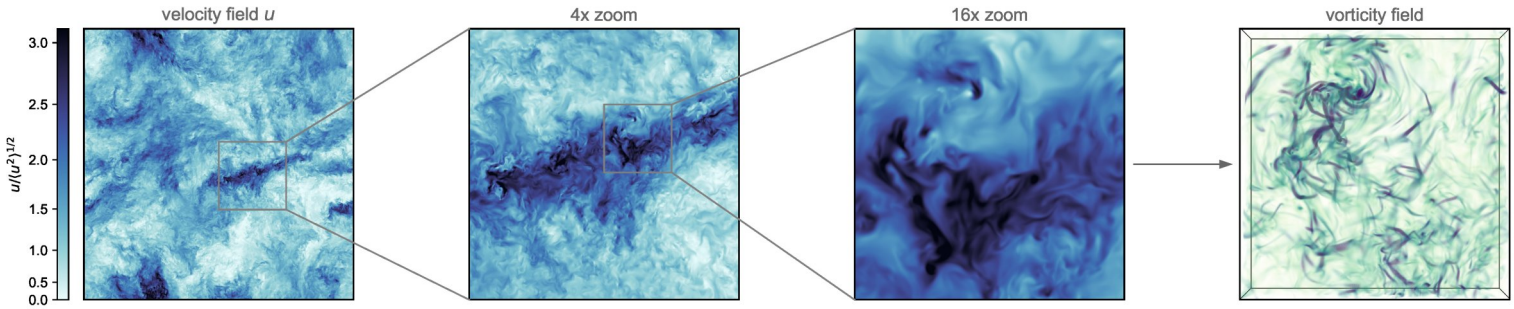

Figure 1: Turbulence is a multi-scale phenomenon. A sequence of zooms into the velocity field (two-dimensional cuts) from one of our simulations with $4{,}096^3$ grid points reveals significant correlations on all scales. Steep gradients in the velocity field are closely related to small-scale coherent structures such as vortex filaments (volume rendering, right panel). The close connection between coherent structures and multi-scale correlations poses a major challenge in developing a statistical theory of turbulence.

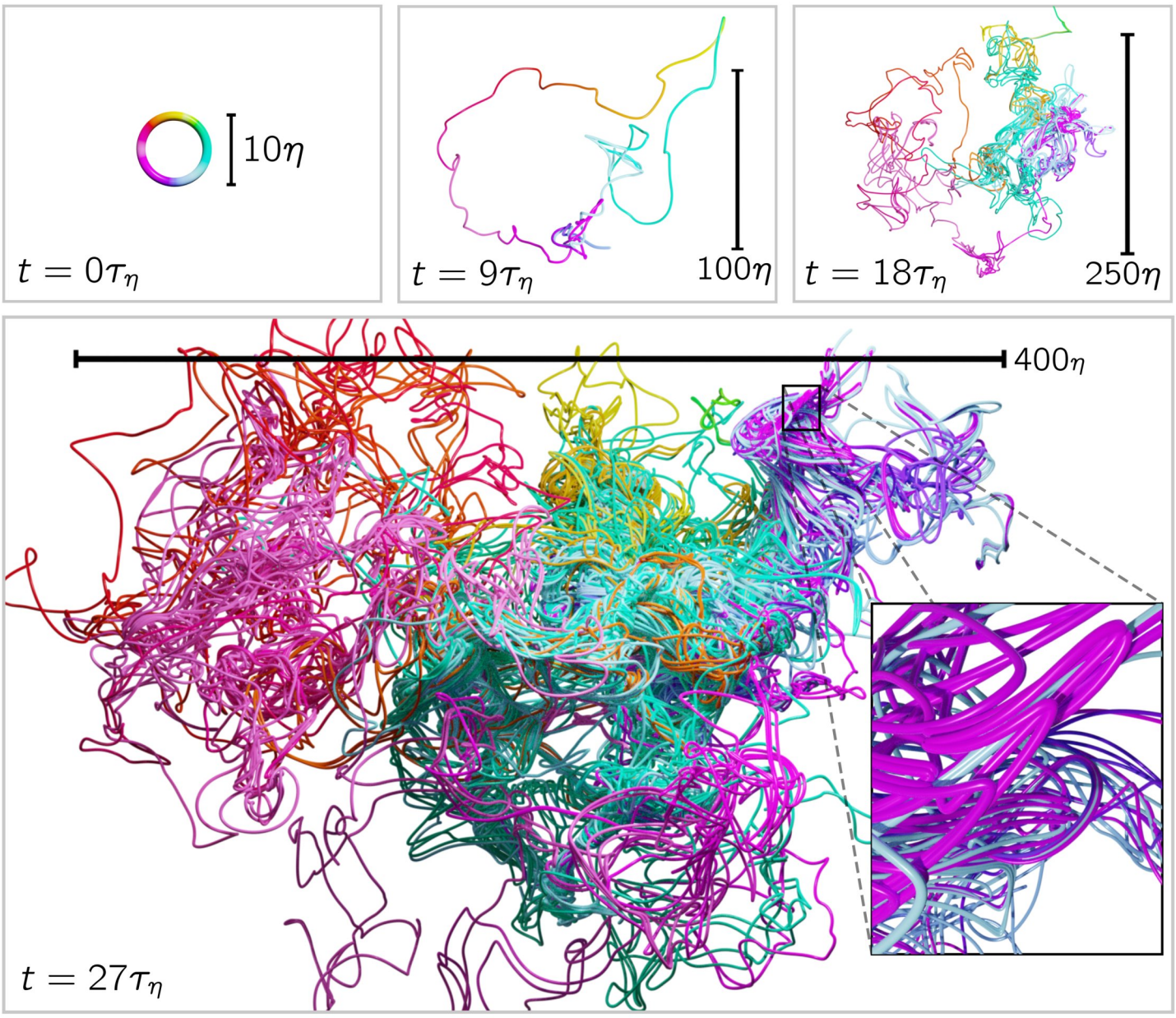

Figure 2: Visualization of an initially circular material loop, advected by a turbulent flow field. The twisting and folding action of the turbulent flow creates a complex loop geometry while the length of the loop on average increases exponentially. Figure adapted from [4] licensed by CC BY 4.0 [5].

of a turbulent flow is already informative about how well turbulence mixes over time.

Recently, we started focusing on geometric features of turbulence. By tracking the evolution of material loops, i.e. closed material lines, we showed how fluid elements are stretched and folded as they go with the flow, leading to very complex shapes, see Fig. 2. Remarkably, we were able to compute robust statistical features of such material lines [4]. This work has implications, for example, for our understanding of magnetic field lines in astrophysical problems or polymer stretching in turbulent flows.

Using the insights of our fundamental turbulence research, we also address a range of application-focused problems. For example, we investigate how turbulence enhances the encounter rates of microorganisms in the oceans. It turns out that small-scale turbulence has a significant impact on their swimming and sedimentation dynamics. This may significantly alter their encounter rates, therefore playing a role for mating, grazing, and the formation of planktonic colonies.

A quite complementary, yet surprisingly similar problem occurs in the formation of rain in clouds. Until today, the microphysical processes that let microdroplets grow to rain drops are not fully understood. In the turbulent environment of clouds, the small-scale vortices act as tiny centrifuges, which accelerate particles into flow regions with less swirl. As a consequence, particles tend to cluster in those regions, significantly enhancing droplet collisions and coalescence. In an ongoing project, we are investigating this process using simulations with the aim of developing better predictions.

These are a few examples from our recent and ongoing work, which illustrate that modern high-performance-computing infrastructures such as the ones provided by the LRZ are an indispensable tool for pursuing simulation-driven theoretical research. Extensive large-scale simulations will continue to provide the computational foundation for such investigations.

References and Links

[1] C. C. Lalescu, B. Bramas, M. Rampp, and M. Wilczek. Comput. Phys. Commun., 278:108406, 2022.
[2] L. Bentkamp, C. C. Lalescu, and M. Wilczek. Nat. Commun., 10:3550, 2019.
[3] C. C. Lalescu and M. Wilczek. New J. Phys., 20:013001, 2018.
[4] L. Bentkamp, T. D. Drivas, C. C. Lalescu, and M. Wilczek. Nat. Commun., 13:2088, 2022.
[5] http://creativecommons.org/licenses/by/4.0/

Earth, Climate and Environmental Sciences

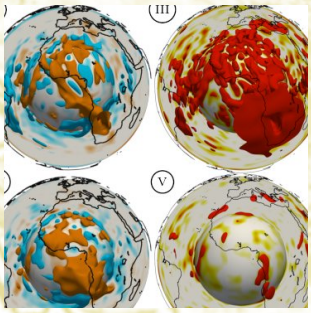

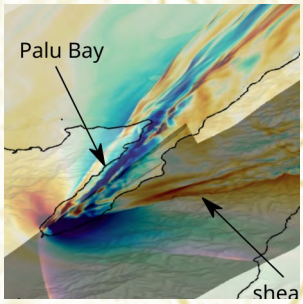

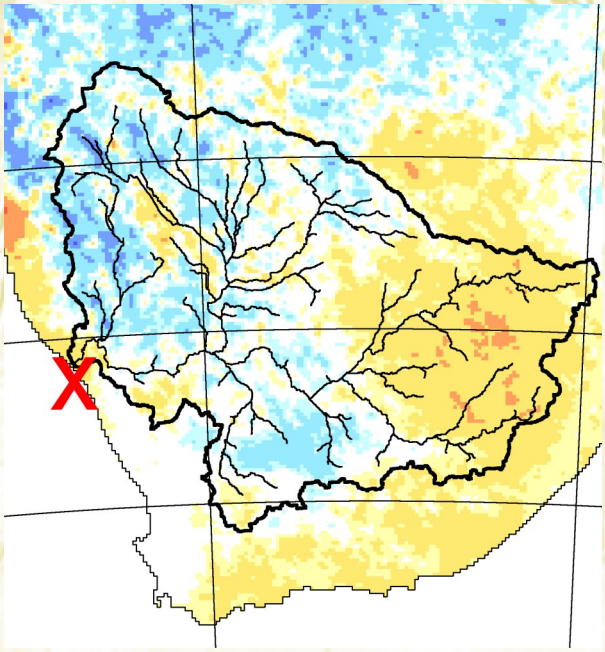

Investigating southern African Holocene climate – bridging from the early Holocene to today

Research Institution
[1]Karlsruhe Institute of Technology, Garmisch-Partenkirchen Research (IMK-IFU), Campus Alpin, Garmisch-Partenkirchen

Principal Investigator
Joël Arnault

Researchers
Harald Kunstmann[1], Kyle Niezgoda[2], Annette Hahn[3], Matthias Zabel[3], Enno Schefuß[3]

Project Partners
[2]Oregon State University
[3]University of Bremen

SuperMUC Project ID: pn29ku

Introduction

Climate variability in Southern Africa is characterized by changes in strength and position of the temperate westerlies, intertropical convergence zone, and Congo air boundary, as well as by sea surface temperature variabilities. The complexity of the climate system is also evident in the isotopic signal of Holocene proxy records, which shows, even over small distances, high regional climate variability [1]. With this project we aim at improving the understanding of the processes that influenced past and present climate variability of Southern Africa and at explaining the isotopic signal of proxy records. For this purpose, we downscale global climate simulations for different past climate time slices with a coupled atmospheric-hydrological regional model equipped with stable water isotopologue [2]. The further consideration of water tracing from two major moisture source regions, namely the Indian and Atlantic Ocean, offers the unique opportunity not only to investigate differences in proxy records, but also to analyze changes in atmospheric dynamics that influence Southern African climate.

Results and Methods

The isotope-enabled regional coupled model WRF-Hydro-iso [2] is enhanced with an isotope-tracing procedure in order to quantify the moisture sources of stable water isotopologues contained in precipitation. WRF-Hydro-iso is used to regionally downscale the isotope-enabled Community Earth System Model [3] for Southern Africa for two 10-year slices, one slice for the mid-Holocene period 6000 years ago, and another slice for the pre-industrial period a few hundred years ago. The isotope tracing procedure is tailored in order to assess the origin of the hydrogen-isotope contained in Southern African precipitation, between the Atlantic and Indian moisture sources. The WRF-Hydro-iso results displayed in Fig. 1 show that the mid-Holocene-to-pre-industrial changes in the Orange river basin in Southern Africa are associated with an increase of the summer Atlantic moisture source contribution to precipitation, with minor differences in the precipitation amounts, and an isotopic enrichment of the precipitation taking place in the western part of the basin. Accordingly, the modeled isotopic enrichment in the Orange region does not indicate that the pre-industrial climate was drier than the mid-Holocene climate in the Orange region, but that the atmospheric circulation has changed with more moisture flow coming from the Atlantic Ocean during summer.

Modeled paleo isotope compositions in precipitation can be compared to isotope compositions of plant materials in sediment archives, as the atoms of hydrogen in plant materials originate from precipitation [4]. The modeled isotopic enrichment in the Orange region matches plant-wax isotope records from a marine sediment core off the Orange river [5], as displayed in Fig. 2. This gives us confidence that the climate change between mid-Holocene and pre-industrial periods in Southern Africa, as simulated by WRF-Hydro-iso, is realistic.

Ongoing Research / Outlook

This study shows the potential of regional downscaling with WRF-Hydro-iso to improve the comparison to isotope records in climate archives, as well as the usefulness of the isotope tracing capability to clarify the physical interpretation of such isotope records. Accordingly, WRF-Hydro-iso can be advised for further paleoclimate reconstructions.

References and Links

[1] B. Chase and M. Meadows, Earth-Sci Rev 84 (2007) 103-138.
[2] J. Arnault et al., J Adv Model Earth Sys 13 (2021) e2021MS002562.
[3] E. Brady et al., J Adv Model Earth Sys 11 (2019) 2547-2566.
[4] D. Sachse et al., Annu. Rev. Earth Planet. Sci., 40 (2012) 221-249.
[5] N. Burdanowitz et al., The Holocene 28 (2018) 1288-1300.

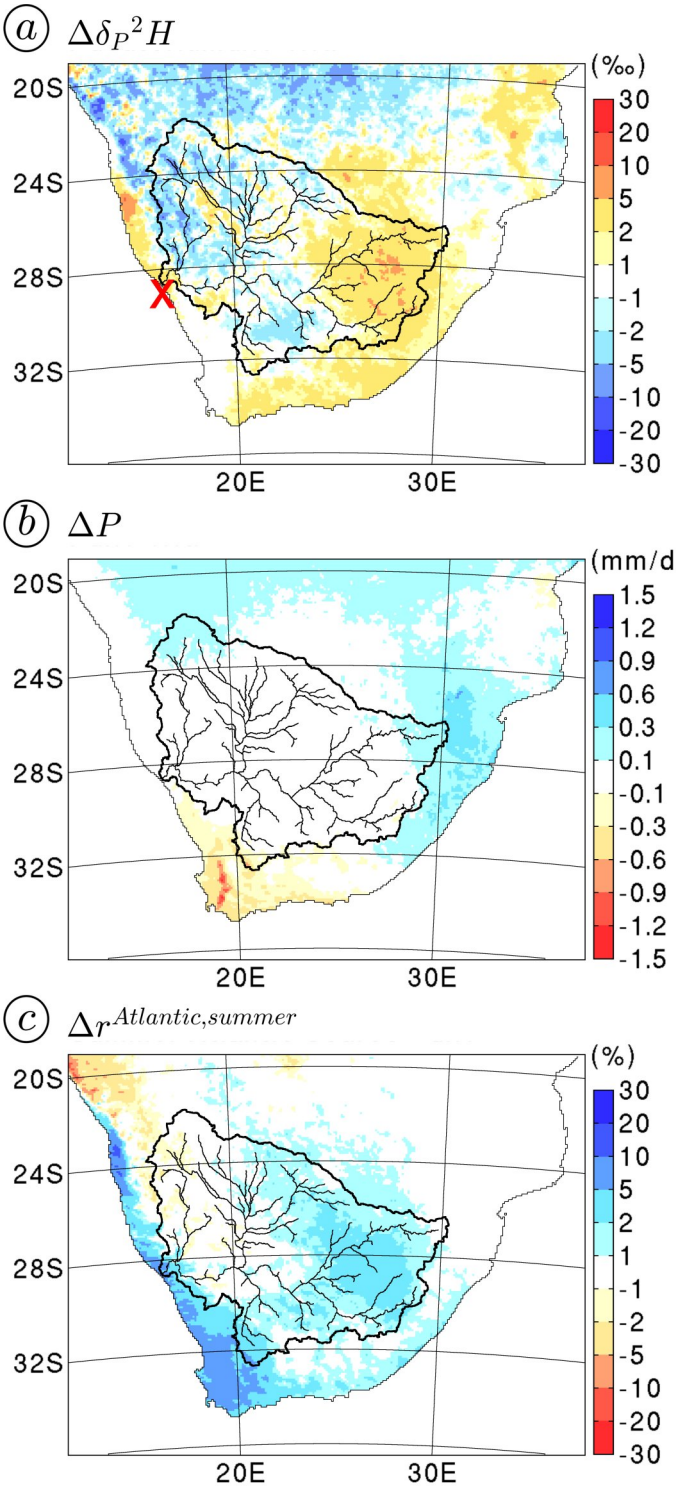

Figure 1:10-year average modeled change in (a) precipitation hydrogen-isotope composition in ‰, (b) precipitation amount in mm/day and (c) summer Atlantic moisture source in % between the mid-Holocene period and the pre-industrial period. The red cross in (a) shows the location of marine sediment core GeoB8331-4 offshore the mouth of the Orange River. The black contour delineates the Orange river basin.

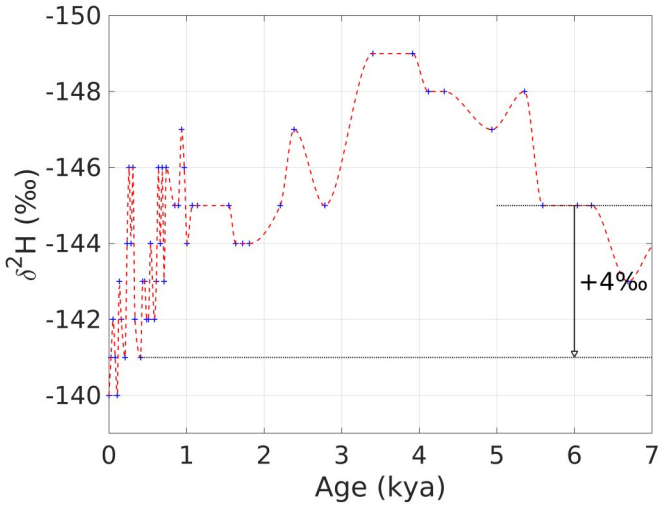

Figure 2: Record of hydrogen-isotope composition of plant waxes from marine sediment cores GeoB8331-4, whose location is shown in Fig. 1a. The x-axis gives the age in kilo years ago (kya) and the y-axis gives the isotopic composition scale in ‰. The isotopic composition-change between the mid-Holocene and pre-industrial periods is highlighted.

Variable resolution meshes in climate research

Research Institution
Karlsruhe Institute of Technology (KIT)
Institute of Meteorology and Climate Research (IMK-IFU)

Principal Investigator
Gerhard Smiatek

Researchers
–

Project Partners
–

SuperMUC Project ID: pr94mi

Introduction

Meshes with different resolutions are employed in simulation of the African Monsoon with the Model for Prediction Across Scales (MPAS). Computational and technical issues of the CPU demanding climate simulations are one aspect of the project. Another is the practical application of the obtained results. Here, after the change of the principal investigator, the focus was moved to an important environmental question of great concern. This is the potential impact of the planned pan-African Great Green Wall (GGW) for the Sahara and Sahel on the regional and continental climate.

The GGW initiative aims at regreening a band in the Sahelian area receiving 100 – 400 mm precipitation per year through afforestation and natural regeneration. The planned wall is at least 15 km wide (Figure 1). Several countries, however, plan reforestations of much wider areas. In total, 30 woody and 22 herbaceous plants are proposed to cultivate in GGW resilient to arid and semi-arid climatic conditions [1]. These species have been selected taking into concern socio-economic values to the population and important ecological functions.

The scientific aims of the present study are provision of simulated climate data for the Saharo - Sahelian region and investigation of the potential influence of the GGW on the Sahelian precipitation. The focus of this report is on the simulation of the precipitation belt migration over the Sahel zone.

Results and Methods

The applied meteorological model is MPAS in the version 7. MPAS is modeling framework that includes an atmospheric, an ocean, and a land-ice model based on unstructured Voronoi meshes and C-grid discretization. The study applies MPAS-atmosphere [2]. It is a global, fully compressible non-hydrostatic model. The performed simulations apply 55 vertical levels up to 30 km heigh and 4 soil levels.

The simulation experiments in the study use three mesh resolutions: The first resolution with a total number of 163,842 model cells is at approximately 60 km. The second resolution is at 30 km with 655,362 cells. Runs with those meshes apply the mesoscale reference physics suite and parameterized convection. The third resolution with 835,586 cells is a variable-resolution mesh. In the area of West Africa (Center: 0°W and 14°N) it extents the resolution in a broad transition zone from the global 60 km to 3 km. In cells with resolution below roughly 4 km MPAS runs in convection permitting mode.

Available precipitation climatologies for the Sahel zone show large differences [3]. The same applies to results of simulations with General circulation models (GCM) as well as regional climate models (RCM) resulting from limitations in representation of the complex physical process driving the African climate[4].

Evaluation of the performed MPAS simulations applies 20 years periods of the CHIRPS (Climate Hazards Group InfraRed Precipitation with Station data) (1996--2015) and CMORPH (NOAA Climate Data Record (CDR) of CPC Morphing Technique) (1998--2017) observational references for the precipitation of the summer season (JJA - June, July, August) and the month August. The investigation area covers the area between -18°W to 40°E and 4°N and 24°N. It is denoted GGW.

Compared to the observational reference of 3.5 mm/d (CHIRPS) and 2.9 mm/d (CMORPH) for the summer season (JJA) and the GGW area, MPAS simulations reveal 2.8 mm/d for the 30 km resolution and 2.6 mm/d for 60 km resolution. This is related to the average of CHIRPS and CMORPH an underestimation in order of 13 % and 19 % respectively. Regional biases are larger. There is a mean overestimation in order of 25 % in the eastern part of the area. In the western part, MPAS simulations underestimate the observations with a mean of over 30 %. Results obtained for August, the month with the precipitation peak in the region, are similar.

Figure 2 shows Hovmöller diagrams of the CHIRPS observed and MPAS simulated daily precipitation amount from 01.06 to 01.10 for the 30 km and 60 km resolutions and from 01.08 to 01.09 for the 60-3km resolution. In this diagram type, each individual column is one day of rainfall across the GGW area

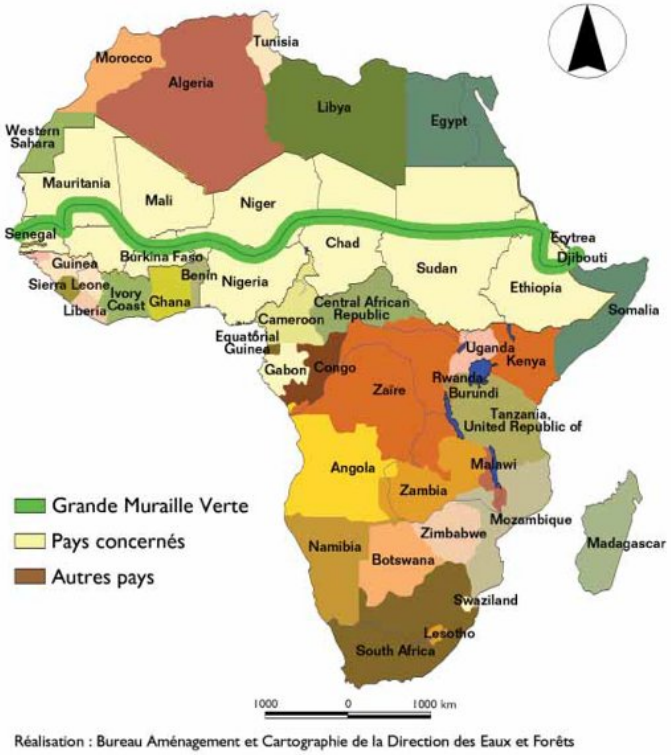

Figure 1: Planned Great Green Wall.

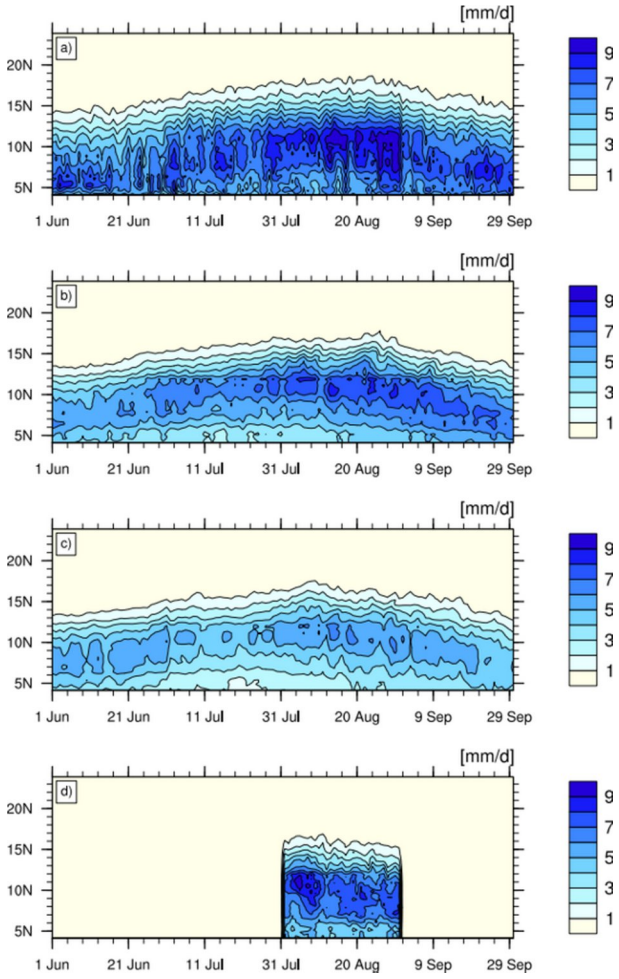

Figure 2: Observed and simulated daily precipitation in the GGW area averaged over the latitude. CHIRPS observed 1996–2015 (a) and mean of all MPAS simulations with 30 km resolution (b), 60 km resolution (c) and variable 60-3 km mesh (d).

(-18°W – 40°E), averaged by latitude. The horizontal axis shows the day if the year and the vertical axis shows the precipitation amount at each latitude as average of all MPAS simulations with the same resolution.

The simulated movement of the rain belt through the JJAS season reveals an extent comparable to the CHIRPS observational reference. In general, the precipitation belt moving to the north is narrower than observed. Also, substantial dry biases are visible south of the main rain belt. MPAS possibly fails in transporting enough moisture from the Atlantic. Only the simulation with 30 km resolution reaches the peak of the northern extent as observed after the 20 August, however this extent is with maximum of roughly 18°N one degree lower as in the CHIPRS observational reference. Simulations with 60 km and 60-3 km reach this peak earlier and extent only roughly to 17°N. In all resolution the underestimation of the northern extent is present throughout the entire considered season.

Ongoing Research / Outlook

Summarizing it can be stated that MPAS runs in all resolutions reasonably reproduce the observed Sahelian precipitation within the range of similar simulations with RCM and GCM models. Therefore, it can be applied in subsequent climate investigations.

However, there are obvious deficiencies present documenting that further improvements in the model formulation, possibly also in boundary input data are needed to reduce the present biases. Increase in the model resolution from 60 km to 30 km seems to reduce the bias.

No significant improvement in the simulated precipitation amount and patterns was reached with the computationally expensive variable 60-3 km mesh. The reason might be the fact that the area in which the convection permitting approach is applied was not sufficiently large and simulations with 3 km resolution covering the entire area are needed here.

References and Links

[1] Ba, A. T., 2010. Grande muraille verte: choix des especes vegetales. In: Dia, a., Duponnois, R. (Eds.), Le projet majeur africain de la Grande Muraille Verte. IRD, Institut de Recherche pour le D'eveloppent, pp. 31–38.
[2] Skamarock, W. C., Klemp, J. B., Duda, M. G., Fowler, L. D., Park, S., Ringler, D. T., 2012. Mon. Wea. Rev. 140, 3090 – 3105.
[3] Dosio, A., I. Pinto, C.Lennard, M.B. Sylla, C. Jack and G. Nikulin (2021), Earth and Space Science, 8, e2020EA001466.
[4] Dosio, A. et al. (2021), Climate Dynamics, 57, 3135-3158.

Fully-coupled simulation of the Palu, Sulawesi 2018 earthquake-tsunami event

Research Institutions
[1]Technical University of Munich
[2]Ludwig-Maximilians-Universität München

Principal Investigator
Michael Bader[1]

Researchers
Lukas Krenz[1], Carsten Uphoff [2], Thomas Ulrich[2], Alice-Agnes Gabriel[2], Lauren S. Abrahams[3], Eric Dunham[3]

Project Partner
[3]Stanford University

SuperMUC Project ID: pn68fi

4

Introduction

ChEESE, the European center of excellence for exascale computing in the domain of solid Earth [1] developed 14 so-called pilot demonstrators that address upcoming services and grand challenges that require exascale performance. As part of the pilot demonstrator on “physics-based tsunami-earthquake interaction”, we developed novel approaches to simulate (and better understand) complex submarine earthquakes and resulting tsunamis.

Results and Methods

Earthquake-tsunami events are commonly simulated using a one-way linking method. First, a simulation (or analytical model) of an earthquake computes the displacement at the seafloor. This displacement data is then used as input for a (typically 2D) tsunami simulation. Such linked models depend strongly on how both simulations are coupled and they make several modeling assumptions that may or may not apply in certain scenarios. As part of the ChEESE demonstrator, we therefore developed the first 3D model that includes earthquake rupture, elastic (in Earth) and acoustic (in the ocean) wave propagation, and tsunami propagation in one simulation [4]. The model has been implemented in SeisSol [2], an open-source earthquake simulation software [3].

The fully-coupled model makes fewer assumptions than the classical coupling strategy. It solves the elastic wave equation in the solid Earth and the acoustic wave equation in the ocean. Earthquake rupture is simulated by dynamic rupture, which uses laboratory-derived non-linear friction laws that model the physics of frictional fault failure. On the moving sea surface, we impose a zero-pressure condition. To avoid the expensive treatment of a moving mesh, we apply a linearization of the boundary condition, which requires solving a (less expensive) ordinary differential equation at each boundary point.

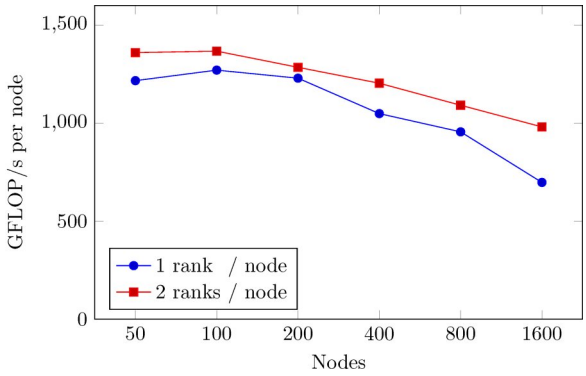

Figure 1: Parallel efficiency on SuperMUC-NG (for a mesh with 89 million elements). From 50 to 1600 compute nodes we achieve a parallel efficiency of ~72%. Figure taken from [3].

Compared to linked simulations, the resulting fully-coupled model includes dispersive effects which can be relevant at greater water depths. In addition, it does not assume that the ocean is incompressible which means that our model can resolve acoustic waves correctly. Acoustic waves do not typically have a large effect on the overall tsunami but can be the dominant wave type when compared with real-world measurements. Furthermore, acoustic waves travel faster than tsunami waves which means that they could be used for an early-warning system.

We demonstrated the capabilities of our model in a large-scale simulation of the Palu, Sulawesi 2018 earthquake, which happened in September 2018. This magnitude 7.5 strike-slip earthquake created a local tsunami that struck the bay of Palu. The event was unusual for two reasons: The earthquake produced very fast (“supershear”) movement along the fault. And, which is our focus, as a strike-slip type of earthquake it would have been expected to lead to predominantly horizontal seafloor displacement, while tsunamis are typically caused by fast vertical displacements. This discrepancy has led to an extensive debate among tsunami scientists.

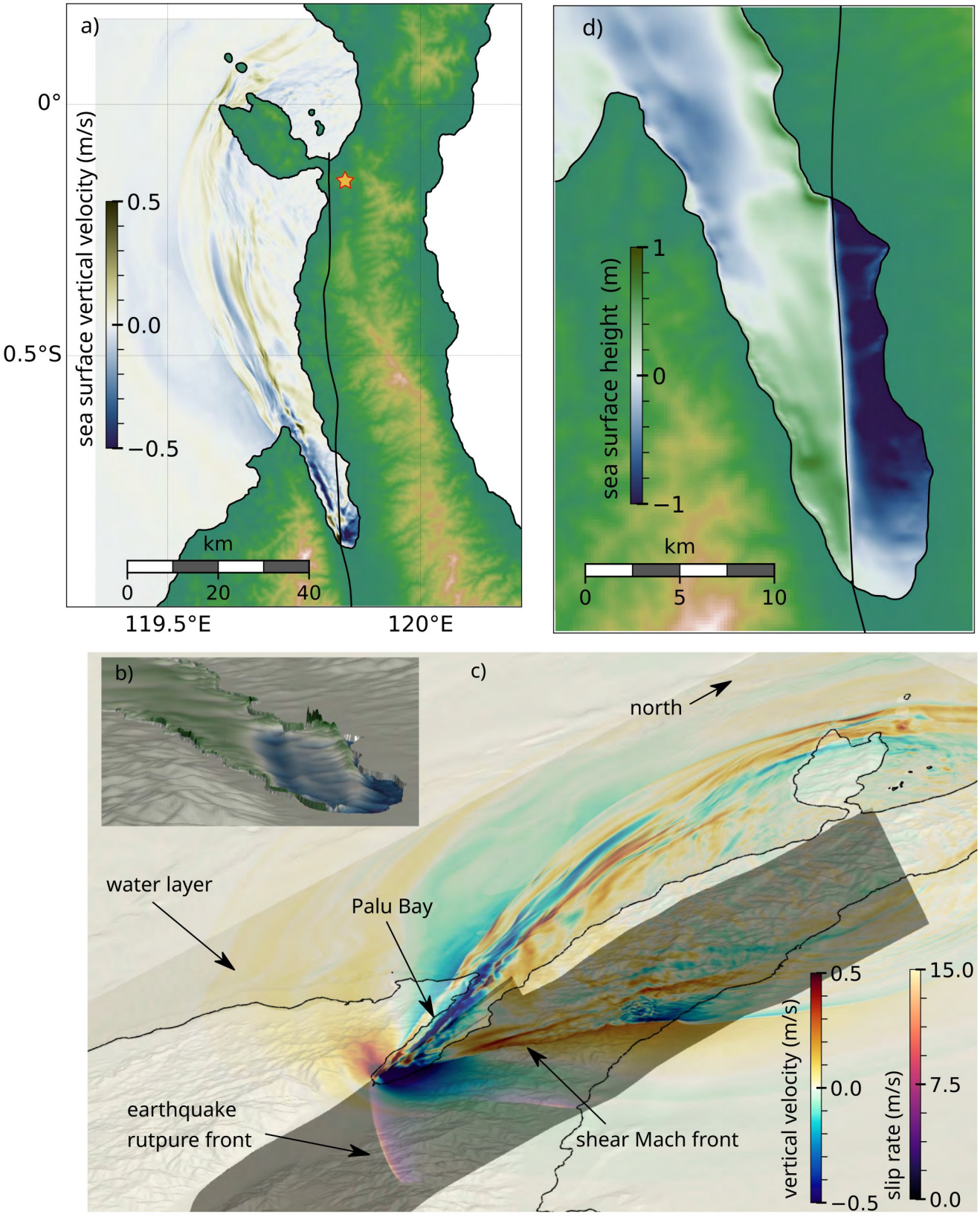

Figure 2: 3D fully coupled model of the 2018 Palu, Sulawesi earthquake-tsunami. a) Map view, vertical sea surface velocity at 15s simulated time (star marks the epicenter, black lines the complex fault system). b) Sea surface height (exaggerated). c) 3D view of vertical velocity at 15s. Note the complicated velocity field. d) Sea surface height of the tsunami at 15s. Figure taken from [3].

For the simulation scenario, we used realistic geometry, including high-resolution topography (and bathymetry), and a complicated fault system. For this, we created computational meshes with various resolutions. The largest mesh, with ~518 million elements (~261 billion degrees of freedom), was the largest SeisSol setup simulated so far. It achieved a resolution of 50m in the water layer and 500m in a refined seismic wave refinement region. With this setup, we were able to observe waves with up to 30Hz frequency content.

We ran the setup on 3,072 nodes of SuperMUC-NG (one half of the machine) and achieved a sustained performance of 3.14 PFLOPS over a total runtime of 5h30min (including all I/O), producing roughly 700 GByte of earthquake- and tsunami-related data. Simulations that additionally output the full 3D-wavefield data produce even more data.

Our model reproduces the overall tsunami of the Palu scenario very well. As shown in figure 3, we noticed interesting differences between our proposed model and the established practice of one-way linking. Briefly, the fully-coupled model produced a smoother wavefield, which may for example be caused by non-hydrostatic effects. Note also the extremely complicated velocity field (Fig. 2), which can only be obtained by very high-resolution modeling.

For a smaller mesh, with 89 Mio elements, we ran performance and scalability tests on SuperMUC-NG, achieving a parallel efficiency of 72% and a performance of up to 1,359 GFLOPS (c.f. figure 1) per node.

Ongoing Research / Outlook

We are currently further investigating the exact reasons for the differences between the results of our fully-coupled and one-way linking models. Furthermore, we are applying the fully-coupled method to additional scenarios from several application areas: new earthquake-tsunami scenarios, as well as earthquake-induced sound signals and lava lake sloshing.

SeisSol uses a hybrid MPI+OpenMP parallelization scheme (together with Pthreads for communication and asynchronous output). We are currently porting and optimizing SeisSol to GPU platforms with a focus on CUDA. In addition, we are considering portability questions for AMD and Intel GPUs.

References and Links

[1] https://www.cheese-coe.eu
[2] https://www.seissol.org
[3] https://github.com/SeisSol/SeisSol
[4] Krenz, L., Uphoff, C., Ulrich, T., Gabriel, A. A., Abrahams, L. S., Dunham, E. M., & Bader, M. (2021, November). 3D acoustic-elastic coupling with gravity: the dynamics of the 2018 Palu, Sulawesi earthquake and tsunami. In Proceedings of the International Conference for High Performance Computing, Networking, Storage and Analysis (SC'21).

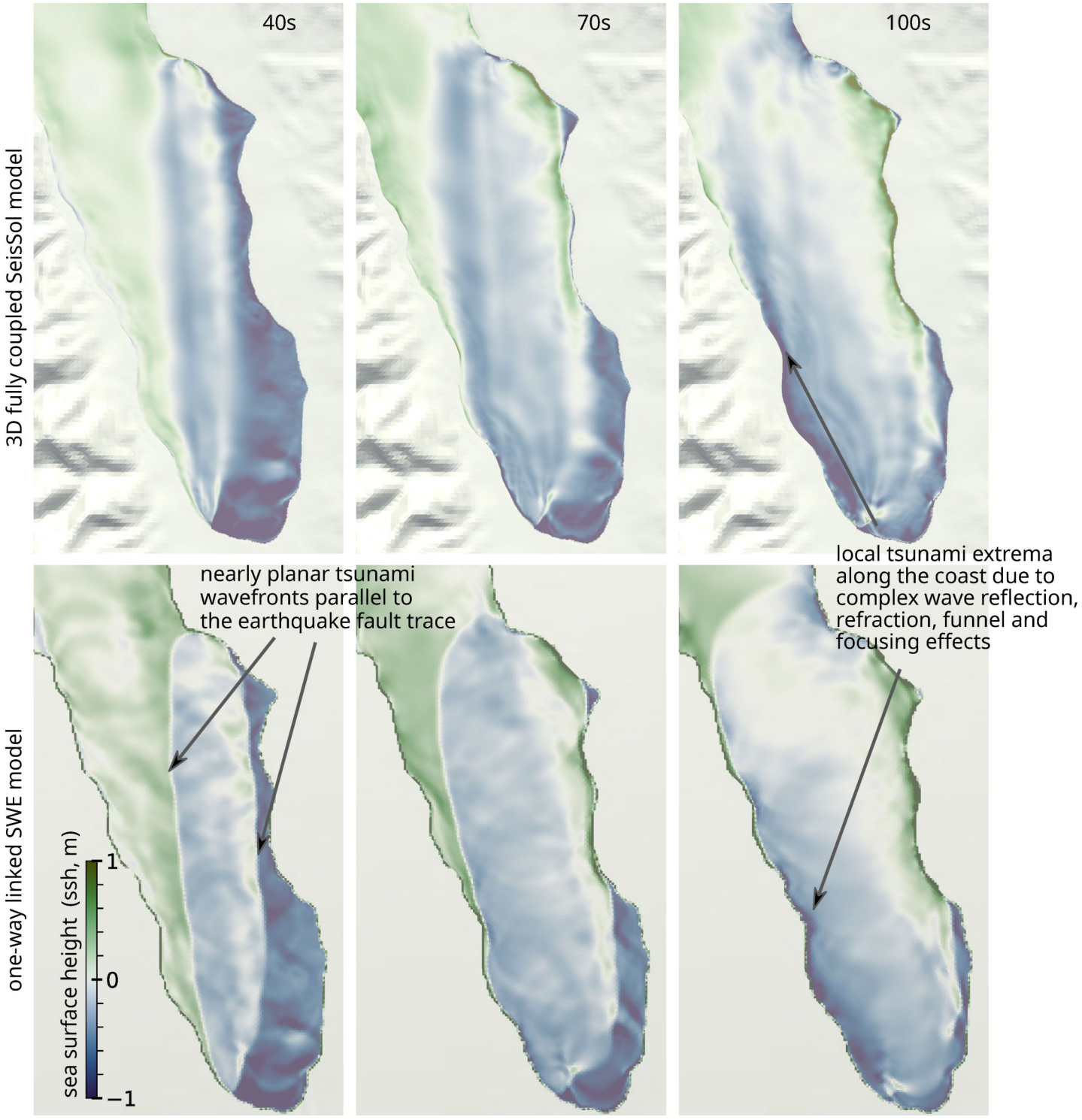

Figure 3: Comparison of the simulated sea-surface height (in Palu bay) of a fully-coupled (top) and a classical two-way linked model (bottom). Both setups used the same earthquake model. Figure taken from [3].

Towards Global Sustainable Water use in Agriculture

Research Institution
Dept. of Geography, Ludwig-Maximilians-Universität Munich

Principal Investigator
Wolfram Mauser[1]

Researchers
Christine Werner[1], Tobias Hank[1], Wolfgang Kurtz[2], Heike Bach[3], Philipp Klug[3]

Project Partners
[2]Leibniz-Rechenzentrum
[3]VISTA Remote Sensing Applications in Geosciences, Munich

SuperMUC Project ID: pn69pe

Introduction

More than 90% of today's human water consumption is for food and energy production in agriculture. More food for a growing human demand needs more water to produce it. Nevertheless, global water resources are limited. Without appropriate action towards most efficient and most sustainable water use in agriculture the world will run into a severe water and food crisis.

With the research project ViWA (Virtual Water Values), funded by the German Ministry for Education and Research (BMBF), we show how High Performance Computing using SuperMUC-NG can open new ways to create the necessary knowledge for action towards more efficient and sustainable water use in agriculture. Complex global crop growth simulations based on climate and environmental data show how water could globally be saved through better farm management. Comparing these complex simulations with actual global crop growth observations using Sentinel-2 satellites creates a global, hybrid, simulation- and observation-based monitoring system, which points at hot-spots of water waste, where improvements in farm management are urgently needed.

Results and Methods

Efficient and sustainable agricutural water use is one of the leading goals of the 2015 Sustainable Development Goals (SDGs) of the United Nations (UN). The SDGs aim at reaching sustainable development and thereby longtime survival of civilisation on the Globe until 2035 through coordinated global efforts.

The central SDG indicator in this context is the agricultural water use efficiency (AWUE, the amount of water evapotranspired to produce a certain amount of food). Unfortunately there is no way to directly observe AWUE. Therefore, to date both efficiency and sustainability of agricultural water use is largely unknown at the global and, in most places on the Globe, the regional and local level. One goal of the research project ViWA (Virtual Water Values) therefore is to develop an innovative global monitoring system for AWUE by combining extensive environmental simulations and new remote sensing Earth observations from the Sentinel-2 satellites.

The specific challenges of global agro-environmental modeling are threefold: 1) large spatial heterogeneity of all relevant variables on the Globe (the planet is diverse), 2) strong non-linearities in almost all processes in nature (the planet is complex), 3) data scarcity for most driving variables and parameters (the planet is largely unknown). As a result, the detailed knowledge on global AWUE requires high spatial and temporal resolution. We developed, adapted to and applied on SuperMUC-NG the sophisticated process-based environmental model PROMET [1,2]. PROMET is an agro-hydrological environmental simulation model, which was favorably compared to other global crop simulation models [3]. In the ViWA project, non-linearity and complexity are addressed by operating the PROMET environmental model globally at a high spatial resolution of 30 arcsec (~1km) and a high temporal resolution of 1 hour. By setting up PROMET in an ensemble constellation, a realistic assessment of uncertainties is obtained.

The main workload of the SuperMUC-Project ViWA consists of executing the PROMET model in parallel scenarios. PROMET, which has been developed at the LMU Department of Geography for the last 25 years, is programmed in FORTRAN. Because of the heavy workload of the specific global research task PROMET was used on SuperMUC-NG to compute ensembles for potential and actual agricultural crop development around the Globe. To do this at the required high spatial and temporal resolution we combined the (OpenMP-) parallelized use of PROMET with running several PROMET instances in parallel: each single PROMET instance simulates plant growth on a small predefined geographical environment on several threads (in this case 1-4 threads, depending on size of the geographical segment).

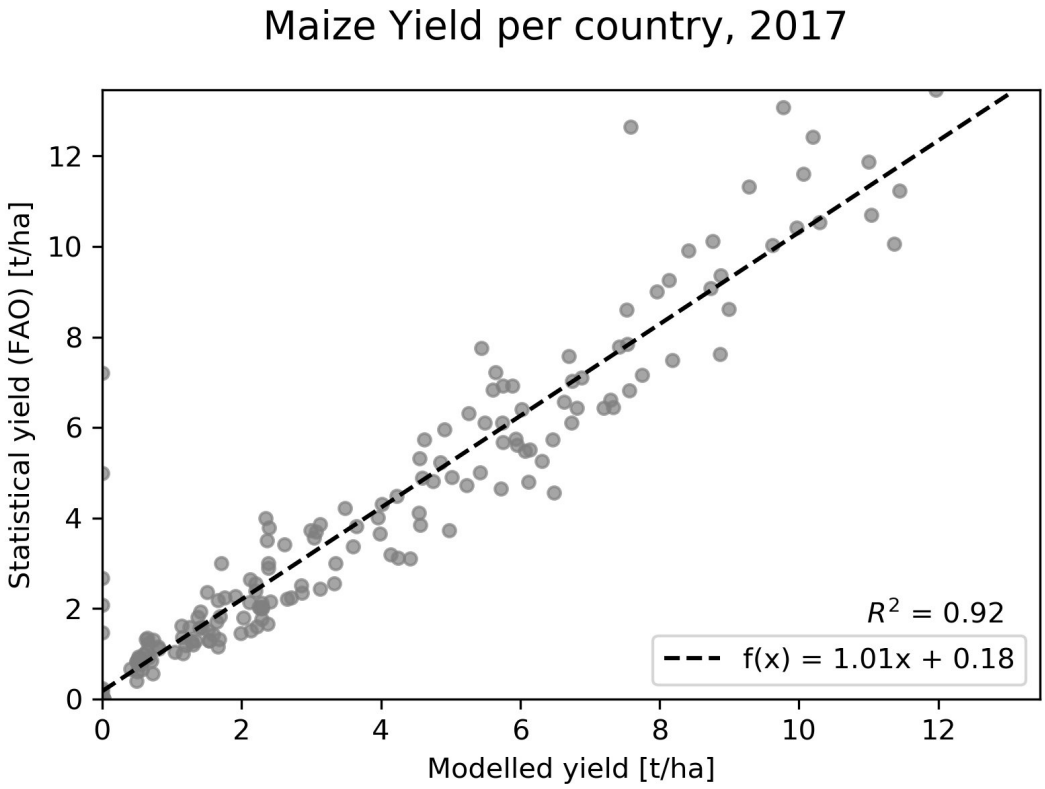

Figure 1: Validation of SuperMUC-NG simulations of crop yield (t/ha) through comparison with national harvest statistics of FAO.

We used ca. 4.5 Mio SuperMUC-NG core hours to simulate the growth and food production of the 17 most important crops globally with a large variety of scenarios regarding fertilization and irrigation during the period of 2017-2018.

Scenarios are necessary as it is a priori unknown how farmers around the Globe manage their fields, use fertilizer or irrigate. On the other hand, new global observation systems using remote sensing based on the EU-COPERNICUS Sentinel-2 satellites continuously record images covering each field on the Globe every 5 days with a resolution of 10m. These Big-Environmental-Data time series contain information on the growth development of the agricultural crops in the form of Leaf-Area-Index (the extent of leaf area per ground area). This information was extracted from all available 100 x 100 km images at 120 representative agricultural locations around the Globe using special image processing routines. By comparing all simulated scenarios using PROMET on SuperMUC-NG with the satellite-based measurements of crop development the most likely simulated management scenario can be identified by finding the closest match. Information on the agricultural water-use efficiency and crop yield can then be extracted from the simulation results of the selected scenario. For a straight foreward scenario simulation a set of two irrigation options (on/off) in combination with a variety of nutrient levels, which represent likely options of farmers around the Globe to fertilize their fields with less or more fertilizer and to irrigate their crops, should theoretically be covered. This would typically lead to a high number of scenarios, which would even exceed SuperMUC-NGs large computing power. In practice we developed an alternative, more efficient way to be able to, for the first time, use this concept of combining Big-Environmental-Data remote sensing observations with HPC-simulations to cover global agriculture. We now vary productive water amount in several steps with the assumption that both, nutrient and water are not independent when used by farmers. It is e.g. highly counterproductive for a farmer to waste large amounts of expensive fertilizer if no water is available because fertilizer cannot be used by water-stressed plants and the resulting agricultural yield is low. Contrary if water is available, temperature may limit plant growth and therefore the need for fertilizers. Thus, we end up with “only” seven scenarios per crop spanning from low management intensity (i.e. low nutrient availability and low amount of productive water required) to high management intensity (i.e. high nutrient availability and high amount of productive water required).

The simulation results for the seven different scenarios indicate that this approach balances out accuracy and computing cost. With our new scenario selection, we are, for the first time, able not only to state if agricultural water use efficiency is increased through irrigation, but also at which amount of irrigation water and yield agricultural water use efficiency is at its optimum. This allows to give local and regional advice to farmers and farming organizations on a possible increase in AWUE and thus a reduction of water waste in agriculture through changing management practices.

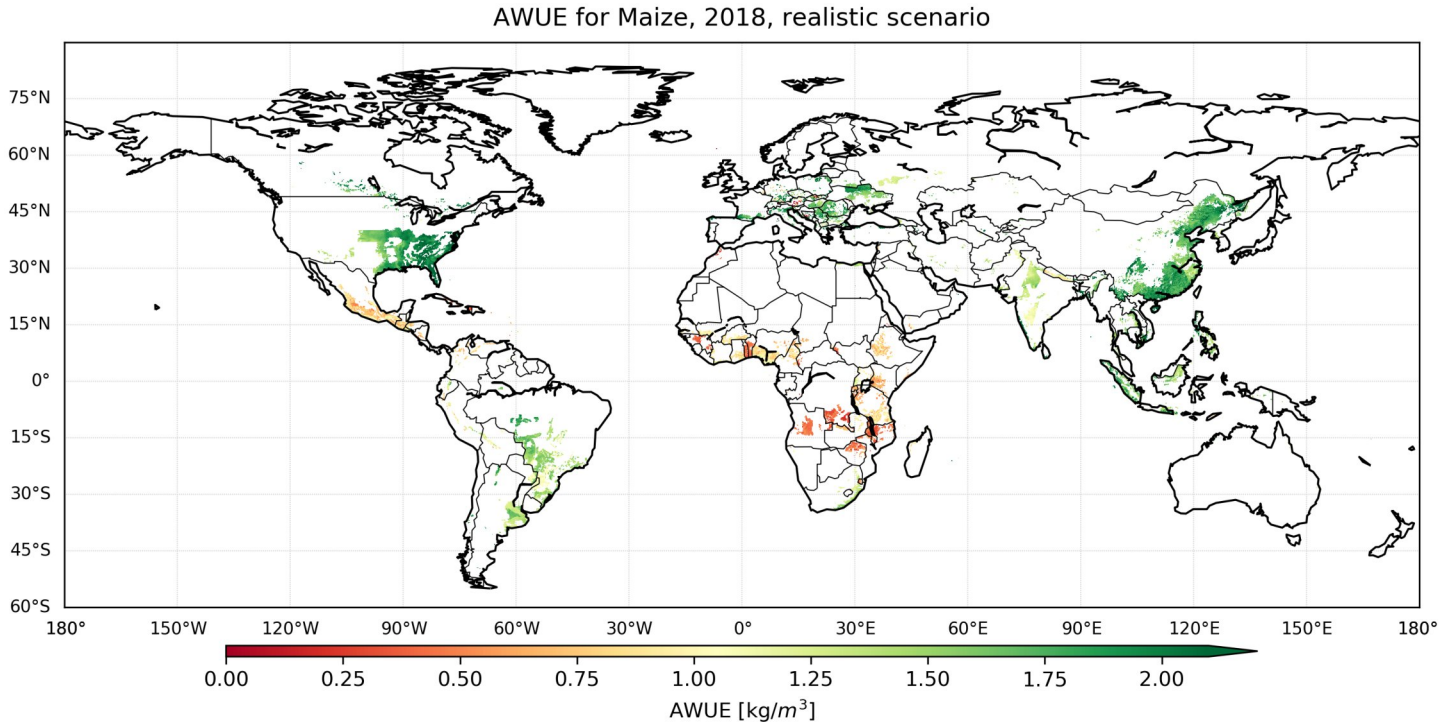

Figure 2: Agricultural water use efficiency (AWUE) for Maize in 2018 based on SuperMUC-NG simulations with ViWA's global monitoring system of agricultural management.

A validation of voluminous results (>100TB) of the 2 years of global PROMET simulations on SuperMUC-NG was carried out through comparison of the aggregated simulated yields of the scenarios, which on a pixel-by-pixel basis best matched the Sentinel-2 observations, with the official national yield statistics of the UN Food and Agricultural Organization (FAO). The results in Fig.1 show the close and convincing match between simulations and statistics.

Ongoing Research / Outlook

The proof of concept of a novel global monitoring saystem for AWUE was achieved thanks to SuperMUC-NG's computing power. Currently we carefully analyze the ca 100 TB of output data from the SuperMUC-NG simulations. As a first result Fig.2 shows the global distribution of AWUE for maize in the year 2018. As can be seen AWUE is high in China, Europe and the US and low to very low in Sub-Saharan Africa. After complete analysis of all years and crops the final results will freely and openly be made available on the European Space Agency(ESA)'s Food Security Thematic Exploitation Platform (FS-TEP, https://foodsecurity-tep.net/). Further development towards application of the described monitoring concept is planned.

References and Links

[1] Mauser, W. & Bach, H., Journal of Hydrology, 376, (2009) 362-377.
[2] Hank, T. et al, Remote Sensing, 7 (2015) 3934-3965.
[3] Müller, C. et al., Geosci. Model Dev., 10 (2017) 1403–1422, https://doi.org/10.5194/gmd-10-1403-2017, 2017.

Global mantle flow retrodictions for the early Cenozoic using an adjoint method

Research Institution
[1]Geophyics Section, Department for Earth and Environmental Sciences, Ludwig-Maximilians-Universität München

Principal Investigator
Hans-Peter Bunge[1], Bernhard Schuberth[1]

Researcher
Siavash Ghelichkhan[2]

Project Partner
[2]Australian National University, Canberra

SuperMUC Project ID: pr48ca

Introduction

The geological history of the Earth is filled with mysterious events that leave fingerprints on vast areas of our planet. The cause and forces behind these events have long kept Earth scientists at work. In the Cenozoic Era (Greek for new life); that is, during the last 65 million years (Ma), the Earth experienced multiple of such events. For example, it is nowadays well known to geologists that the interior of the North American continent has been inundated for tens of millions of years but has dried out at some point around 60 Ma ago. Similarly, the Australian continent has undergone a north-south tilt since its departure from Antarctica as it approaches Southeast Asia. The last century has seen much debate amongst scientists on the potential reasons behind these events with the common understanding that they can only occur due to significant changes of topography over time on each continent. Today, the consensus is that these events are caused by convection in the mantle: the same long-term process of rock deformation in the Earth's mantle that drives plate tectonics. Geophysicists have labelled such changes in topography as dynamic topography, in order to emphasise the nature of such topographic effects and to distinguish it from the actual topography (which results from the combined effects of dynamic and so-called isostatic topography).

Despite the general consensus, understanding the details of the links between dynamic topography variations and the underlying mantle convection remains a grand task in Geodynamics. To this end, geodynamicists have long used high-performance computational models, which are based on a principle mathematical description of the natural world around us: they evolve according to the physical laws that govern motion in the mantle in form of conservation equations for mass, momentum and energy for an extremely viscous fluid. Solving these equations allows one to construct mantle flow histories by integrating solutions forward in time. Over the past decades, there has been enormous progress in computational algorithms and computing resources that enabled the modelling of global mantle flow at earth-like convective vigour. This progress, however, comes with a catch: the governing equations of mantle convection are numerically unstable backward in time and predictions from present-day into the future cannot be tested owing to the large time-scales of millions of years. Adding the fact that the only instant in time for which we have any information on Earth's interior is present day, the instability of the equations backward in time imply that the wealth of data generated at present day, specifically in form of 3-D images from seismic tomography, cannot be directly used to infer past mantle states and their impact on the surface of the Earth.

Results and Methods

To overcome this challenge, geodynamicists have reformulated the problem by turning to optimisation methods such as the adjoint method. In this approach, past mantle states are obtained by optimising flow histories with regards to images from seismic tomography. This way, the (unknown) state of the mantle in the past that naturally evolves into its (known) present-day state is obtained by iteratively minimising the difference between the observed present-day mantle structure and the prediction of a geodynamic model. The Geodynamics group at LMU has pioneered the development of such adjoint models and is at the forefront of current research in this direction. In a recent publication [2], we built upon previous studies and explored the parameter space for reconstruction models of the mantle by generating a suite of geodynamically plausible, compressible, high-resolution Earth models that go back to 50 million years ago. Figure 1 illustrates how a best-fitting model is produced by iteratively minimising the difference between the tomographically observed mantle structure and predictions of a model.

The reconstruction models in [2] clearly demonstrate the importance of the on-going computational growth for developing a deep understanding of natural phenomena. Their models were constructed with the

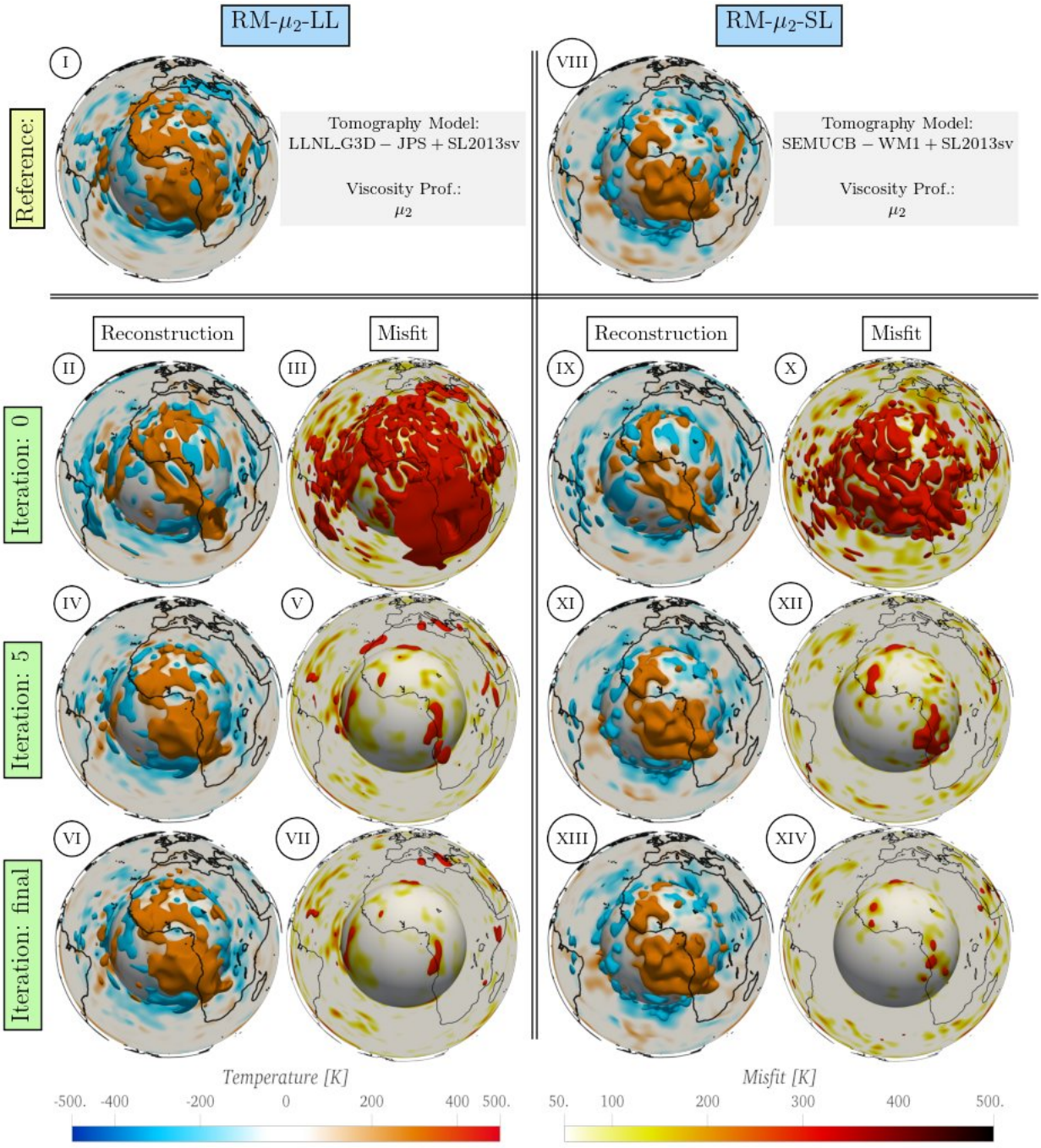

Figure 1: Misfit reduction for two different reconstruction models with different tomographic mantle state estimates. Top row: the estimated temperature field. This "observed" temperature field is used as first guess for the initial condition at 50 Ma. II, IV, VI, IX, XI and XIII are the reconstructed temperature fields at present-day. III, V, VII, X, XII and XIV are the corresponding absolute differences between the modelled and observed temperature fields (i.e., the error), after zeroth, fifth and final iteration. The error iso-surface is chosen at 300 K. Successive model updates improve the reconstructed final temperature field.

parallel finite element code TERRA, using an unprecedented high resolution, which is obtained by dividing the volume of the mantle into ~670 million finite elements, for a maximum grid spacing of ~11 km at Earth's surface. An adjoint iteration for a model of this type, spanning 50 million years, requires between 75 and 150 thousand core hours on SuperMUC-NG of the Leibniz Supercomputing Centre of the Bavarian Academy of Sciences. This constitutes an equivalent of 36-72 hours of computation using 2,048 cores. The initial condition is optimally recovered after 5 to 10 iterations, leading to a total of about a million core hours per reconstruction model. At the moment, there are only a few HPC-facilities in the world that are able to provide the scale and shear amount of computational infrastructure that is necessary for this work.

By choosing a suite of scenarios, combining two different mantle state estimates derived from seismic imaging and four different mantle viscosity profiles, we studied the evolution of dynamic topography and compared the results with the geologic record. The

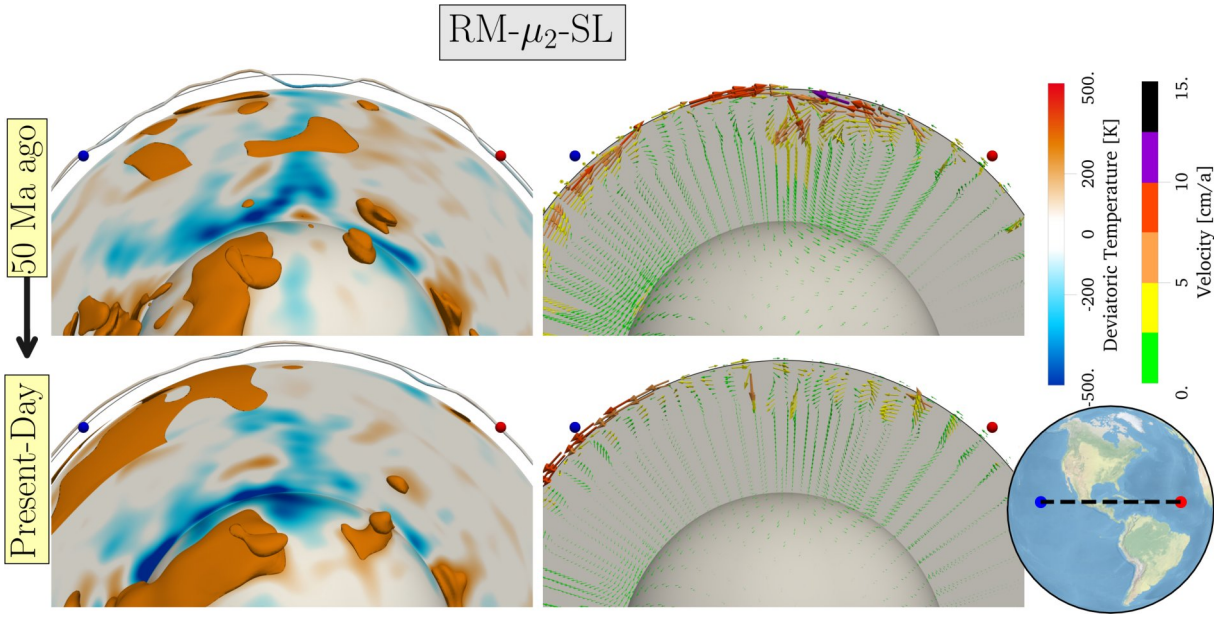

Figure 2: Evolution of mantle temperature and dynamic topography (left column), and velocity field (right column) beneath North America in a reconstruction model. The cross-section is along a great circle passing through 40W,15N and 130W,15N (red and blue points in inset, respectively) visualised together with a spherical surface at the core-mantle-boundary. Point of view is from south, focused on mid-mantle depths.

reconstructions and their associated dynamic topography histories are sensitive to the mantle state estimate and the radial viscosity profile of the Earth model. Most important, the reconstructions are largely in accordance with what geological observations in three major continental areas of North America, Australia and Africa imply. For example, the results show that the long-lasting North American seaway is likely caused by the subducting Farallon plate (an ancient plate that was located west of the continent millions of years ago and which today has largely vanished). The disappearance of the seaway is caused by the waning effect of this ancient slab, as it sinks to greater depths of the mantle. Figure 2 visualises how the evolution of dynamic topography over North America can be linked to the underlying mantle convection currents. The remnant of the ancient Farallon plate in the deep mantle can be seen as blue structure in the centre of the left panels in Figure 2 representing material that is colder than ambient mantle.

Ongoing Research / Outlook

The LMU Geodynamics group has been actively involved in the last years in a number of HPC-related projects. Current efforts focus on the further development of a software framework for extreme-scale simulations of mantle convection in collaboration with the groups of Numerical Mathematics at TUM (Prof. Barbara Wohlmuth) and System Simulation at FAU Erlangen-Nürnberg (Prof. Ulrich Rüde). This framework is able to fully exploit the power of next-generation exascale supercomputers (i.e. reaching 10^{18} floating point operations per second). First exciting results have been achieved in the project *TerraNeo*, supported by the Priority Program 1648 "Software for Exascale Computing" (SPPEXA) of the German Research Foundation (DFG). Using a massively parallel multigrid method, based on the hierarchical hybrid grids (HHG) paradigm and implemented in the open source framework Hybrid Tetrahedral Grids (HyTeG), computations with an unprecedented resolution within Earth's mantle are now possible. In future reconstructions of mantle evolution, we plan to use computational grids that subdivide the entire mantle into domains of about 1 km^3 volume (considering that the volume of the mantle is about 9.06 x $1,0^{12}$ km^3). As a consequence, a large system with over a trillion (10^{12}) degrees of freedom will have to be solved at each time step of a simulation. This demonstrates why mantle convection is regarded as a so-called grand challenge problem.

References and Links

[1] https://www.geophysik.uni-muenchen.de
[2] Ghelichkhan, S., H.-P. Bunge, and J. Oeser (2021), Geophys. J. Int. 226(2), 1432-1460, doi:10.1093/gji/ggab108.

So2Sat - 10^{16} Bytes from Social Media to Earth Observation Satellites

Research Institution
[1]Remote Sensing Technology Institute, German Aerospace Center
[2]Data Science in Earth Observation, Technical University of Munich

Principal Investigator
Xiaoxiang Zhu[1,2]

Researchers
Yuanyuan Wang[1,2], Yilei Shi[3], Vytautas Jancauskas[1], Marie Lachaise[1]

Project Partner
[3]Chair of Remote Sensing Technology, Technical University of Munich

SuperMUC Project ID: pr45ne, pr53ya (Gauss Large Scale project)

Introduction

The rapid urbanization poses fundamental challenges to our societies across the globe. New phenomena of urbanization, such as megaregions and informal settlements, have raced too far ahead of our current understanding of urbanization, which is mostly based on the United Nation's population figure. Therefore, the scientific question of the project *4D City* (pr45ne) and *So2Sat* (pr53ya) [1] is: how does the global urban geographic figures, including geometry, thematic, population density, evolve over time, and in what detail can we observe and measure them?

Our scientific objectives is for the first time systematically fuse the remote sensing data and the massive data available from GIS and social media to map 3D urban infrastructures and their evolution over time, i.e. 4D, in high resolution and on a global scale.

The outcome will create a first and unique global and consistent 3D/4D spatial data set on the urban morphology of settlements, and a multidisciplinary application derivate assessing population density. This is seen as a giant leap for urban geography research as well as for formation of opinions for stakeholders based on resilient data.

Results and Methods

We use a combination of traditional signal processing methods, and deep learning to reconstruction our 3D/4D city models. Previously, we have developed the world's first algorithm to reconstruct urban 3D models from a very small TanDEM-X radar image stack. This is a task usually requires at least 20 images. We employed modern signal processing techniques, including non-local means filtering, as well as compressive sensing (CS), to accomplish this challenging task by using just 5 TanDEM-X interferograms. This algorithm provides the height estimate of buildings in large scale, which has been demonstrated in the last report.

To get the height of individual buildings, previously we have studied the utilization of the building footprint freely available in OpenStreetMap (OSM). However, we found that the OSM footprint is not globally available. In fact, it is estimated that only 10% of the buildings in the world are covered by OSM. Therefore, we started a few years ago developing a new algorithm to automatic extract building footprint from optical imagery [2]. In the last year, we have successfully achieved this goal, and produced the world's first global building footprint map from Planet imagery. Figure 1 demonstrates a small crop of our global building footprint. The upper figure shows the density of the build-up area around Cairo, Egypt. The lower figure shows the individual building footprint in the center of Cairo.

Combining the height estimation and building footprint, we are able to create the so-called Level of Detail 1 (LoD-1) building model in a large scale. Figure 2 and 3 show the LoD-1 model of New York and Santiago de Chile, created and rendered using our algorithm on SuperMUC-NG. We have created such 3D model for over a thousand cities whose population is larger than 300,000 according to the United Nation's population figure in 2014. Those LoD-1 urban models in a global scale are a great leap from the state of the art.

Ongoing Research / Outlook

Currently, we are improving and finalizing the global 3D model reconstruction. After finishing mapping the largest cities, we intend to apply this algorithm to everywhere we are able to detect a human settlement.

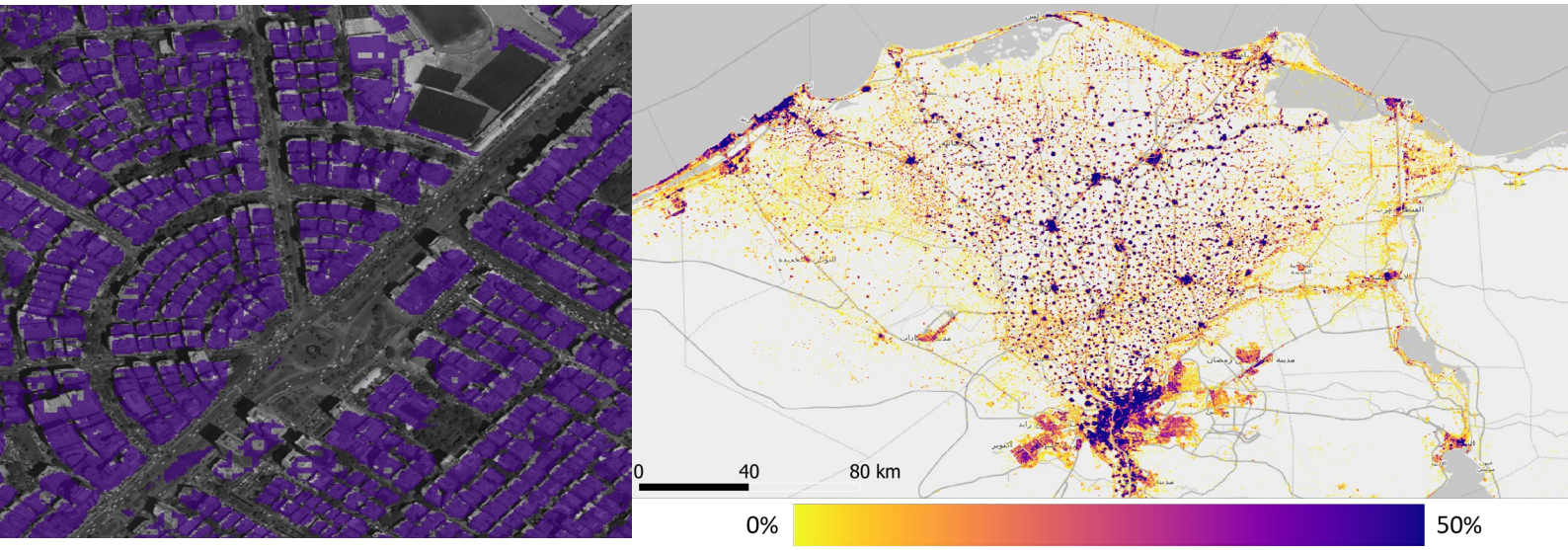

Figure 1: Left: buildup density around Cairo, Egypt, and right: individual building footprint in the center of Cairo.

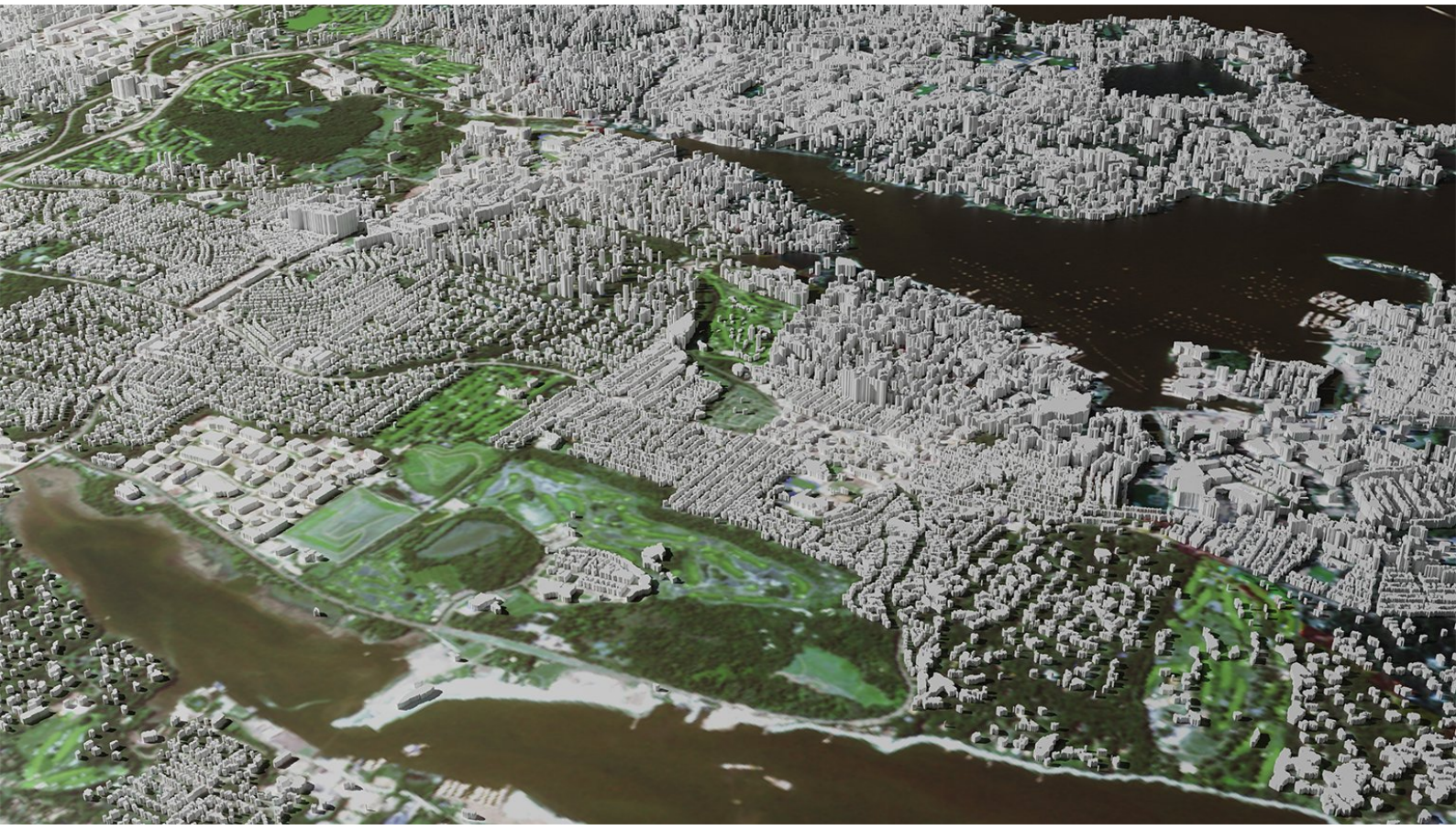

Figure 2: The LoD-1 building model of New York calculated and rendered on SuperMUC-NG.

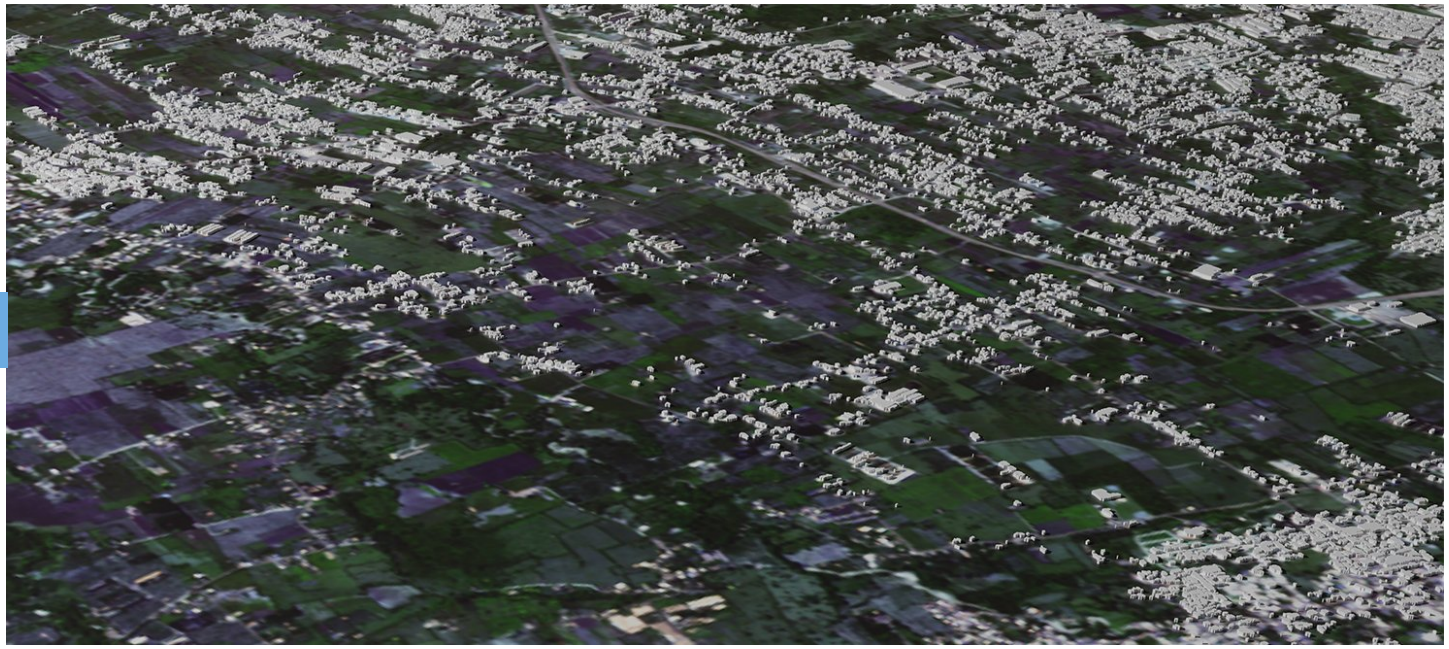

Figure 3: The LoD1 building model of Santiago de Chile calculated and rendered on SuperMUC-NG.

This will create a full global coverage of the 3D building model. In addition, we have finished the mapping of local climate zones of 1692 largest cities in the world [3]. In the future, we aim at a global local climate zones classification.

SuperMUC-NG is vital for the success of our projects, because the sheer data volume and the processing hour required by our projects can only be accommodated in SuperMUC-NG. Our projects currently takes more than 1 petabytes of storage in SuperMUC-NG, to which we are grateful. This biggest challenge in our project is also its big data nature.

References and Links

[1] http://www.so2sat.eu
[2] Q. Li, L. Mou, Y. Hua, Y. Shi, and X. X. Zhu, “Building Footprint Generation Through Convolutional Neural Networks With Attraction Field Representation,” IEEE Trans. Geosci. Remote Sens., vol. 60, pp. 1–17, 2022, doi: 10.1109/TGRS.2021.3109844.
[3] X. X. Zhu et al., “The urban morphology on our planet – Global perspectives from space,” Remote Sens. Environ., vol. 269, p. 112794, Feb. 2022, doi: 10.1016/j.rse.2021.112794.

Elementary Particle Physics

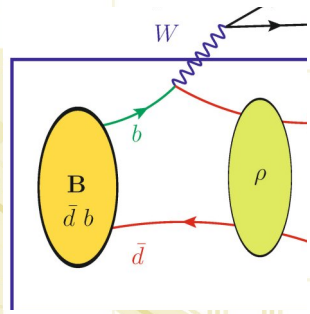

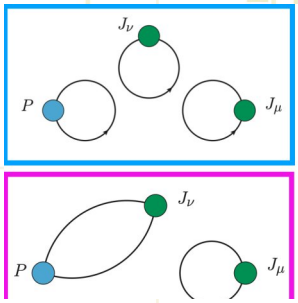

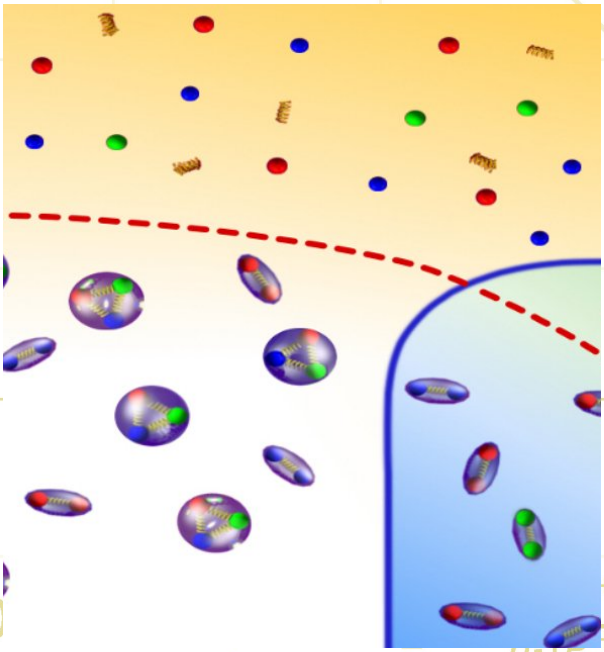

Matter Anti-Matter Annihilation in Charmonium

Research Institution
[1]Bergische Universität Wuppertal

Principal Investigator
Francesco Knechtli[1]

Researchers
Roman Höllwieser[1], Vanessa Koch[1], Tomasz Korzec[1], Michael Peardon[2], Juan Andrés Urrea Niño[1]

Project Partner
[2]Trinity College Dublin

SuperMUC Project ID: pn29se (Gauss Large Scale project)

Introduction

Quantum Chromodynamics (QCD) is the sector of the standard model describing the strong nuclear force, which binds quarks and gluons inside hadrons. The theory confines these constituents, which are never observed directly in experiment.

In this project we study charmonium, a system containing a charm quark-anti-quark pair. These studies underwent a revolution after a number of entirely unexpected narrow resonances called the X, Y and Z states were discovered by the Belle and BaBar experiments at the start of the new millennium. In spite of almost two decades of theory investigations, no clear picture of the internal mechanics of these resonances has emerged. Excitations of constituent gluons are likely to be an important part of some candidate hybrid states. Extensive experimental studies of charmonium and the XYZ states are underway at LHCb at CERN and there are significant plans at new experiments such as Belle II at the SuperKEKB B-factory and BESIII at BEPC and a future Super-c-tau factory. Moreover, the PANDA (Anti-Proton ANnihilation in DArmstadt) experiment at FAIR (Facility for Antiproton and Ion Research), GSI in Darmstadt plans a first anti-proton beam in 2025. PANDA will search for exotic states in charmonium and glueballs, which are states made predominantly of gluons.

Lattice QCD provides a framework to study charmonium from first principles. A rich spectrum is seen, including candidate hybrids in recent calculations however these use an approximation where states are assumed to be stable and charm-quark annihilation effects are neglected. The mass of charmonia are extracted from the exponential fall-off of the correlator in the Euclidean time separation between source and sink of the meson. Charm annihilation contributions are quark-line disconnected diagrams where the charm quark and anti-quark annihilate at the source and sink. They constitute the significant remaining uncertainty in precise calculations of the low-lying charmonium states. Charm-annihilation effects are suppressed by the Okubo-Zweig-Iizuka (OZI) rule, but these dynamics are poorly understood. For example, they contribute to a shift in the mass of the pseudoscalar particle, the η_c meson. This shift has the wrong sign in leading order perturbation theory. Charmonium has the same energy scale as the pseudoscalar glueball. The quantum mechanical mixing of charmonium with glueball states occurs through these charm-annihilation diagrams. This mixing affects the validity of the OZI rule beyond perturbation theory and is studied in this project.

The investigations reported here are part of the research programme of project 1 “The confined gluon: precision spectroscopy with charm quarks” in the Research Unit “Future methods for studying confined gluons in QCD” (FOR 5269) [1] funded by the Deutsche Forschungsgemeinschaft (DFG).

Results and Methods

We have analysed 4,800 gauge configurations of lattice size $48x24^3$ and lattice spacing a=0.066 fm. We employ a technique called distillation [2] which we have improved in this project [3]. The computationally most intensive part of the calculation requires solving the Dirac equation with the right-hand sides given by 200 eigenvectors of the 3D gauge Laplacian on each of the 48 time-slices of the lattice. The number of solutions of the Dirac equations (inversions) per gauge configuration equals 38,400. The quark mass in the Dirac operator corresponds to approximately half of the value for the charm quark in nature.

Figure 1 shows the effective masses of the ground state in the pseudoscalar channel. They plateau for large values of the time separation t/a between source and sink of the meson to the value of the mass of the particle, which in this case corresponds to the η_c meson in nature. The points marked by circles are obtained from the iso-scalar correlator, which includes the contribution of charm-annihilation and the points marked by stars are obtained from the iso-vector correlator, where charm-annihilation is absent. For the data points coloured in red we used our optimised distillation technique. The black data points are

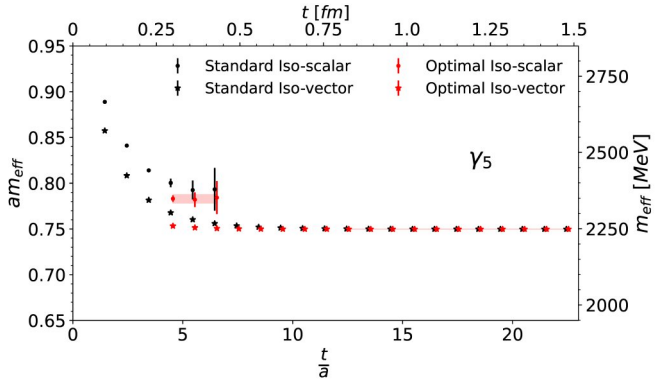

Figure 1: Effective masses of the pseudoscalar meson η_c. Comparison of the iso-scalar and iso-vector mesons. The iso-scalar meson includes the effects of charm-annihilation.

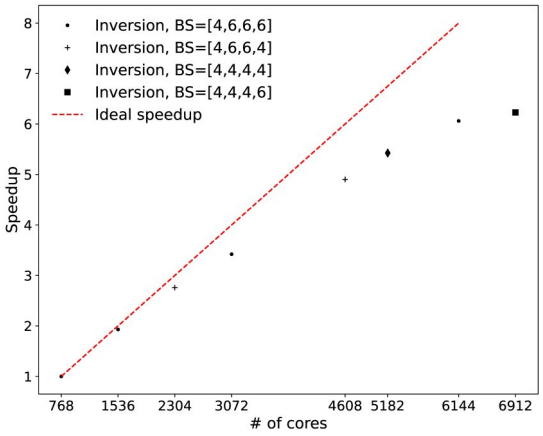

Figure 2: Strong scaling of the inversion of the Dirac operator on a lattice of size 96x48^3. We show the ratio of the run-time the inversion takes on SuperMUC-NG with 768 cores to the run-times it takes using more cores (speedup). The red dashed line is the ideal speedup. In the legend BS means the block size in the deflated SAP GCR solver.

obtained with standard distillation and are shown for comparison. It is evident that with the optimal distillation method the effective masses reach their plateau at earlier times than they do with the standard distillation method. This is crucial to determine the mass of the iso-scalar meson. Due to the charm-annihilation effects the statistical errors of the data for the iso-scalar meson increase rapidlly with the time separation t/a. The charm-annihilation effects lead to an upward shift in the iso-scalar meson mass compared to the iso-vector meson mass. We estimate this shift to be 99 MeV with an uncertainty of 15 MeV. In nature this shift has been indirectly estimated to be about 7 MeV. We expect that the number and the mass of the charm quarks in our model calculation, which differ from their values in nature together with the absence of light quarks account for the difference in the mass shift. For the future we plan a calculation in a physical setting.

To achieve this precision, we developed a software package for the measurement of correlation functions using the improved distillation method. Our programs are based on “QCDlib”, a library written by us in C+MPI, that facilitates massively parallel QCD calculations. The inversions of the Dirac operator are performed by calling the package openQCD [4], namely a deflated SAP GCR solver with AVX instructions enabled for SuperMUC-NG. The computations for 4,800 gauge configurations of lattice size 48x24^3 ran on 384 cores (8 nodes) of SuperMUC-NG and required about 17 millions core-hours.

We have applied our method to 16 times larger gauge configurations of lattice size 96x48^3. The setup is the same as described above but with a smaller lattice spacing a=0.049 fm and using 325 eigenvectors of the 3D Laplacian per time-slice. Figure 2 shows the timings for one inversion of the Dirac operator as a function of the number of cores used on SuperMUC-NG. We plot the ratio of the run-time on 768 cores to the run-times using more cores (speedup). The red dashed line corresponds to the ideal speedup. The performance of our code is close to the ideal line and shows its good scalability. Using different block sizes (BS) corresponds to changing this parameter in the deflated SAP GCR solver used. We have analysed 250 gauge configurations of lattice size 96x48^3. These computations ran on 6,912 cores (144 nodes) and required about 20 millions core-hours. The number of cores 6,912 was chosen because, even though we begin to see deviations from the ideal speedup in the inversion times, it allows for more parallelisation in the temporal direction.

Ongoing Research / Outlook

We plan to compute the charmonium spectrum with hybrid candidates and the effects of charm-annihilation on close-to-physical gauge configurations of size 144x48^3 which include the dynamics of three light degenerate quarks, whose mass is the same as the average light quark mass in nature and a physical charm quark [5]. This will provide information on mass and quark content dependence of the spectrum of charmonium. The Research Unit FOR 5269 [1] will develop new numerical algorithms for calculations of glueballs and charmonium including their mixing and decays. We will also apply some of the new techniques to compute the potential between a static (infinitely massive) quark and anti-quark pair. The latter is a first principle input to effective theories to study the spectrum and decays of charmonium including exotic XYZ candidates.

References and Links

[1] https://confluence.desy.de/display/for5269
[2] M. Peardon et al. [Hadron Spectrum Collaboration], Phys. Rev. D 80 (2009), 054506.
[3] F. Knechtli, T. Korzec, M. Peardon, J.A. Urrea Niño, arXiv:2205.11564.
[4] http://luscher.web.cern.ch/luscher/openQCD/
[5] R. Höllwieser, F. Knechtli, T. Korzec [ALPHA Collaboration], Eur. Phys. J. C 80 (2020) no.4, 349.

Quantum Chromodynamics at finite isospin density

Research Institution
[1]University of Bielefeld

Principal Investigator
Bastian B. Brandt[1]

Researchers
Francesca Cuteri[2], Gergely Endrődi[1]

Project Partner
[2]Goethe University, Frankfurt

SuperMUC Project ID: pn34qe

Introduction

Quantum Chromodynamics (QCD) describes the strong interactions in the Standard Model of particle physics. In contrast to the other elementary forces in nature, QCD is strongly coupled at typical energy scales in today's Universe. Consequently, predictions for strong interaction dominated physical systems, such as nuclei and hadrons, but also neutron stars, cannot be obtained using perturbative methods. In contrast, the numerical study of QCD discretized on a space-time lattice, lattice QCD, has proven to be a viable tool to study the properties of QCD in the strongly coupled regime.

At low energies, quarks and gluons are confined into hadrons, while asymptotic freedom implies the existence of a phase with quasi-free quarks and gluons at high energies, represented by large temperatures or quark densities, for instance. The phase transition between these two phases is the subject of intense theoretical and experimental research. Of particular interest for astrophysics and cosmology are the thermodynamic properties of QCD at small and intermediate temperatures and non-zero quark densities. The same region will also be probed by contemporary heavy-ion collision programs at the Relativistic Heavy Ion Collider (RHIC) and future efforts. For lattice QCD simulations, however, the regime at non-zero baryon density remains inaccessible due to the so-called complex action problem.

Apart from a non-zero baryon density, the aforementioned physical systems typically also feature a finite isospin density, i.e. an asymmetry between the numbers of up and down quarks, or, equivalently, of protons and neutrons. QCD at non-zero isospin density but vanishing baryon and strangeness density has a real action and is amenable to Monte-Carlo simulations [2]. In the grand canonical ensemble, which is conveniently used in lattice QCD simulations, this corresponds to simulations at non-zero isospin chemical potential, but vanishing baryon and strange-quark chemical potentials. In most of the physical situations the effects due to non-zero baryon chemical potential are expected to dominate, but there are some cases where isospin might play a major role, for instance in the early universe at large lepton asymmetry [3].

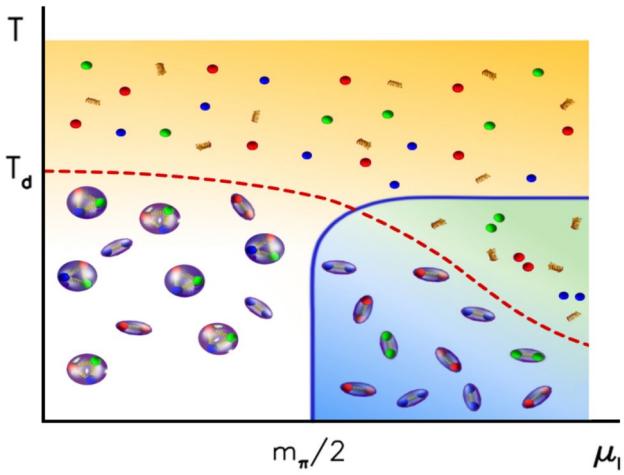

Figure 1: Schematic phase diagram of QCD in the plane of isospin chemical potential and temperature (from Ref. [4]).

Furthermore, studying QCD at pure isospin chemical potential is interesting in its own right. It has a rich phase diagram, shown schematically in Fig. 1, featuring a phase with Bose-Einstein condensation (BEC) of charged pions and a potential superconduct-ing (BCS) phase at large chemical potential on top of the standard hadronic and quark-gluon plasma phases [4]. For a large number of colors the phase diagram was also argued to be related to the phase diagram with finite baryon chemical potential via the so-called orbifold equivalence. In general, studying the effect of a non-zero isospin chemical potential and the Bose-Einstein condensation of pions on the thermodynamic properties of QCD provides important insight for all of the aforementioned physical systems.

Results and Methods

We began the systematic study of QCD with isospin chemical potentials by determining the phase diagram in the temperature-isospin chemical potential plane in [4]. Based on the methodical developments and the generated lattice configurations, we could make further progress in understanding the physics of quarks and gluons under these type of extreme conditions. In

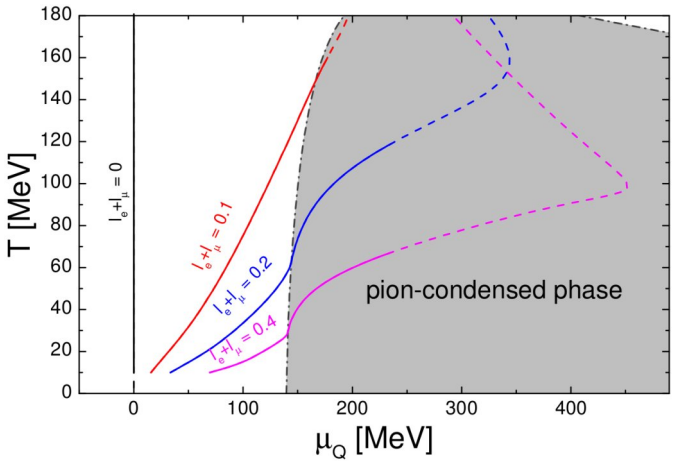

Figure 2: Cosmic trajectories for different values of the initial lepton flavor asymmetry from an effective model improved by lattice QCD input (from Ref. [3]).

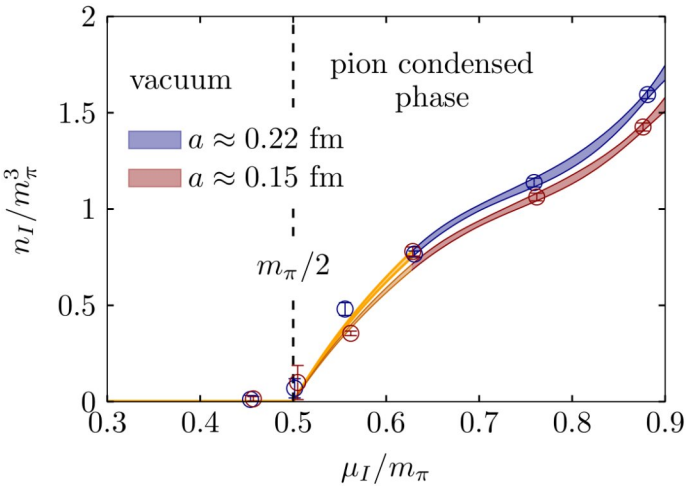

Figure 3: Tentative interpolation of the isospin density for the two coarser lattice spacings. The differently colored lines indicate fits to chiral perturbation theory close to the phase transition (see Ref. [5] for details).

our latest result [3] we calculated the equation of state throughout the phase diagram and used it to validate improved effective models of QCD. The resulting equation of state was employed to calculate the cosmic trajectory of the early Universe for different initial conditions. Our most intriguing finding was that for lepton flavor asymmetries within the range allowed by current experimental bounds, the early Universe enters the pion condensed phase. The cosmic trajectories for different values of the lepton flavor asymmetry are shown in Fig. 2, marking the temperatures where the pion condensation sets in during the evolution. The presence of the pion condensed phase leads to prominent effects for the formation of primordial black holes as well as in the spectrum of primordial gravitational waves, to be detected in future pulsar timing arrays like the SKA experiment.

The above results all rely on the lattice determination of the equation of state (EoS). A precise calculation of the latter is a numerically very demanding task already at zero isospin asymmetry. In the interior of the phase diagram, it becomes more challenging due to the need for the inclusion of a pion source parameter in the simulations and an extrapolation to remove it at the end of the analysis. We have worked out an improved method for this extrapolation in [4].

In this project we focus on the determination of the EoS at non-zero isospin and (small) baryon chemical potentials but vanishing temperatures. The EoS in this regime is of direct relevance for modelling the impact of the isospin asymmetry on the EoS of compact stars and as a further interpolation point for the calculation of the cosmic trajectories. The continuum limit for the EoS demands the use of large lattices (as large as 48^3x72) and simulations of 21 ensembles at different parameters for each lattice spacing. This makes it a similar factor more expensive than comparable projects for the determination of standard vacuum observables. The granted simulation time has been allocated for the generation of the ensembles on the two finest lattice spacings, and the computation of the leading order Taylor coefficients (the most costly measurements). Our code is optimized for large scale cluster architectures and single-GPU applications. For the large lattices used in this study it has been necessary to use SuperMUC-NG due to the memory demands as well as the acceleration of the simulations through parallelization. For both measurements and the generation of configurations on all our ensembles we have used 32 nodes with 48 tasks per node.

In Fig. 3 we show the results for the isospin density at zero temperature for the two coarser lattices together with a tentative interpolation from which eventually the EoS can be computed (see [5]). For the finest lattice spacing the analysis is still ongoing. We have also computed the leading order Taylor expansion coefficients for all our lattices and are currently analyzing them.

Ongoing Research / Outlook

We are currently working on the continuum limit for the EoS, both at vanishing and non-zero temperature. For the vanishing temperature case this includes the finalization of the analysis on the generated lattices. At zero temperature we are still analyzing the leading order Taylor expansion coefficients in the BEC phase to determine the EoS at large isospin and small baryon chemical potentials. The Taylor expansion coefficients measured also allow some hints concerning the prolongation of the BEC phase boundary into the direction of baryon chemical potential. Eventually our simulations will allow for the first analysis of the EoS at large isospin chemical potentials and small Baryon chemical potentials.

References

[1] https://crc-tr211.org/#a08
[2] D. T. Son and M. A. Stephanov, Phys. Rev. Lett. 86 (2001), 592-595.
[3] V. Vovchenko et al., Phys. Rev. Lett. 126 no.1, 012701, 2021.
[4] B. B. Brandt et al., Phys. Rev. D 97 (2018) no.5, 054514.
[5] B. B. Brandt et al., Phys. Rev. D 98 (2018) no.9, 094510.

The role of the charm quark for the QCD coupling constant

Research Institution
[1]Technische Universität München

Principal Investigator
Nora Brambilla[1]

Researchers
Alexei Bazavov[2], Rafael Delgado[3], Andreas Kronfeld[4], Viljami Leino[1], Peter Petreczky[5], Sebastian Steinbeißer[1], Antonio Vairo[1], Johannes Heinrich Weber[6]

Project Partners
[2]Michigan State University
[3]Universidad Politecnica de Madrid
[4]Fermi National Accelerator Laboratory
[5]Brookhaven National Laboratory
[6]Humboldt-Universität zu Berlin

SuperMUC Project ID: pn56bo

Introduction

The modern theory of the strong interactions, quantum chromodynamics (QCD), is a key component of the Standard Model of Particle Physics (SM) and, as such, the foundation of nuclear physics. In the context of the SM, in which quark masses arise from interactions with the Higgs boson, QCD introduces only one free parameter: the strong coupling, usually denoted α_s. The accurate determination of α_s is needed for predictions of the Higgs boson branching ratios, stability of the SM vacuum, and searches for physics beyond the SM, and thus is of great importance.

The static energy of an infinitely heavy quark-antiquark pair is the QCD representative of the well-known central potential problem. The static energy is a theoretically clean observable, which is known to next-to-next-to-next-to-leading order (N^3LO). The static energy is a function of the distance r between the immobile quark and antiquark, which is a well-defined quantum number that can be made small enough to serve as the (inverse) high energy scale. Other than that the static energy only depends on the QCD Lambda parameter Λ_{QCD}, which is directly related to α_s through the QCD beta function. Among the lattice determinations of α_s the static energy is one of the most precise results.

The TUMQCD collaboration [1] has a long history of extracting the strong coupling from the static energy computed in (2+1)-flavor lattice QCD. In this work, we are expanding this program to (2+1+1)-flavor QCD. The inclusion of the dynamic charm quark allow us to compare our results to perturbative charm quark effects. These charm quark effects also affect the determination of the strong coupling. The preliminary results presented here were recently presented in a conference [2] and will be published in more detail in a forthcoming publication [3].

Results and Methods

For our simulations we have used the publicly available code of the MILC collaboration [4], which is a hybrid MPI-OpenMP code written in C and in steady development since the 80ies. The most computationally intensive part of the code is the Rational Hybrid Monte Carlo (RHMC) algorithm, which realizes the Markov process. In the RHMC, the degrees of freedom are coupled to a heatbath and evolved along molecular dynamics trajectories followed by a Metropolis-type accept/reject step.

We employ the (2+1+1)-flavor ensembles from MILC, that use (rooted) highly improved staggered quark (HISQ) action for the sea quarks and 1-loop Symanzik improved gauge action. The static energy, $E_0(r)$, is extracted from the correlator of two Wilson lines in Coulomb gauge, and we extract the ground state by employing single and multi-exponential fits. We always take the distance r to be the distance inferred from the leading-order lattice gluon propagator, which we refer to as tree-level improvement of the static-energy data. Given the high quality of the ensembles, these data are by far the most statistically precise results on $E_0(r)$ to date. This precision, however, has exposed the insufficiency of earlier approaches to account for non-perturbative discretization artifacts beyond the tree-level improvement, which in turn required the development of novel analysis strategies.

We have used SuperMuC-NG for these simulations and measurements. In total we have used 24 million core hours for this project. We have also started a data science storage (DSS) project for the generated research data that we have stored about 250TB so far. Most of our ensembles are reused by us and also by our collaborators using different HPC systems.

The static energy and potential are known to N^3LO order only in the case of massless dynamical quarks.

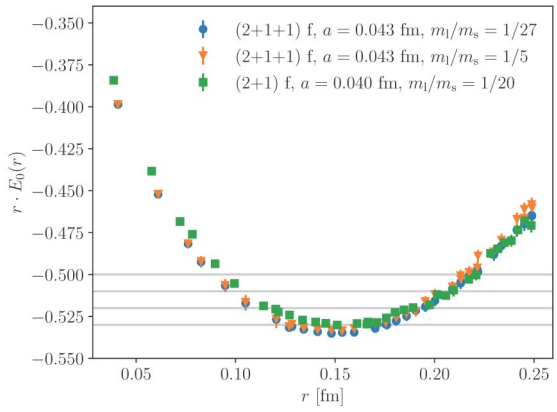

Figure 1: Effects of charm quark are visible from the difference between 2+1 and 2+1+1 flavor QCD data.

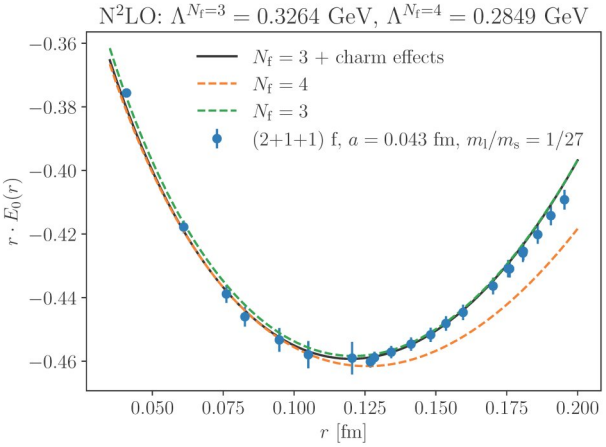

Figure 2: Perturbative curves with and without massive charm quark compared to the lattice data.

Including a massive quark of mass m to the static potential with N_f massless flavors yields a correction to the energy. This correction is known at N²LO. The influence of the charm quark in the sea can be resolved by plotting the (2+1)- and (2+1+1)-flavor QCD results together in Fig 1, which provides clear evidence of a significant contribution from the charm quarks in the sea in the full window of interest for the determination of α_s as indicated by a clear difference between data of the (2+1)- and the (2+1+1) flavor ensembles. Furthermore, in Fig. 2, we show that the data from (2+1+1)-flavor QCD are better described by the curve including N²LO massive charm effect than by curves of same order describing the static potential with N_f =3 or 4 massless quarks only.

In summary, our lattice QCD data show effects of a nonzero charm-quark mass in the static energy. Moreover, these effects are in agreement with perturbation theory at two-loop accuracy. We stress that the static energy with massive charm contributions is known in perturbation theory one order in α_s less than the static energy with just massless quarks, which limits the accuracy of the analysis. That said, the two-loop perturbative description with 3 massless and one massive flavor interpolates between the limiting cases of the (2+1+1)- and (2+1)-flavor lattice data. More specifically, we observe the approach to the massless charm limit at short distances, where the data can be described by the expression of the static energy with 4 massless quarks, and the decoupling of the massive charm quark in the long distance limit, where both (2+1+1)- and (2+1)-flavor results are consistent with the static energy with 3 massless quarks.

Ongoing Research / Outlook

The static energy based lattice scales r_0, r_1, r_2, and the string tension σ have not been determined in (2+1+1)-flavor QCD yet. These quantities are determined by performing local fits to regions relevant for each scale respectively. Our preliminary results for the scales r_0 and r_1, that are not affected by the charm quark, are in agreement with the measurements performed on 2+1 flavors. For the scale r_2, which is affected by the charm quark, our preliminary (2+1+1)-flavor analysis shows a slight deviation from the (2+1)-flavor result.

The static energy at fixed lattice-spacing *a* contains an unphysical term that scales as 1/*a*. In the work above, we have dealt with it by introducing a constant shift so that the data is matched at some distance. In the future work, we will remove this unphysical term completely by subtracting off twice the mass of a heavy-strange meson, where the heavy quark is in the static limit. This will allow for a more precise determination of the static energy, and hence, the strong coupling constant α_s.

To further improve the accuracy of α_s determination, we augment our effort by providing a more robust correction of the discretization artifacts of the static energy at small distances. The static energy on the lattice at distances *r* of the order of the spacing a is affected by significant, non-smooth discretization artifacts that have to be removed in a continuum extrapolation before comparison to the continuum perturbation theory is possible. These discretization artifacts are known from a field-theoretically rigorous calculation only at the leading order, which is insufficient for the accuracy of current lattice simulations. By performing a rigorous lattice perturbation theory calculation at NLO, we aim at reducing the remaining uncertainty to a level where it becomes subleading.

References and Links

[1] https://einrichtungen.ph.tum.de/T30f/tumqcd
[2] S. Steinbeißer, N. Brambilla, R. L. Delgado, A. S. Kronfeld, V. Leino, P. Petreczky, A. Vairo and J. H. Weber, The static energy in 2+1+1-flavor QCD,' [arXiv:2111.02288 [hep-lat]], Contribution to: Lattice 2021.
[3] N. Brambilla, A. S. Kronfeld, R. L. Delgado, V. Leino, P. Petreczky, S. Steinbeißer, A. Vairo, and J. H. Weber (TUMQCD), arXiv:2206.03156 [hep-lat].
[4] MILC code: http://www.physics.utah.edu/~detar/milc/

The QCD phase diagram in the quark mass plane

Research Institution
[1]University of Wuppertal

Principal Investigator
Zoltan Fodor[1,2,3,4]

Researchers
S. Borsányi[1], J. N. Guenther[1], R. Kara[1], P. Parotto[3], A. Pásztor[4], D. Sexty[5]

Project Partners
[2]Jülich Supercomputing Centre, Forschungszentrum Jülich
[3]Pennsylvania State University, State College
[4]Eötvös University, Budapest
[5]University of Graz, Graz

SuperMUC Project ID: pn72tu (Gauss Large Scale project)

Introduction

Quarks are the constituents of the massive basic building blocks of visible matter. These building blocks are the hadrons, more precisely protons and neutrons, which are about 2,000 times heavier than electrons. The most important of these quarks are the up and the down quarks, whereas the strange quark also plays some role in these hadrons. A proton contains two up and a down quarks, whereas the neutron consists of one up and two down quarks (so-called valence quarks). In normal conditions, as on earth or even in the sun, the quarks are confined in hadrons, they cannot get out. The confining force is called the strong force, the underlying theory is the theory of the strong interactions or in other words Quantum Chromo Dynamics, or in short QCD.

It is important to note, that quark masses are constants of nature. They are what they are and experiments cannot change them. In nature the up and down quark masses are just a few per-mill of the proton's mass, whereas the strange quark mass is about one tenth of the proton's mass.

In the early universe, at very high temperatures, the quark ingredients of protons and neutrons were freed. We call this state the deconfined phase. They were not confined in protons or neutrons, in some way these hadrons were boiled and the ingredients got liberated. As the universe expanded and cooled down the quarks got confined in hadrons. We call this state the confined phase. It is an interesting question to tell the order of the transition between these two — confined and deconfined — phases. Is it a first order phase transition as in the case of boiling water? Or is it a second order phase transition? Or it is not a phase transition at all, just an analytic transition as in the case of melting butter? It was believed for a long time that the transition between free quarks and confined quarks is a first order phase transition. It is easy to understand why physicists conjectured this sort of transition type. When we boil water the attractive forces between the water molecules are not strong enough to keep them together and the water molecules get liberated. Similarly, it was believed that the qualitative difference between the confined and liberated quarks is so huge that it must be accompanied by a first order phase transition. What would it mean for the early and even for the present universe? A first order phase transition is always a place for dramatic changes. Bubbles or droplets appear, they grow and finally fill out the whole space. This happens for the water vapor phase transition and this would be the case for a first order QCD phase transition, too. Bubbles would appear, they would collide and the low temperature confining phase would fill the whole universe. During the course of the phase transition various remnants would appear, such as quark nuggets or primordial black holes, just to mention two of them. These remnants could have cosmological consequences or they could be even detectable by experiments. Despite the efforts of three decades no such remnants were detected. Are our experiments not sensitive enough (this is the more plausible scenario)? Or even worse: is the underlying picture false (this seemed to be a less plausible scenario)?

It was a heroic effort to determine the nature of the phase transition for physical quark masses, which our group carried out in 2006 and published in Nature [1] (this publication turned out to be the most cited lattice paper of the present century). This finding has fundamental consequences for the early universe and for the possible remnants we might detect even today. Note however, the result has not only relevance for the early universe (Big Bang) but also for heavy ion collisions (Little Bang), which are carried out at the RHIC (Brookhaven, USA) and LHC (Geneva, Switzerland) accelerators.

Results and Methods

Since the nature of the transition is an extremely crucial, fundamental information and all of the quantitative features (transition temperature, equation of state etc.) depend on it, it is very important to pin down the transition's nature for various points on a hypothetical light quark versus strange quark mass

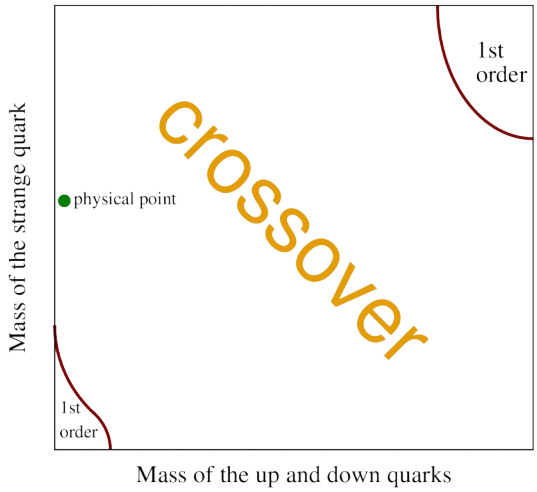

Figure 1: Location of three exemplary potential decentralized retention basins. The basins are situated on the brook and are dammed up by notional dams.

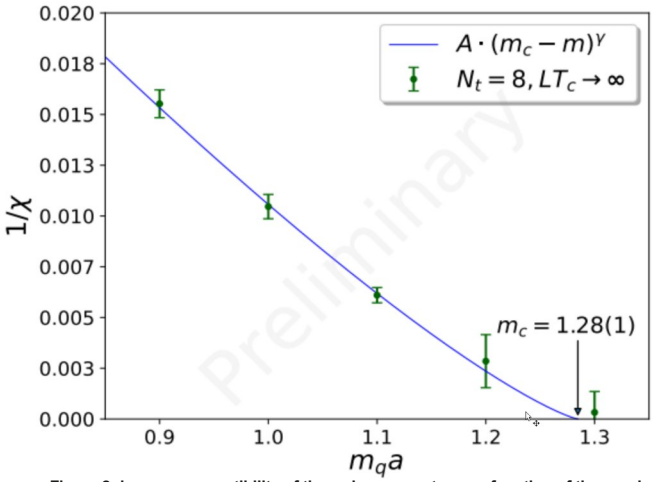

Figure 2: inverse susceptibility of the order parameter as a function of the quark masses in lattice units. The simulated systems seem to get more and more critical as the quark masses are increased since the inverse susceptibility vanishes according to a power law. The results fit well to previous findings based on different methods such as the matrix model [4] or the Binder cumulant analysis [5].

plane. This will embed the finding for the physical point and gives it further support. Here it is of particular importance to locate two characteristic points. The small mass and the large mass degenerate cases. For zero mass we expect a first order phase transition, which becomes second order if we increased the masses after which it is an analytic cross over probably all the way to the physical point. For infinitely large masses the transition is known to be first order. Again reducing the masses all the way down to the physical point with analytic cross over one should find a mass value with a second order phase transition. These cases are illustrated on the attached figure. Our goals are threefold. a) Determine the nature of the transition at the physical point with chiral fermions and with very fine lattices using so-called staggered formalism; b) locate the small mass second order phase transition point (this task needs probably chiral fermions, too, but the first steps can be done with staggered fermions); c) locate the large mass second order phase transition point (in this case chiral symmetry is not important staggered fermions can be used).

Figure 1 is a modern version of what was first sketched by Columbia group in Ref. [2]. Nature with its given quark masses represents a single point in this representation. This physical point is in the region where the confined and plasma phases are not separated by a real transition. Those quark masses where the transition is to be expected to be second order are marked red in the diagram. Our project aims to calculate these lines, since the position of these are, at present, unknown in the continuum limit.

Our first preliminary results concerning the upper right corner of the Columbia plot can be found in Ref [3]. Since real phase transitions can only appear in infinite large systems, we perform simulations with different spatial lattice extensions to calculate the infinite volume extrapolation. Thus we use staggered fermions on lattices of the size: 24^3x8, 28^3x8, 32^3x8, 40^3x8, 48^3x8 and 64^3x8.

If the transition is a real phase transition and not an analytic crossover, the susceptibility of the order parameter is expected to diverge in the infinite volume limit. In the case of a second order transition this behavior is accompanied by a critical exponent.

Figure 2 shows the inverse susceptibility of the order parameter as a function of the quark masses in lattice units. The simulated systems seem to get more and more critical as the quark masses are increased since the inverse susceptibility vanishes according to a power law. The results fit well to previous findings based on different methods such as the matrix model [4] or the Binder cumulant analysis [5].

Ongoing Research / Outlook

Our goal is to calculate the corresponding critical mass on finer lattice discretizations in order to achieve a reliable continuum limit. The result will be the critical point along the diagonal of the Columbia plot located on the 2nd order line in the upper right corner.

Thus we make simulations on LRZ's SUPERMUC-NG system on wide range of lattice resolutions and sizes. The order of the transition we determine by monitoring the fluctuations of the order parameter in a finite volume scaling analysis.

Through the study of the phase structure of the strongly interacting matter in this enlarged parameter space we will also learn something on QCD with Nature's choice of the quark masses. We'll be able to make connection to the phase structure of the strongly interacting matter in actual collider experiments. For this we'll quantify the relation of the critical quark masses (red lines in the diagram above) and the quark densities in high energy accelerator experiments.

References and Links

[1] Y. Aoki et al, Nature 443 (2006).
[2] F. R. Brown et al, Phys.Rev.Lett. 65 (1990).
[3] S. Borsányi et al, PoS 38th Int. Symposium on lattice field theory (2021). arXiv:2112.04192.
[4] K. Kashiwa et al, Phys. Rev. D (2012).
[5] F. Cuteri et al, Phys. Rev. D (2021).

Flavor-singlet meson physics from lattice QCD

Research Institution
[1]Jülich Supercomputing Centre, Forschungszentrum Jülich

Principal Investigator
K. K. Szabo[1]

Researchers
A. Gerardin[2], L. Parato[2], F. Stokes[1], L. Varnhorst[2], W. Verplanke[2]

Project Partner
[2]Aix Marseille Univ, Université de Toulon

SuperMUC Project ID: pn73xi (Gauss Large Scale project)

Introduction

Mesons have played an important role in the development of high-energy physics. The existence of such particles were proposed in the 1930s to describe the nuclear force and they were subsequently found in experiments. Later a large variety of such particles were discovered, eventually they were organized into multiplets. These developments ended in the discovery of quarks and of the color charge, a property similar to the electric charge.

From all the mesons the so-called flavor-singlet mesons are special, most notable flavor-mesons are the π_0, η and η' mesons. They behave strikingly different from what one would expect naively. Physicist call such behaviour an anomaly. There is for example the anomalous electromagnetic decay of the π_0 or the anomaly in the $\eta - \eta'$ mass splitting. The explanation of these anomalies sparked many important theoretical developments.

We now know the masses of these particles to a relatively good precision from experiments and we also have a solid qualitative understanding of the mass generating mechanisms. There are several observables beyond the masses of these particles, which have a huge phenomenological importance. In some cases the experimental determination is not precise enough or not yet possible. Here enters the ab-initio approach to these problems: lattice QCD.

Results and Methods

The ab-initio calculation means in the above context lattice quantum field theory. A space-time grid is introduced and and at every point of it the time evolution of various quantum operators are determined (to be more specific a path integral formalism is applied to that end). In some sense it reminds us to meteorology. Usually, people also introduce a three-dimensional grid, temperatures, pressures and wind velocities are measured and using the underlying equations the time evolution is determined. In both cases it is a heroic effort.

The determination of flavor-singlet meson properties in lattice QCD is difficult. Implementing the above mentioned anomalies on the lattice is a highly non-trivial problem. The computations face large statistical errors due to discon- nected diagrams. The pn73xi allocations aims to address these challenges.

Masses, mixing angles, decay constants
Our first target is to compute the masses and mixing angles in the $\pi_0 - \eta - \eta'$ system. Though these quantities are known experimentally to a high precision, it is interesting to see, if lattice QCD can reproduce them. This would demonstrate, that the anomalous mass generating mechanism is working as expected. There has been a lot of activity in lattice QCD in this area, state of the art computations achieve about 2% accuracy on the masses [1].

Ours will be the first full computation with so-called staggered fermions. These type of fermions are used in many high precision studies, but computing flavor-singlet mesons has only been of exploratory type. It is an open question, if staggered fermions can reproduce the experimentally measured masses. This part of the project is important to validate the staggered framework, in particular the choice of the lattice action and the range of lattice spacings. In particular the fourth-root trick, that we employ for the sea quarks, has been questioned in the past. The η' meson is of interest, since it can provide us evidence, pro or contra, if staggered fermions are able to reproduce the corresponding anomaly in the continuum limit.

In addition, the decay constants of the flavor-singlet mesons are also interesting phenomenologically. These can be extracted from the experimental scattering and decay processes of the η and η'. There are some disagreements in these results, hence ab-initio calculations would be helpful here. We plan to have results on decay constants and mixing angles, too.

In our approach we plan to work directly with physical pion masses and eliminate the uncertainty related to the pion mass extrapolation in previous works. We use several lattice spacings with the staggered

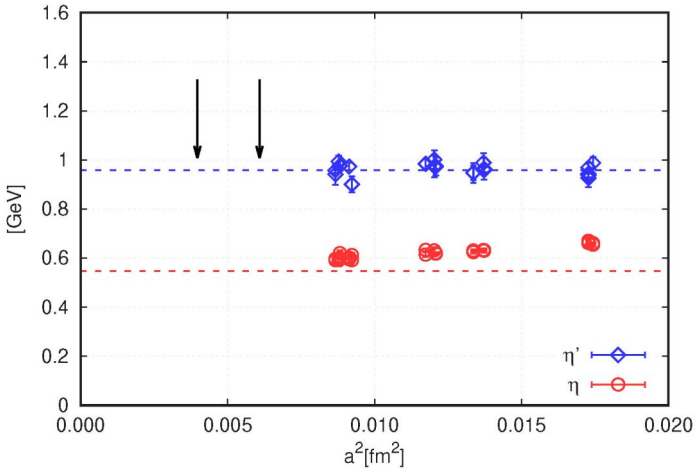

Figure 1: Preliminary results for the η and η/ masses, obtained in the currently running grant period.

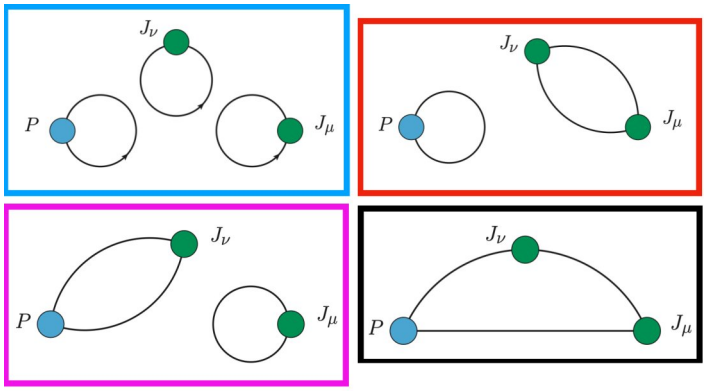

Figure 2: Different topologies, connected and disconnected, which summed up give the total three-point function. The four insets correspond to the correlators P-J-J, PJ-J, P-JJ and PJJ. The hyphen indicates a disconnection. We have implemented these diagrams in our computer codes and are currently in the process of computing them [2].

discretization. Our preliminary results for the η and η/ masses, obtained in the currently running grant period, are shown in Figure 1. For more details see [2].

The major source of systematics in our case is the continuum extrapolation, so we plot the points as the function of lattice spacing squared. On the individual points we reach somewhat better statistical precision than those most recent lattice QCD computations. So we are in a good way to reach a precision on our final result, which is at least as precise as the current state-of-the-art [1].

Hadronic light-by-light scattering

Our second target is to compute the hadronic light-by-light (HLbL) scattering contribution to the magnetic moment of the muon g_μ. There is large attention surrounding this quantity with the hope of a discovery of a new physical interaction. The experimental and theory determinations of g_μ have been choosen to one of the '10 Breakthroughs of the Year in 2021' by the Science Magazine [3].

The current picture on the hadronic contributions to the magnetic moment is far from being settled. The HLbL con- tribution is small, but currently its error is one of the largest in the error budget of the theory determination of g_μ. Independent determinations of the HLbL are therefore highly welcome.

Our strategy relies on the so-called dispersive framework: one considers contributions from all-possible intermediate states in the corresponding scattering amplitude. It turns out that by far the largest contributions among all possible intermediate states are given by the flavor-singlet mesons: π_0, η and η'.

These contributions can be given in terms of so-called transition form factors (TFF). These describe the interaction of these flavor-singlet mesons with two photons. There is very little experimental information on these amplitudes and an ab-initio computation, that we are currently carrying out, would be extremely helpful. Our goal is to perform the first complete lattice calculation of the TFF for all three flavor-singlet mesons.

On the lattice these TFFs are represented as a three-point function. It contains one insertion of a meson (P) and two insertions of a photon (J). Figure 2 shows the different topologies, connected and disconnected, which summed up give the total three-point function. The four insets correspond to the correlators P-J-J, PJ-J, P-JJ and PJJ. The hyphen indicates a disconnection. We have implemented these diagrams in our computer codes and are currently in the process of computing them [2].

References and Links

[1] Bali et al, JHEP 08 (2021) 13.
[2] Gerardin et al, arXiv:2112.08101.
[3] https://www.science.org/content/article/breakthrough-2021

Strong interactions with adjoint and fundamental matter

Research Institution
[1]Institute for Theoretical Physics, University of Jena

Principal Investigator
Georg Bergner[1]

Researchers
Gernot Münster[2], Istvan Montvay[3], Philipp Scior[5], Stefano Piemonte[4], Sajid Ali[5], Juan Camilo Lopez[1]

Project Partners
[2]University of Münster
[3]DESY Hamburg
[4]University of Regensburg
[5]University of Bielefeld

SuperMUC Project ID: pr27ja, pr27re

Introduction

The strong interactions of Quantum Chromodynamics (QCD) describe the formation of nuclear matter from the constituents of the fundamental theory, the quarks and gluons. Unique features of this theory are confinement of color charges and asymptotic freedom. Due to confinement, quarks and gluons are not observed at low energies, but instead a number of bound states are the relevant degrees of freedom of the strongly coupled matter. In the low energy strongly coupled confined state, a perturbative analysis is not possible and the understanding of the confinement mechanism is still a challenging open problem of theoretical physics. At high energies, there is a transition to a deconfined state described by a gas of gluons and quarks. Despite the ongoing effort for a deeper understanding of the confinement mechanism, the only way to compute the formation of bound states and the deconfinement transition are based on large scale numerical methods of lattice gauge theory. These have provided confidence in the consistency of the fundamental theory with experimental observations. Two important questions, however, remain. The first one is whether the numerical methods can also provide a deeper understanding of the confinement mechanism. The second question is whether strongly interacting gauge theories can be a more general guiding principle for new theories beyond the standard model of particle physics. Both of these questions motivate our investigations of strongly interacting gauge theories different from QCD. These theories provide additional analytic insights for example due to an enhanced symmetry. Strong interactions beyond the Standard Model of particle physics require also theories, which are quite distinct from QCD. Our goal is the investigation of supersymmetric gauge theories, like supersymmetric QCD and supersymmetric Yang-Mills theory. Supersymmetric Yang-Mills theory is the simplest supersymmetric gauge theory. It contains the gluons and their supersymmetric partners, the gluinos, which are Majorana fermions in the adjoint representation of the gauge group. We have published our final results for supersymmetric Yang-Mills theory in [1]. Supersymmetric QCD adds a supersymmetric multiplet of matter fields to this theory, consisting of quark fermion fields and their supersymmetric partners, the squarks, which are bosonic scalar fields. Quark and squark fields transform in the fundamental representation of the gauge group. The theory plays an important role in supersymmetric extensions of the Standard Model. Based on the symmetries of the theory, theoretical conjectures have been made that provide insights into the strongly coupled dynamics of this theory. Even without the scalar squark fields, aspects of phase transitions and the running of the gauge coupling in general can be studied in numerical lattice simulations. For this reason we are investigating SU(2) Yang-Mills theory coupled to adjoint and fundamental fermions. Supersymmetric QCD without scalar fields is also a candidate for a composite Higgs theory, in which a strongly coupled sector leads to the formation of the Higgs particle as a bound state. These strongly coupled extensions of the Standard Model are quite constrained by experimental data. Recently theories with fermions in two different representations have been studied as possible candidates. One interesting example is an SU(2) gauge theory with an adjoint fermion and two fermions in the fundamental representation. In the end, only lattice simulations will provide enough information about the confined theory to understand whether such theories are realistic candidates for an extension of the Standard Model.

Results and Methods

The method of numerical lattice simulations is based on a discretized space time. The observables of quantum field theory are evaluated from the path integral with a discretized action of field theory. The configuration space of the quantized fields is sampled using Markov chain Monte Carlo methods. The simulation of dynamical fermion fields requires larger computational resources. The fermions are integrated out leaving a fermionic determinant or, in case of Majorana fermions, a Pfaffian. These contributions in the path integral connect all fields on the lattice and require cost intensive algorithms, like the hybrid Monte Carlo (HMC) algorithm. Due to this complication, only recently theories with fermions in multiple representations have

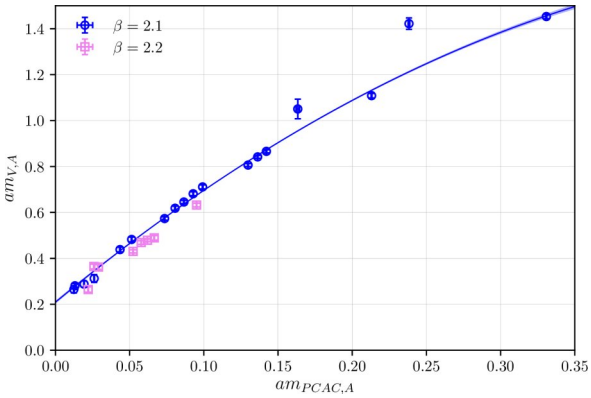

Figure 1: Chiral fit of the vector meson mass as a function of the renormalized (PCAC) mass of the adjoint fermion.

been considered. In our projects, we aim to investigate a very general set of theories, which requires a generalizable approach including variants of the HMC algorithm like the rational HMC. The final simulation results have been obtained from different lattice spacings and are extrapolated to the continuum and infinite volume limit. In most cases, the fermion masses need to be extrapolated as well. In particular, the gluino masses need to be extrapolated to the chiral limit, where the bare gluino mass vanishes. We have simulated the theory with fermions in two different representations. We have verified the consistency with earlier results in the limits where one of the fermion species is removed. We have excluded possible unphysical phases in the simulations. Based on this verification of our methods, we have investigated the theory with one adjoint fermion and two fermions in the fundamental representation. We have determined the bound state masses and determined an effective fermion mass. The most interesting first question is whether the theory is QCD like with a confining low energy effective theory and the formation of a chiral condensate. In QCD the small mass regime close to the chiral limit is determined by chiral perturbation theory. The renormalized coupling runs from low values at high energies (asymptotic freedom) to high values at lower energies (confinement). By contrast, some gauge theories with a larger fermion content are infrared conformal, which means that the running of the gauge coupling stops at a conformal infrared fixed point and the theory becomes approximately scale invariant. A finite fermion mass deforms the conformal theory, but all bound state masses are expected to scale to zero with the same mass anomalous dimension, if the mass tends to zero. We have investigated these two possible scenarios for the infrared regime of the theory. The fermion content seems to be large enough to induce an almost conformal behavior with nearly constant mass ratios, further details are in [2]. However, our results indicate that it is still chirally broken in the infrared (see Figure 1). This means that supersymmetric QCD and related theories can be analyzed in a similar way as QCD in the regime accessible by numerical lattice simulations. Further investigations are required to obtain a more general understanding of the theory. The optimal way to study chiral symmetry breaking is a lattice action that respects chiral symmetry in terms of the Ginsparg-Wilson relation. From the theoretical point of view, these fermion formulations provide a much better

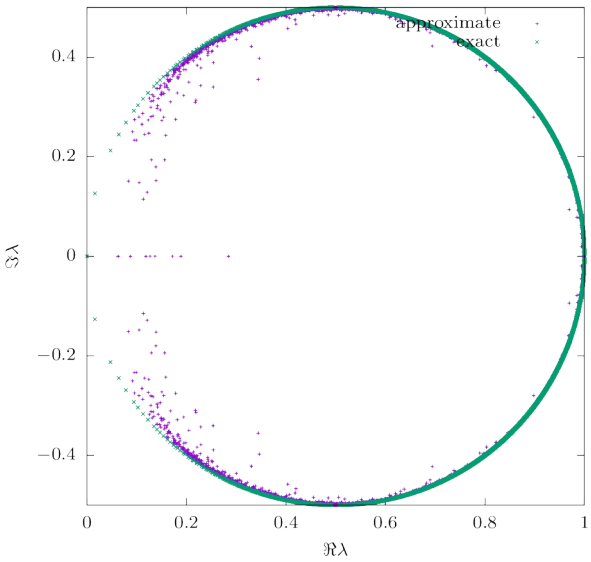

Figure 2: Eigenvalue spectrum of the overlap Dirac operator on a lattice with 8 points in all directions. The Ginsparg-Wilson relation implies that the eigenvalues are on a circle. In addition a polynomial approximation is shown that is used in the simulations.

representation of the theory, but in numerical simulations they are very costly. We have recently investigated a numerical implementation of the overlap fermions and simulated gauge theories with a different number of adjoint fermions using this improved action (Figure 2 shows the implemented approximation, see also [3]). This will provide a better understanding of the formation of a chiral condensate and dynamical chiral symmetry breaking for the considered theories. A further important benefit of the chiral symmetric lattice formulation is also the reduced fine tuning need to restore supersymmetry. Supersymmetry is generically broken by the lattice discretization. Counterterms need to be added to the lattice action and tuned to recover the continuum limit. Possible counterterms are reduced by the symmetries of the lattice action.

Ongoing Research / Outlook

We have done the first investigations of a SU(2) Yang-Mills theory coupled to one fermion in the adjoint and two fermions in the fundamental representation. Our investigations cover only the first basic properties of the theory. Other aspects like phase transitions and possible relations to the Standard Model need a larger currently under investigation. We have implemented and extended our numerical methods with overlap fermions, which allow for a much cleaner representation of the continuum symmetries on the lattice. All of these investigations will in particular help with the simulation of gauge theories with extended supersymmetry.

References and Links

[1] S. Ali et al., Phys. Rev. Lett. 122 (2019) no.22, 221601. arXiv:1902.11127.
[2] G. Bergner and S. Piemonte, Phys. Rev. D 103 (2021) no.1, 014503. arXiv:2008.02855.
[3] S. Piemonte et al., Phys. Rev. D 102 (2020) no.1, 014503. arXiv:2005.02236.

A strong side of weak decays: How beauty and charm resonate in pions and kaons

Research Institution
[1]Helmholtz-Institut für Strahlen- und Kernphysik, Rheinische Friedrichs-Wilhelms-Universität Bonn

Principal Investigator
Marcus Petschlies[1]

Researchers
Constantia Alexandrou[2], Stefan Krieg[3], Luka Leskovec[4], Thomas Lippert[3], Stefan Meinel[5], John Negele[6], Srijit Paul[8], Andrew Pochinsky[6], Gumaro Rendon[7], Giorgio Silvi[3]

Project Partners
[2]Cyprus Institute & University of Cyprus
[3]Forschungszentrum Jülich & Bergische Universität Wuppertal
[4]Thomas Jefferson National Accelerator Facility & Old Dominion University
[5]University of Arizona
[6]Center for Theoretical Physics, Massachusetts Institute of Technology
[7]Brookhaven National Laboratory
[8]Johannes Gutenberg-Universität Mainz

SuperMUC Project ID: pr27yo (Gauss Large Scale project)

Introduction

The B and D mesons, which are built each form a pair of bottom and light or charm and light quarks, are among the more exotic particles observed in the realm of high energy physics. However, they play an eminent role in our present-day efforts to probe our understanding of the fundamental strong and electroweak forces in Nature, which we describe in the Standard Model of elementary particle physics. Both mesons are unstable under the electroweak interaction, and the transition amplitudes

for their decays to states including two pions or a pion and a kaon (denoted for brevity as e.g. $B \to \pi\pi l\bar{\nu}$ and $B \to K\pi ll$) are an essential ingredient

to the investigation of semileptonic B and D decays in the effective electroweak sector of the Standard Model. These flavor changing processes, involving transitions at the quark level of heavy bottom and charm quarks to lighter up and strange quarks (for short, e,g. $b \to ulv$ and $b \to sll$, plus leptons and neutrinos), are gold-plated candidates at the high-precision frontier for testing the Standard Model, as well as in the search for physics beyond the Standard Model: the transition $B \to \pi\pi$ pertains to the precision estimate of the element of the Cabibbo-Kobayashi-Maskawa (CKM) quark mixing matrix , a fundamental parameter of the Standard Model.

The *flavor anomalies* in $b \to sll$ observed as tensions between measured B-meson decays and their Standard Model prediction allow for exciting investigations of New Physics scenarios.

The decay $B \to \pi\pi lv$ is illustrated in Figure 1. The transition matrix elements factorize in an electroweak part, and in one part that is governed by the strong interaction and determined numerically in pure Quantum Chromodynamics (QCD). The latter factor is pictorially defined by the blue box frame. Being subject to the strong force, the theoretical physics investigation of this process requires the High Performance Computing methods of Lattice QCD and thus the computational power of the supercomputer SuperMUC-NG. Studying the process $B \to \pi\pi$ becomes even more challenging, when the elastic pion-pion scattering in the final state, which features the famous ρ resonance is taken into account. (Or the κ and K^* resonances for the transition $B \to K\pi$.)

The rigorous calculation of such matrix elements with an unstable final state must include the proper conversion of our Lattice QCD data obtained in a finite box of size L^3 to the infinite volume of the physical world. Thus the study of $\pi\pi$ and $K\pi$ scattering in Lattice QCD forms an integral part of our computational project.

Results and Methods

The major steps in our Lattice QCD calculation are spectroscopy and mapping to scattering amplitudes (1) for $\pi\pi$ isospin I = 1 with focus on the P -wave (ρ resonance) channel and (2) for $K\pi$ I = 1/2 with focus on S-wave (κ resonance) and P-wave (K^* resonance). Step (3) is the production of 3-point correlation functions for B, D-meson and $\pi\pi$ and $K\pi$ initial and final states, and mapping of extracted matrix elements to infinite-volume amplitudes, based on items (1) and (2) with the Lellouch-Lüscher method and its generalization by Briceno, Hansen and Walker-Loud. The required Wick contractions to construct 2-point correlation functions and matrices thereof for variational analysis of the Lattice QCD spectrum are

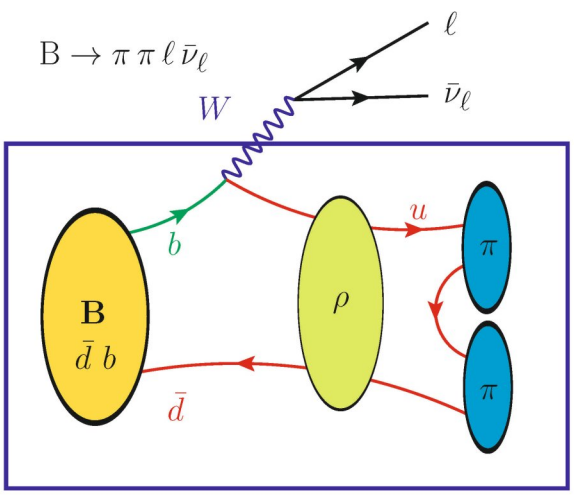

Figure 1: Illustration of the B-decay to a 2-pion state via the rho resonance.

calculated based on SuperMUC-NG partitions with up to 2,592 cores and approximately 25,000 core-hours per job, and using the C/C++ QLUA software suite [3] and QOPQDP-multigrid solver for numerically solving the large sparse linear system of the Dirac equation. With the help of SuperMUC-NG resources we could investigate the $\pi\pi$ and $K\pi$ elastic scattering amplitudes for 2 values of the pion mass (320 MeV label “C13” and 180 MeV with label “D6”). The phase shifts δ_1 (P-wave) and δ_0 (S-wave) are shown in Fig. 2, with ample details about their practical computation given in Refs. [1,2].

Ongoing Research / Outlook

With pion-pion and kaon-pion scattering amplitude information in hand, we simulate the beauty and charm meson 3-point functions for the transitions $B/D \to \pi\pi/K\pi\pi$ and extract the infinite-volume matrix elements in analogy to the case of $\pi\gamma^* \to \pi\pi$ in [4]. In the near future, the resources of SuperMUC-NG allow us to continue our simulation ever closer to the conditions of the physical world, including lighter pions, larger lattice volume, smaller lattice discretization, and to probe such intricate effects as coupled decay channels (mixing of 2-kaon and 2-pion states, and of kaon-pion and kaon-eta states), towards a rigorous contact with experment.

References and Links

[1] C. Alexandrou, L. Leskovec, S. Meinel, J. Negele, S. Paul, M. Petschlies, A. Pochinsky, G. Rendon and S. Syritsyn, Phys. Rev. D 96 (2017) no.3, 034525.
[2] G. Rendon, L. Leskovec, S. Meinel, J. Negele, S. Paul, M. Petschlies, A. Pochinsky, G. Silvi and S. Syritsyn, Phys.Rev.D 102 (2020) 11, 114520.
[3] USQCD software Qlua package, https://usqcd.lns.mit.edu/w/index.php/QLUA
[4] C. Alexandrou, L. Leskovec, S. Meinel, J. Negele, S. Paul, M. Petschlies, A. Pochinsky, G. Rendon and S. Syritsyn, Phys. Rev. D 98 (2018) no.7, 074502.

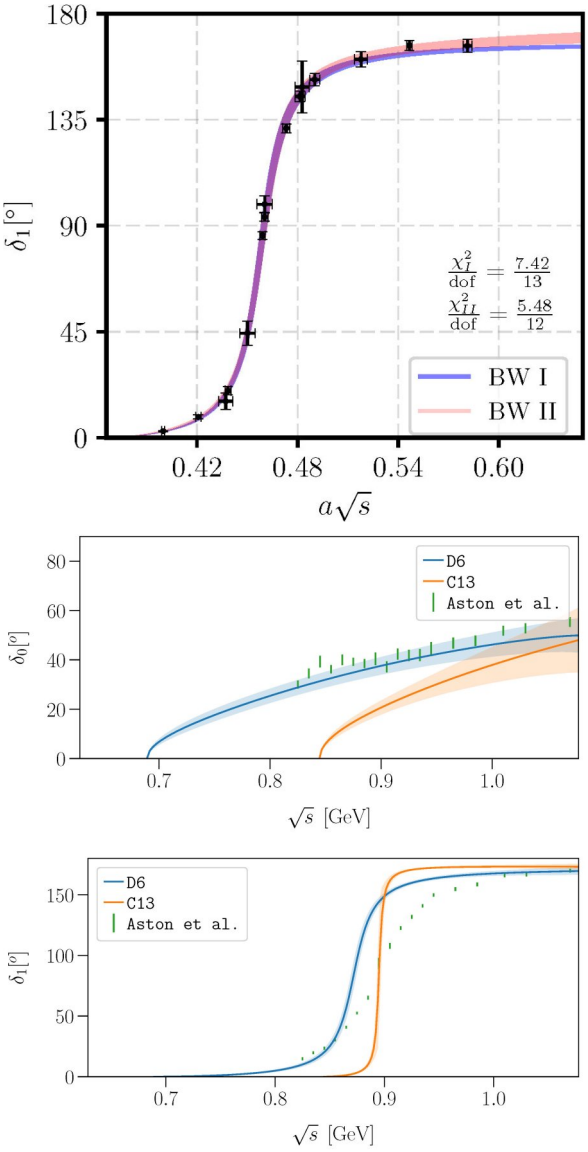

Figure 2: Phase shift fit results for pion -pion P-wave at 320 MeV pion mass (top), kaon- pion S-wave (center) and P-wave (bottom) elastic scattering at 180 MeV and 320 MeV pion mass, determined from Lattice QCD [1,2]

Nucleon observables as probes for physics beyond the standard model

Research Institution
[1]NIC, DESY, Zeuthen

Principal Investigator
Karl Jansen[1]

Researchers
C. Alexandrou[2,3], S. Bacchio[2], M. Constantinou[4], J. Finkenrath[2], K. Hadjiyiannakou[2,3], B. Kostrzewa[5], G. Koutsou[2], M. Petschlies[5], C. Urbach[5], A. Vaquero[6]

Project Partners
[2]The Cyprus Institute
[3]University of Cyprus
[4]Temple University
[5]University of Bonn
[6]University of Utah

SuperMUC Project ID: pr74yo (Gauss Large Scale project)

Introduction

In high-precision low energy particle physics experiments, small but significant discrepancies have been found when compared to expectations from theory. This has substantially increased the interest in precision nucleon structure measurements. This so-called *precision-frontier* of particle physics is serving a complementary role to new physics searches in the *high-energy frontier*, such as those pursued by experiments at the Large-Hadron Collider (LHC) at CERN. A major challenge in such searches is determining the precise contribution from the strong force component of the Standard Model. Experimentally, the proton, which is stable and abundantly available, is an optimal probe for studying strong interaction phenomena and is thus the target of several ongoing experiments such as at MAMI in Mainz, Jefferson Lab, and Fermi Lab as well as at the planned Electron-Ion Collider (EIC) in the US, where an extensive program to map out the proton's rich sea structure is foreseen. Theoretically, strong interaction phenomena are governed by Quantum Chromodynamics (QCD), and at energy scales relevant to the proton structure, the only known way of studying QCD from first principles is via large scale simulations using the lattice formulation.

Our project on SuperMUC-NG targets such simulations, using the so-called twisted mass fermion formulation of lattice QCD, which has the advantage that observables, such as nucleon structure observables we are targeting here, converge faster to the continuum limit. Using the resources provided at LRZ, our Extended Twisted Mass Collaboration (ETMC) [1] has simulated QCD gluon configurations which include dynamical mass degenerate up and down, as well as the strange, and charm quark flavors (N_f = 2+1+1) with masses tuned to their physical values and at three values of the lattice spacing parameter. These state-of-the-art ensembles are being used as building blocks for a wide range of lattice QCD studies in addition to nucleon structure which we highlight here.

Results and Methods

Physical point N_f = 2+1+1 ensembles
Lattice QCD refers to the discretization of the Lagrangian of QCD on a 4-dimensional Euclidean grid that allows to generate representative configurations via a Markov chain Monte Carlo process. The generated gauge configuration ensembles are then used to calculate hadronic quantities of interest. Continuum physics requires extrapolating using ensembles with multiple values of the lattice spacing and volume to the continuum and infinite physical box length limit. Several algorithmic improvements we have implemented during our allocations on SuperMUC include better integration schemes that scale more favorably with the lattice volume and advanced linear solvers [2, 3]. These algorithmic improvements complement the increased availability of computational resources to allow for the simulation of ensembles with larger volumes and with finer values of the lattice spacing, as we document in terms of SuperMUC core-hours over the years in Figure 1.

Nucleon axial form-factors
The ensembles generated on SuperMUC have been used to obtain the axial form factors of the nucleon [4], and in particular to obtain the individual up-, down-, strange-, and charm-quark contributions [5]. The axial structure of the nucleon is important for both understanding strong interaction dynamics and in revealing new physics. For example, neutrino elastic scattering on protons is sensitive to the strange axial form factor of the proton which at zero momentum transfer determines the strange quark contribution to the proton spin. Contributions from the strange quark, such as

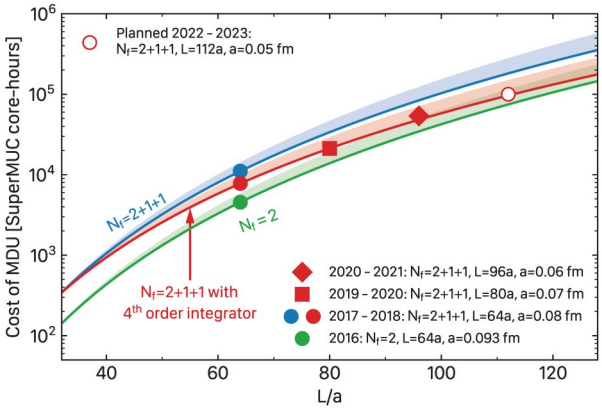

Figure 1: Simulation points carried out on SuperMUC since 2016. The red curve shows improvements achieved by our project to reduce computational cost while increasing the lattice volume.

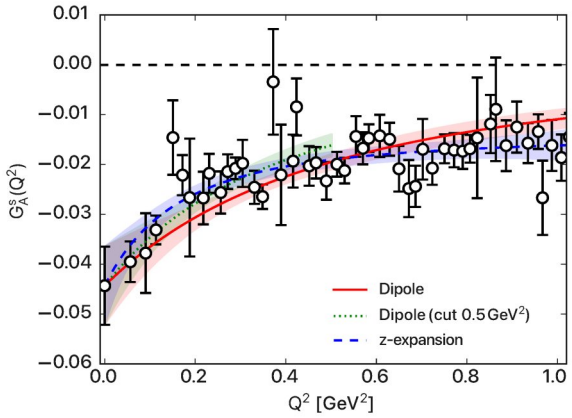

Figure 2: Strange quark contribution to the axial form factor vs the momentum transfer squared (Q^2). We also show fits to the form factor using a dipole form as well as the so-called z-expansion, as explained in Ref. [5].

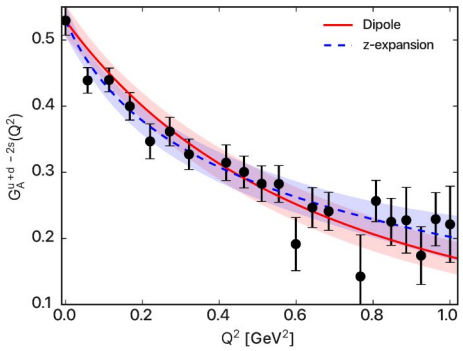

Figure 3: Octet quark combination of the axial form factor vs the momentum transfer squared (Q^2).

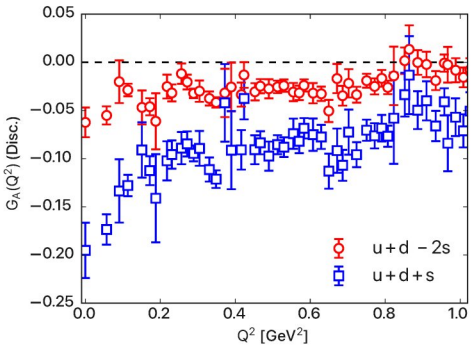

Figure 4: Disconnected quark contribution to the octet (red circles) and singlet (blue squares) combinations of the axial form factor.

the so-called strange σ-term, also enter in the determination of cross sections for a class of popular cold dark matter candidates.

In Figure 2 we show our calculation of the strange axial form factor computed for the first time using N_f = 2+1+1 configurations at the physical point. Our result confirms a negative strange contribution to the nucleon axial form factor and the value in the forward limit (Q^2 = 0) that is compatible with results from phenomenology.

Combining the individual up-, down-, and strange-quark contributions, we construct the SU(3) flavor octet combination, i.e. the combination u+d-2s, as shown in Figure 3. Of interest in particular are the so-called disconnected quark loop contributions to this combination: The strange-quark component of the SU(3) octet combination is disconnected, while the u+d component has both connected and disconnected contributions. A non-zero disconnected u+d-2s combination signals deviation from the SU(3) flavor symmetric point. This is shown in Figure 4, where we see that the deviation from zero is up to 10% for the octet axial form factor at low values of Q^2 and decreasing at larger values. The significance of this result, beyond that it is the first such calculation at the physical point, is also reflected by the fact that in many phenomenological studies the SU(3) flavor symmetric point is assumed to extract such quantities.

Ongoing Research / Outlook

Our analysis for the extraction of the full set of nucleon structure observables on the ensembles generated on SuperMUC is ongoing. In particular, the axial form factors presented here have been carried out using one N_f = 2+1+1 ensemble at the physical point. While this removes the most significant systematic, namely that introduced by the extrapolation to physical quark masses that was required when simulating at heavier-than-physical quark masses, the full analysis on the ensembles shown in Figure 1 will allow us to extrapolate to the continuum limit thus also eliminating any systematics introduced by the finite lattice spacing. Of particular significance is the planned simulation shown in Figure 1 with the open circle, which will allow us to break new ground in terms of the lattice spacing, which will be the smallest ever simulated with this action, as well as in terms of the lattice volume, which will be the largest and for which large-scale resources such as SuperMUC are crucial.

References and Links

[1] ETMC: https://github.com/etmc; http://www-zeuthen.desy.de/~kjansen/etmc/
[2] C. Alexandrou, S. Bacchio, J. Finkenrath, Comput. Phys. Commun., 51-64 (2019), doi:10.1016/j.cpc.2018.10.013. arXiv:1805.09584.
[3] C. Alexandrou et al., Phys. Rev. D98, no.5, 054518 (2018) doi: 10.1103/ PhysRevD.98.054518. arXiv:1807.00495.
[4] C. Alexandrou et al., Phys. Rev. D103, no.3, 034509 (2021) doi:10.1103/PhysRevD.103.034509. arXiv:2011.13342.
[5] C. Alexandrou et al., Phys. Rev. D104, 074503 (2021), doi:10.1103/ PhysRevD.104.074503. arXiv:2106.13468 .

Non-perturbative Heavy Quark Effective Theory and the Strong Coupling

Research Institution
[1]Westfälische Wilhelms-Universität Münster, Institut für Theoretische Physik
[2]Deutsches Elektronen-Synchrotron DESY, Zeuthen

Principal Investigators
Jochen Heitger[1], Rainer Sommer[2]

Researchers
Patrick Fritzsch[3], Antoine Gérardin[4], Fabian Joswig[1,5], Simon Kuberski[1,6,7], Stefan Schaefer[2], Hubert Simma[2], Ben Strassberger[2]

Project Partners
[3]School of Mathematics, Trinity College Dublin
[4]Aix-Marseille-Université, Université de Toulon, Marseille
[5]Higgs Centre for Theoretical Physics, School of Physics and Astronomy, The University of Edinburgh
[6]GSI Helmholtzzentrum für Schwerionenforschung, Darmstadt
[7]Helmholtz-Institut Mainz, Johannes Gutenberg-Universität Mainz

SuperMUC Project ID: pr84mi, pn98ya

Introduction

Decades of research have led to the Standard Model of particle physics. This theory describes the structure of matter at length scales below the diameters of nuclei to an astonishing level of precision. Equivalently, it successfully predicts particle decays and scattering cross sections of high-energy processes up to the energies reached at the Large Hadron Collider (LHC) at CERN in Geneva. Indeed, we also believe that physics at larger length scales, i.e., nuclear and atomic physics, would emerge from the fundamental equations of the Standard Model, if we were able to solve them directly.

A very attractive feature of the Standard Model is that it has very few free parameters. These are – as far as we presently know – fundamental parameters of Nature. Their precise determination is thus an important part of particle physics and physics in general. It is also essential in order to put the Standard Model to tests of ever increasing precision. Such tests are especially motivated by observations that go beyond the physics described by the Standard Model, such as the existence of dark matter or the degree of matter - antimatter asymmetry in the universe. Thus, despite its tremendous success, the Standard Model must be incomplete! In the quest for a more complete theory, precision tests of the Standard Model complement direct searches for dark matter candidates and other effects of “new” physics at the LHC and other experiments.

Both the determination of the fundamental parameters and robust tests of the Standard Model require precision experiments on the one hand and a precise solution of the theory on the other hand. The ”strong” interaction part of the theory is called Quantum Chromo Dynamics (QCD). It describes the structure of the smallest nucleus, the proton, in terms of constituents, called quarks and gluons. At low energies, the dynamics due to the strong interaction cannot be determined analytically. Instead, we need to solve the theory numerically on a *finite space-time grid* on super-computers such as SuperMUC-NG. This is achieved via stochastic evaluation of *Feynman’s path integral*, which provides the quantization of the fundamental fields, the quarks and the gluons. It thus leads to systematically improvable, non-perturbative predictions of the theory.

Small deviations between experiment and theory have been found in quantities related to bound states of heavy quarks. So far, these deviations are not significant enough to claim the discovery of new physics beyond the Standard Model. To improve the theory predictions, we investigate the decays of B-mesons, i.e., bound states of a b-quark with a large mass of around 5 GeV and a light anti-quark. Even on modern supercomputers, the properties of B-mesons cannot be computed straight-forwardly in physically large volumes, because they require fine resolutions resulting in very large, not yet affordable system sizes. Therefore, we employ an expansion in the inverse quark mass, called *Heavy Quark Effective Theory* (HQET). Taking into account the next-to-leading order of the expansion, this effective theory can provide reliable predictions within our precision goals [1].

Results and Methods

A lattice QCD computation comprises two steps: first, ensembles of gauge field configurations are generated according to the distribution dictated by the Boltzmann weight in the path integral. Second, physical observables are computed on these configurations. Both tasks have been performed in our project. We have generated a set of 30 gauge ensembles in small physical volumes with very fine resolutions using the publicly available openQCD code [2]. The largest

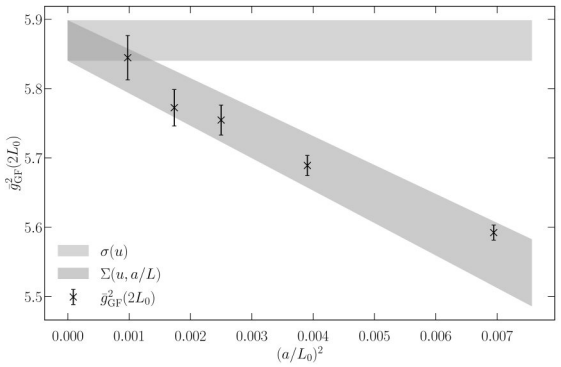

Figure 1: Gradient flow coupling computed on five ensembles with a physical extent of about 0.5 fm. We show the dependence of the coupling on the resolution $(a/L_0)^2$ together with the parametrization Σ and the continuum limit σ of [4].

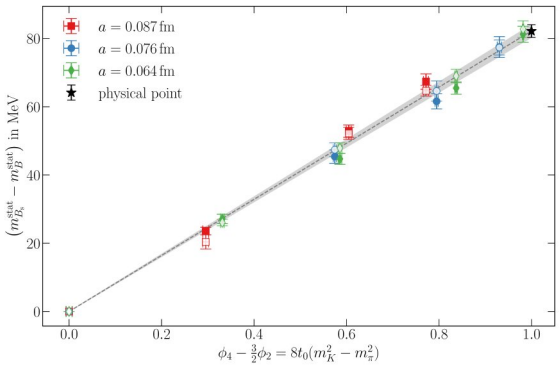

Figure 2: Splitting between B_s- and B-meson at lowest order of HQET depending on the difference of squared kaon and pion masses. Colored symbols show the results obtained at three resolutions, a, and for two discretizations of the static quark. The gray error band indicates the functional form in the continuum. The black star shows the extrapolated value at the physical point.

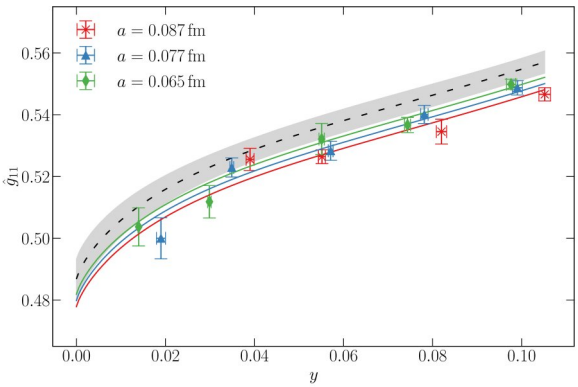

Figure 3: Coupling ĝ depending on the squared pion mass, parameterized by the variable y. We depict results at three resolutions, a, together with the functional form in the continuum limit.

lattices have up to 64^4 sites and each site contains the information of 72 double-precision numbers. Each Monte Carlo chain has a length of up to 100,000 molecular dynamics units. On SuperMUC-NG, we have used up to 2,048 cores for the ensemble generation. The code scales excellently up to this number of MPI tasks due to state-of-the-art methods, such as domain decomposition which reduces inter-core communications considerably.

The generated set of gauge configurations is to be used in a number of projects. First of all, they provide the basis to compute the parameters of HQET at very fine resolutions but small physical volumes. This is done via a matching between HQET and QCD with relativistic valence b-quarks. We consider a large range of kinematical choices to optimize this procedure.

The new ensembles may also be employed to improve our computation of the strong coupling constant of QCD in [3]. In figure 1 we illustrate our results for the finite-volume gradient flow coupling on five gauge ensembles generated at constant physical lattice size of 0.5 fm in each direction, which differ by their resolution. Together with the data, we show the parametrization of this coupling in terms of the lattice spacing, previously computed in [4] using data from coarser lattices. The comparison shows excellent agreement and indicates that the newly generated data will improve the continuum limit.

Having determined the HQET parameters in small volumes, we investigate the properties of B-mesons based on HQET in physically large boxes, generated by our colleagues within the CLS effort [6]. The computations are performed using a code that is again based on the openQCD package. Here, we deal with lattices with up to 192×96^3 sites and physical quark masses. Such calculations are only possible on massively parallel computers such as SuperMUC-NG. In figure 2 we show the results for our computation of the mass difference between a B_s-meson, composed of a b-quark and a strange anti-quark, and a B-meson, composed of b-quark and an up- or down-type anti-quark. This computation is performed at leading (static) order of HQET. The results from the individual gauge ensembles are jointly extrapolated to the physical point. The procedure may be improved by going to the next order of the expansion, using our HQET parameters. The ensemble with physical quark masses allows us to tightly constrain the extrapolation that serves as test of our ability to describe full QCD through HQET.

Further improvements in the quality of such extrapolations in the context of B-meson decays may be achieved by the knowledge of the B*-B-pion coupling ĝ. In figure 3, we show results of [5] for our computation of this quantity using HQET on SuperMUC-NG. We are able to significantly reduce some of the systematic uncertainties that are present in current results.

Ongoing Research / Outlook

We are currently extending the set of observables that is investigated in the effective theory. This includes the mass of the b-quark, decay constants of B-mesons and the form factors of semileptonic decays of B-mesons. SuperMUC-NG enables us to consider a large set of ensembles close to the physical point. This will help us to make precise theory predictions with reliable error estimates.

References and Links

[1] J. Heitger and R. Sommer, JHEP 0402 (2004) 022.
[2] M. Lüscher and S. Schaefer, openQCD, https://luscher.web.cern.ch/luscher/openQCD/
[3] M. Bruno et al., Phys. Rev. Lett. 119 (2017) 102001.
[4] M. Dalla Brida et al., Phys. Rev. D 95 (2017) 1, 014507.
[5] A. Gérardin et al., PoS LATTICE2021 (2021) 540.
[6] https://www-zeuthen.desy.de/alpha/public-cls-nf21

Hadronic corrections to the muon magnetic moment; Isospin breaking effects in QCD

Research Institution
[1]Department of Physics, University of Wuppertal
[2]Jülich Supercomputing Centre

Principal Investigator
K. K. Szabo[1,2]

Researchers
Sz. Borsanyi[1], Z. Fodor[1,2,3,4,5], J. N. Guenther[6], C. Hoelbling[1], S. D. Katz[3], L. Lellouch[7], T. Lippert[1,2], K. Miura[7,8,9], L. Parato[7], F. Stokes[2], B. C. Toth[1], Cs. Torok[2], L. Varnhorst[1]

Project Partners
[3]University of California, San Diego
[4]Institute for Theoretical Physics, Eötvös University
[5]Pennsylvania State University, Department of Physics
[6]Department of Physics, University of Regensburg
[7]Aix Marseille Univ, Université de Toulon
[8]Helmholtz Institute Mainz
[9]Kobayashi-Maskawa Institute, Nagoya University

SuperMUC Project ID: pn68ne, pn56bu (both Gauss Large Sacale projects)

Introduction

The muon is an elementary particle, a short-lived cousin of the electron. For many years the calculation of its magnetic moment has disagreed with its measurement, suggesting that a not-yet-known particle or force perturbs the muon. Such a discovery would have profound consequences on our understanding of Nature.

An experiment at the Fermi National Accelerator Laboratory (FNAL) near Chicago recently confirmed this puzzling discrepancy [3] at an event that received significant media attention.

On the same day, our ab-initio calculation was published in Nature [1], challenging previous computations and bringing the theoretical prediction closer to the experimental value: no new forces or particles may be needed to explain the FNAL measurement.

Ours is the most precise ab-initio calculation so far, with uncertainties comparable to those of the measurement and of the reference, data-driven computations. These computations were carried out -among other resources- using two allocations on SUPERMUC-NG, pn68ne and pn56bu.

Results and Methods

The ab-initio calculation means in the above context lattice quantum field theory. A space-time grid is introduced and and at every point of it the time evolution of various quantum operators are determined (to be more specific a path integral formalism is applied to that end). In some sense it reminds us to meteorology. Usually, people also introduce a three-dimensional grid, temperatures, pressures and wind velocities are measured and using the underlying equations the time evolution is determined. In both cases it is a heroic effort.

In this long term project, which lasted for 6 years and had two stages, we computed the leading order hadronic vacuum polarization contribution to the anomalous magnetic moment of the muon, a^{LO-HVP}, using lattice quantum field theory.

In the first stage [1] we were able to reach a relative precision of 2.7%. The results were published in Physical Review Letters, which was then highlighted by the editors as Editors' Suggestion.

In the second stage [2] we were able to improve the precision by several means and we finally obtained the result

$$a_{\mu}^{LO-HVP} = 707.5(2.3)(5.0)[5.5] \qquad (1)$$

with statistical, systematic and total errors. The relative uncertainty is 0.8%, which is far less than that of other lattice determinations, and is comparable to the errors of dispersion relation-based computations. The result are published in Nature [2] and shown in Figure 1.

Figure 1 shows a comparison of recent results for the leading-order, hadronic vacuum polarization contribution to the anomalous magnetic moment of the muon. Green squares are lattice results: the result obtained in the current project is denoted by BMWc'20 [2], whereas the result of the first stage of this project is denoted by BMWc'17 [1].

As a comparison, the results of other lattice collaborations are also listed: Mainz Fermilab-HPQCD-MILC and European Twisted Mass, all from 2019, and RIKEN-Brookhaven-Columbia from 2018.

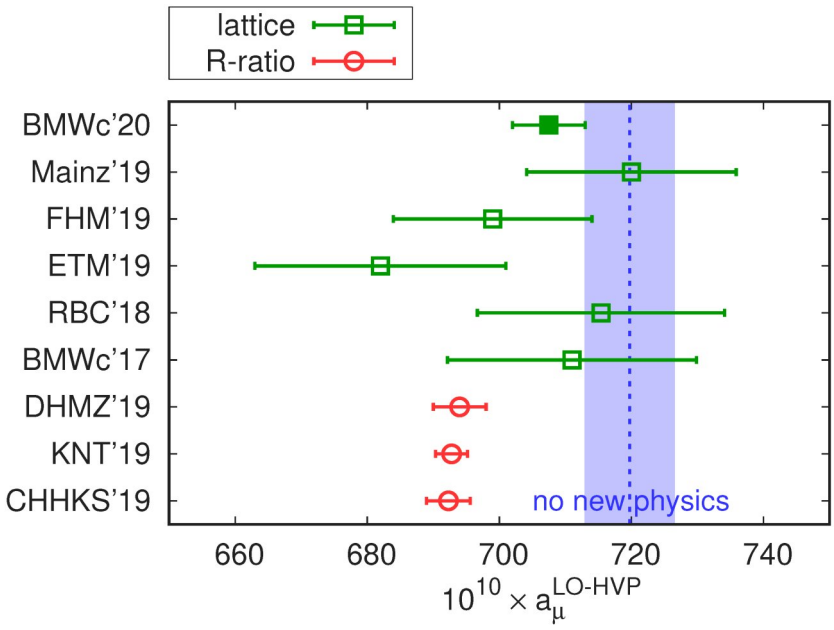

Figure 1: comparison of recent results for the leading-order, hadronic vacuum polarization contribution to the anomalous magnetic moment of the muon. Green squares are lattice results: the result obtained in the current project is denoted by BMWc'20 [2], whereas the result of the first stage of this project is denoted by BMWc'17 [1]. As a comparison, the results of other lattice collaborations are also listed: Mainz Fermilab-HPQCD-MILC and European Twisted Mass, all from 2019, and RIKEN-Brookhaven-Columbia from 2018. Red circles were obtained using the pheonmenology based R-ratio method. The blue shaded region is the value that $a_\mu^{\text{LO-HVP}}$ would have to have to explain the experimental measurement of the magnetic moment, assuming no new physics.

Red circles were obtained using the pheonmenology based R-ratio method. The blue shaded region is the value that $a_\mu^{\text{LO-HVP}}$ would have to have to explain the experimental measurement of the magnetic moment, assuming no new physics.

Key aspects of the computation

To achieve this improvement in precision, we addressed several important problems:

- The largest uncertainty in the first stage result [1] originated from the finite volume correction. In the present accounting period we were able to finish dedicated simulations in order to determine the size of this contribution.
- We reduced the statistical uncertainty of the light connected contribution by applying low mode averaging and increasing the number of configurations.
- For the first time in the literature, we included all leading order QED and strong isospin breaking corrections in our calculations. These are essential in order to reach sub-percent accuracy.
- In order to reach a sub-percent precision the lattice spacing has to be known to a few per-mil accuracy.

The first two of these were carried out in the framework of the "pn68ne: Hadronic corrections to the muon magnetic moment" application, the third using the "pn56bu: Isospin breaking effects in QCD". The computer time for the last ingredient (scale-setting) was provided by PRACE on a supercomputer outside Germany.

The methods developed here will be useful to continue improving the accuracy of the standard model prediction, as will be required to pursue the search for new physics in ongoing and future experiments designed to measure the magnetic moment of the muon.

Finite volume effects

Here we computed the finite size correction that is to be added to our results obtained in a box size with spatial and temporal extents of L_{ref} = 6.272 fm and T_{ref} = 3/2 L_{ref}. We call this the reference box.

In the present grant period we have finished the dedicated runs with the 4HEX action, designed to have small taste violations. One set of runs were performed on 56 × 84 lattices with the reference box size and another set on 96 × 96 lattices with box size L_{big} = T_{big} = 10.752 fm. We call this "big" box, it is much larger than what is used in contemporary lattice field theory simulations.

Using supercomputer resources we measured the $a^{\text{LO-HVP}}$ on these two volumes and for the difference we find:

$$a_\mu(\text{big}) - a_\mu(\text{ref}) = 18.1(2.0)(1.4),$$

where the first error is statistical, the second is systematic, this latter is our estimation for the size of lattice artefacts on this quantity.

The remaining, tiny difference between the big box and the infinite volume, is computed analytically in next-to-next-to- leading-order chiral perturbation theory (XPT). Then the complete finite volume correction, which is to be added to the result obtained in the reference box, is obtained as the sum

$$[a_\mu(\text{big}) - a_\mu(\text{ref})]_{\text{4HEX}} + [a_\mu(\infty) - a_\mu(\text{big})]_{\text{XPT}}$$

for which we find 18.7(2.5), where the error in the brackets is the combined, statistical and systematic, uncertainty of this correction. Compared to our work from the first stage [1] we reduced the uncertainty of the finite size error by more than a factor of five.

Noise reduction

In the present grant period we have finished the evaluation of the current correlator on our ensembles

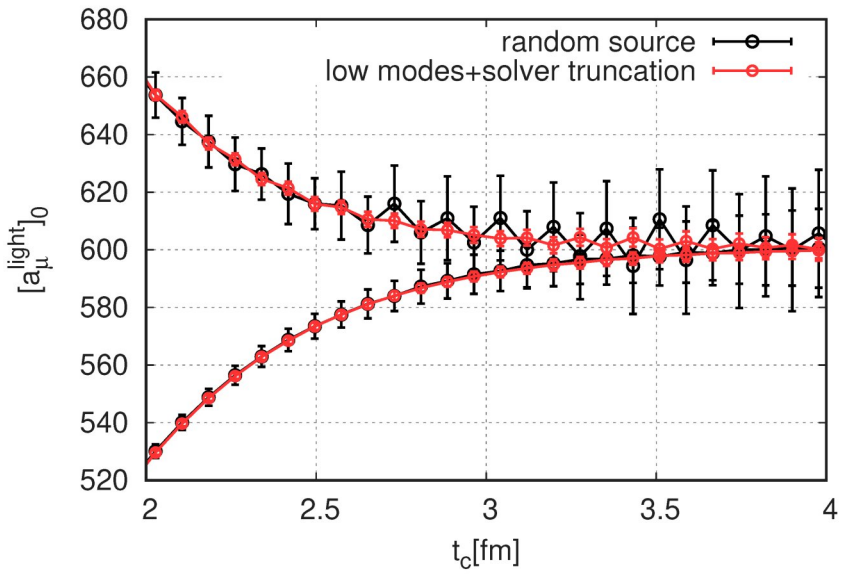

Figure 2: Comparison of the conventional random source based technique, as we applied it in the first stage of this project [1] and the low mode utilizing technique of the second stage [2] for the case of upper and lower bounds on a^{LO-HVP}.

using the noise reduction technique utilizing the low modes of the Dirac operator.

We are projecting out the lowest eigenmodes up to around half the strange quark mass. In the reference of box around 6 fm this means the lowest 1,000 eigenvectors, whereas on the lattice with size around 11 fm the number of modes required is around 6,000. Figure 2 shows a comparison of the conventional random source based technique, as we applied it in the first stage of this project [1] and the low mode utilizing technique of the second stage [2] for the case of upper and lower bounds on a_μ^{LO-HVP}. As a consequence of increasing the number of configurations, and applying the noise reduction techniques, the statistical error on a_μ^{LO-HVP} has reduced by about a factor of three. From 7.5 units obtained in the first stage in [1] to 2.3 units in the second stage [2].

Isospin breaking

Obviously, the most important goal is to reach an accuracy, which is compatible with the expected experimental errors. Only reaching this accuracy guarantees that the experimental findings of several hundred million dollars are fully utilized and only with this accuracy can we decide if and what sort of new physics is there. When we speak about precision a sub-percent error is needed.

Electromagnetic and strong isospin-breaking (IB) effects arise from from

1. the presence of the electromagnetic interaction,
2. the mass difference between up and down quarks.

The most prominent consequence of these effects is the mass difference of the neutron and the proton.

IB effects are on the percent level in general. Thus any reasonable result needs the inclusion of these effects. This is a very hard task. The electromagnetic interaction is weak and long-ranged, whereas the strong interaction is strong and short-ranged. Keeping both of them in a system is more than just challenging.

In our work [2] IB effects are implemented by taking derivatives of QCD+QED expectation values with respect to the bare parameters, electromagnetic coupling and quark mass difference, and computing the resulting observables on isospin-symmetric configurations. The rationale behind this choice is the possibility to optimally distribute the computing resources among the various IB contributions.

IB effects are included in all the observables that enter our analysis: current-current correlators, meson masses needed to fix the physical point, and scale setting. Not only do we account for QED and strong isospin-breaking effects in our results, we also perform a separation of isospin symmetric and isospin breaking contributions. This separation is scheme dependent and requires a convention.

Figure 3 shows the various contributions, whose sum gives the final value a^{LO-HVP}, including examples of the corresponding Feynman diagrams. Solid lines are quarks and curly lines are photons. Gluons are not shown explicitly, and internal quark loops, only if they are attached to photons. Dots represent coordinates in position space, a box indicates the mass insertion relevant for strong-isospin breaking.

The contributions in the first line of the Figure are isospin-symmetric, the other Feynman-diagrams correspond to the isospin-breaking terms. There are three different types electromagnetic IB contributions, depending on whether the photon connects two valence-quark lines, a valence-quark and a sea-quark line or two sea-quark lines. There is also a term representing strong IB effects. Each of the IB terms comes in two varieties: a connected and a disconnected one, the latter refers to contributions, in which there is sea-quark loop involved with single insertion of the external current.

The numbers give our result for each contribution, they correspond to our “reference” system size given by L_{ref} = 6.272 fm spatial and T_{ref} = 9.408 fm temporal lattice extents. We also explicitly compute the finite-size corrections that must be added to these results,

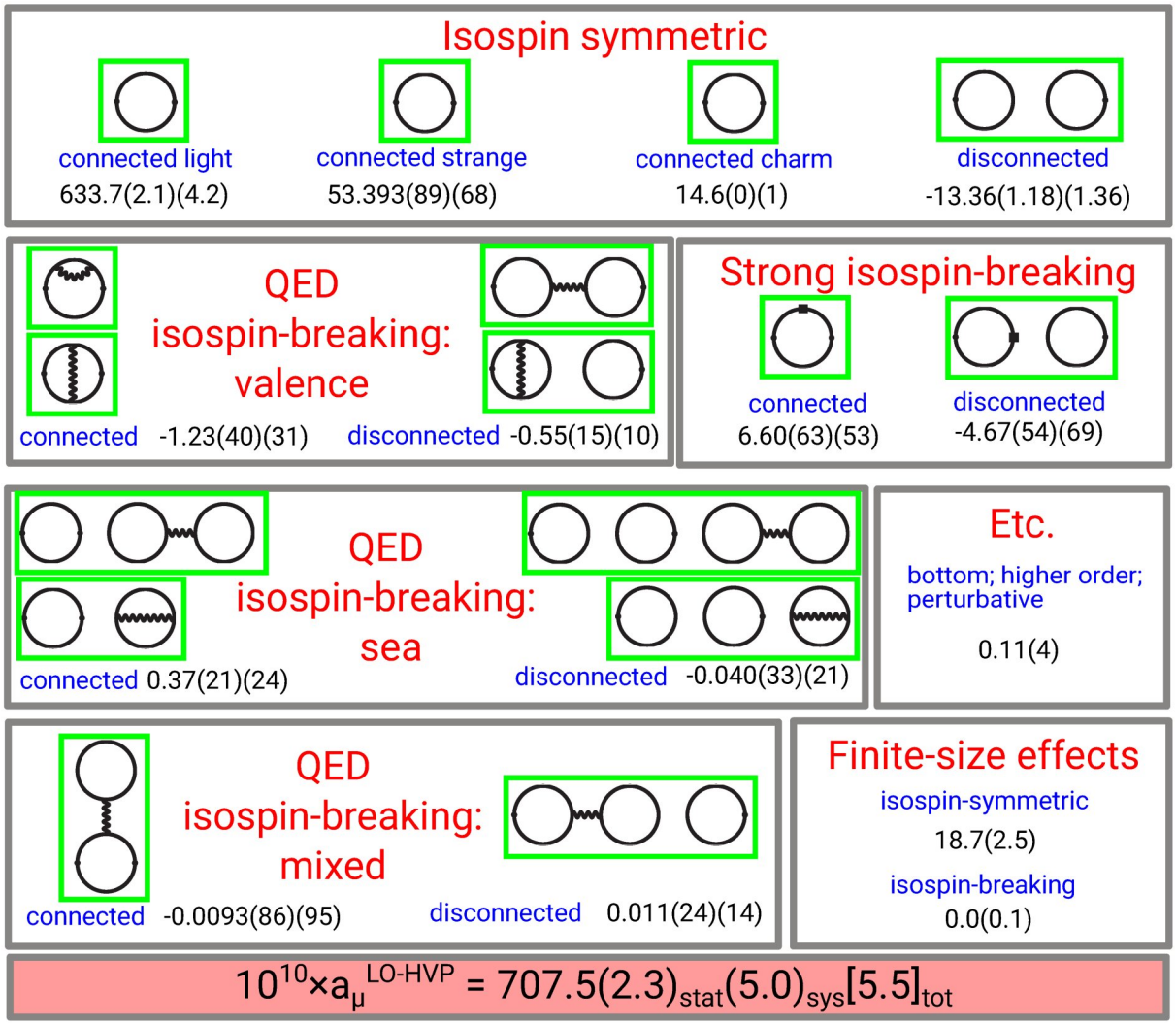

Figure 3: Various contributions, whose sum gives the final value $a^{\text{LO-HVP}}$, including examples of the corresponding Feynman diagrams. Solid lines are quarks and curly lines are photons. Gluons are not shown explicitly, and internal quark loops, only if they are attached to photons. Dots represent coordinates in position space, a box indicates the mass insertion relevant for strong-isospin breaking. The contributions in the first line of the Figure are isospin-symmetric, the other Feynman-diagrams correspond to the isospin-breaking terms. There are three different types electromagnetic IB contributions, depending on whether the photon connects two valence-quark lines, a valence-quark and a sea-quark line or two sea-quark lines. There is also a term representing strong IB effects. Each of the IB terms comes in two varieties: a connected and a disconnected one, the latter refers to contributions, in which there is sea-quark loop involved with single insertion of the external current. The numbers give our result for each contribution, they correspond to our "reference" system size given by Lref = 6.272 fm spatial and Tref = 9.408 fm temporal lattice extents. We also explicitly compute the finite-size corrections that must be added to these results, these are given separately in the lower right panel. The first error is the statistical and the second is the systematic uncertainty; except for the contributions where only a single, total error is given.

these are given separately in the lower right panel. The first error is the statistical and the second is the systematic uncertainty; except for the contributions where only a single, total error is given.

Ongoing Research / Outlook

Interestingly our computation, Equation (1), disagrees with previous phenomenology results, while it seems to require no new physics to explain the magnetic moment of the muon, which is in contrast with earlier belief. This discrepancy between our result and previous determinations were intensively discussed at many conferences, workshops and round tables.

The current status has been pointedly summed up by Nobel Prize Laureate Frank Wilczek at the Lattice conference, in July 2021: "The theoretical community is going to have to get its act together in coming years, to see which is correct, [the phenomenological or our lattice result], if either."

Let us also cite here Edward Witten, another prominent theoretical physicist, from the December 2021 edition of the CERN Courier magazine: "I think it is very important to improve the lattice gauge theory estimates of the hadronic contribution to the muon moment, in order to clarify whether the fantastically precise measurements that are now available are really in disagreement with the SM."

To this end we started to improve our previous lattice QCD determination in [2]. In the current grant period of pn56bu, we took the first steps to move the IB computations towards finer lattices.

References and Links

[1] Borsanyi et al, Phys.Rev.Lett. 121. (2018) 2.
[2] Borsanyi et al, Nature 593 (2021) 7857, 51-55.
[3] Muon g-2 Collaboration, Phys.Rev.Lett. 126 (2021) 14.

Life Sciences

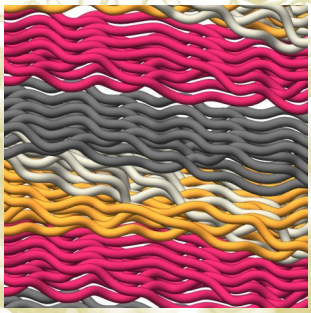

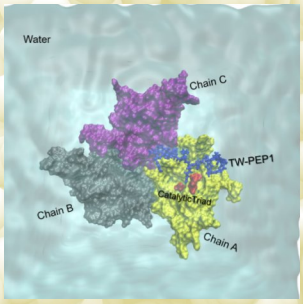

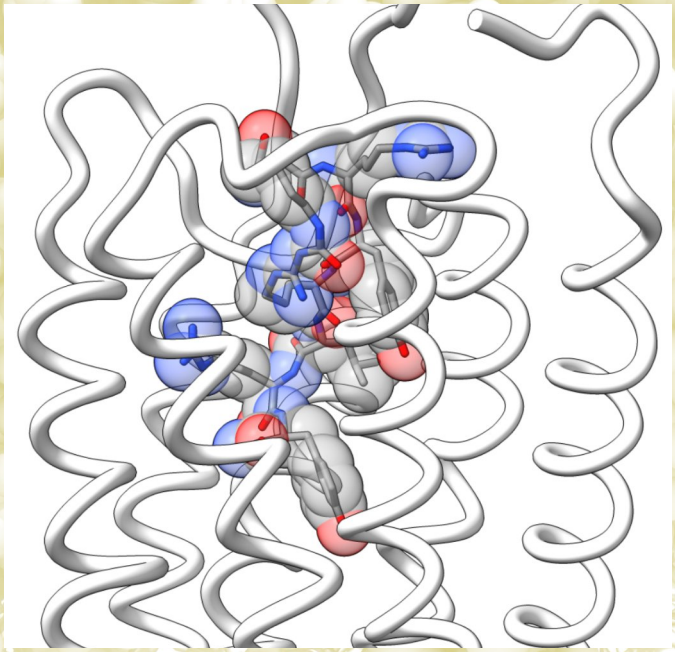

ParBigMen: ParSMURF application to Big genomic and epigenomic data

Research Institution
[1]AnacletoLab – Dipartimento di Informatica, Università degli Studi di Milano

Principal Investigator
Alessandro Petrini[1], Giorgio Valentini[1]

Researchers
Tiziana Castrignanò[2], Peter Robinson[3], Marco Frasca[1], Elena Casiraghi[1], Sara Bonfitto[1]

Project Partners
[2]Department of Ecological and Biological Sciences (DEB) - Università della Tuscia
[3]The Jackson Laboratory for Genomic Medicine, Farmington

SuperMUC Project ID: pn29lu (Prace project no. 2020225452)

Introduction

Variant identification and analysis of Next-Generation Sequencing (NGS) data play a central role in Genomic and Personalized Medicine. In this context, disease-associated variants occurring in protein-coding areas of the DNA are well studied, but the understanding of the impact of variants occurring in the non-coding regions of the genome is for most part incomplete. However, the scientific community shifted its attention towards the understanding of the latter regions, as several recent studies state that most of the potential pathogenic and deleterious variants do not lie in the coding areas of the genome. We contributed to this emerging field of Genomic Medicine by developing machine learning tools for the detection of pathogenic and deleterious variants in the non-coding genome. This task has been proven to be particularly challenging for several reasons, most of which are related with the sparsity of pathogenic mutations which are outnumbered by neutral variants: when tackled with an automated learning approach, this ultimately translates to a high unbalance between classes of examples to be learned, leading to a very challenging classification problem. With HyperSMURF [1] and ParSMURF [2] we proposed two state-of-the-art Machine Learning solutions for dealing with such ill-posed datasets; in particular, HyperSMURF is the evolution of ReMM (Regulatory Mendelian Mutation), the Machine Learning core of Genomiser [3] used for the diagnosis and discovery of genetic variants causative of Mendelian disorders. The main objective of this project is to improve the results obtained so far for providing the scientific community with ever more reliable means for the prioritization of variants associated with Mendelian diseases. The core idea of the project is to improve the prediction performance of the base classifier by using a largely expanded dataset. This improvement of data coverage is done by i) adding new epigenomic features with data from publicly available repositories for increasing the characterization of each sample, and ii) adding newly discovered deleterious and pathogenic samples. However, this increase of data cardinality, along with the high complexity of ParSMURF and the fine tuning of its learning parameters, comes with an increase of computational costs, making this project feasible only on a Tier-0 supercomputing facility. To summarize, the goals of *ParBigMen* are:

1) the release of a new highly parallel version of ParSMURF (called ParSMURF-NG) able to scale with big data and to fully exploit the High-Performance Computing architectures for relevant prediction problems in the context of Personalized and Precision Medicine.
2) the application ParSMURF-NG to big omics data, where many features will be investigated and used to predict pathogenic variants.
3) the evaluation and release of new ReMM scores to the entire scientific community for the prioritization of pathogenic and deleterious SNVs.

	AUROC	AUPRC
Baseline dataset	0.99361	0.34270
New dataset	0.99393	0.42410

Table 1: Comparison of the classifier performance in AUROC and AUPRC when trained with the original and the improved dataset using ParSMURF-NG.

Results and Methods

The main tool developed for this project is ParSMURF-NG. It was specifically developed to improve the scalability and computational efficiency of ParSMURF, thus meeting the computational demand required by *ParBigMen*.

Its scalability and efficiency have been evaluated on three supercomputing systems (Marconi KNL and SKL of Cineca, HLRS Apollo HAWK of HPC Center Stuttgart and SuperMUC-NG) reaching >70% of efficiency even with 128 computing nodes (up to 32k computing cores on Marconi KNL). Fig. 1 reports the strong scaling speed-up and efficiency of ParSMURF-NG on a benchmark dataset of 30M samples and 50 features, also comparing its performance on the three

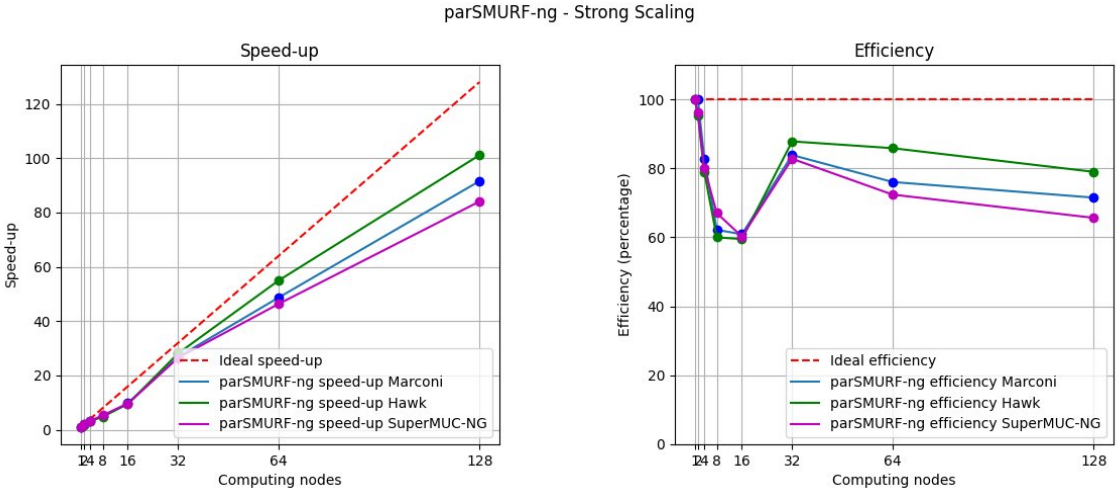

Figure 1: Speed up and efficiency of ParSMURF-NG on Marconi KNL, Apollo HAWK and SuperMUC-NG supercomputing systems, when measured on a strong scaling setup-up over a synthetic dataset.

systems. Although showing a slightly lower speed-up compared to Marconi and Hawk, SuperMUC-NG excelled in the overall execution time, being twice faster than Marconi and approximately four times than Hawk.

ParSMURF-NG is entirely programmed in C++ and is highly optimized for CPUs featuring a high core count such as Intel Xeon Phi processors. All inter-process communication is managed through calls to the MPI library; access to the filesystem is managed in the same way to properly exploit both the shared file system and the high-speed intercommunication infrastructure of contemporary HPC systems. As such, we measured that a pool of 128 ParSMURF-NG processes distributed on 128 nodes of SuperMUC-NG can read the input dataset at a rate of 500 MB/s each. ParSMURF-NG is distributed as source code and is publicly available at [4].

To predict the pathogenicity of genomic variants we trained the classifier of ParSMURF-NG with a dataset consisting of 14 million variants characterized with 26 heterogeneous features. Of all these variants, only 406 are associated with known Mendelian diseases. This dataset has been used in [3] for evaluating the ReMM scores and in *ParBigMen* represents the baseline for comparison.

To provide a more informative dataset to the classifier of ParSMURF-NG we expanded this dataset by adding 80 new pathogenic variants and by characterizing each variant with new epigenomic features extracted from the International Human Epigenomic Consortium data portal. We created more than 500 new features, hence greatly increasing the size of the dataset.

We applied several feature selection strategies to narrow down the number of significant features for this problem: in particular, we considered several classic indexes used for evaluating correlation (Spearman and Pearson correlation coefficient), independence of distribution (Mann-Whitney and Kruskal-Wallis) as well as multivariate methods (MRMR) and a wrapper method (ParSMURF-NG feature importance).

After selecting the set of most significant features, we used SuperMUC-NG for the highly computing intensive operation of finding the set of best learning hyper-parameters of ParSMURF-NG. This model selection task is crucial to properly train a classifier so that it can deliver reliable predictions.

Specifically, in *ParBigMen*, for each combination of the selected features we exhaustively explored a search space of 1,440 configurations. ParSMURF-NG distributed the computation across 2,560 nodes of SuperMUC-NG, delivering the set of best hyper-parameters in less than 12 hours. We estimated that each model selection task performed on a single machine would have taken almost two years to deliver the same results.

Ongoing Research / Outlook

Thanks to the computational power of the SuperMUC-NG system, we managed to find the minimal set of genomic features and the set of best learning hyper-parameters in a feasible amount of time. As briefly reported in Table 1, we increased the performance of the classifier in predicting pathogenic and deleterious variants, by selecting a novel set of epigenomic and conservation features and by finely tuning the hyper-parameteres of our highly parallelized algorithm.

Given the promising results obtained in *ParBigMen*, we plan to expand the experimental set-up by including new highly parallelized methods for multi-variate feature selection and by possibly exploring novel variant features to achieve novel insights into candidate pathogenic variants associated with Mendelian diseases.

References and Links

[1] Schubach M., Re M., Robinson P.N., Valentini G., Scientific Reports 2017;7(1):2959.
[2] Petrini A. et al., GigaScience, vol. 9, 05 2020.
[3] Smedley D. et al., The American Journal of Human Genetics 2016 sep;99(3):595–606.
[4] ParSMURF-NG on AnacletoLab GitHub page: https://github.com/AnacletoLAB/parSMURF-NG

(Bond-)Breaking news: Mechanoradicals in Collagen

Research Institution
[1]Heidelberg Institute for Theoretical Studies
[2]Interdisciplinary Center for Scientific Computing, Heidelberg University

Principal Investigator
Frauke Gräter[1,2]

Researcher
Benedikt Rennekamp[1,2]

Project Partners
–

SuperMUC Project ID: pn34ci

Introduction

Many tissues in our bodies are exposed to mechanical loads. These tendons and many other force-bearing materials, such as bones and skin, consist largely of the structural protein collagen. For instance, imagine your Achilles tendon. It is made of collagen, the virtual rubber band in your body. It is often under extreme pressure, for example, while you play sports or walk, when the Achilles tendon can experience multiple times your body's own weight in pressure. We recently found that excessive mechanical load can lead to covalent bond scissions inside the fibrils, even before macroscopic failure occurs. After a (homolytic) bond breakage, i.e. having an unpaired electron on each fragment side, highly reactive radicals are created in collagen [1,2]. Despite the importance of collagen mechanics and damage, the details of the stress distribution in collagen under load and rupture events at atomistic scale are currently largely unknown.

A major bottleneck in examining the structural changes of collagen under load had been that only low-resolution structures of larger collagen fibril assemblies are available and Molecular Dynamics (MD) simulations have therefore been restricted to small models, which lack many of the important structural features. In this project, we embarked on realistic multi-million atom MD simulations of collagen using the required atomistic structures, which we built in our group and incorporate all structural knowledge available to date. As an intermediate result, we validated representative model sets (from different collagen species and with a set of crosslink types) during this project. This led to the publication of our Webserver ColBuilder [3] as will be discussed below.

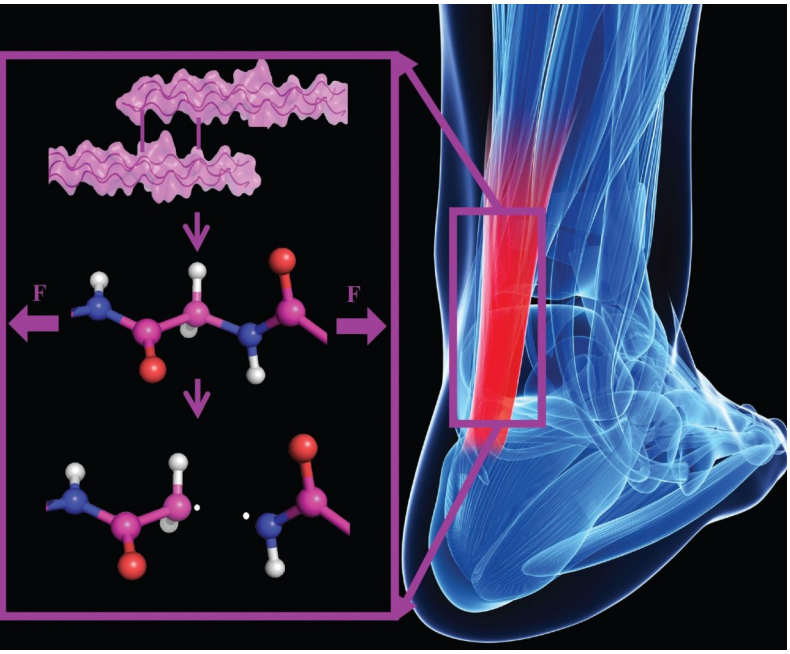

Figure 1: Forces in proteins, as in the displayed Achilles tendon, can lead to bond ruptures inside the molecule. These breakages, which can occur while the whole fibril is still intact, give rise to highly reactive radicals. (Photo credit - for the right part: istockphoto.com/SciePro).

Furthermore, we aim to reveal the molecular basis of mechanical features of collagen by employing steered MD simulations in GROMACS. However, in regular MD simulations, covalent bonds are predefined, and chemical reactions cannot occur. We previously developed a new simulation scheme called KIMMDY (**Ki**netic **M**onte Carlo / **M**olecular **Dy**namics) [4] that can alleviate these issues via a hybrid combination of different simulation methods. Using this technique, we analyzed first rupture sites and found that covalent crosslinks are a potential weak link in the hierarchical collagen structure. The subsequently created radical species could potentially act in signaling processes by converting mechanical forces into oxidative stress. Intriguingly, our determined rupture sites very much overlap with certain amino acids in collagen that can act as a radical sponge.

Results and Methods

Collagen modeling: Simulations of large-scale fibrils with different crosslinks and from different species
Basis of our atomistic simulations is a collagen model that was developed by A. Obarska-Kosinska at HITS and first described in [2]. It integrates a low-resolution structure of collagen with high-resolution structures of short collagen-like peptides from different experimental techniques, respectively. In collagen, 300nm long molecules wind up to large fibril in a distinct pattern. The individual molecules are covalently connected with chemical crosslinks, for which different

Figure 2: Exemplary atomistic model of a Collagen type 1 fibril fragment as obtained from ColBuilder. It comprises 41 triple helices spanning one central overlap and one gap region (in two parts, left and right). Triple helices are colored according to the staggering distance, crosslinks are shown in blue. The regions around these covalent connections turn out to be mechanical weak points in our simulations.

chemistries are known. We modelled collagen fibrils for different species (i.e. different sequences) and crosslink types. An example model is shown in Figure 2. We validated a set of models in equilibrium MD simulations (3 species, each with 2 crosslink types), for which we conducted two 100ns production runs each leading to a total simulation time of 1,200ns on SuperMUC-NG.

Taken together, the atomistic collagen models dynamically explore a conformational space that is close to the x-ray fiber diffraction data and also in line with other experimental observations (gap/overlap ratio and heavy-atom labeling).

This project, combined with the modeling from previous work, led to the publication of the webserver ColBuilder [3]. The repository of collagen models is available at [5]. We expect the repository to facilitate the structural investigation of a wide range of collagen aspects, such as molecular interactions with other proteins, localization of other crosslinks, disease mutants, or others. In the future, we will update — and invite the community to contribute to — the repository with new models and force fields.

Where does collagen break?
Having the overarching question of collagen mechanoradicals in mind, a decisive point is to determine the sites of first breakages. We have conducted steered MD simulations at a constant force for collagen models from three different species, with different crosslink positions, and for different types of loading, as it likely occurs under physiological conditions. The system sizes were in the order of 2-3 million atoms, a size required due to the sparse distribution of crosslinks along the fiber axis, which are important to stabilize the structure. For these large systems, we used on average 768 cores per simulation (amounting to 1,536 logical cores / threads) on SuperMUC-NG. Depending on the system used, this was adjusted to achieve comparable scaling efficiencies. In each instance, the collagen fibrils were pulled for 100ns before executing our simulation scheme of bond rupture as described below. All models and their replica taken together yield a combined total simulation time of more than 6.8 µs in this project.

In these large-scale simulations, we examined the most preferred rupture points by combining Molecular Dynamics (MD) simulations with Kinetic Monte Carlo (KMC) steps, a method we dubbed KIMMDY [4]. This hybrid scheme utilizes all-atom simulation information as input for a Kinetic Monte Carlo step, and in this way can bridge the time scales of MD simulations (microseconds here) and those of the involved chemistry (milliseconds to seconds under force). Qualitatively robust to parameter improvements that we achieved during this project, one finding always remained in our analysis: crosslinked areas are relatively more prone to rupture. As stated above, the crosslinks covalently connect the triple helices in collagen and are, following our analysis, mechanical weak points where stress concentrates. Coming back to our introductory example, one could call these weakest links the “Achilles tendon” of our tendons. The results have direct implications for collagen’s role as radical sponge to prevent further damage of the tendon from mechanoradicals [2]. Intriguingly, redox-active amino acids very much overlap with our determined first rupture sites, giving collagen the means to buffer arising oxidative stress.

Ongoing Research / Outlook

We furthermore started a project on how the crosslink type influences the rupture mechanics. In particular, we look into trivalent crosslinks that connect to two strands of the triple helix in contrast to the previously used divalent crosslinks. These trivalent crosslinks, also known as mature crosslinks, are more common in older collagen and could be a reason for altered mechanics with age.

We expect that the publication based on the aggregated results achieved through usage of SuperMUC will have a large impact for the protein simulation community on the one hand due to the novel scale bridging approach we use, and for the large collagen community on the other hand, given the critical role of collagen tissue in health and disease.

References and Links

[1] https://www.h-its.org/projects/mechanoradicals-in-collagen/
[2] Zapp et al., Nat. Commun. 11, 2315 (2020).
[3] Obarska-Kosinska et al, Biophys. J. 120, 3544–3549, (2021).
[4] Rennekamp et al, J. Chem. Theory Comput. (2020), 16, 1, 553–563.
[5] https://colbuilder.h-its.org

Structure and Dynamics on the Photosynthetic Complex I

Research Institution
Department of Chemistry, Technical University of Munich

Principal Investigator
Ville R. I. Kaila

Researchers
Patricia Saura, Max E. Mühlbauer, Michael Röpke, Hyunho Kim, Ana P. Gamiz-Hernandez

Project Partners
–

SuperMUC Project ID: pn34he

Introduction

Energy conversion in nature is powered by membrane-bound proteins that transform light and chemical energy into an electrochemical gradient across the membrane. These processes are catalyzed by enzymes that transfer electrons and protons across large molecular distances by mechanistic principles that remain poorly understood [1,2]. In this project, we studied key enzymes from the complexes I superfamily that function as redox-driven proton pumps in respiratory and photosynthetic energy conversion [2]. The project had an emphasis on the photosynthetic complex I (Ndh1), the related membrane bound hydrogenases (Mbh), as well the mammalian isoforms of complex I (CI). These systems share common antiporter-like subunits that enable long-range proton pumping across the membrane domain via hydration changes, electrostatic effects, and conformational transitions [2-5]. Of special interest was to unravel how the proton transfer reactions couple to the reduction of quinone (in Ndh1 and CI) or the NiFe-center (in the primordial Mbh isoform).

The cyanobacterial Ndh1 complex (Fig. 1A) has evolved special adaptations that allow it to participate in both respiratory and photosynthetic energy conversion [2]. Ndh1 catalyzes electron transfer from ferredoxin (Fd) to plastoquinone (PQ), and transduces the free energy to pump protons across thylakoid membranes. Remarkably, the Ndh-1MS isoform is utilized for inorganic carbon concentration of CO_2, providing a basis for synthesis of biomass. The latter process takes place in the CupA/S subunits with carbonic anhydrase (CA) activity (Fig. 1D).

The membrane-bound hydrogenase (Mbh) (Fig. 1B) is a redox-driven Na^+/H^+ transporter, that reduces protons to hydrogen gas (H_2) and enables H^+ pumping and Na^+/H^+ exchange across cytoplasmic membranes in archaea. The enzyme comprises a hydrophilic domain, similar to that of Ndh1, while the membrane domain of Mbh drives the H^+ transport and Na^+/H^+ exchange (Fig. 1E). Mbh is a predecessor of the modern CIs, which catalyzes NADH- or Fd-driven quinone (Q) reduction and couples this much larger driving force to proton pumping across the membrane domain [2].

The respiratory complex I (CI) initiates cellular respiration in mitochondrial inner membranes. The intricate mammalian isoforms comprise 14 catalytic core subunits, responsible for coupled electron transfer and proton pumping. These subunits can be surrounded by up to 31 supernumerary subunits with possible relevance for activity and assembly (Fig 1C). The long-range, ca. 300 Å, proton-coupled electron transfer (PCET) process is initiated by electron transfer from NADH to ubiquinone (Q_{10}) via a chain of iron-sulfur centers (FeS). Similar as for Ndh1 and Mbh, this couples this to proton transfer in the antiporter-like subunits of the membrane domain (Fig. 1F) [5]. To gain insight in how these fascinating systems work, we performed large-scale quantum and classical molecular simulations in combination with cryo-electron microscopy (cryo-EM) studies, and biochemical experiments [2-5].

Results and Methods

Our work on these related systems (Fig. 1) resulted in three publications, published in the *Journal of the American Chemical Society* and *Nature Communications* [3-5]. To probe the dynamics of these enzymes during catalysis, we performed atomistic molecular dynamics (MD) simulations on the experimentally resolved structures of Ndh1, Mbh, and CI, that we embedded in lipid membranes, and solvated with water and ions to represent their physiological environment. The models comprise 0.5–1 Mio atoms that we simulated at 310 K and 1 bar pressure within an *NPT* ensemble, using an integration time step of 2 fs, periodic boundary conditions, and long-range electrostatic interactions treated by the particle mesh Ewald

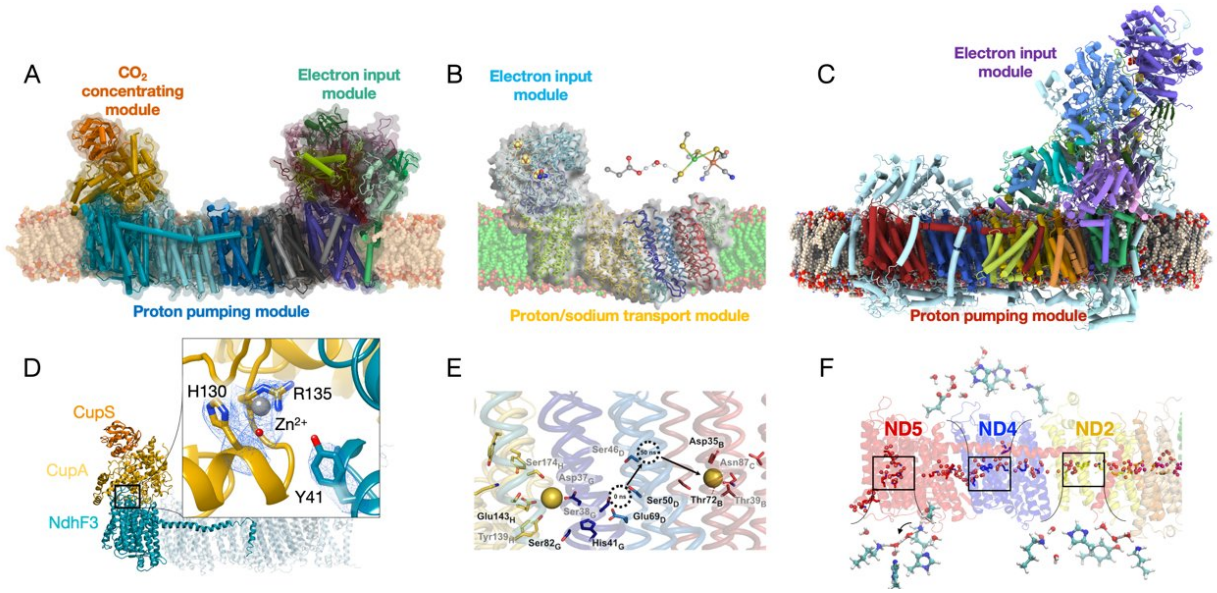

Figure 1: Structure of simulated Complex I systems in this project. A) The photosynthetic Ndh-1MS complex features two soluble domains that catalyze electron transfer (*right*) and carbon concentration (*left*), and a membrane domain that is responsible for proton pumping. B) Mbh consists of a hydrophilic domain responsible for electron transfer and H_2 production, and a membrane domain driving proton transport Na^+/H^+ exchange. *Inset*: the catalytically active NiFe center explored by DFT calculations. C) Structure of the mitochondrial complex I. Electron transfer from NADH to Q couples to proton pumping across the membrane. D) Structure of the carbon-concentration module in CupA/S subunits that associate with the membrane subunit NdhF3. The catalytic site contains Zn^{2+} responsible for carbonic-anhydrase activity according to calculations. E) Sodium transport pathway based on atomistic MD simulations in the membrane domain of Mbh. F) Hydration structure and proton transfer pathways in the antiporter-like subunits of the mitochondrial complex I. The figures are adapted from [2-5].

(PME) approach. All MD simulations were performed with the NAMD program package [6]. To probe the catalytic principles, we also applied quantum chemical DFT and hybrid quantum/classical (QM/MM) calculations. The DFT calculations were performed using the TURBOMOLE program, coupled to QM/MM using a python interface to CHARMM [7].

To understand the molecular principles of the carbon concentration process catalyzed by Ndh1, we resolved the molecular structure of the Ndh-1MS isoform by cryo-EM, and investigated its function by our multi-scale simulation approach in collaboration with Dr. Schuller (Marburg University) and Prof. Nowaczyk (Ruhr-University Bochum). Our findings suggest that Ndh-1MS employs a non-polar cavity in its membrane subunit NdhF3 to concentrate CO_2 around the specialized CupA/S module that has a novel fold. (Fig. 1D). Our calculations suggest that CupA/S converts CO_2 into HCO_3^- in its Zn^{2+}-catalytic site with similar energetics as in canonical CAs (Fig. 1D). We also observed a conserved axis of buried ion-pairs in the membrane domain that could mediate the driving force from the (plasto)quinone reduction to power the CO_2 concentration. These findings show modular adaptations of CI machinery allow cyanobacteria to survive under low CO_2 conditions [3].

For Mbh, we identified conserved water-mediated proton pathways leading across the membrane and to the active site. Our MD simulations showed how conformational changes in a buried ion-pair lead to pKa shifts at the interface between the proton-pumping and sodium-transporting subunit, establishing an electrostatic switch [4]. The simulations also revealed three putative Na^+ binding sites, which could be important for the Na^+/H^+ transport activity, and to understand how the enzyme establishes sodium pathways across the membrane (Fig. 1E).

To obtain complementary information for Ndh1 and Mbh, we also studied the hydration dynamics and proton transfer energetics in the highly intricate mammalian respiratory complex I (Fig. 1C) using a multi-scale approach. Our simulations suggest that the mammalian CI undergoes extensive hydration dynamics that establishes water arrays across the membrane domain and enable proton transfer reactions on a microsecond timescale. The hydration dynamics is modulated by the protonation reactions themselves, whereas the conformations of buried ion-pairs were found to tune the proton transfer barriers along the hydrophilic axis (Fig. 1F) [5].

Our combined findings from this project provide insight into key conserved coupling principles within the complex I superfamily and detailed functional insight into archaeal energy transduction mechanisms.

Ongoing Research / Outlook

The computational resources provided by this SuperMuc project allowed to unravel the molecular basis of key enzymes responsible for biological energy conversion [1-5]. Ongoing work focuses on understanding how electrons are injected into Ndh1 and Mbh based on our multi-scale simulation approach. Our future work will further investigate how these redox-linked processes are coupled to the proton pumping across the membrane domain.

References and Links

[1] http://villekaila.com
[2] V. R. I. Kaila, M. Wikström, Nat. Rev. Microbiol. 19, 319–330 (2021).
[3] J. M. Schuller et al., Nat. Commun. 11, 494 (2020).
[4] M. E. Mühlbauer, et al., J. Am. Chem. Soc. 143, 20873-20883 (2021).
[5] M. Röpke et al., J. Am. Chem. Soc. 142, 21758-21766 (2020).
[6] J. C. Phillips et al., J. Chem. Phys. 153, 044130 (2020).
[7] S. Riahi, C. N. Rowley, J. Comput. Chem. 35, 2076– 2086 (2014).

Supramolecular inhibition of the enzymatic activity of HTRA1

Research Institution
[1]Computational Biochemistry, Center of Medical Biotechnology, University of Duisburg-Essen
[2]Microbiology, Center of Medical Biotechnology, University of Duisburg-Essen

Principal Investigators
Michael Ehrmann[2], Elsa Sanchez-Garcia[1]

Researchers
Julio Cesar Vieyto-Nuñez[1], Joel Mieres-Perez[1]

Project Partners
–

SuperMUC Project ID: pn68da

Introduction

HtrAs (High-temperature requirement A) serine proteases are complex molecular machines that play important roles in protein quality control. HTRA1, a human serine protease of the HtrA family, is an important target for drug development as it is involved in cancer, arthritis, Alzheimer's disease, macular degeneration and cerebral ischemic disease, among other disorders. Therefore, growing efforts are being devoted to the development of inhibitors of HTRA1.

Klärner and Schrader introduced molecular tweezers, synthetic molecules that bind specifically to lysine and arginine residues via hydrophobic and electrostatic interactions [1]. The archetypical molecular tweezer CLR01, which features hydrogen phosphate groups at its periphery (Figure 1, left), is a regulator of protein – protein interactions which also displays anti-amyloid and antiviral activity. On the other hand, peptides containing recognition sequences can be used to regulate protein function. Preliminary experimental results by the Ehrmann's group at the University of Duisburg-Essen showed differences in the activation effect on HTRA1 between peptide fragments (here called PEPs: PEP1 and PEP2) and tweezer derivatives with these peptides as substituents (TW-PEPs: TW-PEP1 and TW-PEP2, Figure 1, right). Motivated by the experimental results, we investigated at the molecular level the binding of PEPs and TW-PEPs to HTRA1. We also investigated the effect of these supramolecular ligands on the structural properties of the serine protease.

Results and Methods

We investigated the dynamics of HTRA1 as well as the binding modes of the peptide (PEPs) and tweezers-peptide (TW-PEPs) ligands to the monomeric and the trimeric structures of HTRA1. To this end, we carried out Gaussian accelerated Molecular Dynamics (GaMD) [2] simulations, using the NAMD package [3]. We performed three replicas of the simulations (3 x 200 ns) for each setup (including control systems with the protein without ligand) for a combined sampling time of approximately 15 µs. The size of the systems, including explicit water molecules as solvent,

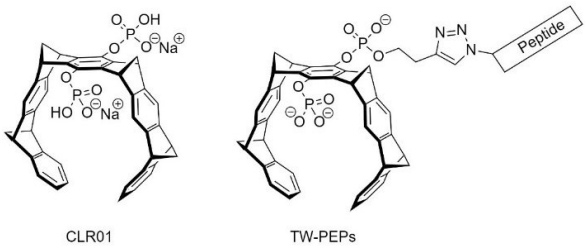

Figure 1: Supramolecular tweezer CLR01 (left). General representation of asymmetric molecular tweezer derivatives with specific peptide sequences as substituents (right).

comprises 60,000 to 112,000 atoms (Figure 2A). The jobs were run for a maximum of 48 h each time, using 1,152 or 2,304 cores depending on the size of the system.

HTRA1 dynamics
The loops LD, L1, L2, and L3 are critical for activating the protease domain of HTRA1 [4] (Figure 2B). Our simulations revealed larger structural variations in these loops in the presence of PEPs and TW-PEPs with respect to the protein alone. L3 showed the highest fluctuations compared to LD, L1, and L2. In addition, representative structures from the simulations indicated that the HTRA1/TW-PEPs complexes displayed the largest structural differences with respect to the experimental X-ray structure of HTRA1 (PDB ID: 3NZI) without ligand. This is important because it is known that the rearrangement of L3 induces the remodeling of the protein [4]. Therefore, the binding of TW-PEPs to HTRA1 could result in the deactivation of the protease domain by favoring the transition to an inactive conformation.

Binding modes of PEPs and TW-PEPs to HTRA1
The activity of HTRA1 is suggested to be regulated by allosteric remodeling [5]. However, the precise activation mechanism is still not fully understood. To provide insights into that mechanism, we studied the binding modes of the ligands that could trigger the allosteric regulation of the activity of the enzyme.

Our results showed that, in the case of TW-PEPs, the hydrogen bond interactions between peptide

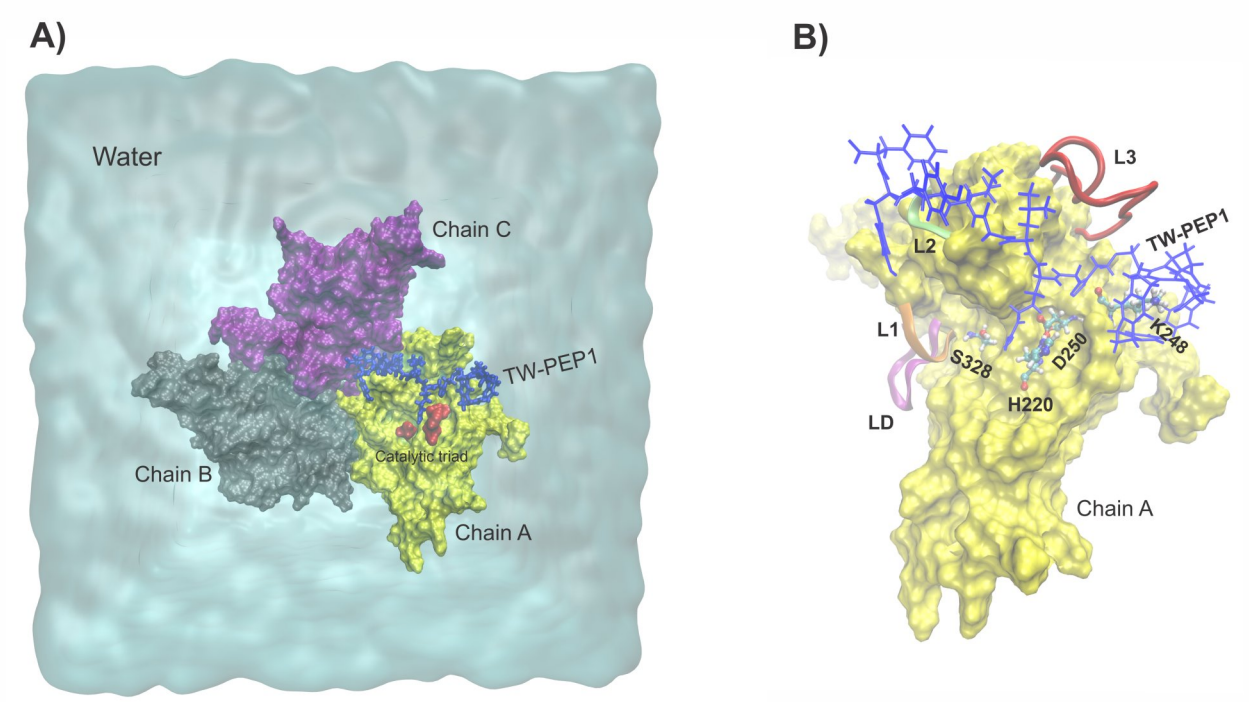

Figure 2: A) Representation of one of the systems under study: HTRA1 trimer, TW-PEP1, explicit water as solvent. B) Favored binding mode of TW-PEP1 (in blue line representation). The loops LD, L1, L2 and L3 are colored in purple, orange, lime and red, respectively. The catalytic residues (H220, D250, S328) and K248 are highlighted in balls and sticks representation.

segments and the residues H220 and D250, which are part of the catalytic triad of HTRA1, are established more frequently compared to the corresponding peptides without tweezers. In contrast, the interactions between catalytic residues (H220 – D250) are less frequent in the presence of TW-PEPs, suggesting the deactivation of the catalytic site.

Based on their proximity to the catalytic domain in the HTRA1 trimeric structure, we selected the residues R190, R227, K248, and K346 as targets for the molecular tweezers. We identified the binding mode associated to K248 as the most promising one based on the high preservation of the inclusion complex with the molecular tweezer (Figure 2B). In this position, one of the residues from the peptide motif in TW-PEPs directly interacts with the catalytic triad (S328, H220, D250), which can negatively affect the enzymatic activity. Digestion experiments by Ehrmann and co-workers demonstrated that the K248A mutant kept the WT inhibitory effect when binding to the TW-PEP1 ligand (unpublished data). Therefore, to gain insight into the tweezers' binding to the alanine mutated HTRA1, we performed additional GaMD simulations of the mutant. We found that, in the K248A mutant, the molecular tweezer binds residue K305 located in the loop L3. This loop is away from the catalytic site and the peptide substituent of the tweezer is mostly involved in intramolecular interactions.

In conclusion, the analysis of our simulations indicates that TW-PEPs have the potential to modulate the catalytic activity of HTRA1 by influencing key structural motifs of the serine protease. The conformation of the loop L3, which plays a crucial role in the catalytic activity of HTRA1, is affected by the binding of TW-PEPs to the protein. In addition, hydrogen bond interactions between the peptide groups of TW-PEPs and the protein may be effective at deactivating the catalytic site of HTRA1. The interactions between the peptide motifs of TW-PEPs and the catalytic site are enhanced in comparison to when only the peptides are used. Moreover, we also observed less frequent interactions between the residues of the catalytic site in the HTRA1/TW-PEPs complexes. We expect that the results of this work will help to unravel the complex inhibition mechanism of HTRA1.

Ongoing Research / Outlook

The resources provided by the SuperMUC-NG infrastructure were crucial to generate the current data and results. This is an ongoing project. Currently, we are performing simulations to estimate the binding free energies of the molecular tweezers to lysine and arginine residues of HTRA1. In addition, we plan to explore alternative binding sites in follow-up projects. We expect that our results will also contribute to the design of new inhibitors of HTRA1.

References and Links

[1] Fokkens M. et al. J. Am. Chem. Soc.127 (2005) 14415–14421.
[2] Pang Y. T. et al. J. Chem. Theory Comput.13 (2017) 9–19.
[3] Philips J.C. et al., J. Chem. Phys. 153 (2020) 044130.
[4] Truebestein L. et al. Nat. Struct. Mol. Biol. 18 (2011) 386–388.
[5] Cabrera A.C. et al. Sci. Rep. 7, (2017),14804.

Simulating Blood Flow in the Virtual Human

Research Institution
[1]Leibniz Supercomputing Centre

Principal Investigator
Dieter Kranzlmüller[1]

Researchers
Alexander Patronis[2], Brian Wylie[2], Thomas Odaker[1], Markus Wiedemann[1], Jon McCullough[4], Peter Coveney[4], Ioannis Zacharoudiou[4], Alfonso Santiago[5], Mariano Vazquez[5], Miguel Zavala[6]

Project Partners
[2]Jülich Supercomputing Centre, [3]University College London, [4]Barcelona Supercomputing Centre, [5]KTH Royal Institute of Technology

SuperMUC Project ID: pn72qu (Gauss Large Scale project)

Introduction

This Large Scale Project was awarded 40 million core-hours and has been focused on the realisation of studying systemic 3D blood flow at full-human scale. To achieve this we have utilised the lattice Boltzmann fluid flow solver HemeLB [1] to conduct simulations within vascular geometries generated from full-scale MRI data. A key feature of this work was that two instances of HemeLB were coupled together to allow arterial and venous flow to be simulated simultaneously.

This work demands the extensive computational resources of a machine like SuperMUC-NG to not only conduct simulations within an acceptable timeframe but also to generate and store the necessary input and output data. At the largest scale of a geometry consisting of multiple billions of data locations, files of multiple terabytes in size are generated. Achieving results at this scale requires a code that continues to scale well to large core counts. HemeLB, both in its single and coupled versions, possesses excellent scaling characteristics and these have been reinforced during this project.

The work of this project contributes to the work of CompBioMed [2], a European Commission funded Horizon 2020 Centre of Excellence, in developing HPC methods in the field of biomedicine and, in particular, the development of a virtual human to assist clinicians in optimising the diagnosis and treatment of patients.

Results and Methods

A key focus of this project has been to continue preparations of HemeLB for execution on upcoming exascale machines. This includes both the incorporation of new physics to the model to better capture blood flow but also technical improvements that will make the code more efficient and easier to use on these upcoming machines.

In [3], we demonstrate how the HemeLB code can be deployed to investigate a problem of clinical relevance. For patients suffering from kidney failure, dialysis may be required to artificially filter waste products from the blood stream. To facilitate this, a surgeon may modify a section of the vasculature to directly connect a major vein to an artery. Bypassing the peripheral vessels increases the flow rate through the vein and can allow it to become a suitable access point for dialysis to take place. Using the self-coupled version of our code we studied the flow through personalized, human-scale arteries and veins of the left forearm. By comparing the flow through key vessels in a healthy (unmodified) configuration to those where an arteriovenous fistula had been created we could study the impact of a chosen surgical intervention (Figure 1).

In many 3D blood flow models, the vessels are represented as rigid walls. By not employing a dedicated solid mechanics model, this choice significantly simplifies the complexity of the simulation and reduces the computational requirements of a job. As part of this project, we have developed a boundary condition [4] for the lattice Boltzmann method that can more accurately capture the effects of an elastic vessel wall on fluid flow than is achieved with a rigid wall model. Importantly, this has been achieved without impacting the computational cost of a simulation or the scaling characteristics of HemeLB. From a qualitative perspective, the shear stress distribution (Figure 2) at the walls of a vascular domain determined by our model is similar to those generated by models with an explicit solid mechanics solver available in existing literature.

With the support of LRZ, we have been able to update the algorithmic implementation of key kernels of HemeLB to newer versions of intrinsics (AVX2 and AVX512). In a block operation held in November 2021, we were able to test the performance of these new implementations on the full partition of SuperMUC-NG. At full-machine scale – 6,400 nodes, 307,200 cores – we observed a 48% speed-up compared to the original implementation (SSE3) and an improvement in parallel efficiency by approximately 35%.

Moving towards the exascale requires all components of the computational workflow to be examined, not just

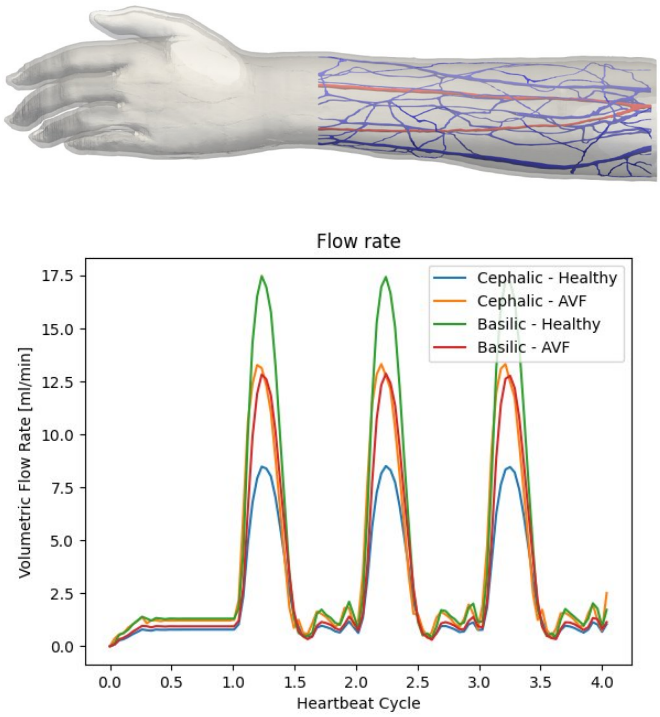

Figure 1: Our model for studying arteriovenous fistula (AVF) illustrated how flow changes in personalized vessels due to surgical intervention.

the performance and scaling characteristics of the code during a simulation. This project has been working with LRZ visualization experts to generate a workflow that makes use of existing HPC resources to efficiently render HemeLB flow simulations. This has been developed using the Intel OSPRay Studio environment and has provided a significant increase in our capability to view very large datasets consisting of billions of datapoints and terabytes of data (Figure 3). A video presentation of this work was selected as a finalist of the Scientific Visualization & Data Analytics Showcase at SC21 [5].

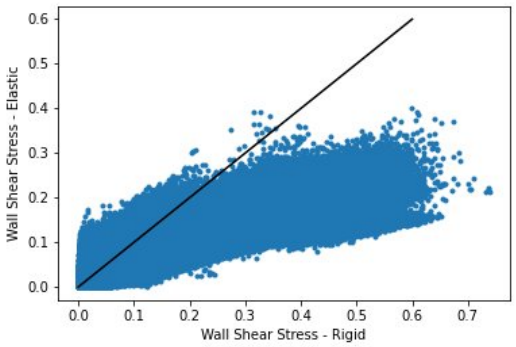

Figure 2: Comparative distribution profile of wall shear stress between our elastic boundary condition and a rigid wall model. This is a qualitatively similar distribution to literature data.

Ongoing Research / Outlook

As this project continues to progress, we will continue to develop our flow algorithms and domains to facilitate simulation of full human vasculatures. The simulation demands of 3D full human blood flow can only be met by HPC infrastructure like SuperMUC-NG. The project will continue by refining our coupling of HemeLB to the 3D heart model Alya. We will also work with LRZ to further develop the visualization workflow to prepare it for the data quantity anticipated for virtual human simulation. It is also anticipated that we will seek to develop virtual reality renderings of HemeLB flow data to showcase how simulations and modelling can be translated and presented in a useful format for end users.

References and Links

[1] http://hemelb.org
[2] https://www.compbiomed.eu/
[3] J. W. S. McCullough and P. V. Coveney, Sci. Rep., 11, 22301 (2021) DOI: 10.1038/s41598-021-01435-8.
[4] J. W. S. McCullough, P. V. Coveney, Sci. Rep., 11, 24260 (2021) DOI: 10.1038/s41598-021-03584-2.
[5] E. Mayer, J. McCullough, J. Gunther, S. Cielo, P. Coveney, SC21 SciViz Showcase presentation (2021), https://www.youtube.com/watch?v=Sd8_cujMP_4.

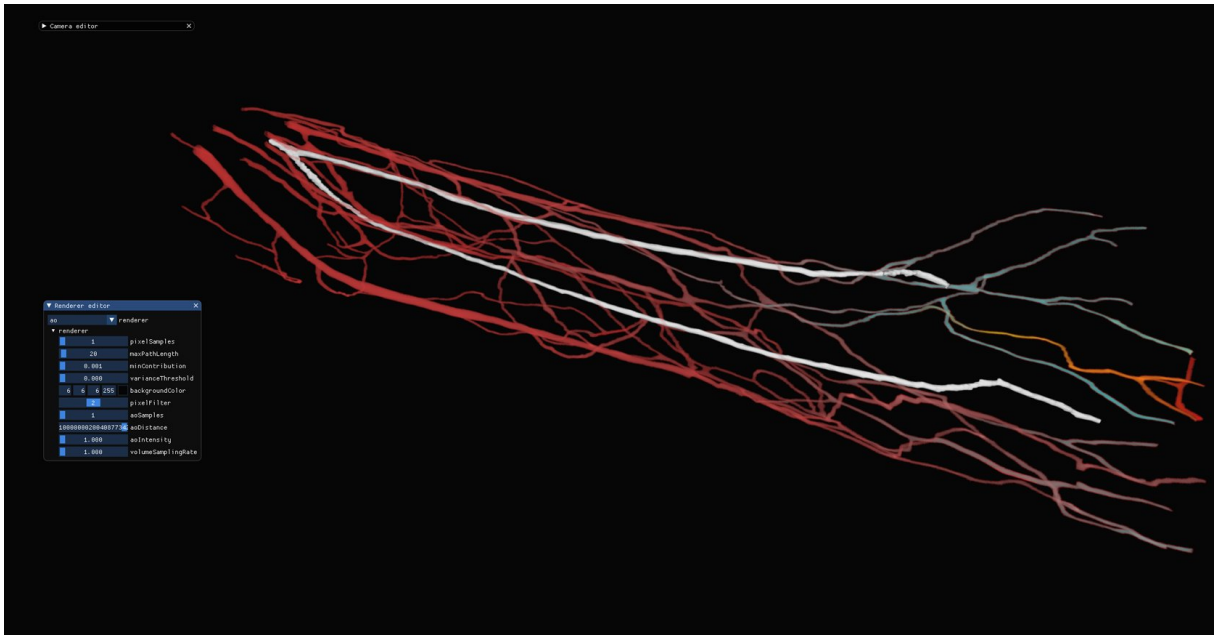

Figure 3: Rendering of HemeLB flow data as generated by the workflow developed in Intel OSPRay Studio. This platform has allowed static images and animations to be produced from the full output generated by a HemeLB simulation.

Biophysical Properties of Zinc-Chloroquine Complexes from Multiscale Simulations

Research Institution
[1]Institute for Advanced Simulation-5, Institute of Neuroscience and Medicine-9, Forschungszentrum Jülich

Principal Investigator
Mirko Paulikat[1]

Researchers
Paolo Carloni[1], Emiliano Ippoliti[1], Florian Karl Schackert[1], Giulia Rossetti[1,5,6], GiovanniMaria Piccini[2], Fabio Arnesano[3], Alessandra Barbanente[3], Daniele Vitone[3], Liliana Quintanar[4], Nils Leopoldo Schuth[4]

Project Partners
[2]Euler Institute, Università della Svizzera italiana, Lugano
[3]University of Bari "Aldo Moro", Bari
[4]Cinvestav, Mexico City
[5]Jülich Supercomputing Center, Forschungszentrum Jülich
[6]Department of Neurology, University Hospital Aachen (UKA), RWTH Aachen University

SuperMUC Project ID: pn73fo (Gauss Large Scale project)

Introduction

The pandemic of Covid-19, the viral infection caused by SARS-CoV-2, started in Wuhan in December 2019. Since then, it has spread leading to almost 430 million infected patients today, with more than 5.9 million deaths as reported by WHO of February 28, 2022.

Major routes to combat the virus include the development of vaccines and drugs. The application of vaccines has been shown to be highly effective in fighting the pandemic. Yet, apart from the difficulties associated with their worldwide distribution, the efficacy is not guaranteed for new viral mutants which may pose an even higher risk of infection. Therefore, it is imperative to foster the discovery of antiviral drugs. One strategy to quickly identify therapeutic agents that can be used in the clinics is to use U.S. Food and Drug Administration (FDA) approved drugs, whose toxicity is well known and controlled. Additionally, some of these drugs can be used in combination with other chemicals. One of them is the zinc ion, which is non-toxic at limited concentrations. Zinc ions have shown antiviral properties and inhibit *in vitro* proteins from specific members of the coronaviruses family [1].

A key issue for the use of zinc ions for antiviral therapy is its difficulty, as a divalent metal ion, to cross the cell membrane and thus reach its targets inside the cell. A variety of ligands, including the FDA approved drug chloroquine (CQ), form complexes with these ions and assist zinc permeation [2], possibly promoting the combined beneficial action of both zinc ions and the drugs against the virus. Here, we studied the permeation of chloroquine and the interaction of the drug with zinc ions in aqueous solution. For the latter, we take advantage of highly scalable *ab initio* molecular dynamics simulations to explore the diverse coordination chemistry of zinc ions.

Results and Methods

The permeation of chloroquine through a lipid bilayer was studied by well-tempered metadynamics enhanced sampling simulations. On SuperMUC-NG, ~180 ns/day could be achieved on 96 cores, exploiting the MPI parallelized GROMACS molecular dynamics package patched with PLUMED.

The simulations provided a detailed picture of the structure and the energetics of the permeating drugs. In addition, they turn out to be fully consistent with experimental data collected several decades ago. Finally, they led to a detailed understanding of the complex dehydration process of the drug upon permeating the membrane.

Next, we investigated how this molecule binds to Zn(II) ions, which display antiviral properties. The resulting zinc-chloroquine complexes in aqueous solution were studied by *ab initio* molecular dynamics simulations, employing the CPMD program package [3]. The density functional theory-based electronic structure is evaluated within a plane wave basis set in combination with norm-conserving pseudopotentials, from which the system is propagated in time via a Born-Oppenheimer scheme. The CPMD implementation uses processor groups to efficiently perform this task. The parallelization within such processor groups is realized through MPI and OpenMP for inter-node and intra-node communication, respectively. Besides the usage of standard GGA functionals (BLYP), we aimed to study zinc complexes also at the more accurate hybrid functional DFT level (B3LYP). The inclusion of exact exchange is computationally extremely demanding, but also highly scalable. On SuperMUC-NG, we were able to efficiently use up to 6,144 cores for these simulations, requiring ~15 min per MD step.

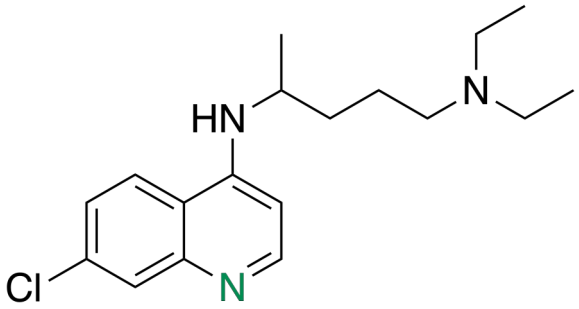

Figure 1: Chemical formula of chloroquine indicating the zinc binding nitrogen.

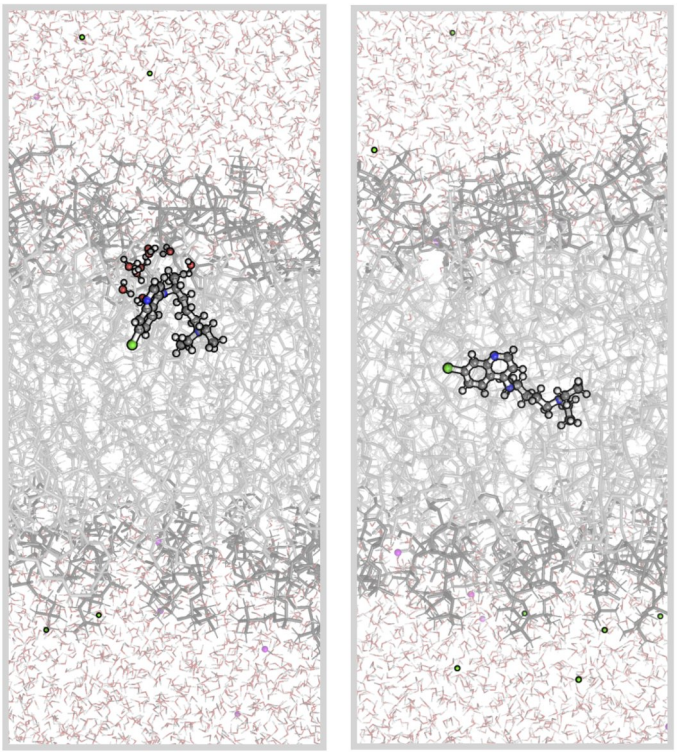

Figure 2: Simulation snapshot of chloroquine permeating across a model membrane.

NMR studies show that zinc binding to chloroquine occurs at its aromatic nitrogen. Thus, the drug's aliphatic side chain bonded to the exocyclic nitrogen was modeled as methyl group to decrease dramatically the system size. The remaining coordination environment of the zinc ion can be composed of water molecules and/or chloride ions under physiological conditions. The ab initio molecular dynamics simulations provide insight on the coordination number and the nature of the ligands in water solution. This information may be useful in understanding how Zn(II) ions and chloroquine, an FDA approved antimalarial drug proposed to be active against Covid-19, may act together.

Ongoing Research / Outlook

Despite the high-performance applicability of *ab initio* molecular dynamics simulations, the sampling time is still limited in the picosecond timescale. A modern route to extend the simulation at quantum chemical accuracy is the usage of neural network potentials. Recently, machine learning potentials trained on *ab initio* data, like in the DeepMD framework, have been proposed [5], which can be used to parametrize the bonded energy terms of isolated molecules or extended systems based on *ab initio* reference data. We explore this methodology for zinc-chloroquine complexes, for which a huge set of configurations needs to be evaluated in parallel. Two papers will be published on these projects.

References and Links

[1] C. C. Lee, C. J. Kuo, M. F. Hsu, et al, FEBS Lett. 581, 5454–5458 (2007).
[2] J. Xue, A. Moyer, B. Peng, J. Wu, B. N. Hannafon, W.-Q. Ding, PloS one 9, e109180 (2014).
[3] CPMD, http://www.cpmd.org/
[4] A. Krężel, W. Maret, Arch. Biochem. Biophys. 611, 3–19, (2016).
[5] L. Zhang, J. Han, H. Wang, R. Car, E. Weinan, Phys. Rev. Lett. 120, 143001 (2018).

Pandemic Drugs at Pandemic Speed

Research Institution
[1]Ludwig Maximillian University, [2]University College London

Principal Investigators
Dieter Kranzlmüller[1], Peter V. Coveney[2]

Researchers
Shunzhou Wan[2], Agastya P. Bhati[2], Alexander D. Wade[2], Dario Alfè[2], Shantenu Jha[3]

Project Partner
[3]Department of Computer Engineering, Rutgers University

SuperMUC Project ID: pn98ve

Introduction

The scale and rapidity of the COVID-19 crisis have challenged existing methods of doing research, not least the current drug design process, which takes about 10 years and $1-3 billion to develop a single marketable drug molecule. The biggest challenge in any drug discovery study is the huge chemical space that needs to be explored amounting to a very large number of potential ligands available (ranging from a few hundred millions to billions) which need to be filtered out based on their binding affinities with the target protein to identify potential drug candidates.

Our effort against coronavirus [1] aims to accelerate the development of antiviral drugs by modelling proteins that play critical roles in the virus life cycle in order to identify promising drug candidates. Our studies deploy both physics-based (PB) techniques including molecular dynamics (MD) based methods, and machine learning (ML) techniques to screen a large set of candidate compounds. The strengths and weaknesses of ML and PB methods complement each other and so it makes sense to couple them in drug discovery.

Results and Methods

BAC (binding affinity calculator) is a free energy workflow we have developed in the last few years, which is designed to automate the end-to-end execution of various free energy approaches, and to handle ensemble calculations. BAC facilitates a physics-based, mechanistic modelling at the level of molecular medicine. An important and interesting application of BAC is as part of a workflow, called IMPECCABLE, that we have developed to accelerate the drug discovery process [2]. It involves constructively combining ML with MD such that they complement each other and allow us to quickly identify potential drug candidates (Figure 1). BAC has been designed to be as generic as possible, and can be used in different settings, independent of the underlying type of diseases.

The iterative nature of the IMPECCABLE workflow with upstream and downstream flow of information allows it to accelerate the sampling of relevant chemical space much faster than traditional methods. We have demonstrated the application of our workflow on four SARS-CoV-2 target proteins [3]. The workflow requires HPC resources for efficient implementation and a dedicated workflow manager to handle the large number of heterogeneous computational tasks on a multitude of supercomputers. We believe that this hybrid ML-PB approach offers potential in long term – with the rise of exascale, quantum and analogue processing – to deliver novel pandemic drugs at pandemic speed. We have already analyzed several million compounds from a set of orderable compound libraries using IMPECCABLE, and filtered out compounds, first using docking and then with ESMACS followed by TIES, to finally select those that bind most effectively to the target under consideration [3].

The COVID-19 pandemic has led to a rush to repurpose existing drugs which can treat the disease or arrest the spread of the virus. Drug repurposing can speed up the traditional process of drug discovery because the drugs have already been proven to be safe in humans. We have used molecular dynamics simulation and an ensemble-based free energy approach to investigate the interactions of a set of existing drugs with the main protease of the SARS-CoV-2 virus (Figure 2). The predicted free energies are compared with experimental results wherever they are available and they are found to be in excellent agreement [4]. Our study also provides detailed energetic insights into the nature of the associated drug−protein binding, in turn shedding light on the design and discovery of potential drugs [4].

We have continued to successfully exploit “block operations” on SuperMUC-NG for a large number of ESMACS simulations, most recently in the period 15-17 November, 2021 when we selected 12 protein kinases and 11 drugs leading to a total 132 drug-kinase complexes for drug ranking and drug selectivity. We used our ESMACS protocol which employs an end-point approach and only simulates the physics states of the drugs and proteins. We were able to use the entire machine, a total of 6,444 nodes, for 11 hours to get all calculations completed. We used a single submission to execute all jobs corresponding

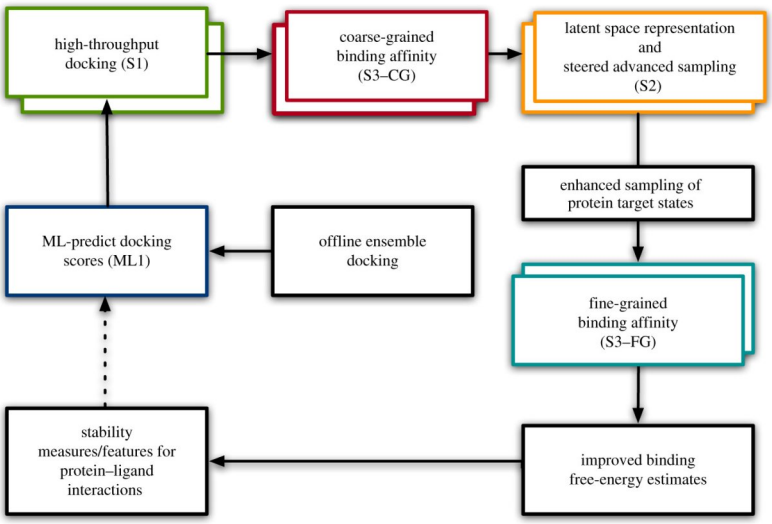

Figure 1: Integrated modelling pipeline for new COVID-19 drug development, where blind ML is made 'smarter' with accurate PB methods. It represents an entire virtual drug discovery pipeline, from hit to lead through lead optimization. The constituent components are ML-based surrogate model for docking (ML1), Autodock-GPU (S1), coarse and fine-grained binding free energies (S3-CG and S3-FG) and S2 (DeepDriveMD). The arrows show the information transferred between the different methods [2,3].

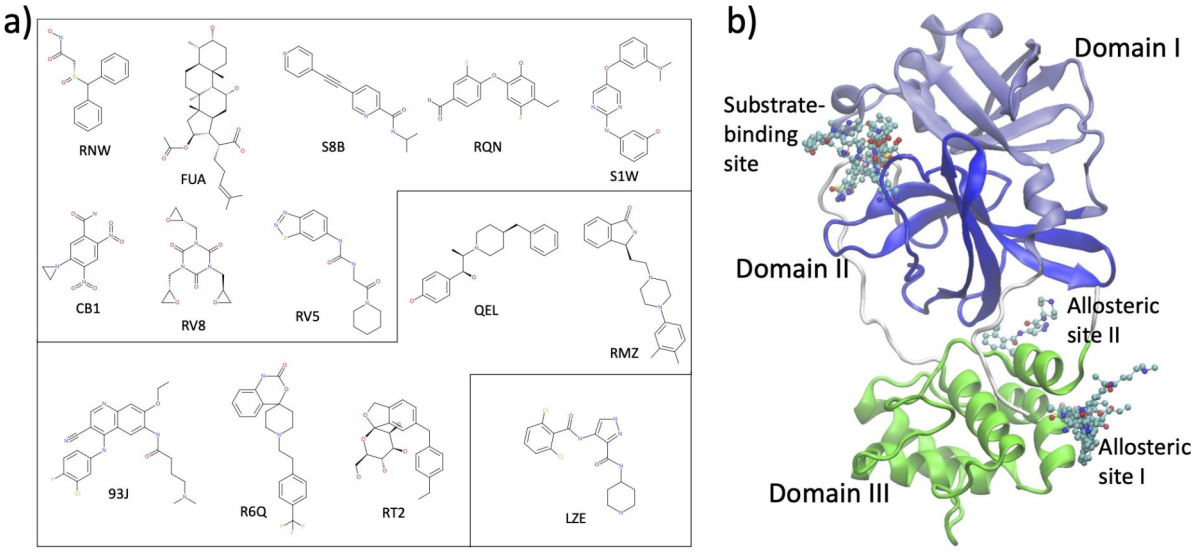

Figure 2: Chemical structures of repurposed drugs targeting SARS-CoV-2 main protease. The drugs (panel a) are grouped according to the sites they bind to: the substrate-binding site, the allosteric site I, and the allosteric site II (panel b). The drugs are also shown in chemical representation bound to 3CLpro (shown in cartoon) at the three binding sites (panel b). The three domains (I, II and III) of 3CLpro are shown in light blue, blue and green, respectively, along with some loops and links (white).

to 132 ESMACS calculations. The job farming function provided by LRZ was successfully used to manage all jobs in the submission. All jobs executed successfully and simulation trajectories were generated and subsequently analysed.

Ongoing Research / Outlook

Many drug resistances are mediated by mutations in target proteins. We are investigating the relative binding affinity changes associated with amino acid mutations in proteins. One of the proteins we are studying is the beta-subunit of RNA polymerase. We are using TIES-PM in conjunction with GROMACS and NAMD to calculate free energy changes associated with hundreds of amino acid mutations in our proteins. Combining the most advanced high-throughput molecular dynamics simulations and associated free energy calculation approaches with rapid sequence analysis technology, BAC and IMPECCABLE offer real-time support for making clinical decisions on patient stratified drug selection.

We are involved in joint co-design efforts with Arm, Atos, Leibniz Supercomputing Centre (LRZ), UCL and Oxford University in the domain of genomics with a specific application to prediction of mutations in Mycobacterium tuberculosis (TB) which confer drug resistance and on how to treat patients on an individual basis in the face of this. The work now underway will first investigate the performance of gene sequencing codes. LRZ is providing the expertise in measuring the performance and scalability of these codes as well as furnishing access to bespoke software solutions to automate these measurements based on our earlier work performed on their own testbed called BEAST which already features some earlier arm hardware.

References and Links

[1] https://www.compbiomed.eu/coronavirus-computational-drug-screening/
[2] A. Al Saadi, et al., "IMPECCABLE: Integrated Modeling PipelinE for COVID Cure by Assessing Better LEads", 50th International Conference on Parallel Processing (ICPP'21), August 9-12 (2021), DOI: 10.1145/3472456.3473524.
[3] A. P. Bhati, et al., Interface Focus, (2021) 11, 20210018. DOI: 10.1098/rsfs.2021.0018.
[4] S. Wan, A. Bhati, A. Wade, D. Alfe, P. V. Coveney, Mol. Syst. Des. Eng., (2022) 7, 123/131. DOI:10.1039/d1me00124h.

Guanylate-binding proteins and their interactions with lipid membranes

Research Institution
Heinrich-Heine-Universität Düsseldorf
Forschungszentrum Jülich

Principal Investigator
Birgit Strodel

Researchers
Jennifer Loschwitz, Wibke Schumann

Project Partners
—

SuperMUC Project ID: pn98zo

Introduction

Toxoplasma gondii is an intracellular parasite which has infected 50% of the German population, and which can be lethal to immune-suppressed people or unborn children. In order to fight off the infection, guanylate-binding proteins (GBPs) are vital. By using fluorescence microscopy, it has been revealed that the membrane of the parasitophorous vacuole, wherein the pathogen *T. gondii* hides after infection of the host, disintegrates after binding of GBPs to the membrane. This is especially the case for the murine guanylate-binding proteins mGBP2 and 7. However, the exact mechanism happens at a smaller length scale than can be observed with microscopes. To fill this gap in knowledge, we perform atomistic molecular dynamics simulations of GBPs.

GBPs bind a form of cellular energetic currency, namely guanylate triphosphate (GTP), which not only enables their oligomerization [1], but gives also rise to large-scale hinge motions [2]. These motions resemble the dynamics occurring in a related group of proteins, called dynamins, whose membrane-remodeling capacities are well studied. The similarities and differences between the motions of GBPs and dynamins are explored in this project. By experimental means, murine GBPs were shown to bind specific lipids, which might aid in curving the parasitophorous vacuole membrane, and in turn might introduce the necessary stress for membrane disintegration. This possibility is tested in this project.

Results and Methods

To reach our goals, we perform molecular dynamics (MD) simulations on SuperMUC, using the software GROMACS. From initial atom positions, forces are iteratively applied, and the motions of the proteins can be captured. Even using massively parallel hardware like SuperMUC, timescales of nano- to microseconds need days of computing time. In order to get closer to laboratory timescales, enhanced sampling methods are employed. These can work by selectively heating up the system or by constraining the system in certain ways, thereby forcing it to perform specified motions. Furthermore, coarse-graining can be used to group several atoms into one bead, which reduces the computational cost and therefore opens up the possibility to simulate larger systems.

One of our research aims is to elucidate how the hinge motion present in dynamins and GBPs can achieve the transition between open and closed protein forms. Of the many dynamins, only the bacterial dynamin-like protein (BDLP) has been structurally resolved in both open and closed state. We first explored the space between these extreme states, then simulated 87 intermediate conformations, for 500 ns each, and determined the energetic barrier of the full conformational change. An energy barrier of about 40 kcal/mol was revealed, an energy accessible by GTP hydrolysis (Figure 2).

Another aim is to unravel the mode of mGBP polymerization, because thousands of these proteins must work together in order to coat the parasitophorous vacuole, which is necessary for a strong enough membrane-damaging effect. We employed an external docking server in order to obtain possible mGBP2 and mGBP7 dimer models. The stability of these models was assessed by MD simulations performed on SuperMUC and their intermolecular binding energies determined. The different models were further compared with experimental data produced by our collaboration partners (Figure 1, point 3). The results of this part of the project were written up in a manuscript draft (for publication in 2022).

Our third aim is to study the membrane binding of mGBP2 and 7 for different membrane compositions. First, we simulated the already membrane-inserted mGBP2 on a single-component lipid membrane at the atomistic scale. However, we observed no effects that, on a larger scale, might cause membrane damage. We therefore switched to a coarse-grained simulation setup, where we consider lipid membranes containing three different lipids and where we make no

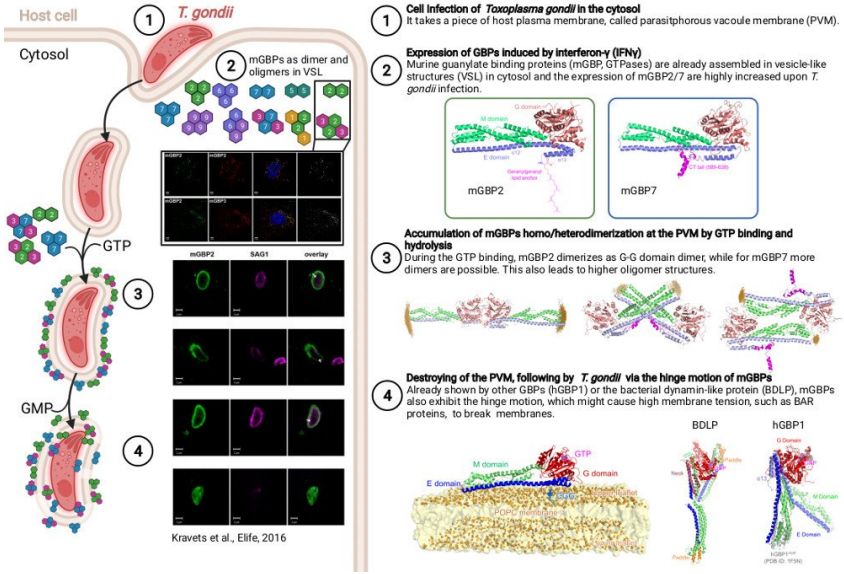

Figure 1: Mode of action of mGBPs following T. gondii infection. (1) The parasite enters the cell and hides in a parasitophorous vacuole from normal degradation. (2) mGBPs, including mGBP2 and mGBP7, are upregulated and organize in vesicle-like structures (VSL) as homo- and hetero-oligomers. The structures of mGBP2/7 are shown on the right side. (3) Upon GTP binding, mGBP2/7 dimerize and accumulate at the of the parasitophorous vacuole membrane (PVM). (4) Disintegration of the PVM is the result of the mGBPs, which might be connected to the large-scale hinge motion by exerting forces on the membrane. This hypothesis is tested here.

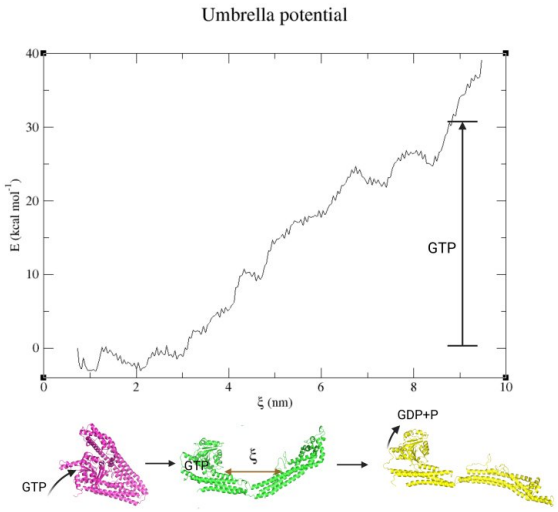

Figure 2: Free energy profile for the close ↔ open transition of BDLP. The closed (purple) and open (yellow) structures along with an intermediate state (green) are shown at the bottom.

assumptions regarding the membrane-protein interaction modes (Figure 3). These setups were all simulated for 10 µs. In most of the cases, mGBP2/7 binds to the lipid membranes. mGBP2 prefers to insert into the membrane via its C-terminal lipid anchor, whereas mGBP7, which lacks such a lipid anchor, uses different parts of its structure to associate with the membrane. This study is still ongoing.

Ongoing Research / Outlook

In the future, we will analyze how GTP binding changes the energetic profile of the close ↔ open transition of BDLP (Figure 2), which is expected to stabilize the open conformation. Afterwards, we will transfer our knowledge to mGBP2. There is evidence that the open form here is achieved by the extension of a long α-helix (shown in blue in Figure 1), which, however, would have to be externally stabilized as the helix is unstable without further contacts [2]. The next step in the membrane project is to start modeling mGBP2/7 dimers at the membrane, in order to evaluate if this oligomer state is able to exert membrane-damaging effects.

References and Links

[1] E. Kravets et al., Elife (2016), 5, e11479.
[2] B. Barz et al., PLOS Computational Biology (2019) 15(10), 1–29.

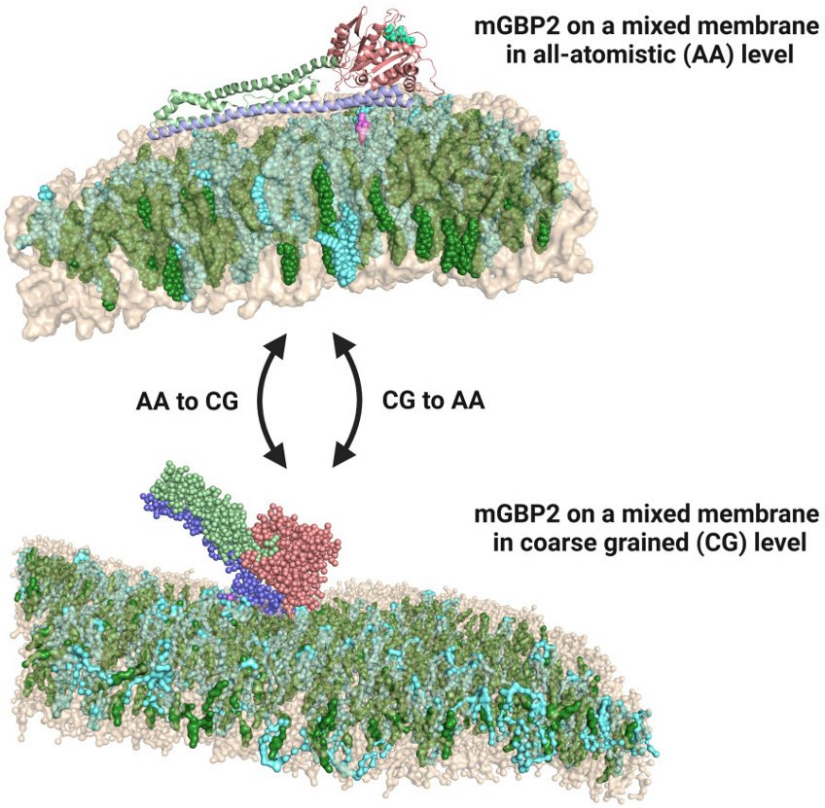

Figure 3: Membrane interactions of mGBP2, simulated at the atomistic (top) and coarse-grained (bottom) level.

Exosite Recognition in Intramembrane Proteolysis

Research Institution
Physics of Synthetic Biological Systems, TU München

Principal Investigator
Christina Scharnagl

Researcher
Simon Menig

Project Partners
–

SuperMUC Project ID: pr27wa

Introduction

Intracellular proteolysis is essential for maintaining the equilibrium between degradation and synthesis of proteins. Whereas proteolysis by soluble proteases is well characterized, there are still open questions about how integral transmembrane proteins are recognized and get cleaved in the cell membrane. Intramembrane proteolysis plays a crucial role in biological processes such as signal transduction, embryonic development, immune response and function of the nervous system. Aberrant cleavage impairs normal functioning and may contribute to diseases. Due to its role in the etiology of Alzheimer's disease (AD), the aspartyl-protease complex γ-secretase (GSEC) is the best studied intramembrane protease in mammals. Understanding the substrate recognition mechanism of GSEC is a key step for establishing substrate specific inhibitors of AD plaque production and is a central aim of the collaborative research project FOR2290 [1] (DFG Forschergruppe, "Understanding intramembrane proteolysis").

Extensive biochemical, cell biological and structural studies provided detailed insights into the cleavage mechanism of the Amyloid Precursor Protein (APP) and, to a lesser extent the NOTCH family of receptors implicated in tumor development [1,2]. In addition to APP and NOTCH1, GSEC cleaves >140 transmembrane protein substrates of type I orientation but only a few non-substrates are unequivocally identified [2]. Currently, the only known prerequisite for a substrate to be bound and hydrolyzed by GSEC is a short ectodomain. In contrast to soluble proteases, GSEC does not appear to recognize a unique sequence motif in its substrates nor are intrinsic local or global flexibility of their transmembrane domain (TMD) the sole determinants for substrate recognition [2,3]. Rather, recruitment of the APP substrate is a multistep process involving several auxiliary binding sites (exosites) spatially separated from the enzyme's active site (see Figure 1) [1,2]. After initial capture by PEN-2 (presenilin-enhancer-2), a non-catalytic subunit of GSEC, the APP substrate is translocated to an exosite on its catalytic subunit (presenilin 1, PS1). Only when the substrate is bound there, its scissile bond can reach the active site. Before moving into the active site (in whole or in part), the substrate makes contact with another exosite located in close proximity to the active site (called docking site [4]). Without coupling to an energy-providing reaction, substrate translocation must involve mechanisms driven by diffusion processes. Since chemical reactions in the cellular membrane take place in a 2d system, the different principles governing diffusion-driven association in 2d versus 3d might contribute to the fundamental differences in substrate recognition by intramembrane-cleaving and soluble proteases.

Results and Methods

Within the research group, experimental methods such as functional assays and structure determinations are complemented by computational approaches. Because most studies focus on APP, crucial points of the recognition mechanism are still not well understood such as the role of exosite-mediated enzyme-substrate interactions for active site docking, whether different substrates use the same or different mechanisms, at which stage non-substrates are rejected, and the impact of the lipid composition. In order to advance our understanding of the initial step in the enzyme reaction – the association of GSEC and its substrate – we apply ensemble-based multi-scale molecular dynamic (MD) simulations using the highly scalable GROMACS 2019.3 code [5]. Coarse-grained (CG) models (MARTINI 2.2 force field, cgmartini.nl) provide the long simulation times and large number of replicates required for an unbiased prediction of substrate-enzyme contacts in membrane using the DAFT approach (Docking Assay For Transmembrane Components [6]). A typical DAFT run consist of 1,000 replicates (1-2 μs length) of a system which corresponds to ~80,000 heavy atoms. With SuperMUC-NG we reached a performance of 3,800 ns/day on 24,000 cores. After validating the *in silico* predicted exosites for APP against the experiments, we studied exosite preferences for 15 substrates, substrate candidates and two non-substrates as well as 5 domain swap constructs in a fully hydrated 1-palmitoyl-2-oleoyl-sn-glycero-3-phosphocholine (POPC) bilayer, the main component of the synaptic plasma membrane. Fur-

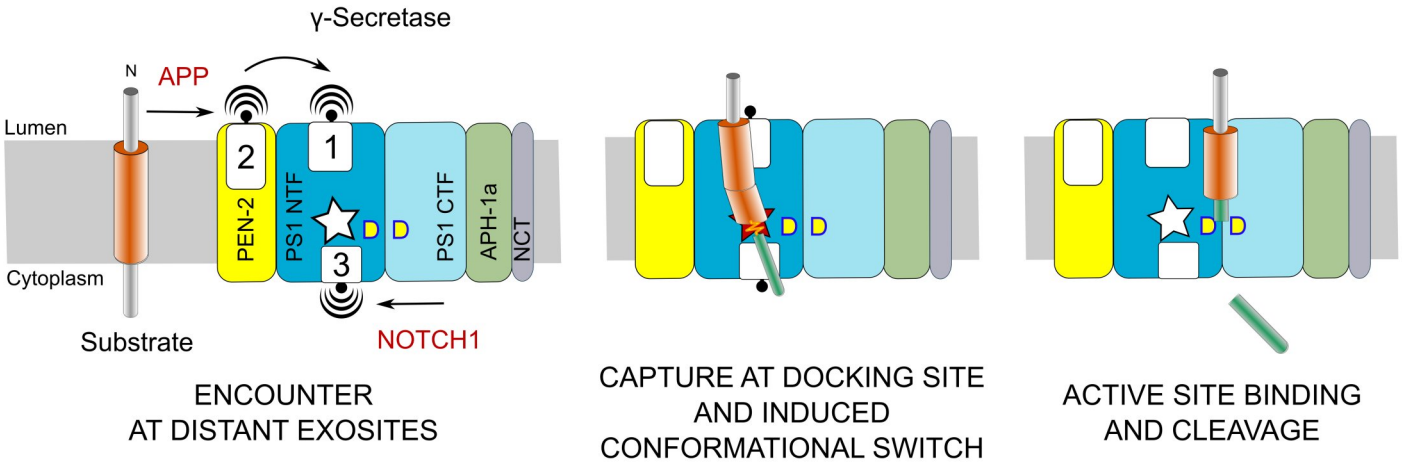

Figure 1: Mutli-site, multi-step recognition by γ-secretase. The substrate transmembrane domain (red) and few juxtamembrane residues (dark grey) are sufficient for high-affinity binding and processing by the intramembrane protease γ-secretase (GSEC). The two catalytic aspartate residues (D) are located in a hydrophilic cleft at the border between the N-terminal (NTF) and the C-terminal (CTF) fragment of the catalytic subunit presenilin 1 (PS1). Exosites distant from the active site are numbered (1-3), a docking site on the outside of PS1 but close to the active site is marked by a star. Recruitment of different substrates follows different pathways. Capture of APP by the non-catalytic subunit PEN-2 (exosite 2) precedes substrate translocation to exosite 1 on PS1. In contrast to APP-like substrates, initial encounter of NOTCH-like substrates takes preferentially place on the intracellular side of PS1 (exosite 3). Non-substrates are trapped at the non-catalytic subunit PEN-2. Dynamic processes contributing to the first two steps were in the focus of the current research project.

thermore, we investigated the impact of more native-like lipid compositions on GSEC-APP and GSEC-NOTCH1 complexes by varying cholesterol concentration, lipid head group charge and hydrophobic tail lengths. After mapping the coarse-grained system back, atomistic resolution MD simulations (CHARMM36 force field, mackerell.umaryland.edu) are used to analyze molecular details of conformational dynamics and interactions in the μs range (210,000 atoms, 960 cores, 110 ns/day) for selected docking poses.

We found that substrates and non-substrates differ by their exosite preferences, where recruitment probability at the non-catalytic subunit PEN-2 is much higher for non-substrates. However, only a subset of the investigated substrates (called APP-like) follows the pattern suggested for APP recruitment. Our analysis revealed an additional exosite at the intracellular border (exosite 3 in Figure 1) dominating initial encounter of NOTCH-like substrates with PS1. Exosite preference can be shifted by the lipid composition towards enhanced encounter at PEN-2 without loosing affinity to PS1.

The analysis of enzyme-substrate interactions suggested a dual functional role of the exosites. During initial encounter they act like an antenna providing electrostatic and stereospecific interactions with substrate juxtamembrane residues. Encounter-complex formation is followed by establishing hydrophobic interactions between substrate and enzyme TMDs. During conformational sampling, exosite binding could act as a guide that restricts the search space and increases the likelihood of contacts between the substrate's cleavage domain and the docking site, where interactions are able to induce instabilities in the substrate TMD. Thus, residues on the surface of GSEC are actively involved in preparation of a partially unwound substrate cleavage domain that permits structures flanking the scissile bond to engage in active site binding. Our results suggest a recognition model where both, exosites and active site contribute to binding specificity and substrate affinity of GSEC. Multiple steps and interactions and the use of different exosites and association pathways might enable binding and processing of dynamically and structurally diverse substrates. Resistance to translocation to the catalytic subunit might be a hallmark of non-substrates.

Ongoing Research / Outlook

Not all of the experimentally observed steps are accessible with the current MD setup. The coarse-grained description of protein-protein and protein-lipid interactions allows a quantitative analysis of competitive exosite binding. However, we were not able to observe substrate hopping between PEN-2 and PS1. This might be a problem of observation time and/or a problem of a too sticky force field. Advanced methods like Brownian dynamics or umbrella sampling will allow to characterize the diffusive processes which govern the spatial correlation between escape and capture at the two exosites in more detail. On the other hand, the *in silico* analysis allows to identify binding interactions within a significantly shorter time compared to biochemical experiments. The simulations greatly benefit from SuperMUC-NG's high performance providing the necessary long simulation times for a large number of replicates. Functional essays can then be used to specifically focus on predicted key steps and interactions.

References and Links

[1] https://www.i-proteolysis.de/
[2] Understanding Intramembrane Proteolysis by γ-Secretase. 2020. Semin Cell Dev Biol, 105. (Ed. Harald Steiner). DOI: https://doi.org/10.1016/j.semcdb.2020.06.204
[3] Manuel Hitzenberger, Alexander Götz, Simon Menig, Barbara Brunschweiger, Martin Zacharias, and Christina Scharnagl. 2020. Semin Cell Dev Biol, 105: 86-101. DOI: https://doi.org/10.1016/j.semcdb.2020.04.008
[4] Anna Kornilova, Frédéric Bihel, Chittaranjan Das, Michael Wolfe. Proc Nat Acad Sci, 102: 3230-3235. DOI: https://doi.org/10.1073/pnas.0407640102
[5] https://gromacs.org
[6] http://cgmartini.nl

Interplay of β_2-adrenergic receptor phosphorylation and membrane composition

Research Institution
[1]Institute of Nanotechnology, KIT

Principal Investigator
Wolfgang Wenzel[1]

Researchers
Kristyna Pluhackova[2], Florian M. Wilhelm[2]

Project Partner
[2]Department of Biosystems Science and Engineering, ETH Zürich

SuperMUC Project ID: pr27wi

Introduction

The broad portfolio of G protein-coupled receptors (GPCRs) mediates rapid cellular responses to diverse extracellular stimuli [1]. On the inside of the cell trimeric G proteins attach to activated receptors and trigger downstream signaling resulting in a physiological response. The interaction of receptors with arrestins results either in arrestin-mediated signaling or in receptor desensitization and endocytosis. Prior to arrestin binding the receptor is specifically phosphorylated on its intracellular loop 3 (ICL3) and/or the C-terminus by a receptor-specific kinase. Different phosphorylation patterns evoke different physiological and pathophysiological responses [2]. Even though the disordered and little conserved ICL3 and C-terminus of the receptors were reported to play an important role in binding of G proteins, GPCR kinases and arrestins, little is known about their structure and dynamics. The structural plasticity and adaptability of ICL3 and C-terminus could explain the promiscuous interactions of more than 800 different GPCRs with 20 different G proteins and only two arrestins. Here, we have studied the interplay between phosphorylation of ICL3 and the C-terminus and native acidic lipids and their impact on the structure and dynamics of a prototypical GPCR (β_2-adrenergic receptor) as well as the consequences for receptor-arrestin binding [3] (see Figure 1).

Results and Methods

Replica exchange solute tempering (REST) simulations (heating up the protein from 310 K to 510 K) were performed to estimate membrane binding probabilities, ensuring sufficient sampling of the conformational space of the ICL3 and C-terminus.

Sequential multiscaling molecular dynamics (MD) simulations spare computational resources by studying time consuming processes (like lipid binding to the protein complex or protein-protein association) using coarse-grained (CG) resolution. After conversion back to all-atom (AA) resolution using the tool backward [4] the simulations were continued atomistically, refining the lipid-protein and the specific protein-protein interactions. In CG MD simulations group of atoms are

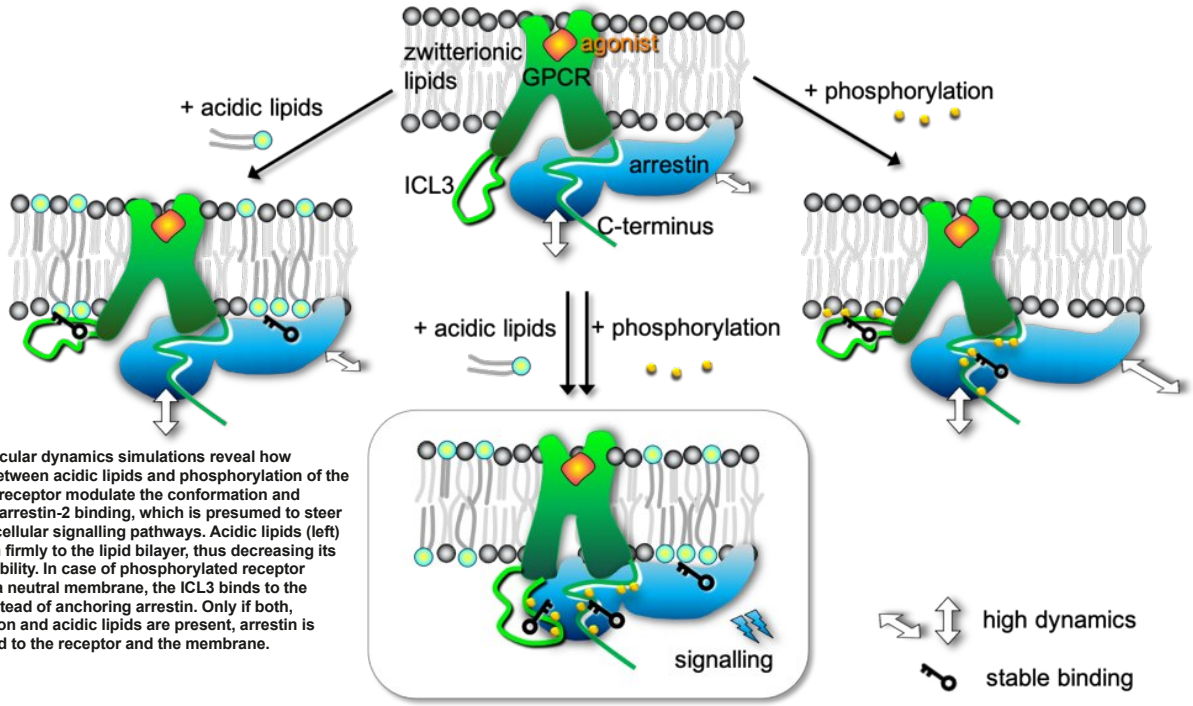

Figure 1: Molecular dynamics simulations reveal how interactions between acidic lipids and phosphorylation of the β_2-adrenergic receptor modulate the conformation and dynamics of βarrestin-2 binding, which is presumed to steer different intracellular signalling pathways. Acidic lipids (left) attach arrestin firmly to the lipid bilayer, thus decreasing its rotational flexibility. In case of phosphorylated receptor embedded in a neutral membrane, the ICL3 binds to the membrane instead of anchoring arrestin. Only if both, phosphorylation and acidic lipids are present, arrestin is stably attached to the receptor and the membrane.

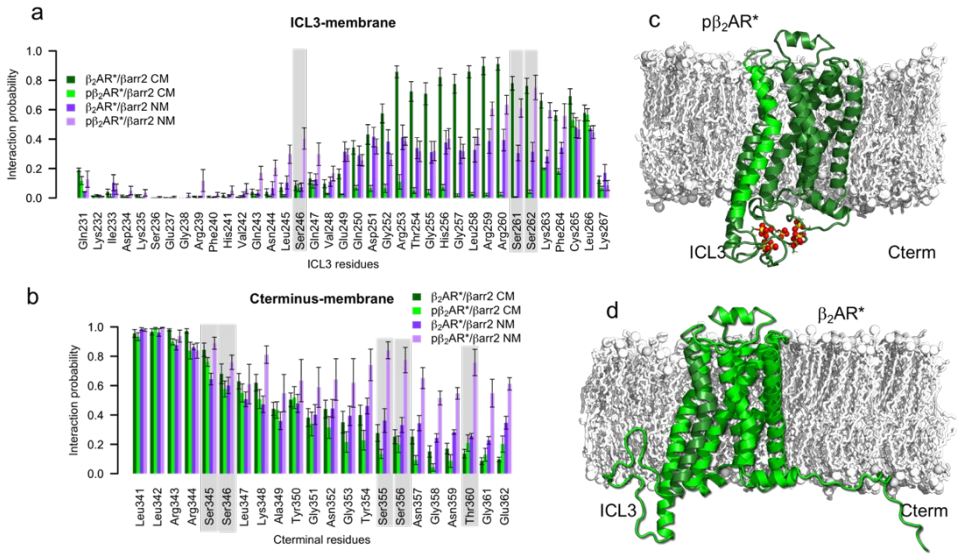

Figure 2: Interplay of membrane composition and β_2AR phosphorylation. Interaction probability per residue of ICL3 (a) and C-terminus (b) with negatively charged membrane (CM) in green tones and with neutral membrane (NM) in purple tones. The phosphorylated receptor (visualised in c) is shown in dark tones and the nonphosphorylated receptor (shown in d) in light tones. The phosphorylatable residues are highlighted by grey background or as yellow/red spheres in c.

bundled into so called beads or particles having average properties of the atoms they represent. The resulting speed-up amounts to a factor of 350 for the here applied methodology and simulation system. However, CG simulations cannot be as well parallelized as AA systems of the same size. In detail, we have used 2 SuperMUC-NG nodes (48 cores each) for CG and 13 nodes for AA simulations, producing ~340 ns and ~6.25 ns simulation time per hour, respectively. All CG simulations were run for 10 μs and all AA simulations for at least 1 μs. All simulations have been performed using the well-established, high performing simulation engine GROMACS [5] in single precision.

GROMACS has only low requirements concerning I/O. The trajectories and other output files are written regularly (every ~20-30 minutes) by appending data to a few binary and text files. All I/O is done by the first MPI rank only. Typical simulations require 2 GB and 12 GB storage, for 10 μs of a CG and 1 μs of an AA simulation, respectively. However, the storage requirements can increase significantly if the output is written out more often or if the storage of forces and velocities is needed.

Our analysis has revealed that phosphorylation does not affect the interactions of the C-terminus with negatively charged lipids (Figure 2). Only in case of a neutral membrane surface, the phosphorylated C-terminus is attracted more to the membrane surface than in all other cases. More surprising was the dramatic effect of ICL3-phosphorylation on its interaction probability with the charged membrane (see Figure 2a), i.e. in the activated but nonphosphorylated state of the receptor (β_2AR*), the transmembrane helix 6 (TM6)-proximal half of ICL3 is almost always attached to the membrane surface. Upon phosphorylation (pβ_2AR*) this interaction is diminished and the ICL3 is almost completely localized in the cytosolic space. This behavior is reversed by embedding the receptor into a neutral membrane. In the nonphosphorylated state, the interaction of the TM6-proximal half of ICL3 with the neutral membrane is less probable than in case of the negatively charged membrane. Upon phosphorylation, the interaction probability increases around ICL3-phosphorylation sites.

In order to reveal whether this tremendous difference in the interaction probability of ICL3 upon phosphorylation with its native negatively charged membrane has an impact on the complex shape with arrestin, multiple complexes of phosphorylated active β_2AR (pβ_2AR*) with its cognate β-arrestin2 were prepared (a spontaneous assembly of the complex at coarse-grained resolution is shown in [3]) and equilibrated atomistically. The simulations have revealed that β-arrestin2 can bind to pβ_2AR* in diverse orientations and insertion depths. Both the conformations and their flexibility are influenced by both the phosphorylation state of the receptor and the membrane composition (Figure 1).

Ongoing Research / Outlook

By steered-MD we have pulled apart diverse complexes (including different activation states of the receptor and diverse membrane compositions) of β_2AR and arrestin and recorded force-time curves and combined them with atomic force microscopy measurements. The acquired results build a solid basis for further investigation of the regulation mechanisms of extracellular signal transmission to the cell. We were able to pinpoint residues that are especially important for stabilisation of the bound states and during unbinding. This knowledge is of special pharmacological importance because currently only the activation state of the receptor is targeted by pharmaceuticals. However, arrestin binding to the receptor competes with binding of its cognate G protein and causes receptor desensitization, thus opening new pathways for pharmacological intervention.

References and Links

[1] Weis, W.I., B.K. Kobilka, Annu. Rev. Biochem., 2014. 87(1): p. 897-919.
[2] Butcher, A.J., et al., Handb Ecp. Pharmacol., 2021, (208), p 79-94.
[3] Pluhackova, K., F.M. Wilhelm, D.J. Müller, Front. Cell Dev. Biol., 2021. 9.
[4] Wassenaar, T.A., et al., J. Chem. Theory Comput., 2014. 10(2): p. 676-690.
[5] https://www.gromacs.org

Secrets of Signaling through Cell Walls

Research Institution
[1]Computer-Chemistry-Center, Friedrich-Alexander-University Erlangen-Nürnberg
[2]Institute for Biochemistry, Friedrich-Alexander-University Erlangen-Nürnberg

Principal Investigators
Timothy Clark[1], Heinrich Sticht[2], Peter Hildebrand[3]

Researchers
Jacqueline Calderon[1], Marcus Conrad[2], Hossein Batebi[3], Guillermo Perez[4]

Project Partners
[3]Institut für Medizinische Physik und Biophysik, Universität Leipzig
[4]Institut für Medizinische Physik und Biophysik, Charité Universitätsmedizin Berlin

SuperMUC Project ID: pr74su (Gauss Large Scale project)

Introduction

G-protein coupled receptors (GPCRs) are membrane proteins that transmit the effects of extracellular ligands to effect changes in the intracellular G-protein signaling system. Approximately 800 GPCRs are encoded in the human genome and approximately half of all marketed drugs target GPCRs. It is therefore not surprising that GPCR-research was recognized by the award of the 2012 Nobel Prize in Chemistry to Robert Lefkowitz and Brian Kobilka. Crystal structures of only 113 different GPCRs are currently available. Importantly, GPCRs can exist in active or inactive conformations and in binary complexes with ligands or intracellular binding partners (IBPs, G-proteins or β-arrestin) or in ternary complexes with both a ligand and an IBP. Crystal structures often deviate from the natural system: Proteins, especially membrane-bound ones, do not necessarily crystallize in their biologically active structures and the measures needed to obtain suitable GPCR crystals tend to increase the diversity between the natural environment and the crystal. It is within this context that molecular-dynamics simulations play a special role in GPCR research as a full-value complement to experimental studies.

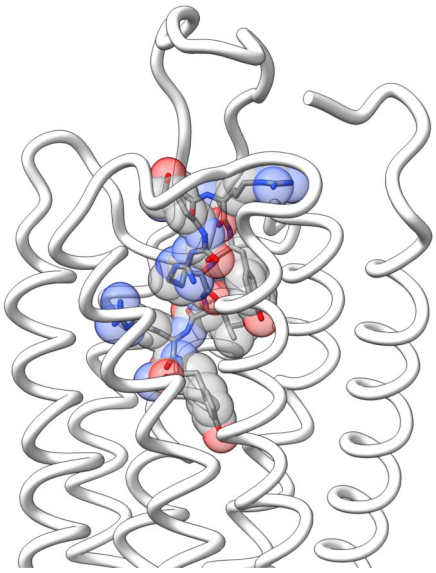

Very long timescale MD simulations can be performed on specialized hardware but are less effective on more conventional massively parallel supercomputers because the simulations only scale up to a relatively limited number of CPUs or GPUs. Luckily, modern variations of metadynamics can make very effective use of massively parallel CPU-based hardware, as has been shown in this project.

Results and Methods

GPCRs were investigated using classical (force-field) molecular-dynamics (MD) simulations on receptors embedded in a model membrane to represent the cell wall. Targeted MD was performed using a metadynamics protocol developed within the project. Most simulations use Gromacs 2019.4 and Plumed 2.5.3. Unbiased MD simulations achieved on average 200 ns/day using 16 nodes (48 cores each) corresponding to ≈ 100 core-h/ns on SuperMUC-ng. Metadynamics simulations perform similarly and converge within 2 µs ≈ 200,000 core-h/run. Performance was optimized via the compute protocol, rather than by modifying software.

Receptor activation
Most of our work has centered on Class A GPCRs but we were able to identify the activation mechanism of a Class B receptor, the glucagon receptor, in very extensive metadynamics simulations with two collective variables [1]. We have now developed a general protocol to simulate the activation/deactivation free-energy profiles of Class A receptors that has proven to be very successful in investigating the effects of different types of ligand on the receptor's conformational equilibria. Protocols have also been established to interpret these results in terms of the specific inter-residue interactions ("microswitches") usually discussed for GPCR-activation.

Receptor-ligand interactions
We have used molecular dynamics simulations to study the interaction between cyclic peptides and the neuropeptide Y Y_4 receptor (Y_4R), which belongs to the Class A GPCRs. [2] These peptides bind Y_4R with picomolar affinity (Figure 1) and exhibit a considerably more pronounced Y_4R selectivity compared to previous ligands. Therefore, they represent promising leads for the development of drug-like Y_4R ligands.

Receptor-catalyzed G protein activation
Our work is focused on the analysis of the formation of a productive complex of active receptor and G protein. Productive means that the receptor is observed

Figure 1: Model of the neuropeptide Y receptor (white tube) illustrating the binding mode of the highest-affinity ligand identified in [2]. The peptide is shown in stick representation and the volume of the atoms is additionally indicated as transparent spheres.

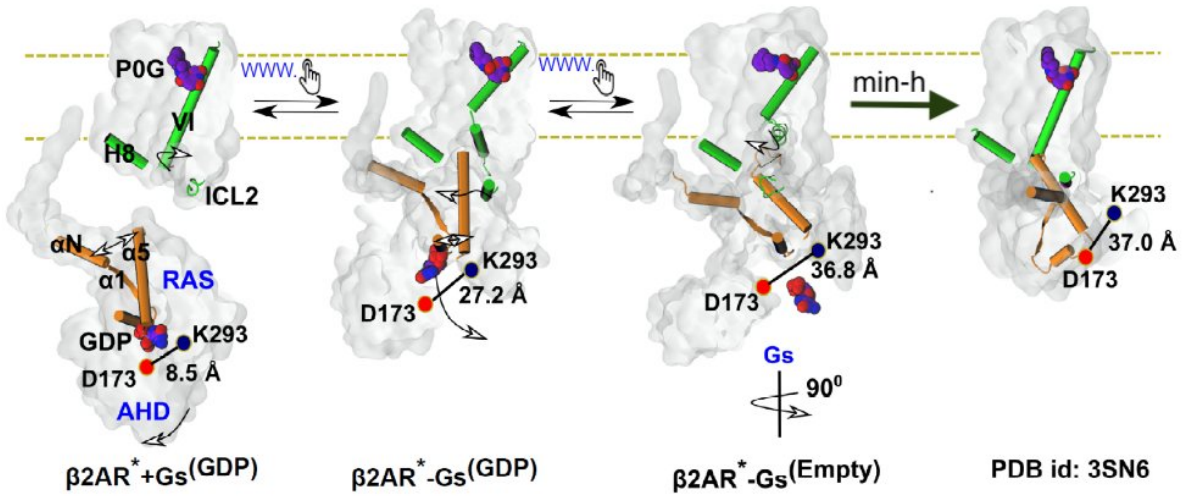

Figure 2: Structural mechanism of receptor catalyzed G protein activation.

catalyzing the nucleotide exchange in the G protein. In our unbiased all-atom MD simulations, the uncoupled receptor and GDP-bound inactive G protein spontaneously form a complex. Long-range allosteric effects are observed from the active receptor to the nucleotide, opening the nucleotide-binding pocket and breaking half of the GDP contacts. In subsequent umbrella sampling MD simulations, we observed the release of GDP from its binding pocket without touching the GDP. Our simulations provide insights into the structural mechanism the universal process of receptor-catalyzed G protein activation (see Figure 2 below).

Ongoing Research / Outlook

As in previous funding periods, project pr94su has made significant advances in the field of GPCR simulations, both in terms of developing computational protocols and in contributing to mechanistic and structural GPCR research in general. In the latter respect, the project has once more underlined the unusual importance in this experimentally very challenging field.

Our studies of the activation of GPCRs have reached a stage at which we now have a powerful tool for studying the activation/deactivation process in atomistic detail and can proceed to production simulations designed to answer open mechanistic questions. Future work will concentrate on the role of the preactive conformation first revealed in atomistic detail in reference [1] and now routinely identifiable for class A GPCRs, and on the roles and conformational effects of different kinds of ligands, with special emphasis on allosteric modulators.

Our close connection with Research Training Center 1910 *Medicinal Chemistry of selective GPCR ligands* provides us with unique opportunities to extend the scope and conclusions of experimental studies by considering new ligand/receptor combinations for which unpublished experimental data are available. In this respect, our studies on receptor-ligand interactions contribute new fundamental knowledge to enhance the ligand-design process. Protocols developed together with Prof. Francesco Gervasio (Geneva) allow us to translate the simulation results into analyses familiar to experimental GPCR researchers.

Finally, our studies go one step further than analyzing the differently active conformations of the receptor itself to investigate the process by which the active conformation(s) of the receptor actually lead to signaling via G-protein activation. These studies represent a significant advance in the scope and applicability of GPCR simulations.

References and Links

[1] G. Mattedi, S. Acosta-Gutiérrez, T. Clark and F. L. Gervasio, Proc. Nat. Acad. Sci. USA (2020) 117, 15414-15422.
[2] A. Konieczny, M. Conrad, F. J. Ertl, J. Gleixner, A. O. Gattor, L. Grätz, M. F. Schmidt, E. Neu, A. H. C. Horn, D. Wifling, P. Gmeiner, T. Clark, H. Sticht and M. Keller, J. Med. Chem. (2021) 64, 16746-16769.

Plasma Physics

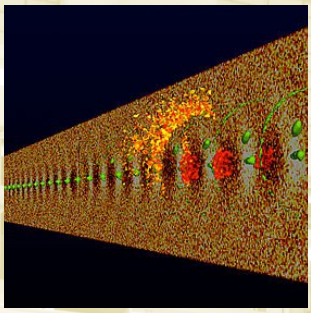

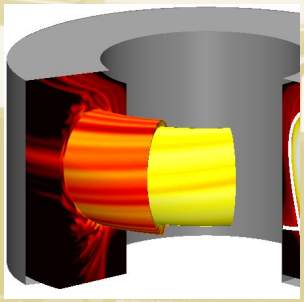

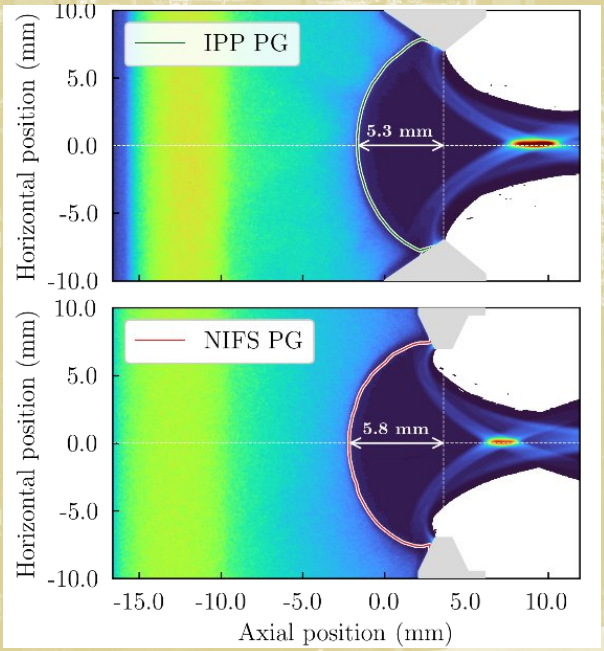

The plasma inside the KATRIN experiment

Research Institution
[1]Institut für Theoretische Astrophysik, Heidelberg

Principal Investigator
Felix Spanier[1]

Researcher
Jonas Kellerer[2]

Project Partner
[2]Institut für Astroteilchenphysik, KIT

SuperMUC Project ID: pn68gi

Introduction

The KATRIN experiment aims at a high precision limit for the electron neutrino mass by measuring the electron spectrum of tritium decay at the endpoint. In order to achieve this precision, it is necessary to have a tritium source with a very high column density. The Windowless Gaseous Tritium Source has a beta decay luminosity of 10^{11} beta decays per second. It consists of a cylindrical tube of 16 m length, which is open at the one side towards the detector, and closed off at the other by the so-called rear wall. Within the WGTS, electrons are guided by a strong magnetic field (up to 3.6 T) to the detector.

The stream of high energy (10 keV and above) electrons through the gas can ionize tritium and through subsequent atomic and molecular processes the electron density becomes non-negligible which leads to a plasma. The plasma has an electric potential in relation to the walls. This in turn changes the potential energy of beta-decay electrons with respect to the detector. For a high-precision measurement of the electron spectrum it is inevitable to understand the plasma potential.

Results and Methods

The plasma physics within the WGTS is a complex interplay of tritium decay, atomic and molecular processes and (kinetic) plasma physics. Additionally, the experiment itself is large in terms of the typical plasma length scales. The complete set of physical equations can therefore not be simulated in one numerical code. Two complementary codes were used in this case:

- *KARL* a Monte Carlo code which generates tritium decay electrons from a given tritium gas density and calculates the spectra and currents of electrons and ions in a given electromagnetic field configuration
- *ACRONYM* is particle-in-cell code that has been adapted for the source geometry of the WGTS. From a given set of particles spectra it calculates the plasma properties and subsequent electromagnetic fields in the WGTS.

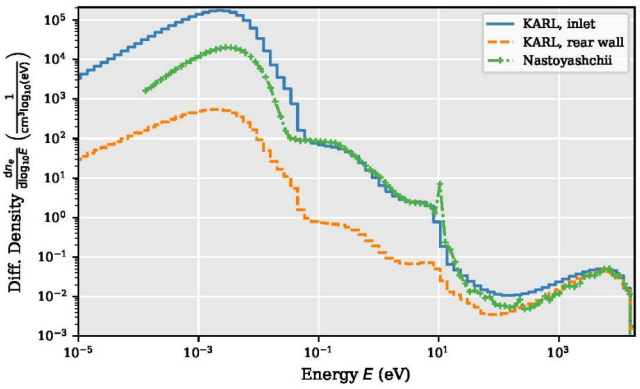

Figure 1: *KARL* simulations showing the energy spectrum of electrons compared to older results by Nastoyashchii [2].

The output parameters of *KARL* can be used as input parameters for *ACRONYM* and vice versa, which leads to an iterative approach until convergence is reached.

The *ACRONYM* code is well described in [1]. The boundary conditions at the WGTS wall have been implemented using the Dey-Mittra-algorithm.

Full simulations of the WGTS are extremely expensive and not necessarily insightful. The interesting physics is taking place near the rear wall. Several simulations have been carried out, where only sections of the WGTS have been simulated and the connection to the rest of the WGTS has been implemented by a free-streaming boundary.

The *KARL* code was developed completely new to allow for Monte Carlo simulations of all charged particles within the WGTS. It includes all relevant physical processes including elastic scattering, ionization, recombination, cluster formation and electric excitation. One major difference to classical Monte Carlo codes is the implementation of density fields that track the density of electrons and ions during simulation, which allows for the correct implementation of recombination processes.

The main goal of *KARL* is to determine particle spectra and densities at any point inside the WGTS. Due to the extreme pressure gradient the spectra differ drastically.

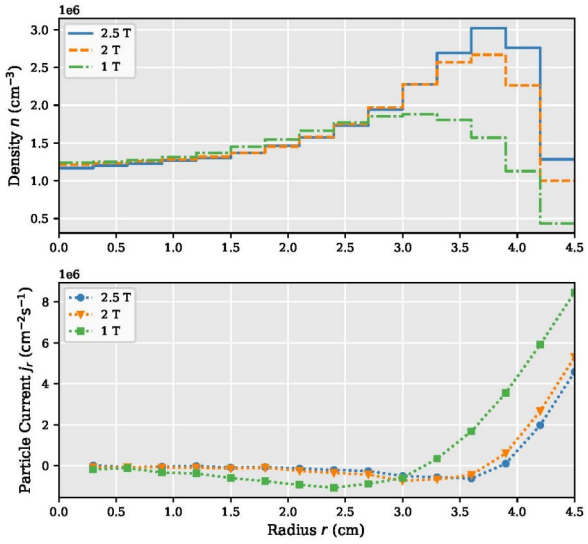

Figure 2: *KARL* simulations showing the ion density as a function of the radius and the ion current in radial direction. A non-negligible radial current and a subsequent loss of particles is imminent.

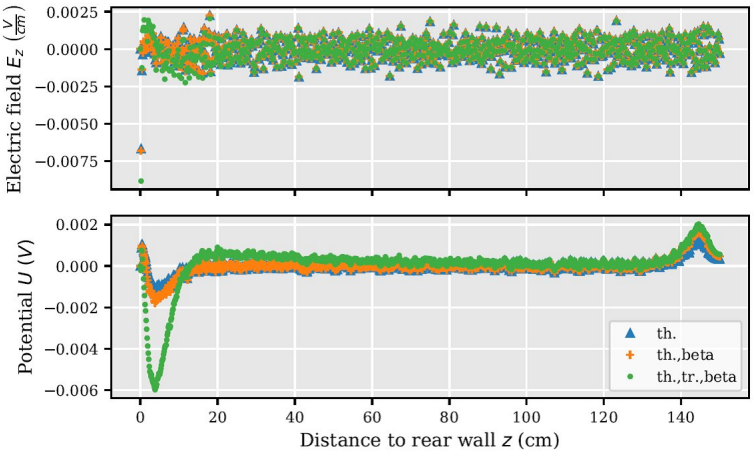

Figure 3: Potential and electric field for varied electron distributions in *ACRONYM* simulations. Green dots include the full spectrum, blue dots include only the thermal electrons.

Figure 1 shows the spectra at the rear end and the center of the WGTS in comparison to older simulations [2]. One key result is that the electron spectrum can be separated in a primary component (electrons from tritium decay), a secondary (nonthermal component), and the thermal background. The ratio of these components is position dependent, but the primary and secondary component are nowhere negligible.

Another important finding is that despite the strong magnetic field there is a non-negligible radial ion current in the center of the WGTS (Figure 2).

As pointed out above, the output of *KARL* simulations is the input for *ACRONYM* simulations. These simulations have taken most of the computing time in the project. One of the most interesting results is the rear wall potential. In Figure 3, the influence of the non-thermal electrons on the plasma potential is shown. Clearly the potential is affected by the particle spectrum of electrons. Simulations shown here are 3d simulations of the first 160 cm next to the rear wall with an inflow boundary on the right. The full source simulations are shown in Figure 4.

Ongoing Research / Outlook

Several open questions followed from the simulations:

- Does the interaction of energetic electrons with the rear wall have an influence?
- The rear wall may be coated with a monolayer of tritium in the course of time turning it from an ideal conductor to a dielectric. How does this affect the plasma potential?
- From experimental side there is still the question of the ideal parameters, which makes a series of simulations in different physical environments necessary.

Two different numerical approaches are tested: A *r-z*-code, which maps the cylindrical source geometry to two dimensions, and 1d Vlasov simulations.

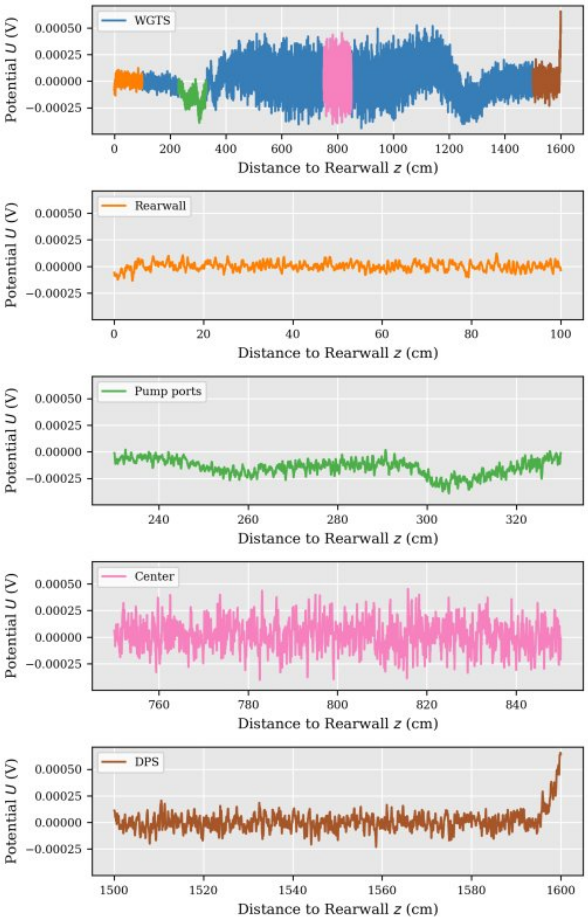

Figure 4: Electric potential for full source simulations including zoom-ins to different regions.

References and Links

[1] P. Kilian, T. Burkart, and F. Spanier. “The Influence of the Mass Ratio on Particle Acceleration by the Filamentation Instability”. In: High Performance Computing in Science and Engineering ’11.

[2] A.F. Nastoyashchii et al. “Effects of Plasma Phenomena….”. In: Fusion Science and Technology 48.1 (2005), pp. 743–746.

SNOX upgrade: improved insight into the physics of particle extraction

Research Institution
[1]Max-Planck-Institut für Plasmaphysik, Garching

Principal Investigator
Dirk Wünderlich[1]

Researchers
Max Lindqvist[1], Alessandro Mimo[1], Serhiy Mochalskyy[1], Adrien Revel[2], Tiberiu Minea[2], Ursel Fantz[1]

Project Partners
[2]Université Paris-Saclay, CNRS, LPGP, Orsay

SuperMUC Project ID: pn69wu

Introduction

Production and acceleration of negative H^- and D^- ions are required for the Neutral Beam Injection (NBI) system used for heating and current drive in the future fusion experiment ITER [1]. The negative ions are produced in large radio-frequency driven ion sources. Present in these ion sources are magnetic fields with a complex 3D topology, with the aim of decreasing the amount of co-extracted electrons. Negative ions are produced via both Volume Production (VP) and Surface Production (SP). SP is enhanced by caesiation of the inner source surfaces, reducing the work function. Negative ions are extracted from the plasma by applying a voltage of up to 10 kV between the Plasma Grid (PG) and the Extraction Grid (EG), the first two grids of the extraction and acceleration system. At steady-state, an equipotential surface between the quasi-neutral plasma and the extracted ion beam, the so-called meniscus, is formed.

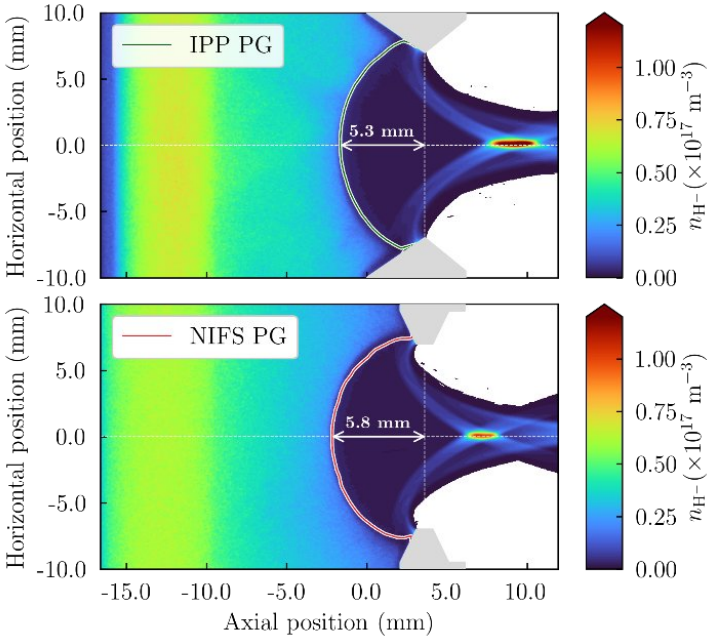

Figure 1: Particle density of SP H^- ions at steady state, averaged over 50 ns. The meniscus is marked by a green or red line, respectively.

Negatively charged particles passing through the meniscus are accelerated by the applied electric field. The magnetic field is generated by a current drawn through the PG and by permanent magnets embedded into the EG. It plays an important role for the electron trajectories and ensures that electrons co-extracted with the ions are dumped onto the EG. The main aim for negative ion sources for ITER NBI is to reach a high current density of negative ions during pulses with a length of up to 1 h while keeping the extracted electron current below that of negative ions. The achievable extracted negative ion current density is limited, in particular in deuterium operation, by the power deposited by the co-extracted electrons onto the EG, i.e. by the co-extracted electron current density of and its increase in time.

Simulations were performed using the 3D-PIC Monte Carlo Particle In Cell (PIC) code ONIX [2] with input plasma parameters (particle densities and temperatures) and grid geometry based on the ELISE ion source, operational at IPP Garching, Germany. ONIX was originally developed at Laboratoire de Physique des Gaz et des Plasmas (LPGP), Orsay, France and allows for performing predictive calculations with complex 3D geometries. Additionally, ONIX allows for taking a full 3D magnetic field as input, being necessary for studying the intrinsically 3D effects which the magnetic field plays on the trajectories of electrons in the plasma. These trajectories are of high relevance for the co-extraction of electrons. PIC codes, in particular in 3D, require a large calculation time and thus typically use small calculation domains only. ONIX interfaces with beam codes such as IBSimu [3], allowing for particles to be tracked through the grid system downstream the end of the calculation domain.

Calculation time at SuperMUC(-NG) was granted for three different topics. In total, 11 simulations were performed: three for the study of PG geometry, 7 for the study of the surface caesiation and one on the investigations of the effect for operation in Deuterium. As summarized in the following, almost all raised questions were answered.

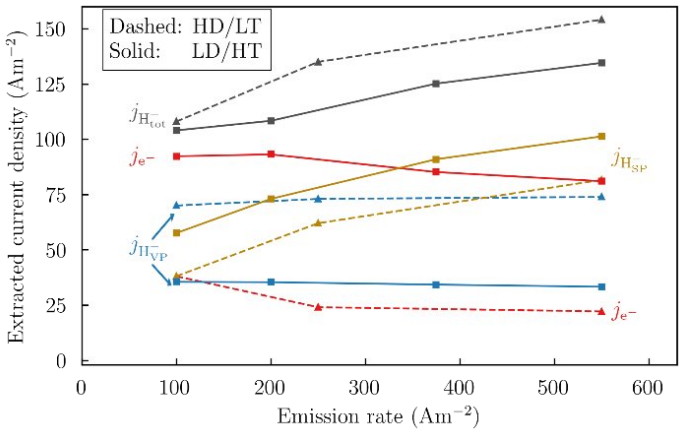

Figure 2: Extracted current densities for the LD/HT case and HD/LT case for a variation of H⁻ SP emission rate varying from 100 to 550 A/m².

Results and Methods

In ONIX, charged particles (electrons, negative ions and positive ions) are tracked self-consistently according to the 3D-PIC algorithm [4]. The simulation domain covers one of the 640 apertures of the PG in the ELISE ion source, starting 21 mm upstream of the knife edge of the chamfered aperture and reaching the EG, 9 mm downstream of the aperture knife (for an illustration of the grid geometry see the upper part of Figure 1). The boundary condition of the electrostatic potential at the plane of the EG is set to the vacuum solution for a potential difference between PG and EG of 10 kV. In order to ensure numerical stability, the size of the used grid cells and the time step need to resolve the Debye length and the inverse plasma frequency, respectively. Fulfilling these requirements necessitates the use of HPC computing for an accurate 3D representation of the plasma. Each of the simulations presented here lasted 921,600 core hours on 4,608 cores.

The PG geometry plays an important role on the meniscus formation and consequently on the optics of the extracted H⁻ ion beam. Simulations were made using two geometries for the PG, the first one (IPP PG) being based on the standard geometry of the ELISE ion source and the smaller BATMAN Upgrade (BUG) machine. The second one is based on the geometry recently used in National Institute for Fusion Science (NIFS) in Gifu, Japan (NIFS PG) and tested in BUG. Figure 1 shows for both cases the particle density of H⁻ ions at steady state along with the shape of the meniscus. The SP H⁻ ions are produced uniformly over the PG surface; however, the majority of the extracted SP H⁻ ions are produced near the knife edge of the PG, which allows the ions to be directly extracted without entering the plasma. In contrast, the VP H⁻ ions are extracted more uniformly over the meniscus. The penetration of the meniscus affects the trajectories of both SP and VP negative ions and thus plays an important role in the beam optics of the extracted negative ion beam as the SP ions are responsible for the halo component. Due to the shallower chamfered area on the plasma side of the NIFS PG, fewer SP H⁻ ions are extracted and the focus point of the extracted ion beam is moved further upstream. These results point out the relevance of the extraction system geometry, in particular close to the knife edge. They are the motivation behind ongoing further investigations with the aim of further reducing the achievable beamlet divergence.

A systematic study on effects of the surface caesiation was performed with two sets of plasma parameters. The first one with electron density n_e=6×10^{16} m^{-3} and electron temperature T_e=2 eV named High Temperature/Low Density (HT/LD) and the second one with n_e=1.2×10^{17} m^{-3} and T_e=1 eV named High Density/Low Temperature (HD/LT). For both cases the extracted negative ion current density is determined for varying the emission rate of SP H⁻ ions from 100 A/m² to 550 A/m², resulting in 7 calculations in total. Figure 2 shows the extracted current density of VP H⁻ ions ($j_{H\text{-}VP}$), SP H⁻ ions ($j_{H\text{-}SP}$), the total ion current density $j_{H\text{-}Tot} = j_{H\text{-}VP} + j_{H\text{-}SP}$ and the co-extracted electron current density (je-). By increasing the emission rate by a factor of 5.5 $j_{H\text{-}SP}$ increases by ~40 A/m² in both cases. The increase of extracted negative ions is correlated with a slight decrease of co-extracted electrons. This effect is small because the majority of SP H⁻ ions is directly extracted without entering the plasma (see Figure 1) and thus does not affect the charge balance close to the meniscus surface. The emission rate variation reflects a variation of the surface work function, taking place in the experiment during the caesium conditioning phase and during plasma pulses. The present results help developing a better understanding in the source performance dynamics, in particular during long pulses and pulses with high RF power.

Investigations on the isotope effect Hydrogen ↔ Deuterium have been performed, indicating an increased depth of the Debye sheath towards the PG compared to hydrogen. In interplay with the magnetic field, the losses of electrons towards the PG surface are reduced, resulting in an increased co-extracted electron current. This result is the first step in developing an improved insight into the physics behind the strong isotope effect observed in negative ion sources based on the surface effect.

Ongoing Research / Outlook

Currently, investigations on the effect of biasing of the PG with respect to the source walls are being conducted. In experiments this has been shown to have a strong impact on co-extraction of electrons, allowing for operation with higher power and higher extraction potential. Moreover, studies on the electron loss along the magnetic field lines, as well as simulations with a two-aperture geometry is in preparation. These projects will provide further insights into the electron transport near the PG which is essential for improving the source performance in the direction of application for ITER and DEMO [5,6].

References and Links

[1] R. Hemsworth, et. al, Nuclear Fusion, 49(4):045006, (2009).
[2] A. Revel, et. al, Journal of Applied Physics, 122(10):103302, 417 (2017).
[3] T. Kalvas, et. al, Review of Scientific Instruments, 455 81(2):02B703, 2010.
[4] C. K. Birdsall and A. B. Langdon. Plasma Physics via Computer Simulation. McGraw-Hill (1991).
[5] Lindqvist et. al., "3D Monte-Carlo PIC modeling of plasma grid biasing and the co-extraction of electrons in negative ion sources", SMuK 2021.
[6] Lindqvist et. al., submitted to Plasma Sources Sci. Technol.

Predictive first-principles simulations of the tokamak boundary

Research Institution
[1]École Polytechnique Fédérale de Lausanne (EPFL), Swiss Plasma Center
[2]École Polytechnique Fédérale de Lausanne (EPFL), SCITAS

Principal Investigators
Paolo Ricci[1], Christian Theiler[1], Gilles Fourestey[2]

Researchers
Davide Galassi[1], Diego Sales de Oliveira[1], Maurizio Giacomin[1]

Project Partners
–

SuperMUC Project ID: pn73si (Prace project no. 2020235617)

Introduction

Fusion energy, the energy source of the stars, is among the very few options to provide safe, clean, abundant, and sustainable electricity. The ITER experimental reactor is being built in southern France to prove the scientific and technological feasibility of fusion energy. In parallel, improved concepts and ideas in view of the first demonstration fusion power plant, called DEMO, are being explored intensively through theory, modeling, and experiments on today's experimental facilities. Both ITER and DEMO are tokamaks, nowadays the most advanced device to provide fusion energy. Tokamaks confines the fusion fuel, which is in the plasma state, magnetically in the center of a donut-shaped vacuum vessel. In the periphery region of a tokamak, the plasma interacts with the solid wall, determining the boundary conditions for the core and the heat load on the vessel walls, a possible showstopper for the entire fusion program, if the material requirements cannot be met. Although the success of ITER and the design of DEMO critically depends on the plasma dynamics at its periphery, the theoretical understanding of plasma dynamics in this region remains a critically open issue. A main reason for the complexity of the boundary plasma is related to the presence of the X point, a region where the poloidal field vanishes. The X point is needed to concentrate plasma-wall interaction to an area spatially separated from the core plasma, called the target plates. A complicated flow pattern is observed around the X-point, where background large-scale flows co-exist and non-linearly interact with complex turbulence dynamics. Turbulence appears in form of structures elongated in the direction of the magnetic field, that regulate the transport of particles and energy in the cross-field direction. Until recently, the numerical simulation of the plasma dynamics in the tokamak boundary region including an X point have been performed exclusively with 2D codes, exploiting the toroidal symmetry of tokamaks. These are useful tools to describe the plasma-wall interaction, but they cannot self-consistently describe transport processes due to turbulence, which is inherently a 3D phenomenon. Thanks to the progress in numerical schemes and the increase in computational resources, "real-size" turbulence simulations of tokamak boundary plasmas in X-point geometry are now possible. First-principles turbulence simulations and a detailed assessment of their agreement with the experiments is of utmost importance to reach the necessary understanding of the plasma physics in the boundary of tokamaks.

Results and Methods

Global simulations of plasma turbulence in the tokamak periphery are carried out within this project with the GBS code [1,2,3]. GBS evolves in time drift-reduced Braginskii equations, a set of fluid equations for electrons and ions in a strong magnetic field. The boundary conditions applied to describe the interaction of the plasma with the solid wall were rigorously derived at the Swiss Plasma Center. The code solves at the same time the kinetic equation for neutral atoms, a unique feature for a first-principles turbulence code. In GBS the plasma dynamics is evolved as the interplay between plasma sources (due to the neutral ionization and the plasma outflow from the tokamak core), turbulent transport, and plasma losses at the walls through recombination processes. Therefore, the simulations evolve self-consistently both the plasma profile and its fluctuations, with no separation between equilibrium and fluctuation scale lengths.

The GBS code is based on a flexible coordinate system that allows simulation of plasma turbulence in arbitrary magnetic geometries. Spatial discretization is based on a non-field aligned fourth-order finite difference scheme that discretizes the radial, vertical and toroidal directions on a regular cylindrical grid. Time stepping is performed by using a standard 4th order Runge-Kutta advancement. The GBS code is written in Fortran 2003 language and parallelized using domain decomposition in the three dimensions with the Message Passing Interface (MPI) library. An iterative solver for the Poisson equation was recently implemented by using the PETSC library, which improved the scaling of GBS. A simulation of a tokamak, such as the one carried out within this

project, requires approximately 10^7 core-hours, that are needed to simulate 50 time units, a typical characteristic time scale of the global evolution of the plasma fields in the tokamak boundary. The GBS code can efficiently run on up to 128 nodes. The code generates a HDF5 result output file per run, containing the snapshots of the plasma and neutral fields, approximately every 50,000 time steps, resulting in a file with a typical size of 10 GB. A typical simulation requires therefore few TB of storage memory. For the neutral part, a memory of 33 GB/node is required for the 128 nodes simulation and 40 GB/node for the 16 nodes simulation, which is largely within the SuperMUC-NG capacity.

At the beginning of the project, we performed simulations of TORPEX, a basic toroidal plasma device at the Swiss Plasma Center. A new scenario featuring an X-point was specifically developed for the comparison with turbulence codes. The relatively low temperatures achievable in TORPEX and its small size allow a thorough comparison between simulations and experiments. The predictive capability of the code were quantified through a rigorous validation procedure, which was applied to several turbulence codes, including GBS [4]. The codes were able to well reproduce experimental background flows, while some discrepancies were found between simulations and experiments in the fluctuation properties. This work has given important guidelines on how to improve turbulence modelling in order to precisely describe the plasma dynamics in the X-point region.

As a next step, we have focused on the simulation of realistic TCV diverted configurations and their validation. TCV (Tokamak à Configuration Variable) is a tokamak located at the Swiss Plasma Center, and one of the main devices operated by the European fusion research community through the EUROfusion consortium. We considered two TCV simulations with different magnetic parameters that we validated against TCV-X21, an experimental dataset developed as a testbed for boundary turbulence codes. The simulations consider L-mode discharges featuring an X-point. In this work, we did not include the self-consistent coupling of the neutral dynamics. These simulations were part of a large validation effort at European level, where the Swiss Plasma Center had a leading role [5]. The codes were found to predict well the plasma profiles at upstream locations, while profiles broader than the experimental ones were predicted by the codes at the target plates, where plasma losses occur. A repository including the experimental dataset, the simulation results and the validation procedure has been published with open access, effectively constituting a benchmark for plasma turbulence codes [6].

A more advanced simulation of the TCV boundary has been started, with the most up-to-dated version of GBS, including the neutral dynamics and electromagnetic effects. Preliminary results show smaller turbulent structures with respect to former simulations, which we expect to lead to narrower heat flux profiles at the wall, thus improving the current agreement between simulations and experiment. The same validation procedure will be applied to these new simulations, allowing to quantify the improvements introduced with the inclusion of neutral dynamics, which is expected to be a key physics element. The results of the GBS validation work will be presented as an invited contribution at the 48th European Conference on Plasma Physics, one of the most important international conferences on this topic.

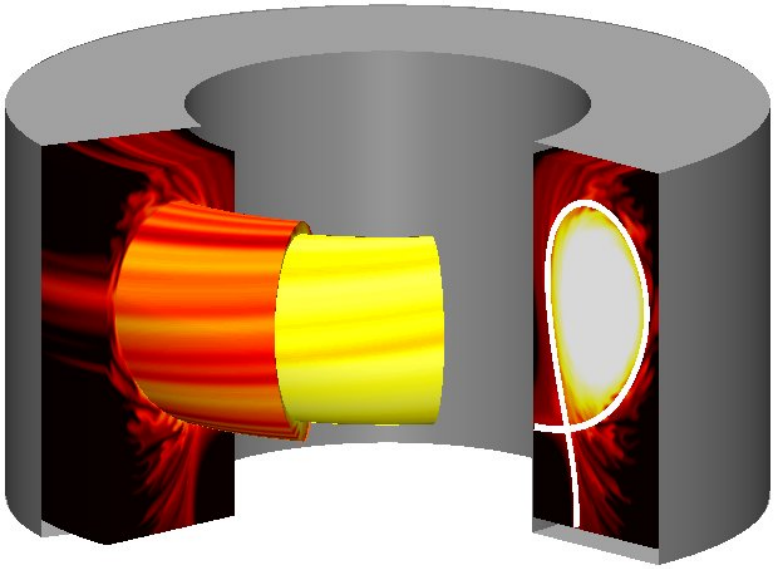

Figure 1: Snapshot of plasma density fluctuations in the TCV tokamak from a GBS simulation. The solid line represents the surface separating the confined region from the region where the heat is exhausted to the walls.

Ongoing Research / Outlook

The multi-scale nature of the physics of turbulence in the tokamak boundary in realistic plasma conditions implies simulations with a high number of degrees of freedom and a relatively long time simulated with respect to turbulence characteristic times. SuperMUC-NG is one of the few supercomputers in the world that allows to run such large-scale simulations as the ones needed for this project, in a human time scale of few months. We plan to continue our validation project by exploring different plasma parameters, starting from the described TCV simulations. In particular, a GBS simulation with high plasma density has been started, aiming at reaching a so-called “detached” plasma regime, which is relevant for future tokamaks since it minimizes the interaction between the plasma and the first wall components. We are also performing a high-power TCV simulation. In these conditions, plasma should access a high confinement regime, which will also be the operating regime of ITER. These new simulations will be validated against dedicated TCV experiments, following the same procedure as in the previous works [4, 5]. This will be an important further step towards the development of a reliable tool for the simulation of the tokamak boundary, that will allow for prediction of the plasma dynamics in future fusion reactors.

References and Links

[1] The GBS code for tokamak boundary simulation http://gbs.epfl.ch/index.html#autotoc_md14.
[2] P. Ricci et al., Plasma Phys Contr Fusion, 54 (2012) 124047.
[3] M. Giacomin, et al., J Comp Phys, 463, 111294 (2022).
[4] D. Galassi et al., Phys Plasmas 29 (2022) 012501.
[5] D. S. Oliveira et al. 2022 Nucl. Fusion in press https://doi.org/10.1088/1741-4326/ac4cde.
[6] https://zenodo.org/record/5776286

PSC Simulation Support for Novel Accelerator Concepts

Research Institution
Chair for Computational and Plasma Physics, Faculty of Physics, Ludwig-Maximilians-Universität München

Principal Investigator
Hartmut Ruhl

Researchers
Karl-Ulrich Bamberg, Patrick Böhl, Fabian Deutschmann, Constantin Klier, Bin Liu, Nils Moschüring, Viktoria Pauw

Project Partner
AWAKE Collaboration (CERN), Max Planck Institute of Quantum Optics (MPQ)

SuperMUC Project ID: pr74si (Gauss Large Scale project)

Introduction

Since the moment ultra-short high-power lasers became available, their potential use for accelerators drew great interest, as the charge separation in plasmas can induce enormous electromagnetic field strengths on a sub-micrometer scale. Accurate modeling of the plasma dynamics is essential for understanding of how the desired acceleration properties can be obtained. Considerable research efforts, both on a theoretical and experimental level, are still needed to achieve ambitious goals, such as medical applications for accelerated protons via laser interaction with mass-limited targets (MLT). These MLTs, such as micro-foils, nano-clusters, needles and wires are potential sources of fast particles and high-energy photons used for purposes such as imaging or treatment planning. The high-energy photons generated in non-linear laser interaction with ultra-thin-foils are of interest e.g. in the context of ultra-short attosecond X-ray pulses (AXP) that are required for the imaging of biological processes like protein folding or the behavior of Rhodopsin in the human retina.

Inspired by the results of larger full kinetic PSC simulations, we also have found a new ion acceleration regime, called Ion Wave Breaking Acceleration (IWBA) [2], where collimated and mono-energetic 200-400 MeV ion beams could be produced with available experimental parameters.

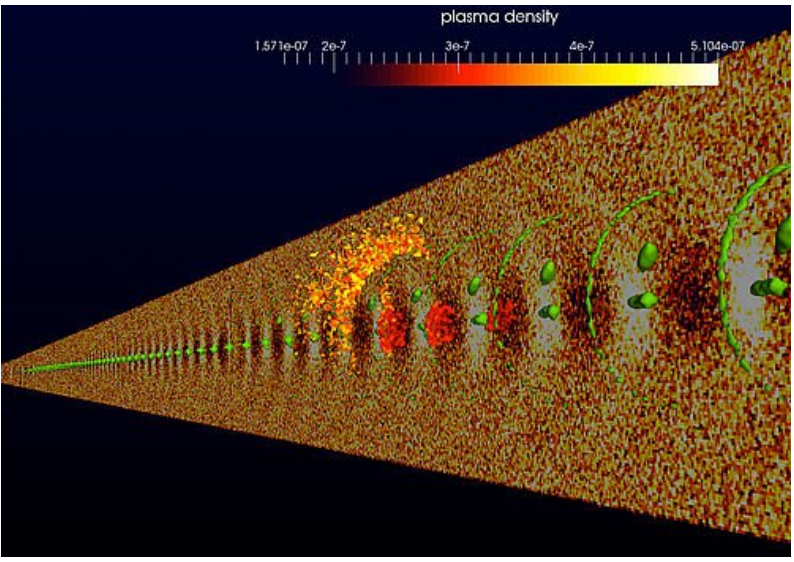

Figure 1: Visualization of the 450 GeV AWAKE ion beam (green), generated by the CERN SPS, inside the plasma (2D slice) and the accelerated electron witness beam (red/yellow). After 5m, micro-bunching and a strong wakefield (black/white pits) can clearly be recognized.

While these approaches use lasers to accelerate electrons which for their part accelerate protons/ions, the AWAKE project in contrast uses highly energetic protons for a new linear lepton accelerator concept for multi GeV electrons on some tens of meters instead of kilometers with the help of wake fields.

In previous projects, the technology necessary to run 10m box size simulations with micrometer resolution was established, such as enhanced memory management, better parallelism and increasing the I/O speed of checkpoints to an average of 105 GB/s to be able to run the simulation for full four weeks of pure wall-clock time on 32,768 cores. In the course of this project, the basic baseline case of AWAKE was simulated, producing dozens of TB with each output step. However, it turned out that instead of simulations with increased density, the experimentalists required several observables/output quantities with much higher temporal resolution. As a consequence, the major effort of the new project was put into increasing global communication efficiency to enable heavy “on-the-fly” data processing and analysis on the scale of tens of thousands of cores. This was a major challenge, but solving some serious issues dramatically increased the performance, so a lot of core hours could be invested in some new complex simulations involving quantum electrodynamical (QED) effects that were originally planned for a later project.

Results and Methods

The Plasma Simulation Code (PSC) [1] is a general-purpose framework to solve the extended Maxwell-Vlasov-Boltzmann system of equations via the PIC approach. The original FORTRAN version evolved to a modern modularized C simulation framework supporting bindings to FORTRAN as well as C/CUDA and features selectable field and particle pushers. The PIC approach is well-known for its good scaling capability

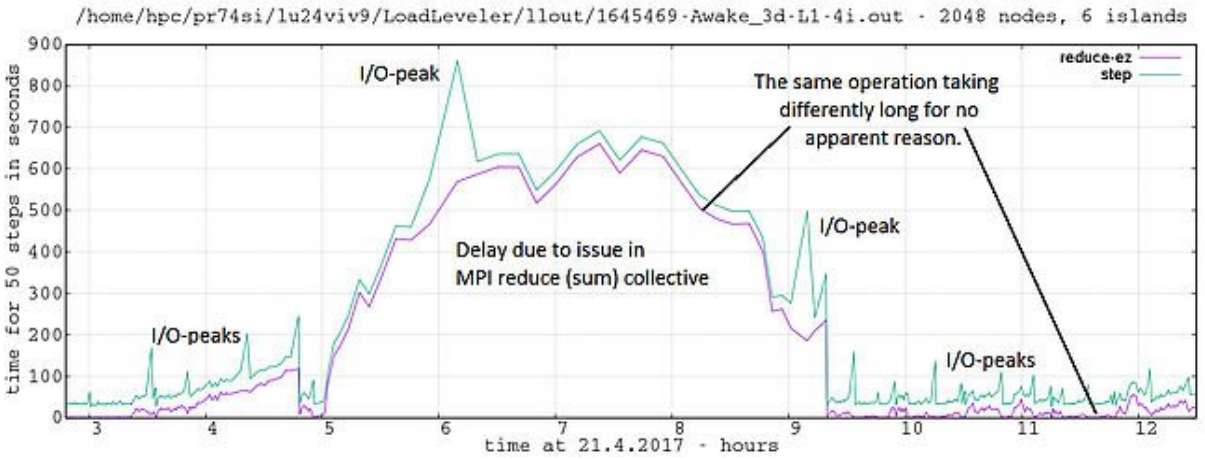

Figure 2: The purple line represents the time for the MPI_reduce (sum) routine used by an important inline analysis. The same analysis was done between the timespan 6 to 8 and 10 to 12. The green line corresponds to the total wall-clock time necessary for a time-step. There is a strong correlation showing that most of the time is spent in this MPI-reduction, blocking the simulation.

via configuration space parallelization. A Hilbert-Peano space-filling curve is used for efficient, dynamic and adaptive load and memory balancing allowing for complex and dynamic geometries.

Ultra-Thin Foils (UTFs): Generation of high energy photons by the "slingshot" effect
A very strong and very short (only a few cycles) – but experimentally available – circularly polarized laser pulse can “press” a major fraction of the electrons out of a 10 nm thick carbon-like foil. The generated electric field strongly accelerates the electrons back to the ions, and relativistic effects create an even shorter AXP useful to “film” protein folding which happens on the time scale of 10^{-18} seconds.

Together with AWAKE (see below), the nano-foil project is one of our biggest simulations requiring half a trillion grid cells. Due to this only few output steps are possible. The video below (Fig. 0) shows a 3D-Volume rendering of such a scenario (reduced resolution). During this project, the focus was placed on frequency analysis, which therefore also requires information from every time step. One goal consisted in the extension of the special output routines for better frequency sampling. In addition, we could reduce memory footprint of the simulation from 16 islands of SuperMUC Phase 1 (requiring “Block Operation”) to 8 islands, making the ultra-thin foil simulations much more feasible.

AWAKE: Linear lepton acceleration on the scale of meters instead of kilometers
The AWAKE project studies the interaction of a 450 GeV proton beam of the SPS pre-accelerator at CERN with a 10 m long plasma. Moving window technology allows for reducing the active memory footprint and the costs by a factor of 30 to about 3% of a full simulation. Nevertheless, every single output dump still takes 3 TB and checkpoints may take even up to 12 TB. For collaboration with experimentalists, these data were still not sufficient, as time-averaged observables requiring information from every single time step were also demanded. Therefore, instead of studying the beam filamentation at higher plasma densities, we redesigned the simulation and implemented heavy inline data processing and analysis in consultation with Dr. Konstantin Lotov (Head of Simulation Efforts of AWAKE).

We also ran a set of simulations with lower plasma density in the linear regime as benchmark with quite convincing results. However, especially the inline data processing on large scales led to a significantly increased amount of collective communication. This revealed an MPI issue most likely related to the IBM-MPI behavior on SuperMUC Phase 1 (Fig. 2).

Exhaustive investigations carried out together with experts from the LRZ Astrolab and engineers from IBM found leads that the problem could be related to the interaction of the collective and point-to-point communication patterns in the PSC with intra-node RDMA transfers. After their elimination the problems did not reappear.

Another big challenge consisted in the fact that the available IBM implementation, “pami_tune” provided only one algorithm for “MPI_GatherV”, which apparently used only “MPI-Root” as receiver. As INTEL did not scale to that many SuperMUC islands (at that time), a custom-tuned tree-like algorithm was written for the PSC, decreasing the wall-clock time from several hundred seconds (on 4-8 islands) to usually less than 40 ms, which is a speed-up factor of more than 2,000.

After having resolved these issues, we were able to provide the experimentalists with all the information they needed (Fig. 3) to reach the initial goal of confirming that the reduced codes (fluid-based and 2D cylindrically symmetric) can accurately represent the relevant physics as well as fully kinetic 3D simulations.

The Head of Simulation Efforts of AWAKE confirmed that the respective results showed high concordance, and by now also coincide with initial experimental results, e.g. the PSC simulations correctly showed that

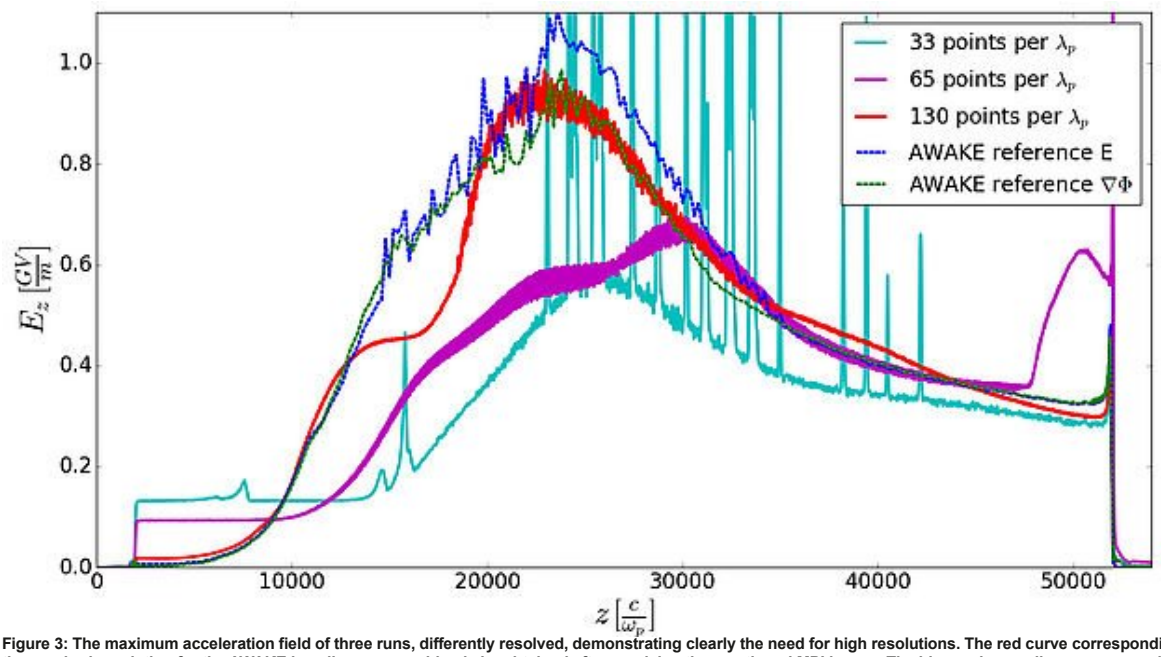

Figure 3: The maximum acceleration field of three runs, differently resolved, demonstrating clearly the need for high resolutions. The red curve corresponding to the required resolution for the AWAKE baseline case could only be obtained after resolving the mentioned MPI issues. The blue and green lines correspond to reference results, obtained by using reduced models (∇Φ as the derivative of the potential denotes sort of an averaged E_z). They show very good agreement [6].

there would be no hosing, a result that can only be predicted with fully kinetic 3D simulations. This represents an unprecedented benchmark at this extreme scale for Particle-in-Cell codes [7].

Mass-Limited Targets (MLTs): Ion acceleration for medical purposes

The approach consists in the long/strong acceleration of the electrons and the use of the thereby generated electric field to “pull” and therefore accelerate the protons. This is the direct contrast to AWAKE, where protons accelerate leptons.

Substantial progress was made in finding a parameter range that offers a higher ratio for the conversion of laser pulse energy into fast ion energy when using MLTs levitated in a Paul trap [5] to produce fast ions. In this project we tested different pulse shapes, field strengths and target geometries and densities.

By altering these parameters, the dynamic of the acceleration process can be shifted between different regimes like target normal sheath acceleration (TNSA), Coulomb Explosion (CE) and Radiation Pressure Acceleration (RPA). We studied the transition between these different dynamics and the properties of their fast ion spectrum and found that the maximum proton energies rise approximately linearly with pulse field strength for the near solid targets that were used in the experiments that were run in parallel to the simulation efforts.

Due to the necessary resolution, a typical simulation requires about 20 billion grid cells and runs approximately 12 hours on one island on SuperMUC Phase 1. Larger ones require up to 4 islands.

The simulations revealed that the absorption of laser energy can be enhanced by lowering the density of the target at primary pulse interaction. Experimentally, this can be achieved by pre-expanding the target with a minor pulse before the main interaction. With a target at roughly critical density (nc), the laser can penetrate the target completely and we have an enhanced RPA effect in addition to the coulomb explosion observed so far in experiments and simulations.

Additionally, the length of the pulse is adjusted to the expansion time of the exploding target. This leads to an increase of maximum proton energy from 100 MeV for solid targets to 400 MeV for less dense targets with a pulse energy of 100 J. If these results can be reproduced in experiment, it will be a significant improvement as compared to the older results, as ion energies of a few 100 MeV are then within reach at much smaller pulse energies that can be delivered by relatively common laser facilities. This set-up also concentrates the accelerated protons much more in the forward direction compared with the Coulomb exploding situation. The work was presented at the GSI-PHEDM conference Hirschegg in January 2020 as "PIC simulation of laser irradiated micro-plasma with varying density" and won the "Laser and Particle Beams" Young Scientist Award. The corresponding paper will soon be published.

Ion Wave Breaking Acceleration (IWBA): Experimentally easy available laser driven ion acceleration in gases and foam

Compared to the results of previous IWBA projects, the goal was to simplify the setup for experimentalists by finding laser parameter sets that should be commonly available for experimental laser physicists. The pulse form is now a pure Gaussian, in time as well as in space, and the laser intensity is lower than 10^{21} W/cm^2. The difficulty to overcome is then the

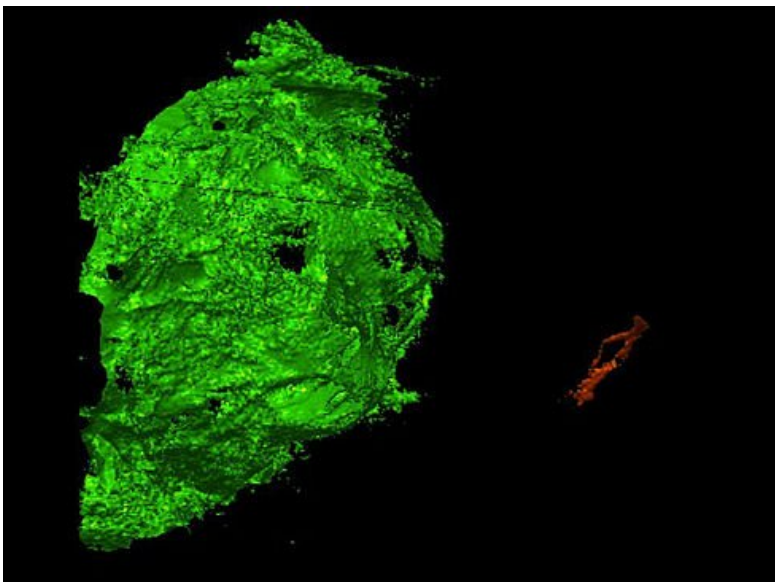

Figure 5: 3D-iso-surface plot for a 3D simulation with a 4 Joule circularly polarized laser pulse with a peak intensity about $6 \cdot 10^{20}$ W/cm². The pure Gaussian profile is common for experimental setups. The marked ions are accelerated to energies in the range of 60-80 MeV.

reduced parameter window for the IWBA regime. For example, with an intensity of $6 \cdot 10^{20}$ W/cm², the optimal initial plasma density has to be in the small range of 6.5 n_c to 8.5 n_c. Up to now, there is no good theory to analytically describe these phenomena. So it is necessary to scan the parameters very carefully to find the small window. Furthermore, the ion trapping happens in a very small region of space, therefore requiring high resolutions of at least 50 cells per micron [2, 3]. Larger runs (Fig. 5) usually require 2,000-2,560 cores taking 24-48 hours resulting in about 100 kilo-core-hours per run. The parameter scan consisted of several hundred runs (also smaller ones) on SuperMUC and also on its "little sister" Hydra (for "throughput"). The typical output is about two Terabyte per run being reduced to some Gigabytes during post-processing.

Some of the core-hours saved due to the change in the AWAKE simulation campaign and the increased communication efficiency were invested in the former mentioned projects (IWBA, MLT and UTFs) with the wonderful results described above and in the mentioned publications.

However, another part of the freed core-hours could be used to address some QED projects that were originally postponed and not part of the grant, due to their complexity but nevertheless succeeded to produce already worthwhile results.

QED Vacuum break down in counter propagating circularly polarized laser pulses: Matter-antimatter production

For very strong laser fields, effects like radiation reaction have to be accounted for. For the PSC a "photon" system was implemented for two reasons: On the one hand, the required resolution to resolve the radiation reaction is way too high even for moderate laser fields. On the other hand, the classic Maxwell equations are insufficient for stronger fields (a_0 ~ 1,000). The photons are generated by event generators for both cases, based on Monte-Carlo methods described in the theses of Constantin Klier and Fabian Deutschmann. Furthermore, adaptive time sub-cycle steps were necessary to implement correct dynamics and rates in very strong acceleration cases.

Because of the high memory requirements due to the dynamic production and rebalancing of particles, these simulations needed a complete island of SuperMUC Phase 1. The need for good statistics and the arithmetically complex equations to be solved required more than 120 wall-clock hours runtime, only for the results shown here.

References and Links

[1] https://www.plasma-simulation-code.net
[2] Liu, B., J. Meyer-ter-Vehn, and H. Ruhl. "Scaling of ion trapping in laser-driven relativistically transparent plasma." arXiv preprint arXiv:1803.06358 (2018).
[3] Liu, B., Meyer-ter-Vehn, J., Ruhl, H. and Bamberg, K.-U. "Laser Acceleration of Electrons, Protons and Ions", SPIE conference proceedings (2017) Volume 10240, IV.
[4] Ostermayr, T. M., et al. "Proton acceleration by irradiation of isolated spheres with an intense laser pulse." Physical Review E 94.3 (2016): 033208.
[5] Ostermayr, T. M., et al. "A transportable Paul-trap for levitation and accurate positioning of micron-scale particles in vacuum for laser-plasma experiments." Review of Scientific Instruments 89.1 (2018): 013302.
[6] Caldwell, A., et al. "Path to AWAKE: Evolution of the concept." Nuclear Instruments and Methods in Physics Research Section A: Accelerators, Spectrometers, Detectors and Associated Equipment 829 (2016): 3-16.
[7] N. Moschuering et al. "First Fully Kinetic 3D Simulation of the AWAKE Baseline Scenario", Plasma Phys. Control. Fusion 61 (2019): 104004.

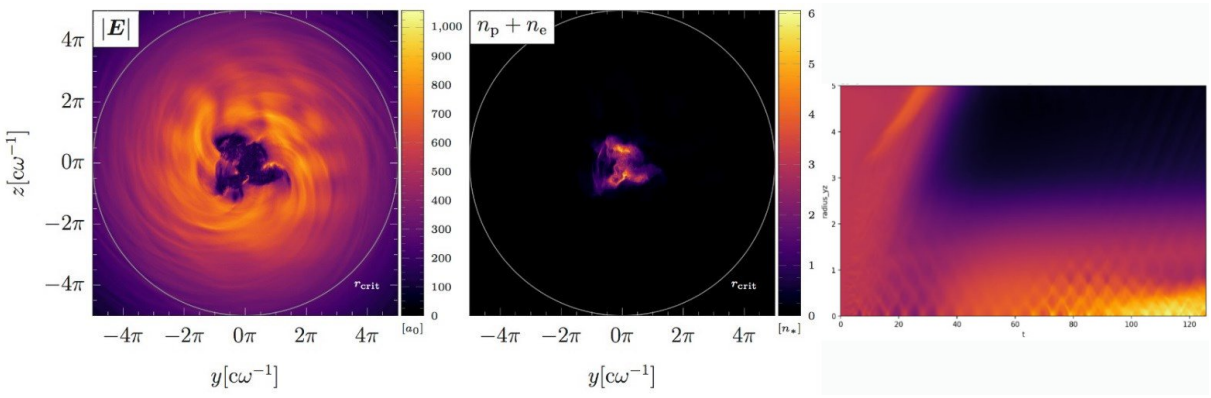

Figure 6: Left a) shows the field strength (Gaussian in space) while the center b) shows the plasma charge density in a rotating electric field (a_0 = 1,000). In the center a patch is clearly masking the field. The patch of clearly over critical density was formed by pair production and holding the particles in the focus, while initial conditions were 10 times under critical. On the right c) the temporal evolution of the density (radius versus time) is plotted, showing that the increasing electric field (Gaussian in time) pushes plasma away into the outer areas, but in the center, where the intensity is high enough, it holds the particles and seeds pair production.

Math and Computer Science

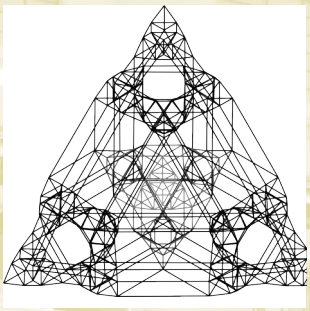

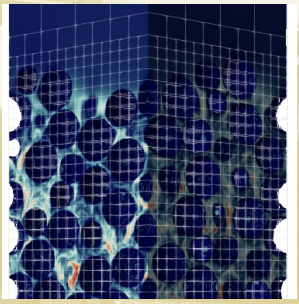

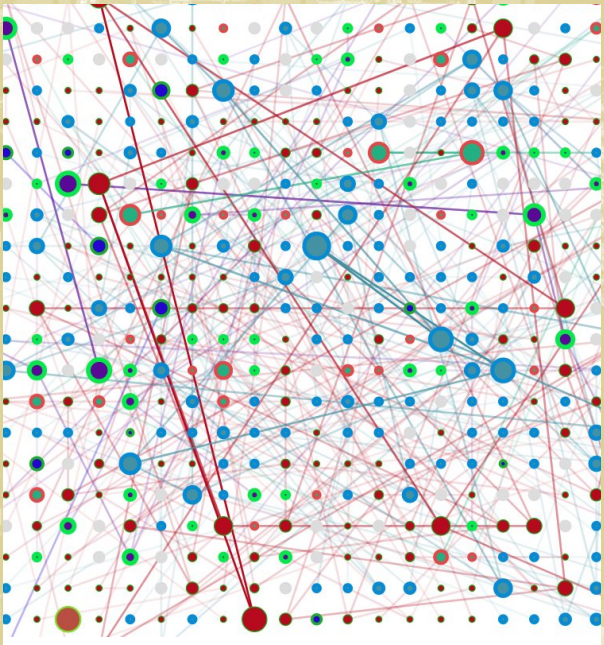

The Next Generation of Benchmarks for Automated Deep Learning

Research Institution
[1]University of Freiburg
[2]Leibniz Supercomputing Centre

Principal Investigator
Frank Hutter[1]

Researchers
Archit Bansal[1], Danny Stoll[1], David Brayford[2]

Project Partners
–

SuperMUC Project ID: pn68xi

Introduction

In recent years, Deep Learning (DL) has been incredibly successful in different areas, from speech recognition and automatic image analysis to prototypes of autonomous driving and world-class level algorithms for playing computer games and board games, such as "Go". The reasons for this success are: (1) the availability of massive training data; (2) advanced DL techniques that can accurately model learning problems by overparameterized large neural networks, called Deep Neural Networks (DNN); and (3) advances in computing software/hardware that made training DNNs affordable. This popularity was promoted by novel DNN architectures for image classification/segmentation tasks, such as ResNet, InceptionNet, DenseNet and U-Net. However, widespread use in other areas is still hindered due to: (1) the lack of sufficient data; and (2) the complex development process of new problem-specific DNN architectures. Our research focuses on the latter. The process of designing DNN architectures is still mostly based on experience and trial-and-error. Inexperienced users are often unable to unlock the power of DL as they struggle to navigate the search space of possible architectures: number of layers, proper operations (e.g, convolution, pooling and skip connection), etc. Our work aims to overcome these issues by investigating Neural Architecture Search (NAS) - a key area in automated DL. The underlying idea is to view the problem of designing a DNN architecture as an optimization problem. A growing body of work now shows that automatically generated DNNs can outperform manually created ones. More generally, NAS is also the natural next step after deep learning: while deep learning automatically learns representations, with NAS we now automatically learn the architectures that allow us to learn those representations. Therefore, NAS has become one of the hottest and most intensely researched directions in deep learning, with an exponentially growing number of publications on the topic. NAS is, however, remarkably costly as it might involve training hundreds of thousands of DNN architectures, taking from days to weeks or even months. Even more concerning is the carbon footprint of such simulations due to the enormous power consumption. In order to fix this, PI Frank Hutter has spearheaded the creation of so-called tabular NAS benchmarks, which train a large number of DNNs architectures and record their validation performance in a table, in order to allow very fast evaluations of NAS algorithms after the one-time cost of creating the tabular NAS benchmark. This line of work has been extremely successful, but current NAS benchmarks are still limited in several ways:

- No logging of side information.
- No variation of hyperparameters.
- Limitation to a single or very few datasets.
- Limitation to simple search spaces.
- Focus on expensive evaluations, rather than cheap multi-fidelity evaluations used by modern NAS optimizers.

In our work we use the SuperMUC-NG cluster to create the next generation of NAS benchmarks to overcome all of these limitations. This next generation of benchmarks will facilitate research on NAS, while reducing the environmental impact of conducting such research and lowering the barrier to entry in this field of research. An exciting aspect of our work for the HPC field is that, due to our focus on cheap multi-fidelity evaluations (reduced network size, reduced image resolutions, etc), in contrast to the predominant use of GPUs in other areas of deep learning, our experiments are actually much more cost-efficient to perform on a large cluster of CPUs; thus, we carry them out on SuperMUC-NG. More information about our research group is available at our website [1] and about our research projects at the project website [2].

Results and Methods

Our on-going project has already resulted in the creation of the largest known benchmark dataset in the field to date, containing 54 million data points each consisting of over 20 metrics about the performance characteristics of the trained models. Our benchmark will facilitate research on automated Deep Learning in

Property	Reference	Ours
# Architectures	~ 1,000	15,625
# Hyperparameters	2 x discrete	2 x discrete, 2 x continuous
# Fidelities	0	4
# Metrics	9	20
# Datasets	1	3
# Trained DL models	48,000	810,000
# Data points	192,000	140,000,000
Extensive logging of side information	No	Yes

Table 1: This table compares the current status of our ongoing project to the most recent work in the field, titled NAS-HPO-Bench-II (October, 2021), that shares a number of common properties with our work but is much more limited in its scope.

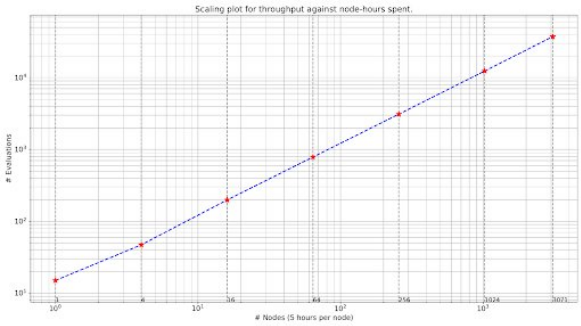

Figure 1: Scaling graph created from scaling studies performed for the block operation.

several ways:

- Since our search space consists of both architectures and hyperparameters, our benchmark supports research for NAS, Hyperparameter Optimization (HPO) and joint NAS and HPO.
- Our dataset contains 5,400 unique fidelity settings spread over 4 different fidelity parameters that control the cost of training a neural network (most benchmarks are limited to 0 or 1 fidelity parameter), a unique feature of our benchmark that would support researchers who want to employ Multi-Fidelity Optimization techniques in NAS and HPO.
- Our dataset also records 20 metrics and heterostructures that could be used by researchers to employ Multi-Objective Optimization techniques for their research.
- Since our dataset also spans a growing number of datasets (3 thus far, more are in progress), researchers will also have an opportunity to employ Transfer Learning techniques with our benchmark.
- Additionally, we have a collection of nearly 10 TB of checkpoint data, which can, e.g., be used when benchmarking algorithms that employ so-called Zero-Cost Proxies, another recent direction in NAS research.

See Table 1 for a comparison with a reference benchmark published in October, 2021. We employed a job setup that is known to be quite possibly the most efficient way to utilize parallel compute resources for running any calculation, known as an “Embarrassingly Parallel” job setup. This allows us to scale-up the number of computations we perform in parallel, thereby increasing cluster usage efficiency, almost infinitely. With this job setup we have, thus far, managed to train 810k unique DL model configurations that consist of unique combinations of architecture, hyperparameter and fidelity choice on three different datasets. To collect this data, we used a total of 27M core hours. Figure 1 illustrates the near linear scaling efficiency of the parallel processing strategy employed. This information was used to by the LRZ to determine if the workflow could be deployed on a significant portion of SuperMUC-NG during the “block operation”. In the “block operation” the project was provided exclusive use of SuperMUC-NG for 2 days. During this time significant amount of compute resource were used and the benchmarks generated are being used by another project that produced interesting results, which will go into future publications [3,4] and a Master’s thesis [5]. Our work offers a staggering amount of cost-savings in the form of DNN evaluations that can be replaced by queries to our benchmark: On the one hand, the average amount of compute-time needed to evaluate the most important class of models in our benchmark is greater than 45 core-hours. On the other hand, a single query to our benchmark produces equivalent data at the cost of less than 0.1 core-seconds. A single research paper may need to evaluate many hundreds of thousands of such models, and using our benchmark will thus both help democratize research in this field and save very substantial compute time & carbon emissions. As a result, other related NAS benchmarks have been cited by hundreds of research papers, and we expect the same for our new benchmark.

Ongoing Research / Outlook

Currently, we use the remaining compute resources of our project to create benchmarks for more datasets, as the inclusion of only one or very few target datasets is one of the limitations of existing NAS benchmarks. For this, we are able to utilize the massive number of parallel compute nodes available on the SuperMUC-NG to run simulations for up to 100k Deep Learning trainings in parallel. The greatest limitation we face is the availability of RAM on a per-node basis, which bottlenecks the number of parallel computations that we can perform. Nonetheless, the SuperMUC-NG provides us with parallel compute resources well beyond what we see in related work (see Table 1). Finally, we plan to create NAS benchmarks based on complex hierarchical search spaces, which are in contrast to the simple search spaces of existing benchmarks. As the NAS research community is only starting to tackle hierarchical NAS, cheap and rigorous ways to benchmark in this area are of dire need. Within our remaining compute resources we aim to create a proof-of-concept for such benchmarks and will apply for a follow-up project focusing on these hierarchical NAS benchmarks.

References and Links

[1] https://ml.informatik.uni-freiburg.de/
[2] https://www.automl.org/
[3] A. Bansal, D. Stoll, M. Janowski, A. Zela, F. Hutter, "JAHS-Bench-201: A Foundation For Research On Joint Architecture And Hyperparameter SearchŁ". Submitted for peer-review at the 36th Conference on Neural Information Processing Systems, Datasets and Benchmarks Track. June, 2022.
[4] https://github.com/automl/jahs_bench_201
[5] Janowski et al., paper in preparation.

Massively Scalable Discrete Algorithms for the Basic Toolbox

Research Institution
[1]Karlsruhe Institute of Technology

Principal Investigator
Peter Sanders[1]

Researchers
Michael Axtmann[1], Demian Hespe[1], Lukas Hübner[1,2], Sebastian Lamm[1], Charel Mercatoris[1], Matthias Schimek[1], Dominik Schreiber[1], Tim Niklas Uhl[1]

Project Partner
[2]Heidelberg Institute of Theoretical Studies

SuperMUC Project ID: pn72pu

Introduction

Algorithms are at the heart of the information age – they control most nontrivial aspects of computer applications. However, algorithm development (and therefore the progress of the information age) is facing a major crisis by the collision of two revolutionary developments. On the one hand, we observe an explosion of the amount of data to be processed (big data). On the other hand, the performance of a single device for executing a sequence of program instructions (a processor core) is stagnating. The widening gap between required and available performance can only be closed by decisively improving the algorithms necessary for computationally-demanding applications. The algorithms must become more efficient for large inputs, and they must be able to efficiently use many processors at once (parallel processing). We therefore target the most frequently used building blocks of algorithms (the basic toolbox) as well as scalability to the largest inputs and the largest machines. More concretely, we address some of the discrete algorithms that play a role in almost all nontrivial computer programs: Sorting and basic algorithms for graphs. Moreover, parallel computing requires additional, equally omnipresent basic toolbox operations such as collective communication (broadcast, reduce, prefix sum,…) and load balancing. We are not considering numerical algorithm which are already covered much better.

To develop massively scalable algorithm for the discrete basic toolbox, we use the methodology of algorithm engineering (AE) that integrates the robustness and scalability guarantees of algorithm theory with careful, practice oriented modelling, implementation, and experimental evaluation. The result of this are algorithms that scale two orders of magnitude better than the state of the art. Most of them are available as open-source software. Although we are not directly targeting the numerical applications that are so far the main users of supercomputers, such applications will also benefit because our algorithms help with load balancing, collective communication, and data analysis.

Results and Methods

We now discuss two of the main sub-projects we investigated: scalable graph algorithms [2] and massively parallel malleable jobs [3,4]. In addition to these sub-projects, we also examined robust and fault-tolerant massively parallel sorting [1] and scalable (hyper-)graph partitioning.

Scalable Graph Algorithms
Most state of the art HPC platforms are heavily designed for numerical simulations that feature fairly regular data access and communication patterns. However, more data intensive and irregular workloads are becoming increasingly popular, i.e. from materials science applications. Graphs are a common representation for the data sets used by these applications. In order to guide the design of modern hardware architectures supporting these types of workloads, the highly successful Graph 500 benchmark was devised. On the downside, the Graph 500 benchmark basically restricts itself to a single problem on a single family of random graphs.To address these issues, we designed

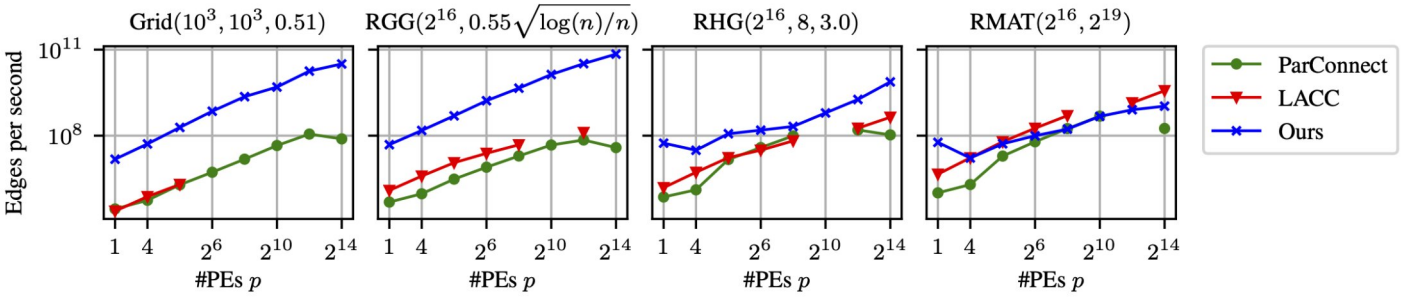

Figure 1: Weak scaling results of the connected component algorithms on synthetic instances.

and implemented multiple basic graph algorithms that scale for tens of thousands of cores on a wide spectrum of input instances. In particular, we investigated connected components, triangle counting and minimum spanning forests. We now briefly present our findings for connected components [2]. We developed a communication-efficient algorithm that scales to graphs with billions of edges and tens of thousands of cores. Our algorithm is based on a recent linear-work shared-memory parallel algorithm by Blelloch et al. and the low diameter graph decomposition by Miller et al. Furthermore, we implemented an approach to distribute high degree vertices that aims to reduce communication bottlenecks. We compared the scaling behaviour (weak and strong) of our algorithm with two state of the art algorithms: LACC by Azad and Buluc, and ParConnect by Flick et al. For our weak scaling experiments, we used different types of random graphs. In our strong scaling experiments, we use a wide spectrum of real-world instances. Overall, our algorithm scaled particularly well for graphs that have a fairly uniform degree distribution, such as grids and geometric graphs. In particular, our algorithm is up to 410 times faster (measured as throughput in edges per second) on grids and up to four orders of magnitude faster for random geometric graphs. Scaling for more skewed degree distributions, such as RMAT graphs, is worse. Nonetheless, performance is still in line with both competitors.

Massively Parallel Malleable Jobs

A parallel algorithm is malleable if it can handle a flexible number of compute nodes during its execution. Malleability is an appealing concept because it allows for continuous redistribution of computational resources in order to make fair and optimal use of a distributed system. In the scope of this sub-project, we have focused on an in-depth case study of applying the concept of malleability to propositional satisfiability (SAT) solving in HPC environments [3,4]. As such, we have designed and implemented a distributed malleable SAT solving engine which we have shown to scale to up to 2,560 cores. Our system, the Mallob SAT engine has won multiple awards at the International SAT Competitions, running on up to 1600 hardware threads at once, despite the fact that the competition rules did not allow us to exploit the malleability of our approach. The central novel feature of our approach from an application perspective is a malleable and succinct approach to the periodic exchange of knowledge among the many individual solver backends. We used our award-winning malleable SAT engine to evaluate a first iteration of our malleable job scheduling and load balancing approach Mallob. We propose to arrange the compute nodes associated to a particular job within a randomised binary tree. Periodically, a lightweight all-reduction enables each node to compute the fair number of nodes its respective job is supposed to have. Depending on this number, the binary tree of each job grows or shrinks as necessary, suspending or (re-)activating particular nodes.

We have shown that our approach commonly schedules incoming jobs within a fraction of a second and is able to reliably redistribute all present jobs in a flexible manner to consistently make best use of the HPC environment at hand. From an application perspective, we showed that SAT solving can profit from this malleability: Using SuperMUC-NG, we found that the time needed to resolve a formula decreases if additional compute nodes sometimes join the solving effort.

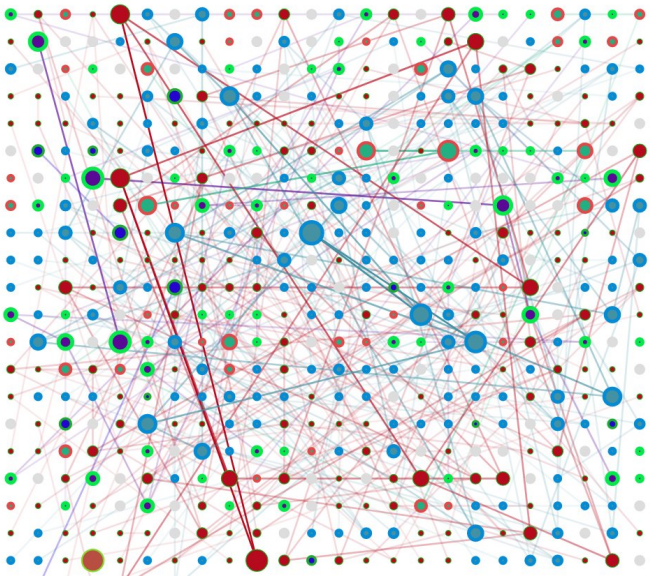

Figure 2: Snapshot of Mallob. Each node is a MPI process, and its color represents the job it works on. Edges between nodes represent communication dependencies.

Ongoing Research / Outlook

All of our sub-projects are actively being worked on. In particular, we are working on publishing results on our in-memory replication mechanism ReStore, which serves as a building block for a diverse set of applications, including fault-tolerant (sorting) algorithms. Furthermore, we are developing additional scalable graph algorithms including hybrid algorithms for both minimum spanning forests and triangle counting. Our job scheduling algorithms are being improved in different aspects including scheduling latencies and balancing fairness. We are also investigating other application besides propositional satisfiability. Finally, we are developing a scalable distributed graph partitioner that scales better for large numbers of blocks and irregular graphs than the current state of the art. This serves as a building block for several applications that require parallel processing.

References and Links

[1] https://algo2.iti.kit.edu/
[2] S. Lamm, P. Sanders: Communication-efficient Massively Distributed Connected Components. Accepted at IPDPS 2022.
[3] D. Schreiber, P. Sanders: Scalable SAT Solving in the Cloud. SAT 2021, pp. 518–534.
[4] D. Schreiber: Mallob in the SAT Competition 2021. SAT Competition 2021, pp. 38–39.
[5] M. Axtmann: Robust Scalable Sorting. PhD thesis, KIT, 2021.

waLBerla – A massively parallel framework for multi-physics simulations

Research Institution
[1]Chair for System Simulation (Informatik 10), Friedrich-Alexander Universität Erlangen Nürnberg

Principal Investigator
Harald Köstler[1]

Researchers
M. Bauer[1], S. Eibl[1], J. Hönig[1], N. Kohl[1], C. Rettinger[1], C. Schwarzmeier[1], D. Thönnes[1], B. Vowinckel[2]

Project Partner
[2]TU Braunschweig

SuperMUC Project ID: pr86ma

Introduction

The open-source massively parallel software framework waLBerla [1,2] (widely applicable lattice Boltzmann from Erlangen) provides a common basis for stencil codes on structured grids with special focus on computational fluid dynamics with the lattice Boltzmann method (LBM).

Other codes that build upon the waLBerla core are the particle dynamics module MESA-PD and the finite element framework HyTeG.

Various contributors have used waLBerla to simulate a multitude of applications, such as multiphase fluid flows, electrokinetic flows, phase-field methods and fluid-particle interaction phenomena.

The software design of waLBerla is specifically aimed to exploit massively parallel computing architectures with highest efficiency. In order to simulate real-world scenarios, waLBerla relies on using the immense compute power available on modern high performance computing systems such as LRZ's SuperMUC-NG.

Results and Methods

Simulation study of particulate flows
Using direct numerical simulations to study particulate flows has become a promising alternative to laboratory experiments. They allow a deeper insight into physical properties, can be controlled more easily, and are more cost efficient for parametric studies. For that reason, we are constantly developing further our fluid-particle coupling module inside the waLBerla framework. As a result, the coupling module has been adapted to now also support waLBerla's newly developed particle simulation module MESA-PD which now allows for much more flexibility regarding the particle-interaction algorithms. We used this gained flexibility to further improve the accuracy of the interaction algorithms. We employ these novel techniques to study particulate flow scenarios, like erosion processes of riverbeds.

To obtain statistically converged results, such systems often require a large amount of particles and long run times for which we employ the SuperMUC-NG supercomputer.

Another topic of our numerical studies is to track down the source that initiates particle erosion. In collaboration with Bernhard Vowinckel, TU Braunschweig, we revisit their recent study on the erosion of single particles in turbulent channel flow. As shown in Figure 1, a movable layer of spheres is placed on top of a fixed layer. An erosion process is characterized by a sphere leaving the top layer and traveling through the domain. It is supposedly triggered by strong fluid vertices hitting the sphere or a former collision by an already moving particle.

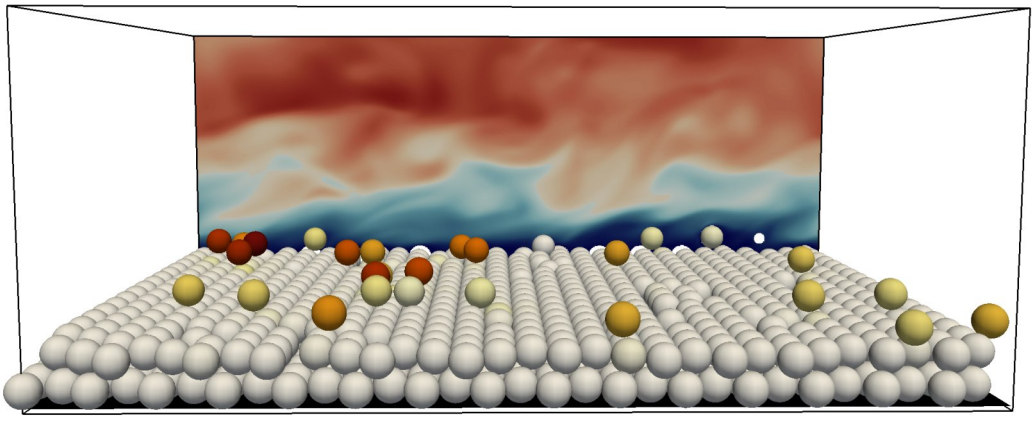

Figure 1: Erosion study of a single movable layer of spheres above a fixed layer inside turbulent flow. The spheres are colored according to their velocity magnitude.

Besides the long run time and the fine spatial resolution, the required logging of all particle positions and velocities at all time steps is a major challenge for massively parallel execution.

This work has been presented at the PARTICLES conference 2019 in Barcelona [3].

Simulations of flow through porous media
Turbulent flow through porous media is of relevance in a large variety of scientific and industrial applications. While numerical simulations of such applications should preferably be simulated with direct numerical simulations, computational limits and costs often only allow using under-resolved numerical simulations with turbulence models.

In collaboration with the group of Vivek Buwa from the IIT Delhi, we have used direct numerical LBM simulations to asses the accuracy of turbulence models that are commonly used for the simulation of flow through complex geometries.

Our model porous medium was constructed by simulating a sedimentation process using waLBerla's rigid body dynamics module. The periodic porous medium is composed of 113 randomly arranged spherical particles. In the fluid simulation, the resulting pore spaces are resolved with a resolution equivalent to 160 computational cells per particle diameter. The total domain consists of about 6e8 computational elements with the computational grid being refined only within the pore spaces to increase efficiency, as shown in Figure 2. Using modern code generation technology, we employ a highly optimized implementation of the cumulant lattice Boltzmann collision operator to increase the numerical stability.

The largest simulation was performed on 768 nodes of SuperMUC-NG and required about 18 h of compute time.

Our findings have been presented at two conferences [3, 4] and in a journal publication [5].

Ongoing Research / Outlook

We are currently preparing for time-dependent runs also in the TerraNeo project [7], and are estimating, that during the next year, these experiments may together with the riverbed experiments, consume the majority of the remaining compute time.

We are grateful, that during the friendly user phase, especially the phase-field simulations could be computed without accounting of core-h on the project. Therefore we saved a lot of resources on our account.

References and Links

[1] https://walberla.net
[2] Bauer et al. "waLBerla: A block-structured high-performance framework for multiphysics simulations". In: Computers & Mathematics with Applications (2020). ISSN: 0898-1221. DOI: 10.1016/j.camwa.2020.01.007.
[3] https://congress.cimne.com/particles2019/admin/files/fileabstract/a118.pdf
[4] AS. Ambekar, C. Schwarzmeier, U. Rüde, VV. Buwa: Particle-resolved simulations of turbulent flow through packed bed reactors: comparison of flow simulations using RANS, LES and DNS approaches, 11th International Symposium on Catalysis in Multiphase Reactors & 10th International Symposium on Multifunctional Reactors (Virtual Conference, 21. March 2021 - 24. March 2021).
[5] C. Schwarzmeier, AS. Ambekar, U. Rüde, VV. Buwa: Fully Resolved Lattice Boltzmann Simulations of Turbulent Flow Through Porous Media, Platform for Advanced Scientific Computing (PASC) Conference (Virtual Conference, 5.-9. July 2021).
[6] AS. Ambekar, C. Schwarzmeier, U. Rüde, VV. Buwa: Particle-Resolved Turbulent Flow in a Packed Bed: RANS, LES and DNS Simulations, In: American Institute of Chemical Engineers Journal (2022). ISSN: 0001-1541, 1547-5905. DOI: 10.1002/aic.17615
[7] https://terraneo.fau.de

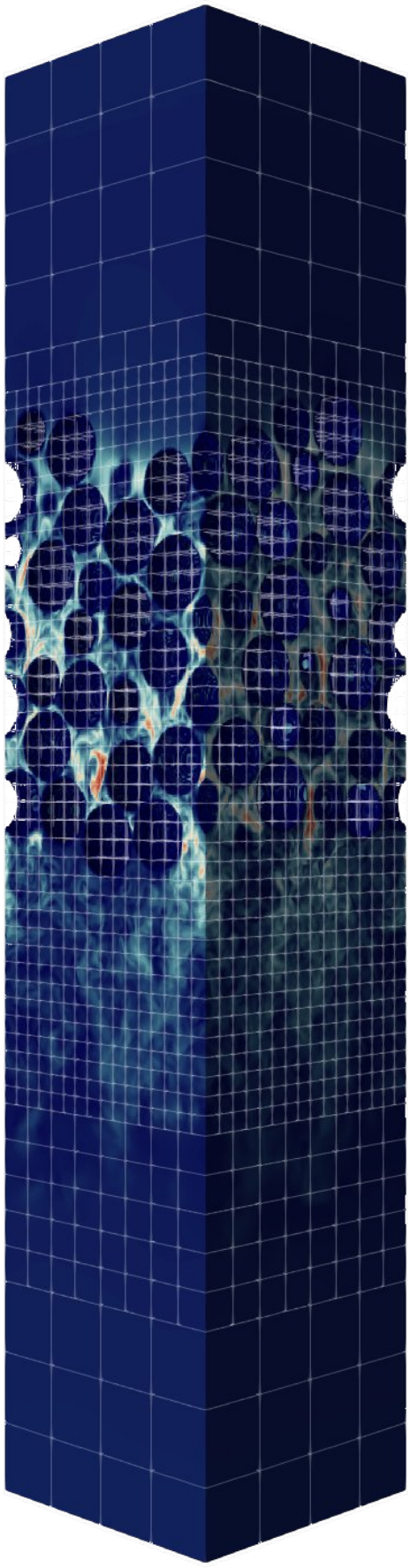

Figure 2: Direct numerical simulation of turbulent flow through a porous medium consisting of spherical particles. The computational grid is statically refined in three levels. For illustration purposes, the grid has been coarsened by a factor of 40. The colors represent the flow velocity with higher velocities being colored red.

Eccentricities in Hanoi Graphs

Research Institution
[1]Mathematical Institute, Ludwig-Maximilians-Universität München

Principal Investigator
Andreas M. Hinz[1,2]

Researcher
Ciril Petr[2]

Project Partner
[2]Institute of Mathematics, Physics and Mechanics, Ljubljana

SuperMUC Project ID: pr87mo

Introduction

The mathematical model of the well-known Tower of Hanoi game, with applications from psychology to computer science, are the *Hanoi graphs* H_p^n (see [2]). The p^n vertices represent the states of the game, i.e. the legal distributions of n discs among p pegs. A single move of one disc is modelled by an edge of the graph. While virtually everything is known for $p = 3$ and many topological graph parameters have been determined for all p, metric properties, referring to the *distance* between two vertices, i.e. the length of a shortest path leading from one to the other, are extremely hard to come by (see Figure 1).

In 1941 B.M.Stewart and J.S.Frame came up with two algorithms and corresponding values, the *Frame-Stewart numbers*, for the length of the solution for the task to get from one perfect state (all discs lie on the same peg) to another in the presence of p pegs, but a minimality proof was missing. The claim that their algorithms indeed lead to optimal move numbers is now known as the *Frame-Stewart conjecture* (FSC). When we started the project, its truth had been established by computer search for $p = 4$ and $n \leq 30$ only. (Meanwhile, the case $p = 4$ has been solved for all n analytically by T.Bousch in 2014.) It came as a big surprise when R.Korf discovered during these computations that for $n = 15$ (but not for smaller n) the *eccentricity* of a perfect state, i.e. the largest distance from a regular state, and consequently the *diameter* of H_4^{15} (this is the largest distance between any two states), is strictly larger than the distance between two perfect states, because everybody had expected that perfect states engender the worst case. Even more surprising was that this *Korf phenomenon*, i.e. excess $ex(n) > 0$, did not occur for $n = 16$ to 19, but reappeared for $n = 20$. The *Korf-Felner conjecture* (KFC) is that Korf's phenomenon happens for all larger n.

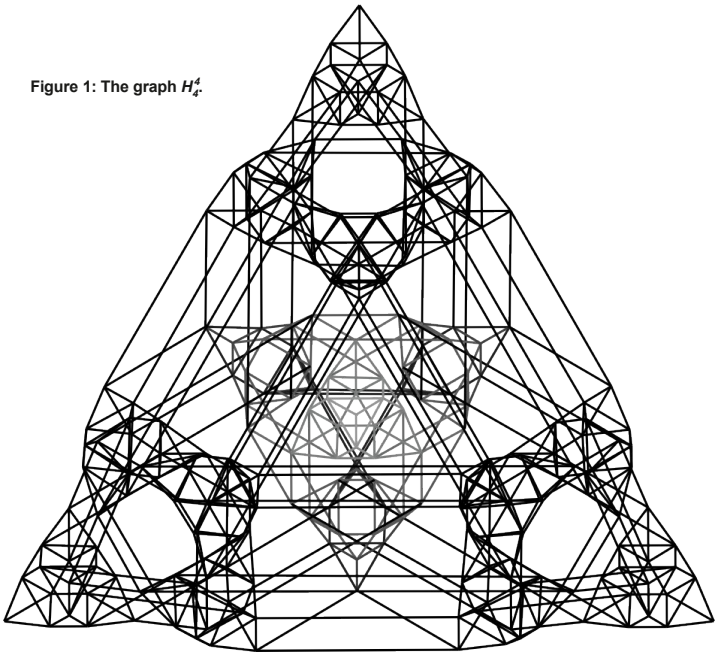

Figure 1: The graph H_4^4.

The main goal of the project was therefore to obtain a better understanding of the metric structure of Hanoi graphs H_p^n by investigating eccentricities of their vertices. E.g., the diameters of H_4^n were known for $n \leq 14$ only. Moreover, Korf's phenomenon appears at $n = 15$, such that this case was a crucial threshold value for which we calculated *all* eccentricities.

Another goal was to address similar questions in variants of the Tower of Hanoi where moves of the discs are restricted, e.g., to neighboring pegs which are arranged in a line (*Linear Tower of Hanoi*), or to a star-like pattern of the pegs (*Star Tower of Hanoi*).

Results and Methods

The diameter of H_4^{15} was found to be 130, not exceeding the eccentricity of a perfect state vertex. The latter value we were able to calculate up to and including $n = 26$ (see Table 1), thereby confirming the KFC up to that number and obtaining all vertices that are further away from a perfect state than another perfect state. Meanwhile, Korf has found in [5], by a different method and without calculating all eccentricities, that for $15 < n \leq 18$ the diameter of H_4^n is equal to the corresponding Frame-Stewart number. We have independently recomputed the diameter for $n = 16, 17, 18$ and succeeded in extending the result also to $n = 19$. So currently no case is known where the perfect states do *not* belong to the periphery.

n	15	16	17	18	19	20
$\varepsilon(0^n)$	**130**	161	193	225	257	**294**
$ex(n)$	**1**	0	0	0	0	**5**
n	21	22	23	24	25	26
$\varepsilon(0^n)$	**341**	**394**	**453**	**516**	**585**	**669**
$ex(n)$	**20**	**9**	**4**	**3**	**8**	**28**

Table 1: Eccentricities of perfect states and their excess in H_4^n; values obtained during our project are in red.

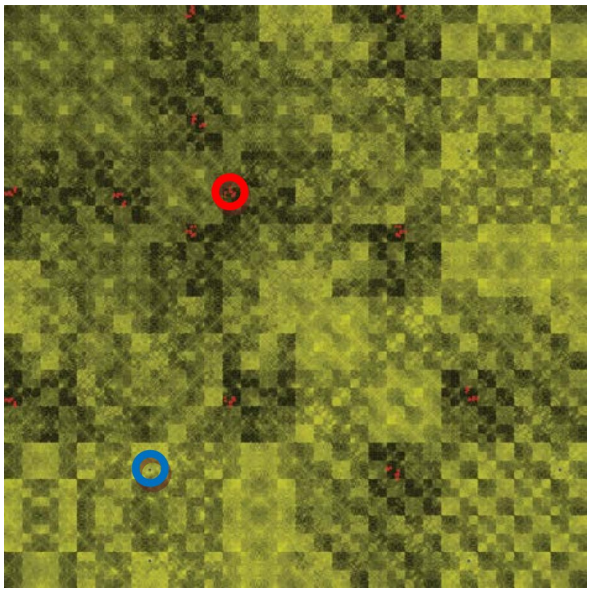

Figure 3: All eccentricities in the graph H_4^{15} represented in a matrix layout (16,384 x 16,384); blue patches mark areas (64 x 64) with center vertices and red patches mark areas with peripheral vertices.

We were able to obtain Korf's result with our DDD BFS algorithm using a single OpenMPI implementation. Since the eccentricities of perfect states are the largest known, they are candidates for being equal to the diameter. If we span a tree rooted in any particular state v, then the union of the first $d(0^n,1^n) - \varepsilon(v) + 1$ tree levels contain states that have lower or equal eccentricity than the perfect state. All these states can be eliminated from further search. So, with each span of a tree we can decrease the set of remaining states to be checked. Lower values of eccentricities give us larger sets of states to be eliminated. In order to accelerate the process of elimination, we have consecutively ran batches of independent parallel spans rooted in randomly chosen starting states from the remaining set of states. A sequence of batches sooner or later exhausted the set of remaining states and at the end of this process we got the information of the largest eccentricity i.e. the diameter. For $n = 16$, 17, 18, 19 we had to execute $8{,}642$ (9), $9{,}028$ (10), $14{,}332$ (46), $57{,}880$ (97) [spans (batches)], respectively, to exhaust the set of all states (Figure 2).

The FSC was confirmed for $p = 5$ up to and including $n = 20$ (see [4]), for $p = 6$ to $n = 16$, and for $p = 7$ to $n = 21$. The latter effort was taken in connection with Conjectures 5.65 and 5.66 in [2]. The list of minimum numbers of disc moves necessary to transfer an n-tower from the center peg to a peripheral one in the Star Tower of Hanoi (sequence A291877 in the *Online Encyclopedia of Integer Sequences*) was extended to

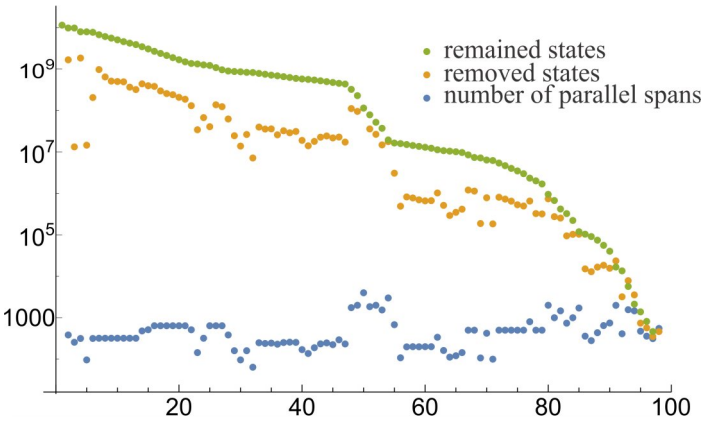

Figure 2: Reduction of search-space through 97 consecutive batches of parallel spans in H_4^{19}.

include the value 1,428 for $n = 22$. This is in agreement with the *Dudeney-Stockmeyer Conjecture* which claims the optimality of a specific strategy related to the Frame-Stewart algorithm; cf. [3]. The conjecture has been tested for other rules for the discs and never failed so far. The only case where it cannot be applied, the Linear Tower of Hanoi, was also investigated for four pegs and up to 23 discs (OEIS A160002); the value obtained for $n = 23$ was strictly better than the one from a sug-gested algorithm.

The basic exploration tool for all our experiments was a breadth-first search (BFS) algorithm, spanning a tree over the graph. Our main concern when implementing BFS for the particular graph H_4^{15} (Figure 3) was its speed and memory footprint. A single span took 350 seconds and had a 690 MB of memory footprint. This enabled us to use all 32 hyperthreads on SuperMUC Phase 2 thin nodes efficiently. The delayed duplicate detection (DDD) BFS algorithm is practical when levels are so large that they cannot fit entirely into the internal memory (RAM). Also there is no need for a special data structure in order to document which vertices have already been visited. Moreover, it is suitable for massive parallelization. Level 565 in a tree rooted in a perfect state in the graph H_4^{26} is the largest (w.r.t. the width of the problem space) and contains $43{,}993{,}240{,}827{,}720$ states.

Ongoing Research / Outlook

We are currently trying to adapt Korf's method to our procedures with the hope to calculate diameters for H_4^n for $n = 20$, where positive excess reappears, and perhaps even for $n = 21$, because as a triangular number this will be the next candidate for some surprise. Computing the diameter of a graph is an interesting and useful problem as such, so implementing an efficient algorithm is a challenge by its own. Other instances of the Dudeney-Stockmeyer Conjecture and the Linear Tower of Hanoi should come into focus in the future.

References and Links

[1] http://www.tohbook.info
[2] A. M. Hinz, S. Klavžar, C. Petr., The Tower of Hanoi-Myths and Maths, Second Edition, Birkhäuser/Springer, Cham, 2018.
[3] A. M. Hinz, B. Lužar, C. Petr., Discrete Appl. Math., in press.
[4] A. M. Hinz, C. Petr., Electron. Notes Discrete Math. 53 (2016), 445-458.
[5] R. E. Korf, Finding the Exact Diameter of a Graph with Partial Breadth-First Searches, Proceedings of the Fourteenth International Symposium on Combinatorial Search (SoCS 2021), 73-78.

Replication-Based Resilience in the ExaHyPE Engine

Research Institution
[1]Technical University of Munich, Department of Informatics

Principal Investigator
Michael Bader[1]

Researchers
Philipp Samfaß[1], Benjamin Hazelwood[2], Tobias Weinzierl[2], Anne Reinarz[1,2]

Project Partner
[3]Durham University

SuperMUC Project ID: pr83no

Introduction

Improving the resilience of simulation software against hardware errors is one of the major challenges for the exascale era. In many fields of computing, replication is the method of choice to overcome hard or soft errors, i.e. errors that either manifest in hard crashes or in data pollution: runs are executed twice (or even more) in parallel, such that silent errors can be detected from different outcomes between the runs, and hard errors can be overcome as long as at least one execution terminates successfully. However, due to the massive increase in computational costs, replication is often unattractive for supercomputing.

In two recent articles [2,3], we have presented approaches to realize replication-based resilience, at significantly reduced overhead, in the ExaHyPE engine for solving hyperbolic PDE systems [1].

Results and Methods

Replication with teaMPI
The library teaMPI developed at Durham University allows the execution of K-fold redundancy for MPI-based simulations. teaMPI plugs into MPI's standard profiling interface (PMPI) and transparently executes simulations in K teams (cmp. Figure 1). Each team executes the MPI application independently. However, short status messages – so-called *heartbeats* – are exchanged between ranks and their replicas, which for example allows to detect whether ranks or entire teams fall behind (or terminate unexpectedly) during the simulation.

Replication and Task Sharing in ExaHyPE
By default, *K*-fold replication increases the computational cost by a factor *K*, which is only acceptable if either hardware is extremely unreliable or if the desired results are required with utmost reliability within a given time. To mitigate this "performance pain", we extended the replication approach offered by teaMPI by sharing of task outcomes between replicated ranks [2].

The hyperbolic PDE engine ExaHyPE follows an MPI+Tasking approach for hybrid parallelization. To improve load balancing in simulations with adaptive mesh refinement, ExaHyPE offers to temporarily migrate tasks between MPI ranks [4]. Combining task sharing and replication allows to share the outcome of tasks between replicas: if an MPI rank finishes a task, it can send the outcome of this task to its replicas, such that the respective task need not be recomputed there. The replicated teams need to follow a different schedule of task computation, such that tasks that are computed in one team are not handled simultaneously in another. We therefore only consider tasks for sharing, if they are not subject to strong task dependencies. While we cannot strictly enforce that tasks are not redundantly computed, we may shuffle their execution order and thus "encourage" non-redundancy. Shareable tasks should also be compute-heavy and exhibit a small memory footprint, to better amortize the costs of task outcome migration.

Experiments on SuperMUC-NG revealed that sharing task outcomes can reduce the overhead (in terms of core hours) for 2-fold redundancy to just 20–40% (40–60% for 3-fold redundancy) compared to a non-replicated run. Task sharing and replication also open new ideas for I/O and checkpointing. For example, we can imagine that while one replica writes a checkpoint, the other team(s) proceed with the simulation. After the checkpoint is written, the respective teams can catch up exploiting the task outcomes shared by its replicas – in the same way as it would catch up after one of the ranks has been temporarily slowed down (cmp. Figure 2), e.g. due to some hardware problem.

Detecting Silent Data Corruption
Silent errors are errors that alter the outcome of the computation, but otherwise remain unnoticed. In the solution of hyperbolic PDEs, for which solutions are characterized by the propagation of features as waves (consider earthquakes, tsunamis, e.g.), such errors are difficult to identify. Silent errors are propagated as waves and thus gradually pollute the solution in large parts of the domain and might only be detected once they lead to blatantly obvious mistakes ("not a number").

Sharing outcomes between replicated solutions allows us to detect discrepancies earlier. In principle, we

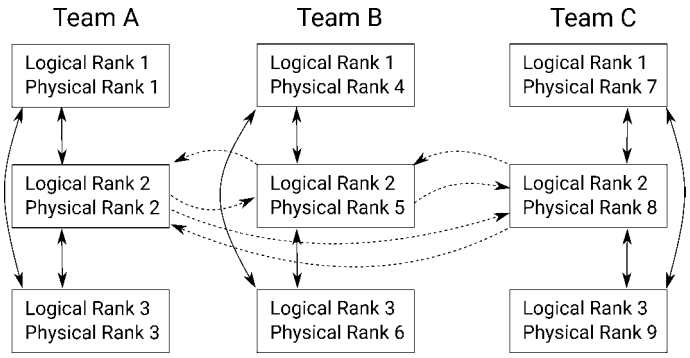

Figure 1: 3-fold replication of MPI ranks in teaMPI. Inter-team communication (vertical arrows) is determined by the MPI applications. Communication between teams is restricted to exchanging small messages (heartbeats, e.g.) between ranks and their replicas.

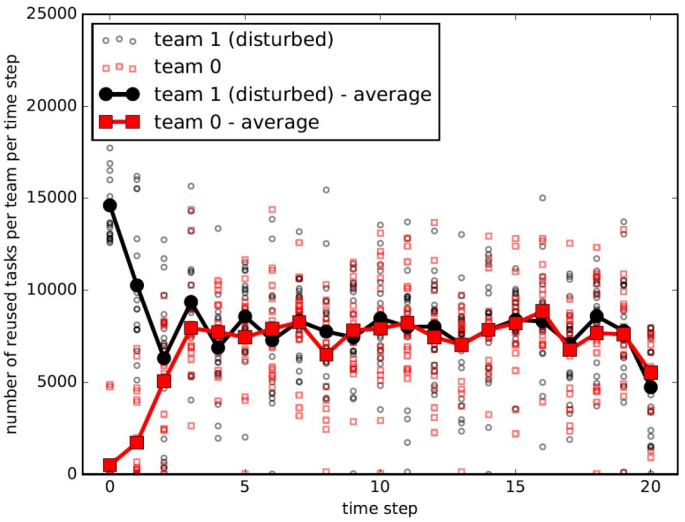

Figure 2: Number of task outcomes obtained from the replica in a simulation with 2-fold redundancy: team 1 has been disturbed and is catching up over a series of simulation time steps (image from [2]).

could compare hash values of computed results between replicas, and thus detect silent errors. However, this would come at a high performance price, again. An improved approach exploits ExaHyPE's specific discontinuous Galerkin discretiza-tion scheme, which applies a so-called *a-posteriori limiter*: After computing a cell-local solution, it checks this solution for physical admissibility – for example, whether certain minimum-maximum principles are satisfied, or whether non-negative physical quantities (e.g., density) actually stay non-negative. We have explored how these admissibility tests can make silent error detection more efficient [3].

We introduced *error criteria*, i.e., functions that characterize how likely a task outcome contains a soft error. Outcomes that include "not a number" values or fail a physical admissibility check are very likely erroneous. Outcomes that violate a minimum-maximum principle could be result of a soft error, but might also just stem from certain features (shocks, etc.) building up in the solution. We therefore combine multiple error criteria into an error indicator. Our approach executes a simulation with 2-fold replication, but restricts sharing of task outcomes to outcomes with a low error indicator score. Otherwise, outcomes are considered "dubious", and are compared with the outcome received from the replica process. The respective control flow for task sharing is illustrated in Figure 3.

By sharing task outcomes, erroneous outcomes can be corrected, if the soft errors are detected early. Transient soft errors can thus be healed. The overhead for soft-error detection and the effectiveness of error correction both depend strongly on the efficiency and sensitivity of the error indicator. Any false-positive declaration of a soft error by the indicators will prevent outcome sharing and force computation of the respective task on both replicated processes, instead. However, if soft errors are not detected in time, they may propagate too far and be detected too late to allow correction. We have shown that several error criteria need to be combined to obtain efficient and sensitive error indicators. We have also demonstrated that the approach scales on up to 35,088 cores of SuperMUC-NG.

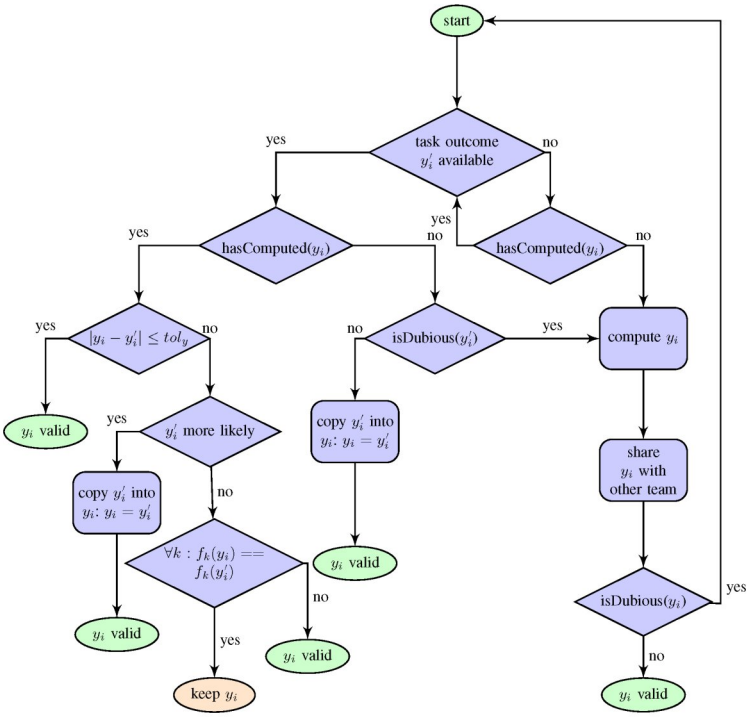

Figure 3: Control flow for computing, sharing, checking and correcting the outcomes of a task execution (image from [3]).

References and Links

[1] ExaHyPE Engine: https://www.exahype.org
[2] P. Samfass, T. Weinzierl, B. Hazelwood, M. Bader: teaMPI – Replication-based Resilience without the (Performance) Pain. ISC'20 (2020). https://doi.org/10.1007/978-3-030-50743-5_23
[3] P. Samfass, T. Weinzierl, A. Reinarz, M. Bader: Doubt and Redundancy Kill Soft Errors—Towards Detection and Correction of Silent Data Corruption in Task-based Numerical Software. FTXS Workshop @SC21 (2021).
[4] P. Samfass, T. Weinzierl, D.E. Charrier, M. Bader: Lightweight task offloading exploiting MPI wait times for parallel adaptive mesh refinement. Conc. Comp. – Pract. E. 32 (24), 2020.

Appendices

SuperMUC-NG: System Description

SuperMUC-NG (Next Generation) completed its installation in September 2018, and started general user operation in August 2019. It replaced the predecessor system “SuperMUC” as the leadership class supercomputer at the Leibniz-Rechenzentrum (Leibniz Supercomputing Centre, LRZ) in Garching near Munich (the MUC suffix refers to the Munich airport code). With more than 311,040 cores, a main memory capacity of 719 TByte and a peak performance of 26.9 petaFLOPS (= 26.9 x 10^{15} floating point operations per second), it is among the fastest supercomputers in the world. SuperMUC-NG entered the TOP500 list of supercomputers in the world at rank 8 in November 2018.

SuperMUC-NG is tightly integrated into the European high-performance computing ecosystem. LRZ is a European Centre for Supercomputing and a Tier-0 Centre for the Partnership for Advanced Computing in Europe (PRACE).

All compute nodes are equipped with Intel Xeon Skylake Platinum 8174 processors. The internal interconnect is a fast OmniPath network with a link bandwidth of 100 Gbit/s. The compute nodes are bundled into 8 domains (islands). Within one island, the OmniPath network topology is a 'fat tree' for highly efficient communication. The OmniPath connection between the islands is pruned with a pruning factor of 1:3.75.

In addition, 65 nodes of the LRZ Compute Cloud were procured with the SuperMUC-NG system to provide services to users that cannot be offered otherwise. The LRZ Compute Cloud currently consists of 82 Cloud Compute Nodes with 40 cores and 192 GB memory, 32 accelerated Cloud Compute Nodes with 40 cores, 768 GB memory and two Nvidia Tesla V100 GPUs with 16 GB high bandwidth memory, and 1 Cloud Huge Node with 192 cores and 6 TB memory.

SuperMUC-NG integrates Lenovo DSS-G for IBM Spectrum Scale (aka GPFS) as building blocks for the storage WORK (34 PiByte, 300 GB/s aggregated bandwidth) and SCRATCH (16 PiByte, 200 GB/s aggregated bandwidth). The LRZ Data Science Storage offers additional 20 PiByte (with 70 GB/s aggregated bandwidth) for long-term storage of project data that can also be shared with the science community throughout the world. The HOME filesystem has a capacity of 256 TiByte.

LRZ's tape backup and archive systems are operated via the Spectrum Protect (formerly Tivoli Storage Manager) software from IBM, providing 260 Petabytes of capacity to the users of SuperMUC-NG. Digital long-term archives help to preserve simulation results. User archives are also mirrored to a remote site for potential disaster recovery.

Like its predecessor, SuperMUC-NG is cooled with hot water with an inlet temperature of up to 50 degrees Celsius and an outlet temperature of up to 56 degrees Celsius. These high temperatures allow to use the waste heat to generate cold water using a large set of adsorption chillers produced by the company Fahrenheit. The adsorption chillers are based on the physical

Figure 1: SuperMUC-NG.

principle of using solid materials of enhanced water vapor adsorption capacity for cooling via the evaporation of water. The cold water from the chillers is used to remove the waste heat of air-cooled components such as network switches, power supplies and storage. In addition, LRZ's buildings are heated re-using SuperMUC-NGs heat dump.

SuperMUC-NG is available to all German and European researchers to expand the frontiers of science and engineering. Collaborations of European scientists can submit proposals to PRACE. Twice per year, the Gauss Centre for Supercomputing has a dedicated call for large scale projects that request more than 45 million core-hours. Smaller proposals by German scientists can be submitted throughout the year directly to LRZ.

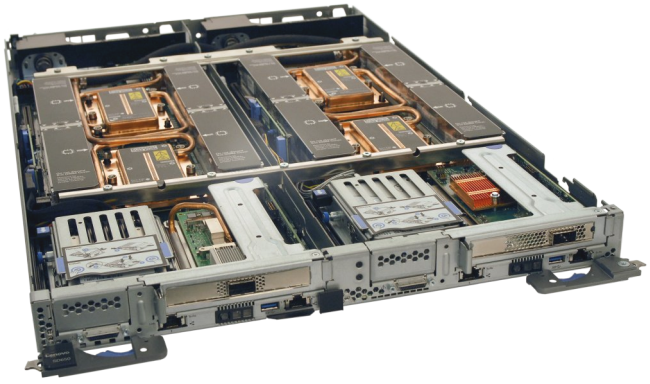

Figure 2: Dual node chassis of SuperMUC-NG.

Technical data

Compute Nodes	**Thin Nodes**	**Fat Nodes**	**Total (Thin + Fat)**
Processor Type	Intel Skylake Xeon Platinum 8174	Intel Skylake Xeon Platinum 8174	Intel Skylake Xeon Platinum 8174
Cores per Node	48	48	48
Memory per Node [GByte]	96	768	N/A
Number of Nodes	6,336	144	6,480
Number of Cores	304,128	6,912	311,040
Peak Performance @ nominal [PFlop/s]	26.3	0.6	26.9
Linpack [PFlop/s]	–	–	19.476
Memory [TByte]	608	111	719
Number of Islands	8	1	9
Nodes per Island	792	144	N/A
Filesystems			
High Performance Parallel Filesystem	50 PiB @ 500 GB/s		
Data Science Storage	20 PiB @ 70 GB/s		
Home Filesystem	256 TiB		
Infrastructure			
Cooling	Direct warm water cooling		
Waste Heat Reuse	For producing cold water with adsorption coolers		
Software			
Operating System	Suse Linux Enterprise Server (SLES)		
Batch Scheduling System	SLURM		
High Performance Parallel Filesystem	IBM Spectrum Scale (GPFS)		
Programming Environment	Intel Parallel Studio XE, GNU compilers		
Message Passing	Intel MPI, (OpenMPI)		

Usage of SuperMUC-NG

After three years of operation, SuperMUC-NG Phase 1 is still one of the fastest CPU-only supercomputers in the world. The current HPC trend to accelerated systems will manifest in the Phase 2 extension coming in 2023, which will incorporate Intel Ponte Vecchio GPU accelerators, yielding a much better FLOP/s per Watt ratio than current CPUs. However, the advantage of CPU-based systems is still a general usability for many fields of scientific computing without having to invest too much effort into code porting.

Figure 1 displays the share of used core hours by the various scientific disciplines according to level two of the DFG classification scheme. The most demanding field of numerical scientific simulations traditionally is computational physics, consuming more than half of the available compute time. Here, large shares of the core hours go to Nuclear and elementary particle physics with, e.g., lattice QCD simulations, astrophysics with simulations of galaxy and star formation, or gravitational waves, as well as condensed matter physics with the computation of quantum effects in solid state matter. The second largest community are engineering applications with computational fluid dynamics simulations of gas and liquid flows, and combustion, which require about 20% of the overall compute time. The rest is utilized by various other scientific areas such as biology, chemistry, computational medicine, geosciences, computer science and mathematics, including machine learning and artificial intelligence methods. The projects in these scientific domains are numerous but typically consume smaller shares because their simulation models do not scale as readily as many physics or engineering applications.

However, the time evolution of the shares displayed in Figure 2 shows that emerging scientific domains have caught up over the time of operation of SuperMUC-NG and enlarged their share. With respect to the origin of the compute time projects, it is not surprising that about 40% of the allocated time has been applied for by researches located in Bavaria. Here, the strong relations LRZ to the Munich and Bavarian universities play an important role, but also the collaboration with researchers of the Max Planck facilities in Garching. Another 50% of the compute time is used by researchers in the other federal states of Germany. About 10% of the available resources have been furnished to European researchers via the PRACE (Partnership for Advanced Computing in Europe) initiative. However, the PRACE project has finished now and will be replaced by allocations offered by EuroHPC pre-exa and exascale machines.

During the three years of operation SuperMUC-NG produced more than 6.6 billion core hours running over 1.8 million jobs. The productive core hours reach about 82% of the theoretically possible value during that time. Idle times are due to regular maintenances and scheduling gaps. Furthermore, in the spring of 2020, security issues required a downtime of more than a month with a strong impact on the productivity. The productivity of about 85% reached in the last year corroborates the expected value due to the long standing experience operating large HPC systems.

For detailed reports on the consumption of the SuperMUC-NG compute time, see [1].

References and Links

[1] https://doku.lrz.de/display/PUBLIC/Usage+Statistics+for+SuperMUC-NG

Year	Months	Usage [M core-h]	Productivity	No. of jobs submitted
2019	5	830.1	83.0 %	181,474
2020	12	2,104.1	77.0 %	659,920
2021	12	2,308.5	84.6 %	684,638
2022	7	1,361.5	86.0 %	333,064
Total	**36**	**6,604.1**	**82.1 %**	**1,859,096**

Table 1: Usage, productivity, and number of submitted jobs on SuperMUC-NG. In 2019, SuperMUC-NG started operation in August, therefore only 5 months are reported. In 2022, there are 7 months reported (the reporting time frame for this book ended in July, 2022). Productivity is <100% due to system mainentance.

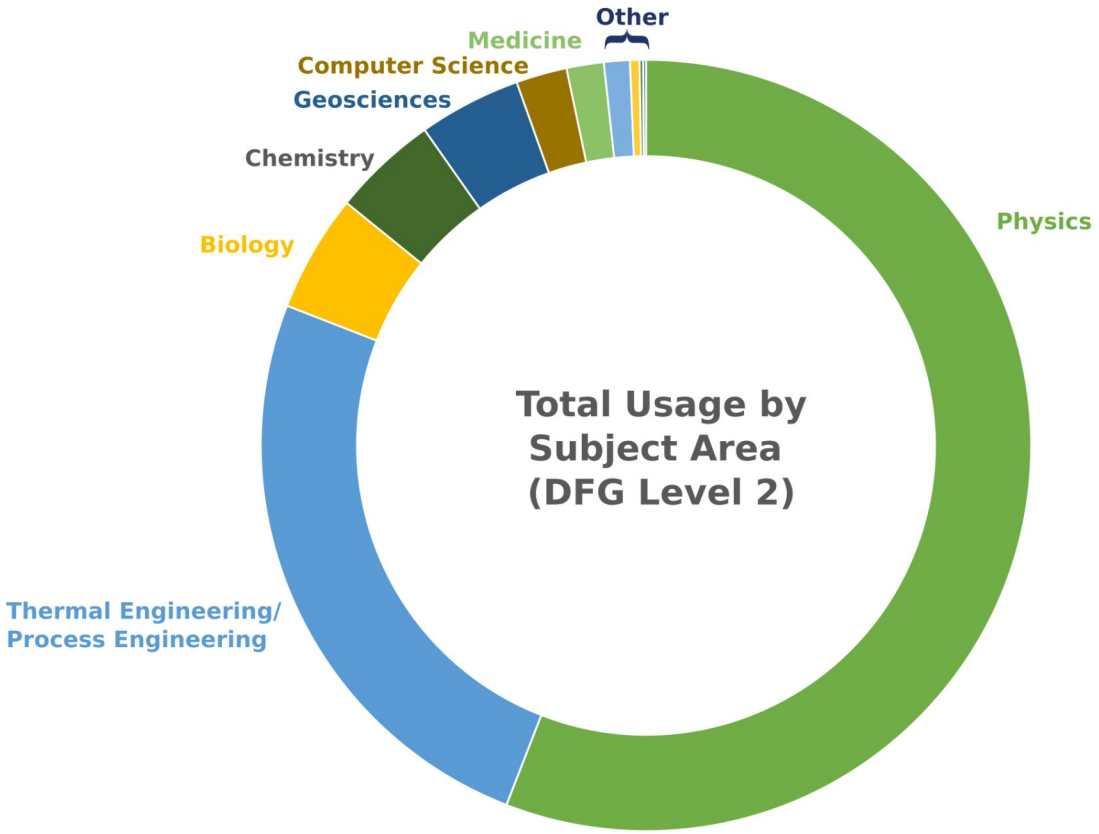

Figure 1: Total usage of SuperMUC NG by subject area (level two of the DFG classification scheme).

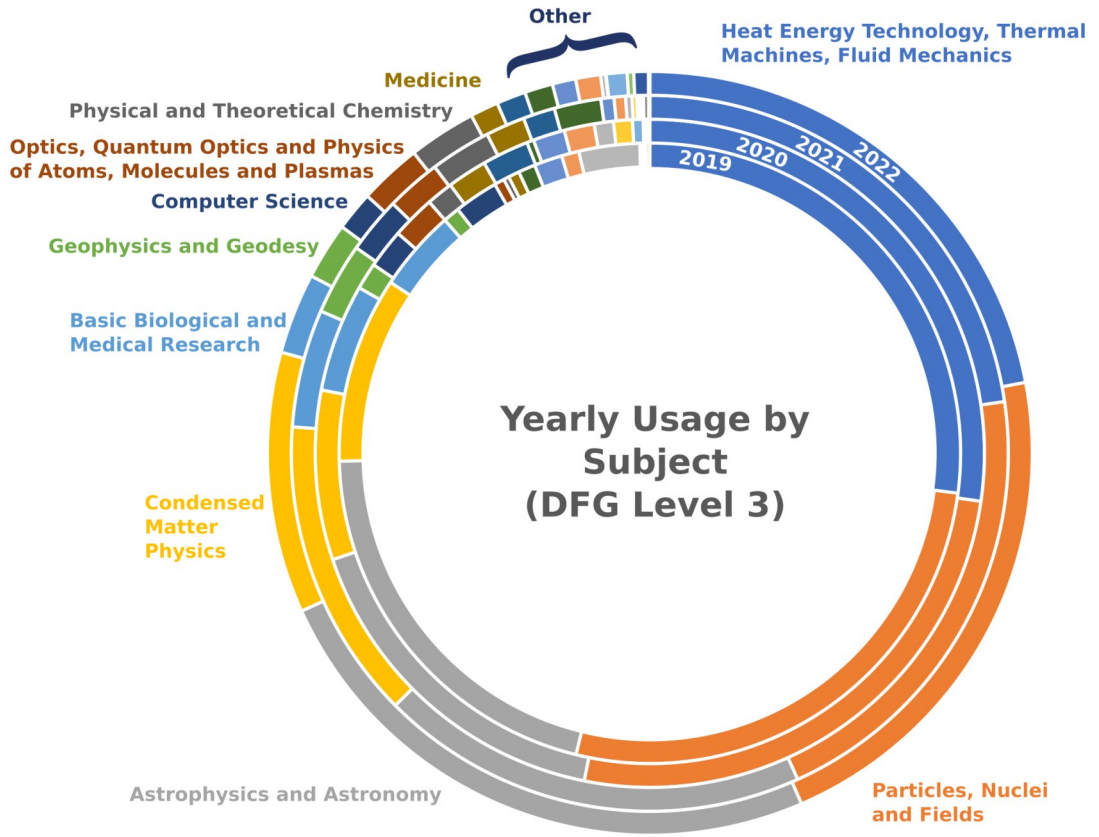

Figure 2: Detailed yearly usage of SuperMUC-NG by subject (level three of the DFG classification scheme).

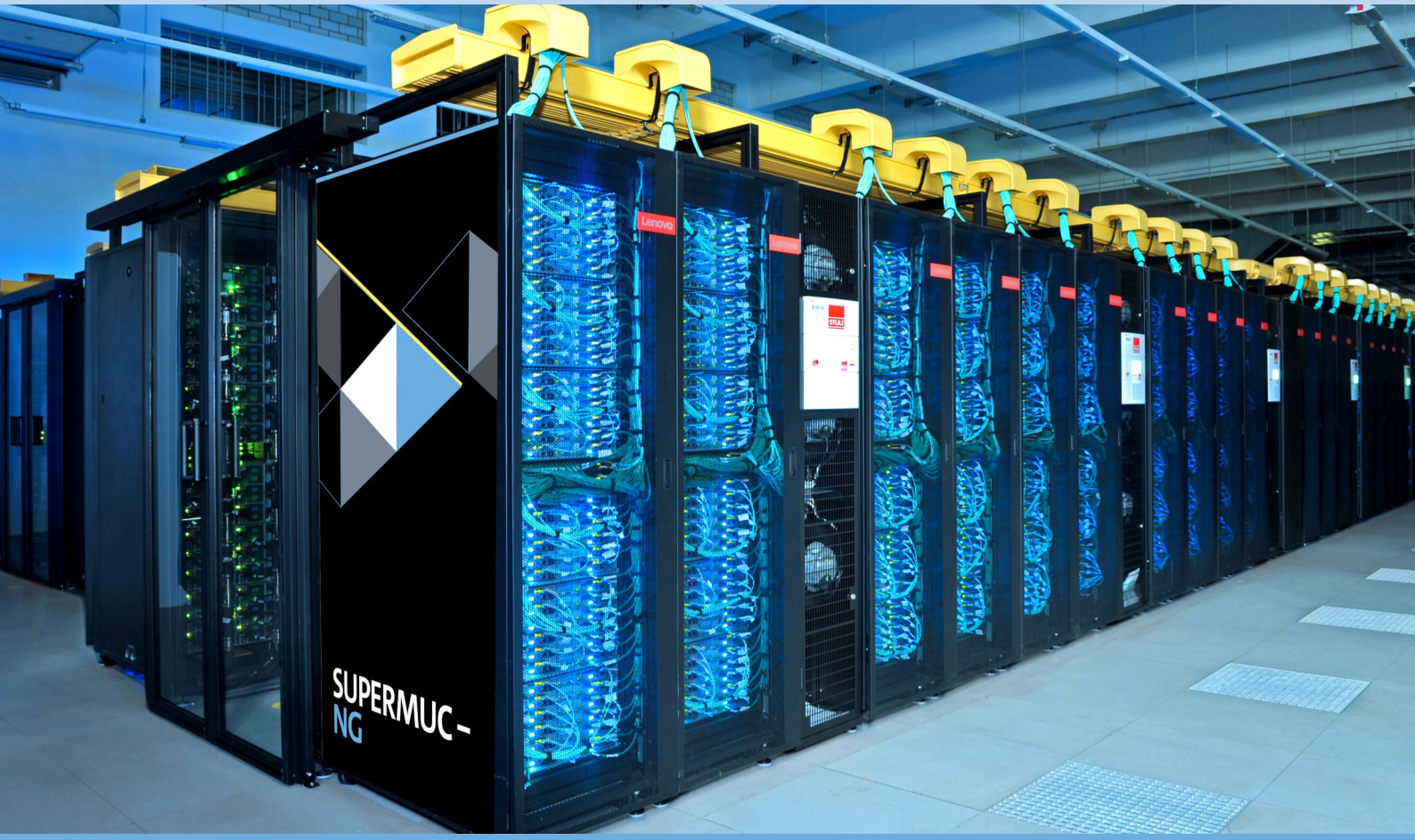

In this book, the Leibniz Supercomputing Centre (LRZ), a member of the Gauss Centre for Supercomputing (GCS), reports on the results of numerical simulations, performed in the time frame June 2020 – December 2021. The 100 project reports give an impressive overview of the utilization of SuperMUC-NG, the Tier-0 system of the Bavarian Academy of Sciences and Humanities.

SuperMUC-NG is based on Lenovo ThinkSystem SD650 DWC compute nodes and equipped with Intel Skylake Xeon Platinum 8174 processors. The machine started user operation in August 2019 and delivered more than 2.5 billion core-hours for numeric scientific simulations up to today. A detailed system description can be found in the appendix.

The articles provide an overview of the broad range of applications that use high performance computing to solve challenging scientific problems. For each project, the scientific background is described, along with the results achieved and the methodology used. References for further reading are included with each report.

GEFÖRDERT VOM

Gefördert durch den Freistaat Bayern

Bundesministerium
für Bildung
und Forschung

ISBN 978-3-9816675-5-4
https://www.lrz.de/hpcbooks